PB81-188542

Effect of Parameters of Filtration on Dust Cleaning Fabrics

Institute of Industry of Cement Building
Materials, Opole (Poland)

Prepared for

Industrial Environmental Research Lab.
Research Triangle Park, NC

Mar 81

U.S. Department of Commerce
National Technical Information Service
NTIS

PB81-188542

EPA-600/7-81-028
March 1981

EFFECT OF PARAMETERS OF FILTRATION ON DUST CLEANING FABRICS

FINAL REPORT

by
Jan R. Kościanowski
Lidia Kościanowska
Eugeniusz Szczepankiewicz
Bronisław Weryński
Stanisław Bethke

Institute of Industry of Cement Building Materials
452-641 Opole
Oświęcimska Str. 21 Poland

EPA Project Officer: James H. Turner
Industrial Environmental Research Laboratory
Office of Energy, Minerals, and Industry
Research Triangle Park, NC 27711

Prepared for
U.S. ENVIRONMENTAL PROTECTION AGENCY
Office of Research and Development
Washington, DC 20460

PRODUCT OF:
NATIONAL TECHNICAL
INFORMATION SERVICE
U.S. DEPARTMENT OF COMMERCE
SPRINGFIELD, VA. 22161

TECHNICAL REPORT DATA
(Please read Instructions on the reverse before completing)

1. REPORT NO.
EPA-600/7-81-028

2.

3. RECIPIENT'S ACCESSION NO.
PB81 188542

4. TITLE AND SUBTITLE
Effect of Parameters of Filtration on Dust Cleaning Fabrics

5. REPORT DATE
March 1981

6. PERFORMING ORGANIZATION CODE

7. AUTHOR(S) J.R.Koscianowski, Lidia Koscianowska, Bronislaw Werynski, Eugeniusz Szczwpankiewicz, and Stanislaw Bethke

8. PERFORMING ORGANIZATION REPORT NO.

9. PERFORMING ORGANIZATION NAME AND ADDRESS
Institute of Industry of Cement Building Materials
452-641 Opole
Oswiecimska Str. 21
Poland

10. PROGRAM ELEMENT NO.
EHE624

11. CONTRACT/GRANT NO.
Public Law 480-5-533-4

12. SPONSORING AGENCY NAME AND ADDRESS
EPA, Office of Research and Development
Industrial Environmental Research Laboratory
Research Triangle Park, NC 27711

13. TYPE OF REPORT AND PERIOD COVERED
Final; 1976-1979

14. SPONSORING AGENCY CODE
EPA/600/13

15. SUPPLEMENTARY NOTES Project officer J.H.Turner is no longer with EPA; for details, contact IERL-RTP's Louis S. Hovis, Mail Drop 61, 919/541-2925. EPA-600/2-76-074 and EPA-600/7-79-031 are related reports.

16. ABSTRACT The report summarizes 4 years of laboratory and large-scale tests on the dust filtration process and the basic filtration parameters that determine performance. Physical parameters describing fabric and dust cake structure were defined and three basic dust filtration mechanisms were considered: selective precipitation, inertial sedimentation, and diffusion. From test results of two Polish polyester fabrics filtering separated fly ash, three-dimensional probabilistic models of dust collection efficiency and filtration resistance were introduced. Also developed was a general filtration model, based on random field theory, that included full mathematical augmentation. The effect of electrostatic phenomena on dust filtration was examined in an attempt to define its influence. Study conclusions included: (1) air flow through a clean fabric and the dust filtration process are normal stochastic processes; (2) dust filtration is a specific dry filtration process, differing from the air filtration process or the high-efficiency air filtration process; (3) dust collection efficiency during the dust filtration process depends on three basic filtration mechanisms related to the aerosol particle size distribution; and (4) woven filtration materials are heterogeneous and anistropic media characterized by periodic structure that, at high face velocity values, exhibit transition region flow of K_1 (resistance).

17. KEY WORDS AND DOCUMENT ANALYSIS

a. DESCRIPTORS		b. IDENTIFIERS/OPEN ENDED TERMS	c. COSATI Field/Group	
Pollution	Caking	Pollution Control	13B	07A,13H
Filtration	Electrostatics	Stationary Sources	07D	20C
Dust Filters	Precipitation	Fabric Filters	13K	
Fabrics	Sedimentation	Poland	11E	14G
Dust	Diffusion	Resistance	11G	
Aerosols	Polyester Fibers			
Fly Ash	Mathematical Models		21B	12A

18. DISTRIBUTION STATEMENT
Release to Public

19. SECURITY CLASS (This Report)
Unclassified

20. SECURITY CLASS (This page)
Unclassified

21. NO. OF PAGES
466

22. PRICE

EPA Form 2220-1 (9-73)

ABSTRACT

This report summarizes 4 years of laboratory and large-scale tests of the dust filtration process and the basic filtration parameters determining performance. Physical parameters describing fabric and dust cake structure were defined and three basic dust filtration mechanisms were considered: selective precipitation, inertial sedimentation, and diffusion. From test results of two Polish polyester fabrics filtering separated fly ash, three-dimensional probabilistic models of dust collection efficiency and filtration resistance were introduced. A general filtration model, based on random field theory, was also developed that included full mathematical argumentation.

Electrical properties of dusts and fabrics were examined to define the influence of electrostatic phenomena on the dust filtration process. This examination led to a quantitative determination of local electric fields in the fabric and dust cake.

The conclusions from this work are:

- Air flow through a clean fabric and the dust filtration process are normal stochastic processes.
- Dust filtration is a specific dry filtration process, differing from the air filtration process or the high-efficiency air filtration process.
- Dust collection efficiency during the dust filtration process depends upon three basic filtration mechanisms related to the aerosol particle size distribution.
- Woven filtration materials are heterogeneous and anisotropic media characterized by periodic structure that, at high values of face velocity, exhibit transition region flow described by a resistance function, K_i'.

Microscale electric fields formed by triboelectrical charge exchange between fibers and dust particles significantly influence the dust filtration process.

TABLE OF CONTENTS

SECTION PAGE

Abstract ii

List of Figures. vii

List of Tables xviii

Acknowledgments. xxii

I Conclusions. 1

Dust Filtration Process 1

True Filtration Process 2

II Recommendations. 3

III Introduction 4

Research Objectives 6

General Program 6

Testing of filtration materials 6

Structural parameters for woven fabrics. 7

Structural parameters of the dust cake 7

Electrostatic properties of dust and fabrics . . 8

Fabric and Dust Selection 8

IV Theoretical Base of Dust Filtration Process. 20

Introduction. 20

Dry Filtration Processes. 23

Description of the Dust Filtration Process. 27

Dust Filtration Type I. 32

Efficiency, Dust Filtration Type I. 33

TABLE OF CONTENTS (con.)

SECTION PAGE

Filtration resistance problems in Dust Filtration Type I 48

Dust Filtration Type III. 53

Dust collection efficiency problems in Dust Filtration Process Type III 56

Filtration resistance problems: Dust Filtration Process Type III 58

Some peculiarities of the Dust Filtration Process Type I. 62

V Effect of Filtration Parameters on Dust Filtration Process Type I 78

Introduction 78

Equipment and Procedures 79

Results. 83

Discussion of Results. 83

The effect of filtration parameters on dust collection efficiency. 83

The effect of filtration parameters on filtration resistance variations. 141

The effect of initial aerosol state parameters on dust collection efficiency and filtration resistances 164

Dust collection efficiencies and filtration resistances in the first phase of Dust Filtration Process Type I. 170

Recapitulation and Conclusions 177

VI Filtration Parameters and Effect on Dust Filtration Process Type III 180

Introduction 180

Equipment and Procedures 181

Results. 188

TABLE OF CONTENTS (con.)

SECTION PAGE

Discussion of Results. 188

The influence of filtration parameters upon dust collection efficiency 188
Effect of filtration parameters on filtration resistance 201

Conclusions 228

VII Comparison Between Dust Filtration Process Type I and Type III. 232

Introduction. 232

Comparison of Dust Collection Efficiencies. 233

Comparison of Filtration Resistances. 246

Conclusions 256

VIII Study of Filter Medium Parameters. 260

Introduction. 260

Fabric Structure: Basic Technological Parameters 263

Secondary Technological Parameters Describing Woven Structure. 270

Physical Parameters Characterizing Woven Filtration Structure 278

Comparison of Some Fabric Parameters. 295

Air Flow Through Clean Filtration Structures. . . . 303

Recapitulation and Conclusions. 313

IX Study of Structural Dust Parameters. 315

Introduction. 315

Equipment and Procedures. 321

Results and Discussion. 321

Conclusions 335

TABLE OF CONTENTS (con.)

SECTION PAGE

X Model of Dust Collection Efficiency. 343

  Theoretical Background. 343
  Model Application to Fabric Filtration. 349

  Conclusions 352

XI Electrostatic Properties of Dusts and Fabrics. 353

  Introduction. 353

  Definition of Forces Between Dust Particles and Fibers Because of Electrostatic Phenomena. 353

  Electrical Properties of Industrial Dusts and Filtration Materials 357

    Determination of the electrical properties of industrial dusts 358

    Determination of electrical properties of filtration materials. 359

    Study of dust-fabric systems 360

  Final Remarks and Discussion of Further Research 369

XII Additional Work. 371

  Introduction. 371

  Measurement Conditions. 371

  Results and Discussion. 373

  Conclusions 375

XIII References 376

Appendix A Data Plots. 379

Appendix B Data Tabulation 393

Appendix C Glossary of Terms 431

Appendix D List of Nomenclature. 435

LIST OF FIGURES

Number		Page
1	Surface of clean fabric style ET-4	9
2	Surface of clean fabric style ET-30.	10
3	Surface of clean fabric style F-tor 5.	11
4	Surface of clean fabric style PT-15.	12
5	Grains of test cement dust	14
6	Grains of test coal dust	15
7	Grains of test talc dust	16
8	Grains of test fly ash dust.	17
9	Particle size distribution of test dust (1-fly ash, 2-talc, 3-cement, 4-coal)	18
10	Initial state parameters of dispersion medium guaranteeing dry filtration process	21
11	General scheme of filtration process	25
12	Types of dust filtration	30
13	Dust collection efficiency in Dust Filtration Process Type I as a function of time.	34
14	Theoretical variation of efficiency in time according to Equation 19.	39
15	Comparison of granular bed structure with dust cake structure	41
16	Filtration mechanisms in ductive filtration.	43
17	Filtration resistance variation in time for Dust Filtration Process Type I	50
18	Changes of K_2 in Dust Filtration Process Type I.	54
19	Dependence of porosity function upon absolute porosity . .	55

LIST OF FIGURES (continued)

Number Page

20 Theoretical variation of efficiency in time. 59

21 Theoretical variation of efficiency vs. dust load. . . . 60

22 Theoretical variation of filtration resistance in time 63

23 Theoretical variation of filtration resistance vs. terminal dust load. 64

24 Surface of dust cake on fabric ET-4. 65

25 Characteristic crater form of ducts/canals 66

26 Process of dust cake structure defects formation in static dust cake. 68

27a Superficial structure of model fabric (vertical view) 70

27b Superficial structure of model fabric (askew view) 71

28a Basket areas and free areas in glass fabric type Q-54-878 (interyarn free area). 72

28b Basket areas and free areas in glass fabric type Q-54-878 (enlargement interyarn free area). 73

28c Basket areas and free areas in glass fabric type Q-54-878 (new "basket free area") 74

28d Basket areas and free areas in glass fabric type Q-54-878 (enlargement of new "basket free area"). . . 75

29 Deformation of filtration resistance characteristics due to dust cake defects. 76

30 Illustration of laboratory stand 80

31 Diagram of the laboratory test stand 81

32 Efficiency as a function of dust covering in Rosin-Rammler coordinate system 85

33 Dust collection efficiency for two interpretations of the mean efficiency of an individual cycle. 88

LIST OF FIGURES (continued)

Number Page

34 Dependence of E_o on q_g. 93

35 Dependence of function F_2 on q_g 94

36 Predicted and experimental efficiences of ET-4 as a function of q_g for average value of $L_o' = 25$ g/m^2 . . . 100

37 Predicted and experimental efficiences of ET-4 as a function of q_g for average value of $L_o' = 35$ g/m^2 . . . 101

38 Predicted and experimental efficiencies of ET-4 as a function of q_g for average value of $L_o' = 50$ g/m^2 . . 102

39 Predicted and experimental efficiencies of ET-4 as a function of q_g for average value of $L_o' = 100$ g/m^2. . . 103

40 Predicted and experimental efficiencies of ET-4 as a function of q_g for average value of $L_o' = 150$ g/m^2. . . 104

41 Predicted and experimental efficiencies of ET-4 as a function of q_g for average value of $L_o' = 200$ g/m^2. . . 105

42 Predicted and experimental efficiencies of ET-4 as a function of q_g for average value of $L_o' = 250$ g/m^2. . . 106

43 Predicted and experimental efficiencies of ET-4 as a function of q_g for average value of $L_o' = 350$ g/m^2. . . 107

44 Predicted and experimental efficiencies of ET-4 as a function of q_g for average value of $L_o' = 400$ g/m^2. . . 108

45 Predicted and experimental efficiencies of ET-4 as a function of L_o' for $q_g = 60$ m^3/m$^2 \cdot$ h 109

46 Predicted and experimental efficiencies of ET-4 as a function of L_o' for $q_g = 70$ m^3/m$^2 \cdot$ h 110

47 Predicted and experimental efficiencies of ET-4 as a function of L_o' for $q_g = 80$ m^3/m$^2 \cdot$ h 111

48 Predicted and experimental efficiencies of ET-4 as a function of L_o' for $q_g = 100$ m^3/m$^2 \cdot$ h. 112

49 Predicted and experimental efficiencies of ET-4 as a function of L_o' for $q_g = 120$ m^3/m$^2 \cdot$ h. 113

50 Predicted and experimental efficiencies of ET-4 as a function of L_o' for $q_g = 140$ m^3/m$^2 \cdot$ h. 114

LIST OF FIGURES (continued)

Number Page

51 Predicted and experimental efficiencies of ET-4 as a function of L_o' for $q_g = 160$ $m^3/m^2 \cdot h$. 115

52 Predicted and experimental efficiencies of ET-4 as a function of L_o' for $q_g = 180$ $m^3/m^2 \cdot h$. 116

53 Predicted and experimental efficiencies of ET-4 as a function of L_o' for $q_g = 200$ $m^3/m^2 \cdot h$. 117

54 Predicted and experimental efficiencies of ET-30 as a function of q_g for average value of $L_o' = 25$ g/m^2 . . . 118

55 Predicted and experimental efficiencies of ET-30 as a function of q_g for average value of $L_o' = 35$ g/m^2 . . . 119

56 Predicted and experimental efficiencies of ET-30 as a function of q_g for average value of $L_o' = 50$ g/m^2 . . . 120

57 Predicted and experimental efficiencies of ET-30 as a function of q_g for average value of $L_o' = 100$ g/m^2. . . 121

58 Predicted and experimental efficiencies of ET-30 as a function of q_g for average value of $L_o' = 150$ g/m^2. . . 122

59 Predicted and experimental efficiencies of ET-30 as a function of q_g for average value of $L_o' = 200$ g/m^2. . . 123

60 Predicted and experimental efficiencies of ET-30 as a function of q_g for average value of $L_o' = 250$ g/m^2. . . 124

61 Predicted and experimental efficiencies of ET-30 as a function of q_g for average value of $L_o' = 350$ g/m^2. . . 125

62 Predicted and experimental efficiencies of ET-30 as a function of q_g for average value of $L_o' = 400$ g/m^2. . . 126

63 Predicted and experimental efficiencies of ET-30 as a function of L_o' for $q_g = 70$ $m^3/m^2 \cdot h$ 127

64 Predicted and experimental efficiencies of ET-30 as a function of L_o' for $q_g = 80$ $m^3/m^2 \cdot h$ 128

65 Predicted and experimental efficiencies of ET-30 as a function of L_o' for $q_g = 100$ $m^3/m^2 \cdot h$. 129

66 Predicted and experimental efficiencies of ET-30 as a function of L_o' for $q_g = 120$ $m^3/m^2 \cdot h$. 130

LIST OF FIGURES (continued)

Number Page

67 Predicted and experimental efficiencies of ET-30 as a function of L_o' for $q_g = 140\ m^3/m^2 \cdot h$. 131

68 Predicted and experimental efficiencies of ET-30 as a function of L_o' for $q_g = 160\ m^3/m^2 \cdot h$. 132

69 Predicted and experimental efficiencies of ET-30 as a function of L_o' for $q_g = 180\ m^3/m^2 \cdot h$. 133

70 Predicted and experimental efficiencies of ET-30 as a function of L_o' for $q_g = 200\ m^3/m^2 \cdot h$ 134

71 Dependence of residual dust load on time and q_g for fabric ET-30 (test dust: fly ash). 139

72 Dependence of residual dust load on time and q_g for fabric ET-4 (test dust: fly ash) 140

73 Variation of coefficient B from Equation 65 as a function of L_o for fabric ET-4 (Series I). 146

74 Variation of coefficient B from Equation 65 as a function of L_o for fabric ET-30 (Series I) 147

75 Variation of coefficient B from Equation 65 as a function of L_o for fabric F-tor 5 (Series I) 148

76 Variation of coefficient B from Equation 65 as a function of L_o for fabric PT-15 (Series I) 149

77 Variation of coefficient B from Equation 65 as a function of L_o for fabrics ET-4 and ET-30 (Series II and III) 150

78 Probable dependence of coefficient B from Equation 65 as a function of FA for fabrics ET-4, ET-30, F-tor 5, and PT-15, tested with fly ash in Series I experiments. 152

79a Filtration resistance as a function of q_g, fabric ET-4. . 156

79b Filtration resistance as a function of q_g, fabric ET-30. 157

80 Filtration resistance and q_g at the moment of ducts/canals formation 159

LIST OF FIGURES (continued)

Number		Page
81	Change of filtration resistance due to ducts/canals formation during testing of fabric style ET-4 with fly ash at $q_g = 120\ m^3/m^2 \cdot h$ (Series I).	161
82	K_2 vs. L_o for fabric style ET-4, tested with fly ash. . .	162
83	K_2 vs. L_o for fabric style ET-30, tested with fly ash . .	163
84	Dust collection efficiency as a function of c_1 for fabric style ET-30 tested with separated fly ash . . .	168
85	Effect of c_1 on filtration resistance during testing of fabric style ET-30 with separated fly ash	171
86	Dependence of specific filtration resistances upon initial concentration during testing of fabric style ET-30 with separated fly ash in two ranges of q_g . . .	172
87	Dust collection efficiency as a function of average value of L_o (low L_o region).	175
88	Filtration resistance variation as a function of average L_o in the low L_o region.	176
89	Large-scale stand	182
90	Diagram of the large-scale test stand	183
91	Diagram of regeneration cycle	185
92	Construction of bags.	186
93	Dependence of $(F_1 \cdot F_3)$ on q_g for fabrics ET-4 and ET-30.	195
94	Dependence of F_4 on q_g for fabrics ET-4 and ET-30	196
95	Predicted and experimental efficiencies of ET-4 as a function of q_g for $L_p = 50\ g/m^2$.	202
96	Predicted and experimental efficiencies of ET-4 as a function of q_g for $L_p = 100\ g/m^2$	203
97	Predicted and experimental efficiencies of ET-4 as a function of q_g for $L_p = 150\ g/m^2$	204

LIST OF FIGURES (continued)

Number		Page
98	Predicted and experimental efficiencies of ET-4 as a function of q_g for $L_p = 200$ g/m²	205
99	Predicted and experimental efficiencies of ET-4 as a function of q_g for $L_p = 300$ g/m²	206
100	Predicted and experimental efficiencies of ET-4 as a function of q_g for $L_p = 400$ g/m²	207
101	Predicted and experimental efficiencies of ET-4 as a function of L_p for $q_g = 60$ m³/m² · h	208
102	Predicted and experimental efficiencies of ET-4 as a function of L_p for $q_g = 80$ m³/m² · h	209
103	Predicted and experimental efficiencies of ET-4 as a function of L_p for $q_g = 100$ m³/m² · h.	210
104	Predicted and experimental efficiencies of ET-4 as a function of L_p for $q_g = 120$ m³/m² · h.	211
105	Predicted and experimental efficiencies of ET-4 as a function of L_p for $q_g = 160$ m³/m² · h.	212
106	Predicted and experimental efficiencies of ET-30 as a function of q_g for $L_p = 50$ g/m².	213
107	Predicted and experimental efficiencies of ET-30 as a function of q_g for $L_p = 100$ g/m²	214
108	Predicted and experimental efficiencies of ET-30 as a function of q_g for $L_p = 150$ g/m²	215
109	Predicted and experimental efficiencies of ET-30 as a function of q_g for $L_p = 200$ g/m²	216
110	Predicted and experimental efficiencies of ET-30 as a function of q_g for $L_p = 300$ g/m²	217
111	Predicted and experimental efficiencies of ET-30 as a function of q_g for $L_p = 400$ g/m²	218
112	Predicted and experimental efficiencies of ET-30 as a function of L_p for $q_g = 60$ m³/m² · h	219
113	Predicted and experimental efficiencies of ET-30 as a function of L_p for $q_g = 100$ m³/m² · h.	220

LIST OF FIGURES (continued)

Number Page

114 Predicted and experimental efficiencies of ET-30 as a function of L_p for $q_g = 100\ m^3/m^2 \cdot h$. 221

115 Predicted and experimental efficiencies of ET-30 as a function of L_p for $q_g = 120\ m^3/m^2 \cdot h$. 222

116 Predicted and experimental efficiencies of ET-30 as a function of L_p for $q_g = 160\ m^3/m^2 \cdot h$. 223

117 Variation of coefficient B´ as a function of L_p 227

118 Predicted and measured filtration resistance for ET-4 at $q_g = 80\ m^3/m^2 \cdot h$ 229

119 Predicted and measured filtration resistance for ET-30 at $q_g = 100\ m^3/m^2 \cdot h$. 230

120 Variation of R_E as a function of L for fabric ET-4. . . . 236

121 Variation of R_E as a function of q_g for fabric ET-4 . . . 237

122 Variation of R_E as a function of L for fabric ET-30 . . . 238

123 Variation of R_E as a function of q_g for fabric ET-30. . . 239

124 Transition from classical filtration to defect filtration 241

125 Variation of coefficient "n" as a function of dust covering 244

126 Large-scale dust collection efficiency calculated from Equation 90 for fabric ET-4 tested with separated fly ash. 247

127 Large-scale dust collection efficiency calculated from Equation 90 for fabric ET-30 tested with separated fly ash. 248

128 Variation of $R_{o_{\Delta P}}$ as a function of L for fabric ET-4. . . 251

129 Variation of $R_{o_{\Delta P}}$ as a function of L for fabric ET-30 . . 252

130 Variation of $R_{o_{\Delta P}}$ as a function of q_g for fabrics ET-4 and ET-30. 254

LIST OF FIGURES (continued)

Number		Page
131	Variation of coefficient "n" from Equation 92 vs. q_g.	255
132	Predicted and measured variations of filtration resistance for fabric ET-4.	257
133	Predicted and measured variations of filtration resistance for fabric ET-30	258
134	View and sections of plain weave fabric.	264
135	Characteristic magnitudes of plain weave composition . .	271
136	Painter's nomogram (diagram)	273
137	Geometric interpretation of fabric thickness	276
138	Draemel's model of woven filtration structure.	279
139	Comparison of cross sections of threads of examined fabrics (along fill).	281
140	Influence of fabric structure deformation on calculated "free area" (FA).	282
141	View of new "basket free area" (BFA) in structure of fabric ET-4	283
142	View of new "basket free area" (BFA) in structure of fabric ET-30.	284
143	View of new "basket free area" (BFA) in structure of fabric F-tor 5.	285
144	View of new "basket free area" (BFA) in structure of fabric PT-15.	286
145	Deformation of yarn sections under external forces . . .	288
146	Basket free area in woven filtration structure	289
147	Influence of certain structural parameters on BFA (cross sections along warp).	291
148	Warp yarn deformation effect on BFA.	292
149	New model of woven filtration structure.	294

LIST OF FIGURES (continued)

Number		Page
150	Characteristic elements of structure for woven materials.	298
151	Comparison of hydraulic resistances during laminar and turbulent flow	307
152	Variation of resistance function of woven filtration materials.	312
153	Four-element configuration of dust grains	316
154	View of dust cake structure made with grains of four-element configuration.	317
155	Eight-element configuration of dust grains.	319
156	View of dust cake structure made with grains of eight-element configuration.	320
157	Scheme of cement dust separation.	322
158	Scheme of coal dust separation.	323
159	Scheme of talc separation	324
160	Scheme of fly ash separation.	325
161	Apparatus for determination of the jogged dust weight	326
162	Theoretical dependence, $S = f(d_{50})$, for cement (Series II).	329
163	Theoretical dependence, $S = f(d_{50})$, for coal (Series II).	330
164	Theoretical dependence, $S = f(d_{50})$, for talc (Series II).	331
165	Theoretical dependence, $S = f(d_{50})$, for fly ash (Series II).	332
166	Variation of Δh vs. shocking time for separated cement	336
167	Variation of Δh vs. shocking time for unseparated cement	337

LIST OF FIGURES (continued)

Number Page

168 Variation of Δh vs. shocking time for separated coal 338

169 Variation of Δh vs. shocking time for unseparated coal 339

170 Variation of Δh vs. shocking time for separated fly ash. 340

171 Variation of Δh vs. shocking time for unseparated fly ash. 341

172 Change of dust layer initial porosity during shocking (separated and unseparated fly ash). 342

173 Diagram of stand for charge accumulated on fabric measurement. 361

174 Particle size distribution of test dusts. 372

175 Correlation between two methods of measuring absolute dust density 374

LIST OF TABLES

Number		Page
1	Fabric Parameters	
2	Initial Statistical Efficiency, E_0, as a Function of q_g (Series I and Previous Experiments).	87
3	Values of F_2 as a Function of q_g (Series I and Previous Experiments	90
4	Values of F_1 as a Function of q_g (Series I and Previous Experiments).	91
5	Initial Statistical Efficiency, E_0, Values of F_1 and F_2 as a Function of q_g (Series II and III)	92
6	Coefficients of the Parabolic Equation: $E_0 = a(q_g)^2 + bq_g + c$ (Series I and Previous Experiments)	96
7	Coefficients of the Parabolic Equation: $F_2 = n = a_2(q_g)^2 + b_2q_g + c_2$ (Series I and Previous Experiments)	97
8	Coefficient of the Parabolic Equation: $E_0 = a(q_g)^2 + b \cdot q_g + c$ (Series II and III)	98
9	Coefficients of the Parabolic Equations: $F_1 = a_1(q_g)^2 + b_1 \cdot q_g + c_1$ and $F_2 = a_2(q_g)^2 + b_2 \cdot q_g + c_2$ (Series II and III).	98
10	Values of Face Velocity Corresponding to E_{MIN}	136
11	Values of Coefficient B From Equation 65 as a Function of L_0 (Series I and Previous Experiments)	144
12	Values of Coefficient B From Equation 65 as a Function of L_0 (Series II and III)	145
13	Coefficients of the Parabolic Equation: $B = A_1L_0{}^2 + B_1L_0 + C_1$ (Series I and Previous Experiments). . . .	153
14	Coefficients of the Parabolic Equation: $B = A_1L_0{}^2 + B_1L_0 + C_1$ (Series II and III).	154

LIST OF TABLES (continued)

Number Page

15 MMD and δ_g for Test Dusts (μm) 154

16 Laboratory Efficiency (%) of Polyester Style ET-30 Tested With Separated Fly Ash Under Conditions of the Change Concentration (at q_g = 120 m^3/m^2h) 166

17 Laboratory Efficiency (%) Of Polyester Style ET-30 Tested With Separated Fly Ash Under Conditions of the Change Concentration (at q_g = 180 m^3/m^2h) 166

18 Final Pressure Drop in Laboratory Testing (in mm H_2O) for Polyester Style ET-30 Tested with Separated Fly Ash Under Conditions of the Change Concentration 167

19 Laboratory Efficiency of ET-30 During Testing With Separated Fly Ash in the Range of Low Values, L_o (at q_g = 60 m^3/m^2h) 174

20 Large-Scale Efficiency (%) of Polyester Style ET-4 and ET-30 Tested With Separated Fly Ash 189

21 Final Pressure Drop in Large Scale (mm H_2O) for Polyester Style ET-4 and ET-30 Tested With Separated Fly Ash 190

22 Filling of Fabric Structure With Dust for Large-Scale Experiments 191

23 Real Values of Characteristic Parameter of Dust Cake, L_p (in g/m^2), for Large-Scale Experiments 191

24 Values of $F_1 \cdot F_2$ and F_4 From Equation 39. 193

25 Coefficients of Parabola Equations: $F_1 \cdot F_3 = a_{1\ 3} q_g{}^2 + b_{1\ 3} q_g + c_{1\ 3}$ and $F_4 = a_4 q_g{}^2 + b_4 q_g + c_4$ . . . 193

26 Hopper Efficiency (%) Calculated by Dust Balance 198

27 Values of Coefficients A´ and B´ From Equation 82. . . . 226

28 Coefficients of Equation: $A' = a_3 L_p^2 + b_3 L_p + c_3$ and $B' = A_3 L_p^2 + B_3 L_p + C_3$ 226

29 Values of Function R_E. 235

30 Values R_{E_o} and $n(\bar{L}_o)$ From Equation 87. 242

LIST OF TABLES (continued)

Number Page

31 Coefficients a_{R1}, b_{R1}, C_{R1}, and a_{R2}, b_{R2}, c_{R2}, From Equation 89 245

32 Values of Function $R_{\Delta P}$ 249

33 Values of $R_{o_{\Delta P}}$ and $n(q_g)$ From Equation 92 253

34 Coefficients a_{p1}, b_{p1}, c_{p1}, and a_{p2}, b_{p2}, c_{p2} From Equation 93 253

35 Values of Characteristic Factor "C" 265

36 Kinds of Elementary Fibers. 268

37 Yarn Characteristics of Fabrics Used in Laboratory and Large-Scale Tests 269

38 Similarity Table of Fabrics Under Assumption of Circular Cross Section of Yarns 301

39 Similarity Table of Fabrics Under Assumption of Elliptical Cross Section of Yarns. 302

40 True Forms of Flow Resistance Function (for Low Values of Flow, $\Delta P > 10$ mm H_2O). 309

41 True Forms of Flow Resistance Function (for High Values of Flow, $\Delta P > 10$ mm H_2O) 310

42 Kinetic and Static Specific Surface for Dusts: Cement and Coal (Series I). 327

43 Coefficients a and b for Equation 148 333

44 Changes of Dust Layer Porosity During Shocking 333

45 Charge Accumulating on Filtration Fabrics During Dusting With Talc Air Flow 363

46 Charge Accumulating on Filtration Fabrics During Dusting With Cement Flow 364

47 Charge Accumulating on Filtration Fabrics During Dusting With Fly Ash Air Flow. 365

48 Charge Accumulating on Filtration Fabrics During Dusting With Coal Air Flow 366

LIST OF TABLES (continued)

Number | | Page
49 Electric Charge Accumulating on Fabric ET-4 at the Moment of Dust Cake Removal From Fabric Surface. . . . 368

50 Electric Charge Accumulating on Fabric ET-30 at the Moment of Dust Cake Removal From Fabric Surface. . . . 368

X1

ACKNOWLEDGMENTS

The authors would like to thank employees of the U.S. Environmental Protection Agency who participated in this endeavor. The authors extend special thanks to Project Officer Dr. James H. Turner, who throughout the program provided help and insight concerning the interpretation of test results. We would also like to thank EPA consultants, Professor M. W. First from Harvard University and Dr. R. Dennis from GCA/Technology Division, whose cooperation made our work richer. We acknowledge with thanks the cooperation of Professor A. T. Szaynok and her staff at the Institute of Physics of Wrocław Polytechnic; and Dr. K. Skudlarski, the Head of the Laboratory of Scanning Microscopy, and his staff, who performed microscopic examinations, provided interesting illustrations, and identified certain problem areas.

SECTION I

CONCLUSIONS

Both experimental testing and theoretical analyses formed the basis for the conclusions reached during this project.

DUST FILTRATION PROCESS

- Three types of dust filtration occur during laboratory testing:

  Filtration Type I: filtration beginning with the virgin fabric and ending at the initiation of the first regeneration cycle;

  Filtration Type II: filtration by the fabric and accumulating dust but before the equilibrium state is reached (the quantity of dust collected during the filtration cycle exceeds that removed during the subsequent regeneration cycle); and

  Filtration Type III: steady state filtration by the fabric and its dust cake characterized by stable pre- and post-regeneration conditions (the quantity of dust removed during regeneration is approximately equal to that collected during the filtration cycle--the large-scale test conditions representative of industrial dust filtration).

- Dust collection efficiency and filtration resistance, apart from the type of filtration, are determined by initial aerosol state parameters, filtration parameters, and structural parameters of the dust-fabric system.

- Dust collection efficiency and filtration resistance can be adequately described by probabilistic mathematical models over the range of the empirical data.

- Mean dust collection efficiency during a filtration cycle (Filtration Types I and III) depends on the time required to build a dust cake and its thickness.

- The collection efficiency of the dust cake cannot be compared to the collection efficiency of the filtration layer (the fabric) because of the physically different filtration media.

- Consideration of the effect of the particle size distribution of the aerosol on the dust collection efficiency permits a correlation of the dust-fabric system efficiency with important, initial aerosol state parameters.

- The main mechanisms that determine filtration process efficiency in the dust cake are selective precipitation, inertial sedimentation, and diffusion.
- Dust collection efficiency and filtration resistance depend upon the pore size distribution of the dust-fabric system.
- The pore size distribution function is a characteristic of each fabric dust cake system and has a log normal distribution.

TRUE FILTRATION PROCESSES

- The dust collection efficiency for Filtration Process Type I depends on the degree of dust pulverization, the dust concentration, the shape of the aerosol particles, the face velocity (q_g), and the areal dust loading of the filter (L_o).
- Areal mass density of the dust in or on a dust-covered filter (the terminal dust load, L_o) is a reliable parameter for estimating filtration effects.
- Increases in q_g and the degree of dust pulverization decrease dust collection efficiency and increase filtration resistance.
- Increases in dust concentration and L_o both increase dust collection efficiency.
- Dust collection efficiency for Filtration Process Type III depends upon q_g and the areal mass density of the dust cake, L_p.
- Increasing q_g decreases efficiency and increases filtration resistance.
- Increasing L_p increases efficiency and shifts process performance toward higher filtration resistance.
- The functional dependence of dust collection efficiency on q_g is determined by the kind of fabric included in the dust-fabric system.
- Both Filtration Processes Type I and Type III are characterized by dust cake defects, which influence dust collection efficiency and filtration resistance.
- The formation of dust cake defects is related to disturbed equilibrium between the dust particles comprising the dust cake, resulting in the dislocation of the dust particles and the formation of ducts/canals after a certain pressure drop is reached.

SECTION II

RECOMMENDATIONS

The results of this project point to the need for further investigation in the following areas:

- Development of the relationship between the porosity of woven materials and their free area (FA) and basket free area (BFA) distribution, and empirical verification of this relationship over a wide range of materials;
- The relationship between the pulverization state of suspended dust and the specific area of the dust layer formed from it, including the role of particle shape and the hydraulic properties of the layer; and
- Empirical verification of the role of fabric properties in the process of filtration through a dust layer.

Investigation of these areas would help perfect, qualitatively and quantitatively, mathematical models of the dust filtration process.

SECTION III

INTRODUCTION

For many years the dust filtration process has used textile filtration media in industrial dust collection devices; i.e., filter bags, pocket dust collectors, bag houses, and pulse-jet dust collectors. While all these dust collection devices perform the same overall function, there are considerable differences in their individual process mechanisms.

The dust removal process is very efficient and dust collection efficiency usually exceeds 99 percent. This property promoted the rapid use of fabric filters, despite the fact that their performance has only a weak theoretical base. Different fabric dust collectors were designed during a short time and were optimized for:

- Longer life of the filtration fabrics (mainly by application of less severe regeneration systems);
- Automation; and
- Reliability, low pressure drop, and architecture.

As dust collection devices developed, so did the production of improved filtration materials. Filtration materials produced from natural fibers (cotton and wool) were gradually replaced with synthetic fibers (i.e., polyester, polyamide, and polyacrylonitrile), which had better mechanical properties and chemical resistance. The higher temperature resistance of the synthetic fibers led to greater industrial use of fabric filters.

However, it is noteworthy that the development of new raw fiber materials with improved physicochemical properties did not lead to new production methods for woven filtration materials. The new filtration materials were similar in structure to those produced from the natural raw materials. This situation may have been caused by failure to communicate the importance of fiber spatial structure to fabric producers. Such requirements were difficult to define because of fragmentary research and limited understanding of the dust removal process. Moreover, early research focussed primarily on quantitative process data.

The situation is paradoxical because contemporary industrial-scale filters are nearly perfectly constructed and successfully operate as highly automated systems. No systematic theoretical base for the dust filtration process exists, however, from which to direct further research on industrial gas filtration with woven filtration materials and to further optimize the process and the filtration medium. Further improvement in filter construction without compromising the filtration process constitutes progress in dust removal because it does not jeopardize clean air. Knowing what changes will interfere with dust collection requires theoretical understanding of the dust filtration process, so such a theoretical base must be developed.

Theoretically, dust filtration is a multiparameter process differing from other filtration processes. Some researchers have tried to explain the peculiarities observed with industrial dust collectors by resorting to the classical filtration theory and especially the single fiber theory. This approach led to confusion in research planning and in interpreting results. Many papers are incomprehensible because the authors did not know what type of filtration process they were studying.

At present scientists agree, however, that the basic mechanisms of dust particle precipitation from an aerosol stream that determine the process effectiveness in the classical theory of filtration are also observed in dust filtration. However, their physical interpretation is different because of differences in the basic assumptions of the two processes.

In the phase I and II reports of this project we proposed standardized process nomenclature and defined our initial assumptions. Our proposal was based on a theoretical physical model of dust filtration, which is presented in Section IV of this report. The efficiency of dust collection, the primary qualitative parameter of the process, was examined as a function of filtration parameters; i.e., face velocity and dust flux. We also tried to correlate filtration efficiency with some structural parameter of the filtration medium.

The preliminary mathematical model of dust filtration, based on experiments conducted in our Institute and further analyzed at the Institute of Mathematics of WSP Opole, is an integral part of this report. Some experimental results obtained in other projects are also included in an attempt to make this report as complete a description of filtration as possible and hence as useful as possible in planning further research.

RESEARCH OBJECTIVES

The basic objectives of the program financed by EPA and conducted by the Institute of Cement Building Materials in Opole were:

- To describe the effects of fabric structural parameters on the pressure drops associated with gas flow through the clean fabric;
- To describe the effects of structural parameters of both the fabric and the dust cake on pressure drops during the filtration process;
- To describe the functional dependence between dust collection efficiencies and the variables of the dust filtration process; and
- To test, by mathematical modeling, fabric structures with the best filtration properties.

Total program research includes the following:

- Laboratory testing, including testing of dust and fabrics;
- Large-scale testing;
- Auxiliary studies; and
- Application of mathematical methods, including modeling.

GENERAL PROGRAM

Testing of Filtration Materials

The program concentrated on determining the effects of filtration parameters on dust collection efficiency for specific filtration materials produced in Poland and tested with certain kinds of dusts. Laboratory and large-scale testing was performed. Initial dust concentration, the same for all experiments, was $c_1 = 10\ g/m^3 \pm 10$ percent. Dust loadings on the fabric and face velocities were as follows:

- For the laboratory-scale tests,
  $L_o = 100, 400, \text{ or } 700\ g/m^2$; and
  $q_g = 60, 80, \text{ or } 120\ m^3/m^2h$;
  with pressure drop $\Delta P < 250$ mm H_2.
- For the large-scale tests:
  $L_o = 400 \text{ or } 700\ g/m^2$, and
  $q_g = 60 \text{ or } 80\ m^3/m^2h$,
  with pressure drop $\Delta P < 250$ mm H_2O.

However, after laboratory tests were statistically analyzed, the program appeared too narrow for adequate modeling. Consequently, the large-scale research program was enlarged to include results more useful for statistical analysis. Only two filtration materials were tested with one kind of dust, but the tests were expanded to five levels of q_g (60, 80, 100, 120, and 160 m^3/m^2h) and six levels of L_o (L_{NK} + 100, + 200, + 300, + 400, + 600, + 800 g/m^2).

Moreover, for comparative results, auxiliary testing was conducted for two filtration materials on the laboratory scale. The dispersion medium for both laboratory and large-scale testing was ambient air with normal humidity, pressure, and temperature. The relative humidity of the dispersion medium was controlled to about 40 percent ± 10 percent, and the temperature, 20° to 30° C.

Structural Parameters For Woven Fabrics

Work concentrated on the effect of structural parameters of woven fabrics; i.e., the effect of permeability and free area (FA) on the dust filtration performance and the determination of a new structural parameter having physical sense but related to the technological properties of the fabric materials. Examination of woven structures included:

- Study of simplified, physical, geometrical models of woven structures;
- Determination of the variation of technological parameters and their effect on woven material structure (on geometrical model of fabric);
- Determination of the effect of fiber composition on the spatial structure of the fabric; and
- Statistical analysis of the effect of structural deformation phenomena on filtration.

During the first phase of research we studied clean air flow through porous structures; during the next phases we examined dusty air flow.

Structural Parameters of the Dust Cake

The object of this research was to correlate the parameter characterizing dust in a suspended state (in front of the filtration structure) with the physical parameter characterizing the dust cake. This correlation is of great importance in qualitative and quantitative prediction of dust filtration. Tests and statistical analyses were conducted in the laboratory.

Electrostatic Properties of Dusts and Fabrics

The effect of electrostatic phenomena on the dust filtration process is widely described in the literature and is observed during industrial testing. Consequently, preliminary measurements of the electrostatic properties of the dusts, fabrics, and dust-fabric systems used in this research were carried out at the Institute of Physics of Wrocław Polytechnic, under direction of Professor Dr. A. Szaynok (except for tests performed with dusts collected directly from a technological line; i.e., without storage). The range of examination included:

- Measurement of natural dust electrification,
- Determination of the effect of gas medium on dust electrification,
- Measurement of the electrical properties of fabrics,
- Study of the kinetics of charge formation on the fabric surface, and
- Study of the interaction between the dust and the fabric.

These studies stimulated several hypotheses concerning the influence of electrification during the dust filtration process.

FABRIC AND DUST SELECTION

Selection of fabrics and dusts was not random but resulted from concepts developed during auxiliary studies of dust effects and the effects of fabric structural properties on the dust filtration process. If only the main research objective; i.e., determining the effect of filtration parameters on dust-cleaning fabrics, were considered, the test could be conducted with randomly selected fabrics and dusts.

Four types of Polish filtration fabrics composed of synthetic fibers--polyester and polyamide--were examined. The polyester fabrics were fabric ET-30 (staple fiber), fabric ET-4 (staple fiber), and fabric F-tor 5 (continuous filament). The one polyamide fabric was fabric PT-15 (continuous filament).

The polyester fabrics represented a heterogeneous group with respect to raw materials, an important factor in the interaction between dust particles and fibers (e.g., electrostatic phenomena), and they also differed with respect to superficial and spatial structure (see Figures 1 through 4).

The selection of polyamide fabric PT-15 of structure similar to fabric F-tor 5 permitted observation of the effect of fiber type, with respect to raw

Photo credit: SEM by K. Skudlarski, Electronic Microscopy Laboratory of Wrocław Polytechnic.

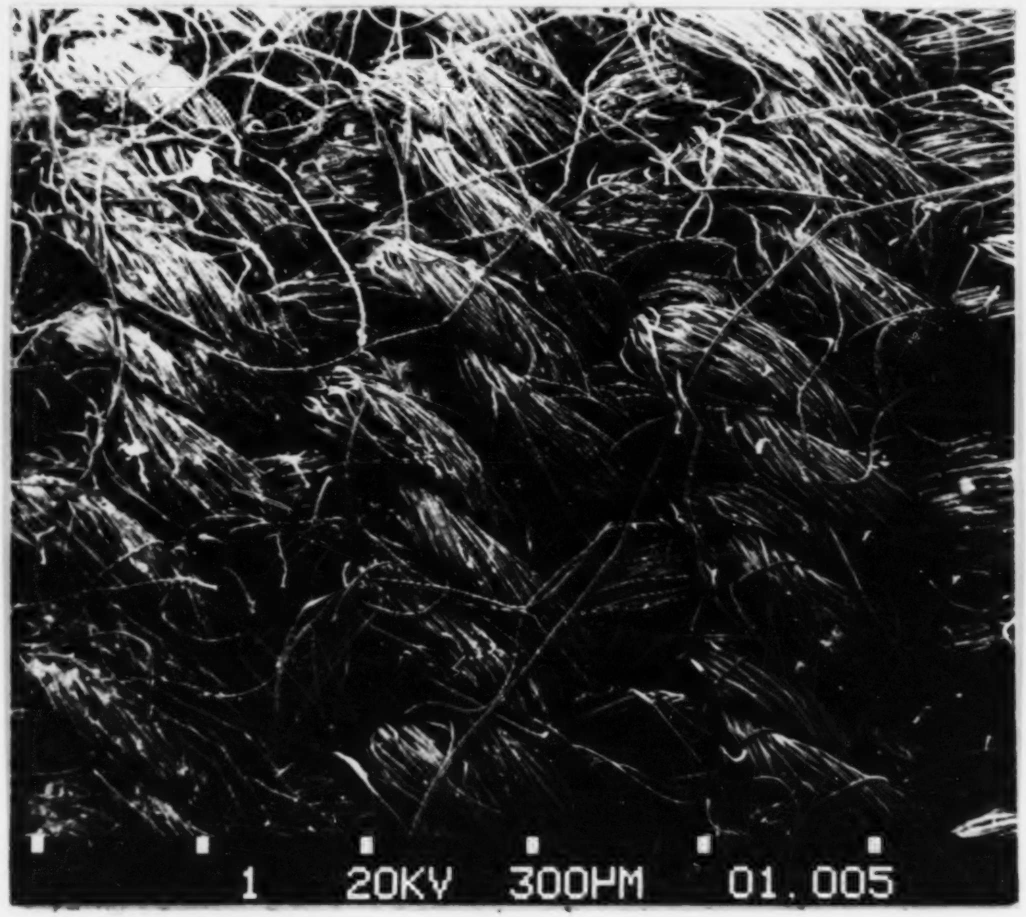
1 20KV 300PM 01.005

Figure 1. Surface of clean fabric style ET-4.

Photo credit: SEM by K. Skudlarski, Electronic Microscopy Laboratory of Wrocław Polytechnic.

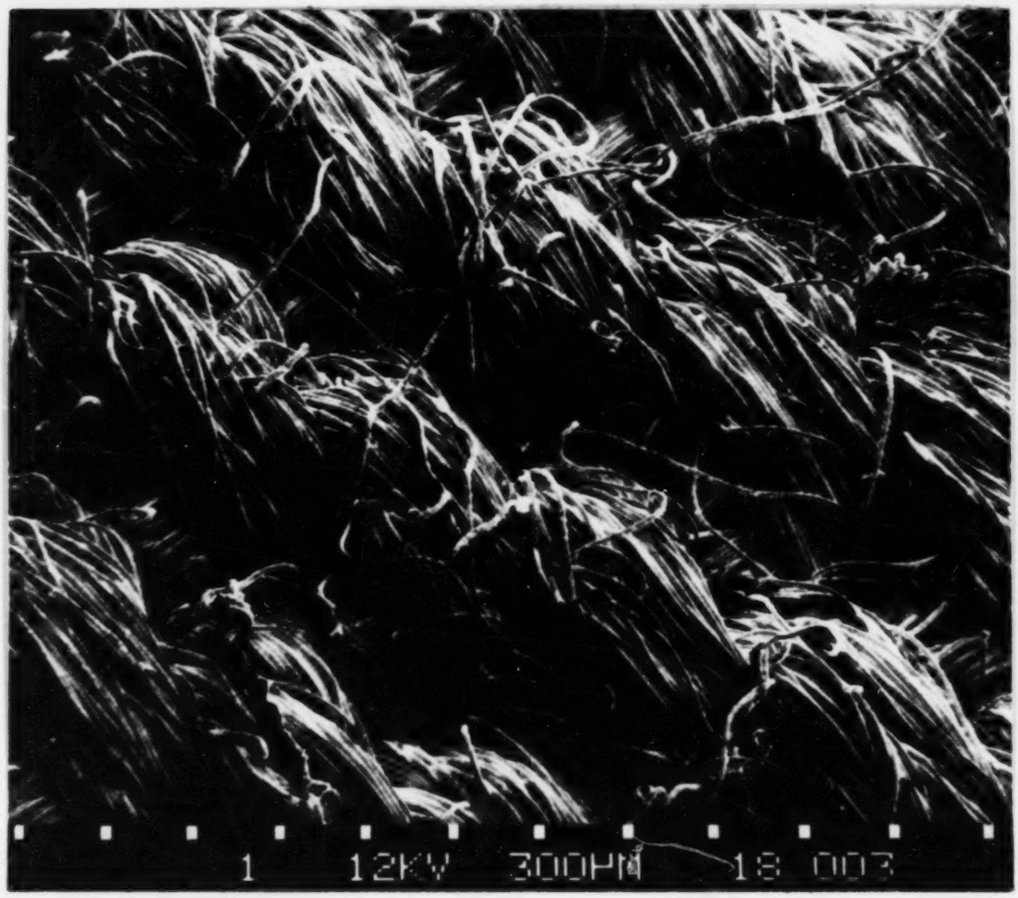
1 12KV 300PM 18 003

Figure 2. Surface of clean fabric style ET-30.

Photo credit: SEM by K. Skudlarski, Electronic Microscopy Laboratory of Wrocław Polytechnic.

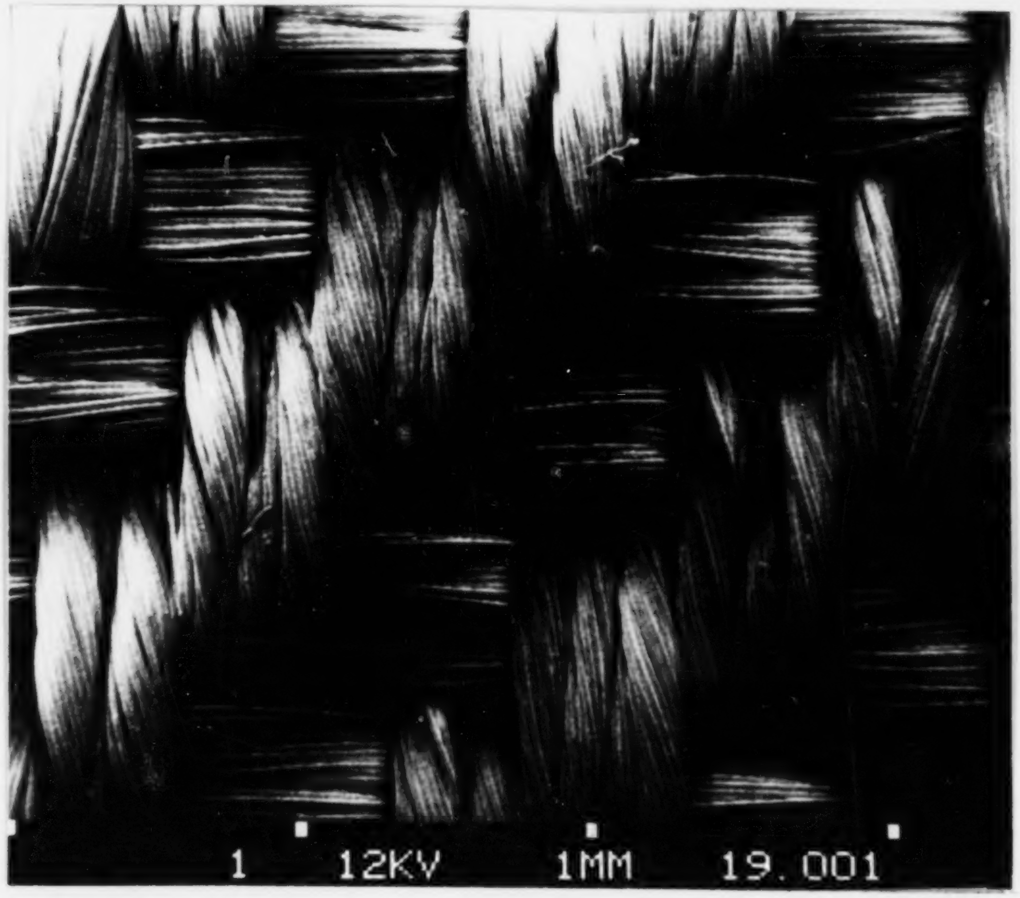
1 12KV 1MM 19.001

Figure 3. Surface of clean fabric style F-tor 5.

Photo credit: SEM by K. Skudlarski, Electronic Microscopy Laboratory of Wrocław Polytechnic.

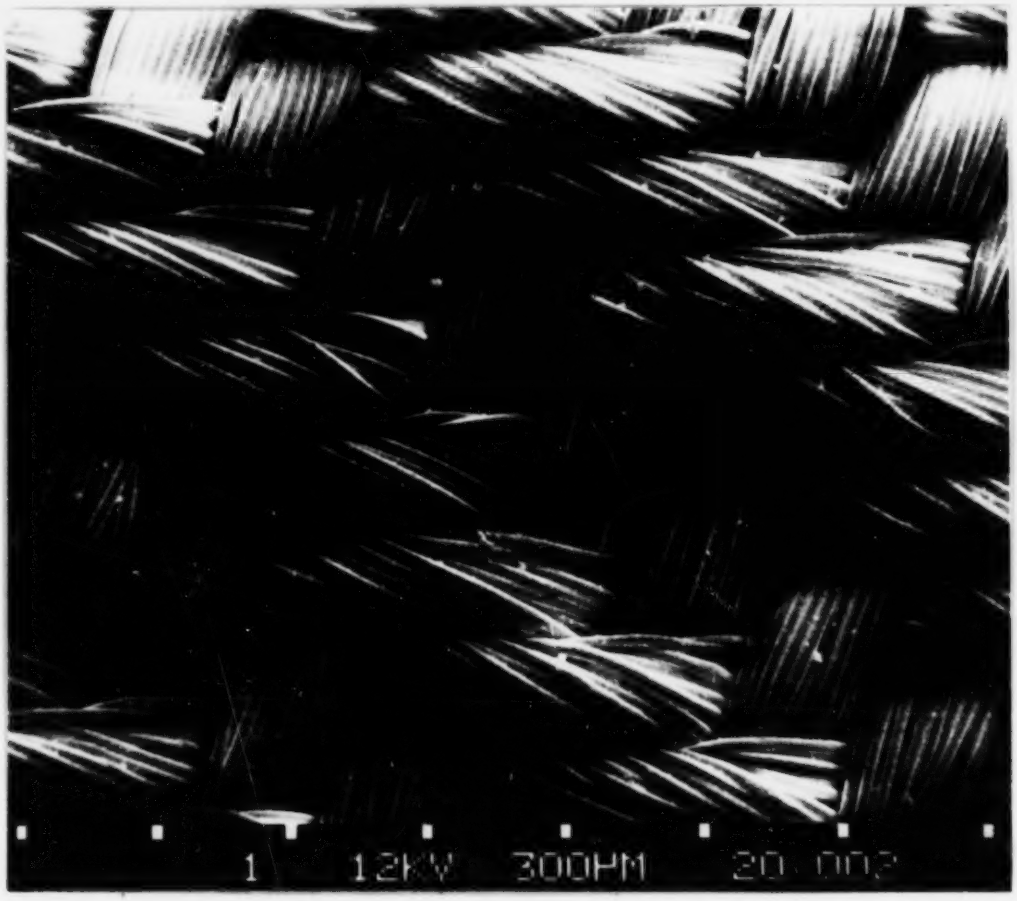
1
12KV
300HM
20 002

Figure 4. Surface of clean fabric style PT-15.

TABLE 1. FABRIC PARAMETERS

		Fabrics							
		ET-4		ET-30		F-tor 5		PT-15	
Parameter	Unit	PS*	Measured	PS*	Measured	PS*	Measured	PS*	Measured
Width of fabric	cm	as required	36	140 ± 4	135	140 ± 4	140	85 ± 1	85
Kind of yarn:									
warp		50 Tex Z × 2 S	45.21 Tex × 2	21 Tex Z × 2 S	22.15 Tex × 2	Td 125/2	Td 136.37	Td 210/1	Td 228.43
fill		180 Tex Z	178.25 Tex	21 Tex Z × 2 S	21.99 Tex × 2	Td 250/1	Td 253.52	Td 210/1	Td 233.77
Thread count in 10 cm:									
warp		180 ± 5	180	477 ± 10	488	540 ± 12	528	564 ± 12	545
fill		126 ± 5	126	276 ± 6	274	376 ± 12	360	360 ± 11	363
Fabric weight	g/m²	450 ± 31	428.1	365 ± 25	361.6	271 ± 13	307.5	272 ± 14	247
Thickness (pressure 100 g/cm²)	mm	-	0.92	-	0.74	-	0.50	-	0.39
Tensile strength, less than:									
warp	kg/5 cm width	220	240	250	323	346	310	300	336
fill	kg/5 cm width	260	310	130	182	276	225	200	233
Elongation during tension, no more than:									
warp	%	70	51	60	60	30	37	60	43
fill	%	50	35	50	48	20	15	40	28
Permeability	m³/m² min at 20 mm H_2O	18-24	20.73	12-18	7.54	-	14.6	-	3.65
Weave	-	$\frac{1}{3}Z$	$\frac{1}{3}Z$	$\frac{2}{1}Z$	$\frac{2}{1}Z$	$\frac{2}{2}Z$	$\frac{2}{2}Z$	$\frac{3}{3}$	$\frac{3}{3}$
Finishing	-	Steaming	Steaming	Thermal stabilization, washing	Thermal stabilization, washing	Crude	Crude	Stabilized	Stabilized

*Polish standards.

Photo credit: SEM by K. Skudlarski, Electronic Microscopy Laboratory of Wrocław Polytechnic.

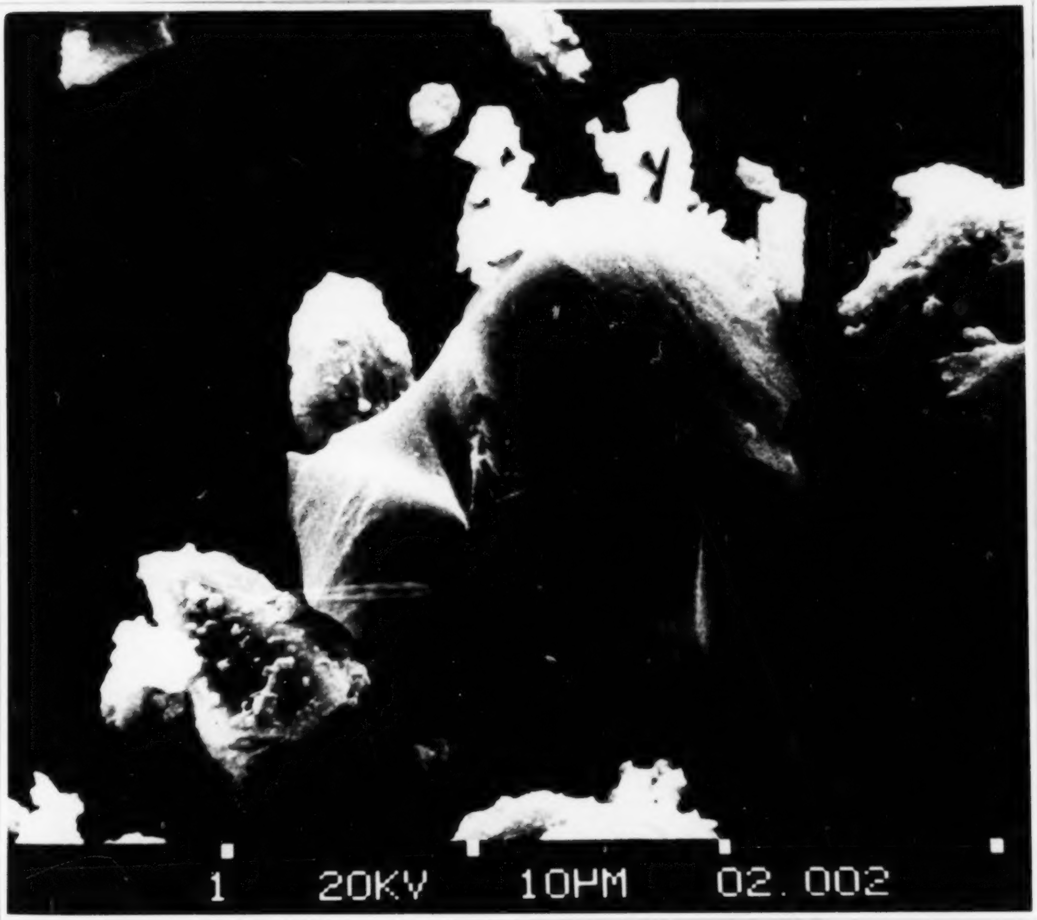
1 20KV 10PM 02.002

Figure 5. Grains of test cement dust.

Photo credit: SEM by K. Skudlarski, Electronic Microscopy Laboratory of Wrocław Polytechnic.

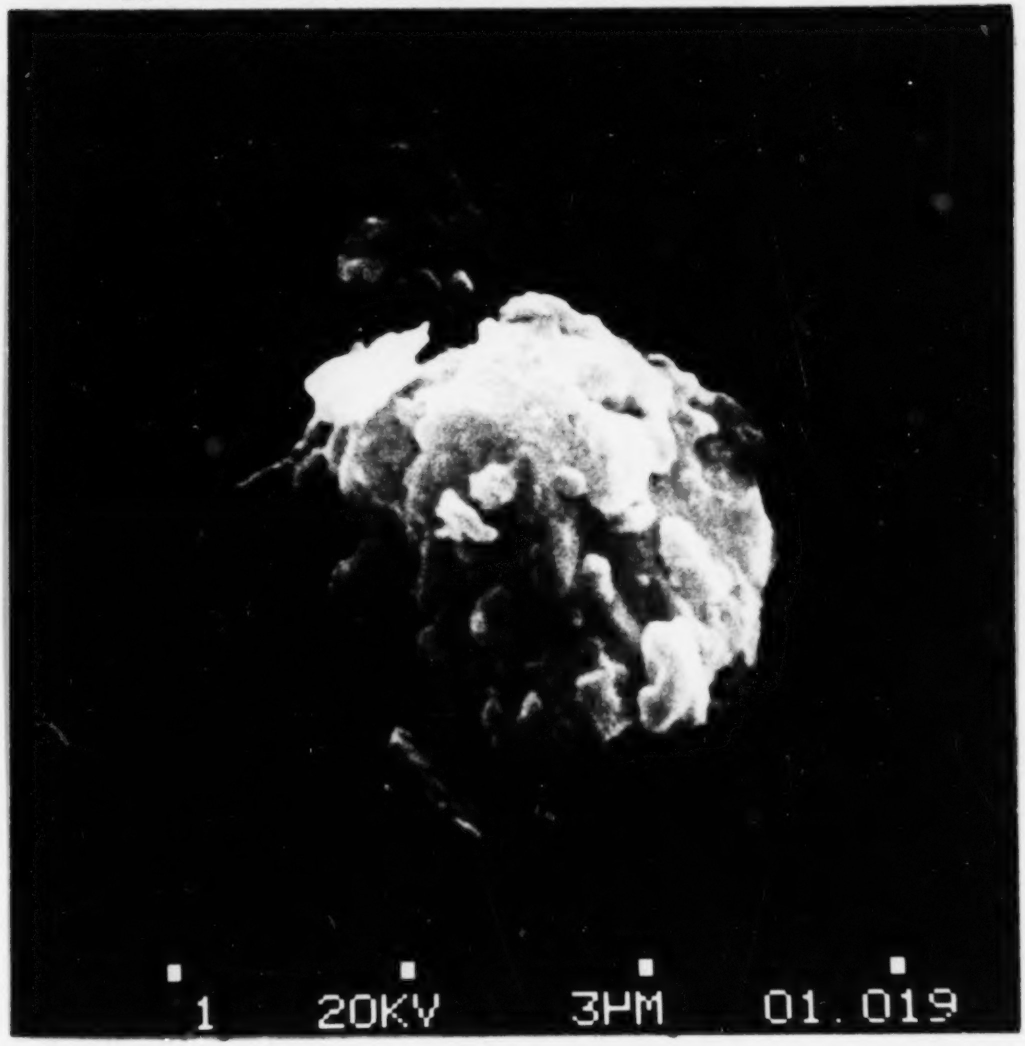
1 20KV 3µM 01.019

Figure 6. Grains of test coal dust.

Photo credit: SEM by K. Skudlarski, Electronic Microscopy Laboratory of Wrocław Polytechnic.

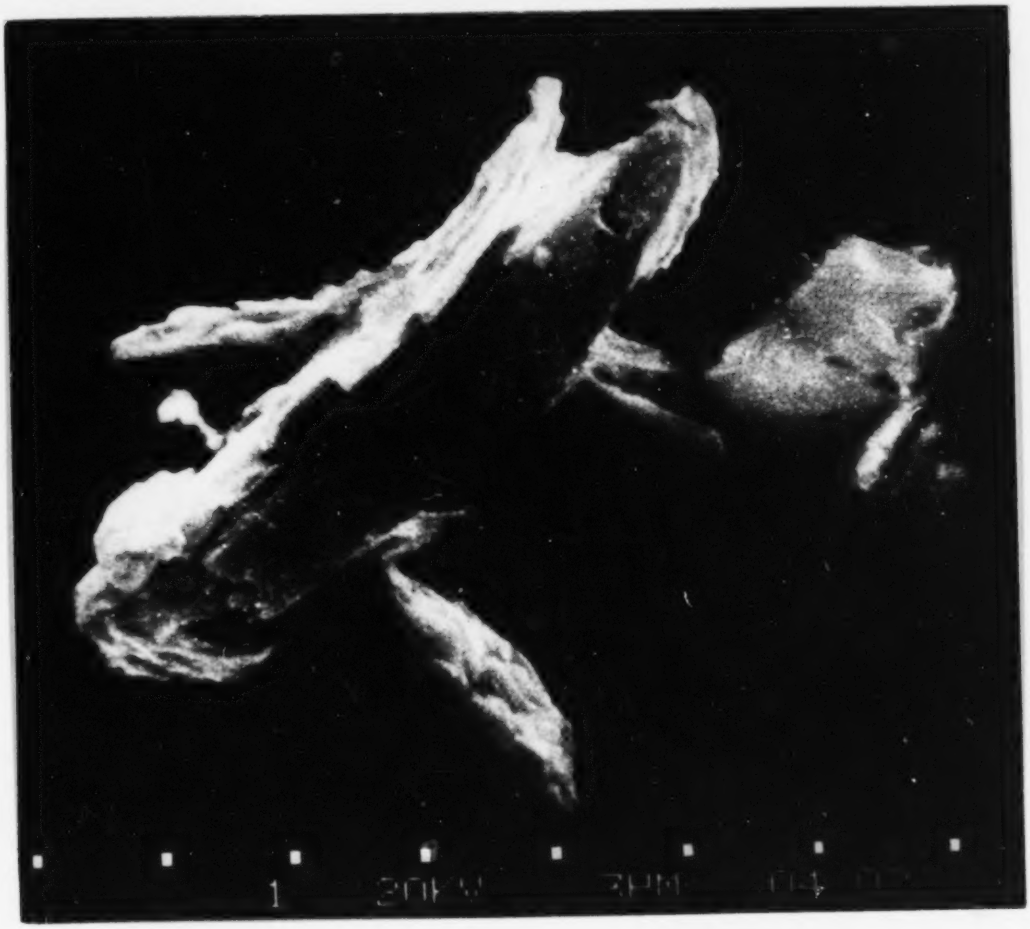

Figure 7. Grains of test talc dust.

Photo credit: SEM by K. Skudlarski, Electronic Microscopy Laboratory of Wrocław Polytechnic.

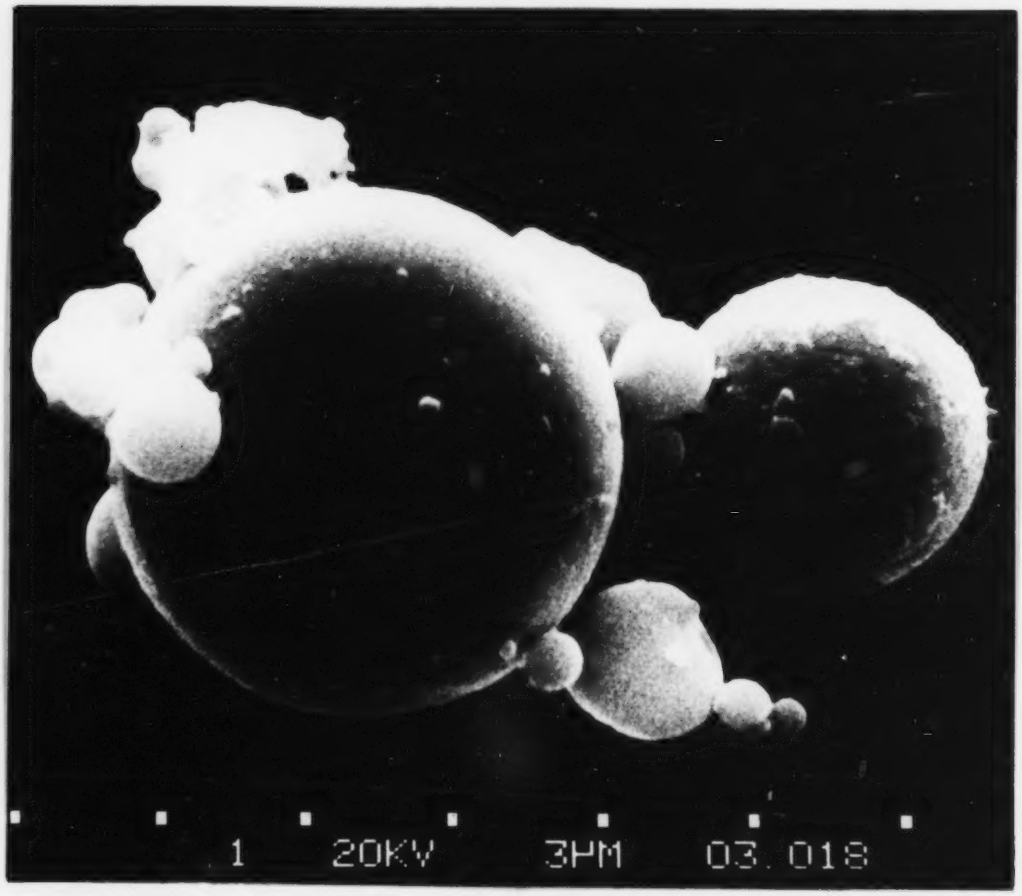
1 20KV 3μM 03.018

Figure 8. Grains of test fly ash dust.

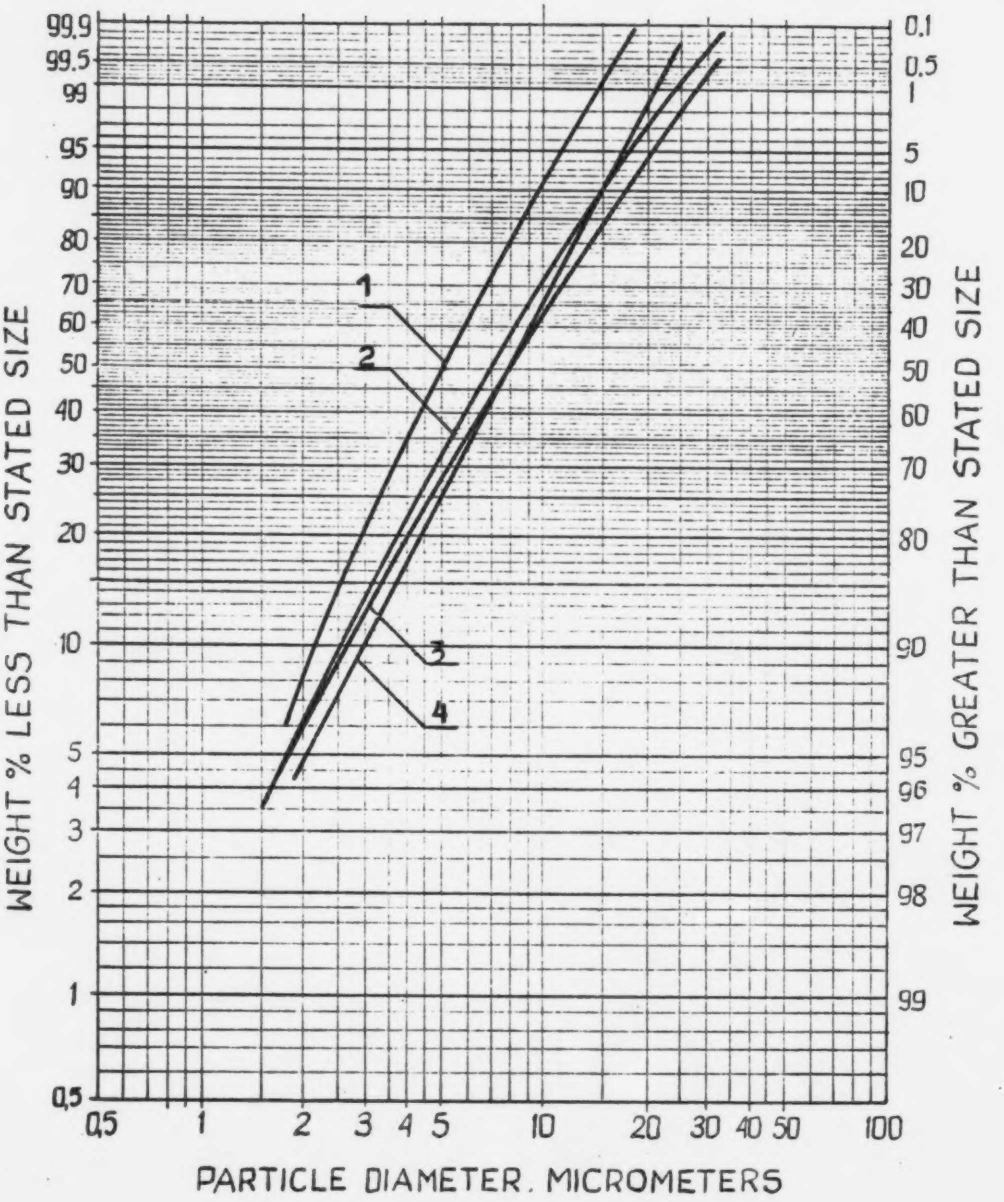

Figure 9. Particle size distribution of test dust (1-fly ash, 2-talc, 3-cement, 4-coal).

material, on dust filtration material. Table 1 lists the basic parameters of the tested fabrics.

The test dusts were industrial dusts taken from appropriate points on the production processing line. They were cement dust, coal dust, talc, and fly ash. These dusts differ in physicochemical properties and in particle shape.

The dust samples were separated to obtain a particle size distribution containing no more than 10 percent (by weight) of particles with diameters greater than 20 μm. Laboratory dusts were processed by an Alpine separator; the dusts used in the large-scale tests were separated by subcontractors.

The particle size distribution of the dusts after separation was similar:

Cement	MMD = 8 μm	$\sigma_g = 2.2$ μm
Coal	MMD = 8 μm	$\sigma_g = 2.2$ μm
Talc	MMD = 7 μm	$\sigma_g = 2.2$ μm
Fly ash	MMD = 5.5 μm	$\sigma_g = 1.9$ μm

However, the test dusts differ significantly in particle shape (see Figures 5 through 8).

Under the original research program schedule, selected fabrics were tested in the laboratory with these four kinds of dusts. Because of the wider test range of the present research program, all laboratory and large-scale tests were conducted only with fly ash. Tested filtration structures were represented by fabrics ET-30 and ET-4. Particle size distributions for the test dusts are shown in Figure 9 and Table B-1.

SECTION IV

THEORETICAL BASE OF DUST FILTRATION PROCESS

INTRODUCTION

Most studies of theoretical and empirical filtration problems begin with a general definition of the filtration process that includes the effect of the porous structure of the filtration medium on the aerosol flowing through it. Such a general definition of the filtration process is as follows: filtration is the precipitation of dispersed solid state particles, suspended in a movable fluid dispersion medium, onto or into a filtration medium through which the dispersion medium flows. This definition distinguishes two basic filtration processes according to the thermodynamic state of the dispersion medium:

- Wet filtration (a liquid dispersion medium), and
- Dry filtration (a gas or an atmospheric air dispersion medium).

This report assumes only dry filtration; i.e., those processes that operate in the area of superheated steam, in which only gases make up the filtration medium. The above assumption, for processes performed at atmospheric pressure, can be presented as:

$$T_{PR} \geq t_R + \Delta t_{PR} \,, \qquad (1)$$

where

T_{PR} = initial temperature of the dispersion medium, °C;

t_R = the highest possible dew point temperature of the process, °C;

Δt_{PR} = the empirical temperature change of the dispersion medium during the filtration process (proportional to heat losses in an actual dust collection device) °C.

Temperatures above the heavy curve in Figure 10 define the operating temperatures of the dispersion medium that are needed to maintain dry filtration according to the above condition. Maintaining dry filtration operation, when

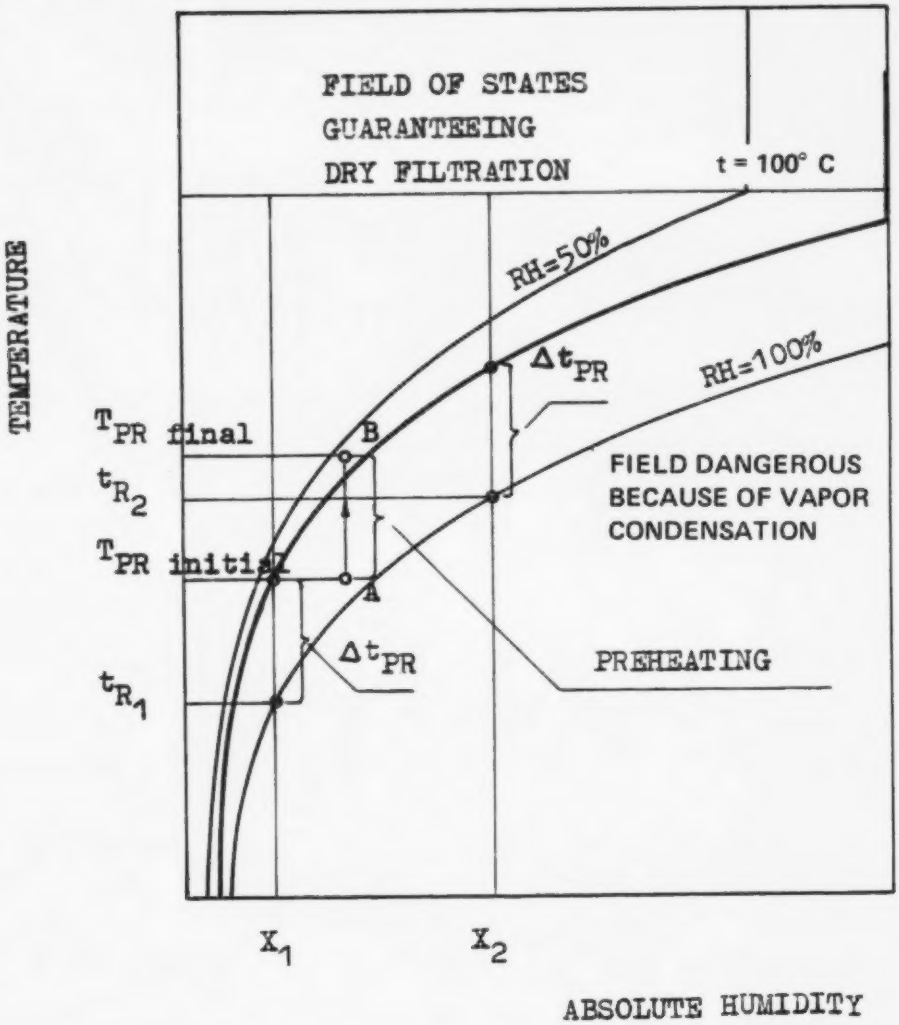

FIELD OF STATES GUARANTEEING DRY FILTRATION
t = 100° C
RH=50%
RH=100%
TEMPERATURE
T_{PR} final
t_{R_2}
T_{PR} initial
t_{R_1}
B
A
Δt_{PR}
Δt_{PR}
FIELD DANGEROUS BECAUSE OF VAPOR CONDENSATION
PREHEATING
X_1
X_2
ABSOLUTE HUMIDITY

Figure 10. Initial state parameters of dispersion medium guaranteeing dry filtration process.

the dispersion medium humidity varies with time (a phenomenon observed in realistic technological processes) necessitates added heat to the aerosol stream before it enters the dust collection device. This case is illustrated in Figure 10 by the preheating step that shifts the dispersion medium temperature from below the heavy curve (point A) to above it (point B).

Equation 1, specifying the initial thermodynamic state of the dispersion medium for dry filtration, determined the assumptions used in the aerosol definition adopted for further studies.

Friedlander[1] identifies difficulties in writing a general definition for aerosol because of properties unique to its formation. Aerosol definitions quoted in the literature [2] [3] [4] are not precise enough to be considered universal. For this research, a modified definition of aerosol was accepted, which is right only for problemsolving.

Because the liquid phase was excluded in the assumption of a dry filtration process, aerosol is a two-phase system composed of a gas dispersion phase and a solid dispersed phase. Under certain conditions, the system can be regarded as stable or quasi-stable.[5]

External and internal forces affecting aerosol particles are regarded as local conditions. For aerosol in motion, under the influence of external forces and subject to diffusion effects, the following equation can be written:

$$\frac{\partial n}{\partial t} + V\nabla n = D\nabla^2 n - \nabla c\ n\ , \qquad (2)$$

where

n = particle size distribution,

t = time,

V = gas velocity distribution,

D = diffusion coefficient,

c = velocity of particle migration affected by external forces.

The particle size distribution of Equation 2 is a characteristic function of the aerosol that depends on time and position. It describes the state of comminution of the dispersed phase in the dispersion medium and is influenced by the internal processes of sedimentation, diffusion, coagulation, and growth, as well as by external forces.

Assuming the particles to be spheres, their size distribution can be described by the relationship:

$$n_d\ (d_p,\ \vec{r},\ t) = \frac{dN}{d\ (d_p)}\quad , \tag{3}$$

where

dN = number of particles per unit volume of fluid having diameter between d_p and $d_p + d(d_p)$,

d_p = particle diameter,

$\vec{r}$ = polar coordinate, and

t = time.

If the terms in Equation 2 that contain the contribution of external forces and diffusion are neglected, the particle size distribution depends directly on the gas velocity distribution in the aerosol stream; i.e., for any given velocity distribution, a particle size distribution can be found.

When these ideas are introduced to the aerosol definition development for given local conditions consisting of fixed internal and external forces, the particle size distribution is assumed to be stable or quasi-stable.

$$n_d\ (d_p,\ \vec{r},\ t) = \frac{dN}{d(d_p)} = \text{constant}\quad . \tag{4}$$

The above assumption; i.e., the particle size distribution is independent of time and position, may be valid over specific time spans, depending upon the internal and external forces affecting the aerosol (the "local" conditions).

DRY FILTRATION PROCESSES

By the general definition of filtration each filtration process can be characterized by a set of internal and external parameters. External parameters are the measurable manifestations of a continuous process that can be determined independently of the physical phenomena that determine their absolute values. External parameters depend on filtration time, so it is difficult to pinpoint their instantaneous values. Average values are usually associated with specific stages of the process; these average values also depend on time.

A second characteristic of external parameters is their existence independent of other process parameters. External parameters of the filtration process are:

- Average total efficiency of dust collection,
- Fractional efficiency, and
- Filtration resistance.

These external process parameters can all be measured in a real filtration process.

Internal parameters are factors determined by process physical phenomena and do not depend on filtration time. Their absolute value determines the measured values of the external parameters. The internal parameters of filtration are:

- The state parameters, SP;
- The filtration parameters, FP; and
- The structural parameters of the filtration medium, SPFM.

State parameters characterize the aerosol before and after the filtration structure and are the thermodynamic and physicochemical properties of the dispersion and dispersed mediums. The main parameter is a function of particle size distribution. Filtration parameters are the independent process variables that allow comparison of filtration effects. Structural parameters of filtration describe, from a physical point of view, the filtration structure as characterized by the technological parameters of its production and also by the physiochemical properties that depend on the raw materials from which it was manufactured.

Each filtration process takes place at a specific efficiency and incurs energy losses resulting from the aerosol flow through the porous structure of the filtration medium. The driving force for filtration, then, is a specific value of pressure drop across the filtration medium structure.

If a constant value of filtration efficiency is assumed, the effect of groups of parameters on the filtration process can be discussed. With this assumption, Figure 11 schematically illustrates the theory of dry filtration. The transition from the initial aerosol state (1) to the final state (2) does not depend on the path but only on the initial and final parameters of the aerosol state (e.g., dust concentration). Many processes can yield the same efficiency but with different filtration structures and parameters.

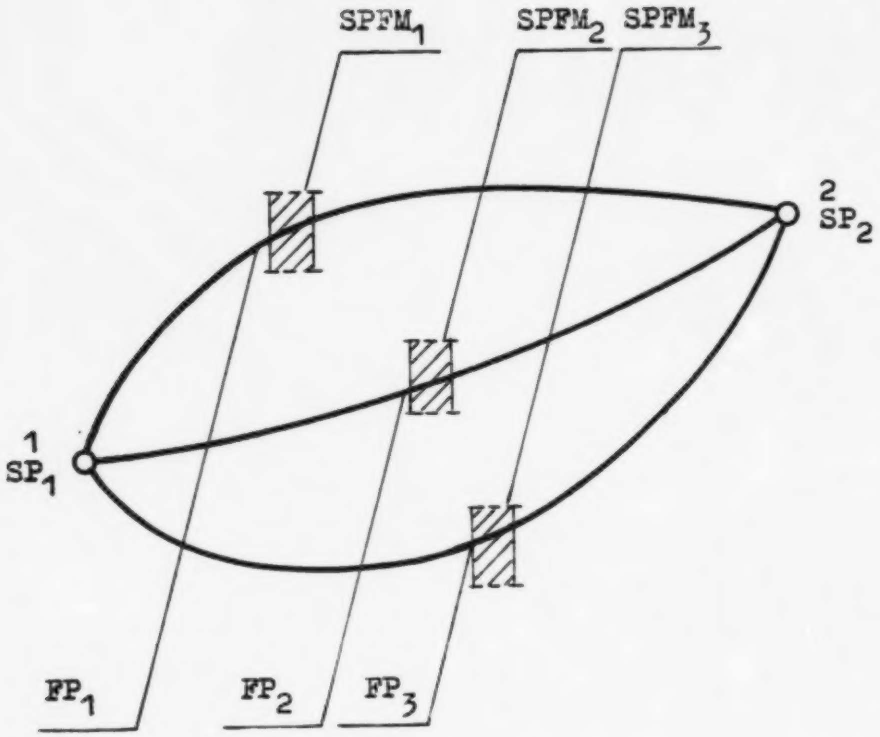
SPFM$_1$
SPFM$_2$
SPFM$_3$
2
SP$_2$
1
SP$_1$
FP$_1$
FP$_2$
FP$_3$

SP_1, SP_2 = state parameters

FP_1, FP_2, FP_3 = filtration parameters

$SPFM_1, SPFM_2, SPFM_3$ = structural parameters of filtration medium

$SP_1 \neq SP_2$

FP_1 and $SPFM_1 \neq FP_2$ and $SPFM_2 \neq FP_3$ and $SPFM_3$

E = constant

Figure 11. General scheme of filtration process.

If filtration efficiency depends only on the initial and final dust concentration, the following equation can be written:

$$E = \left[1 - \frac{c_2}{c_1}\right]100 \quad , \tag{5}$$

where

E = filtration efficiency,

c_1 = initial dust concentration, and

c_2 = final dust concentration.

Equation 5 indicates that dust collection efficiency is a good quantitative parameter that describes the filtration efficiency of a given filtration structure, in terms of initial concentration.

Performed with low initial dust concentrations, the process differs physically from a process performed with high initial dust concentrations. Moreover, if particle size distribution is considered for characterizing the differences between different aerosols, three types of dry filtration processes can be delineated:

- High-efficiency air filtration: initial solid particle concentration in the aerosol is below 1 mg/m^3; particle size distribution is characteristic of aerosols found indoors;[6] and
- Air filtration: initial concentration of solid particles in the aerosol is below 50 mg/m^3; particle size distribution is that characteristic of atmospheric aerosols.
- Dust filtration: initial concentration of solid particles in the aerosol is above 50 mg/m^3; particle size distribution is that characteristic of industrial aerosols.

Air filtration, and especially high-efficiency air filtration, is based on the classical theory of filtration. When certain assumptions are applied, physical and mathematical modeling is simplified.

On the other hand, the physical processes occurring in industrial dust filtration (Filtration Process III) are poorly understood. Dust filtration has an inadequate theoretical base.

DESCRIPTION OF THE DUST FILTRATION PROCESS

The primary property distinguishing the dust filtration process from other dry filtration processes is its cyclic time behavior. Both the high-efficiency filtration process and the air filtration process usually consist of just one filtration cycle, during which the filtration medium is filled with dust to a certain predetermined level of filtration drag. After this final state is reached, the filtration medium is replaced.

During dust filtration, the filtration medium is periodically cleaned and the filtration cycles are repeated in set time periods and sequences. Practically speaking, the influence of the clean filtration medium on process efficiency can be neglected because the time during which the aerosol contacts the clean filtration medium is short compared to the total filtration time. However, interactions between the clean structure and the solid particles of the dispersed phase play an important role in the dust filtration process because of their influence on the structural properties of the composite, partially dust-filled filtration medium.

The time necessary to reach a state that requires filtration structure regeneration depends on the internal parameters of the process. The basic state parameters (SP) most often considered are the following:[7] [8]

- The thermodynamic parameters of the dispersion medium:

  Temperature,
  Humidity, and
  Pressure.

- The chemical property of the dispersion medium:

  Chemical composition.

- The physical parameters of the dispersed phase:

  Particle size distribution,
  Density,
  Concentration,
  Electrification, and
  Particle shape.

- The chemical properties of the dispersed phase:

  Chemical composition, and
  Mineral composition.

The main filtration parameters (FP) are:

- Face velocity, m^3/m^2h;
- Dust flux, g/m^2h;
- Terminal dust load, g/m^2;
- Residual dust load, g/m^2; and
- Filtration time, min.

The main structural parameters of filtration materials (SPFM) are:

- Porosity;
- Mean pore size, μm, and its geometric standard deviation;
- Specific surface;
- Free area (FA); and
- Diameter of the basic fiber.

In practice, filtration velocity is not measured; its average value is determined based on the total volume of gas flowing through the filtration structure during a certain time (or by an intermediate measurement of the dispersion medium flow). Therefore, the term "filtration velocity" is used to refer to the velocity field and its distribution during gas flow through the porous layers. This velocity field is a vector, but the magnitude used in many papers on gas filtration is a scalar, being an average value calculated from the ratio:

$$\frac{Q}{F} \quad m^3/m^2h \quad , \tag{6}$$

where

Q = mean flow intensity, m^3/h; and

F = active fabric surface area, m^2.

Use of the term "gas loading of the filtration area" (face velocity) to describe the ratio given in Equation 6 recognizes its physical attributes, although its dimensions are those of velocity. The difference may be more clearly distinguished by using m/h for velocity and m^3/m^2h for gas loading of the filtration area (face velocity is the term used in this report).

An analogous quantity is the "dust loading of the filtration area" (dust flux), which is defined according to the following equation:

$$q_p = q_g \; c \quad , \tag{7}$$

where

q_p = dust loading of the filtration area, g/m^{2}h;

q_g = face velocity, m^3/m^{2}h; and

c = concentration of the dispersed phase in the dispersion medium, g/m^3.

The term "dust loading of the filtration area" describes the calculated rate of dust buildup on the filtration structure; the term used in this report is dust flux.

The best way to describe the filtration process is to follow pressure drops with time (Figure 12). Assume the process starts with a clean fabric and is characterized by constant regeneration time (of fixed energy), constant initial state parameters of the aerosol, and constant filtration parameters with a predetermined value of ΔP_K, at which regeneration of the filtration medium occurs. The pressure drop characterizing the process is marked by a solid line. The functional dependencies of certain stages of the process are indicated by dashed lines. The differing pressure drop behavior represented by the dashed lines reflects differing amounts of the dispersed phase in or on the filtration structure for each phase of the process, leading to the delineation of the following states of the filtration medium:

- Pure filtration structure (virgin fabric),
- Structure partly filled with dust (virgin fabric plus dust not removed by cleaning and before the steady state operation is reached),
- Structure fully filled with dust (virgin fabric plus dust not removed by cleaning and after the steady state operation is reached), and
- Structure covered with dust (fabric plus dust just before cleaning).

A pure filtration structure is characterized by the pressure drop, ΔP_o, at a constant value of face velocity during clean air flow; i.e., $q_p = 0$.

A structure partly filled with dust is characterized by successive values of ΔP_N increasing towards ΔP_{NK} as a result of a constant, q_p. The filling of the filtration structure with dispersed medium (dust) is described by the areal dust load and the fabric, L_i, where $i = N_1 \dots N_K$ are the cycle numbers, and L_i is the areal dust load after the i^{th} cycle. This fabric state exists immediately after the regeneration cycle but before the equilibrium state is achieved.

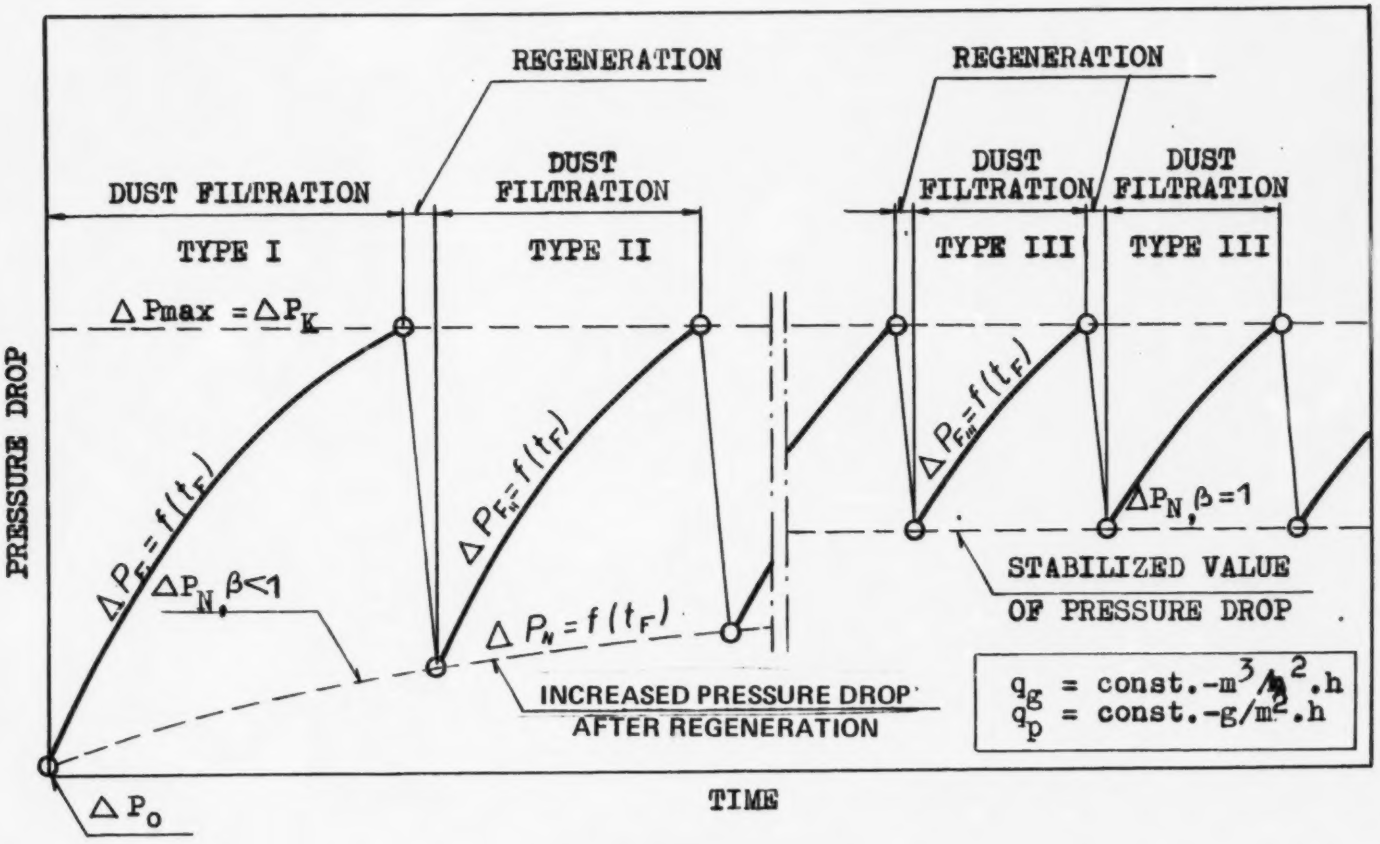
REGENERATION
REGENERATION
DUST FILTRATION
DUST FILTRATION
DUST FILTRATION
DUST FILTRATION
TYPE I
TYPE II
TYPE III
TYPE III
Δ Pmax = ΔP_K
PRESSURE DROP
$\Delta P_F = f(t_F)$
$\Delta P_{F_{II}} = f(t_F)$
$\Delta P_{F_{III}} = f(t_F)$
$\Delta P_N, \beta<1$
$\Delta P_N = f(t_F)$
$\Delta P_N, \beta=1$
INCREASED PRESSURE DROP AFTER REGENERATION
STABILIZED VALUE OF PRESSURE DROP
q_g = const.-m^3/m^2.h
q_p = const.-g/m^2.h
ΔP_o
TIME

Figure 12. Types of dust filtration.

A fully filled structure is characterized by ΔP_{NK}, the pressure drop associated with an areal dust load of L_{NK}. This state represents the equilibrium state for which $L_{NK_1} = L_{NK_2} = \ldots. = L_{NK}$; i.e., L_{NK} = constant independent of the cycle numbers.

A structure covered with dust is a fully filled structure with a dust cake on its working surface. The pressure drop of this state is indicated by ΔP_K, and the magnitude of the dispersed phase on the fabric is indicated by $L = L_{NK} + L_p$, where L_p is the areal density of the dust cake.

Intermediate states of filtration between startup and equilibrium can be described by the term "fabric-filling" according to Equation 8:

$$\beta_i = \frac{L_i}{L_{NK}} \quad , \tag{8}$$

where

β_i = fabric filling after regeneration cycle i;

L_i = fabric dust load after "i" regeneration cycle, g/m^2; and

L_{NK} = equilibrium fabric dust load, g/m^2.

The "fabric filling" can also be described by the relationship:

$$\beta_{r_i} = \frac{\Delta P_{Ni}}{\Delta P_{NK}} \quad , \tag{9}$$

where

β_{r_i} = relative fabric filling after regeneration cycle, i;

ΔP_{Ni} = pressure drop of partly filled structure, after "i" regeneration cycle, mm of water; and

ΔP_{NK} = pressure drop of fully filled structure (after an equilibrium state is achieved), mm of water.

All filtration cycles of the complete filtration process are characterized by different values of B_{r_i} and β_i (< 1, until the equilibrium state is achieved, after which $\beta_i = 1$). Until $\beta_i = 1$, each filtration cycle is qualitatively and quantitatively different from the previous one.

Three main types of dust filtration occur in dry dust filtration: Dust Filtration Types I, II, and III[9] (Figure 12).

Dust Filtration Type I initiates the filtration process as the fabric first contacts the aerosol. This phase ends when a certain dust load on the fabric is reached as measured by a predetermined pressure drop.

Dust Filtration Type II includes those filtration processes between the first regeneration cycle and the equilibrium state. Dust Filtration Process Type II performs with $\beta_i < 1$.

Dust Filtration Type III is the filtration process characteristic of the equilibrium state. It is characterized by constant L_{NK} and L from cycle to cycle and by constant pressure drops after regeneration. Dust Filtration Type III Processes perform with $\beta_i = 1$. These Type III processes occur in industrial fabric dust collectors.

The differing, initial states of the filtration medium between successive filtration cycles with differing degrees of fabric filling (β) lead to the conclusion that the various dust filtration processes represent physical processes that cannot be compared. Thus, the external parameters of these processes (efficiency and filtration resistance) for a given set of filtration materials and operating conditions also differ:

$$E_I \neq E_{II} \neq E_{III} \quad \text{, and} \qquad \qquad (10)$$

$$\Delta P_{FI} \neq \Delta P_{FII} \neq \Delta P_{FIII} \quad .$$

The equivalent of Equation 10 can be obtained after the corresponding regression functions are defined:

$$E_I = R_E \cdot E_{III} \quad \text{, and} \qquad \qquad (11)$$

$$\Delta P_{FI} = R_{\Delta P} \, \Delta P_{FIII} \quad .$$

DUST FILTRATION TYPE I

Dust Filtration Type I is a process characteristic of laboratory-scale experiments in which the test material is dusted in only a one-cycle operation without regeneration. As with all filtration processes, this process can be characterized by definite values of external parameters (efficiency, filtration resistance) related to the filtration parameters.

EFFICIENCY, DUST FILTRATION TYPE I

Dust collection efficiency is the most important external filtration parameter, and it varies qualitatively with process conditions. Efficiency is usually calculated by weighing the increase of dust on the test filtration material and on an absolute filter. Mathematically, it is an average value as determined by a single measurement.

When the effect of varying process parameters on material filtration efficiency is studied, average values of dust collection efficiency are obtained for a succession of differing parameter values, which permits a plot of dust collection efficiency as a function of time and the examined parameter. Usually, in an interpretation of laboratory-scale results, mean values of dust collection efficiency are related to the final states of individual measurement cycles, which then delineate the dependence.

This procedure, for dust collection efficiency variations as a function of time (the duration of a single experiment), is illustrated in Figure 13. Assuming fixed filtration materials and operating conditions, dust collection efficiencies E_1, ..., E_4 correspond to filtration times t_1, t_2, t_3, and t_4, respectively. When each experiment's efficiency is plotted against its final state (time), points "a" to "d" are obtained, which yields the $E = f(t)$ function labelled curve 1.

It should be noted that efficiency E_1 is a mean efficiency of the process from $t = 0$ to $t = t_1$, and E_2 is a mean efficiency from $t = 0$ to $t = t_2$. True efficiency obtained during the process from $t = 0$ to $t = t_1$ and related to the final state of process E_1 must be by nature higher than the mean, empirically determined efficiency.

Because the dependence, $E = f(t)$, is generally curvilinear, the following equation can be obtained through application of the theorem of average, integral value:

$$\bar{E}\Big|_{t=0}^{t=t_n} = \frac{1}{t_n}\int_0^{t_n} f(t)dt = f(c) \quad , \tag{12}$$

where

$\bar{E}\Big|_{t=0}^{t=t_n}$ = experimentally determined mean dust collection efficiency between $t = 0$ and $t = t_n$;

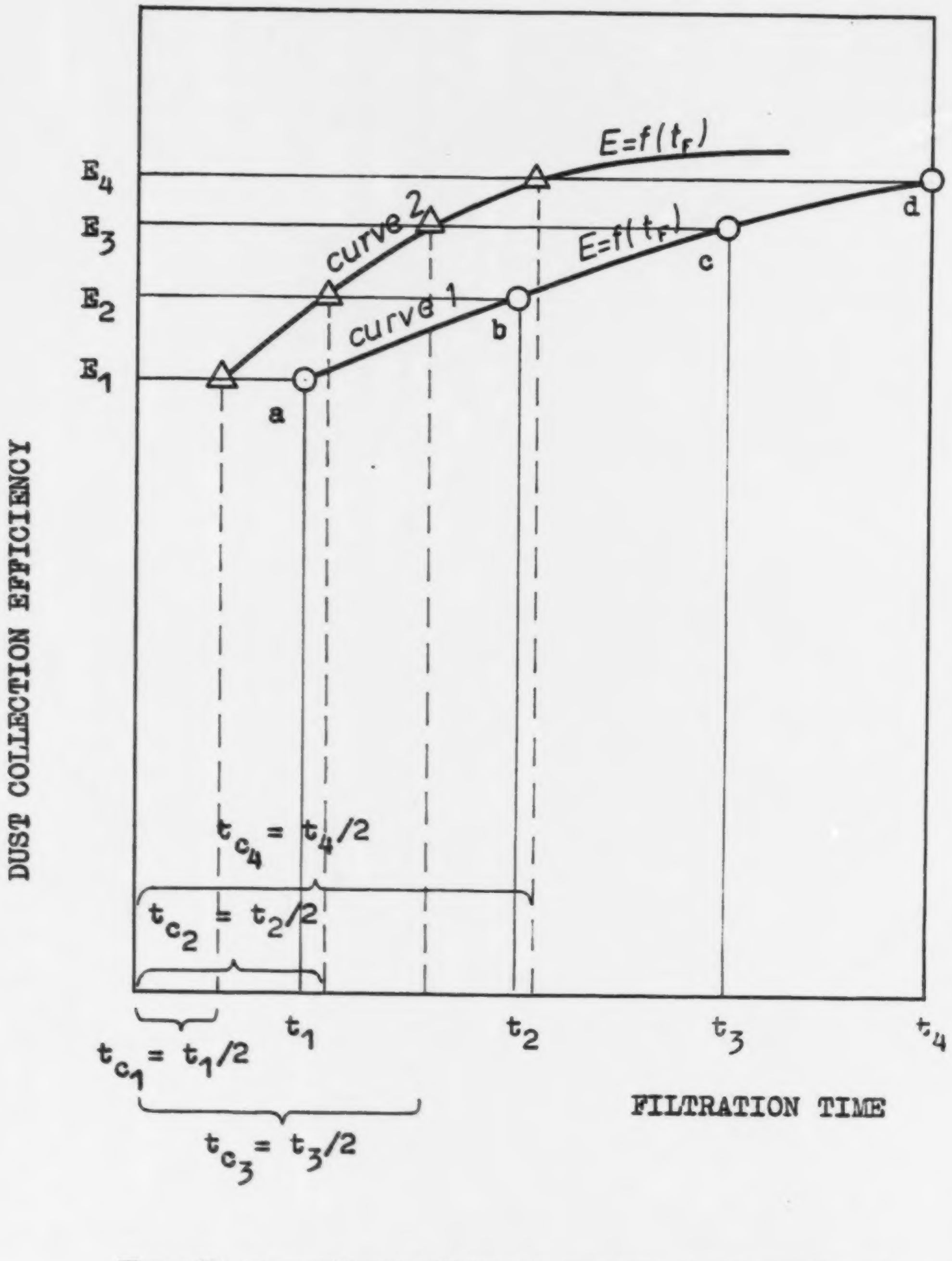
DUST COLLECTION EFFICIENCY
FILTRATION TIME
E_4
E_3
E_2
E_1
$E=f(t_F)$
curve 2
$E=f(t_F)$
curve 1
a
b
c
d
t_1
t_2
t_3
t_4
$t_{c_4} = t_4/2$
$t_{c_2} = t_2/2$
$t_{c_1} = t_1/2$
$t_{c_3} = t_3/2$

Figure 13. Dust collection efficiency in Dust Filtration Process Type I as a function of time.

t_n = successive times of experiments at n = 1, 2, 3 ...;
$f(t)$ = time dependence of dust collection efficiency; and
$f(c)$ = average integral value of function $f(t)$ over the range, $t = 0$ to $t = t_n$.

The abscissa value corresponding to the mean efficiency of a given filtration cycle during which a mean value is determined can be calculated by:

$$f(t) = f(c) \; . \tag{13}$$

Equation 12 shows that if the f(t) curve tends toward a straight line, the f(c) value becomes a mean arithmetic value. For a linear f(t) function, the value, f(c), is calculated as the mean arithmetic value from the equation:

$$f(c) = \bar{E}\Big|_{t=0}^{t=t_n} = \frac{E(t=0) + E(t=t_n)}{2} = \frac{E_o + E_n}{2} \quad , \tag{14}$$

where

$\bar{E}\Big|_{t=0}^{t=t_n}$ = mean dust collection efficiency over the range, $t=0$ to $t=t_n$;
t_n = successive times of experiments, n = 1, 2, 3 ...;
E_o = true initial dust collection efficiency at $t = 0$; and
E_n = true efficiency at $t = t_n$.

Because the dust collection efficiency function, $E = f(t)$, is usually unknown, the calculation of t_c, based on Equation 13, is not generally possible. The E curve can be calculated, however, by the method of successive approximations.

Because the curve, $E = f(t)$ for $L_o > 50\ g/m^2$, is linear, Equation 14 can be used to calculate t_c. For successive filtration cycles, $t_c = t_n/2$ where n = 1, 2, 3, ..., k. Although this simplification introduces approximation errors, it provides a quick assessment of laboratory experiments. The efficiency of curve E obtained by such an approximation process is shown as curve 2 in Figure 13.

The following conclusions result from the discussion and measurements of variations in laboratory dust collection efficiency.

- Dust collection efficiency as a function of time is characterized by discrete, random variability of mean values.
- Mean values of dust collection efficiency obtained in each experiment show the time dependence of dust collection efficiency in the form of a continuous function. The assumption of a continuous function reflects the process, which is continuous in the physical sense.
- Mean values determined experimentally for a specific final state of the process give an incorrect functional dependence, $E = f(t)$, because the instantaneous efficiency of the final stage of the process is higher than the mean value calculated over the particular time span.
- Efficiency variation in time should be determined from experimental data for the mean values of dust collection efficiency assigned to intermediate rather than final stages of the process.
- The character of the filtration process does not permit an experimental determination of the initial process efficiency. The mean initial efficiency may be determined only by back extrapolation from the empirical function, $E = f(t)$.

Research carried out in the second phase of this project allows a determination of the functional relationship between dust collection efficiency for Dust Filtration Type I and the basic filtration parameters; i.e., face velocity, q_g; and areal dust loading, L_o. The dependence is the following relationship described by Valentine:[10]

$$E_I = 100 \left[E_o \right]^{-L_o^{n}} , \qquad (15)$$

where

E_I = laboratory dust collection efficiency, %;
E_o = initial efficiency, %;
L_o = areal dust density, g/m^2; and
n = direction coefficient.

A more general form of Equation 15 is:

$$E_I = 100 \left[F_1 \right]^{-L_o^{\left[F_2 \right]}} , \qquad (16)$$

where

F_1 and F_2 = functions of q_g.

Equations 15 and 16 are valid for $L_o > 0$ because of the properties of the general functional form, $y = a^{-x}$.

For large values, L_o increases with time, according to the following equation:

$$L_o = c_1\, q_g\, t_F = q_p\, t_F \quad , \qquad (17)$$

where

L_o = areal dust density, g/m²;
c_1 = initial dust concentration, g/m³;
c_2 = final dust concentration, g/m³ (assumed = 0);
q_g = face velocity, m³/m²h;
q_p = dust flux, g/m²h; and
t_F = filtration time, h.

Dust collection efficiency as a function of time is described by combining Equation 17 and Equation 16:

$$E = 100 \left[F_1\right]^{-(q_p\, t_F)^{F_2}} \quad , \qquad (18)$$

For certain process performance parameters, Equation 18 has the following simple analytical form, which can be easily interpreted geometrically:

$$E = 100 \cdot A^{-\left(B \cdot t_F\right)^{C}} \quad , \qquad (19)$$

where

A, B, C = experimental constants, and
t_F = filtration time.

If these criteria are accepted for mean dust collection efficiency in one experiment, the t_C value calculated from Equation 13 for a given set of process parameters should be inserted in Equations 18 and 19.

The model presented in Equations 15 and 16, describing dust collection efficiency as a function of the basic parameters, q_g and L_o, is a three-dimensional, probabilistic model of Dust Filtration Type I. The range of its validity is determined by the range of the parameters considered. Moreover, the constant values (or coefficients of functions F_1 and F_2) in this model depend on filtration material, dust, and other process parameters. These statements are based on the model's empirical data.

The model has some limits, but it permits a description of the effects of certain process parameters on laboratory-scale dust collection efficiency.

It is also possible to analyze the process physically over the range of values assumed by the process parameters. The extrapolation of process performance outside the assumed range is possible with certain limits resulting from the physical model.

Theoretical variation of efficiency in time according to Equation 19 is shown in Figure 14. The variation is characterized by a fast increase in dust collection efficiency until the filtration structure fills with dust. Later, the increase in efficiency is slower; i.e., the structure is being covered with dust, which forms the dust cake, but the filtration effects are small. During this time, the porous structure of the dust cake has a smaller effect on the process than the structure of the filtration material. The filtration material acts only as a base for the dust layer.

The nomenclature of classical filtration theory is used to describe a single cycle of filtration, which represents Dust Filtration Type I, and three phases of filtration can be delineated:

- Stationary filtration, which does not play any practical role in the complete process because of its short duration;
- Nonstationary filtration, which occurs as the filtration structure is being filled with dust; and
- "Ductive" filtration, which characteristically occurs when the dust cake is being formed.

Stationary and nonstationary filtration phases influence the initial efficiency, E_o, of the process. The efficiency of the two phases depends strongly on the structural parameters of the filtration material, the particle size distribution, and the raw materials making up both the fabric and the dust.

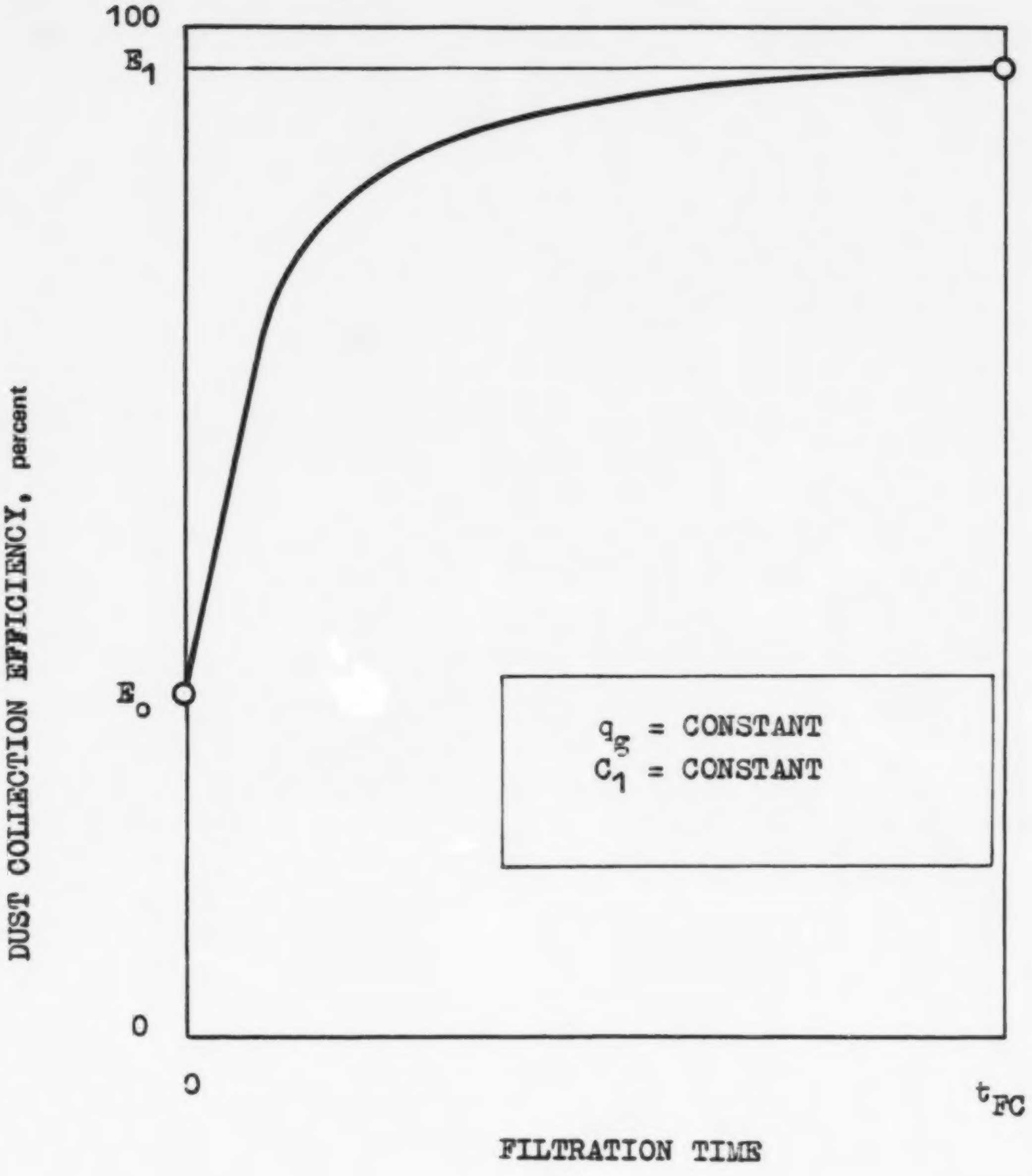

Figure 14. Theoretical variation of efficiency in time according to Equation 19.

Dust migration[11] through the filtration material structure due to the hydromechanic effect of the flowing gas stream is avoided in the "ductive" filtration phase because the efficiency is determined mainly by the filtration properties of the dust cake.

In research of dust cake filtration properties and the study of basic physical filtration mechanisms on the overall dust collection efficiency, the tendency is to compare the process with filtration through granular beds. However, although filtration through the dust cake is physically similar to filtration through granular beds, the processes are not identical and should be studied separately.

The principle of flow around a single filtration element applied to the estimated efficiency of the process through filtration beds with assumptions for the classical filtration theory for flow around elementary fiber cannot be applied in the case of dust cake. The basic assumptions of the isolated fiber theory are not satisfied in dust filtration. Moreover, if structural properties and the mechanisms of dust particle precipitation in granular beds and dust cake are compared, considerable differences are observed, leading "ductive" filtration to be regarded as a separate process. The differences between "ductive" filtration and filtration through granular beds (Figure 15) are:

- In "ductive" filtration, the porous filtration layer is formed from the same raw material as the aerosol, so the physical interactions between the structural elements of the filter and the dust particles differ from those of the classical granular bed, for which the filter and dust in raw materials are, in general, different.
- Thickness of the dust cake varies as a function of time, while thickness of the classical granular bed is constant.
- The relative particle size of the dust cake is comparable to that of the precipitated polydisperse aerosol, while in classical granular bed filtration the relative size ratio approaches 100 to 400.

The range of this project was too narrow to serve as a base for a precise hypothesis concerning the dust cake filtration process. However, a physical model of the dust cake filtration process was built based on results from earlier testing of industrially classified (fractionated) dusts.[12] [13]

The basic total assumptions for the proposed physical model of the dust cake filtration process are:

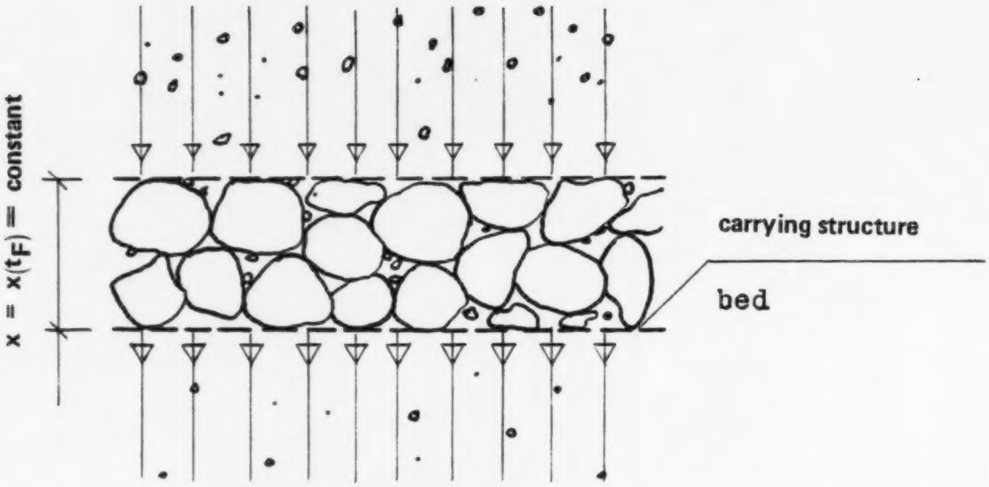
x = x(t_F) = constant
carrying structure
bed

a. Filtration through granular bed.

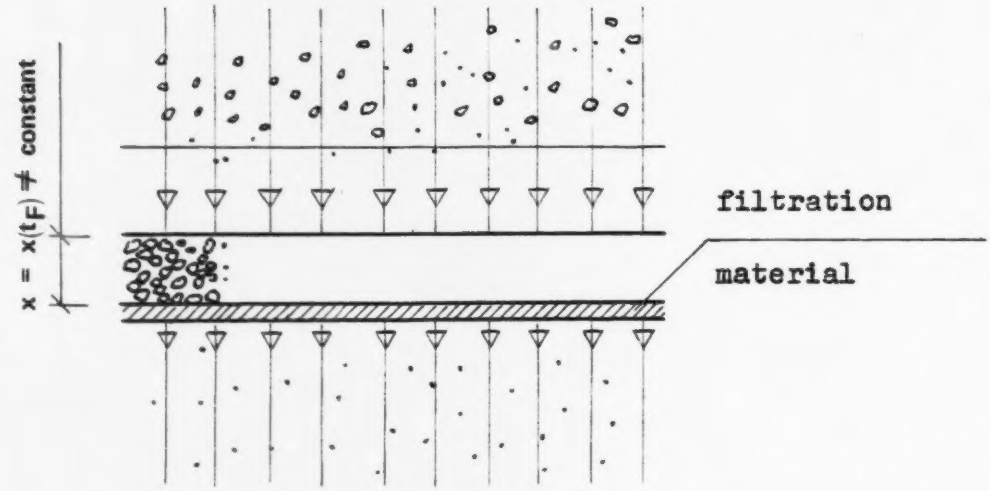
x = x(t_F) ≠ constant
filtration
material

b. "Ductive" filtration.

Figure 15. Comparison of granular bed structure with dust cake structure.

- The particle size distribution in the aerosol upstream of the filtration structure is independent of time and position,
- The velocity distribution in the aerosol upstream of the filtration structure is independent of time and position,
- The particle size distribution in the aerosol is log normal,
- The spatial structure of the dust cake formed on the surface of the filtration material is not affected by dislocations or structural defects in a geometrical sense, and
- The dust concentration upstream of the filtration is constant.

During the first phase of the study it is assumed that dust particles are spherically shaped.

With these assumptions, the dust cake increases in thickness by the value, dh, in the time period, dt, so the total dust cake layer has a new thickness of h + dh. Assuming that $dh = \sim \bar{d}$ ($\bar{d}$ = mean particle diameter), the thickness of successive static layers of growing dust cake can be described.

The superficial porosity of the dust cake (individual layers of thickness, dh) is the ratio between pore area and total dust cake surface and is closely related to the particle size distribution of the aerosol. Like aerosol particles, the equivalent pore size distribution is also log normal; thus, superficial porosity and pore size distribution are determined by functions similar to the aerosol particle size distribution.

Consider an element of dust cake (Figure 16) and assume for simplicity that the diameter of all elements of its structure is the same. The following mechanisms of aerosol particle deposition can be delineated:

- Selective precipitation, which causes the dust cake to grow;
- Inertial deposition in the dust cake structure because of acceleration of dust particle in pores to velocity, $V_p > > V$, where V_p is the gas velocity in the pore, and V is the mean gas velocity upstream of the dust cake structure;
- Diffusion inside the dust cake structure; and
- Electrostatic precipitation inside the dust cake structure because of local electric fields.

Selective precipitation includes a sieving effect, but a major difference is the fact that the openings of a sieve are of constant dimensions, while in the dust cake filtration process pore size is a function of aerosol particle size distribution.

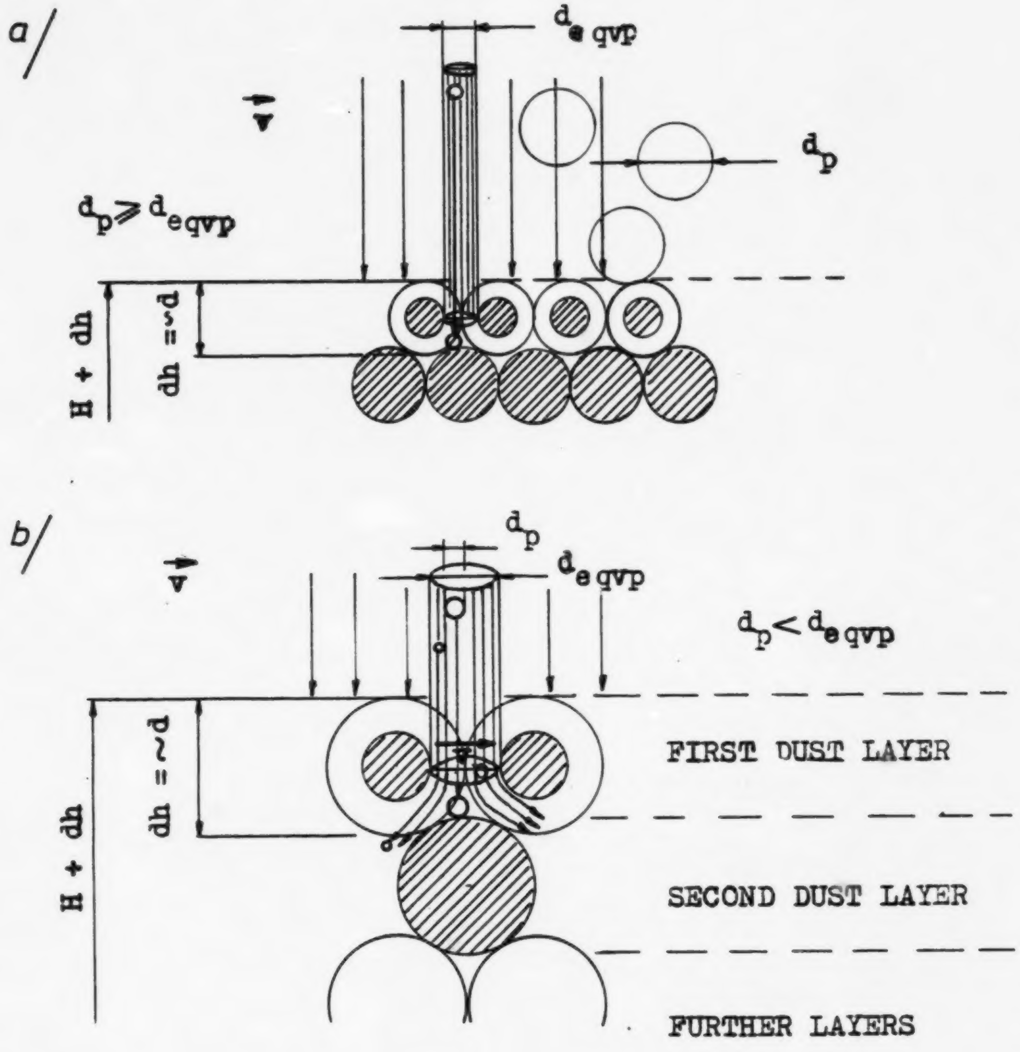
a/
d_e qvp
v
d_p
d_p ≥ d_eqvp
H + dh
dh =~ d
b/
d_p
d_e qvp
v
d_p < d_e qvp
H + dh
dh =~ d
FIRST DUST LAYER
SECOND DUST LAYER
FURTHER LAYERS

a. Selective precipitation of dust particles on dust cake structure.

b. Impaction precipitation of dust particles in dust cake structure.

Figure 16. Filtration mechanisms in ductive filtration.

Selective precipitation also includes the mechanisms of simple inertial deposition and interception in the velocity field, $\vec{V}$. These selective precipitation mechanisms depend on the particle size distribution, the mean velocity upstream of the dust cake structure, the densities of the dispersion medium and the dust, and the gas viscosity. The collection efficiencies of these mechanisms depend on the Stokes number, which is regarded as a characteristic number for inertial deposition of dust particle.

Based on the analysis of dust cake structure to be presented in Section IX, the condition for dust particles not to be precipitated by selective precipitation mechanisms is:

$$d_p^1 < d_{eqv.p} = \frac{4F}{0} \quad , \qquad (20)$$

where

d_p^1 = dust particle diameter, μm;
$d_{eqv.p}$ = equivalent pore diameter, μm;
F = pore area, (μm²); and
0 = wetted perimeter of pore, μm.

All dust particles in a stream tube of diameter $d_{eqv.p}$ can penetrate the first dust layer. However, dust particles that flow through the first layer pores are accelerated from velocity, $V \to V_p$. Because a four-element configuration of particles in the dust cake structure is most probable (the problem is discussed more closely in Section IX), some dust particles penetrating the first dust layer are precipitated by inertia on the dust particles of the second layer. Dust particles with diameters under the size limit, $d_p < d_{lim}$, penetrate to further layers. The size limit results directly from the gas velocity in the pores, (V_p), the densities of the dust and the gas, and viscosity.

Precipitation of dust particles under the size limit is performed in the dust cake structure and is caused by interception and diffusion. Accordingly, the efficiency of the diffusion precipitation process depends on the flow time of the dust particle through the dust cake and thus on the total thickness of the dust cake.

Equivalent pore size in a single monodisperse layer of dust particles, for a four-element configuration, is related to dust particle diameter according to:

$$d_{epv.p} = \sim 0.200\ R \quad , \tag{21}$$

where

$d_{eqv.p}$ = equivalent pore size, μm; and

R = particle radius, μm.

So, the condition expressed by Equation 20 is an inequality:

$$d_p' < 0.1\ d_p \quad . \tag{22}$$

Dust cake collection for monodisperse dust can be 100 percent efficient because of the selective precipitation mechanism.

For polydisperse aerosols, selective precipitation efficiency depends on the degree of dispersion of the dust particles. If Equation 21 is assumed true for certain aerosol particle size classes, pore size distribution can be expressed by:

$$f(d_{eqv.p}) = \frac{1}{\sigma_p\sqrt{2\pi}}\ \exp\ -\left[\frac{(d_{eqv.p} - d^M_{eqv.p})^2}{2\sigma_p{}^2}\right] \quad . \tag{23}$$

Mean $d^M_{eqv.p}$ and standard deviation, σ_p, are distribution parameters. The mean can be determined based on the following equation, which results from previous deliberations:

$$\begin{aligned} d^M_{eqv.p} &= 0.1\ (d_{50}) = 0.1\ (\mathrm{MMD}) \quad , \text{ and} \\ \sigma_p &= 0.1\ \sigma_g \quad , \end{aligned} \tag{24}$$

where

$d^M_{eqv.p}$ = mean diameter of equivalent pore size distribution, μm;

MMD = d_{50} = mass mean diameter of dust particle distribution, μm;

σ_p = standard deviation of equivalent pore size distribution, μm; and

σ_g = standard deviation of mass dust particle size distribution, μm.

If $d^M_{eqv.p}$ is determined from the cumulative curve of dust particle size, the percent of dust fraction, f_1, satisfying Equation 22 can be calculated. The dust fraction related to the dust loading upstream of the dust cake structure, $q_{p^1} = c_1 \cdot q_g$, gives the dust flux flowing through the first dust particle layer:

$$q_{p^2} = q_{p^1} \cdot f_1 \quad . \tag{25}$$

According to Fourier's equation, the gas velocity in the pores is:

$$Q = F_c \cdot V = F_p \cdot V_p \quad , \text{ and}$$

$$V_p = \frac{F_c}{F_p} \cdot V = \frac{1}{\varepsilon_p} \cdot V \quad , \tag{26}$$

where

Q = flow rate, m^3/s;

F_c = dust cake area, m^2;

F_p = pore area corresponding to F_c, m^2;

V = aerosol velocity upstream of the dust cake structure, m/s;

V_p = velocity in pores, m/s;

ε_p = superficial porosity; and

ε_p = 0.09 for a four-element configuration of dust cake structure.

The Reynold's number corresponding to flow conditions through the first dust particle layer is:

$$Re_p = \frac{d_{eqv.p} \cdot V_p}{\nu} \quad , \tag{27}$$

where

$d_{eqv.p}$ = equivalent pore diameter, cm;

V_p = velocity in pores of the first layer, cm/s; and

ν = viscosity, poise.

For the four-element configuration, the condition for geometrical inertia deposition of dust particles from the aerosol flowing out of the nozzle is satisfied:

$$d_{eqv.p} / L \sim 1 \quad , \tag{28}$$

where

L = length of nozzle from static element on which the dust is precipitated (particles of the second dust layer), µm.

Thus, the limit for particle size can be determined by the equation:[14] [15]

$$d_{lim} = \left[\frac{18 \cdot \Psi \cdot \nu \cdot d_{eqv.p}}{C \cdot c_p \cdot V_p} \right]^{1/2} \quad , \tag{29}$$

where

d_{lim} = diameter of particle impacting on the second layer, cm;
Ψ = Stokes impaction parameter;
ν = viscosity, poise;
$d_{eqv.p}$ = diameter of pore, cm;
C = Cunningham correction factor;
c_p = particle density, g/cm^3; and
V_p = velocity of gas through pore, cm/s.

Thus, the dust flux leaving the second layer is a smaller fraction of dust characterized by size $d_p < d_{lim}$ according to:

$$q_{p^3} = q_{p^2} \cdot f_2 \quad , \tag{30}$$

where

q_{p^3} = dust loading of the third layer, g/m^{2}h;
q_{p^2} = dust loading of the second layer, g/m^{2}h; and
f_2 = dust fraction precipitated in the second layer.

The physical model presented above, based on a qualitative analysis of filtration in the dust cake and the application of some relationships introduced by the classical filtration theory, permits an estimation of the effect of internal process parameters on process efficiency.

Assuming that the filtration properties of the dust cake determine the efficiency of the dust-fabric system in the second phase of Dust Filtration Process Type I (and also during Dust Filtration Type III after the system reaches a state of equilibrium), the present model can predict the physical parameters of the aerosol leaving the system.

The particle size distribution of dust leaving the system is the most technologically interesting. This function may be determined from the above equations.

The model does not consider electrostatic effects occurring in the process. However, the presence of these effects can be determined by comparing the theoretical and experimental results. This theory confirms results obtained by J. H. Turner and R. Dennis[16] [17] concerning the time dependence of the particle size distribution in the aerosol leaving the dust collection device. Both authors point out the decrease in small particles accompanying the increase in dust cake. The effect of selective precipitation after dust cake formation and the decrease of submicron fractions attributable to diffusion and interception mechanisms is clear.

This physical model can be the basis for further research quantifying the model predictions.

Filtration Resistance Problems in Dust Filtration Type I

Deposition of gas-dispersed particles in and on the filtration medium structure is accompanied by an increased flow resistance of the dispersion medium, as determined by filtration resistance. Filtration resistance is measured by the static pressure drop difference before and after the filtration structure, according to the equation:

$$\Delta P_F = (\Delta P_K - \Delta P_0) \quad , \qquad (31)$$

where

ΔP_F = filtration resistance, mm H_2O;
ΔP_K = final pressure drop, mm H_2O; and
ΔP_0 = initial pressure drop (resistance of pure fabric), mm H_2O.

Filtration resistances are functions of the filtration time, t_F, under certain process conditions.

Based on tests conducted on various dust fabric systems, it was ascertained that for filtration fabrics, filtration resistance variation in time has the form of a parabola with the following variable coefficients:

$$\Delta P_F = \begin{cases} -a_1 t_F^2 + b_1 t_F + c_1 & \text{for} \quad t_F \epsilon [0, t_{FA}] \\ a_1' t_F^2 + b_1' t_F + c_1' & \text{for} \quad t_F \epsilon [t_{FA}, t_{FC}] \end{cases} , \qquad (32)$$

where

ΔP_F = filtration resistances, mm H_2O;
t_F = filtration time, min;
t_{FA} = time corresponding to the point of inflection, min;
t_{FC} = filtration time for a given filtration cycle, min;
a_1, b_1, c_1 = coefficients; and
a_1', b_1', c_1' = coefficients.

Equation 32 is illustrated in Figure 17. The curve includes two parts that identify two phases of increasing filtration resistance.

The first phase is characterized by a rapid increase in filtration resistance, which stops after inflection point A is reached. The length of the first phase depends mainly on face velocity but also on the kind of filtration material, the kind of dust, and the particle size distribution.

Based on an examination of filtration material samples tested in short intervals, the hypothesis can be offered that the rapid increase of resistance during the first phase of the process is related to filling the filtration material structure with dust, and thus to its decreased porosity, variation of pore diameter distribution, and average pore diameter. The above hypothesis is confirmed by a discussion of Hagen Poiseuile's equation of laminar flow through a capillary:

$$\Delta P = \frac{8 \quad \cdot Q \cdot L}{10 \cdot \pi \cdot R^4} , \qquad (33)$$

where

ΔP = pressure drop,
ν = gas viscosity,
Q = flow rate through pore,
L = length of pore, and
R = average pore radius.

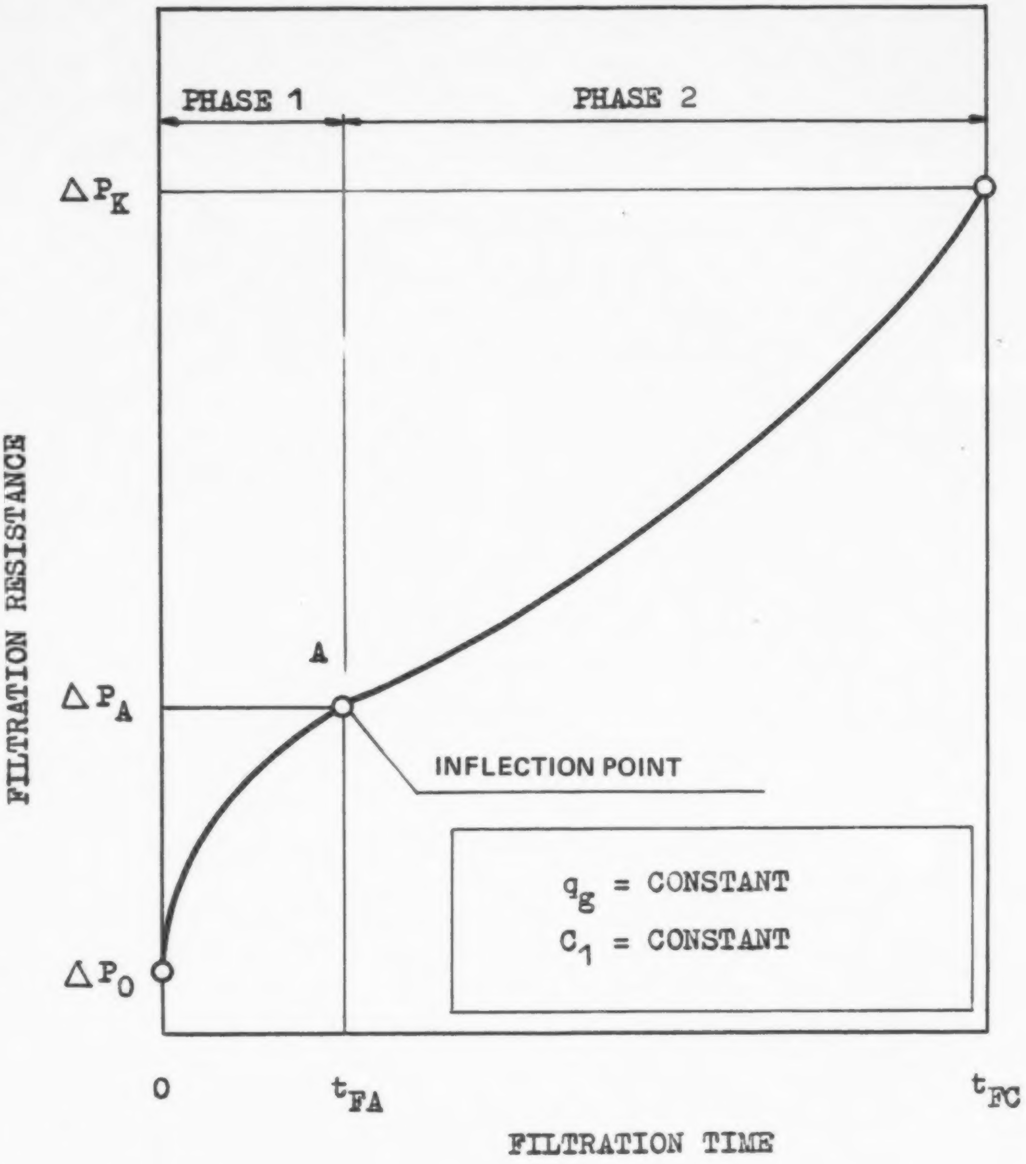

Figure 17. Filtration resistance variation in time for Dust Filtration Process Type I.

Assuming constant values of ν, Q, and L, the pressure drop, ΔP, depends strongly on R. Thus, at the inflection point, the fully filled filtration material structure is characterized not only by a definite value of filling (amount of dust filling the structure) but also by a certain value of mean pore diameter.

From the inflection point, a slower increase in filtration resistance is observed corresponding to a parabola with positive direction coefficients. The shape of the parabola in the second phase of the curve, $\Delta P = f(t_F)$, is different for various dust-fabric systems. The effect of the structural parameters of the filtration material and the dust parameters on properties and spatial structure of the dust cake can be seen.[18]

It is noteworthy that no research explains the peculiarities and physics of the phenomena that determine the process by which the filtration structure fills with dust or the effect of the filtration medium structure on dust cake properties. Most work concerning these problems deals with the results of these effects rather than with the physics of the phenomena itself.

Dust filtration research with artificially charged dusts supports the conclusion that this phenomenon can play an important role in the dry filtration process.[19]

These deliberations and actual measurements of filtration resistance variation in time show that the laboratory and industrial-scale models of filtration resistance represented by Kozeny-Carman's equation are, for Dust Filtration Type I, not good predictors.

The resistance coefficient, K_2, for the dust-fabric system defined as an inverse of the permeability coefficient of the system, according to Kozeny-Carman's theory, can be presented in the form of the following equation:

$$K_2 = \frac{1}{K} = k \cdot \nu \cdot S_o^2 \; (1 - \varepsilon) / \rho_p \cdot \varepsilon^3 \quad , \qquad (34)$$

where

K_2 = resistance coefficient for dust-fabric system,

K = permeability for dust-fabric system,

k = Carman constant,

ν = gas viscosity,

S_o^2 = kinetic specific surface,

ε = porosity, and

ρ_p = dust density.

Assuming a homogeneous system and constant process parameters, the resistance coefficient, K_2, is usually calculated from the equation:

$$K_2 = \frac{d(\Delta P)}{d(t_F)} = \frac{d(S)}{d(L_o)} \quad , \tag{35}$$

where

$S = \Delta P/q_g$ = system drag, and

L_o = areal dust density.

Equation 34 can be written:

$$K_2 = f\left(\frac{1 - \varepsilon}{\varepsilon^3}\right) \quad , \tag{36}$$

where

$(1 - \varepsilon)/\varepsilon^3$ = a porosity function.

From Equation 35 and the known parabolic dependence of filtration resistance upon time confirmed by experiments in the range of Dust Filtration Type I, the porosity function, $(1 - \varepsilon)/\varepsilon^3$, is concluded not to have a constant value. Equation 32 results in the following for the second phase of filtration resistance increase:

$$K_2 = \frac{d(\Delta P)}{d(t_F)} = 2a_1' \, t_F + b_1' \quad , \tag{37}$$

where

b_1 = an empirical coefficient equal to the value of K_2 at the inflection point, A (or the K_2 value of the linear portion of the filtration resistance vs. time plot),

a_1' = an empirical coefficient, or

$t_F = (t_{FC} - t_{FA})$.

Equation 37 can be noted to be of the following form:

$$K_2^* = K_2 + 2a_1' \, (t_{FC} - t_{FA}) \quad , \tag{38}$$

where

K_2'' = the resistance coefficient of the second phase of Dust Filtration Process Type I, and

K_2 = the resistance coefficient of the phase of Dust Filtration Process Type I, assuming a linear dependence.

The dependence described by Equation 38 is illustrated in Figure 18.

Equation 38 results in an increase in the value of resistance coefficient with filtration time, which implies an increase in the porosity function, $(1-\varepsilon)/\varepsilon^3$, or a decrease in the dust-fabric system porosity, ε. The above results show that in the second phase of Dust Filtration Process Type I some structural changes lead to decreased porosity of the dust-fabric system. The hypothesis may be offered that the structural changes are connected with compression effects of the dust cake caused by an increased drop in static pressure.

These deliberations are right for applying the Kozeny-Carman theory; i.e., for laminar flow. The absolute value of porosity can be determined from the value of K_2. Variation of the porosity function with absolute porosity is illustrated in Figure 19.

If the results of the discussion of physical mechanisms occurring during dust cake growth are considered, the hypothesis can be offered that the superficial porosity of the fully filled structure is equal to the mean superficial porosity of the dust cake at the inflection point of the filtration resistance curve (point A, Figure 17). Superficial porosity of the dust cake results mainly from the selective precipitation mechanism and is determined by the dust particle size distribution in the aerosol.

Although difficult to verify experimentally, this hypothesis results directly from scientific deliberations and experimental trends of dust collection efficiency and resistance in time during Dust Filtration Process Type I.

The physical meaning of the constants in Equation 32 is discussed in a later section on problems of dust cake structural parameters.

DUST FILTRATION TYPE III

Dust Filtration Process Type III applies to industrial gas filtration by fabric filters, so it is the most practically important filtration process.

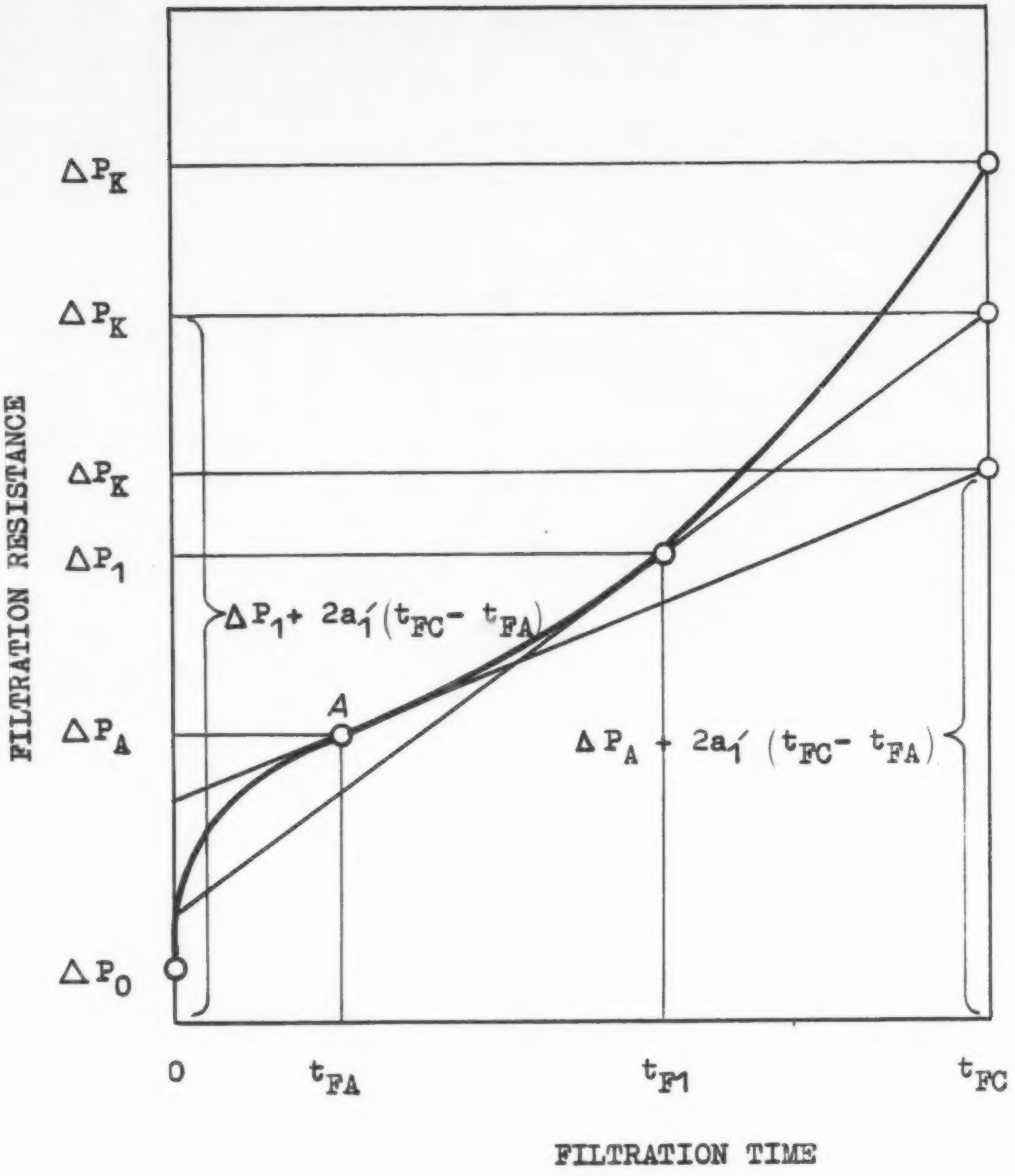

ΔP_K
ΔP_K
ΔP_K
ΔP_1
$\Delta P_1 + 2a_1'(t_{FC} - t_{FA})$
A
ΔP_A
$\Delta P_A + 2a_1'(t_{FC} - t_{FA})$
ΔP_0
FILTRATION RESISTANCE
0
t_{FA}
t_{F1}
t_{FC}
FILTRATION TIME

Figure 18. Changes of K_2 in Dust Filtration Process Type I.

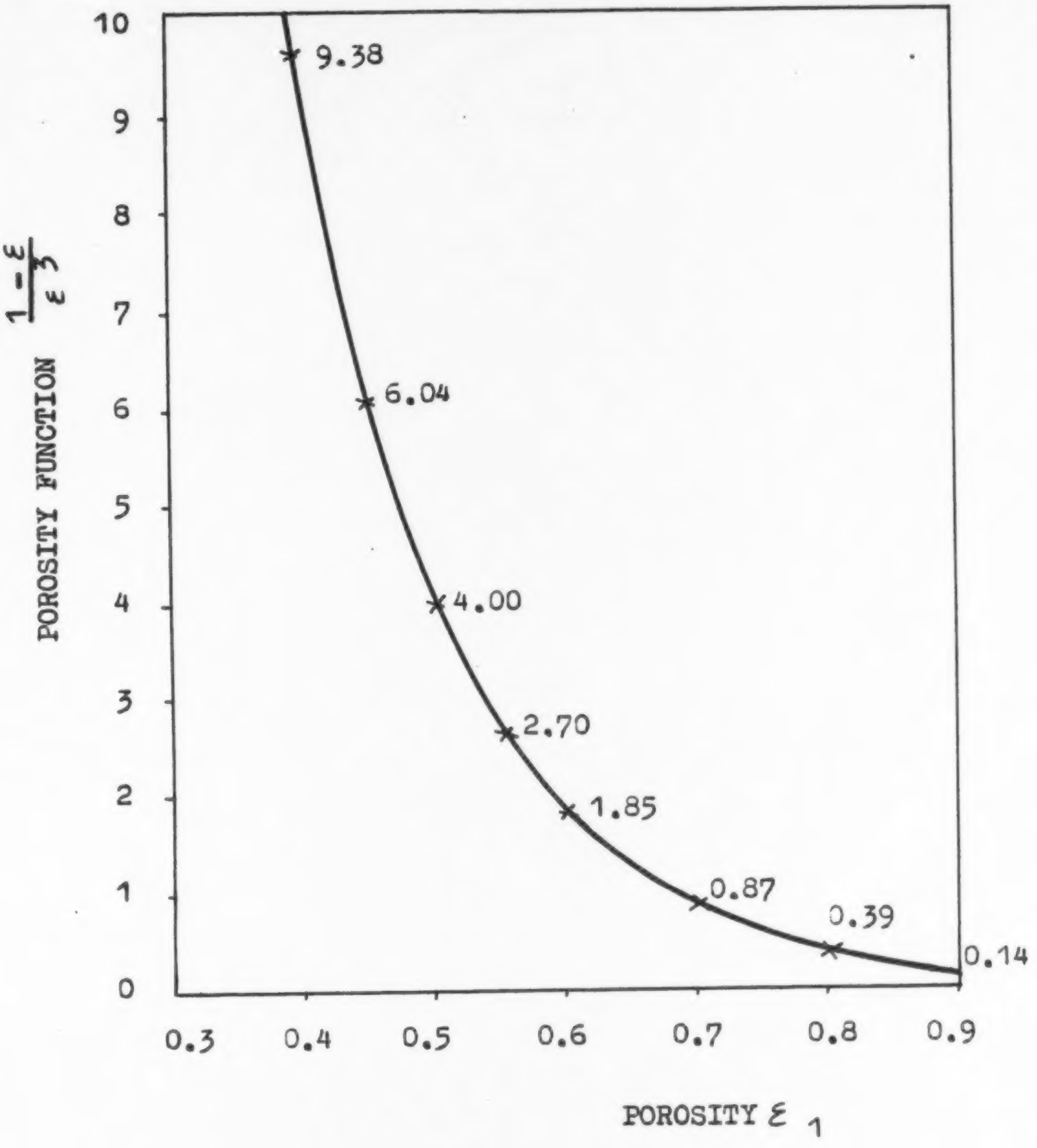

Figure 19. Dependence of porosity function upon absolute porosity.

Dust Collection Efficiency Problems In Dust Filtration Process Type III

Like Dust Filtration Process Type I, the dust collection efficiency of Dust Filtration Type III was determined by the weighing method based primarily on dust balance over a specific filtration time. Thus, the interpretation of these results is identical with the interpretation of the previous section.

The initial efficiency of Dust Filtration Process Type III is higher than the initial efficiency of Dust Filtration Process Type I because of the higher efficiency of the filtration material structure and its residual dust load. In that situation, Equation 14 can be applied to determine filtration time corresponding to the mean value of the dust collection efficiency.

Based on previous and current research, a three-dimensional model of the dust collection efficiency of Dust Filtration Process Type III was developed. This model shows the dependence of efficiency on q_g and L_o. The model further develops the exponential dependence explained by Valentine and described by the following:

$$E_{III} = 100 \left[F_3 \; F_1 \right]^{-L_p^{F_4}} \quad , \qquad (39)$$

where

E_{III} = dust collection efficiency of Dust Filtration Process Type III, %;
F_3 and F_4 = functions depending on internal process parameters;
L_p = dust cake parameter, g/m^2;
F_1 = $100/E_I^o$; and
E_I^o = Initial dust collection efficiency, Dust Filtration Process Type I, for corresponding filtration parameter.

Initial process efficiency, corresponding to a specific steady state residual dust load, L_{NK} (depending on the properties of the filtration material and process parameters) and filtration time, $t_F = 0$, is described by the following formula:

$$E_{III}^o = 1/F_1 \cdot F_3 \cdot 100 \quad . \qquad (40)$$

Generally, functions F_1 and F_3 heavily depend on q_g and the structural parameters of the filtration material. Moreover, F_3 depends on L_{NK}. The above statements can be presented mathematically as follows:

$$F_1 = f\,(q_g,\ \mathrm{SPFM})\quad,\ \text{and}$$
$$F_3 = f\,(q_g,\ L_{NK},\ \mathrm{SPFM})\quad. \tag{41}$$

The value of function F_4 (Equation 39) depends mainly on q_g and the parameters characterizing the dust cake structure.

Similar to the discussion of dust collection efficiency of Dust Filtration Process Type I, the three-dimensional model can be shown as an equation of dust collection efficiency in filtration time, assuming $c_2 = 0$:

$$E_{III} = 100 \left[F_3 \cdot F_1 \right]^{-(q_p \cdot t_F)^{F_4}} \quad. \tag{42}$$

Equation 42 has the following analytical form:

$$E_{III} = 100 \cdot A_{III}^{-(B_{III} \cdot t_F)^{C_{III}}} \quad, \tag{43}$$

where

A_{III}, B_{III}, C_{III} = experimental constants, and

t_F = filtration time.

The following equation offers one hypothetical assumption for the three-dimensional probabilistic model of dust collection efficiency of Dust Filtration Process Type III:

$$L_o = L_{NK} + L_p \quad, \tag{44}$$

where

L_o = total areal density of dust on or in the fabric, g/m^2;

L_{NK} = equilibrium areal mass density of residual dust, g/m^2; and

L_p = areal mass density of the dust cake, g/m^2.

According to R. Dennis,[20] who conducted experiments on glass fabrics and fly ash, aside from the dust that fills the fabric, some additional dust remains on the fabric after each regeneration. This amount of dust was not considered. Thus, a corrected version of Equation 44 is:

$$L_p = L_o - L_{NK} - f_L \cdot L_p \quad , \tag{45}$$

where

f_L = fraction by weight of dust cake, which is not regenerated.

The amount of dust not regenerated depends on many factors, but mainly on dust and fabric properties. Its percentage by weight can be easily determined experimentally and is a constant for a given geometry of filtration elements and conditions of filtration and regeneration.

The physical model of the dust cake presented previously permits an estimation of filtration mechanisms influencing process efficiency. This estimation was confirmed by conclusions of an analysis of Dust Filtration Process Type III. Dust Filtration Process Types I and III are not equivalent because of the differing state of the filtration media. This nonequivalence is apparent in Figure 20 and Figure 21, which show the theoretical variation of efficiency with filtration time (Figure 20) and areal dust density (Figure 21).

Filtration Resistance Problems: Dust Filtration Process Type III

Filtration resistances in Dust Filtration Process Type III are higher than those observed in Dust Filtration Process Type I because the filtration material is filled with dust when the filtration process begins. Filtration resistances can be described by:

$$\Delta P_F = \Delta P_K - \Delta P_{NK} \quad , \tag{46}$$

where

ΔP_K = final pressure drop (pressure drop across the fabric and dust cake immediately prior to regeneration), mm H_2O; and

ΔP_{NK} = initial pressure drop (pressure drop across the dust-filled fabric immediately after regeneration).

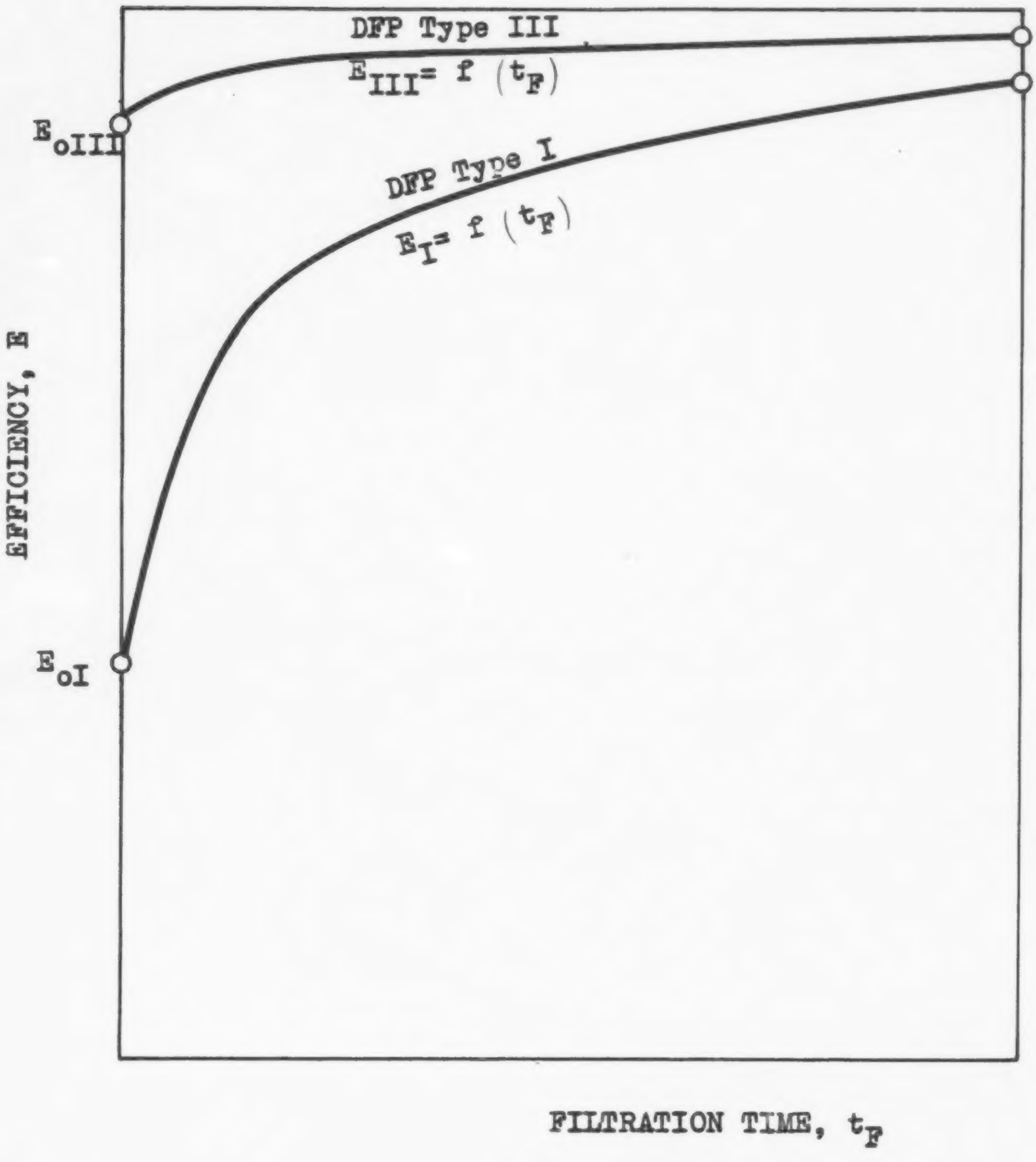

Figure 20. Theoretical variation of efficiency in time.

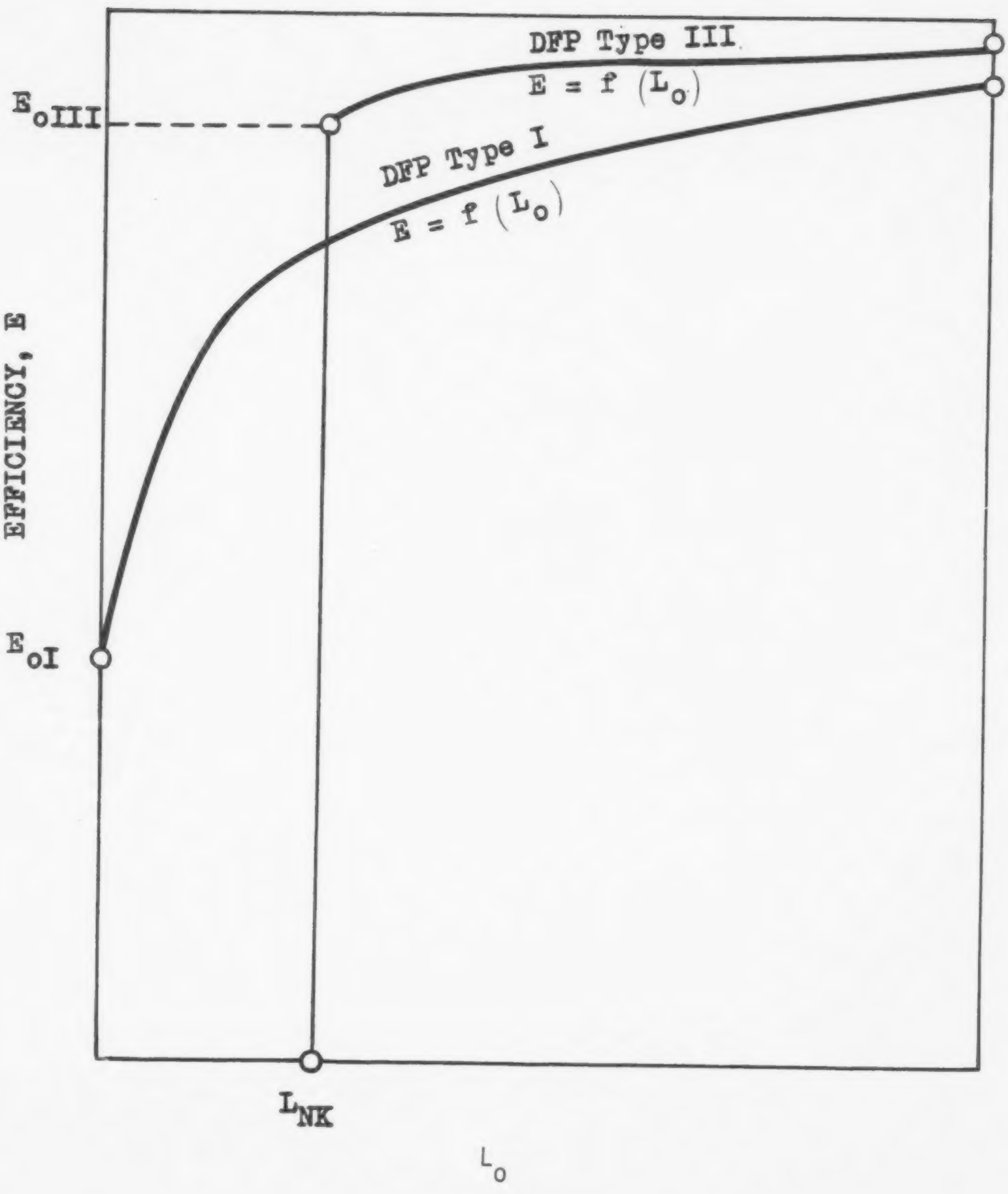

Figure 21. Theoretical variation of efficiency vs. terminal dust load.

However, in most papers[21] [22] that deal with filtration resistance problems, the approximate resistance variation as a function of time is regarded as linear. Based on our experience and theory, the following model of filtration resistance increase in Dust Filtration Process Type III was adapted:

$$\Delta P_F = \begin{cases} -a_3 t_F^2 + b_3 t_F + c_3 & \text{for} \quad t_f \epsilon \left[0,\ t_{FB}\right] , \\ a_3' t_F^2 + b_3' t_F + c_3 & \text{for} \quad t_F \epsilon \left[t_{FB},\ t_{FC}\right] , \end{cases} \tag{47}$$

where

ΔP_F = filtration resistances, mm H_2O;
t_F = filtration time, min;
t_{FB} = time corresponding to inflection point, min;
t_{FC} = time of a given filtration cycle, min; and
$\left.\begin{matrix} a_3, b_3, c_3 \\ a_3', b_3', c_3' \end{matrix}\right\}$ = coefficients characteristic of Dust Filtration Process Type III.

The model shows that during dust filtration, the resistance coefficient, κ_2, for a dust-fabric system is not constant but increases as filtration time increases. This increase demonstrates structural changes of the dust cake, which are mainly connected with changes in the porosity of the system. These changes are examined in detail in the discussion of Dust Filtration Process Type I.

Based on the probabilistic model of filtration resistance variation, the functional dependence of the resistance coefficient, K_2, can be presented as:

$$K_2^{III} = K_2 + 2a_3' \left(t_{FC} - t_{FB}\right) , \tag{48}$$

where

K_2^{III} = the resistance coefficient of the dust-fabric system for the second phase of Dust Filtration Process Type III;
K_2 = the resistance coefficient of the dust-fabric system for the second phase, assuming a linear increase of resistance in time;
t_{FB} = filtration time necessary for reaching the inflection point B;
t_{FC} = time at end of filtration cycle; and
a_3' = empirical coefficient.

So, the final resistance of the dust-fabric system, for a specific t_F, can be expressed by :

$$\Delta P_K = \Delta P_{NK} + K_2^{III} \cdot t_F \quad . \tag{49}$$

The designations are the same as the designations in previous relationships (Equation 36 and Equation 48).

Because many factors influence the coefficients in Equation 47, a physical explanation of these coefficients is difficult. Figure 22 and Figure 23 show the theoretical variation of filtration resistance with time and areal dust density, respectively. It should be emphasized, that from a mathematical viewpoint, a nonlinear model of filtration resistance is more general than a linear model.

Some Peculiarities of the Dust Filtration Process Type I

Dust Filtration Process Type I occurs in most laboratory experiments according to the previously presented three-dimensional probabilistic models of dust collection efficiency and filtration resistance. However, under certain test conditions and with certain test filtration materials (continuous filament fabrics), the empirical data differ from the predicted theoretical behavior.

More detailed examination of this phenomenon resulted in the discovery of defects in the dust cake formed during filtration. The defects occur in the form of "ducts-canals" randomly covering the dust cake area (Figure 24). "Ducts-canals" are spherical and characteristically have a crater form (Figure 25), which proves their rapid formation. In most cases the "ducts-canals" are observed in places of low fiber density, so their formation is accompanied by a rapid decrease in dust collection efficiency and filtration resistance. "Ducts-canals" formation was first observed in 1969 during research of the hydraulic properties of the dust cake.

Based on many experiments conducted to explain the origin and conditions of formation of dust cake defects, two types of defects were delineated:

- Defects formed in the static dust cake during clean air flow, and
- Defects formed in the dust cake built during continuous dust filtration.

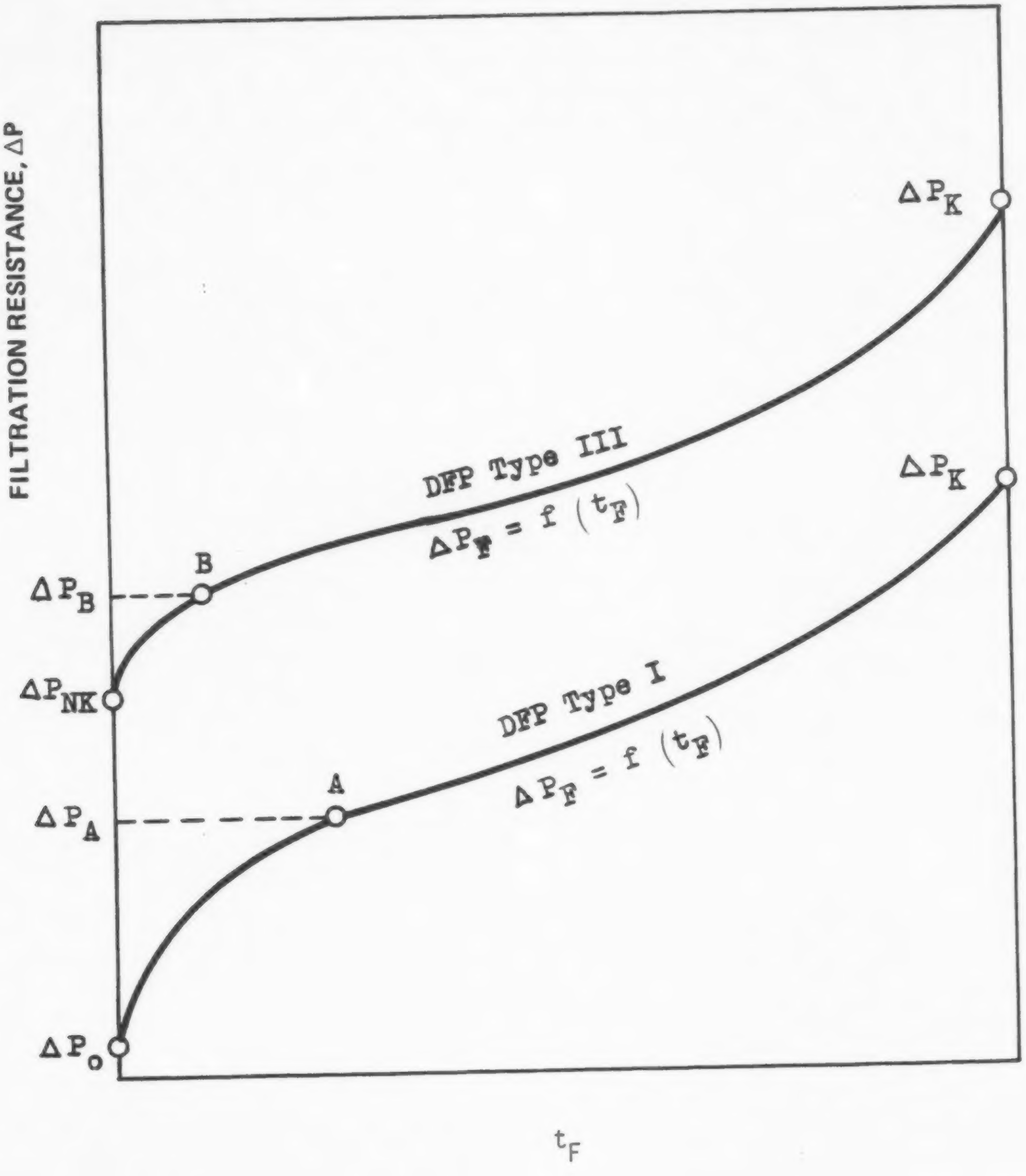

Figure 22. Theoretical variation of filtration resistance in time.

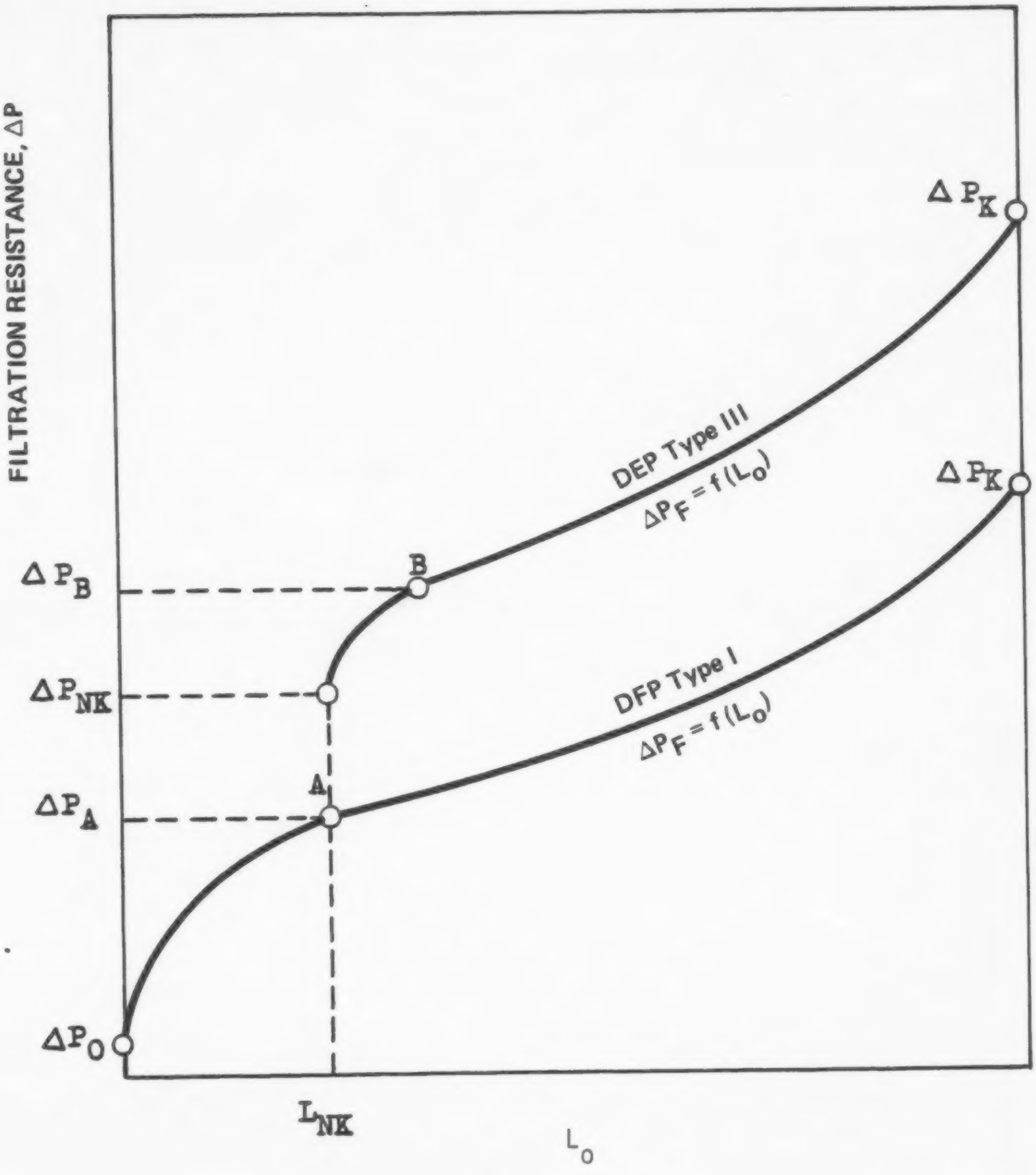

Figure 23. Theoretical variation of filtration resistance vs. terminal dust load.

Reproduced from
best available copy.

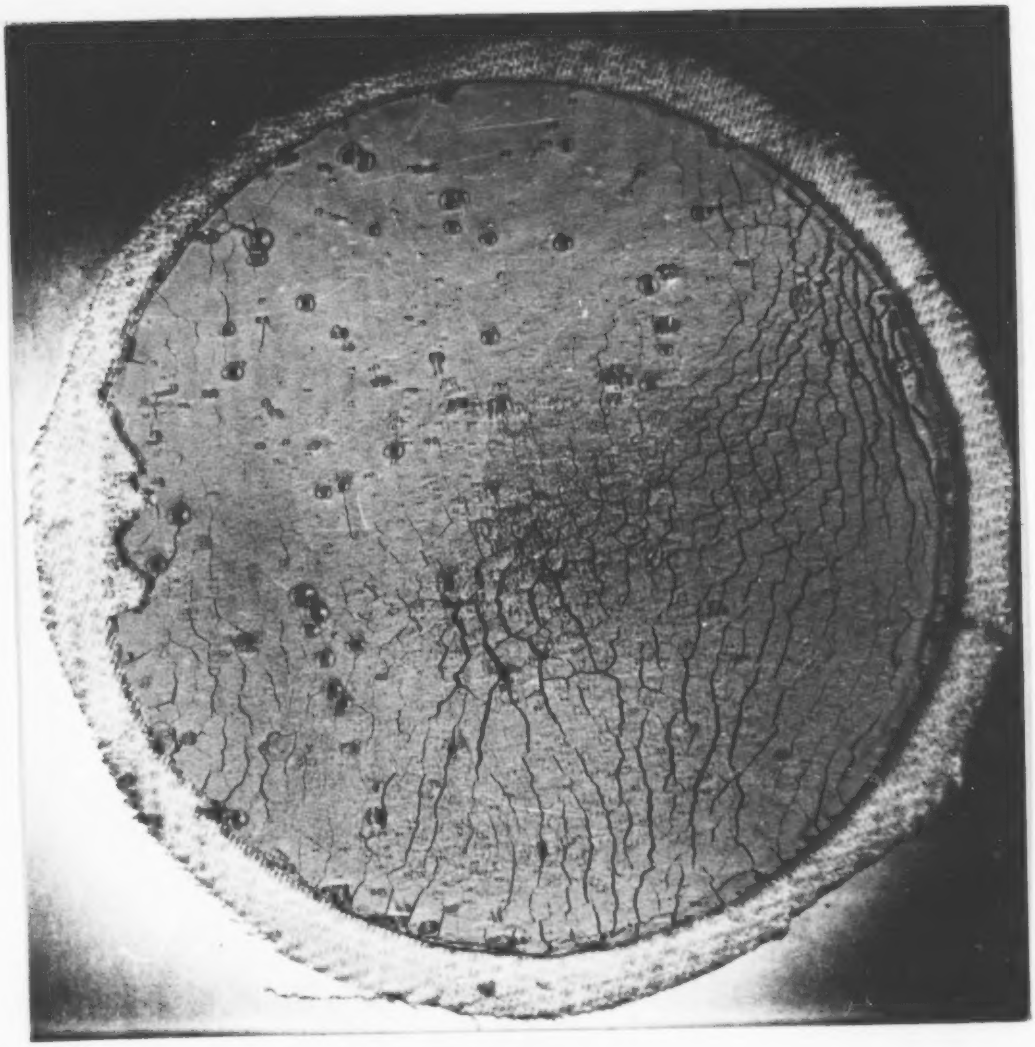

Figure 24. Surface of dust cake on fabric ET-4.

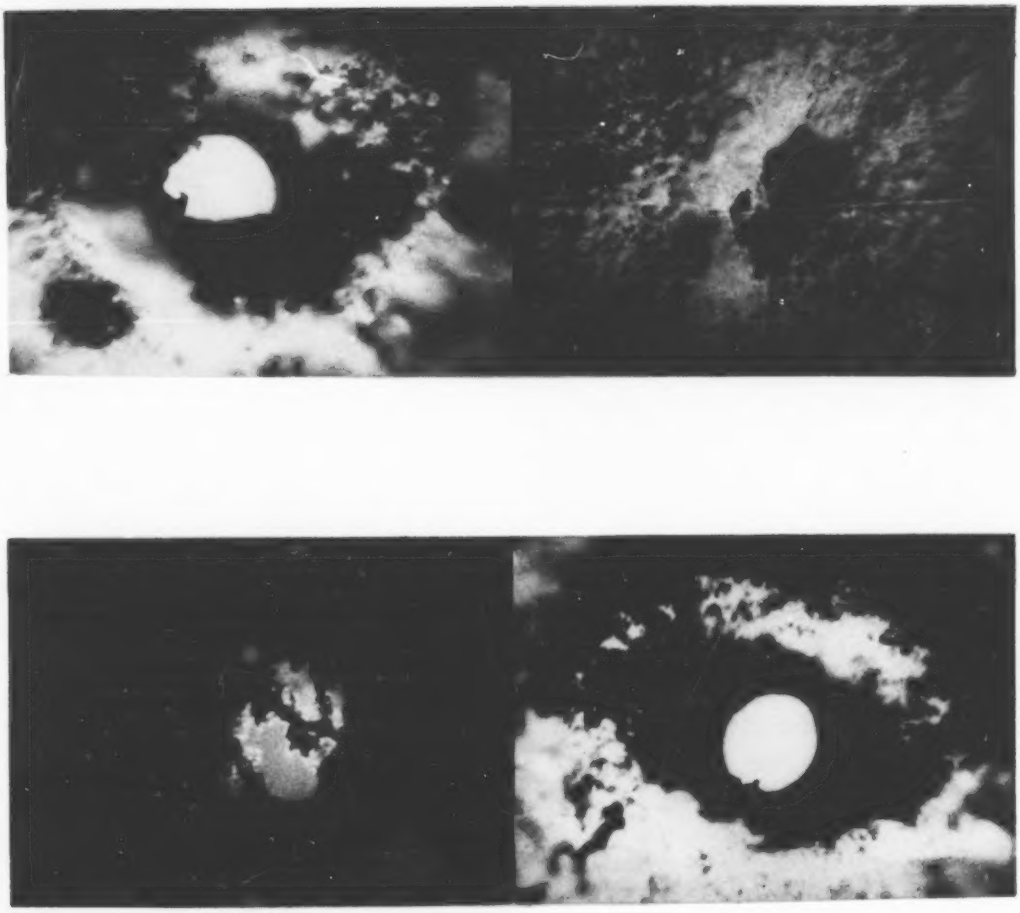

Figure 25. Characteristic crater form of ducts/canals.

Defects of the static dust cake are observed during subsequent clean air flow in excess of the face velocity maintained during its dust cake formation. Over the range of 0 - q_{gA} (q_{gA} is the face velocity at which the static dust cake was formed) increasing face velocity produces a parabolic increase in pressure drop. After value q_{gA} is exceeded, the increased resistance during clean air flow through static dust cake first has parabolic character and then a nonproportionate decrease comparable to values of the face velocity. Flow resistance variation in the range of $q_g > q_{gA}$ deviates considerably from that predicted by the function, $\Delta P = f\ (q_g)$. These unexpected variations of flow resistance with increasing q_g are accompanied by the formation of dust cake structure defects in the form of "ducts-canals."

If a higher face velocity is used to build the static dust cake, defects in the dust cake occur at a corresponding higher face velocity. This situation is illustrated in Figure 26.

Research on the hydraulic properties of static dust cake shows that the structure of a static dust cake--and thus its mechanical properties--depends mainly on the face velocity at which the dust cake is built (q_{gA}). The conclusion is reached that the mechanical properties of the dust cake are determined by the conditions of its spatial, structural formation.

It is interesting that the static dust cake defects of a particular filtration material and dust appear at similar values of pressure drop independently of the face velocity employed during dust cake formation. A definite limit in value of static pressure gradient seems to exist above which local disturbances appear between the elements of the dust cake structure. The limiting value of the static pressure gradient is presumed to depend on the physical properties of the dust and the filtration material.

The curves in Figure 26 lead to an interesting conclusion; i.e., that decreasing sections representing definite pressure drop differences, B_1B_1', B_2B_2', prove the existence of a value of face velocity for dust cake formation (q_{gA}), at which dust cake cannot be formed without structural defects. So, for a specific dust the varying values of q_gA reflect the influence of the filtration material structure.

During regeneration structural defects can also occur in the pseudo-static dust cake of the chambers not being cleaned (but subjected to an increased

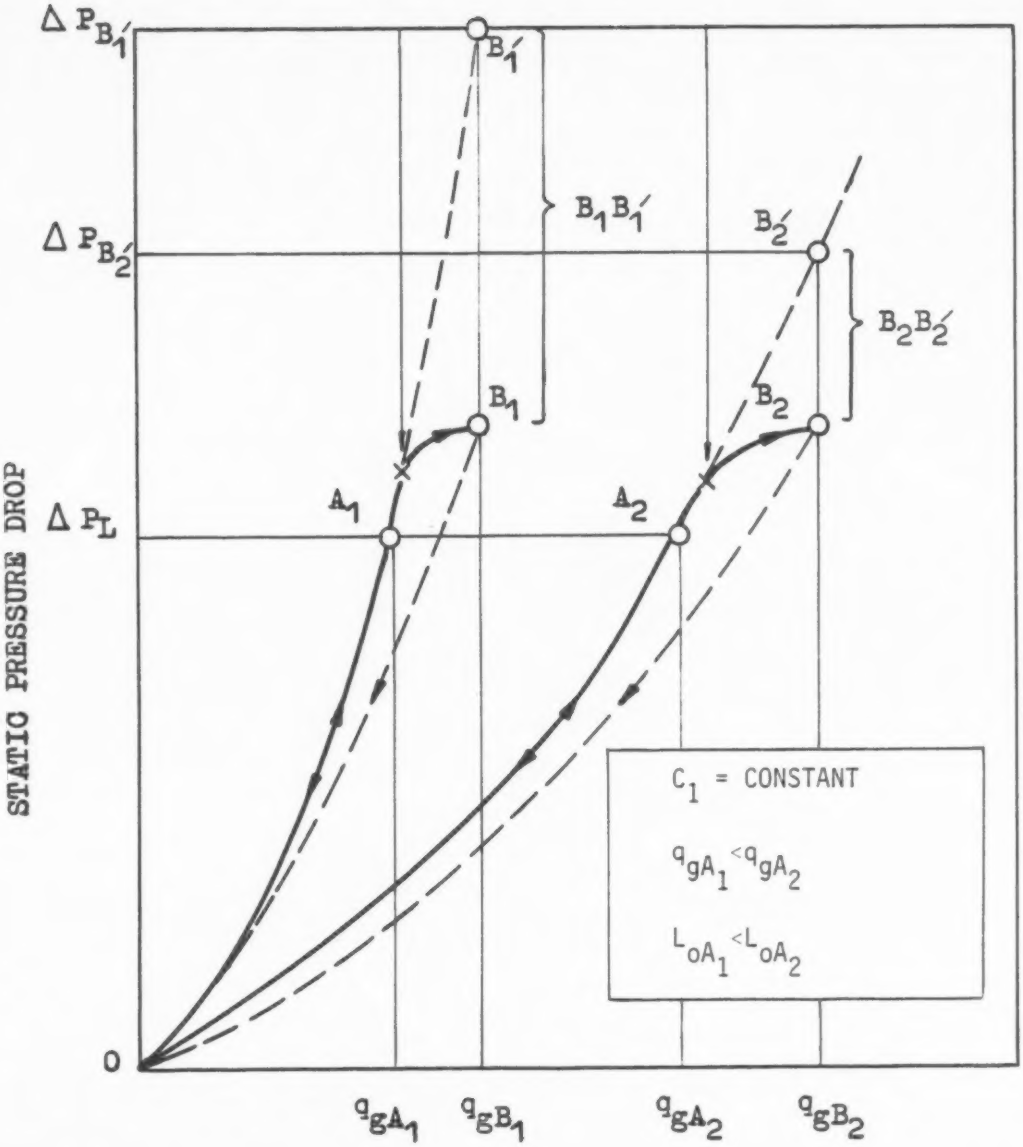

Figure 26. Process of dust cake structure defects formation in static dust cake.

q_g). Dust cake defects formed during continuous filtration probably have physical mechanisms of formation similar to those of the static dust cake defects. The difference is that they occur in the dynamic process.

In the previous case, the well-formed dust cake structure was subjected to forces resulting from an increased gradient of static pressure because of an increased q_g. Now, defects appear at a constant value of q_g and an increased gradient of pressure because of deposition of dust on the filtration material structure.

Also in this case, the limit gradient of pressure, ΔP_{LIM}, at which the structural defects appear, can be observed. The above phenomenon, observed during testing of glass fabrics, can be explained only by the existence of spaces in the filtration material structure that remain unfilled with fiber. The mechanical strength of the dust cake in these spaces is much lower than its mean mechanical strength.[23] A more detailed examination of this phenomenon confirmed this hypothesis and stimulated discovery of new free areas called "basket elements." These elements are situated at the interlace of the warp and fill yarns and are askew to the fabric plane. They are distinct from the "free areas" (FAs) also situated between the warp and fill yarns but in the plane of the fabric.

The basket elements caused the rapid decrease in dust collection efficiency of tested materials, so their influence was termed a "basket effect," which differs from the FA effect. The FA effect on dust collection efficiency was examined by Draemel.[24]

Basket elements are characterized by a comparatively large effective dimension of approximately 85 μm, at a standard deviation of 60 μm. For q_g = 60 m^3/m^2h and 200 m^3/m^2h, the number of canals formed because the basket effect was 10 and 26,000/m^2, respectively. Examination of the effective dimension distribution proved the distribution was normal.

Dennis obtained similar results[20] during laboratory testing of glass fabrics with fly ash, confirming the existence of the "basket effect." The "basket effect" is characteristic of continuous filament fabrics and depends on the kind of weave and yarn diameter (and also fiber diameter).

Figures 27 and 28 compare the basket effect with FA for a model fabric made of cord (Figure 27) and an actual fabric filter (Figure 28). The limitations caused by the basket effect can be minimized by mixing staple yarns with

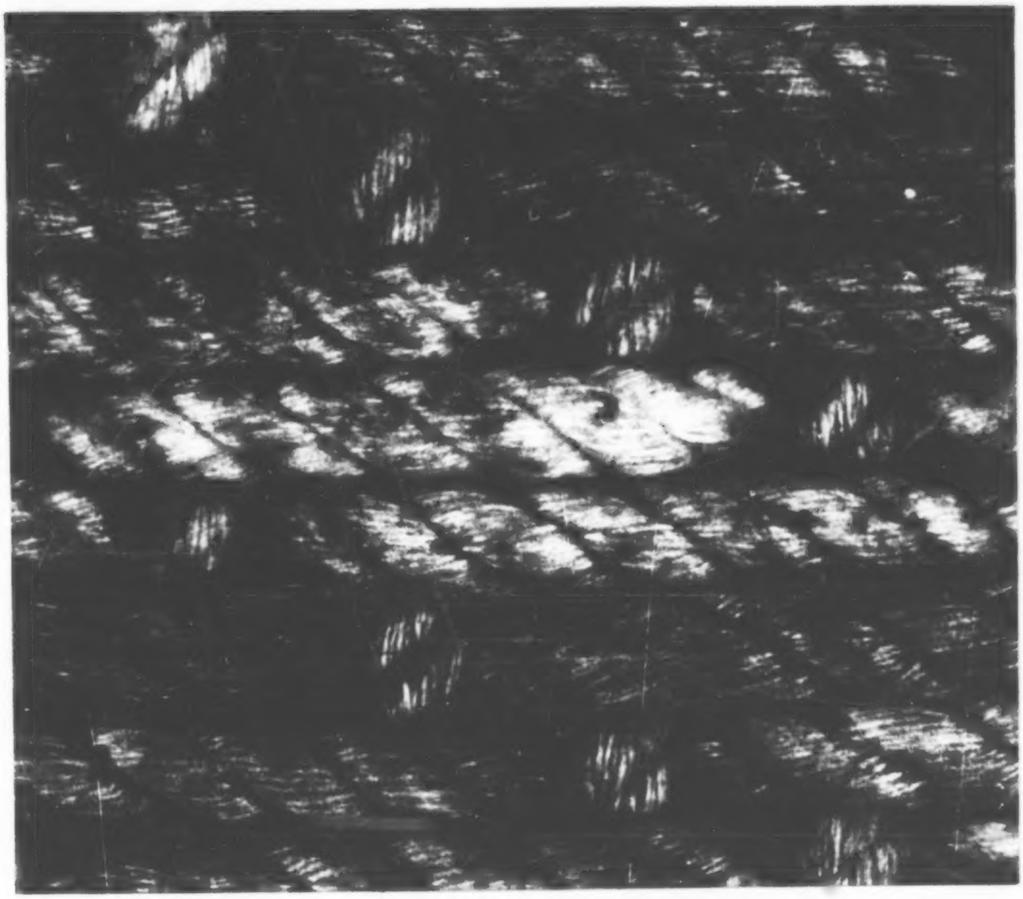

Figure 27a. Superficial structure of model fabric (vertical view).

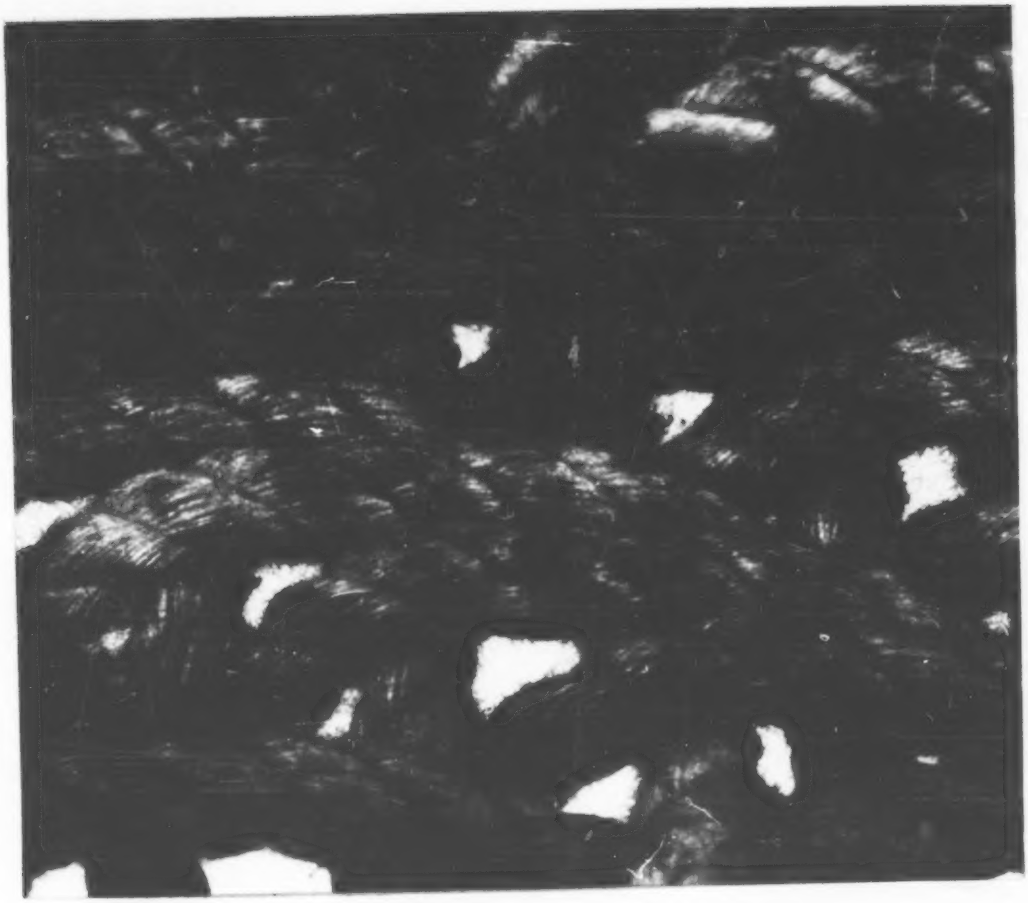

Figure 27b. Superficial structure of model fabric (askew view).

Photo credit: SEM by K. Skudlarski, Electronic Microscopy Laboratory of Wrocław Polytechnic.

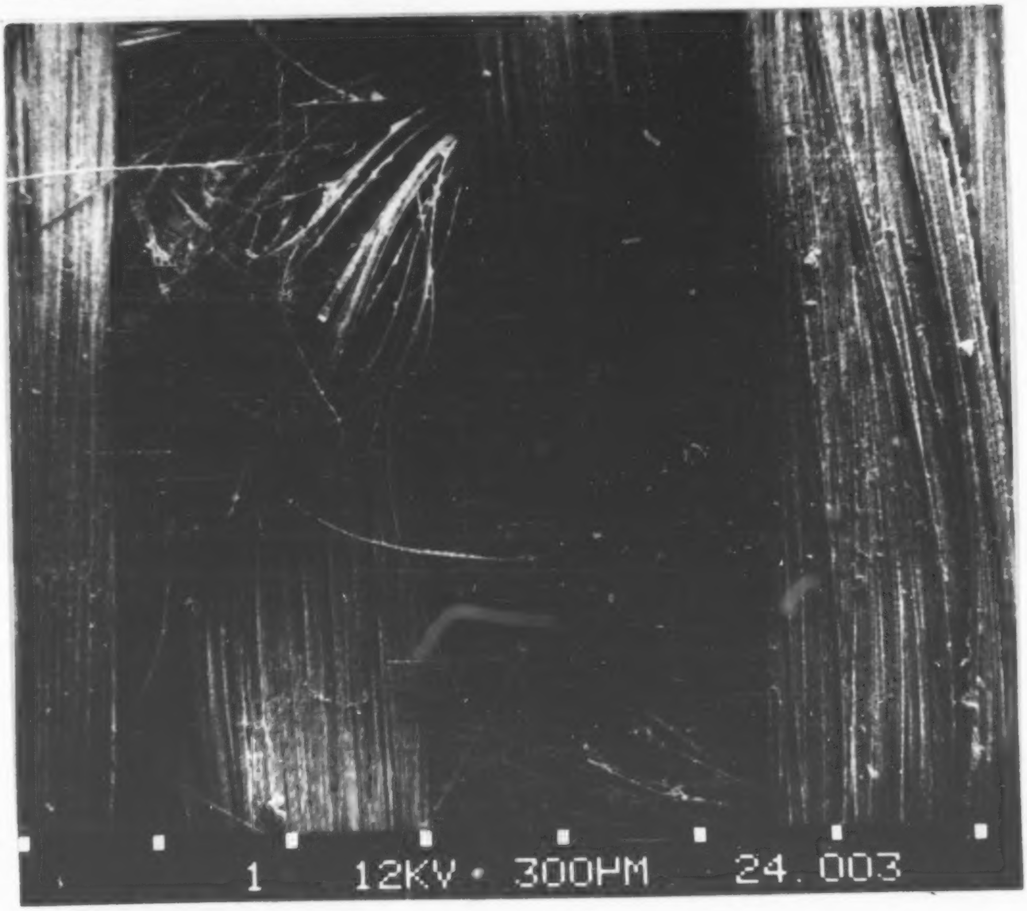

Figure 28a. Basket areas and free areas in glass fabric type Q-54-878 (interyarn free area).

Photo credit: SEM by K. Skudlarski, Electronic Microscopy Laboratory of Wrocław Polytechnic.

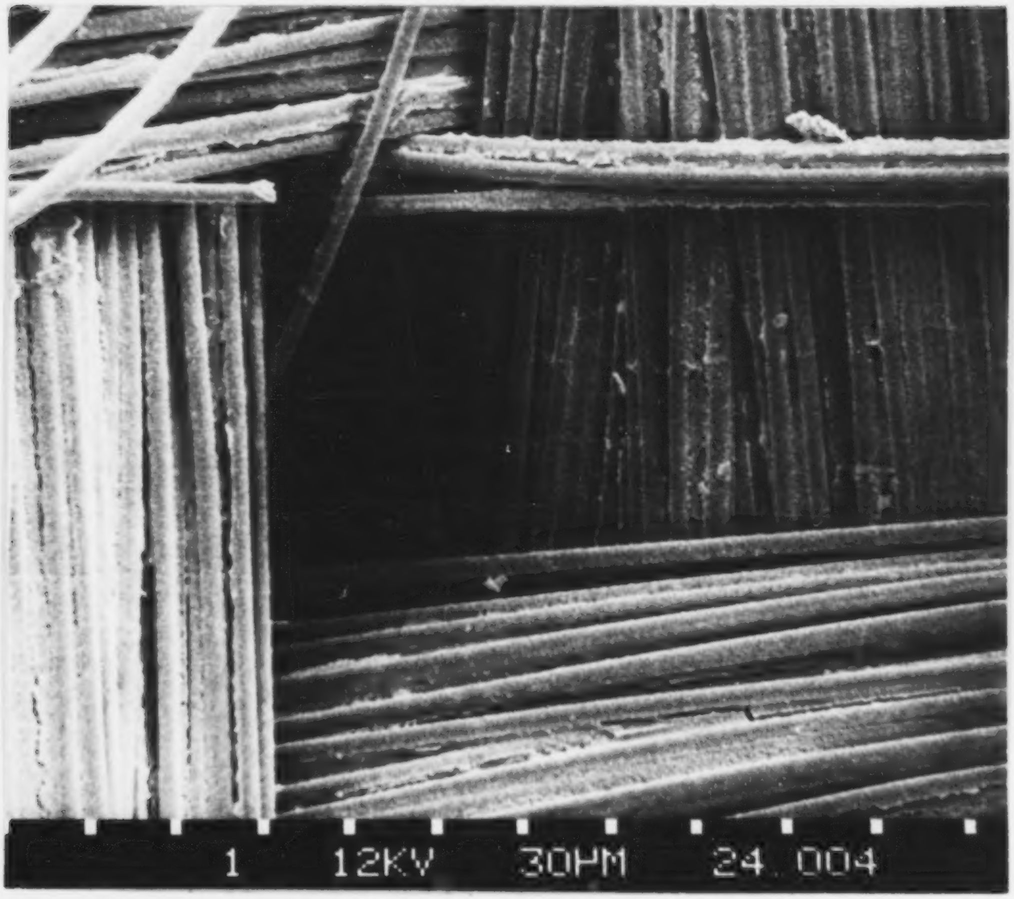

Figure 28b. Basket areas and free areas in glass fabric type Q-54-878 (enlargement interyarn free area).

Photo credit: SEM by K. Skudlarski, Electronic Microscopy Laboratory of Wrocław Polytechnic.

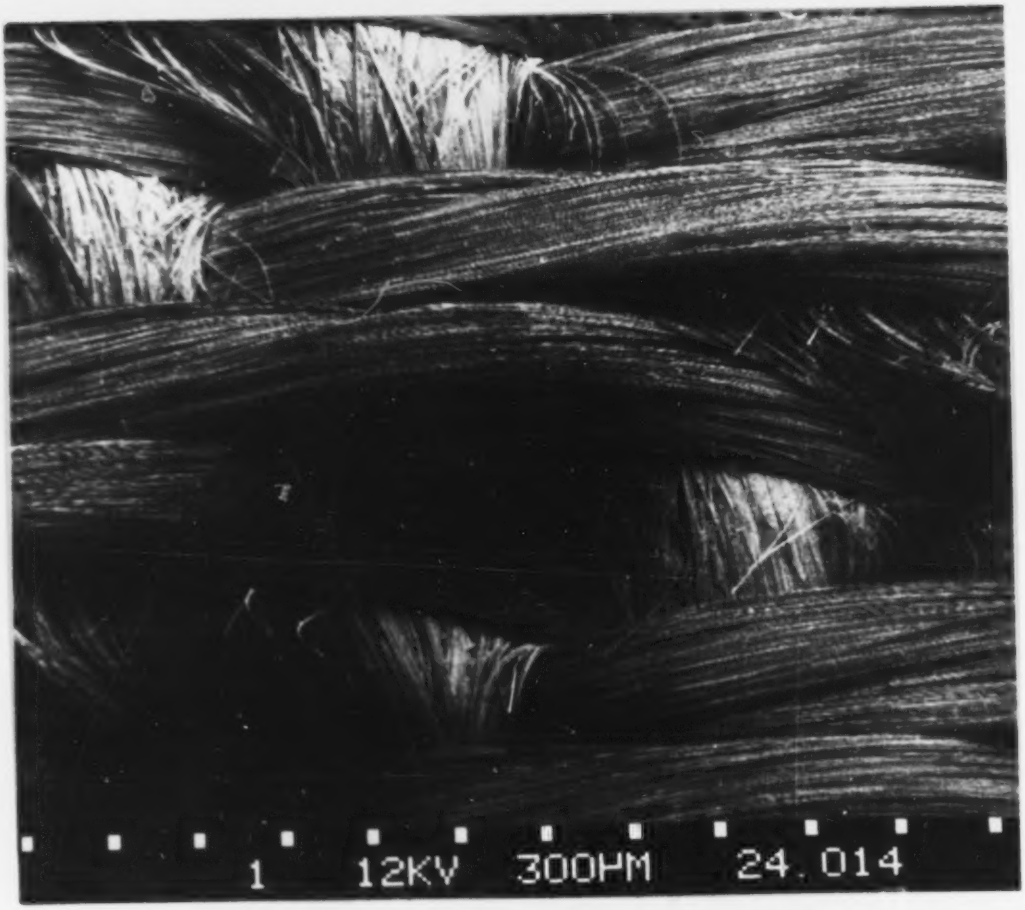

Figure 28c. Basket areas and free areas in glass fabric type Q-54-878 (new "basket free area").

Photo credit: SEM by K. Skudlarski, Electronic Microscopy Laboratory of Wrocław Polytechnic.

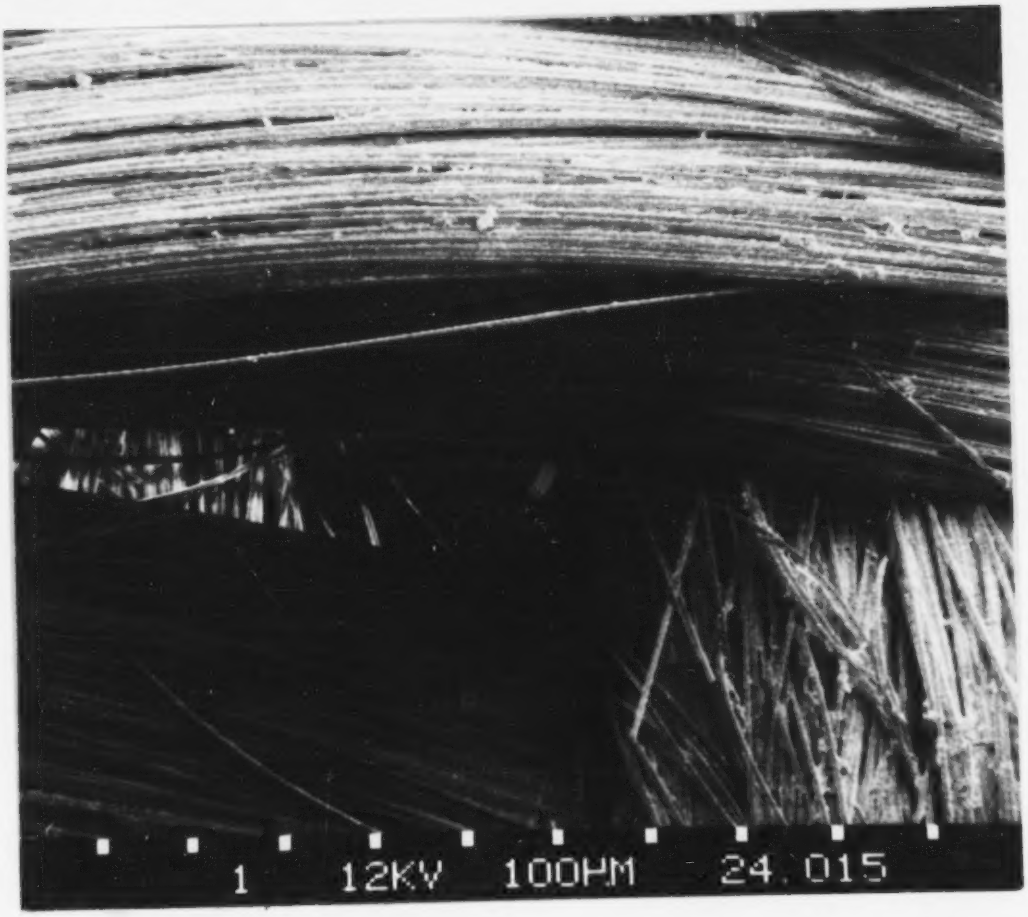

Figure 28d. Basket areas and free areas in glass fabric type Q-54-878 (enlargement of new "basket free area").

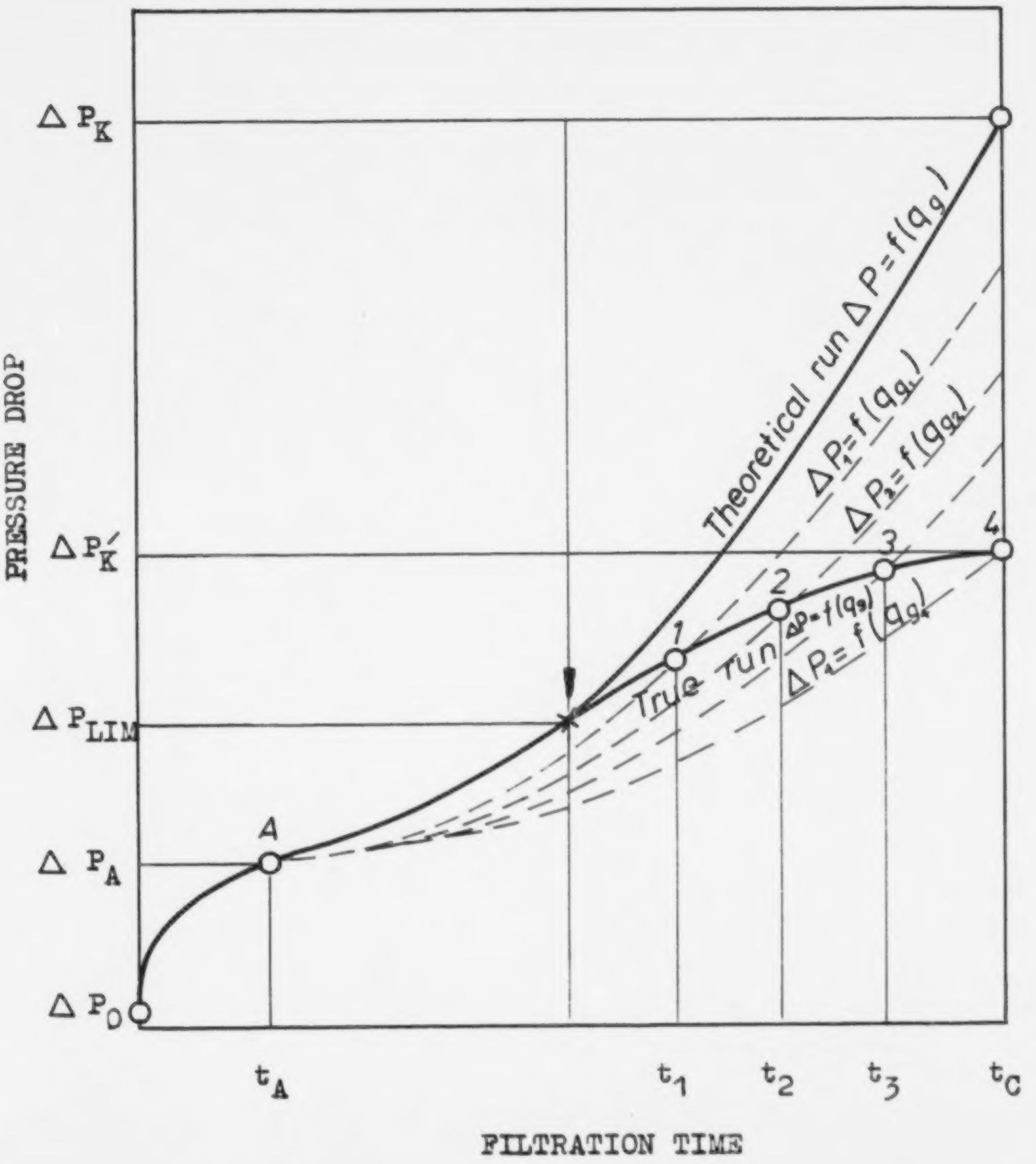

Figure 29. Deformation of filtration resistance characteristics due to dust cake defects.

filament yarns in the thread systems (warp and fill), forming a mixed fabric structure.

The formation of dust cake defects during filtration results in decreased dust collection efficiency and in deviation of the hydraulic characteristics from the theoretical prediction. Figure 29 shows filtration resistance variation in time, including the effect of defects of the dust cake structure. The observed differences between the actual and theoretical behavior of filtration resistances are caused by a decreased mean value of q_g.

However, the number of canals depends on q_g and is constant for a given value of q_g. Increasing resistance differences, resulting from increasing dust cake thickness, cause stronger and stronger flow through the canals. Thus, for definite time periods, t_1, t_2 ..., etc., the process occurs according to:

$$\left.\begin{aligned} \Delta P_1 &= f(q_{g^1}) \text{ for } t_1 \\ \Delta P_2 &= f(q_{g^2}) \text{ for } t_2 \\ &\ldots\ldots\ldots\ldots \\ \Delta P_n &= f(q_{gn}) \text{ for } t_n \end{aligned}\right\}$$

where

$$t_1 < t_2 < \ldots < t_n$$

$$q_{g^1} < q_{g^2} < \ldots < q_{gn} \quad .$$

At the end of the filtration cycle a final resistance, $\Delta P_K' < P_K$, is obtained, where ΔP_K is the theoretical final filtration resistance.

The above variations in the time dependence of filtration resistance are characteristic of filtration processes through continuous filament fabrics in the presence of defects in the dust cake structure. Staple fiber fabrics, characterized by a high fiber filling of the spatial and superficial structure, also show dust cake defects at high q_g. The basket effect is not clearly observed here, however, and the "canals-ducts" formation is caused rather by low mechanical strength of the dust cake in the interthread space, where the influence of FA can be observed.

SECTION V

EFFECT OF FILTRATION PARAMETERS ON DUST FILTRATION PROCESS TYPE I

INTRODUCTION

Dust Filtration Process Type I is characteristic of laboratory-scale experiments in which small area, flat filtration specimens are subjected to a single dust cycle (no regeneration). This process is crucial to developing basic research of dry filtration because it enables researchers to obtain information quickly about dust collection efficiency and filtration resistances for an arbitrary range of filtration parameters and filtration material. Although the process is not equivalent to the process performed by industrial dust collection devices, it is possible to extrapolate from laboratory experiments to industrial-scale experiments if definite interpretive methods are applied. Moreover, it should be emphasized that in laboratory-scale experiments it is possible to control operating conditions, which is not always true for large- or industrial-scale experiments.

Laboratory examinations conducted for this project were not typical tests in which the process parameter levels were predetermined and fixed but rather were exploratory of the dust filtration process. The levels of examined parameters depended on an interpretation of requirements and procurement of statistically correct results.

Among the five main filtration parameters discussed in Section IV, two basic parameters were considered: face velocity, q_g, and the terminal dust load, L_o. The other filtration parameters--dust flux, q_p, and filtration time, t_F--are related to previous parameters according to the following relationships (assuming that final dust concentration, c_2, = 0):

$$q_p = q_g \cdot c_1 \text{ , and} \qquad q_g = q_p/c_1 \; . \tag{50}$$

$$L_o = q_g \cdot c_1 \cdot t_F \; . \tag{51}$$

Equations 50 and 51 show the relationship between the independent filtration parameters and the dependent process parameters. The steady state residual dust load, L_{NK}, is a key parameter correlated to characteristic properties of the superficial and spatial structure of the filtration materials. Although the effect of L_{NK} on the external process parameters was not considered initially, it was later determined to be important. The problem of the fabric loading up with dust is addressed in the section that discussed the test problems associated with the structural parameters of the filtration material.

EQUIPMENT AND PROCEDURES

Laboratory testing of selected filtration fabrics was conducted on a stand (illustrated in Figure 30) specially designed by the Instytut Przemysłu Wiążących Materiałów Budowlanych (IPWMB) and adapted for the testing of flat fabric specimens under ambient air conditions. This stand includes the following (see Figure 31):

- Testing chamber,
- Rotameter for measuring flow intensity,
- Needle valve for controlling flow intensity,
- Vibrato-injecting dust feeder,
- Micromanometer for measuring pressure drop, and
- Vacuum pump.

The testing chamber, which is the main part of the stand, is equipped with:

- Diffuser at the inlet,
- Fabric specimen table, and
- Control filter table at the outlet end.

A round fabric specimen of 100 cm^2 test area was positioned in the middle of the table, supported by wire net screening (4 cm along one side).

In testing, dusty air flows through the fabric from the top downward, with the inlet diffuser providing a uniform flow throughout the entire test area of the fabric. After passing through the fabric specimen, the air circulates through a control filter of soft batting and paper (a disc with a 200-cm^2 test area). The control filter is positioned on the table at the outlet end, supported by wire and screening (1 cm along one side).

Average dust collection efficiency was determined by weighing the fabric specimen and the control filter and applying the following equation:

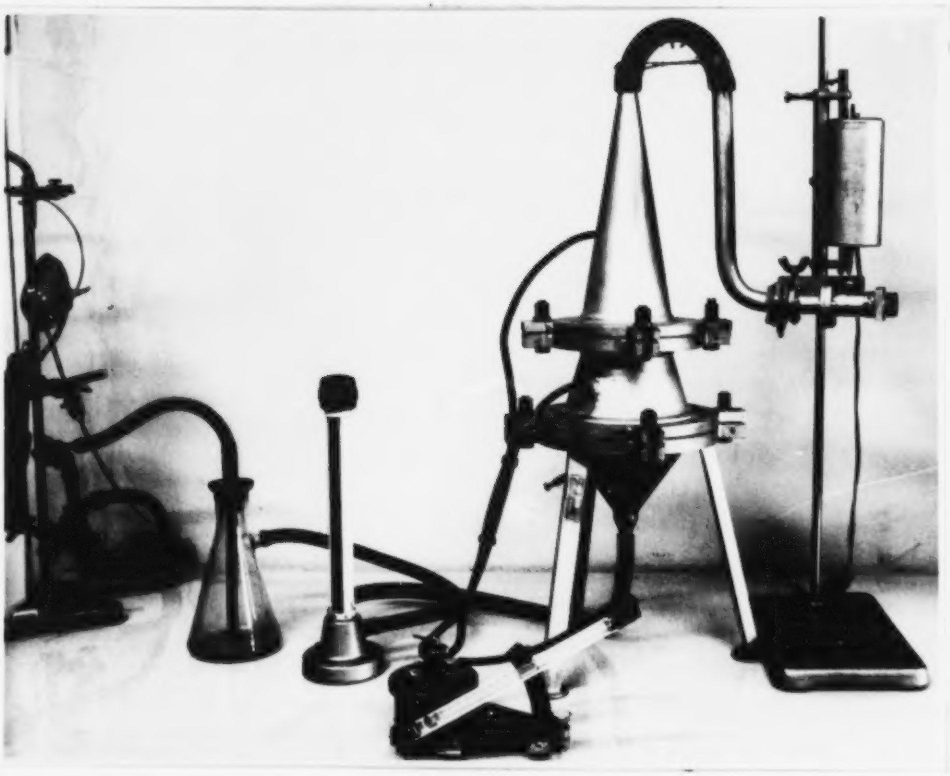

Figure 30. Illustration of laboratory stand.

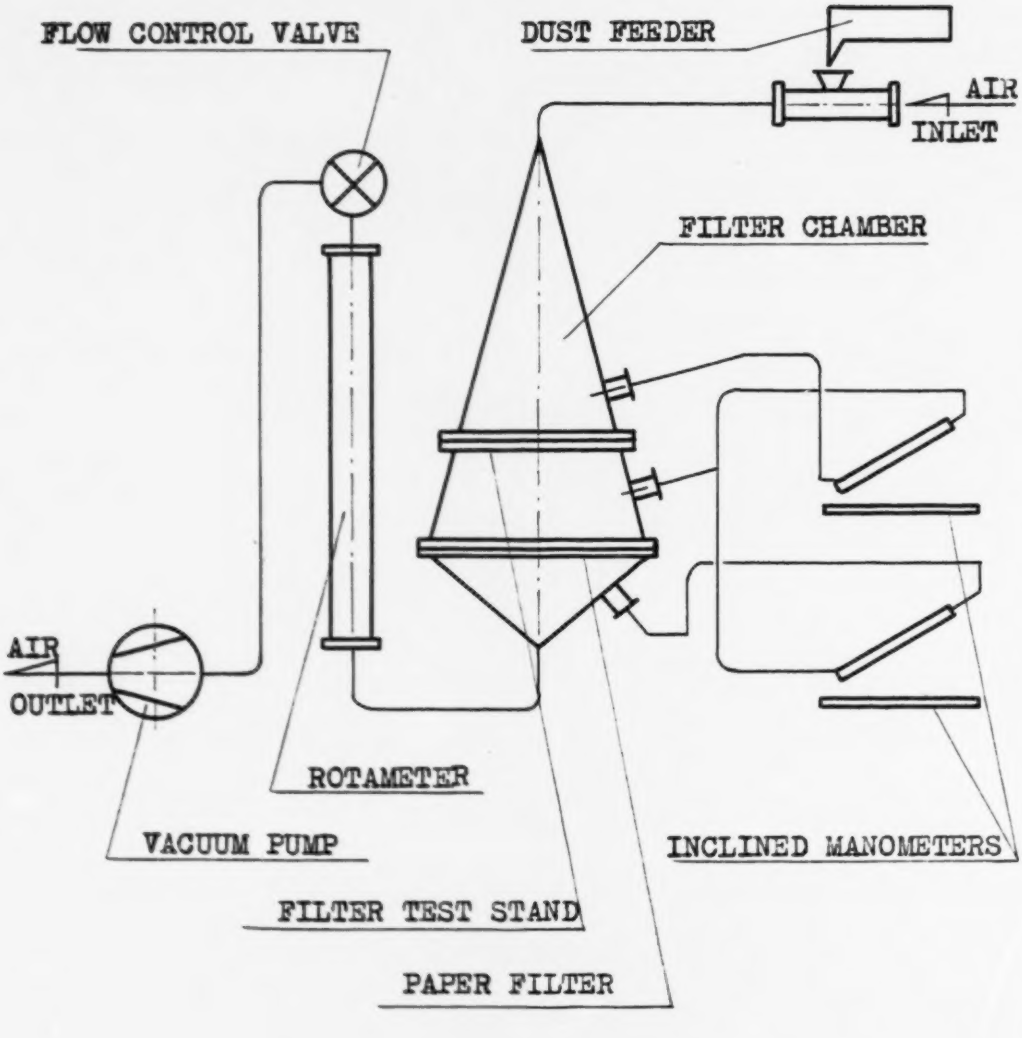
FLOW CONTROL VALVE
DUST FEEDER
AIR
INLET
FILTER CHAMBER
AIR
OUTLET
ROTAMETER
VACUUM PUMP
INCLINED MANOMETERS
FILTER TEST STAND
PAPER FILTER

Figure 31. Diagram of the laboratory test stand.

$$E = \frac{G_z}{G_c} = \frac{G_c - G_o}{G_c} = \frac{G_z}{G_z + G_o} \cdot 100 \quad , \qquad (52)$$

where

E = dust collection efficiency in percent,

G_z = weight in grams of dust collected on the fabric,

G_o = weight in grams of dust collected on the control filter, and

G_c = weight in grams of dust fed into the testing chamber.

During testing the temperature and humidity of the ambient air were recorded. The fabric samples and control filters were conditioned in ambient air over a period of 72 hours. Under these conditions the following data can be obtained:

- Mean filtration efficiency,
- Hydraulic characteristics of filtration materials during clean air flow,
- Hydraulic resistance variation during dusty air flow, and
- Degree of dust filling of filtration materials.

Though specially designed for the laboratory testing of woven filtration fabrics, this stand can also be used for laboratory testing of other filtration materials (e.g., felt). Five randomly chosen filtration material samples were independently tested to obtain the most reliable experimental data at constant q_g and L_o. From these data, a mean dust collection efficiency and a mean value of filtration resistance were calculated. Thus, mistakes resulting from the heterogeneous structure of the filtration material were eliminated.

The value of q_g was constant during the experiment because the system regulated the gas flow through the apparatus. Because the vibrating dust feeder tends to have an irregular dust feeding rate, the dust concentration entering the test chamber varied slightly. However, the deviations fell within 10 percent of the assumed dust concentration. These fluctuations in dust concentration caused deviations between the assumed and the actual values of the terminal dust load, L_o. These deviations were accounted for during statistical analysis of the data.

Because of irregular temperature and gas humidity during the experiments, some scatter may have been introduced by these parameters. However, such effects are difficult to determine because of the narrow range of variation.

RESULTS

All filtration material test data are included in Appendix B. Tables B-2 through B-9 include test results of fabrics ET-4 and ET-30 obtained in previous experiments conducted with unseparated dusts (cement and coal). These results are interesting because they show the effect of dust pulverization on dust filtration. The earlier experiments were conducted on the same apparatus used in this project. Moreover, both dust samples were taken from the same point of the technological line with the second sample subsequently separated prior to use in the test series of the current project.

Tables B-10 through B-17 include results of testing four kinds of fabrics: ET-4 and ET-30, F-tor 5, and PT-15. These fabrics were tested according to the initial research program with four kinds of separated dusts: cement, coal, talc, and fly ash. This set of results comprises Series I of the experiment. Tables B-18 through B-21 include the results of fabrics ET-4 and ET-30 tested with separated fly ash under conditions determined during the modified, broadened research program. This set of results forms Series II of the experiment.

After these results were analyzed, a recommendation was made to conduct additional testing (under conditions assumed for Series II) at q_g = 140, 160, and 180 m^3/m^2h. The results of these tests are contained in Tables B-22 and B-23, as Series III of the experiment.

DISCUSSION OF RESULTS

The effect of q_g and L_{NK} on the external process parameters, the dust collection efficiency, and the filtration resistances was studied based on a three-dimensional probabilistic model presented in Section IV.

The Effect of Filtration Parameters on Dust Collection Efficiency

Equation 18, a three-dimensional model of dust collection efficiency for Dust Filtration Process Type I, can be reduced to linear form as follows:

$$E = [F_1]^{-L_o^{F_2}} \cdot 100 \quad ,$$

$$\frac{100}{E} = [F_1]^{L_o^{F_2}} \quad ,$$

$$\log \frac{100}{E} = L_o^{F_2} \log F_1 \quad , \text{ and}$$

$$\log \log \frac{100}{E} = F_2 \log L_o + \log \log F_1 \quad . \qquad (53)$$

Equation 53, in the Rosin-Rammler coordinate system ($\log \log \frac{100}{E}$ vs. $\log L_o$), is a straight line with directional coefficient F_2. The intercept of the straight line with the ordinate axis determines the value, F_1, which corresponds to the hypothetical, initial process efficiency, E_o; that is, at $L_o = 1$, $\log L_o = 0$, so:

$$\log \log \frac{100}{E_o} = \log \log F_1 \quad ;$$

thus

$$\frac{100}{E_o} = F_1 \quad . \qquad (54)$$

Substituting Equation 54 into Equation 18 yields:

$$E = \left[\frac{100}{E_o}\right]^{-L^{F_2}} \cdot 100 \quad , \qquad (55)$$

where

$$E_o = \frac{1}{F_1} \cdot 100 \quad . \qquad (56)$$

A geometrical interpretation is contained in Figure 32.

The modified relationship for dust collection efficiency in Dust Filtration Process Type I (Equation 55) shows that, for negative values of the function F_2, the hypothetical initial efficiency, E_o, is the lowest efficiency of the process.

Positive values of function F_2 indicate abnormal process performance; from Equation 55, positive F_2 implies that increased dust cake (increasing values of L_o) is accompanied by a decrease in values of dust collection efficiency. This situation occurs when defects in the dust cake, such as ducts/canals, are observed.

For any specific set of experimental conditions, F_1 and F_2, the coefficients of a straight line in the Rosin-Rammler system, are conjugate functions. They are therefore concluded to depend on the same filtration parameters that

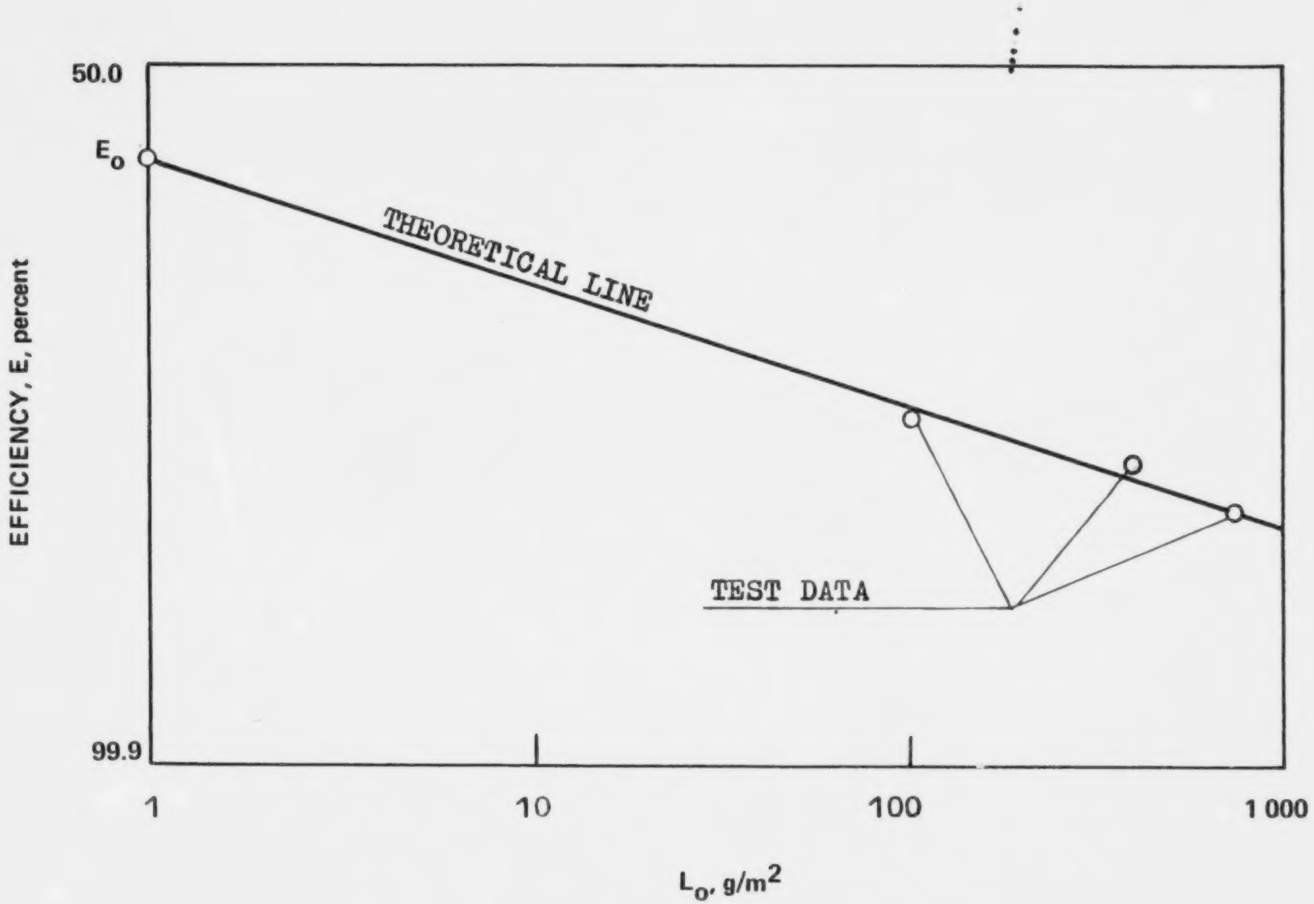

Figure 32. Efficiency as a function of dust covering in Rosin-Rammler coordinate system.

determine process performance. It is noteworthy, however, that although this conclusion is mathematically correct, it is not derived empirically, but from extrapolation of the data in the operating range of the filtration parameters.

Based on the classical filtration theory, the initial dust collection efficiency, E_o, depends mainly on filtration material structure, dust type, dust particle diameter, and gas velocity in front of the filtration structure (Table 2). Thus, this efficiency depends also upon the initial aerosol state parameters and the structural parameters of the filtration medium. But it does not depend on time.

However, if the true dust filtration process described in the theoretical discussion of this report is considered, the true value of initial dust collection efficiency has only a small effect on the mean efficiency of the measurement cycle, so determination of its absolute value has no practical use. Thus, although the method of interpretation is valid for filtration in the dust filtration range (high initial dust concentration), the inverse of F_1 (the initial efficiency, E_o) has no practical meaning.

Equation 53 was used in a statistical analysis of the test results. The results that varied significantly from mean values or deviated from the predicted straight lines in the Rosin-Rammler coordinate system were eliminated. In contrast to calculations presented in the second-phase report, the calculations in this report used the interpretation of mean value of dust collection efficiency presented in Section IV. The first approximation was applied; i.e., the mean value of dust collection efficiency for the measurement cycle was assigned to an abscissa value equivalent to one-half the value of areal dust density built up during the measurement cycle.

The two interpretations of mean cycle efficiency, $E = f(L_o)$, are illustrated in Figure 33 for fabric ET-4, tested with separated fly ash at $q_g = 60\ m^3/m^2h$ according to Series II of the experiments. The regression lines for empirical data were determined according to:

$$\begin{aligned} &y = a + bx \quad , \text{ where} \\ &y = \log \log \frac{100}{E} \text{ , and} \qquad\qquad (57) \\ &x = \log \frac{L_o}{2} = \log \bar{L}_o \text{ at } q_g = \text{constant} \quad . \end{aligned}$$

The coefficients, a and b, for regression lines were determined according to:

TABLE 2. INITIAL STATISTICAL EFFICIENCY, E_o, AS A FUNCTION OF q_g

(Series I and Previous Experiments)

Type of filtration fabric	q_g (m^3/m^2h)	Kind of dust					
		Separated cement	Unseparated cement	Separated coal	Unseparated coal	Separated talc	Separated fly ash
ET-4	60	78.25	99.95	99.95	91.90	66.84	83.19
	80	98.89	61.61	99.69	79.43	96.48	83.75
	120	98.86	77.76	99.44	98.34	98.87	88.03
ET-30	60	93.94	58.41	96.59	94.98	99.10	14.95
	80	83.06	79.87	77.76	94.65	90.01	92.71
	120	97.97	97.72	38.59	93.88	97.97	90.25
F-tor 5	60	91.08	88.73	0.16	99.52	97.72	85.69
	80	30.35	46.79	0	83.82	58.62	89.60
	120	0	0	98.17	0	76.16	87.11
PT-15	60	80.06	81.50	93.12	99.45	99.61	99.58
	80	86.06	0	84.46	99.98	71.74	83.19
	120	96.63	99.47	99.46	99.87	96.93	96.88

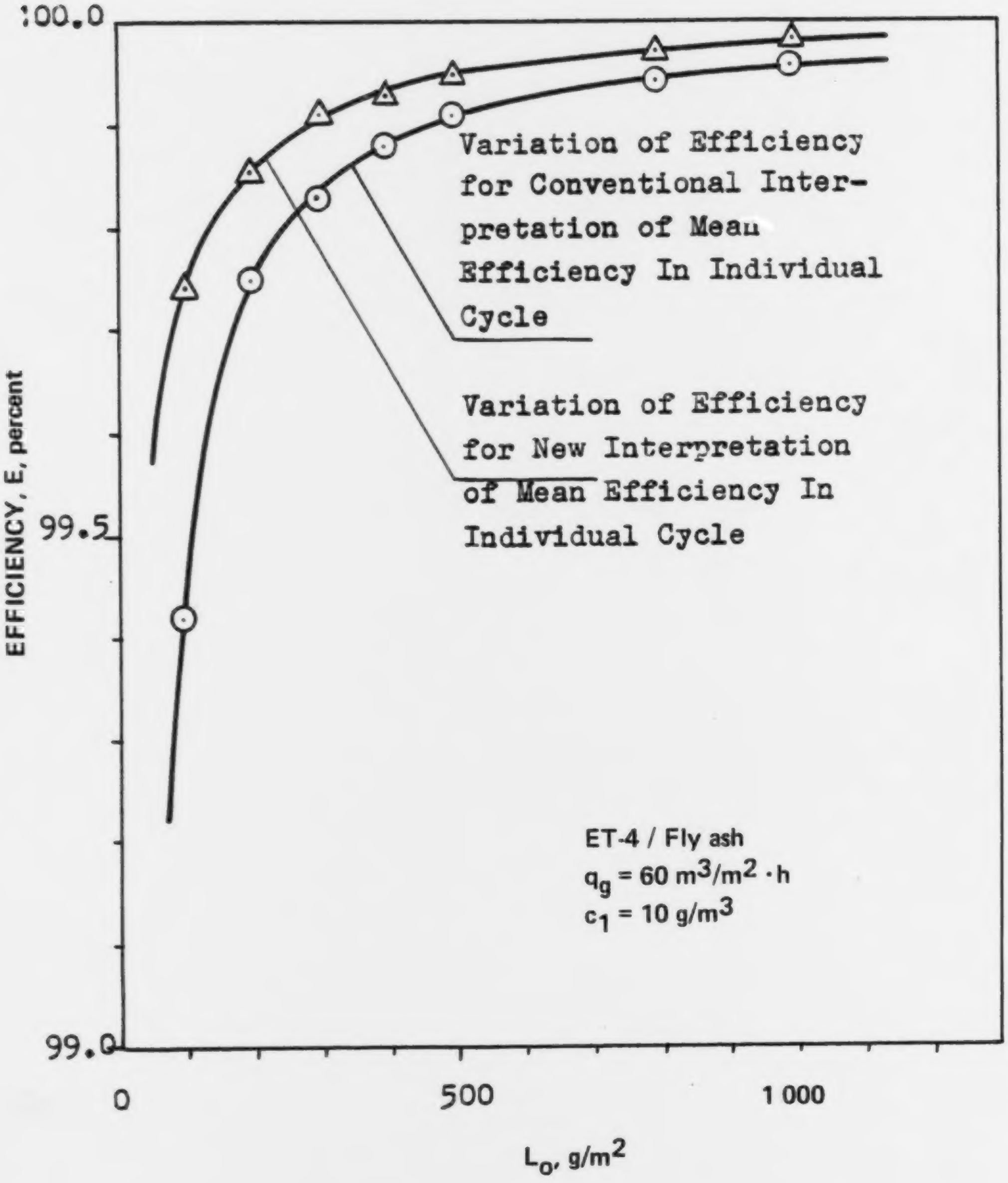

Figure 33. Dust collection efficiency for two interpretations of the mean efficiency of an individual cycle.

$$a = \log\log\frac{100}{E_o} = \frac{(\Sigma y)\,(\Sigma x^2)-(\Sigma x)\,(\Sigma xy)}{n(\Sigma x^2)-(\Sigma x)^2}\text{ , and} \tag{58}$$

$$b = F_2 = \frac{n(\Sigma xy) - (\Sigma x)\,(\Sigma y)}{n(\Sigma x^2) - (\Sigma x)^2}\ ,$$

where

n in the numerator and denominator of the right-hand side of the equation is the number of points to which the regression line was fitted.

Values of initial static dust collection efficiency, E_o, and directional coefficients of regression b (depending on F_2 for a specific q_g) are shown in Tables 3 through 5. Calculations were based on the assumption that empirically determined values of dust collection efficiency are averages for a particular measurement cycle, corresponding to the value of $\frac{t_{FC}}{2}\left(\text{or } \frac{L_o}{2}\right)$. The values differ from those presented in the second-phase report of this project, where calculations were based on the assumption that dust collection efficiency corresponds to the final state of the measurement cycle; i.e., to t_{FC} (or L_o). When this new interpretation of mean dust collection efficiency is applied, initial efficiencies, E_o, are higher in all cases (Figure 33); but the values of the directional coefficient, $b = f_2$, are lower.

The determination of E_o and F_2 in the Series II and III tests (broader program) used only the new interpretation of mean efficiency. Figure 34 shows the dependence of E_o upon q_g, for fabric ET-4 and ET-30 both filtering fly ash. Figure 35 shows the corresponding F_2 values. The shape of these curves is parabolic, with clearly defined extremes. It is significant that curves of both fabrics show minimum in a similar range of q_g:

- Fabric ET-4 $q_g = 110\ m^3/m^2h$, and
- Fabric ET-30 $q_g = 140\ m^3/m^2h$.

In this range, the fabrics show the lowest initial dust collection efficiency, and the function F_2 has the lowest value. Thus, for these values of q_g the mean process efficiency depends mostly on L_o.

The effect of dust cake defects, causing deformation of the parabolic dependencies depicting E_o and F_2, is shown in the diagrams. From the calcula-

TABLE 3. VALUES OF F_2 AS A FUNCTION OF q_g (Series I and Previous Experiments)

Type of filtration fabric	q_g (m^3/m^2h)	Kind of dust					
		Separated cement	Unseparated cement	Separated coal	Unseparated coal	Separated talc	Separated fly ash
ET-4	60	-1.13	-0.52	-0.44	-0.79	-1.26	-1.09
	80	-0.55	-1.09	-0.41	-1.03	-0.47	-0.98
	120	-0.08	-0.92	-0.48	-0.33	-0.16	-0.74
ET-30	60	-0.85	-1.38	-0.80	-0.96	-0.64	-1.51
	80	-1.15	-1.04	-1.18	-0.94	-0.89	-0.84
	120	-0.67	-0.65	-1.37	-0.79	-0.65	-0.87
F-tor 5	60	-0.85	-0.90	-1.50	-0.33	-0.37	-0.97
	80	-1.00	-1.25	-2.20	-0.60	-0.96	-0.80
	120	-1.36	-1.58	-0.03	-1.41	-0.46	-0.73
PT-15	60	-1.19	-1.36	-0.98	-0.50	-0.43	-0.47
	80	-1.16	-2.39	-1.26	-0.48	-1.31	-1.04
	120	-0.92	-0.40	-0.53	-0.16	-0.75	-0.75

TABLE 4. VALUES OF F_1 AS A FUNCTION OF q_g
(Series I and Previous Experiments)

Type of filtration fabric	q_g (m^3/m^2h)	Kind of dust					
		Separated cement	Unseparated cement	Separated coal	Unseparated coal	Separated talc	Separated fly ash
ET-4	60	1.278	1.01029	1.00047	1.0981	1.496	1.202
	80	1.01125	1.623	1.00309	1.259	1.03648	1.194
	120	1.01148	1.286	1.00567	1.01686	1.01138	1.136
ET-30	60	1.06449	1.719	1.03528	1.05286	1.00909	6.69
	80	1.204	1.252	1.286	1.05651	1.111	1.07862
	120	1.02073	1.02332	2.591	1.06523	1.02069	1.108
F-tor 5	60	1.09792	1.127	609.6	1.00479	1.02329	1.167
	80	3.295	2.197	-	1.193	1.706	1.116
	120	-	-	1.01864	-	1.313	1.148
PT-15	60	1.249	1.227	1.07391	1.00537	1.00396	1.00421
	80	1.162	-	1.184	1.00024	1.394	1.202
	120	1.0348	1.00536	1.00541	1.00134	1.03169	1.03219

TABLE 5. INITIAL STATISTICAL EFFICIENCY, E_o, VALUES OF F_1 AND F_2 AS A FUNCTION OF q_g (Series II and III)

Type of filtration fabric	q_g (m^3/m^2h)	Value		
		E_o (%)	F_1	F_2
ET-4	60	61.96	1.6140	-1.1329
	70	54.52	1.8340	-1.1273
	80	62.89	1.5900	-1.0998
	100	50.68	1.9730	-1.1266
	120	52.60	1.9010	-1.1090
	140	65.40	1.5290	-1.0692
	160	-	-	-
	180	37.12	2.694	-1.2403
	200	97.28	1.028	-0.0619
ET-30	70	90.91	1.0999	-0.8403
	80	88.50	1.1300	-0.8841
	100	76.75	1.3030	-0.9727
	120	65.57	1.5250	-0.0152
	140	-	-	-
	160	-	-	-
	180	70.42	1.4200	-0.8282
	200	84.39	1.1850	-0.4130

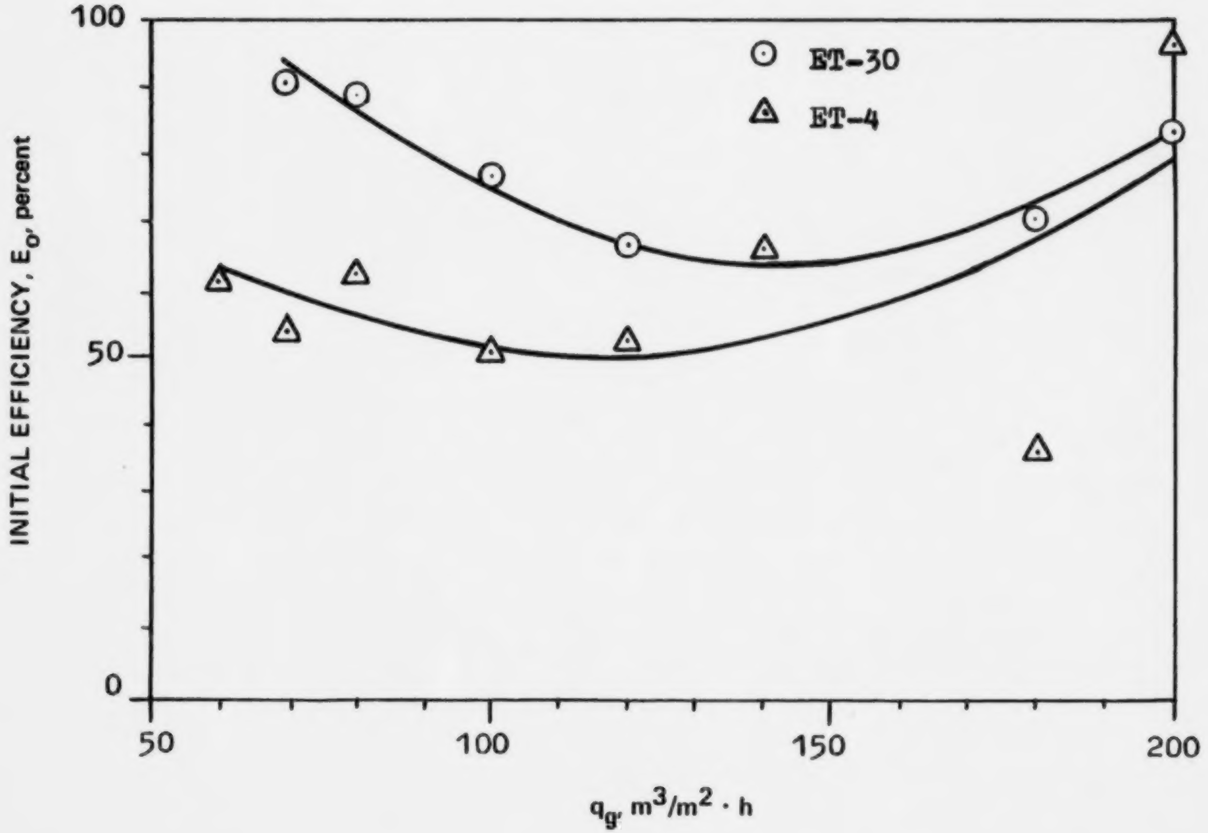

Figure 34. Dependence of E_o on q_g.

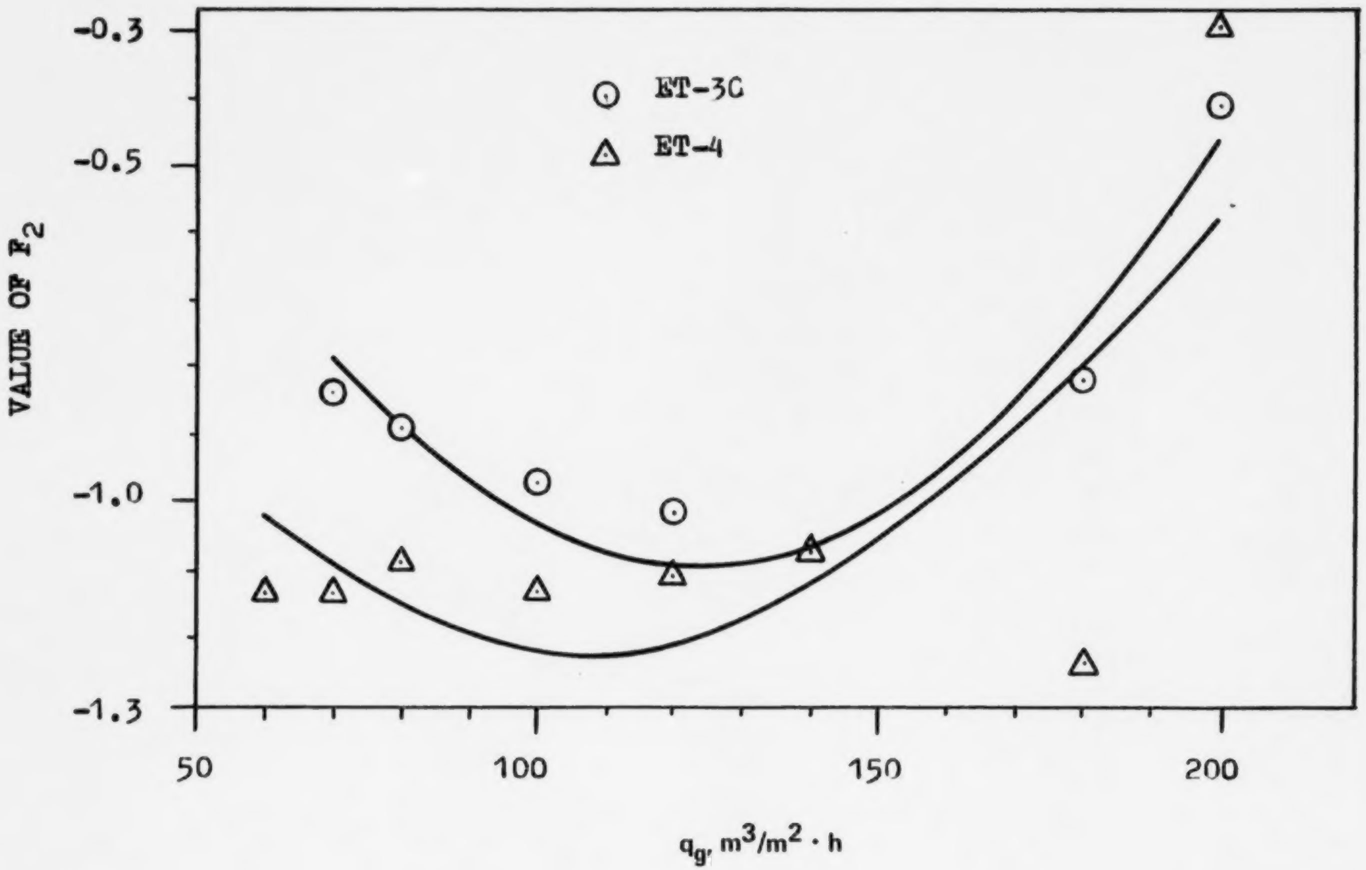

Figure 35. Dependence of function F_2 on q_g

tions, we obtain the set of straight lines in the Rosin-Rammler coordinate system for a specific filtration material and dust and for different values of q_g. Equation 18 has the following form:

$$E_I = [F_1(q_g)]^{-\bar{L}_o^{\,F_2(q_g)}} \quad . \tag{59}$$

The least squares method was used to calculate that functions F_1 and F_2 are quadratic and best fitted by parabolas. The following general form of the probabilistic model of dust collection efficiency for Dust Filtration Process Type I was obtained:

$$E_I = 100\,[a_1 q_g^2 + b_1 q_g + c_1]^{-\bar{L}_o^{\,[a_2 q_g^2 + b_2 q_g + c_2]}} \quad , \tag{60}$$

or

$$E_I = 100\,[(\,{}_a\;q_g^2 + bq_g + c]^{-\bar{L}_o^{\,[a_2 q_g^2 + b_2 q_g + c_2]}} \quad , \tag{60a}$$

where

a, a_1, a_2, b, b_1, b_2, c, c_1, and c_2 are constants depending upon the kind of dust and the structural parameters of the fabric.

The coefficient values from Equations 60 and 60a are shown in Tables 6 through 9. When the coefficients were calculated, data taken at higher q_g (i.e., for fabric ET-4, q_g = 160 m^3/m^2h and for fabric ET-30, q_g = 140 and 160 m^3/m^2h) were not considered because of dust cake defects. Three-dimensional models for individual fabrics and dusts are obtained by substitution.

The first part of the equation corresponds to function F_1, which describes the statistical, initial dust collection efficiency, E_o:

$$F_1 = a_1 q_g^2 + b_1 q_g + c_1 \quad . \tag{61}$$

The parabolic nature of the relationship indicates the presence of a maximum or a minimum. The value of q_g, where the extreme of the function F_1 appears, can be determined according to:

TABLE 6. COEFFICIENTS OF THE PARABOLIC EQUATION: $E_o = a(q_g)^2 + bq_g + c$ (Series I and Previous Experiments)

Type of filtration fabric		Kind of dust					
		Separated cement	Unseparated cement	Separated coal	Unseparated coal	Separated talc	Separated fly ash
ET-4	a	$-1.7213 \cdot 10^{-2}$	$3.8679 \cdot 10^{-2}$	$1.1250 \cdot 10^{-4}$	$1.8271 \cdot 10^{-2}$	$-2.3704 \cdot 10^{-2}$	$1.3167 \cdot 10^{-3}$
	b	3.4418	-7.3321	$-2.8750 \cdot 10^{-2}$	-3.1814	4.8006	$-1.5633 \cdot 10^{-1}$
	c	$-6.629 \cdot 10^{1}$	$4.0063 \cdot 10^{2}$	$1.0127 \cdot 10^{2}$	$2.1701 \cdot 10^{2}$	$-1.3586 \cdot 10^{2}$	$8.783 \cdot 10$
ET-30	a	$1.5279 \cdot 10^{-2}$	$-1.0446 \cdot 10^{-2}$	$-6.2917 \cdot 10^{-4}$	$-4.5833 \cdot 10^{-5}$	$1.0892 \cdot 10^{-2}$	$-6.5825 \cdot 10^{-2}$
	b	-2.6831	2.5354	$-8.5342 \cdot 10^{-1}$	$-1.0083 \cdot 10^{-2}$	1.9793	$1.3104 \cdot 10$
	c	$1.9992 \cdot 10^{2}$	$-5.611 \cdot 10$	$1.5006 \cdot 10^{2}$	$9.575 \cdot 10$	$1.7865 \cdot 10^{2}$	$5.3429 \cdot 10^{2}$
F-tor 5	a	$3.7963 \cdot 10^{-2}$	$1.5454 \cdot 10^{-2}$	$4.1038 \cdot 10^{-2}$	$-2.1842 \cdot 10^{-2}$	$3.9892 \cdot 10^{-2}$	$-4.2958 \cdot 10^{-3}$
	b	-8.3513	-4.2606	-5.7533	2.2728	-7.5398	$7.9692 \cdot 10^{-1}$
	c	$4.5549 \cdot 10^{2}$	$2.8873 \cdot 10^{2}$	$1.9762 \cdot 10^{2}$	$4.1780 \cdot 10$	$4.065 \cdot 10^{2}$	$5.3340 \cdot 10$
PT-16	a	$-5.9583 \cdot 10^{-4}$	$1.0936 \cdot 10^{-1}$	$1.3467 \cdot 10^{-2}$	$-4.875 \cdot 10^{-4}$	$3.3721 \cdot 10^{-2}$	$1.9663 \cdot 10^{-2}$
	b	$3.8342 \cdot 10^{-1}$	$-1.9385 \cdot 10$	-2.3183	$9.475 \cdot 10^{-2}$	-6.1144	-3.5303
	c	$5.92 \cdot 10$	$8.5094 \cdot 10^{2}$	$1.8374 \cdot 10^{2}$	$9.5520 \cdot 10$	$3.4508 \cdot 10^{2}$	$2.4169 \cdot 10^{2}$

TABLE 7. COEFFICIENTS OF THE PARABOLIC EQUATION: $F_2 = n = a_2(q_g)^2 + b_2q_g + c_2$
(Series I and Previous Experiments)

Type of filtration fabric		Kind of dust Separated cement	 Unseparated cement	 Separated coal	 Unseparated coal	 Separated talc	 Separated fly ash
ET-4	a_2	$-2.875 \cdot 10^{-4}$	$5.4583 \cdot 10^{-4}$	$6.4167 \cdot 10^{-5}$	$4.8945 \cdot 10^{-4}$	$-5.2917 \cdot 10^{-4}$	$6.875 \cdot 10^{-6}$
	b_2	$6.925 \cdot 10^{-2}$	$-1.0491 \cdot 10^{-1}$	$9.0833 \cdot 10^{-3}$	$-8.0427 \cdot 10^{-2}$	$1.1358 \cdot 10^{-1}$	$4.600 \cdot 10^{-3}$
	c_2	-4.25	3.81	$-7.900 \cdot 10^{-1}$	2.2729	-6.1700	-1.3912
ET-30	a_2	$4.500 \cdot 10^{-4}$	$-1.2083 \cdot 10^{-4}$	$2.3750 \cdot 10^{-4}$	$4.5833 \cdot 10^{-5}$	$3.0833 \cdot 10^{-4}$	$-5.7083 \cdot 10^{-4}$
	b_2	$-7.800 \cdot 10^{-2}$	$3.3917 \cdot 10^{-2}$	$-5.225 \cdot 10^{-2}$	$-5.4167 \cdot 10^{-3}$	$-5.5667 \cdot 10^{-2}$	$1.1342 \cdot 10^{-1}$
	c_2	2.21	-2.9800	1.4800	$-7.9999 \cdot 10^{-1}$	1.5900	-6.26
F-tor 5	a_2	$-1.1617 \cdot 10^{-4}$	$1.5417 \cdot 10^{-4}$	$1.4875 \cdot 10^{-3}$	$-1.125 \cdot 10^{-4}$	$7.00 \cdot 10^{-4}$	$-1.125 \cdot 10^{-4}$
	b_2	$8.8333 \cdot 10^{-3}$	$-3.9083 \cdot 10^{-2}$	$-2.4325 \cdot 10^{-1}$	$2.25 \cdot 10^{-3}$	$-1.275 \cdot 10^{-1}$	$2.4250 \cdot 10^{-2}$
	c_2	$-9.6000.10^{-1}$	$8.9000 \cdot 10^{-1}$	7.7400	$-6.0000 \cdot 10^{-2}$	4.760	-2.0200
PT-15	a_2	$2.2569 \cdot 10^{-5}$	$1.6875 \cdot 10^{-3}$	$5.3750 \cdot 10^{-4}$	$1.1667 \cdot 10^{-4}$	$9.6667 \cdot 10^{-4}$	$5.9583 \cdot 10^{-4}$
	b_2	$6.5528 \cdot 10^{-4}$	$-2.8775 \cdot 10^{-1}$	$-8.9250 \cdot 10^{-3}$	$-1.5333 \cdot 10^{-2}$	$-1.7933 \cdot 10^{-1}$	$-1.1192 \cdot 10^{-1}$
	c_2	-1.3304	9.8300	2.4400	$1.3767 \cdot 10^{-8}$	6.8500	4.1000

TABLE 8. COEFFICIENT OF THE PARABOLIC EQUATION:
$E_o = a(q_g)^2 + b \cdot q_g + c$
(Series II and III)

Parabola coefficient	Kind of fabric	
	ET-4	ET-30
a	$4.1311 \cdot 10^{-3}$	$5.6333 \cdot 10^{-3}$
b	-0.9635	-1.6035
c	$1.0691 \cdot 10^{2}$	$1.7830 \cdot 10^{2}$

TABLE 9. COEFFICIENTS OF THE PARABOLIC EQUATIONS:
$F_1 = a_1(q_g)^2 + b_1 \cdot q_g + c_1$ AND
$F_2 = a_2(q_g)^2 + b_2 \cdot q_g + c_2$
(Series II and III)

Parabola coefficient	Kind of fabric	
	ET-4	ET-30
a_1	$-0.8018 \cdot 10^{-4}$	$-0.9370 \cdot 10^{-4}$
b_1	$2.0775 \cdot 10^{-2}$	$2.6558 \cdot 10^{-2}$
c_1	$6.1932 \cdot 10^{-1}$	$-3.5436 \cdot 10^{-1}$
a_2	$0.9448 \cdot 10^{-4}$	$1.0801 \cdot 10^{-4}$
b_2	$-2.0108 \cdot 10^{-2}$	$-2.6631 \cdot 10^{-2}$
c_2	$-1.5864 \cdot 10^{-1}$	$5.4055 \cdot 10^{-1}$

$$q_{g\ extr} = -\frac{b_1}{2a_1} \quad . \tag{62}$$

The existence of an extreme value of q_g has implications for interpreting Dust Filtration Process Type I because it divides the process into two parts, in which the predicted dust collection efficiency can be either higher or lower, depending on the character of the extreme value, $q_{g\ extr}$. Concerning fly ash filtration through ET-4 and ET-30, $q_{g\ extr}$ is:

- For fabric ET-4,

$$q_{g\ extr} = \frac{2.0775 \times 10^{-2}}{2(8.0180 \times 10^{-5})} = 129.6\ \mathrm{m^3/m^2h} \quad \text{, and}$$

- For fabric ET-30,

$$q_{g\ extr} = \frac{2.6558 \times 10^{-2}}{2(9.3702 \times 10^{-5})} = 141.7\ \mathrm{m^3/m^2h} \quad .$$

This approach was used to analyze the experimental results of Series I (the second-phase report of the project). We found that using too few values of filtration parameters leads to ambiguous results.

The analysis of Dust Filtration Process Type I presented in this report and based mainly on experimental results of Series II and III verifies the conclusions presented in the second-phase report, which were based on results obtained in the initial research program (Series I). When Equation 60 and Equation 60a are solved for specific values of L_o and q_g, a set of results depicting dust collection efficiency as a function of these parameters is obtained.

Theoretical dust collection efficiency variations as a function of q_g and L_o are shown in Figures 36 through 70. Dust collection efficiencies obtained during laboratory experiments in Series II and III are depicted by points. The agreement between values of dust collection efficiency resulting from the model and those obtained experimentally was good. The effect of q_g on dust collection efficiency was considered, and results that agree with data published by other authors[25 26] were obtained. Data show that dust collection efficiency decreases as q_g increases.

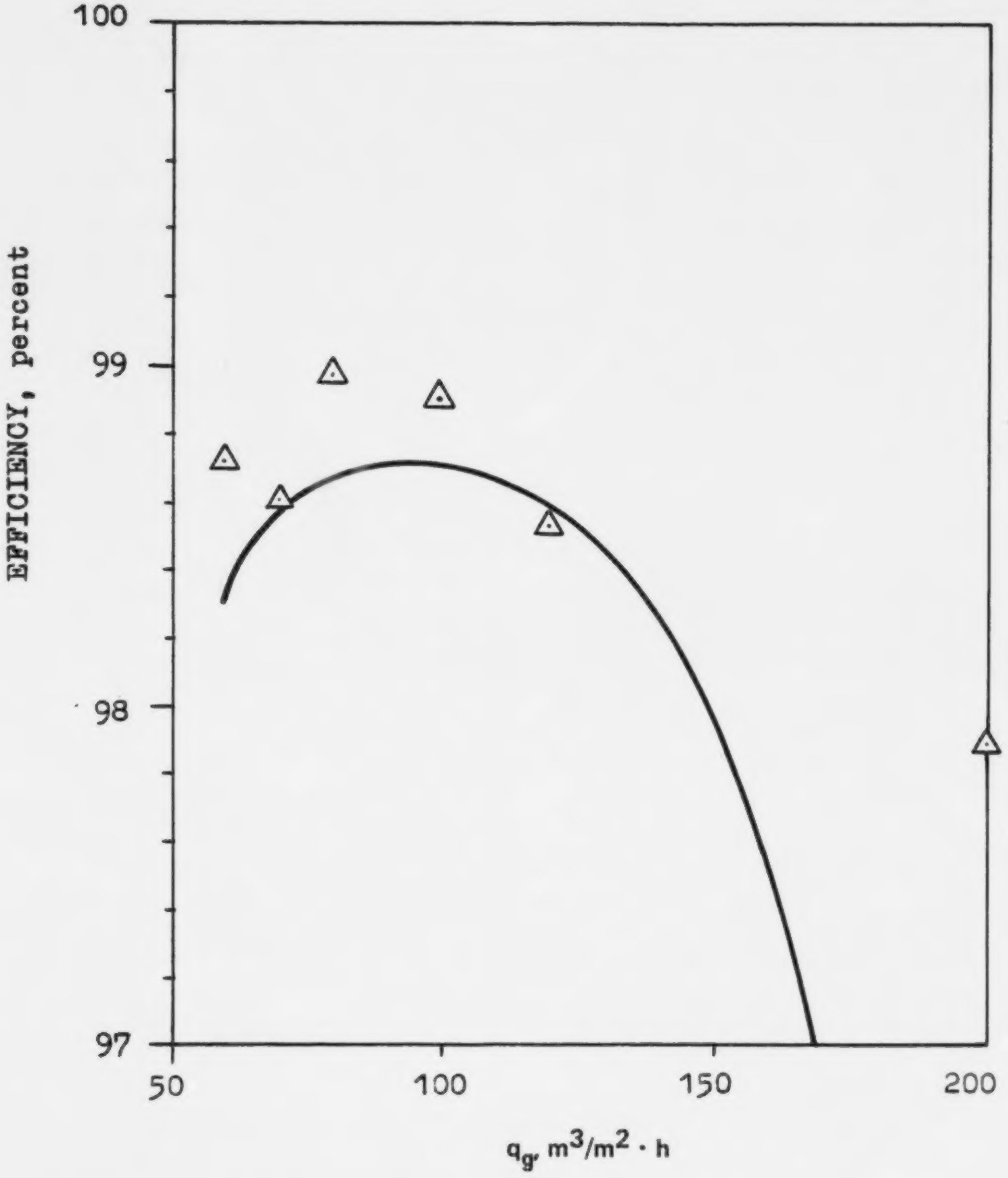

Figure 36. Predicted and experimental efficiencies of ET-4 as a function of q_g for average value of $L_o' = 25$ g/m^2.

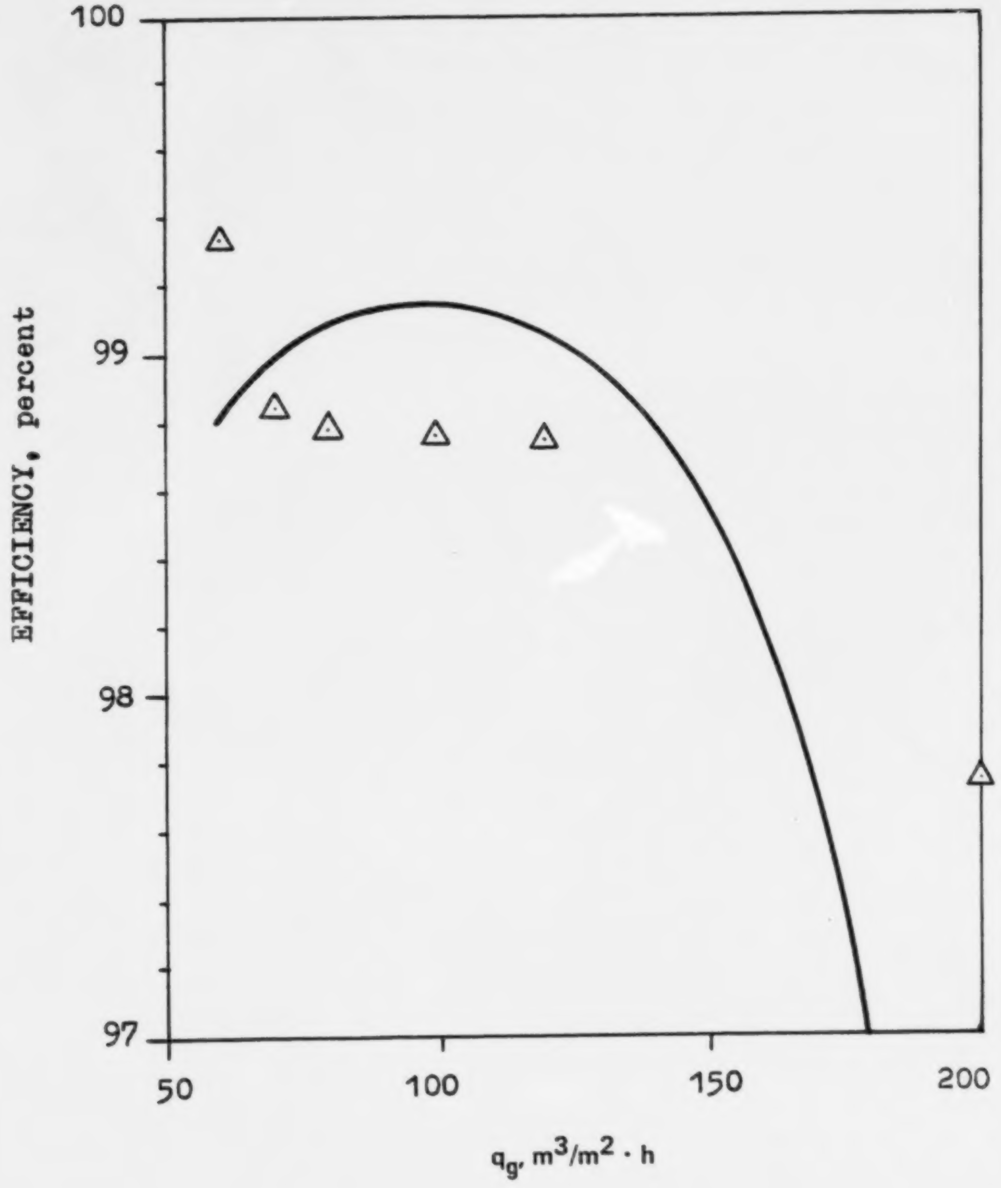

Figure 37. Predicted and experimental efficiencies of ET-4 as a function of q_g for average value of $L_o' = 35\ g/m^2$.

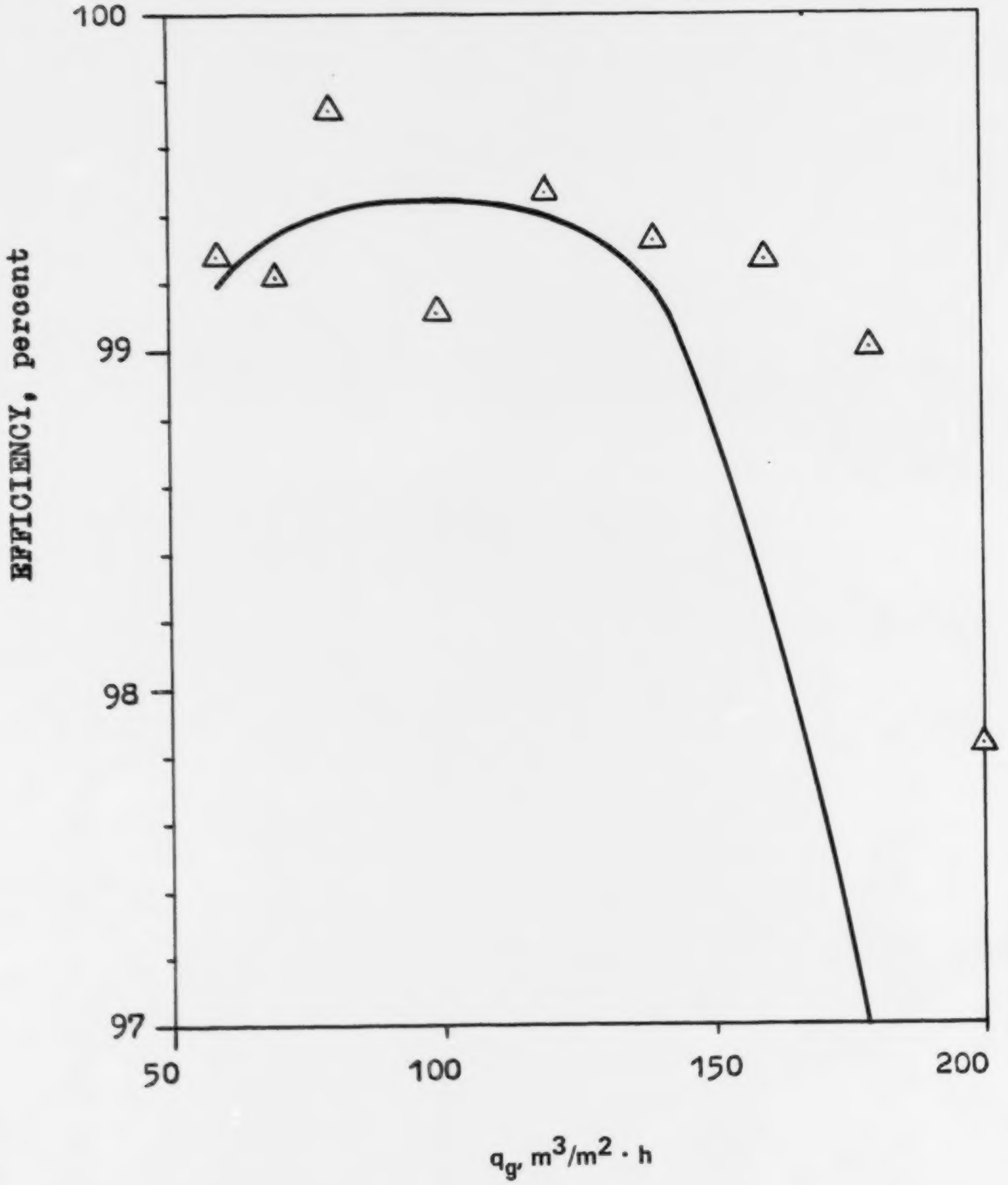

Figure 38. Predicted and experimental efficiencies of ET-4 as a function of q_g for average value of $L_o' = 50\ g/m^2$.

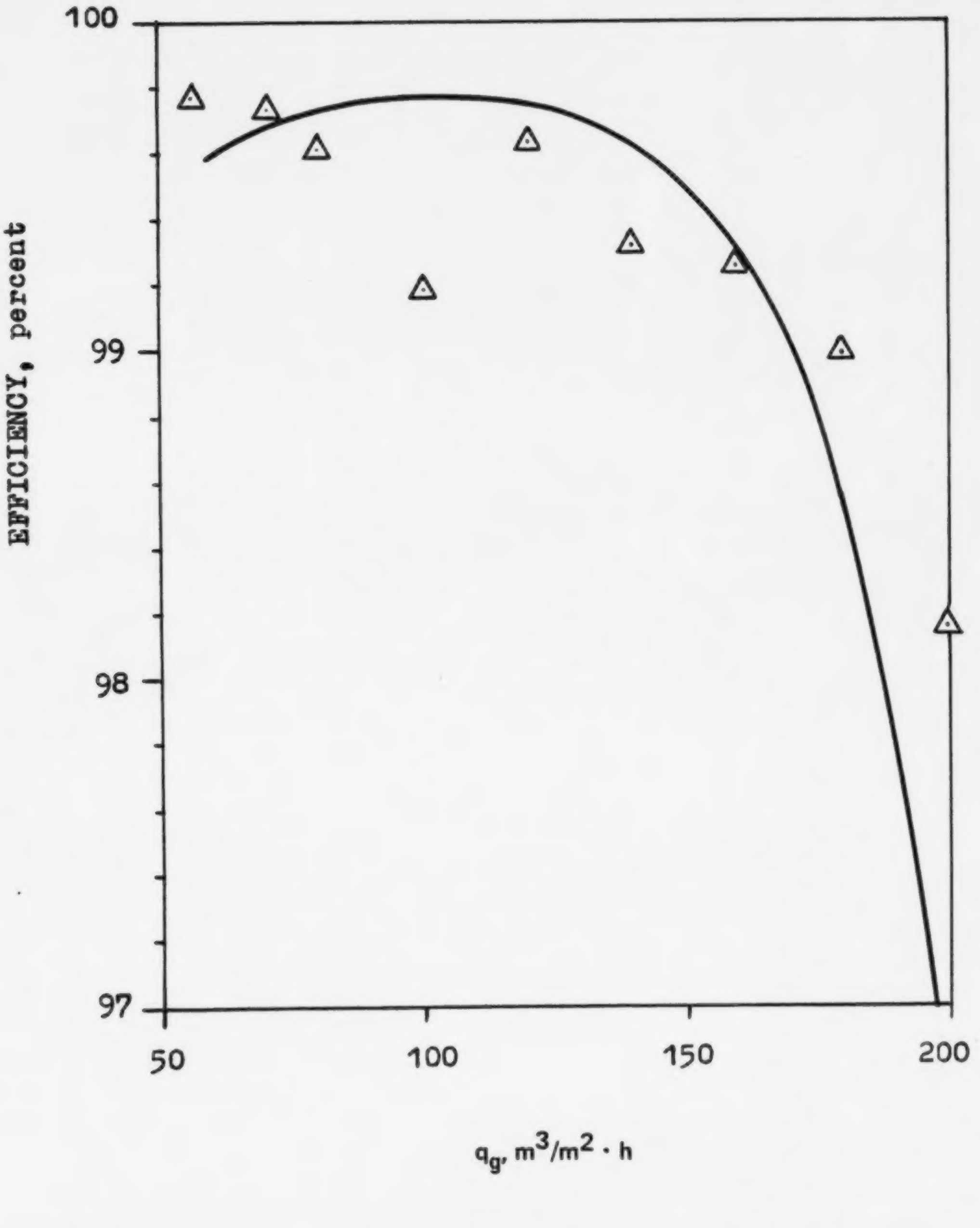

Figure 39. Predicted and experimental efficiencies of ET-4 as a function of q_g for average value of $L_o' = 100$ g/m^2.

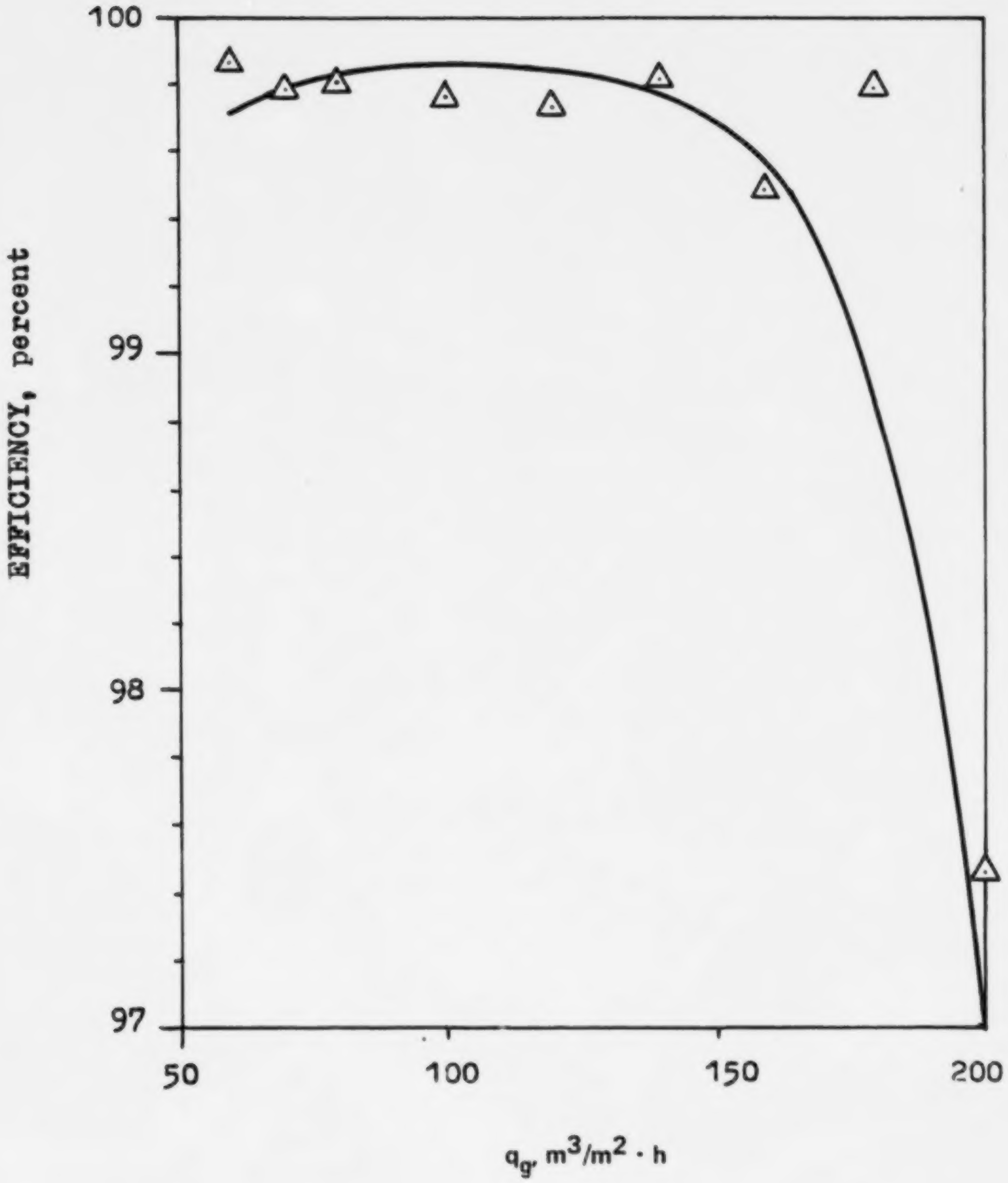

Figure 40. Predicted and experimental efficiencies of ET-4 as a function of q_g for average value of $L_o' = 150$ g/m^2.

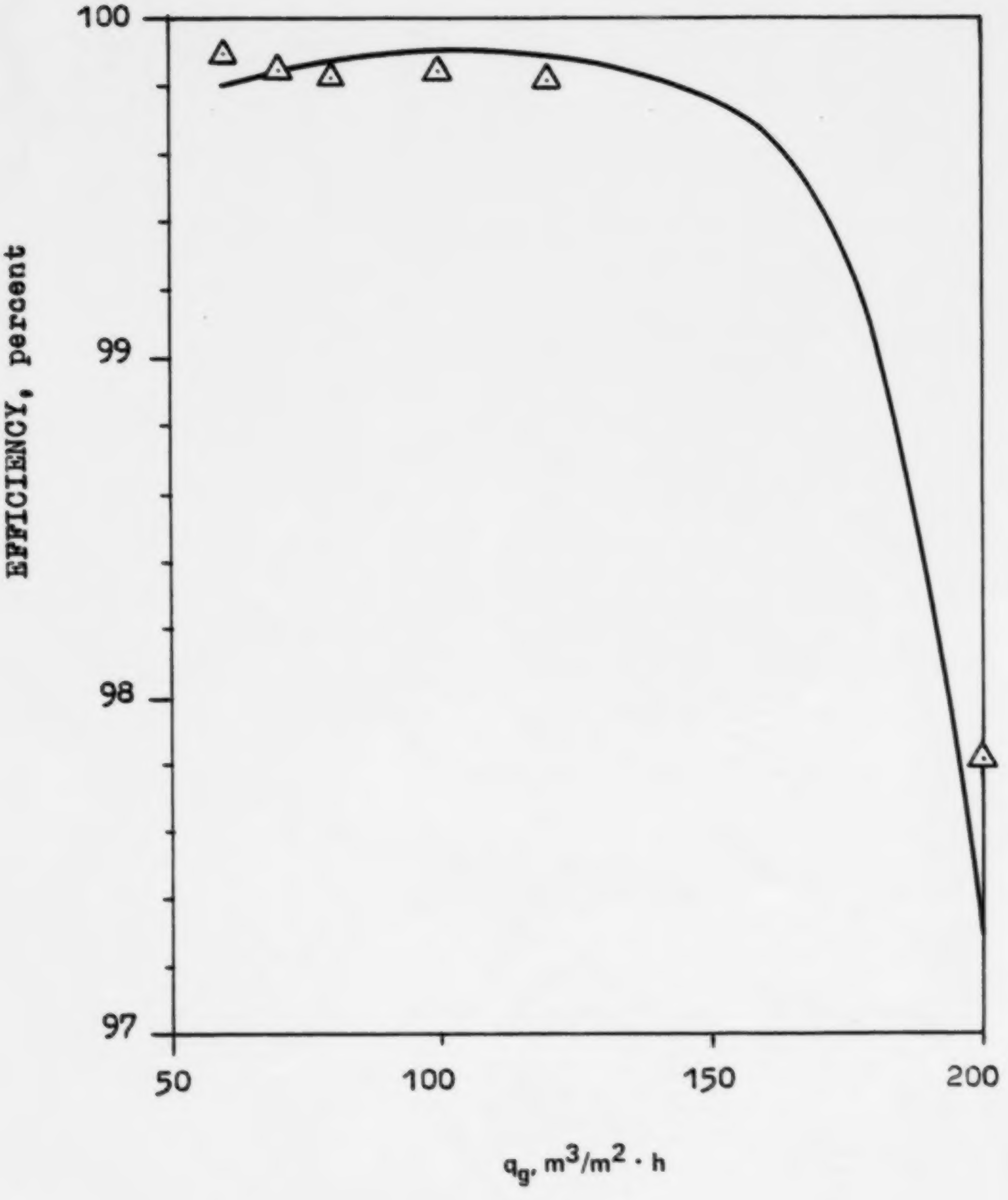

Figure 41. Predicted and experimental efficiencies of ET-4 as a function of q_g for average value of $L_o' = 200$ g/m^2.

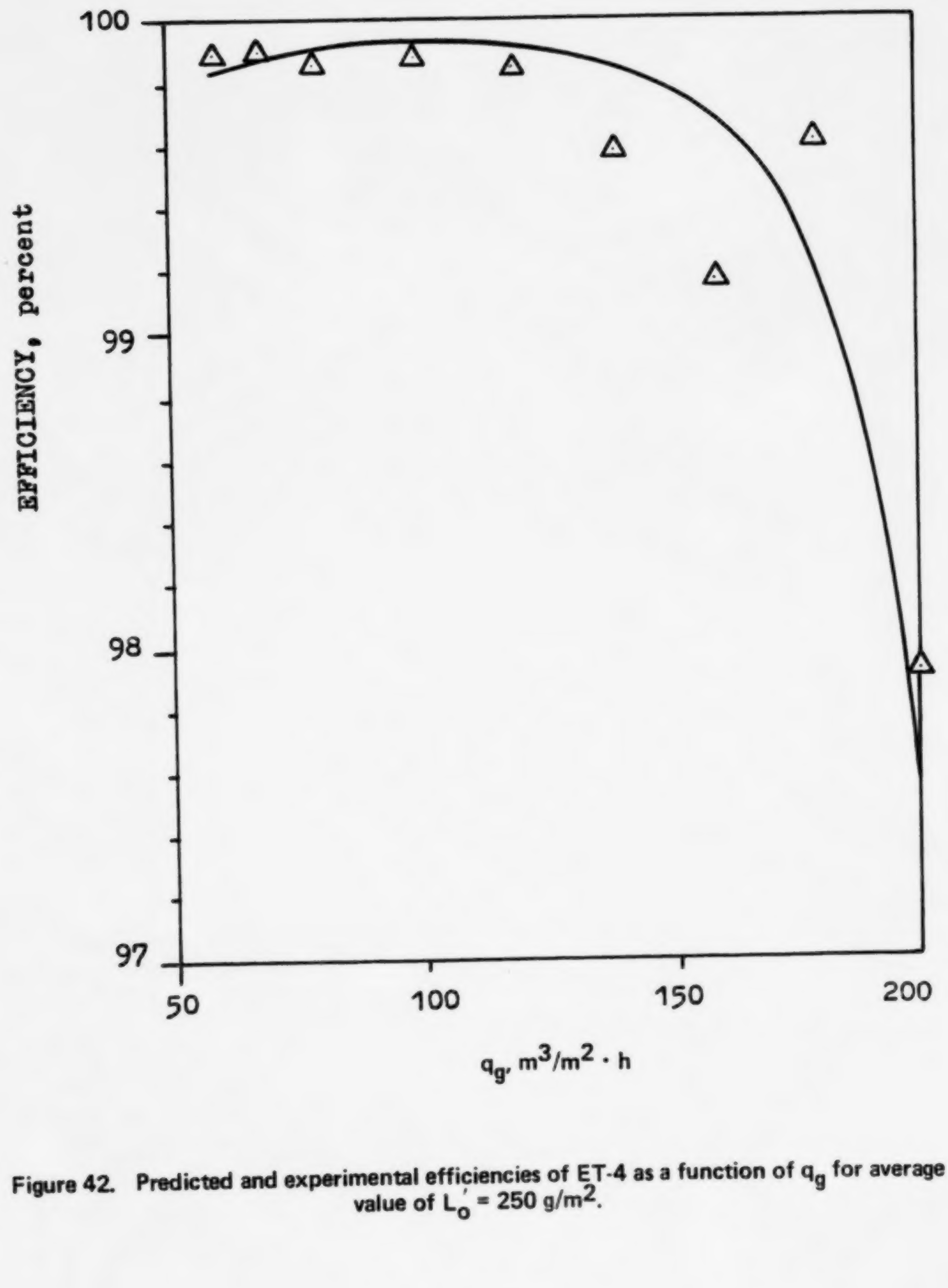

Figure 42. Predicted and experimental efficiencies of ET-4 as a function of q_g for average value of $L_o' = 250\ g/m^2$.

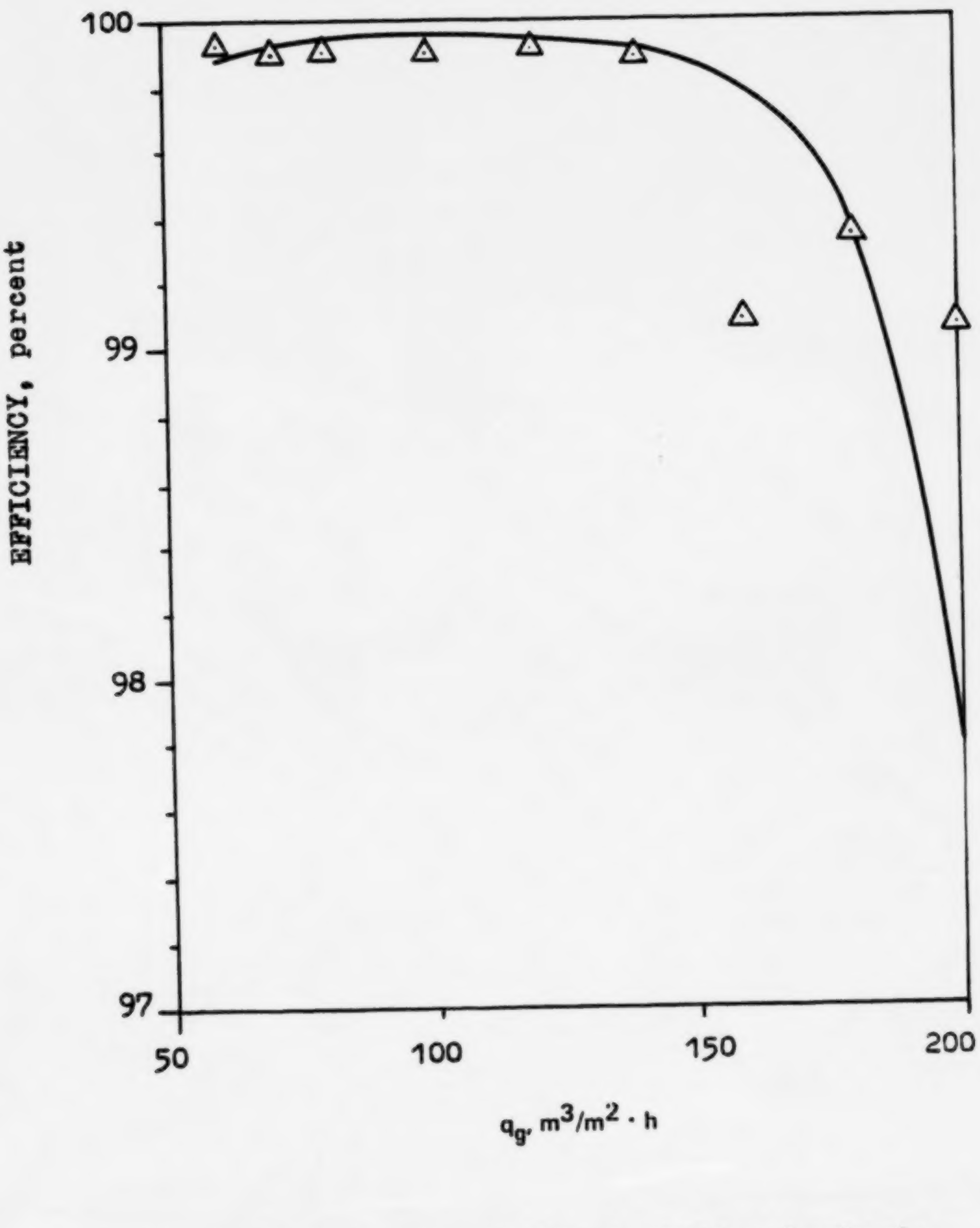

Figure 43. Predicted and experimental efficiencies of ET-4 as a function of q_g for average value of $L_o' = 350$ g/m^2.

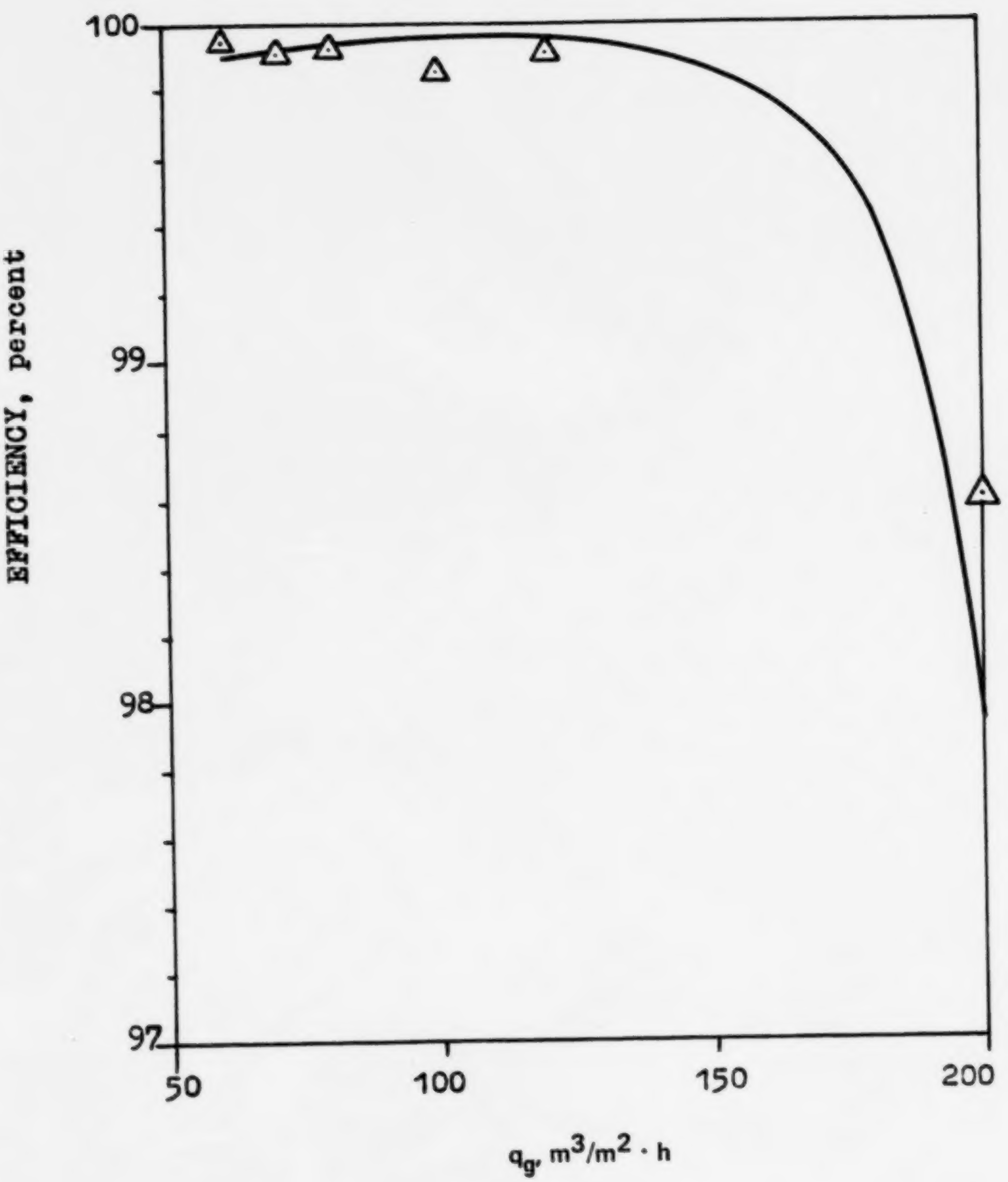

Figure 44. Predicted and experimental efficiencies of ET-4 as a function of q_g for average value of $L'_o = 400\ g/m^2$.

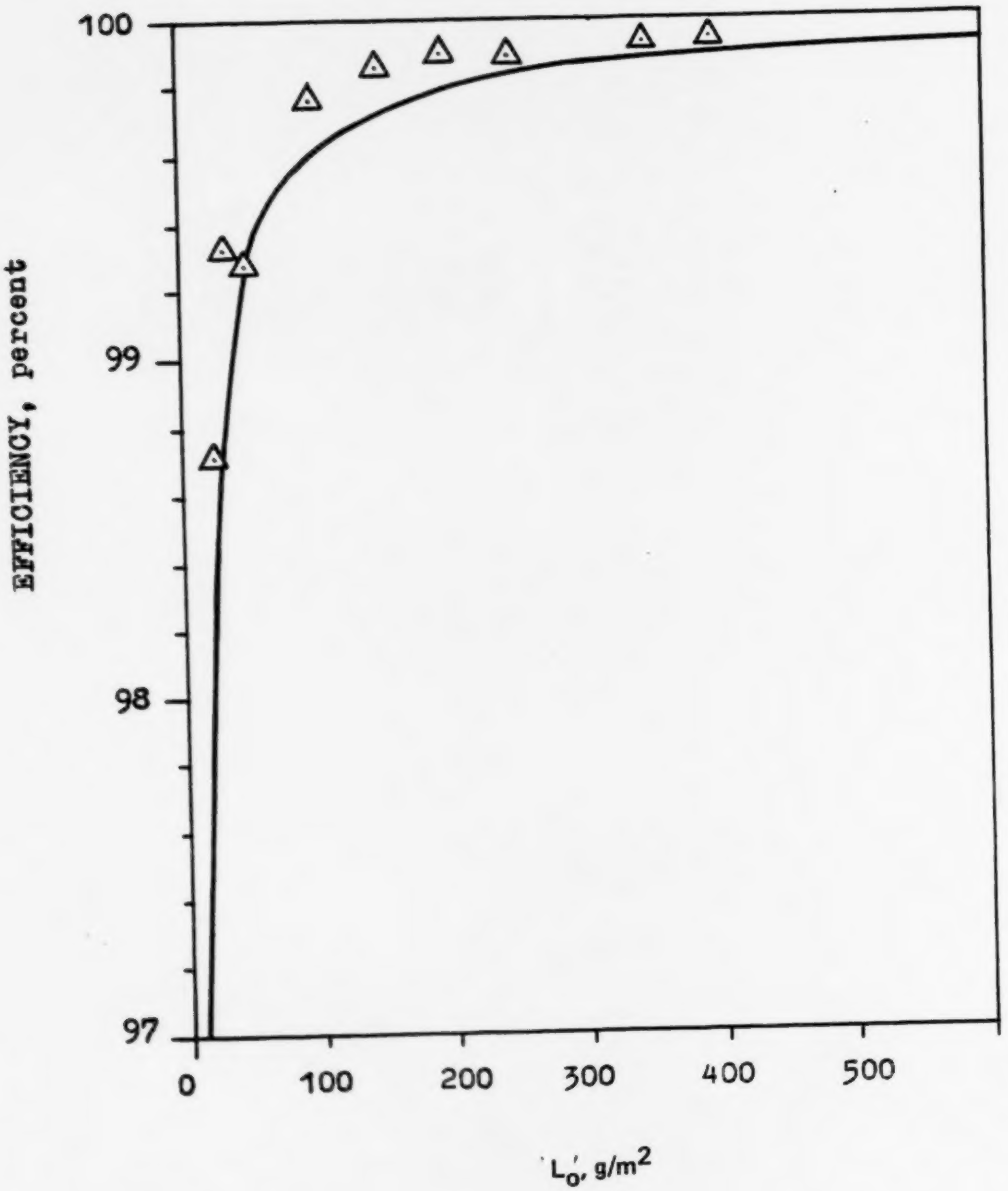

Figure 45. Predicted and experimental efficiencies of ET-4 as a function of L_o' for q_g = 60 m^3/m^2 · h.

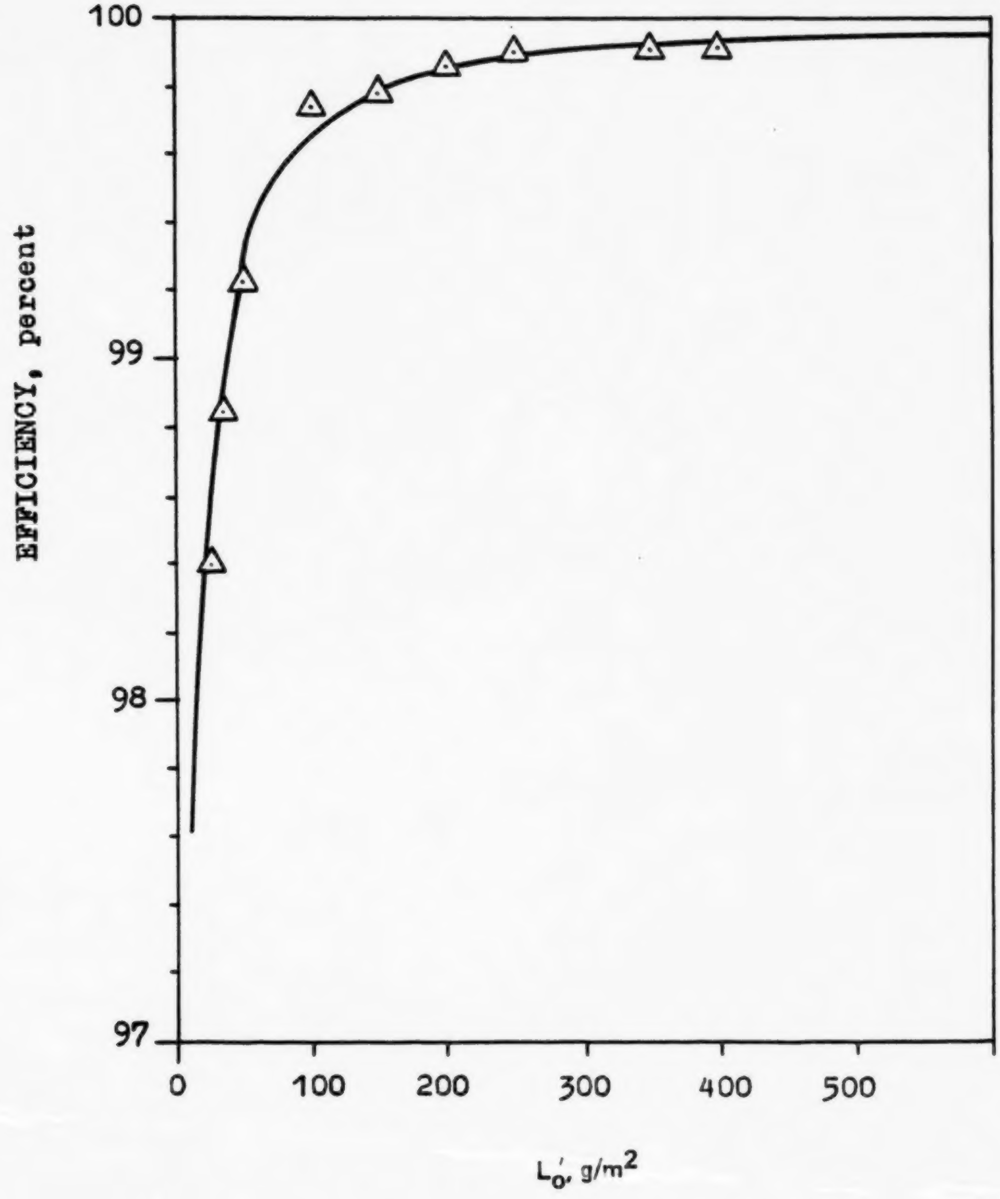

Figure 46. Predicted and experimental efficiencies of ET-4 as a function of L_o' for $q_g = 70\ m^3/m^2 \cdot h$.

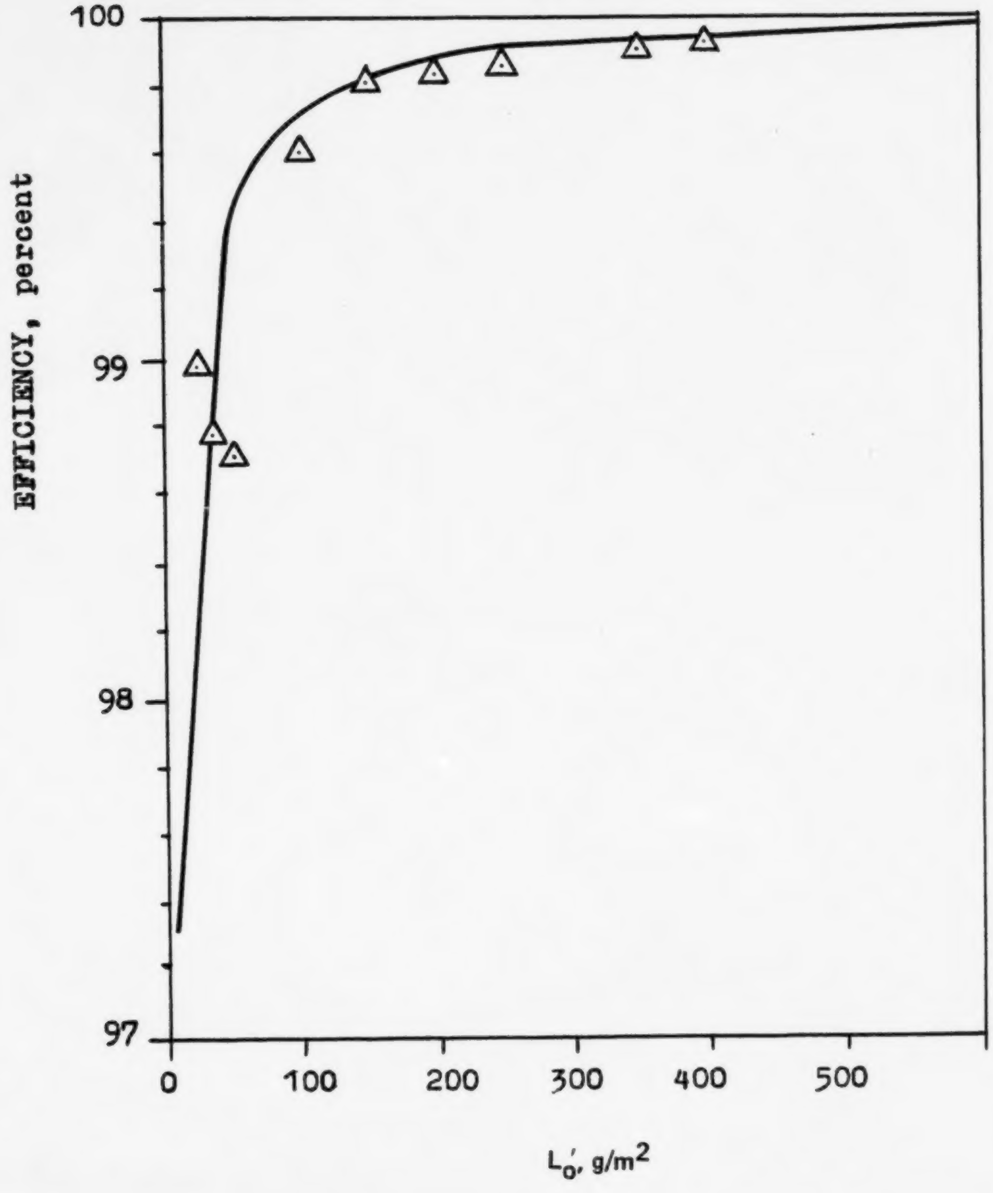

Figure 47. Predicted and experimental efficiencies of ET-4 as a function of L_o' for $q_g = 80\ m^3/m^2 \cdot h$.

112

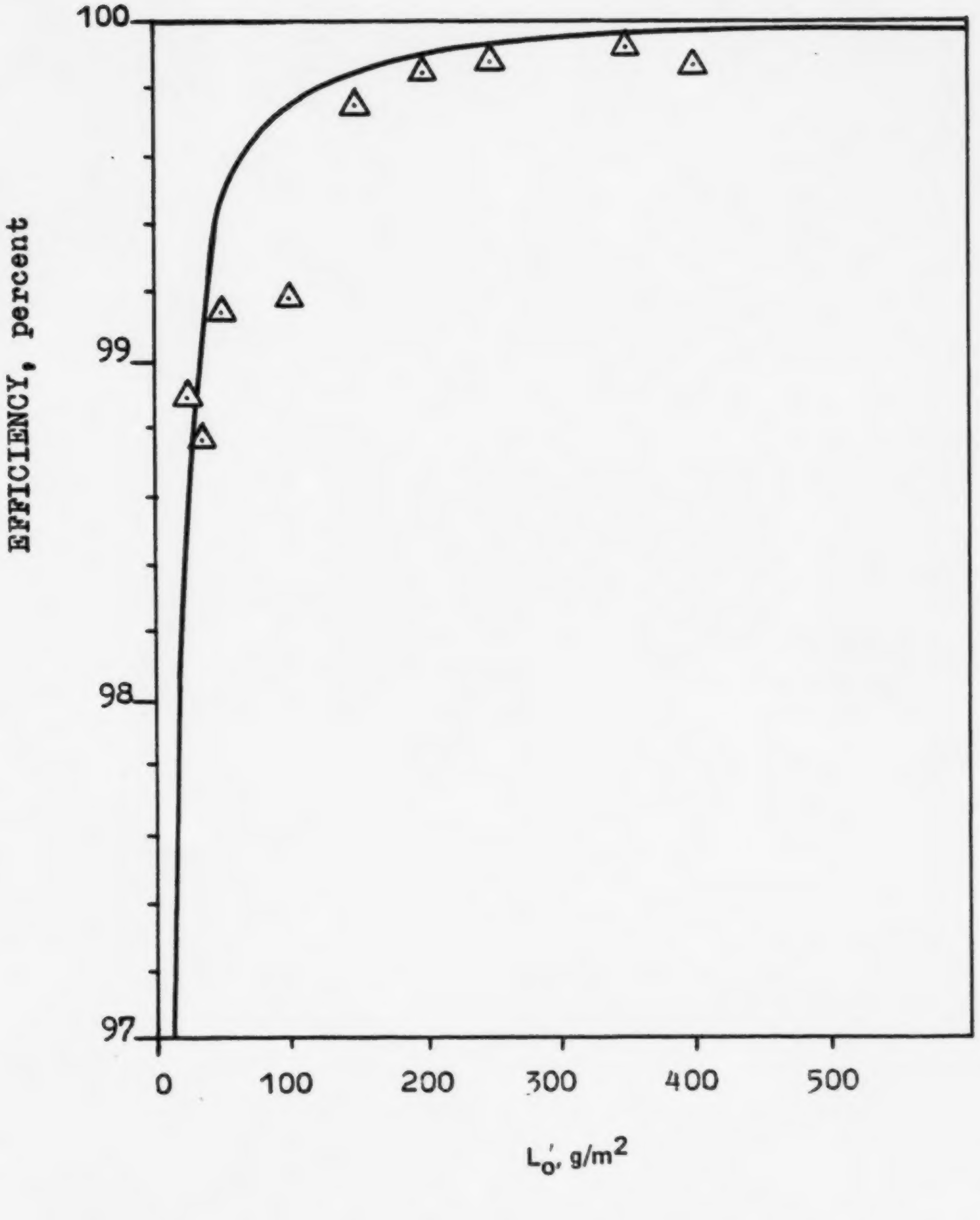

Figure 48. Predicted and experimental efficiencies of ET-4 as a function of L_o' for $q_g = 100\ m^3/m^2 \cdot h$.

113

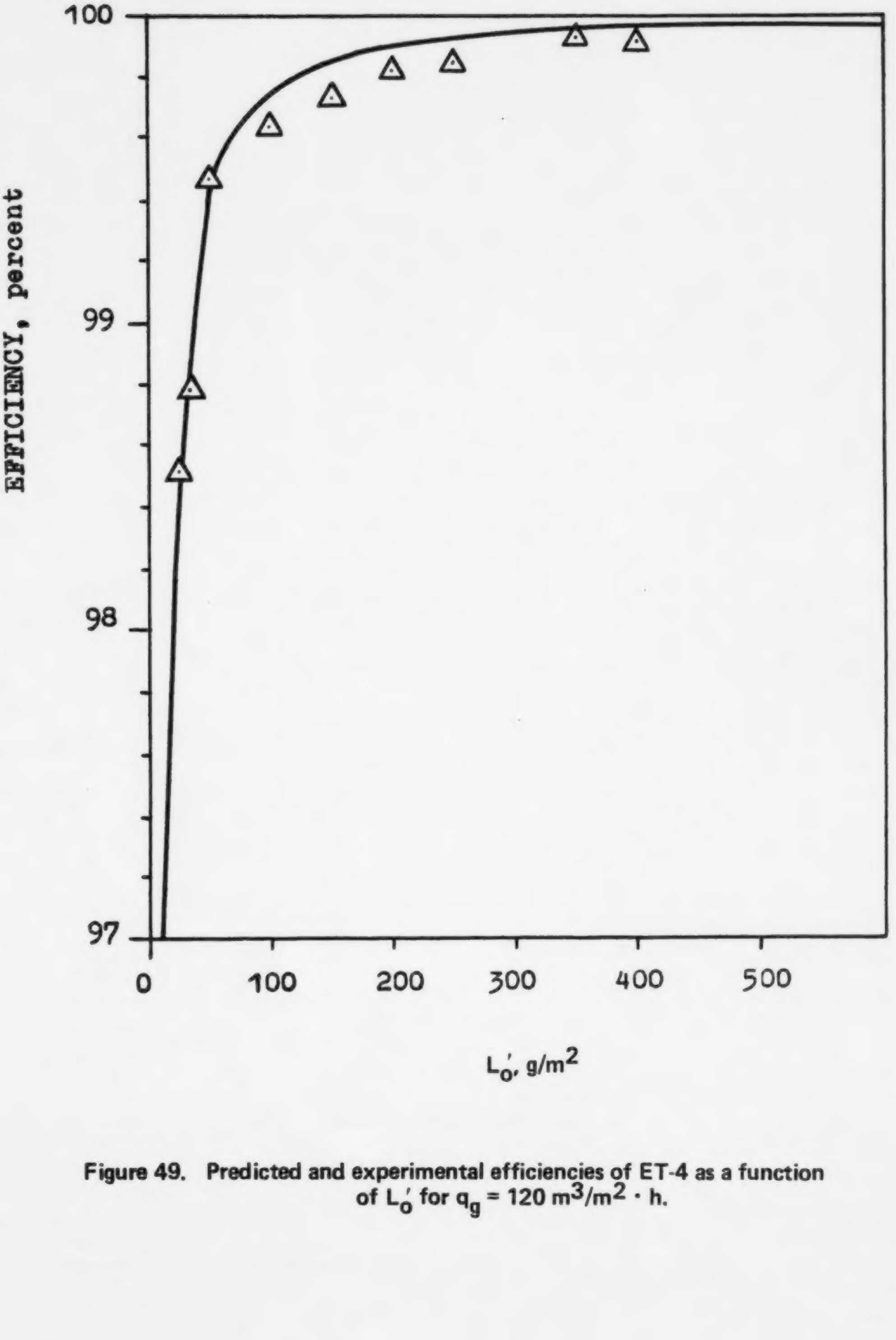

Figure 49. Predicted and experimental efficiencies of ET-4 as a function of L_o' for $q_g = 120\ m^3/m^2 \cdot h$.

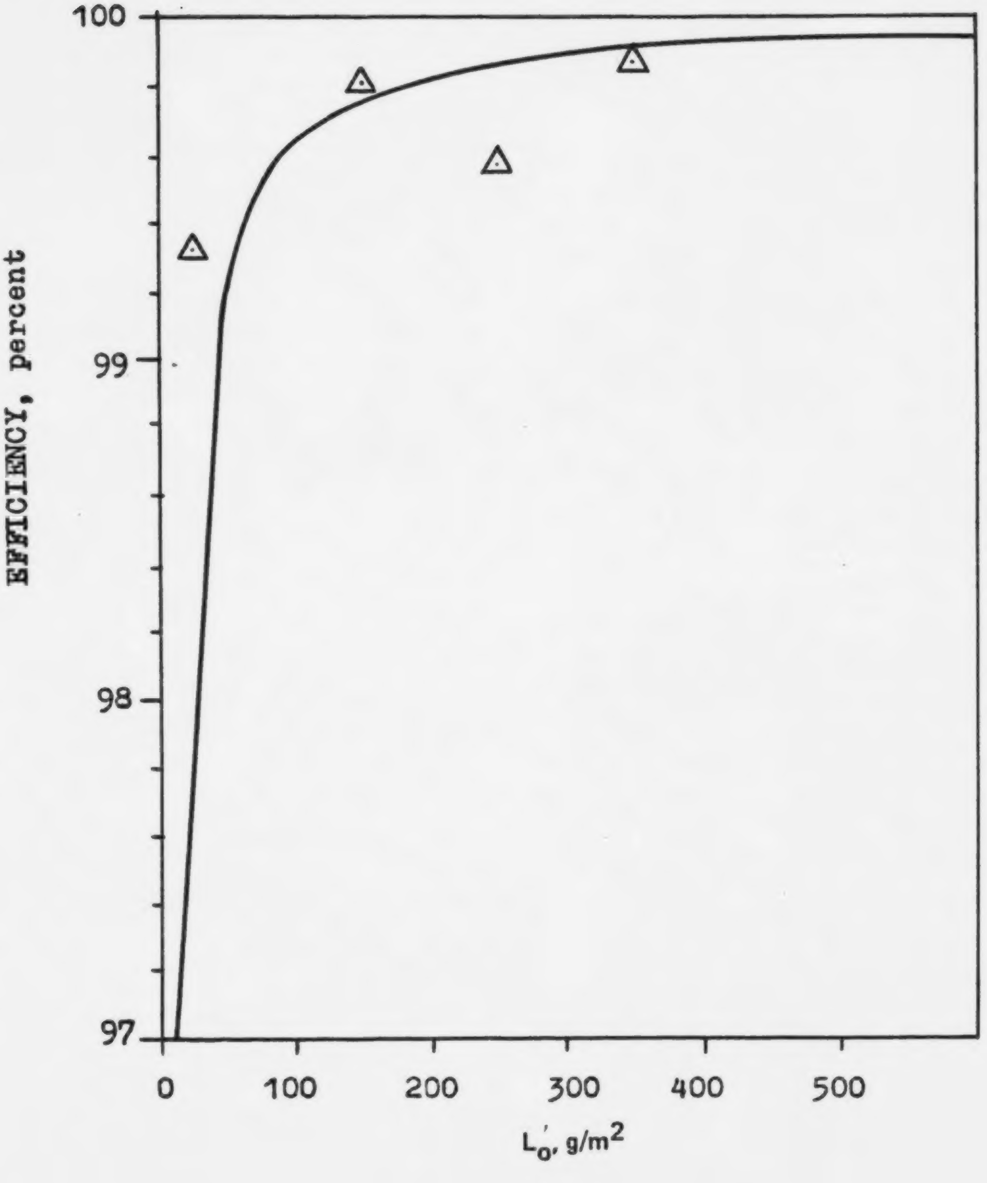

Figure 50. Predicted and experimental efficiencies of ET-4 as a function of L_o' for q_g = 140 m^3/m^2 · h.

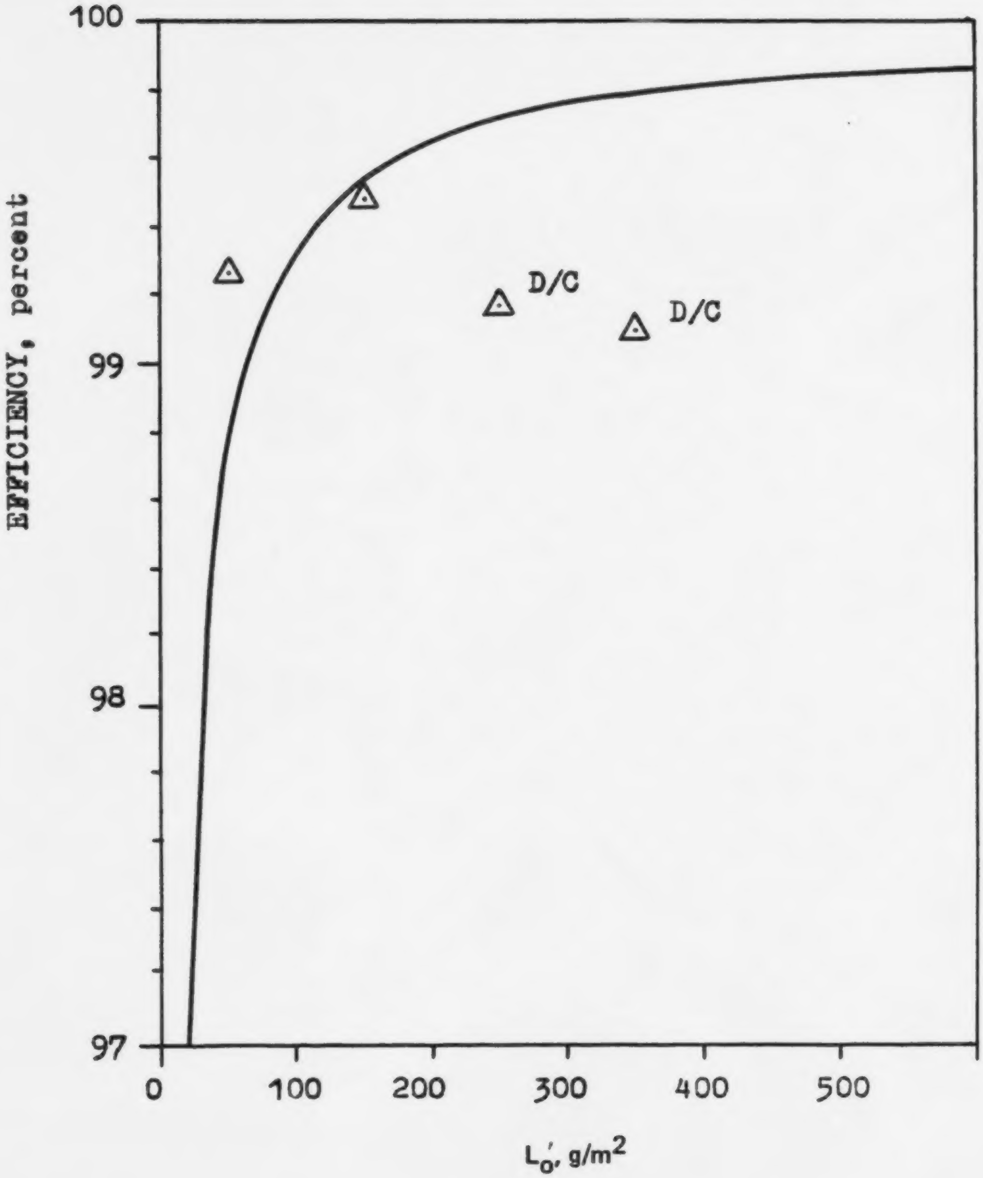

Figure 51. Predicted and experimental efficiencies of ET-4 as a function of L_o' for $q_g = 160\ m^3/m^2 \cdot h$.

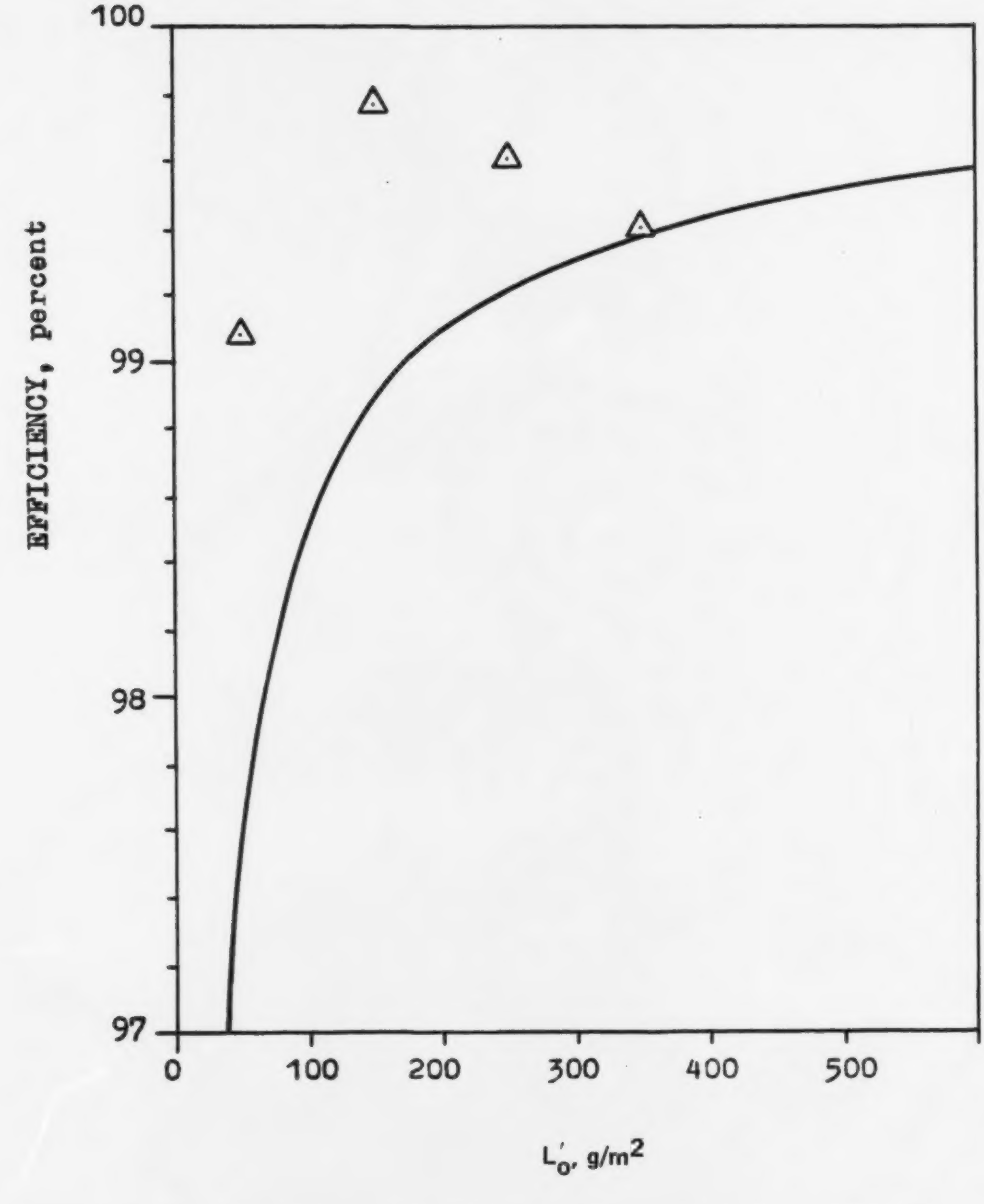

Figure 52. Predicted and experimental efficiencies of ET-4 as a function of L_o' for q_g = 180 $m^3/m^2 \cdot h$.

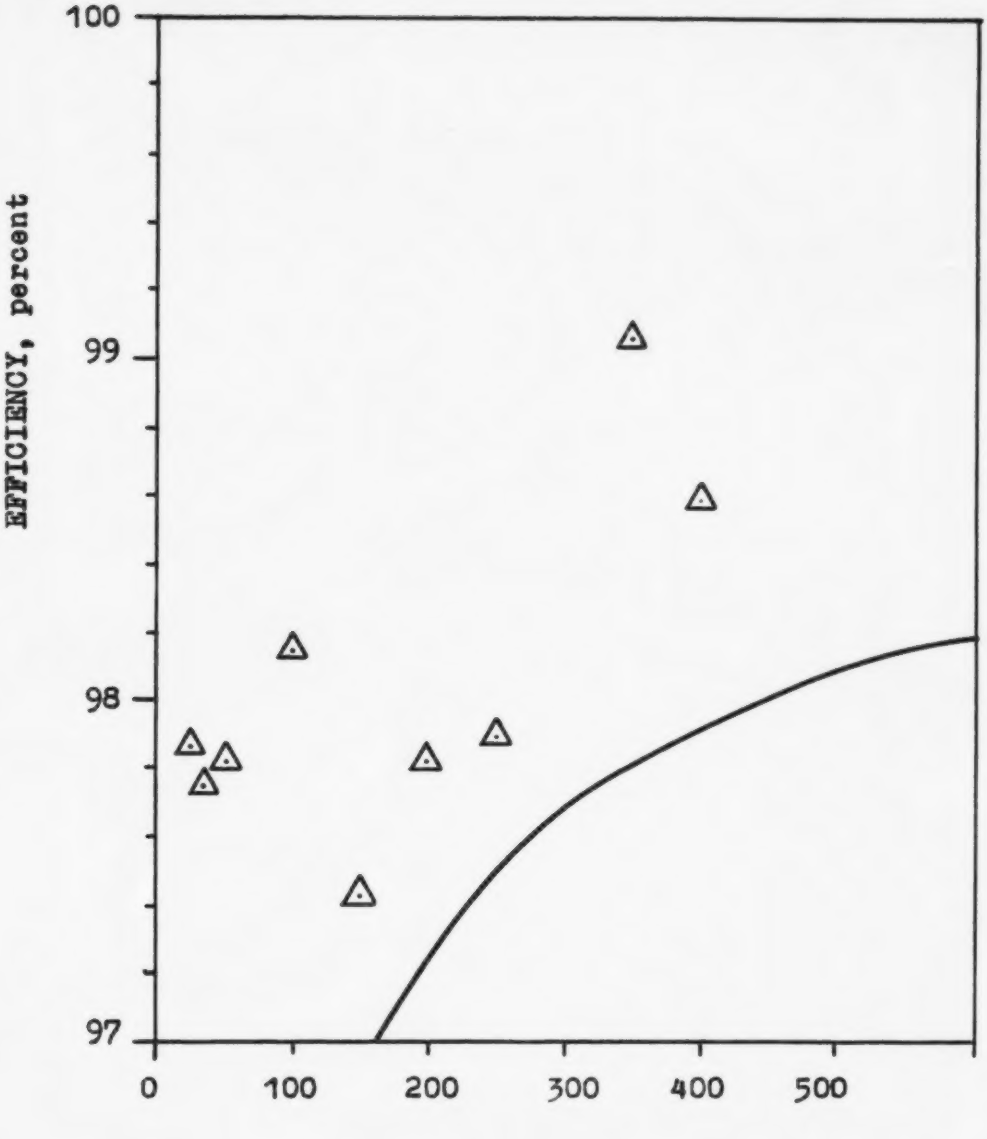

Figure 53. Predicted and experimental efficiencies of ET-4 as a function of L_o' for $q_g = 200$ m^3/m^2 · h.

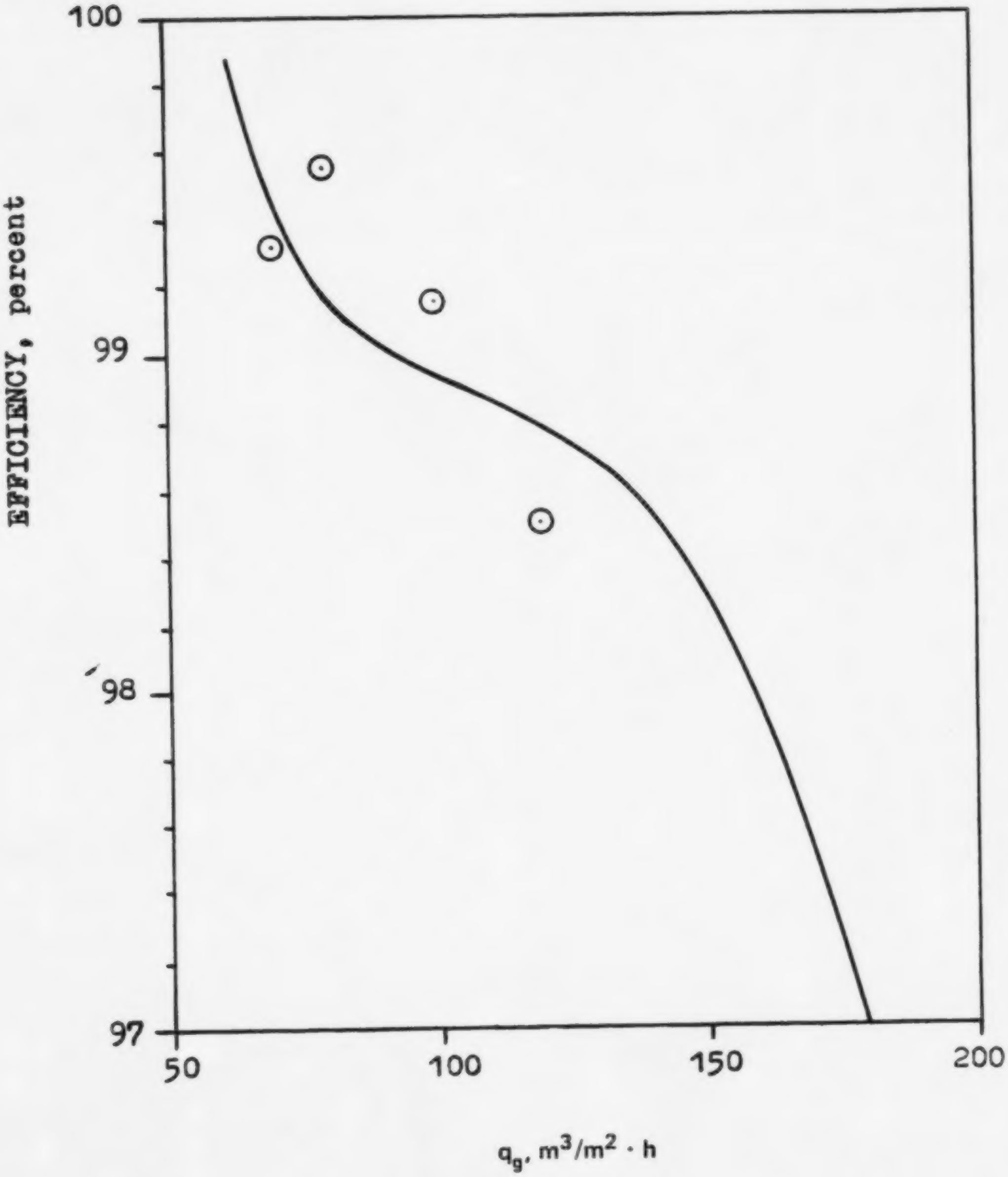

Figure 54. Predicted and experimental efficiencies of ET-30 as a function of q_g for average value of $L_o' = 25$ g/m^2.

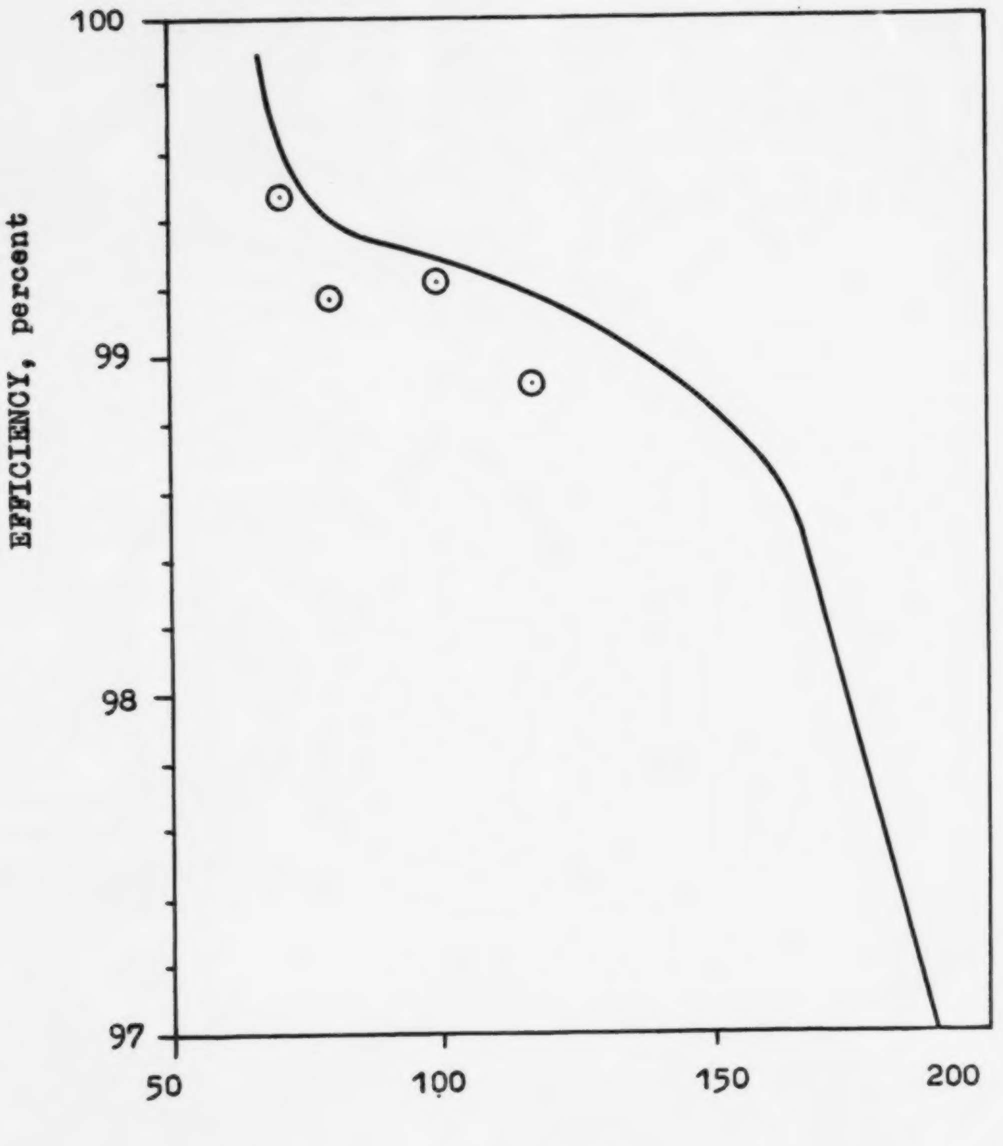

Figure 55. Predicted and experimental efficiencies of ET-30 as a function of q_g for average value of $L_o' = 35$ g/m^2.

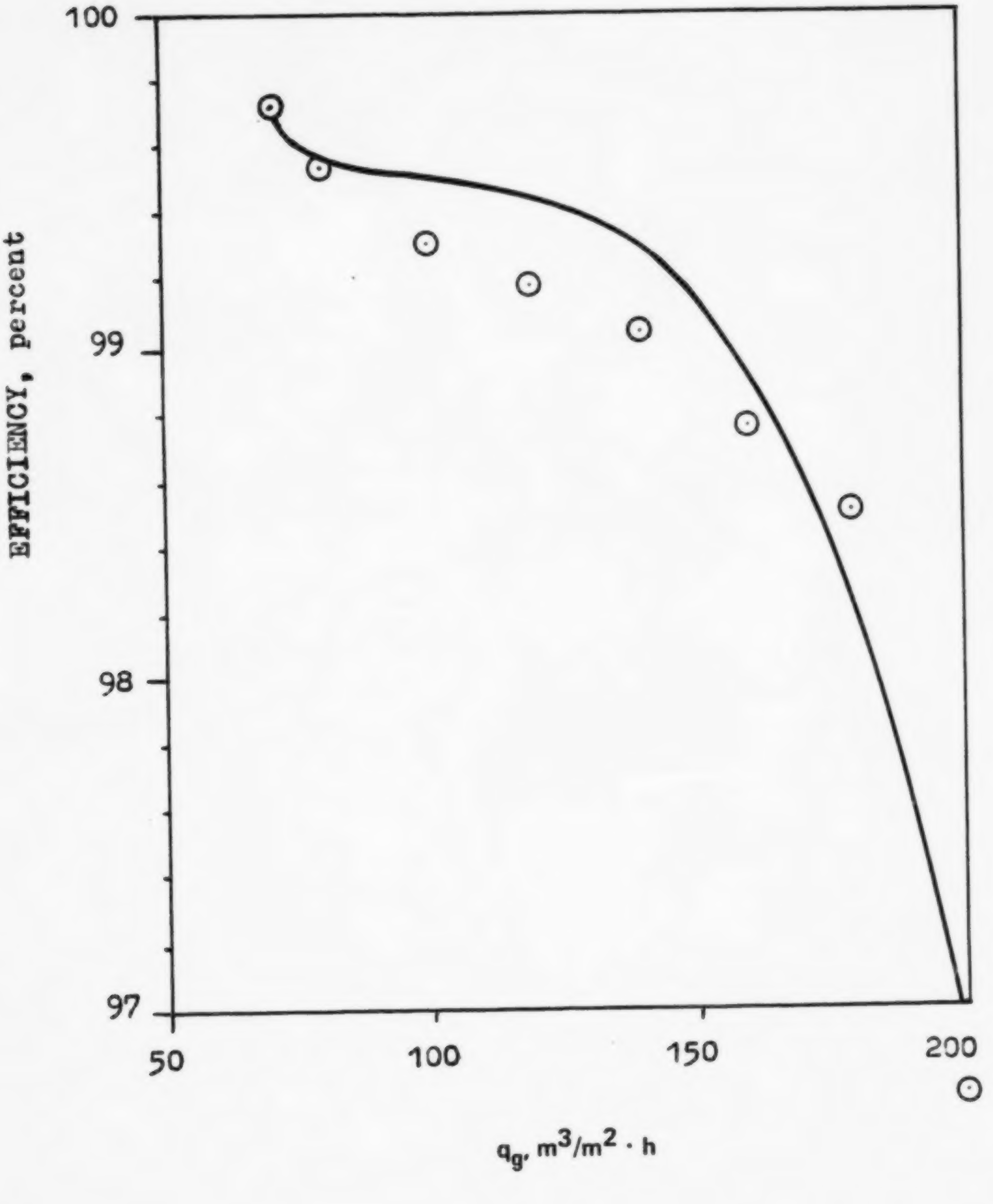

Figure 56. Predicted and experimental efficiencies of ET-30 as a function of q_g for average value of $L_o' = 50$ g/m^2.

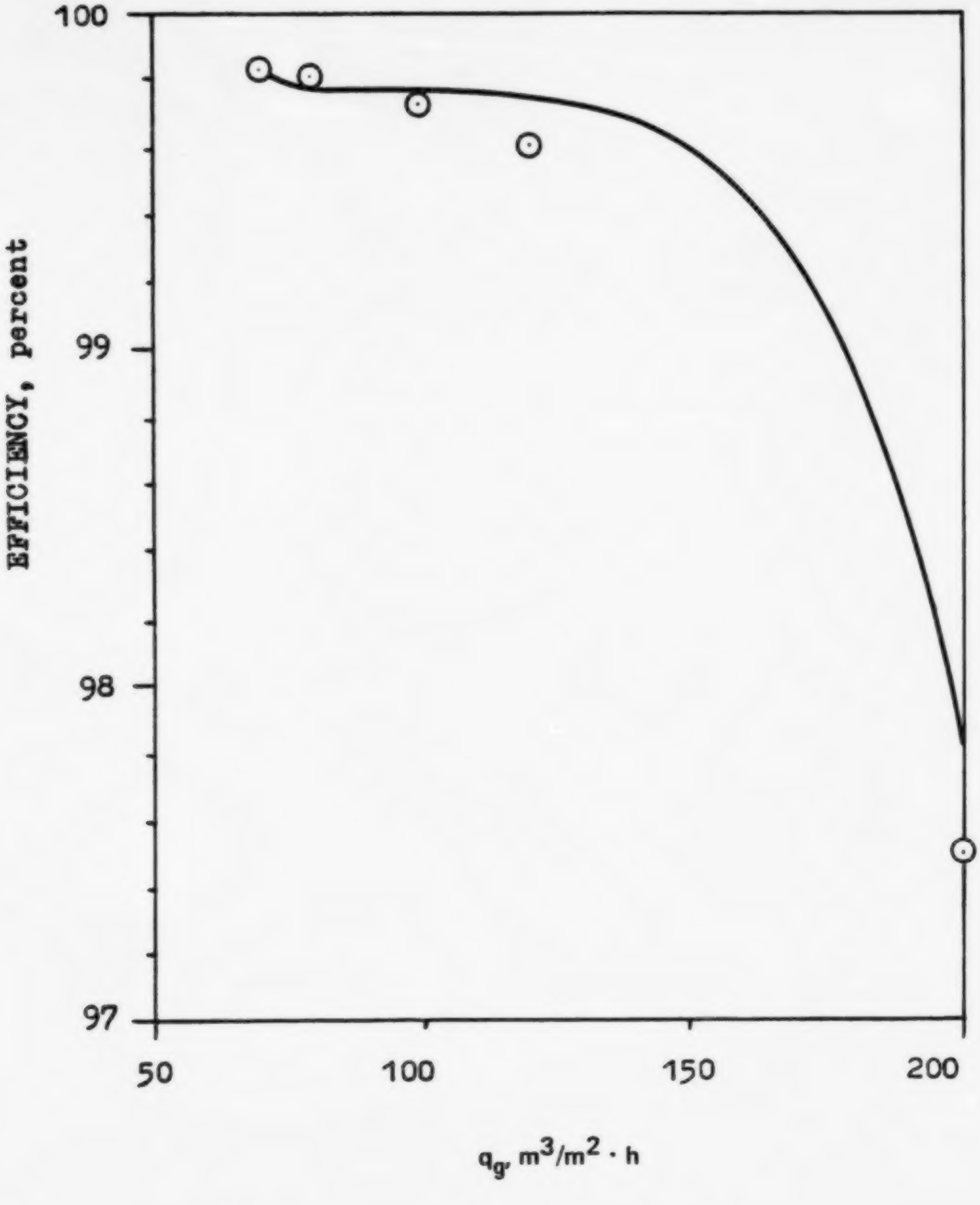

Figure 57. Predicted and experimental efficiencies of ET-30 as a function of q_g for average value of $L_o' = 100$ g/m^2.

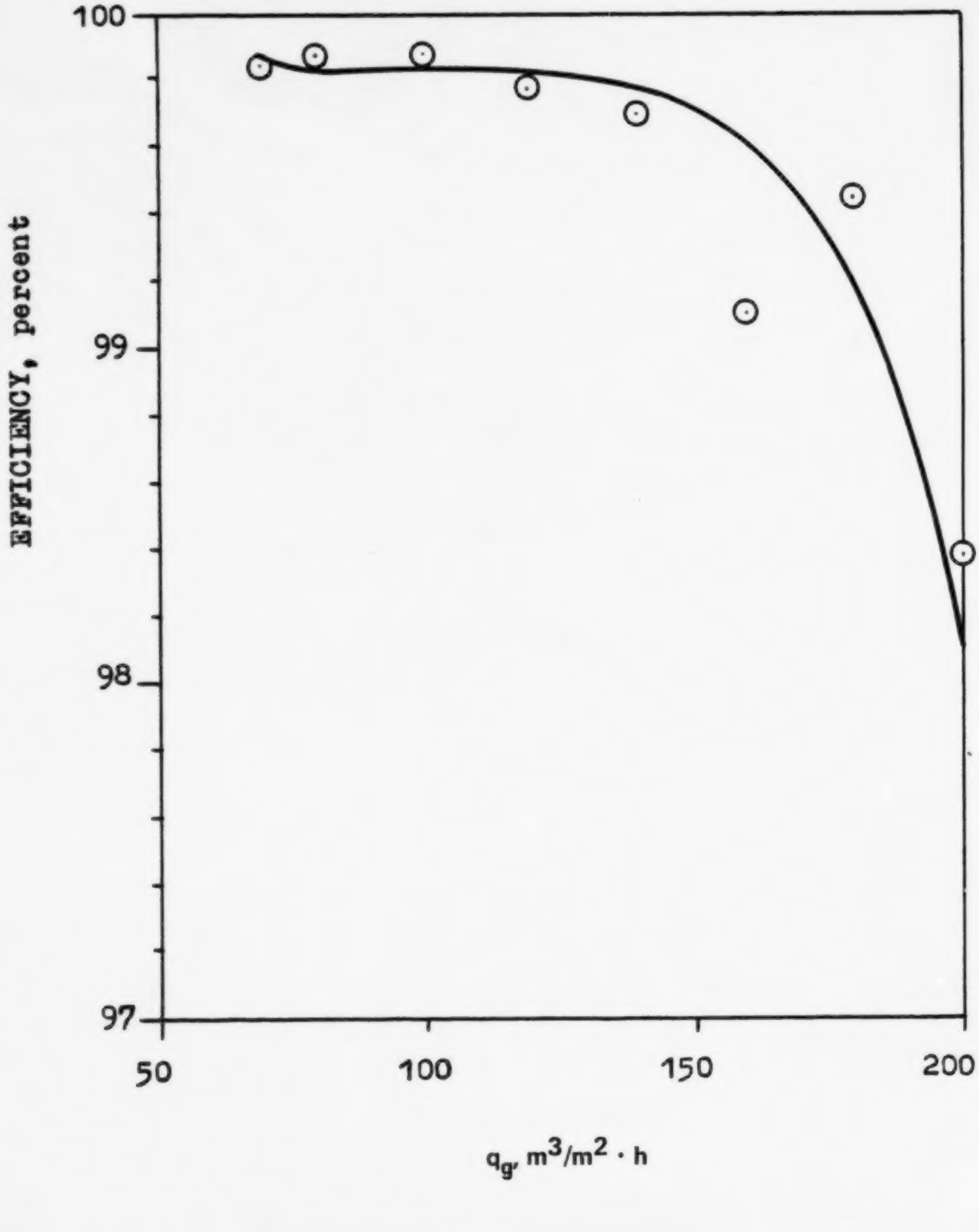

Figure 58. Predicted and experimental efficiencies of ET-30 as a function of q_g for average value of $L_o' = 150$ g/m^2.

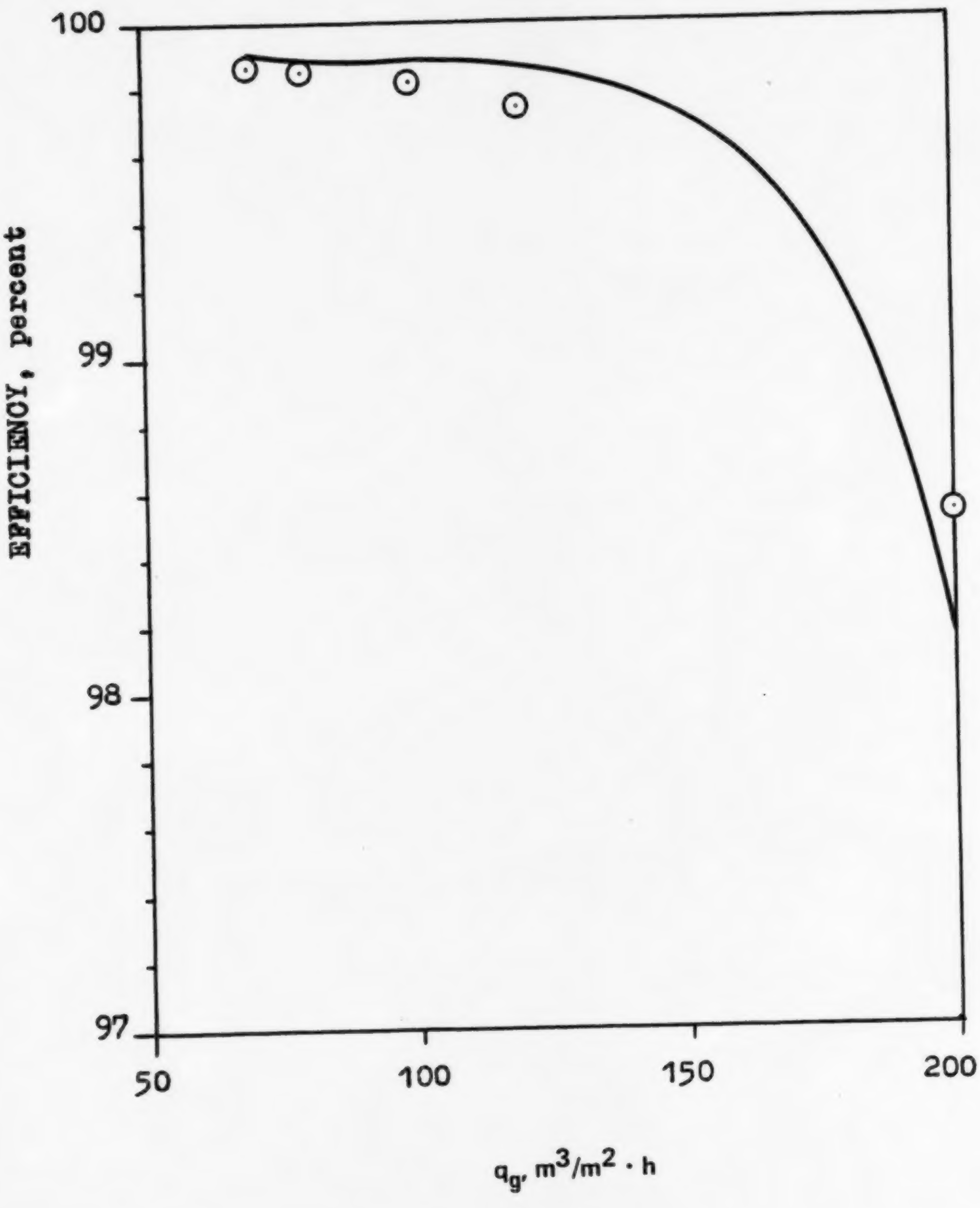

Figure 59. Predicted and experimental efficiencies of ET-30 as a function of q_g for average value of $L_o' = 200$ g/m^2.

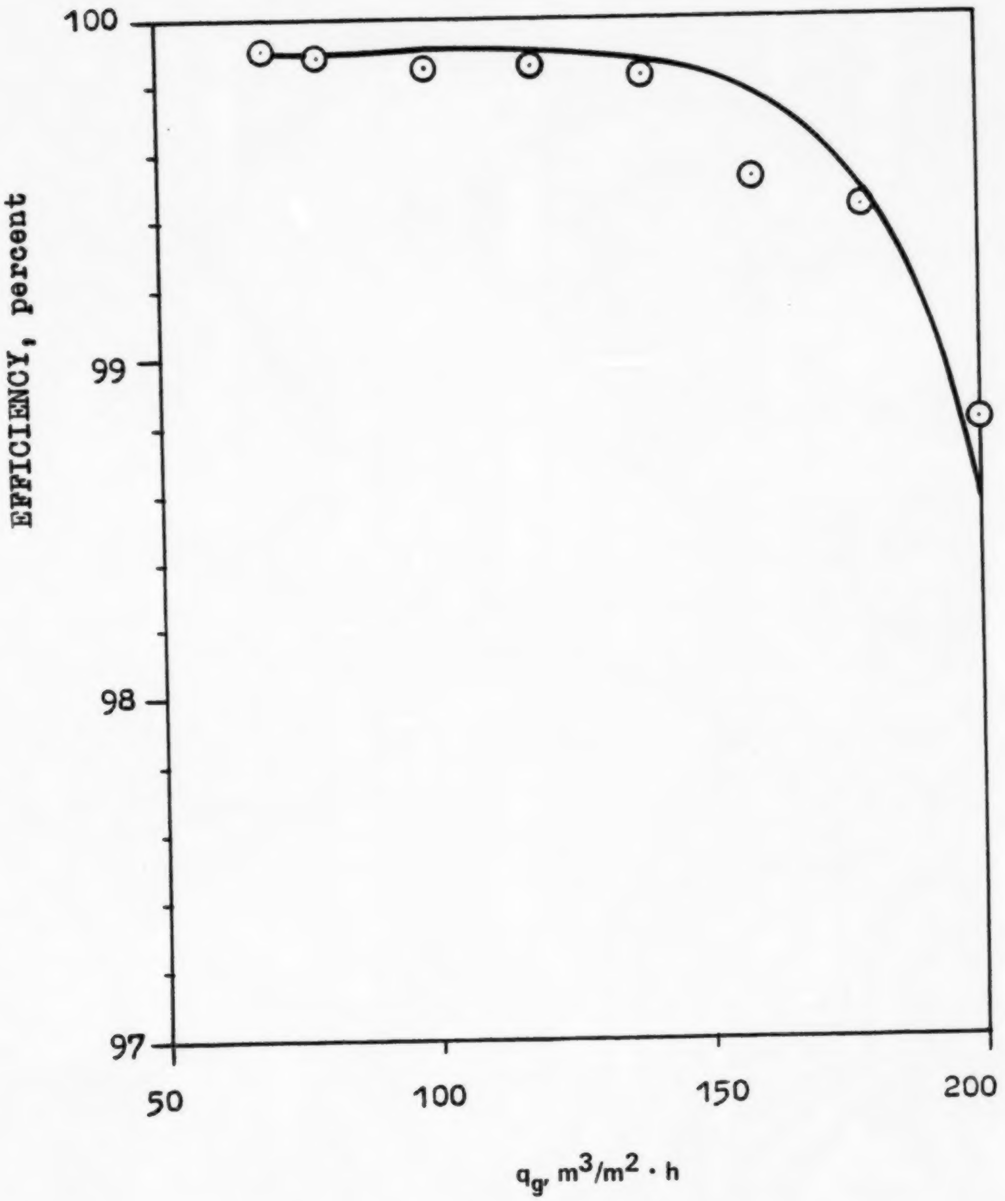

Figure 60. Predicted and experimental efficiencies of ET-30 as a function of q_g for average value of $L_o' = 250$ g/m^2.

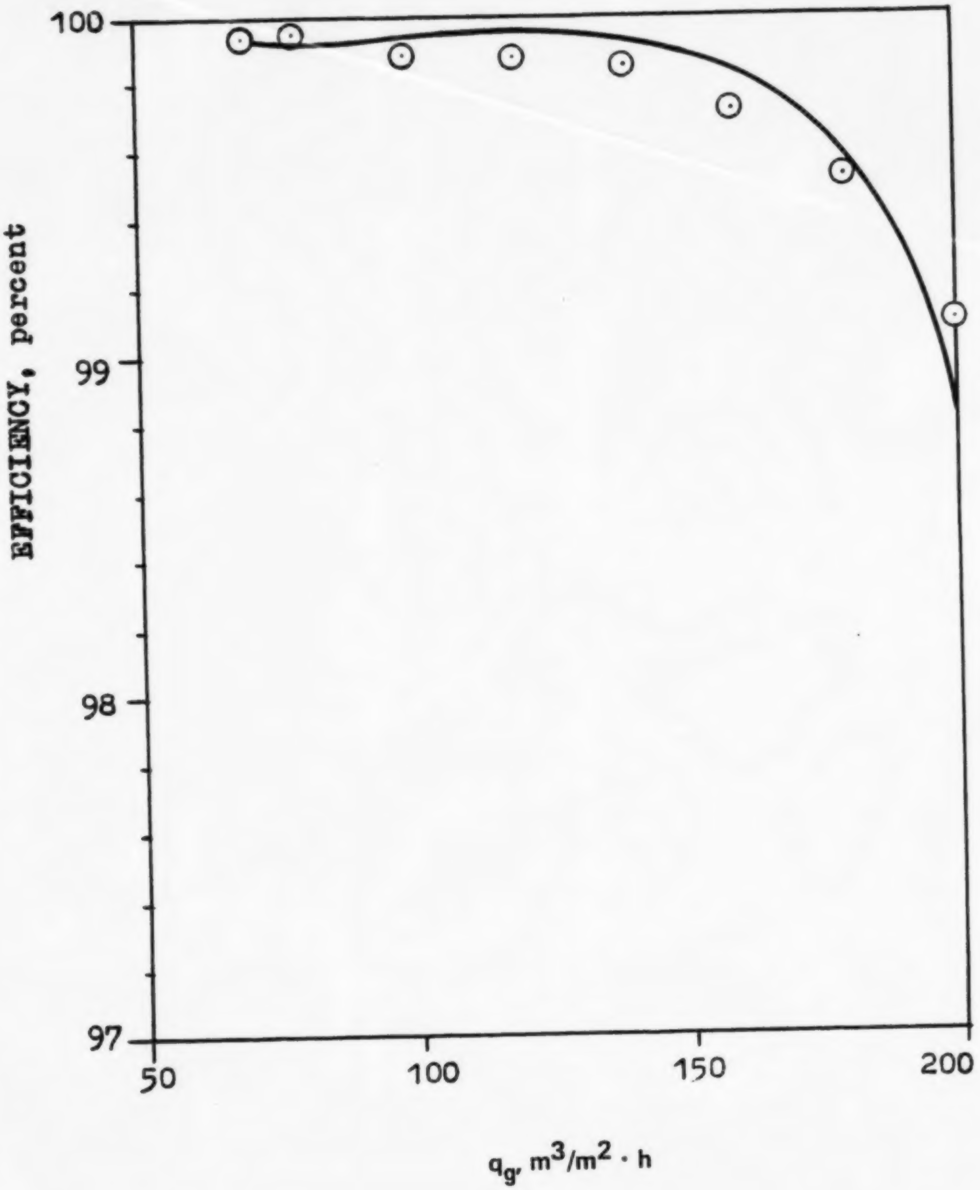

Figure 61. Predicted and experimental efficiencies of ET-30 as a function of q_g for average value of $L_o' = 350$ g/m^2.

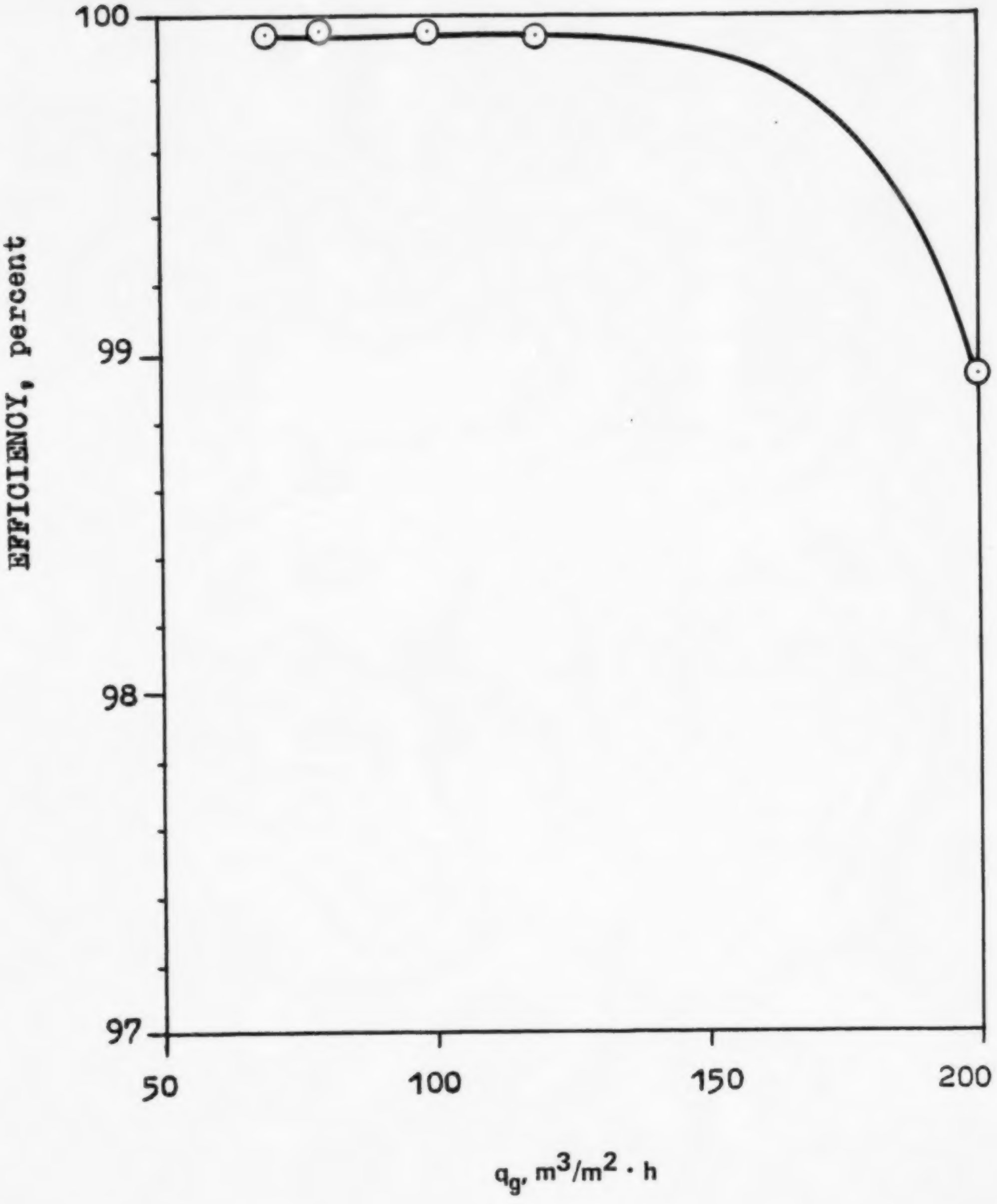

Figure 62. Predicted and experimental efficiencies of ET-30 as a function of q_g for average value of $L_o' = 400\ g/m^2$.

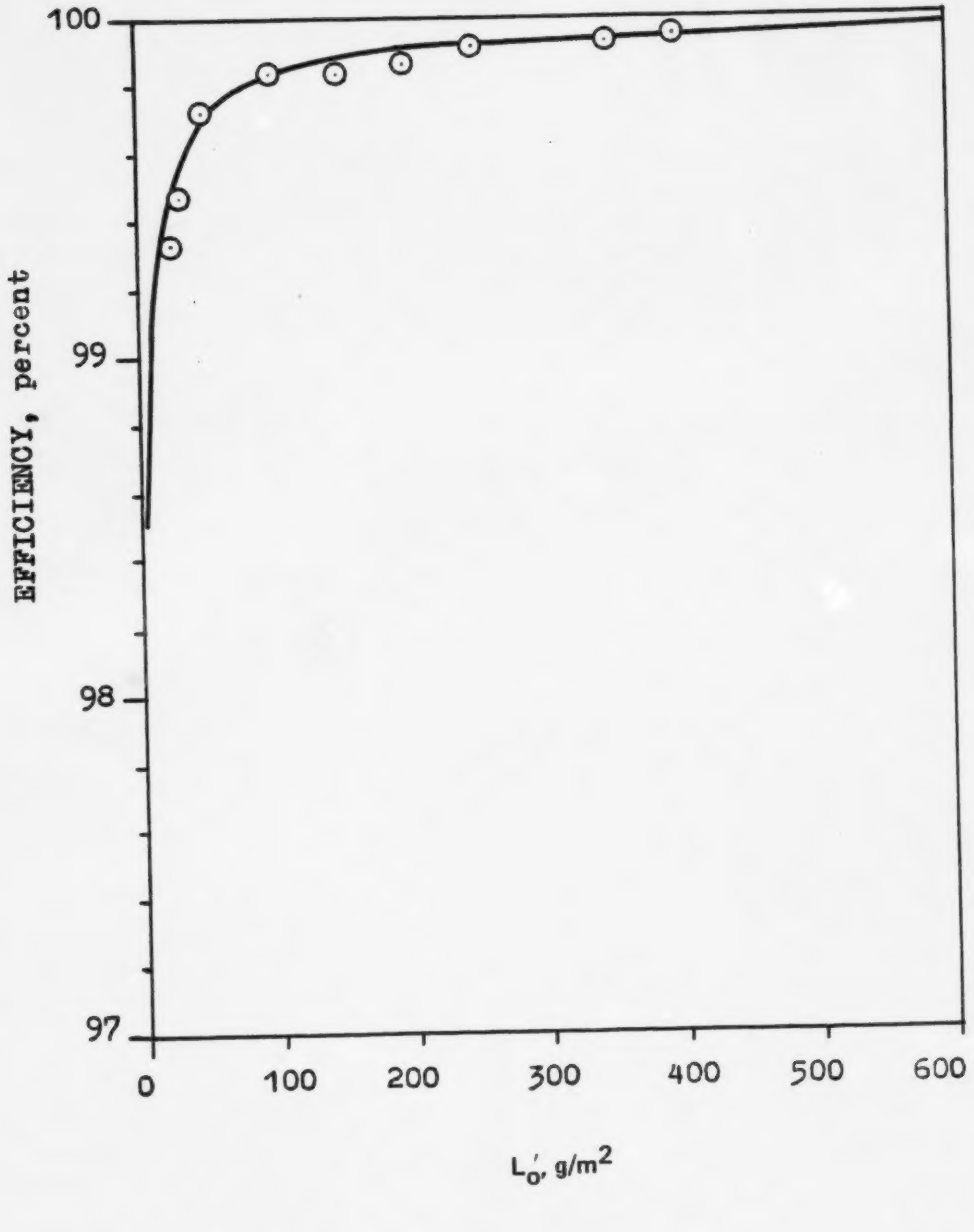

Figure 63. Predicted and experimental efficiencies of ET-30 as a function of L_o' for $q_g = 70\ m^3/m^2 \cdot h$.

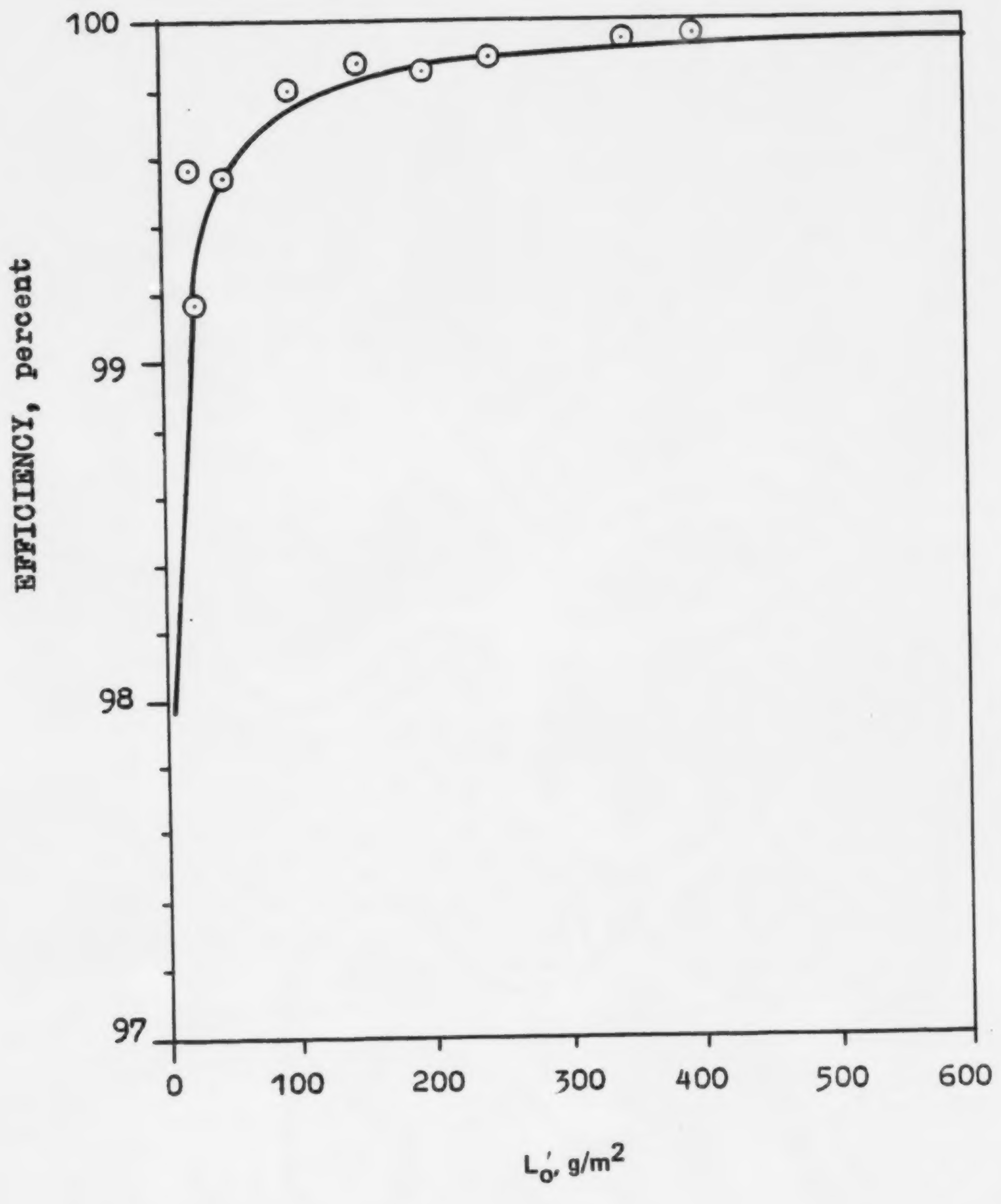

Figure 64. Predicted and experimental efficiencies of ET-30 as a function of L_o' for $q_g = 80\ m^3/m^2 \cdot h$.

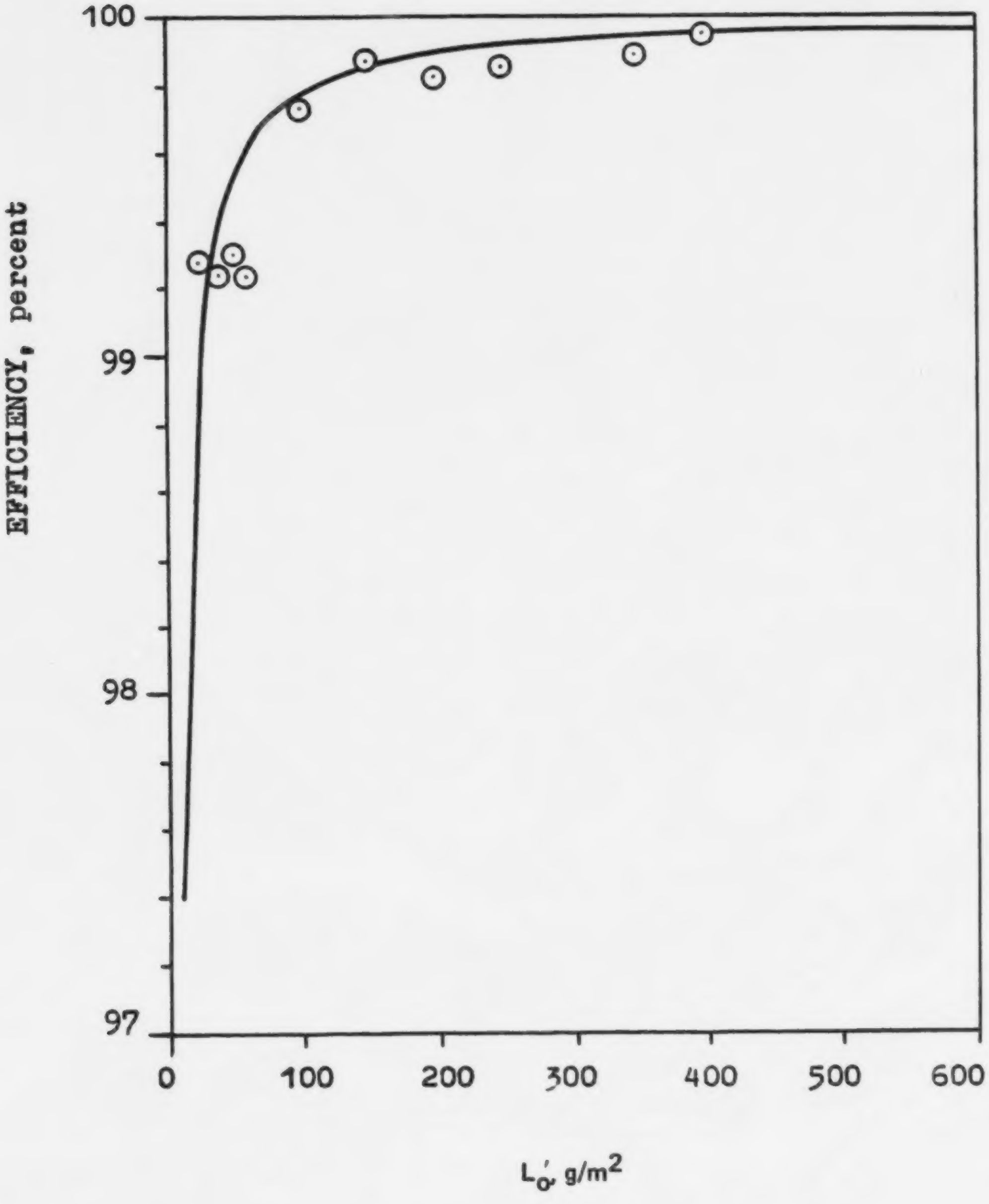

Figure 65. Predicted and experimental efficiencies of ET-30 as a function of L_o' for $q_g = 100$ m^3/m^2 · h.

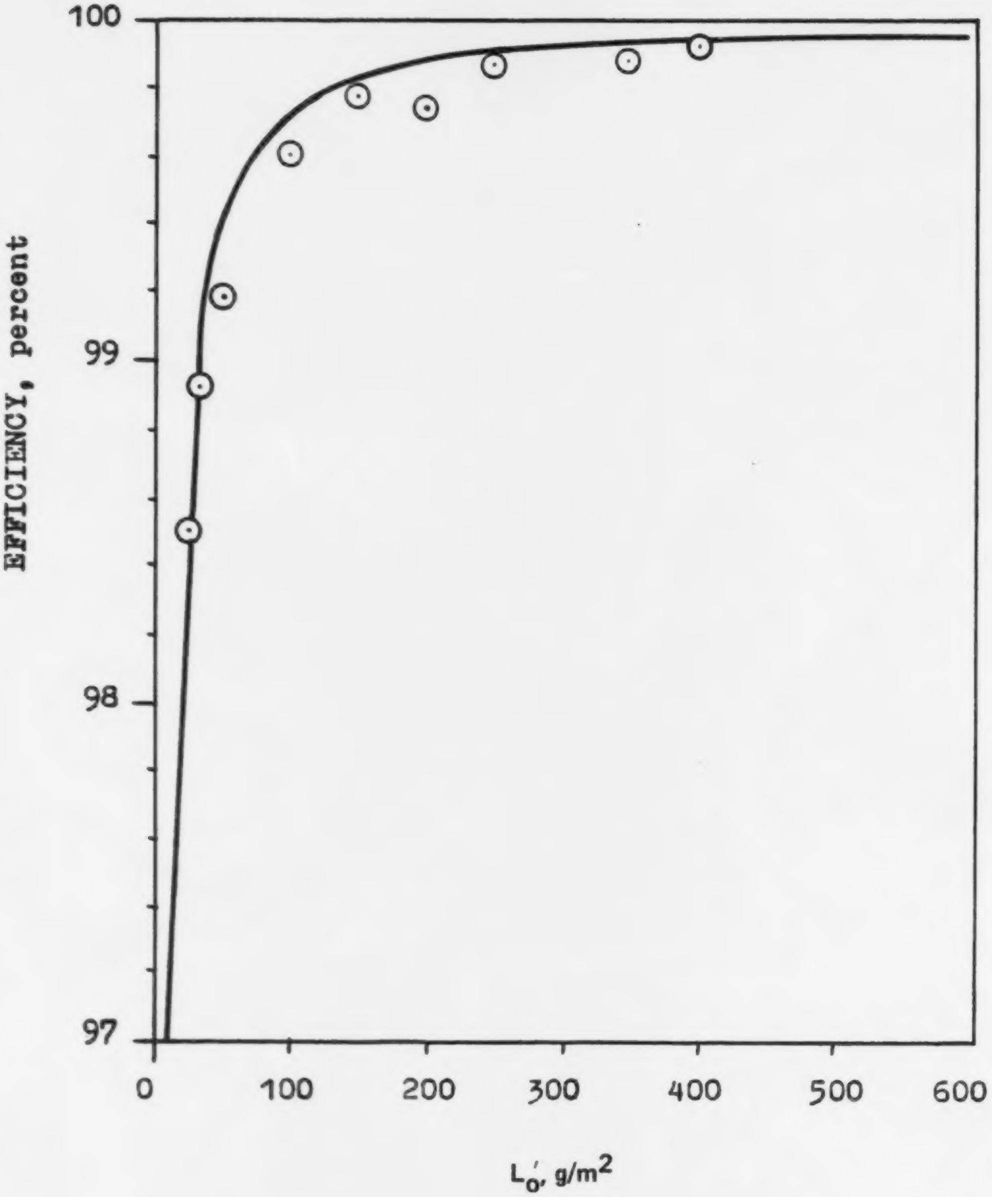

Figure 66. Predicted and experimental efficiencies of ET-30 as a function of L_o' for $q_g = 120\ m^3/m^2 \cdot h$.

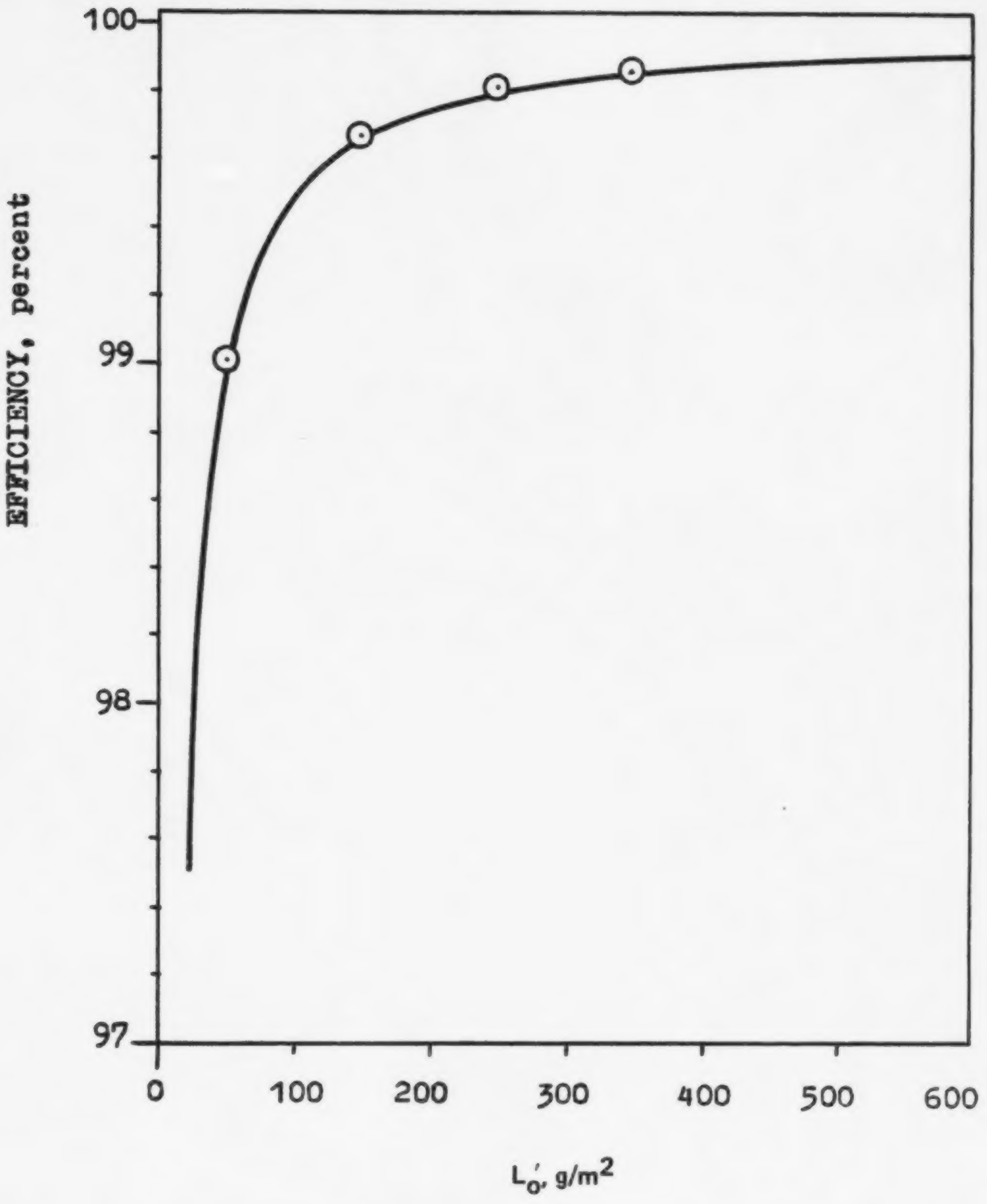

Figure 67. Predicted and experimental efficiencies of ET-30 as a function of L_o' for $q_g = 140$ m^3/m^2 · h.

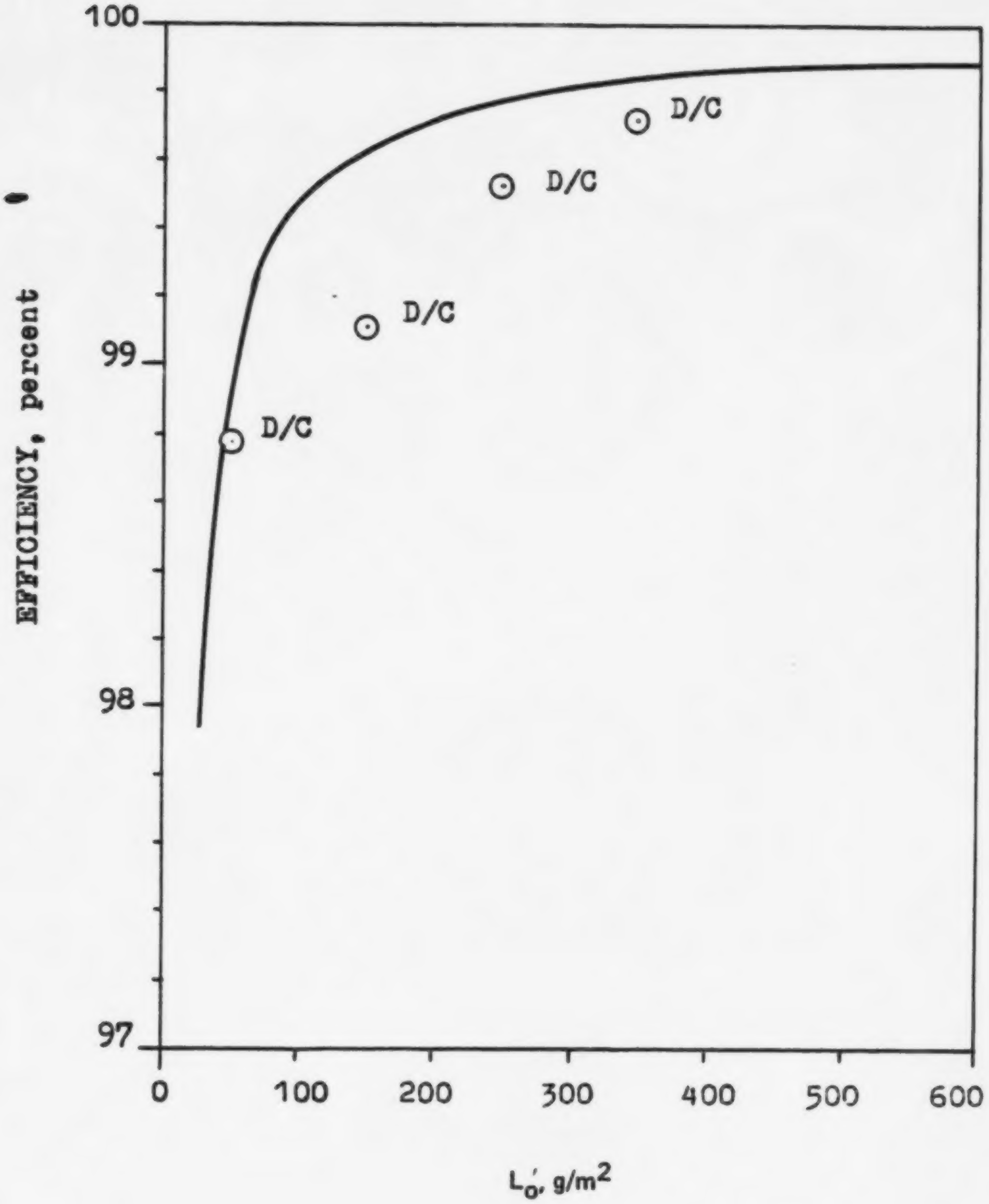

Figure 68. Predicted and experimental efficiencies of ET-30 as a function of L_o' for $q_g = 160\ m^3/m^2 \cdot h$.

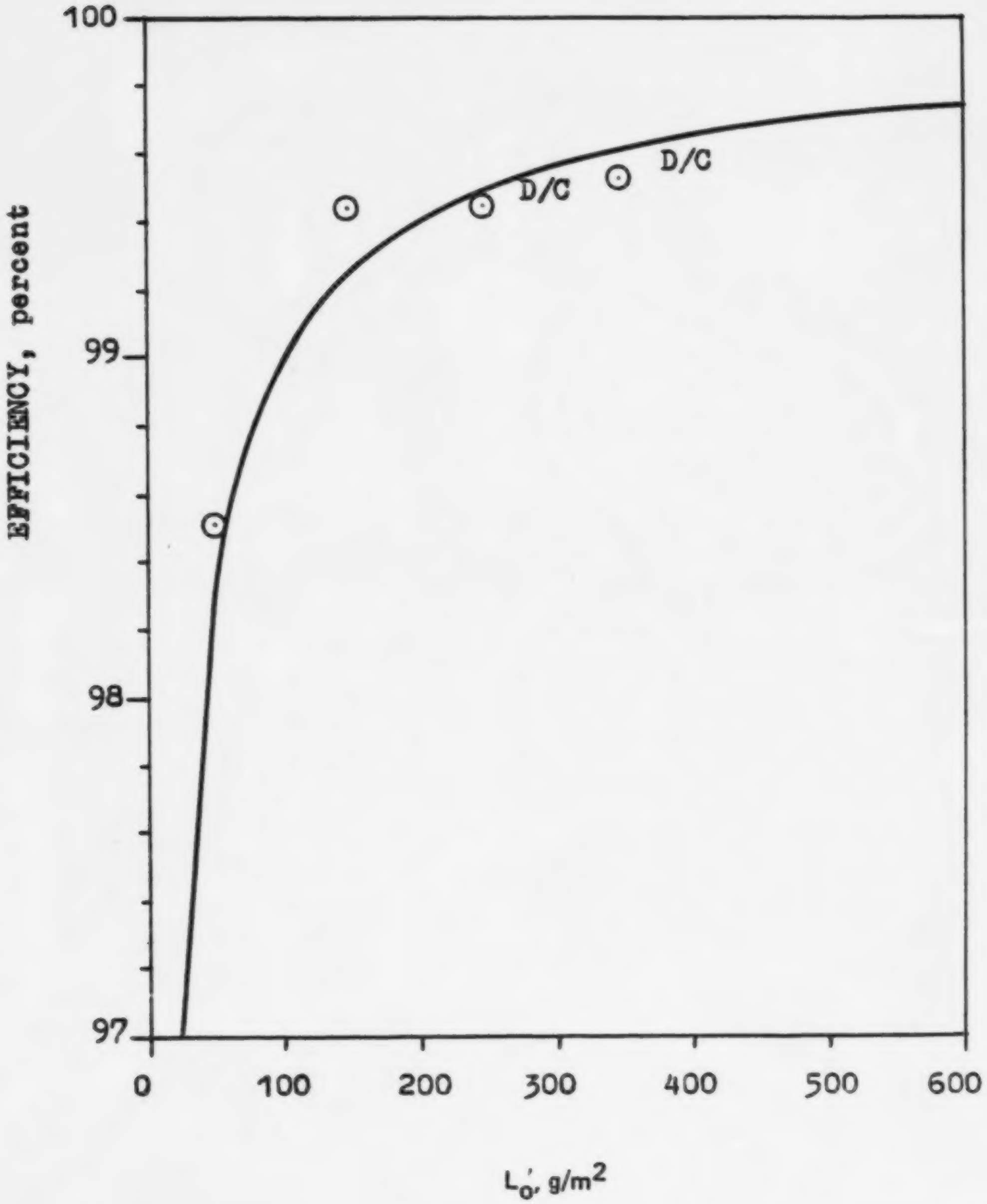

Figure 69. Predicted and experimental efficiencies of ET-30 as a function of L_o' for q_g = 180 m^3/m^2 · h.

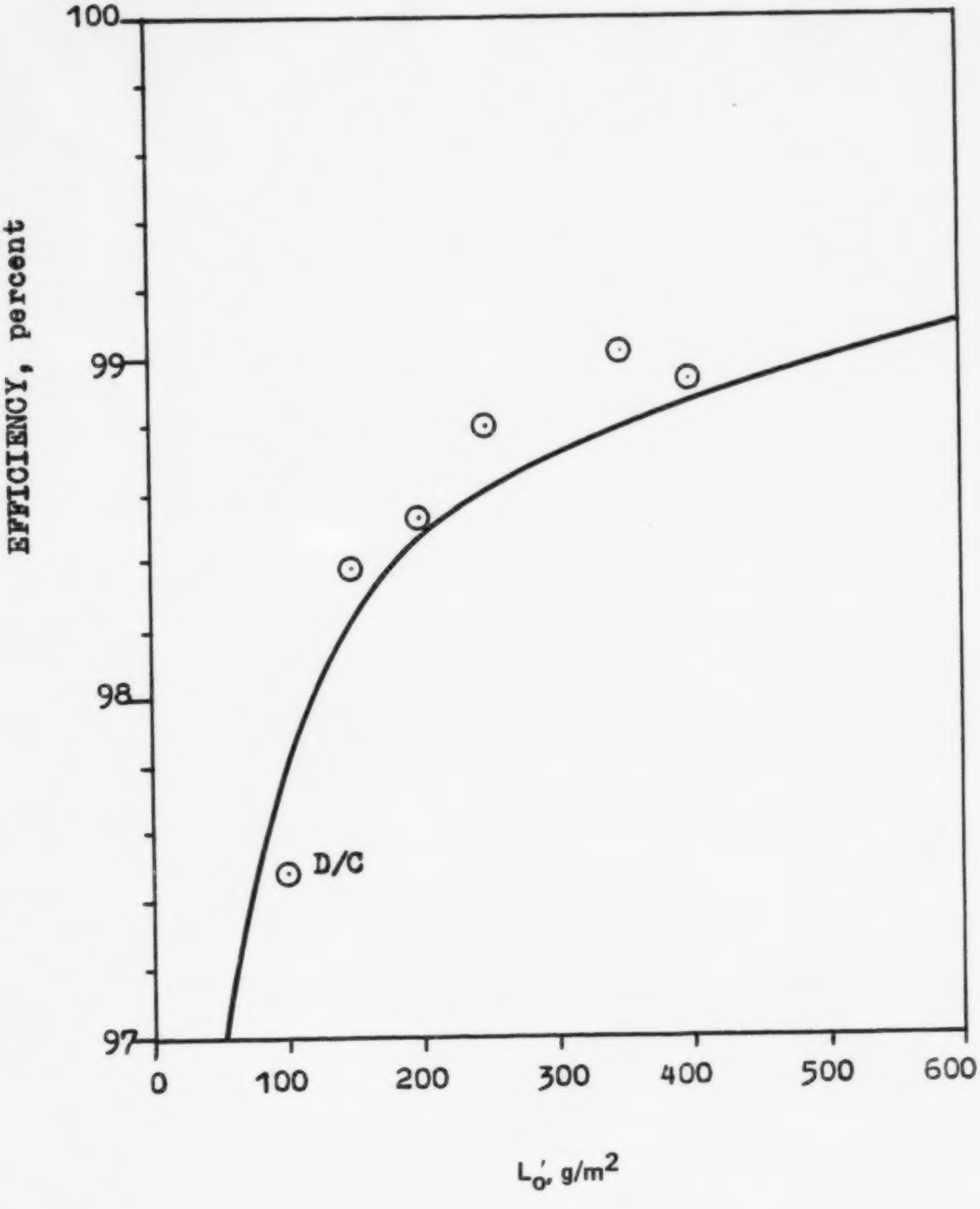

Figure 70. Predicted and experimental efficiencies of ET-30 as a function of L_o' for $q_g = 200\ m^3/m^2 \cdot h$.

However, the shape of the dust collection efficiency curve as a function of q_g differed for fabric ET-4 and fabric ET-30. Equation $E_I = f(q_g)$ for fabric ET-4 apparently has a maximum in the range of $q_g = 80$ to 120 m^3/m^2h, made especially clear at low values of L_o. Curve $E_I = f(q_g)$ for fabric ET-30 has no maximum, but rather an inflection point at $q_g \cong 80$ m^3/m^2h. From this point, dust collection efficiency decreases rapidly as values of q_g increase.

Assuming the existence of a minimum dust collection efficiency, $E_{I\ min}$, it is possible, based on the model, to determine a maximum q_g value for each level of L_o, at which E_I still exceeds $E_{I\ min}$. Table 10 includes q_g values for an assumed level of $E_{I\ min} = 99.8$ percent. Fabric ET-4 first achieves dust collection efficiency greater than $E_{I\ min}$, at a terminal dust load, L_o = 150 g/m^2 in the range of $q_g = 70$ to 130 m^3/m^2h. Fabric ET-30 achieves efficiency above $E_{I\ min}$ for all examined levels of dust covering, and with increasing L_o, the range of q_g over which $E_I \geq E_{I\ min}$ increases slightly. Data compiled in Table 10 show the effect of the filtration material structure on the external parameters of the process (E_I and ΔP_F).

Fabric ET-4 is more porous than fabric ET-30 (Table 1), so it needs more time to build a dust cake sufficiently thick to achieve higher efficiencies. The behavior of fabric ET-4 confirms theoretical deliberations previously presented concerning the effect of superficial porosity of the filtration material on Dust Filtration Process Type I performance.

Examinations of the fractional efficiency for both filtration materials, conducted at low values of dust covering, would probably show a decreased dust collection efficiency for almost the entire range of grain diameters for fabric ET-4. But for fabric ET-30, the collection efficiency at a certain grain diameter might be nearly 100 percent. Until fabric ET-4 reaches L_o = 150 g/m^2, it operates at lower efficiency than $E_{I\ min}$, which results in lower average dust collection efficiency over the filtration cycle. Therefore, the duration of the filtration cycle and the time needed for reaching a certain average dust load, $\bar{L}_o$, also influence the average dust collection efficiency in the filtration cycle. At the time assumed for the filtration cycle only the time needed for reaching a certain $\bar{L}_o$ (at which $E_I = E_{I\ min}$) influences the average dust collection efficiency. For a given filtration material, this time depends on the dust flux, $q_p = q_g \cdot c_1$, g/m^2h, describing a specific

TABLE 10. VALUES OF FACE VELOCITY CORRESPONDING TO E_{MIN}

Kind of fabric	Mean values of dust covering, $\bar{L}_o$ (g/m^2)	Value of face velocity that corresponds to $E_{I\ min}$ = 99.8	
		Above	Below
ET-4	25	-	-
	35	-	-
	50	-	-
	100	-	-
	150	70	130
	200		145
	250		150
	350		160
	400		162
ET-30	25		60
	35		65
	50		65
	100		75
	150		120
	200		135
	250		155
	350		160
	400		165

dust stream upstream of the filtration structure. Because c_1 is usually fixed, the only variable parameter is q_g.

In the first period of filtration (low L_o) the efficiency of fabric ET-4 depends only slightly on q_g (in the range of 60 to 140 m^3m^2h). But after L_o = 150 g/m^2 is achieved, a limiting value of q_g is noticeable, characteristic of this fabric and shown by the model.

Fabric ET-30 has different, more advantageous qualities than fabric ET-4. Operating fabric ET-30 below $q_g = 60\ m^3/m^2h$ permits an average filtration efficiency greater than $E_{I\ min}$ to be achieved over almost the entire range of applied dust loads.

The model allows not only a determination of the dust collection efficiency during any period of Dust Filtration Process Type I but also the characterization of the properties of the filtration material structure.

The variations of the equation, $E_I = f(\bar{L}_o)$, contained in Figures 45 through 53 and 63 through 70 for each level of q_g are in accordance with the results of this project and others. These variations show increased efficiency with increased dust loads. Good agreement exists between the model and the experiments. Some disagreement at higher levels of q_g was caused by the use of high q_g experimental data, which resulted in modification of $F_1(q_g)$ and $F_2(q_g)$ (see Figure 34 and Figure 35).

When the relationship, $E_I = f(\bar{L}_o)$, is analyzed over different ranges of q_g, the hypothesized effect of q_g on the dust cake structure is confirmed. If the measurement results at which dust cake defects were observed are avoided (causing a decrease in dust collection efficiency), the efficiency decrease with increasing q_g (over all ranges of L_o) leads to the conclusion that the dust cake structure at high values of q_g is characterized by higher spatial and superficial porosity. This higher porosity can be caused by gas flow disturbance through the filtration structure, which results from the occurrence of microcanals of higher effective pore diameters than those from the particle size distribution alone. Alternatively, the force distribution in the dust cake structure may cause fluidization. Confirmation of this hypothesis requires additional, detailed examinations.

The preceding discussion of the effect of basic filtration parameters on dust collection efficiency in Dust Filtration Process Type I results in the following conclusions:

- An increase of terminal dust load, L_o, improves dust collection efficiency over all ranges of q_g.
- An increase of q_g decreases dust collection efficiency in Dust Filtration Process Type I.
- Two levels of q_g can be distinguished in this process, according to value $q_{g\ extr}$, which is a characteristic of a specific dust-fabric system. The first range, at values of $q_g < q_{g\ extr}$, is characterized by either an increase or a very small decrease in dust collection efficiency as a function of increasing q_g and by the absence of defects in the dust cake structure. The second range, at values of $q_g > q_{g\ extr}$, is characterized by a rapid decrease in dust collection efficiency with increasing q_g, resulting from increased dust cake porosity until defects appear. Dust filtration in the first range can be regarded as classical because of the dependence of E_I upon L_o.

The object of interest during the overall research program was the determination of the degree of dust filling of fabrics ET-4 and ET-30 during a single laboratory test cycle. After each experimental run, the single-dusted sample was cleaned manually in a standardized manner and reused. A wide range of empirical material was obtained, shown in Figures 71 and 72.

Each point on the plot is an average of five measurements made for a given q_g and L_o (filtration time, because c_1 = constant). At short filtration times the points are scattered, but for lengthy filtration times they tend to equal L_N = 28 g/m^2 to 30 g/m^2. It is interesting that this value of L_N is similar for both fabrics despite the fact that the fabrics are differently structured. Differences in $L_N = f(t_F)$ are clear for $q_g > 120$ m^3/m^{2}h. The filling of the more porous structure (ET-4) reaches maximum values for $q_g = 140$ to 180 m^3/m^{2}h, while in the case of the more packed structure (ET-30), the filling curves are ordered according to increasing q_g. Because the equation, $L_N = f(t_F)$, is not precise and because the measured values of L_N are lower than those for structures dusted several times to a state of equilibrium, these L_N values cannot presently be interpreted more completely.

The conclusion is reached, however, that, for Dust Filtration Process Type I, an important parameter is the terminal dust load, L_o.

At the project's end, the authors will use the coefficients of parabolic equations, $E_o = f(q_g)$ and $F_1 = f(q_g)$ in Table 6 and Table 7 (Series I), for a

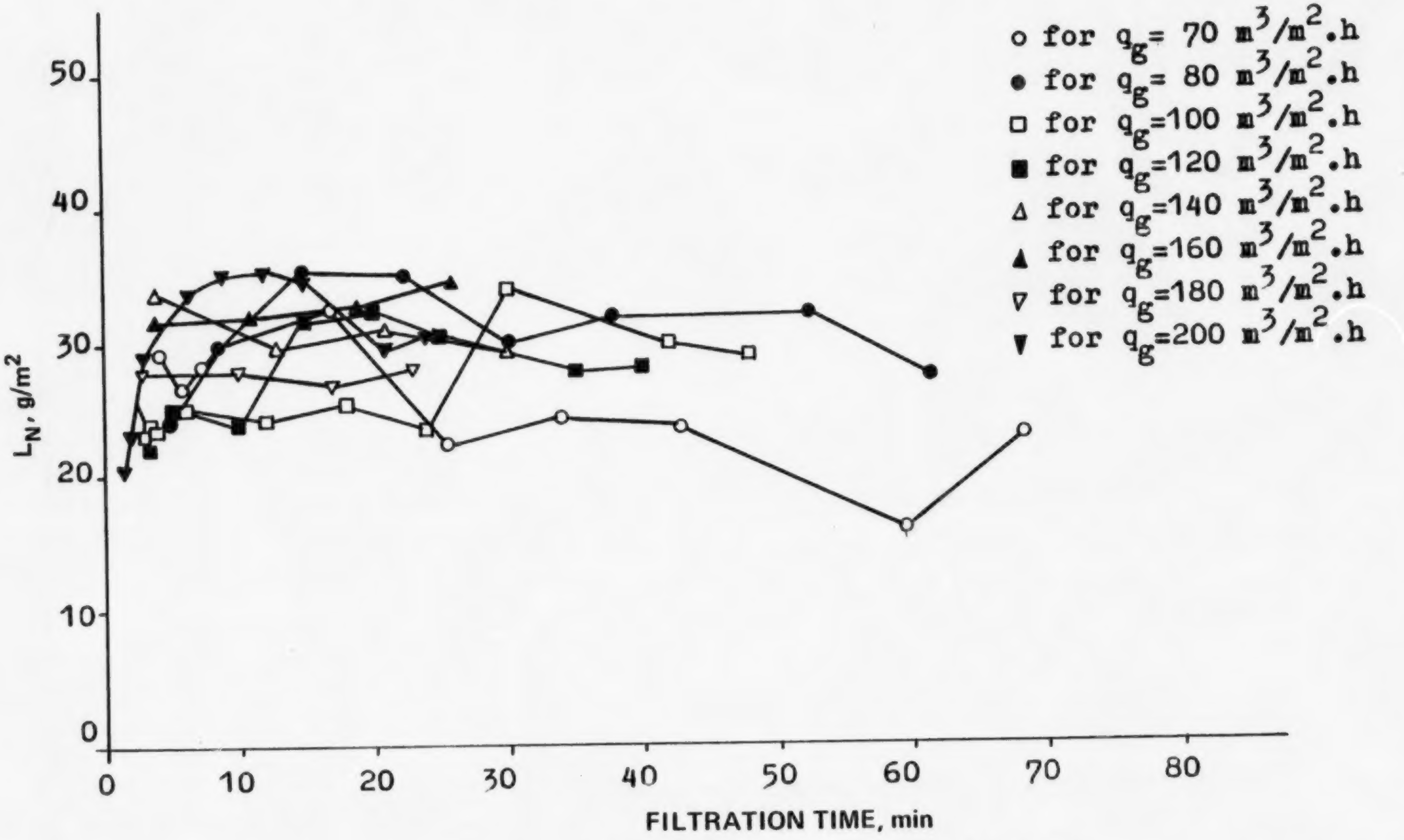

Figure 71. Dependence of residual dust load on time and q_g for fabric ET-30 (test dust: fly ash).

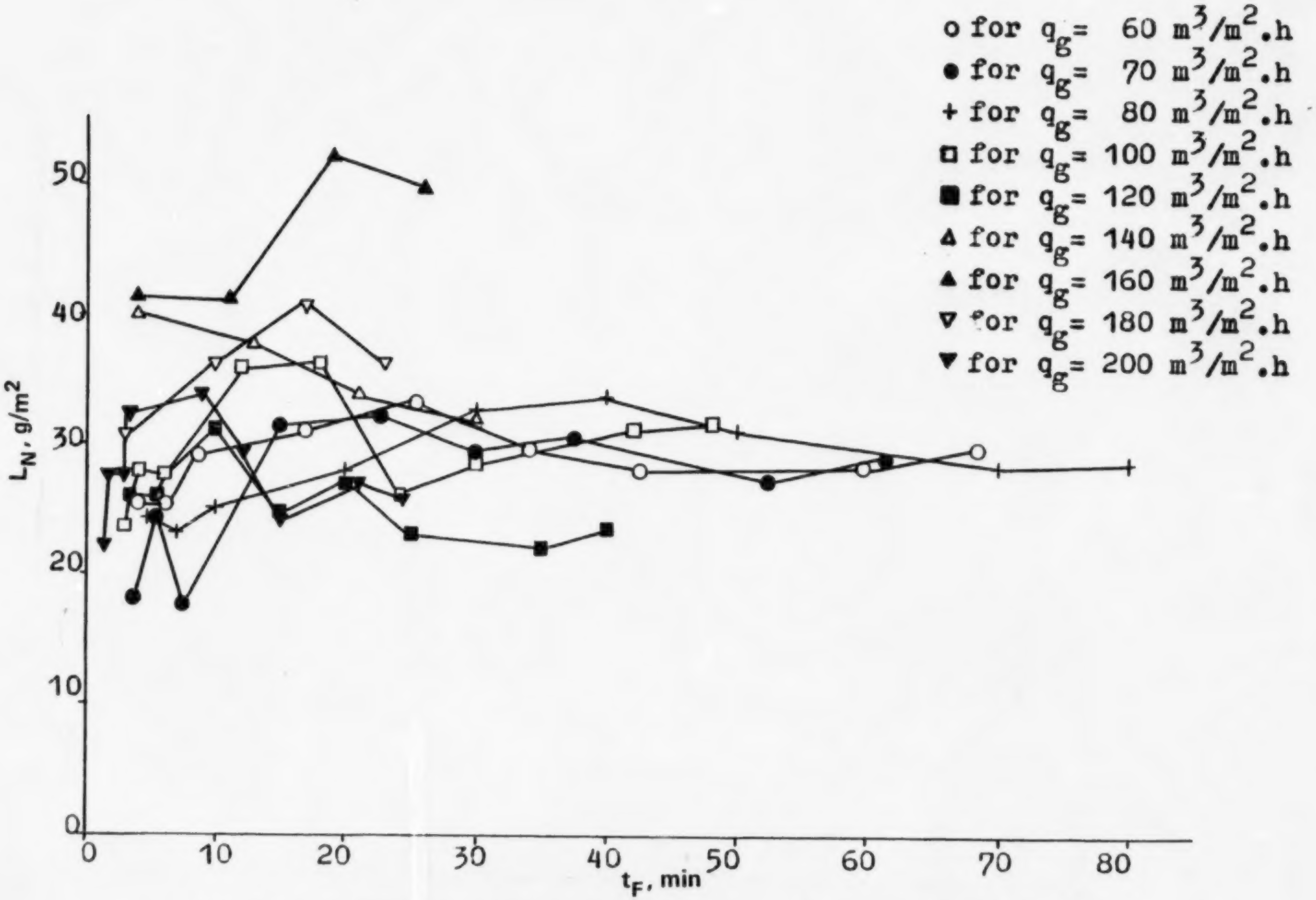

Figure 72. Dependence of residual dust load on time and q_g for fabric ET-4 (test dust: fly ash).

new interpretation of the mean from the measurement cycle. The material, which was presented in the second-phase report, cannot be a base for developing dust collection efficiency models. These empirical curves are imprecise because they were defined by only three measurement points for each level of filtration parameters.

Examination of fabrics ET-4 and ET-30 shows that in the second phase of the research program, a precise determination of modifications of F_1 (or E_0) and F_2 is instrumental in obtaining a correct efficiency model. This precise model, however, is only possible based on extensive empirical material.

This conclusion is fully confirmed by the empirical character of the dust collection efficiency model. Because of the heterogeneity of the woven fabric structure, it is necessary to conduct several tests to obtain a mean value of a specific parameter that will best approximate its true value. Taking the number of measurements, n, = 5 provided a sufficiently precise estimate of functions F_1 and F_2 for q_g = 80 to 140 m^2/h.

The Effect of Filtration Parameters on Filtration Resistance Variations

Detailed examinations of the increase in filtration resistance as a function of L_0 and filtration time, in the range of Dust Filtration Process Type I, do not confirm the linearity of this dependence postulated in some models.[21] [22]

During earlier examinations, both with unseparated and separated dusts (Series I, II, and III), the filtration resistance increase was found to be curvilinear and parabolic during the second phase of the filtration cycle (after inflection point A).

The above leads to the following general functions:

$$\Delta P_F = f(L_0^{b_1}) \quad ,$$
$$\Delta P_F = f(t_F^{b_2}) \quad , \text{ and} \qquad (63)$$
$$\Delta P_F = f(q_g^{b_3}) \quad ,$$

assuming

c_1 = constant.

From a broad empirical data base the development of a three-dimensional probabilistic model describing filtration resistance variation in the second phase of Dust Filtration Process Type I, was undertaken.

Three main independent variables were considered: face velocity, q_g; the terminal dust load, L_o; and filtration time, t.

Because of the relationship between L_o and filtration time with constant dust concentration, the general form of the model is:

$$\Delta P_F = f[q_g, L_o (t_F)] \quad . \qquad (64)$$

The relationship expressed by Equation 63 is modified as the following empirical model of filtration resistance:

$$\Delta P_F = A[q_g]^B \quad , \qquad (65)$$

where

$$B = f[L_o (t_F)] = A_1 \cdot L_o{}^2 + B_1 L_o + C_1$$

$$= A_1 (q_p \cdot t_F)^2 + B_1 (q_p \cdot t_F) + C_1 \quad ,$$

where

ΔP_F = filtration resistance, mm H_2O;
q_g = face velocity, m^3/m^2h;
q_p = dust flux, g/m^2h; and
A, A_1, B_1, C_1 = empirical constants, characterizing the dust-fabric system.

The empirical data were fitted to Equation 65.

From Equation 65 the following equation is obtained:

$$\log \Delta P_F = \log A + B \log q_g \quad . \qquad (66)$$

In a log log plot, Equation 66 forms a straight line with directional coefficient B. The values of coefficient B depend on L_o and filtration time, so from a series of experiments, a set of straight lines is obtained.

When $q_g = 0$, $\Delta P_F = 0$; when $q_g = 1$ and $\Delta P_F = 1$, $\log q_g = 0$ and $\log \Delta P = 0$; so $\log A = 0$. Thus, coefficient A should equal 1. With these assumptions, the set of lines should start at the beginning of the logarithmic coordinate system (1, 1). But from empirical data, $A = 0.01$, so the lines cross the ordinate axis at $q_g = 10$. If the origin of the coordinate system is moved to point 10, 1 the final form of the three-dimensional model describing the variation of filtration resistance is:

$$\Delta P_F = [q_g/10]^{A_1 L_o^2 + B_1 L_o + C_1} , \tag{67}$$

$$\text{or} \quad \Delta P_F = [q_g/10]^{A_1 (q_g \cdot t_F)^2 + B_1 (q_g \cdot t_F) + C_1} . \tag{67a}$$

The relationships in Equation 67 and 67a are the same as those in Equation 65. The values of coefficient B for individual experiments were determined from Equation 66 and the use of the linear regression method; i.e., the coefficients a and b in Equation 68 were determined as in Equation 58:

$$y = a + bx , \tag{68}$$

where

$y = \log \Delta P_F$,
$x = \log q_g$,
$a = \log A$, and
$b = B$ (Equation 65).

Table 11 includes the values of coefficient B, both for experiments in Series I and experiments conducted earlier with unseparated dusts. Table 12 includes the values of coefficient B for Series II and III; i.e., experiments according to the broadened research program. The results obtained in Series II and III experiments provide a better estimation of coefficient B because they were conducted over a wider range of filtration parameters.

The variation of the equation, $B = f(L_o)$, for the Series I experiments illustrated in Figures 73 through 76, shows the dependence of coefficient b upon L_o (and also B's dependence on the kind of dust and filtration material). Similar behavior was observed for the Series II and III experiments (Figure 77).

The effect of the filtration material structure on filtration resistance, observed by many authors,[13] [27] is usually discussed on two levels:

- The initial resistance value for a given q_g (effective drag), and
- The increase of resistance coefficient of the dust-fabric system, K_2 (assuming a linear increase of filtration resistances in time).

TABLE 11. VALUES OF COEFFICIENT B FROM EQUATION 65 AS A FUNCTION OF L_o
(Series I and Previous Experiments)

Kind of fabric	L_o (g/m^2)	Kind of dust					
		Separated cement	Unseparated cement	Separated coal	Unseparated coal	Separated talc	Separated fly ash
ET-4	100	1.3033	1.0932	1.2912	1.0084	1.1895	1.1482
	400	1.9003	1.6342	1.9707	1.5663	1.9291	1.6627
	700	2.1892	1.8348	2.2085	1.7257	2.2391	1.9431
ET-30	100	1.6064	1.5475	1.5982	1.3422	1.4825	1.4485
	400	1.9966	1.8648	2.0947	1.7215	2.0484	1.7819
	700	2.2464	1.9764	2.3781	1.8427	2.2958	2.0246
F-tor 5	100	1.6234	1.6121	1.6906	1.4674	1.5428	1.4928
	400	2.0555	1.8320	2.1525	1.7228	2.0867	1.7998
	700	2.2805	1.9876	2.3949	1.9810	2.3498	2.0261
PT-15	100	1.8803	1.6862	1.8985	1.6254	1.7240	1.7148
	400	2.1561	1.9339	2.2532	1.8631	2.1279	1.9256
	700	2.3341	2.0778	2.4643	2.0101	2.3368	2.1345

TABLE 12. VALUES OF COEFFICIENT B FROM EQUATION 65 AS A FUNCTION OF L_o (Series II and III)

L_o (g/m²)	Kind of fabric	
	ET-4	ET-30
50	1.02	1.15
70	1.06	1.20
100	1.16	1.28
200	1.35	1.47
300	1.53	1.61
400	1.62	1.74
500	1.75	1.82
700	1.95	1.98
800	1.97	2.05

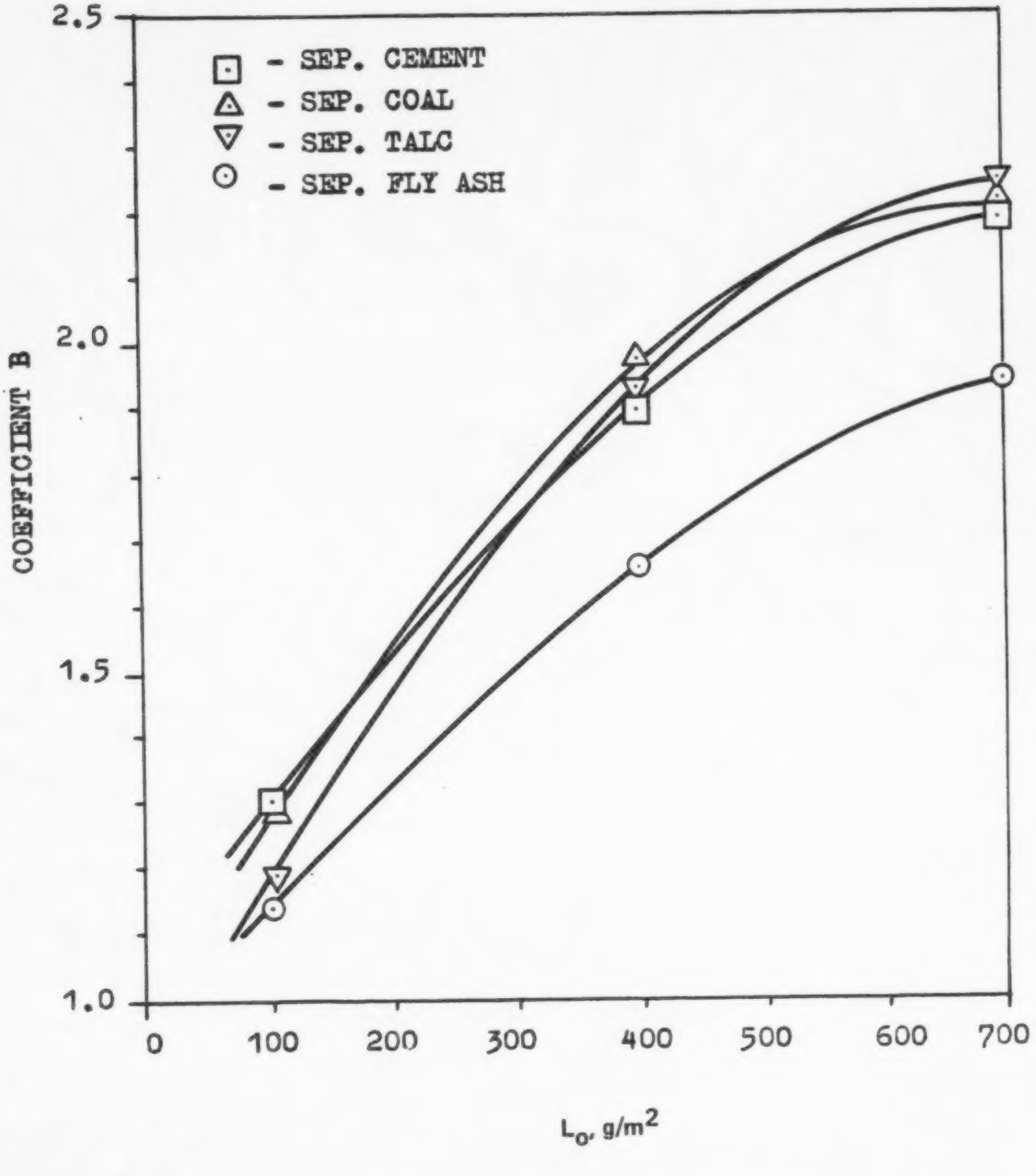

Figure 73. Variation of coefficient B from Equation 65 as a function of L_o for fabric ET-4 (Series I).

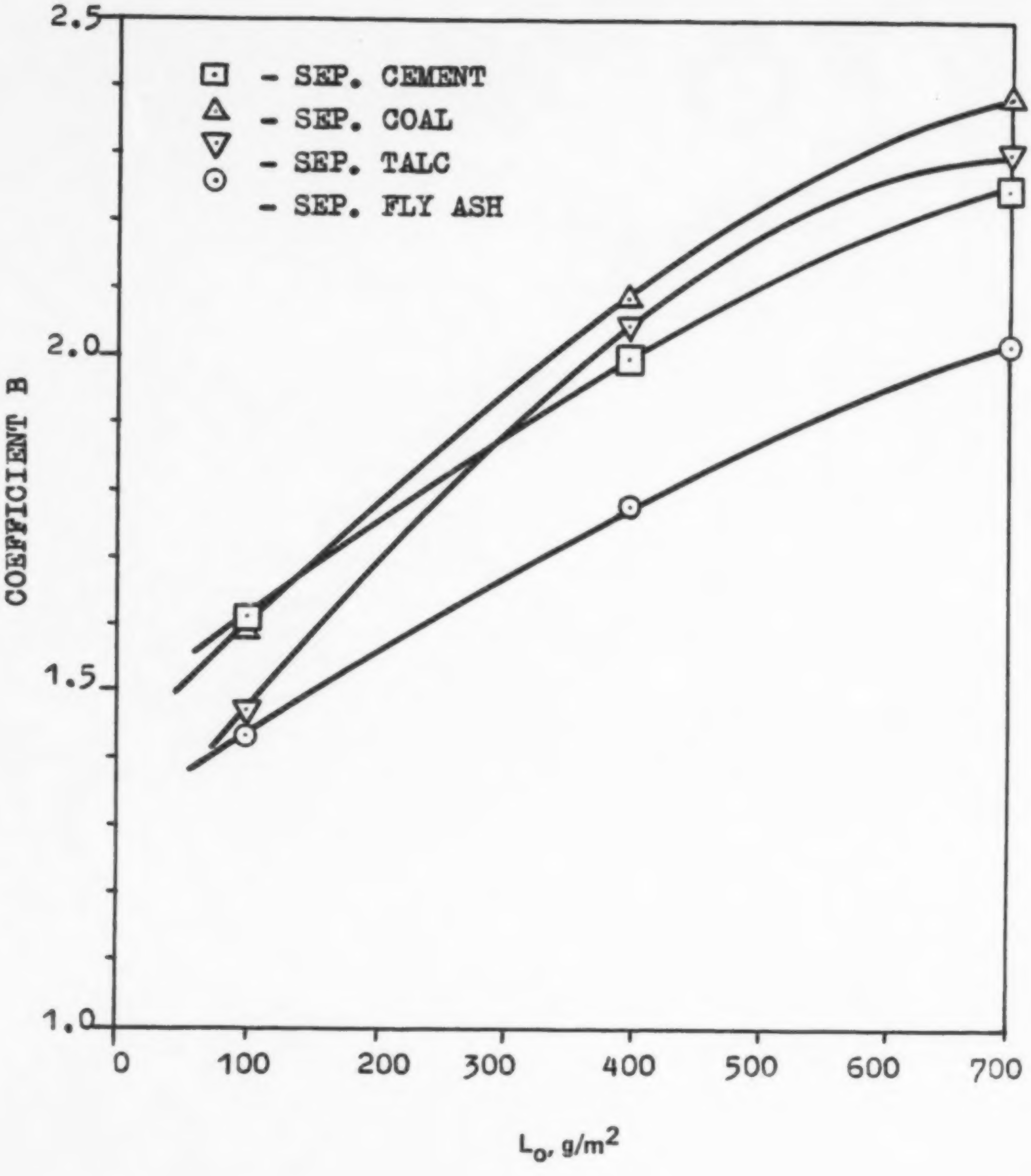

Figure 74. Variation of coefficient B from Equation 65 as a function of L_o for fabric ET-30 (Series I).

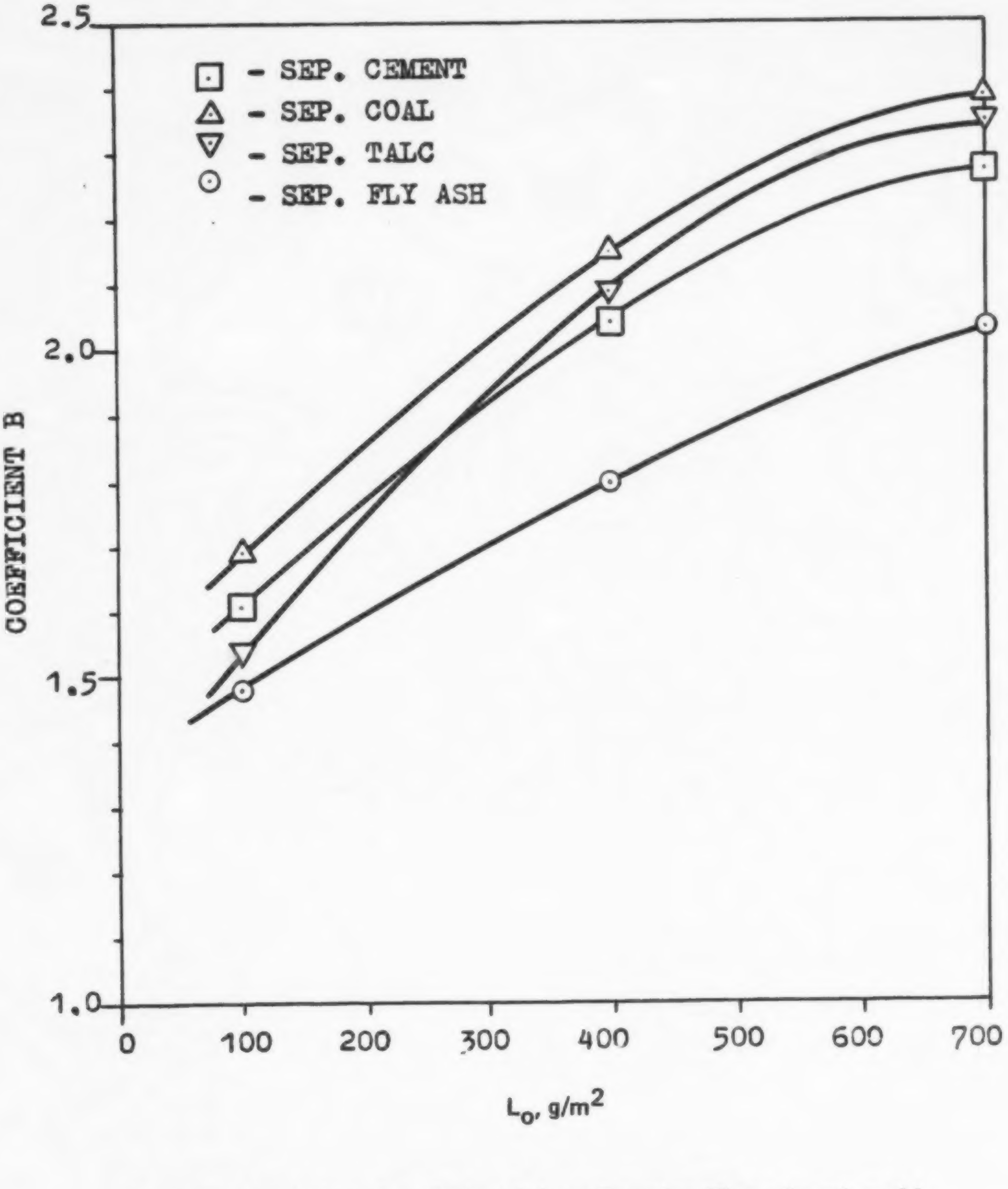

Figure 75. Variation of coefficient B from Equation 65 as a function of L_o for fabric F-tor 5 (Series I).

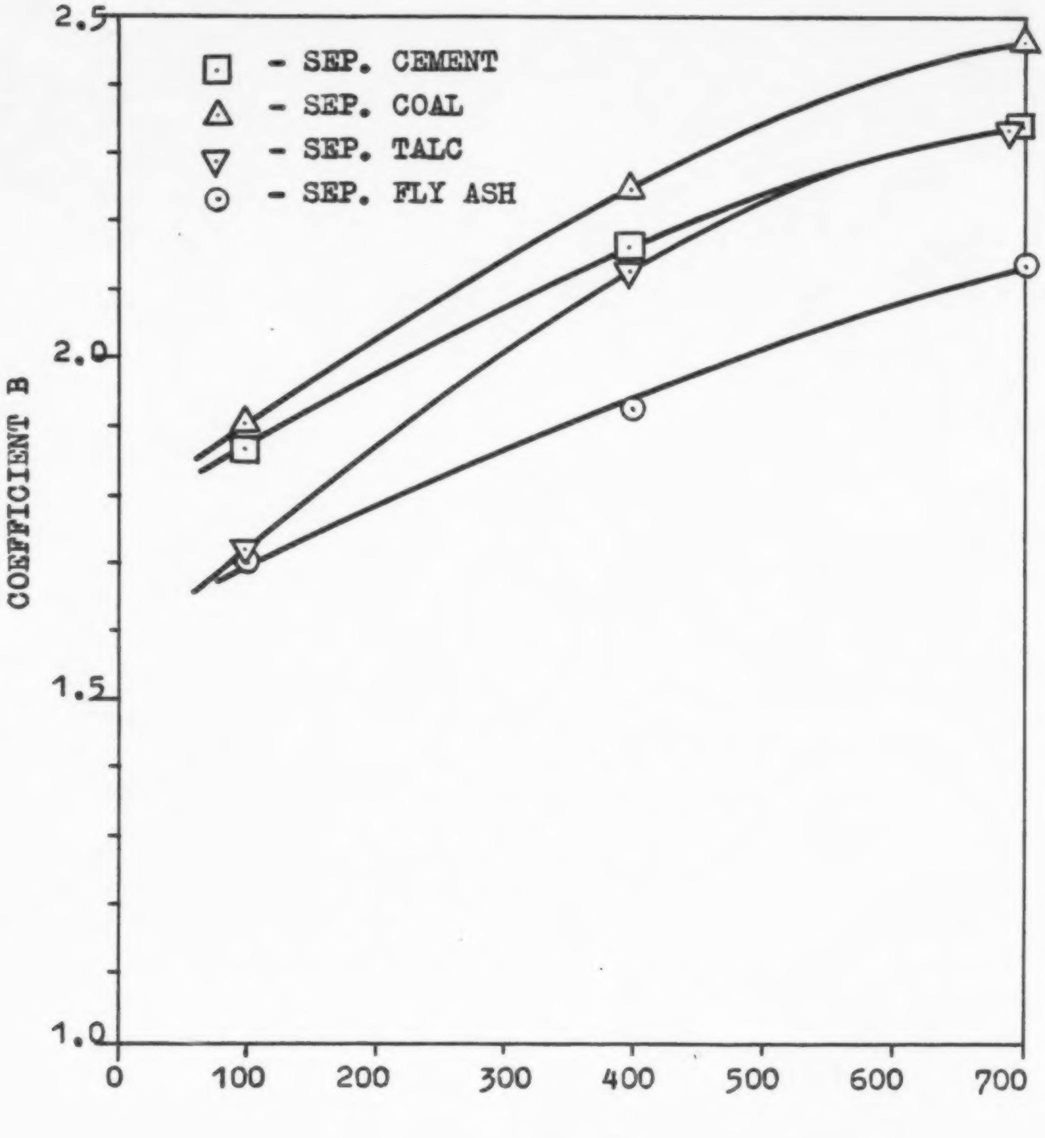

Figure 76. Variation of coefficient B from Equation 65 as a function of L_o for fabric PT-15 (Series I).

150

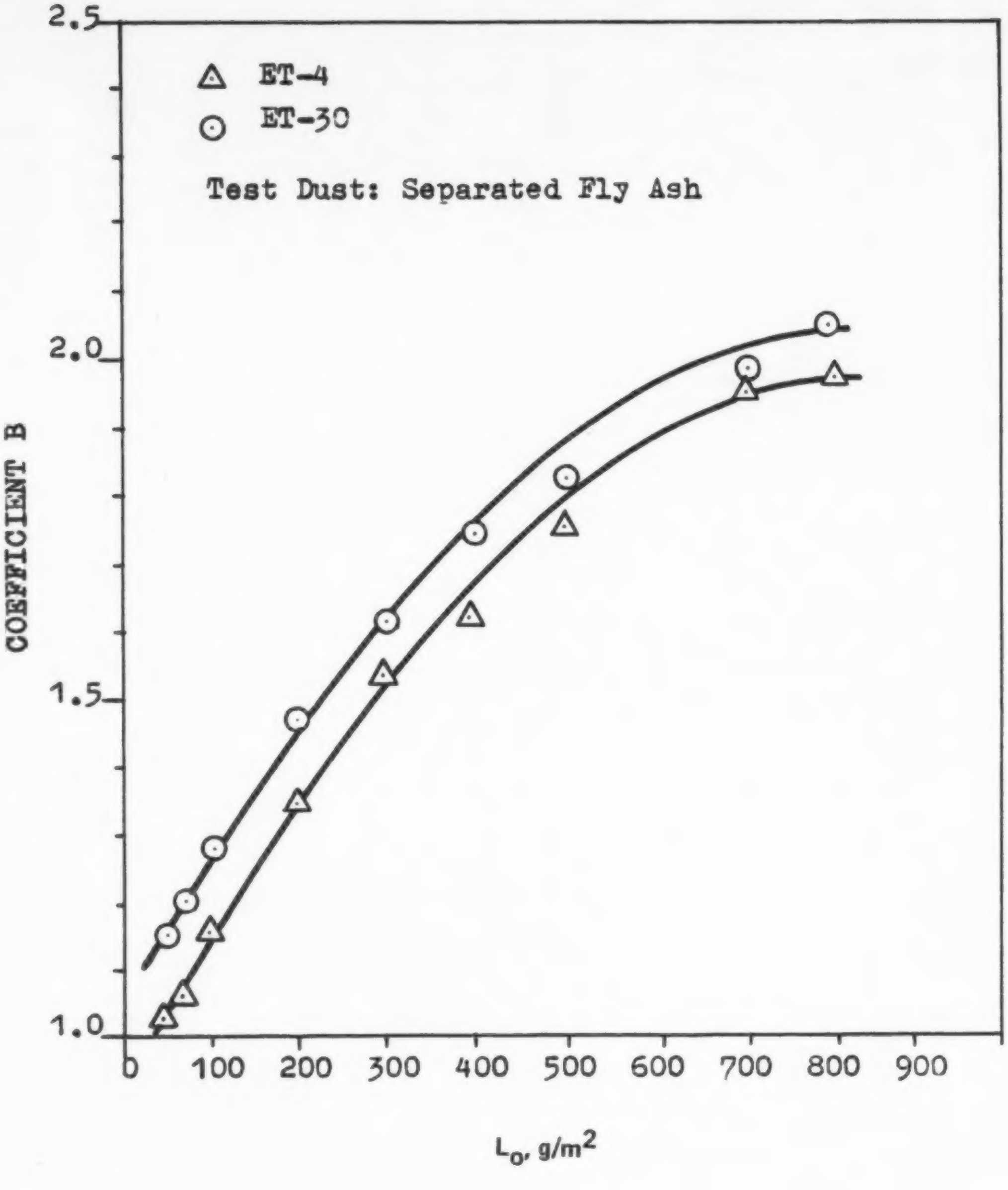

Figure 77. Variation of coefficient B from Equation 65 as a function of L_o for fabrics ET-4 and ET-30 (Series II and III).

Generally, the homogeneity of the dust cake is assumed, and any deviations from a linear dependence of ΔP_F with time are averaged as measurement errors.

With consideration of the strongest statistical structural parameter of the filtration medium--free area (FA)--it can be concluded that:

- The dust cake structure is heterogenous, varying with the dust-fabric system; and
- The effect of filtration material decreases as dust cake thickness increases.

These conclusions result from analysis of the probable dependence between FA and coefficient B, illustrated in Figure 78. This plot was prepared from experimental data using fly ash and the calculated values of FA for these test fabrics. With increasing dust cake thickness (higher values of L_0), the curves become more parallel to the abscissa, indicating a weakened dependence. It is noteworthy that the fabrics selected for these experiments differ mainly in their spatial and superficial structure because of different initial material (staple fiber vs. continuous filament) and technological parameters (see Table 1).

The superficial fabric structure affects only the first dust layers formed on its surface. By selective precipitation the dust cake structure becomes more uniform in the direction of gas flow--the influence of elementary dust layers on themselves. Compressive forces favor homogeneous isotropic structure in the gas flow plane.

Because dusts of similar particle size distribution were used in the experiments (all test dusts were separated similarly), observed differences in the dependence of B upon L_0 for various dusts result from dust particle shapes that influence the spatial structure of the dust cake. This hypothesis was confirmed by microscopic observation of dust particle shapes. Based on these observations, the cement and coal dust particles were found to be similar; the fly ash was spherical.

The behavior of talc (plate-shaped particles) is interesting. With little dust cake (small L_0) the talc layer exhibits properties similar to properties of fly ash; but at higher L_0, the layer exhibits hydraulic properties similar to cement and coal dust layers.

Application of the least squares method was used to ascertain that the discussed equation, $B = f(L_0)$, is best fitted by the parabola from Equation 65. A, B, and C are contained in Table 13 for the Series I experiments and in Table 14 for Series II and III experiments.

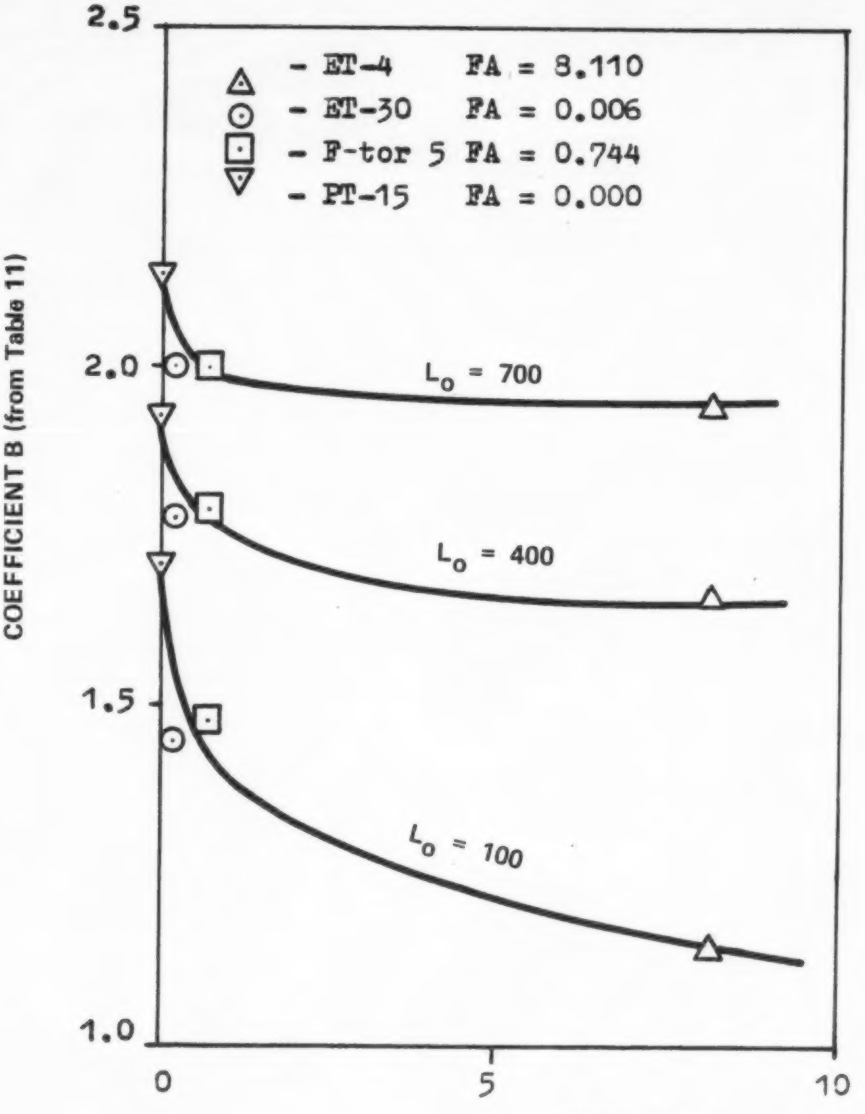

Figure 78. Probable dependence of coefficient B from Equation 65 as a function of FA for fabrics ET-4, ET-30, F-tor 5, and PT-15, tested with fly ash in Series I experiments.

153

TABLE 13. COEFFICIENTS OF THE PARABOLIC EQUATION: $B = A_1 L_o^2 + B_1 L_o + C_1$

(Series I and Previous Experiments)

Kind of fabric		Kind of dust					
		Separated cement	Unseparated cement	Separated coal	Unseparated coal	Separated talc	Separated fly ash
ET-4	$A_1=$	$-1.7117 \cdot 10^{-6}$	$-1.8911 \cdot 10^{-6}$	$-2.4539 \cdot 10^{-6}$	$-2.2139 \cdot 10^{-6}$	$-2.3867 \cdot 10^{-6}$	$-1.3006 \cdot 10^{-6}$
	$B_1=$	$2.8458 \cdot 10^{-3}$	$2.7489 \cdot 10^{-3}$	$3.4919 \cdot 10^{-3}$	$2.9666 \cdot 10^{-3}$	$3.6587 \cdot 10^{-3}$	$2.3653 \cdot 10^{-3}$
	$C_1=$	1.0358	$6.3722 \cdot 10^{-1}$	$9.6654 \cdot 10^{-1}$	$7.3388 \cdot 10^{-1}$	$8.475 \cdot 10^{-1}$	$9.2468 \cdot 10^{-1}$
ET-30	$A_1=$	$-7.8 \cdot 10^{-7}$	$-1.1428 \cdot 10^{-6}$	$-1.1839 \cdot 10^{-6}$	$-1.4339 \cdot 10^{-6}$	$-1.7694 \cdot 10^{-6}$	$-6.0389 \cdot 10^{-7}$
	$B_1=$	$1.6907 \cdot 10^{-3}$	$1.6291 \cdot 10^{-3}$	$2.2469 \cdot 10^{-3}$	$1.9813 \cdot 10^{-3}$	$2.7711 \cdot 10^{-3}$	$1.3633 \cdot 10^{-3}$
	$C_1=$	1.4451	1.396	1.3853	1.1584	1.2231	1.3172
F-tor 5	$A_1=$	$-1.1506 \cdot 10^{-6}$	$-3.5722 \cdot 10^{-7}$	$-1.2194 \cdot 10^{-6}$	$1.5556 \cdot 10^{-8}$	$-1.56 \cdot 10^{-6}$	$-4.4833 \cdot 10^{-7}$
	$B_1=$	$2.0156 \cdot 10^{-3}$	$9.1161 \cdot 10^{-4}$	$2.1494 \cdot 10^{-3}$	$8.4355 \cdot 10^{-4}$	$2.593 \cdot 10^{-3}$	$1.2475 \cdot 10^{-3}$
	$C_1=$	1.4333	1.5245	1.4879	1.3828	1.2991	1.3725
PT-15	$A_1=$	$-5.4333 \cdot 10^{-7}$	$-5.7667 \cdot 10^{-7}$	$-7.9778 \cdot 10^{-7}$	$-3.3722 \cdot 10^{-7}$	$-1.0833 \cdot 10^{-6}$	$-1.0556 \cdot 10^{-8}$
	$B_1=$	$1.191 \cdot 10^{-3}$	$1.114 \cdot 10$	$1.5812 \cdot 10^{-3}$	$8.6094 \cdot 10^{-4}$	$1.888.10^{-3}$	$7.0794 \cdot 10^{-4}$
	$C_1=$	1.7666	1.5806	1.7484	1.5727	1.546	1.6441

TABLE 14. COEFFICIENTS OF THE PARABOLIC EQUATION:
$B = A_1 L_o^2 + B_1 L_o + C_1$
(Series II and III)

Kind of fabric	Values of coefficients		
	A_1	B_1	C_1
ET-4	$-1.2356 \cdot 10^{-6}$	0.00231	0.9209
ET-30	$-1.1588 \cdot 10^{-6}$	$2.1383 \cdot 10^{-3}$	1.0649

TABLE 15. MMD and δ_g FOR TEST DUSTS (μm)

	Before separation		After separation	
Kind of dust	MMD	δ_g	MMD	δ_g
Cement	34.0	5.15	8.0	2.2
Coal	19.0	2.71	8.0	2.2
Talc	9.0	2.37	7.0	2.2
Fly ash	8.5	2.24	5.5	1.9

Constants from Equations 67 and 67a were used to obtain the parabolic models of filtration resistance for the test filtration materials and dusts (Dust Filtration Process Type I).

The parabolic coefficients calculated from the Series I, II, and III tests were similar for fabric ET-4, but not for fabric ET-30.

The statistical validity of results from the Series II and III experiments is higher than that from the Series I experiments, so the models for both fabrics and fly ash are:

for fabric ET-4,

$$\Delta P_F = [q_g/10]^{[-1.2356 \times 10^{-6} L_o^2 + 2.31 \times 10^{-3} L_o + 9.209 \times 10^{-1}]} \quad , \qquad (69)$$

and for fabric ET-30,

$$\Delta P_F = [q_g/10]^{[-1.1588 \times 10^{-6} L_o^2 + 2.1383 \times 10^{-3} L_o + 10.649 \times 10^{-1}]} \quad . \qquad (70)$$

The theoretical filtration resistance curves as a function of q_g for three levels of L_o were determined based on the above models (see Figure 79).

Analysis of the values of coefficient B was derived from the effect of the particle size distribution function on filtration resistance variation (Table 11). This analysis showed that unseparated dusts characterized by higher values of MMD have lower filtration resistances. Degree of dust dispersion is compared in Table 15. Filtration resistance models permit an estimate of filtration resistance in Dust Filtration Process Type I for an arbitrary point of the process; i.e., after required filtration time or after achievement of a specific L_o (using examined fabrics and dust). The models also permit analysis of the effect of the basic process parameters on filtration resistance.

However, like other probabilistic models, the models do not address the phenomena in a physical sense. Using test data to develop cause and effect relationships is important supplementary work. In later sections of this report, laboratory test data are discussed in this sense.

The filtration resistance models indicate good agreement between theoretical and experimental values, provided the experiments are conducted to avoid dust cake defects. The problem of ducts/canals formation is discussed in the theoretical section of this report.

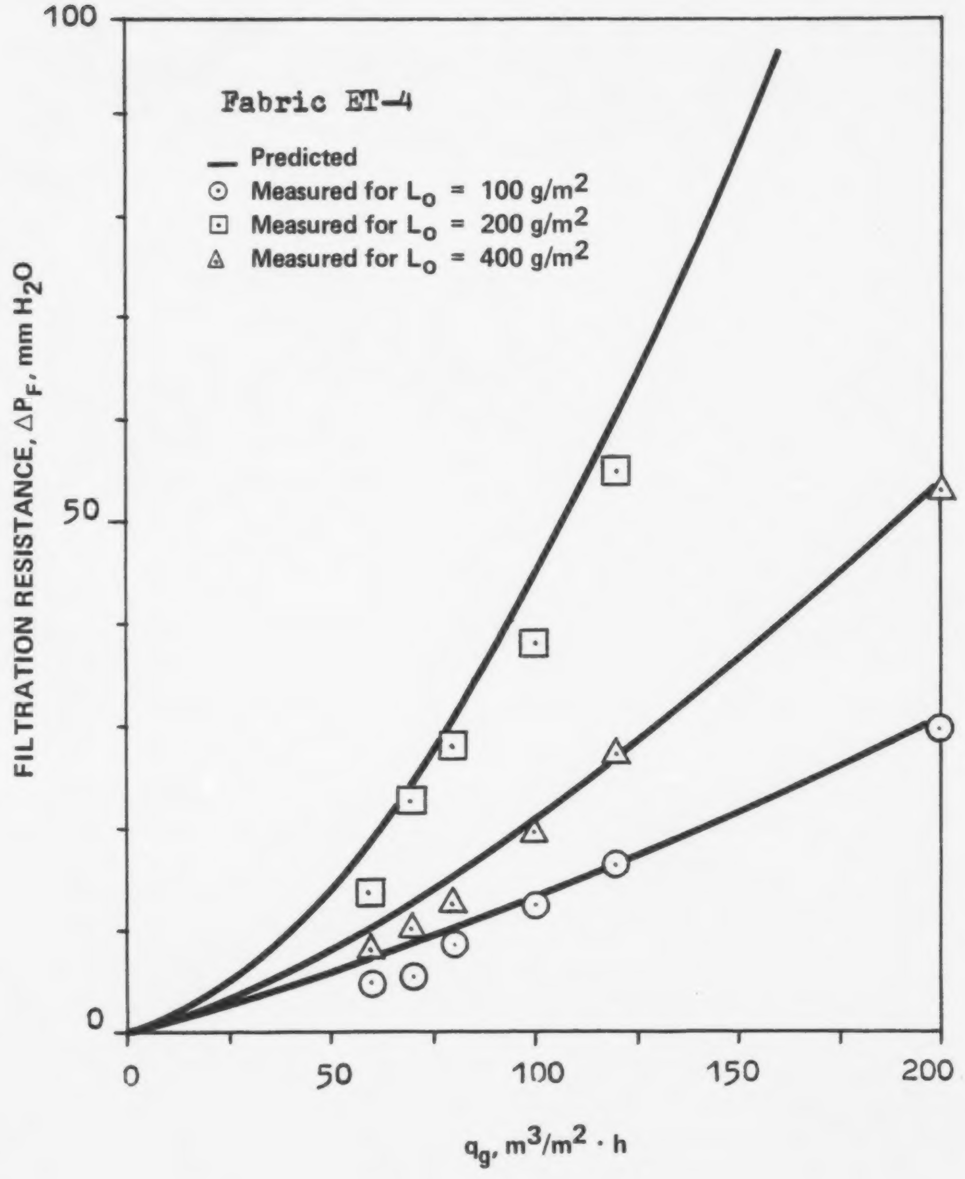

Figure 79a. Filtration resistance as a function of q_g, fabric ET-4.

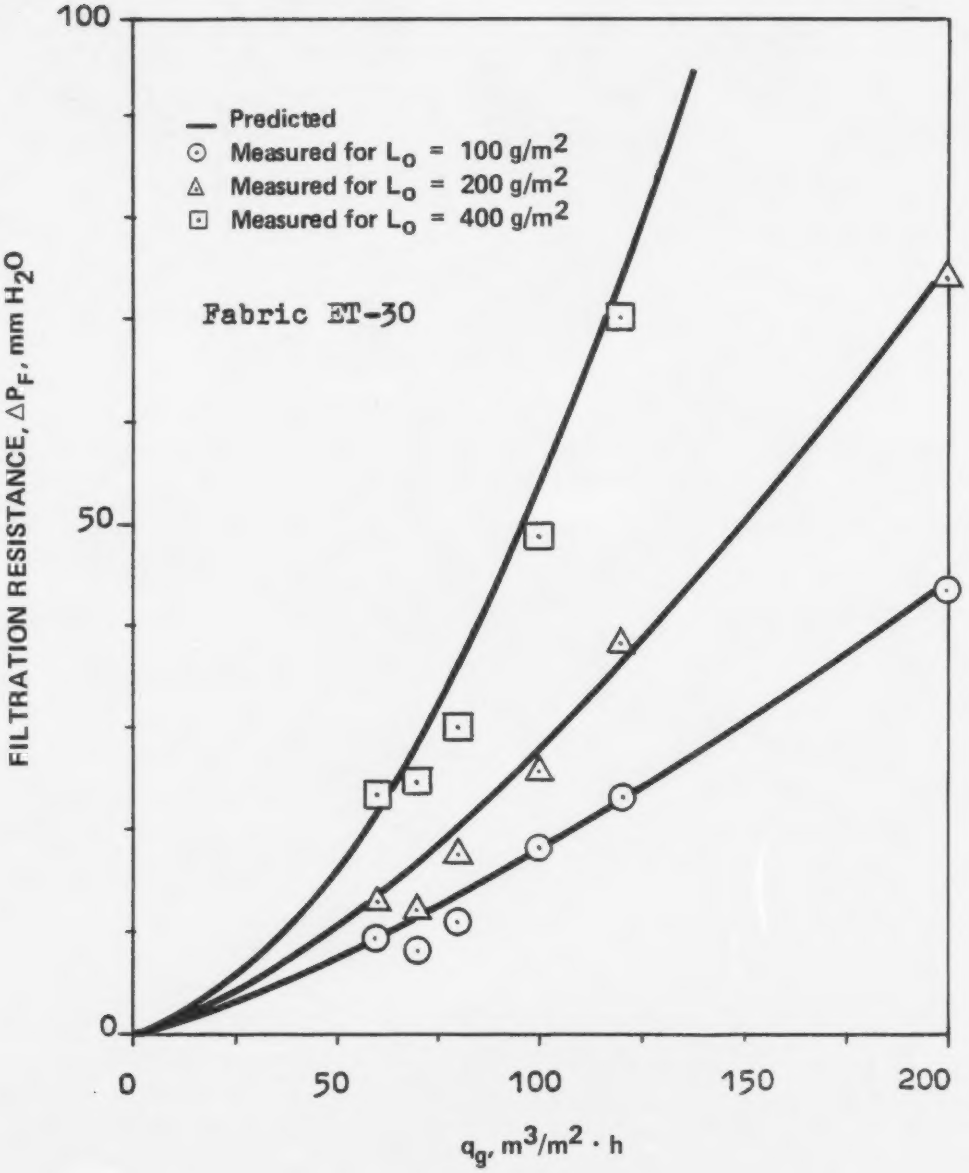

Figure 79b. Filtration resistance as a function of q_g, fabric ET-30.

During some experiments conducted in Series I, II and III, ducts/canals in the dust cake structure were observed. In Series I experiments, dust cake defects are observed for the following levels of filtration parameters:

- Fabric ET-4: tested at q_g = 120 m^3/m^2h with cement dust (L_o = 400 and 700 g/m^2), talc (L_o = 100, 400, and 700 g/m^2), and fly ash (L_o = 700 g/m^2);
- Fabric F-tor 5: tested at q_g = 120 m^3/m^2h with cement dust (L_o = 700 g/m^2) and talc (L_o = 100, 400, and 700 g/m^2).

In Series II and III experiments structural defects of the dust cake were observed for q_g above 100 m^3/m^2h:

- Fabric ET-4 tested with separated fly ash showed dust cake defects for the following values of filtration parameters:

  q_g = 140 m^3/m^2h for L_o = 300 and 500 g/m^2;
  q_g = 160 m^3/m^2h for L_o = 300 and 700 g/m^2;
  q_g = 180 m^3/m^2h for L_o = 500 and 700 g/m^2; and
  q_g = 200 m^3/m^2h for L_o = 200, 300, 400, 500, 700, and 800 g/m^2.

- Fabric ET-30 tested with separated fly ash showed dust cake defects for the following values of filtration parameters:

  q_g = 160 m^3/m^2h for L_o = 300 and 500 g/m^2;
  q_g = 180 m^3/m^2h for L_o = 500 g/m^2; and
  q_g = 200 m^3/m^2h for L_o = 200, 300, 400, 500, 700, and 800 g/m^2.

Identification of structural defects of the dust cake was made organoleptically after a particular measurement cycle, suggesting that ducts/canals can form at lower filtration resistances than those corresponding to the L_o indicated above.

Figure 80 was plotted from empirical data to explore the hypothesis of a limiting value of filtration resistance for each filtration material and dust type (dust particle size distribution) below which dust filtration occurs without forming dust cake defects. The plot shows the values of hydraulic resistances at which dust cake defects and the corresponding values of q_g were observed. For fabric ET-4, the data points at q_g = 120 and 180 m^3/m^2h should be lower because, according to the dust collection efficiency curve results, dust cake defects were formed before the final state was reached.

Based on experimental data, approximate values of the limiting pressure drop for separated fly ash, at which filtration occurs without defects in the dust cake structure, were determined:

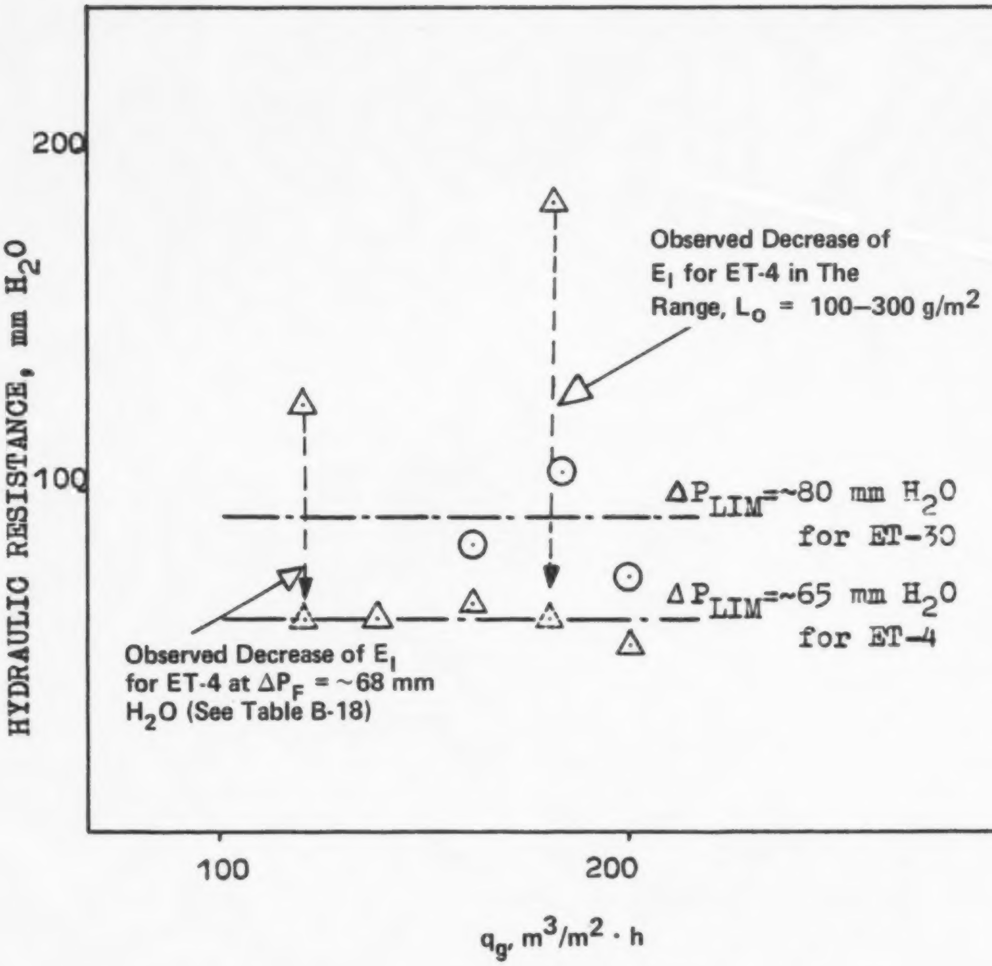

Figure 80. Filtration resistance and q_g at the moment of ducts/canals formation.

$$\Delta P_{LIM} = \sim 65 \text{ mm } H_2O \quad \text{for ET-4} \quad , \text{and}$$
$$\Delta P_{LIM} = \sim 80 \text{ mm } H_2O \quad \text{for ET-30} \quad .$$

These values correspond to q_g values for polyester fabrics of about 80 m^3/m^2h (Tables B-20 and B-21).

Complementary studies concern the formation and effect of filtration structure defects on filtration resistances; the hydraulic variation of the ET-4/separated cement dust system (at q_g = 120 m^3/m^2h) is illustrated in Figure 81 (Series I--Table B-14). Because L_o = 400 g/m^2, ducts/canals formation was observed. The theoretical equation, $\Delta P_F = f(t_F)$, determined from the three-dimensional model of filtration resistance is marked by a continuous line; the dotted line connects measured points and shows the deviations from the theoretical equation. The inflection point of both curves shows the moment when canals/ducts are formed. The limiting value of filtration resistance can also be read from the diagram, $\Delta P_{LIM} = \sim 55$ mm of water. This example confirms the theoretical deliberations explained earlier concerning distortion of filtration resistance variation as a function of time (or as a function of L_o) caused by dust cake defects.

Data analysis from this project and examination of the origin of dust cake defect formation during dust filtration through glass fabric (Project 5-533-4) lead to the conclusion that the basic elements determining formation of dust cake defects are free spaces not filled with fiber and defined either as free areas (FAs) or basket free areas (BFAs).

The demonstrated effect of filtration material structure on ducts/canals formation suggests that the design of filtration material structure should seek to incorporate the smallest mean pore size compatible with the elements of the structure. Structural packing influences the absolute value of the hydraulic resistance of the fabric. Thus, the correct construction should be characterized by a specific permeability, which can be obtained by suitable construction and integration of fill and warp yarns.

It is theoretically interesting to determine the value of resistance coefficient K_2 (from Equation 35) over the ranges of L_o. All experimental data obtained in Series I, II, and III were analyzed. The calculated results (Table B-24) mark those measurements at which dust cake defects were observed. Based on Table B-24, the diagram of the equation, $K_2 = f(L_o, t_F)$, for experimental data obtained in Series II is shown in Figure 82 and Figure 83. The analysis

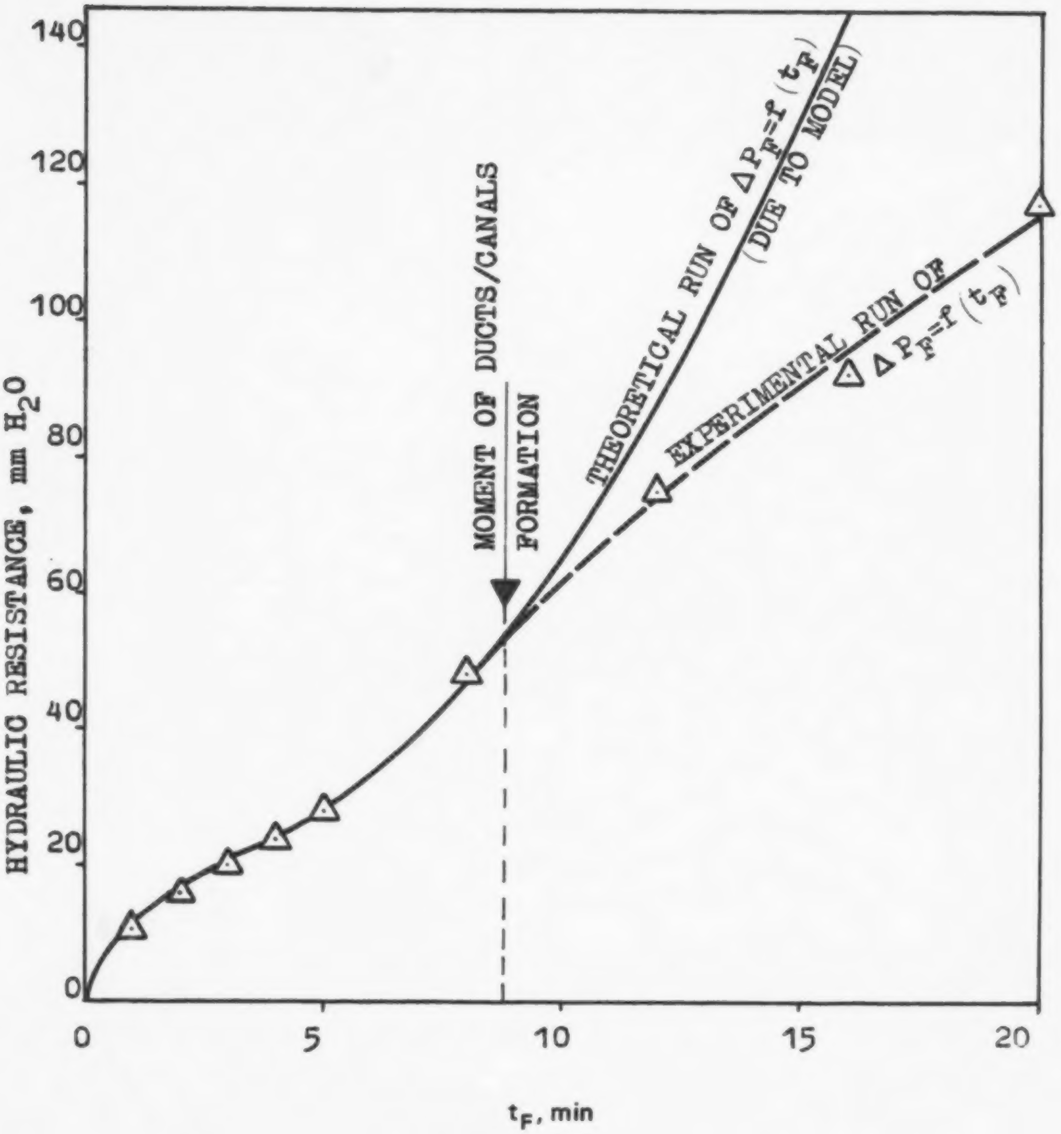

Figure 81. Change of filtration resistance due to ducts/canals formation during testing of fabric style ET-4 with fly ash at $q_g = 120\ m^3/m^2 \cdot h$ (Series I).

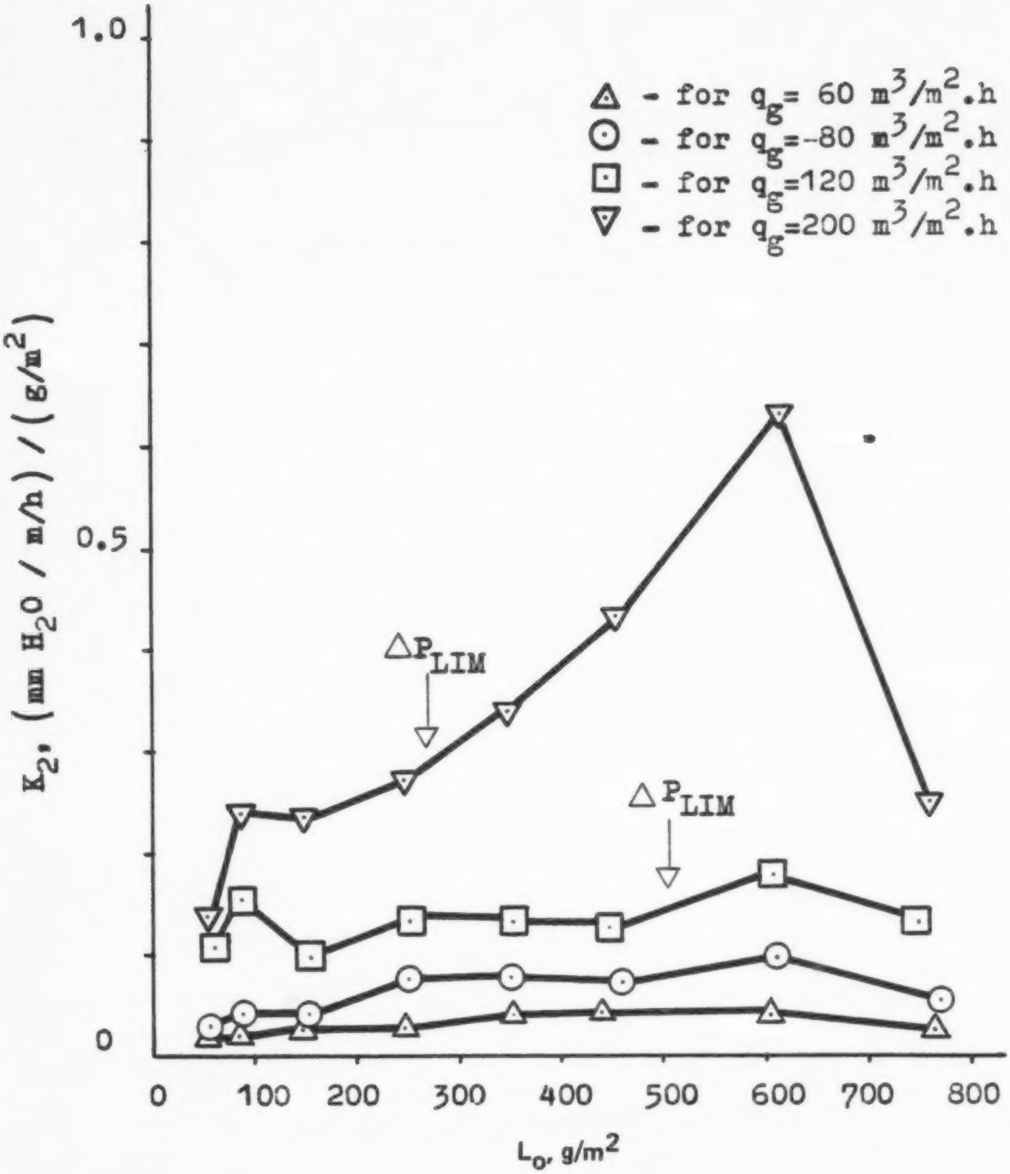

Figure 82. K_2 vs. L_o for fabric style ET-4, tested with fly ash.

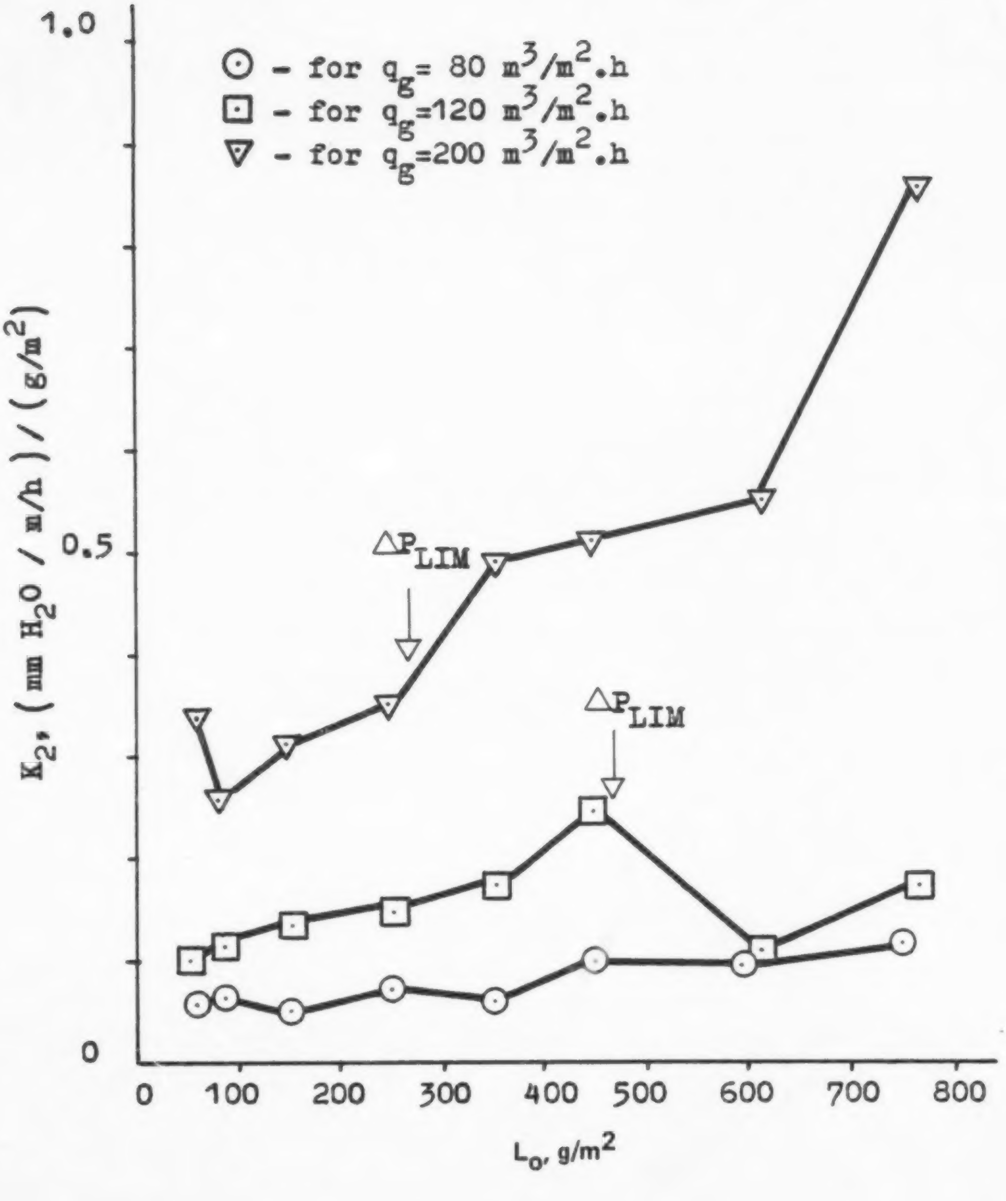

Figure 83. K_2 vs. L_o for fabric style ET-30, tested with fly ash.

was conducted only for the tests carried out at q_g = 60 (70), 80, 120, and 200 m^3/m^2h; i.e., permitting a detailed examination of the relationship.

As shown in the diagram, the points do not fall in a regular pattern. Their distribution suggests the presence of a variation in dust cake structure conditioned by discrete forces, caused by an increasing difference in static pressure. The diagram exhibits the dependence of resistance coefficient K_2 on q_g for a given dust-fabric system. Deliberations from the theoretical section concerning the dependence of K_2 on filtration time, expressed by Equation 37 and Equation 38, are also confirmed.

For fabric of low dust load ($L_o \sim 600$ g/m^2), a linear dependence ($K_2 = f[L_o (t_F)]$, according to Equation 37) can be easily extrapolated. For higher L_o values, K_2 displays values below this linear relationship (Figure 82 and Figure 83). According to Equation 36, lower K_2 implies a decreased value of the porosity function, which means that the porosity of the dust-fabric system increases. However, microscopic examinations of dusted material samples do not show structural defects of the dust cake for this range of q_g even though the K_2 curve proves their existence. The defects are presumed to be minute, but they strongly affect the examined dependencies. At high q_g (q_g = 120 to 200 m^3/m^2h), K_2 is linear only in the first phase of dust cake buildup, after which departures from linearity occur because of the mechanism described. When definite filtration resistances were ascribed to definite values of L_o, departures from the linear relationship, $K_2 = f[L_o (t_F)]$, appeared after a certain filtration time or after the structure was covered with dust. These departures occur at filtration resistances corresponding to the empirical limiting values of filtration resistances, ΔP_{LIM}, previously determined. However, this fact confirms the theory concerning peculiarities of quasi-static dust cake, produced during Dust Filtration Process Type I on the surface of the filtration material.

The Effect of Initial Aerosol State Parameters on Dust Collection Efficiency and Filtration Resistances

The effect of initial aerosol state parameters on dust filtration is usually discussed from the viewpoint of preserving dry filtration conditions, the thermal and chemical resistance of the filtration material, and correlations between times of the filtration cycle and the initial dust concentration. No one, however, has discussed it from the viewpoint of the effect these parameters have on the physical phenomena occurring during the process.

Because this project includes an estimation of the effect of filtration parameters on process performance--yielding narrow information about the effect of initial aerosol state parameters on filtration--additional random laboratory tests concerning the effect of varying dust concentrations on dust collection efficiency and filtration resistances were undertaken. The problem was interesting because of the complex description of Dust Filtration Process Type I and the confirmation of theoretical studies through experiments.

Tests were conducted with fabric ET-30 and fly ash at two levels of q_g and one level of L_o (400 g/m^2). Dust concentration varied over the range, 10 to 60 g/m^3. The results are presented in Tables 16 through 18. The primary question that must be answered is, "What is the effect of dust flux, q_p, on process performance?"

Dust flux, q_p, is controlled by filtration parameters; i.e., describing the manner of filtration is an interesting parameter because it depends on the concentration of initial state parameters.

When the problem of the effect of face velocity, q_g, on dust collection efficiency at a constant initial concentration was discussed, efficiency was proven to decrease with increasing q_g. When q_p values are considered for these conditions (which also increase with increasing q_g), dust collection efficiency is determined to decrease with increasing q_p. This conclusion conflicts with theoretical considerations. Increased dust flux, which implies an increased rate of dust cake formation, should increase dust collection efficiency.

When the results presented in Tables 16 and 17 are analyzed, it appears that, for constant q_g, an increase in efficiency with increasing q_p (increase of dust concentration) is observed, compared to the model efficiency for a particular value of dust covering, L_o. Dust flux cannot be regarded as an unequivocal filtration parameter. Its value must be defined each time for the value of q_g for which it is taken (e.g., $q_p \big|_{q_g} = 120 = 1\ 200\ g/m^2h$).

The effect of dust concentration on dust collection efficiency obtained for examined ranges of q_g is shown in Figure 84.

TABLE 16. LABORATORY EFFICIENCY (%) OF POLYESTER STYLE ET-30 TESTED WITH SEPARATED FLY ASH UNDER CONDITIONS OF THE CHANGE CONCENTRATION (at q_g = 120 m^3/m^2h)

C_1 (g/m^3)	q_p (g/m^2h)	L_o (g/m^2)	t_F (min)	Laboratory efficiency (%)
10.24	1228.8	409.08	20	99.78
20.54	2464.8	410.07	10	99.82
29.41	3529.2	412.17	7	99.83
40.73	4887.6	406.82	5	99.87
50.63	6075.6	404.53	4	99.88
60.85	7302.0	364.59	3	99.85

TABLE 17. LABORATORY EFFICIENCY (%) OF POLYESTER STYLE ET-30 TESTED WITH SEPARATED FLY ASH UNDER CONDITIONS OF THE CHANGE CONCENTRATION (at q_g = 180 m^3/m^2h)

C_1 (g/m^3)	q_p (g/m^2h)	L_o (g/m^2)	t_F (min)	Laboratory efficiency (%)
9.91	1783.8	395.24	13.33	99.69
20.00	3600.0	397.79	6.66	99.55
30.36	5464.8	408.60	4.50	99.68
38.90	7002.0	388.50	3.33	99.77
49.32	8877.6	393.56	2.75	99.75
61.48	11066.4	404.92	2.17	99.78

TABLE 18. FINAL PRESSURE DROP IN LABORATORY TESTING (in mm H_2O) FOR POLYESTER STYLE ET-30 TESTED WITH SEPARATED FLY ASH UNDER CONDITIONS OF THE CHANGE CONCENTRATION

q_g (m^3/m^2h)	L_o (g/m^2)	C_1 (g/m^3)	Final pressure drop (mm H_2O)
120	409.08	10.24	84.10
	410.07	20.54	82.72
	411.17	29.54	81.94
	406.82	40.73	80.05
	402.89	50.44	79.11
	364.59	60.85	65.61
180	395.24	9.91	153.36
	397.79	20.00	156.06
	408.60	30.36	171.45
	388.50	38.90	144.99
	393.56	49.32	148.23
	404.92	61.48	158.76

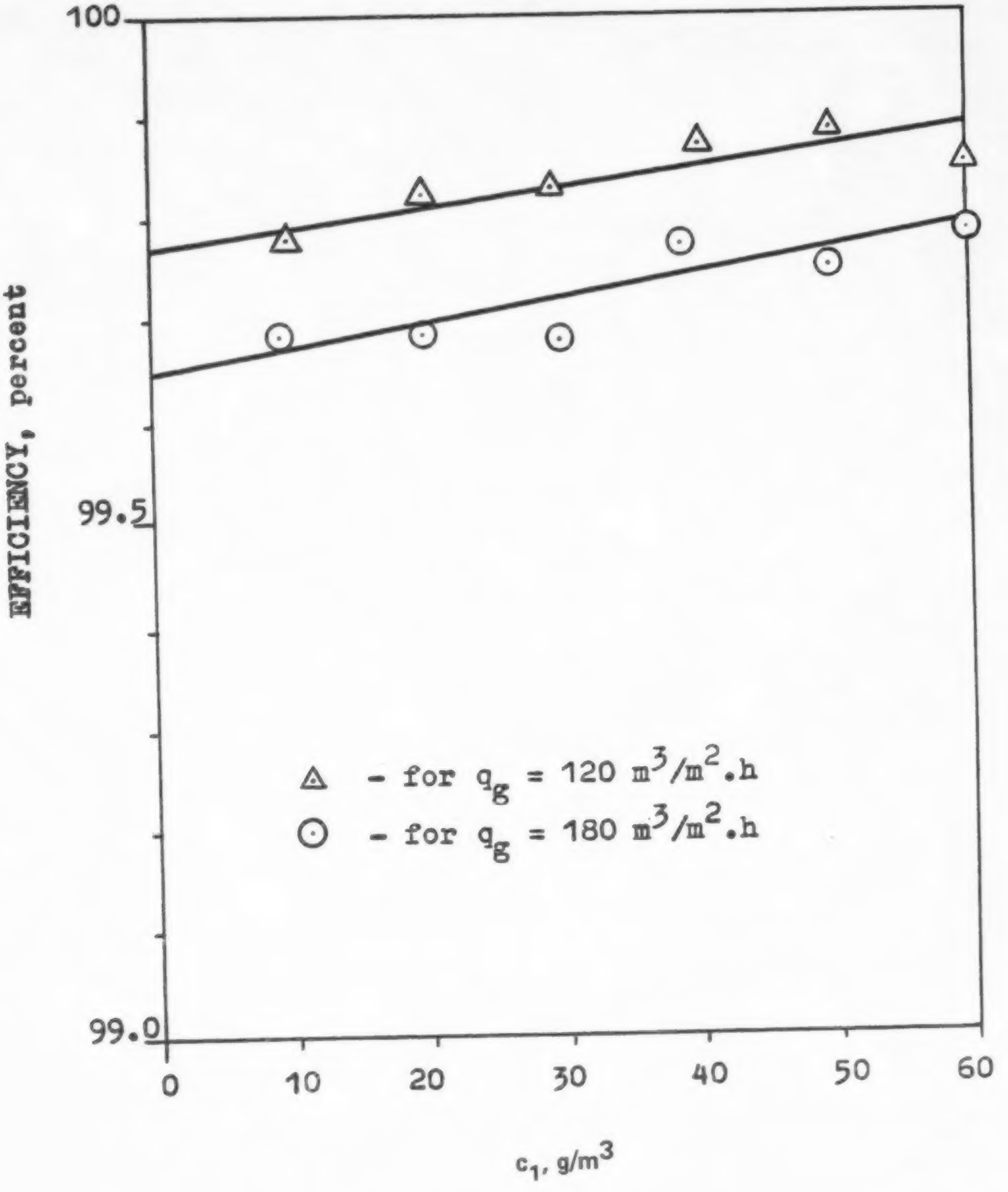

Figure 84. Dust collection efficiency as a function of c_1 for fabric style ET-30 tested with separated fly ash.

The relationships concerning individual levels of q_g can be approximated to straight lines. The directional coefficients for the lines are:

$$\text{for}\quad q_g = 120\ \text{m}^3/\text{m}^2\text{h} \qquad n_1 = 0.0016\ , \text{ and}$$
$$q_g = 180\ \text{m}^3/\text{m}^2\text{h} \qquad n_1 = 0.0021\ .$$

When relationships between initial concentration and dust collection efficiency are examined, the following models for fabric ET-30 at the assumed levels of q_g can be determined:

for $q_g = 120$,

$$E_I = [1 + 0.0016\ (c_1 - 10)]\ E_{I(c_1 = 10)}\ , \text{ and} \tag{71}$$

for $q_g = 180$,

$$E_I = [1 + 0.0021\ (c_1 - 10)]\ E_{I(c_1 = 10)}\ , \tag{72}$$

where

$E_I\ (c_1 = 10)$ = the theoretical dust collection efficiency in Dust Filtration Process Type I determined by Equation 60.

Because the directional coefficient of the curve, $E = f(c_1)$, depends on q_g, a generalized model of dust collection efficiency for Dust Collection Efficiency Type I, including the effect of initial concentration, can be presented in the following form:

$$E_I = \left\{1 + n(c_1)\ [c_1 - 10]\right\} [a_1 q_g^{\ 2} + b_1 q_g + c_1]^{-L_o\ [a_2 q_g^{\ 2} + b_2 q_g + c_2]}\ , \tag{73}$$

where

$n(c_1)$ = the characteristic function.

The model distinguishes two aspects of the effect of increasing q_p on process performance. On one hand increasing q_p results from an increase in q_g (i.e., in the changing distribution of flow velocity through the filtration structure) and, on the other hand, with increasing dust concentration (and, thus, increasing dust stream at a definite flow velocity distribution through the filtration structure). Distinguishing between the two effects is important for a physical interpretation of phenomena occurring during Dust Filtration Process Type I.

Filtration resistances as a function of time recorded during experiments provide interesting plots. Figure 85 shows the filtration resistance increase in time at $q_g = 120$ m^3/m^{2}h.

At a similarly thick dust cake, as measured by the constant value, L_o, a decrease in final resistance with increasing dust concentration was observed.

For an examination of the effect of varying dust concentration on dust cake structure, specific filtration resistances ($\Delta P_K/L_o$) obtained during experiments were compared. Results of this analysis are illustrated in Figure 86. During the experiment conducted at $q_g = 120$ m^3/m^{2}h, a continuous decrease in specific filtration resistance with increasing dust concentration was observed. This decrease means that greater dust concentration causes an increase in dust cake porosity. Thus, an examination of fractional efficiency in dust cakes formed in this manner would be interesting.

The $q_g = 180$ m^3/m^{2}h curve shows the effects of dust cake compression and discrete structural variation, probably resulting from interferences among the various forces operating in the dust cake.

The effect of aerosol particle size distribution on dust collection efficiency and filtration resistance can be discussed only by comparing results of testing fabrics with separated and unseparated dusts (cement, coal). The results confirm the theory of selective dust particle precipitation on the fabric structure and on the dust cake in dust filtration. The increase in collection efficiency and decrease in filtration resistances at increasing mean grain size is the result of the physical model presented in the theoretical section.

Dust Collection Efficiencies and Filtration Resistances in the First Phase of Dust Filtration Process Type I

Fabric ET-30 was tested to confirm the hypothetical dust collection efficiency as a function of time (terminal dust load, L_o, at c_1 = constant) that results from the probabilistic model and its connection with structural changes of the dust-fabric system in the first phase of Dust Filtration Process Type I.

Fly ash was used as the test dust. The tests were conducted at $q_g = 60$ m^3/m^{2}h, and initial dust concentration, 20.42 to 20.7 g/m^3. Because of the low values of q_g, comparatively low values of q_p were obtained, which allowed

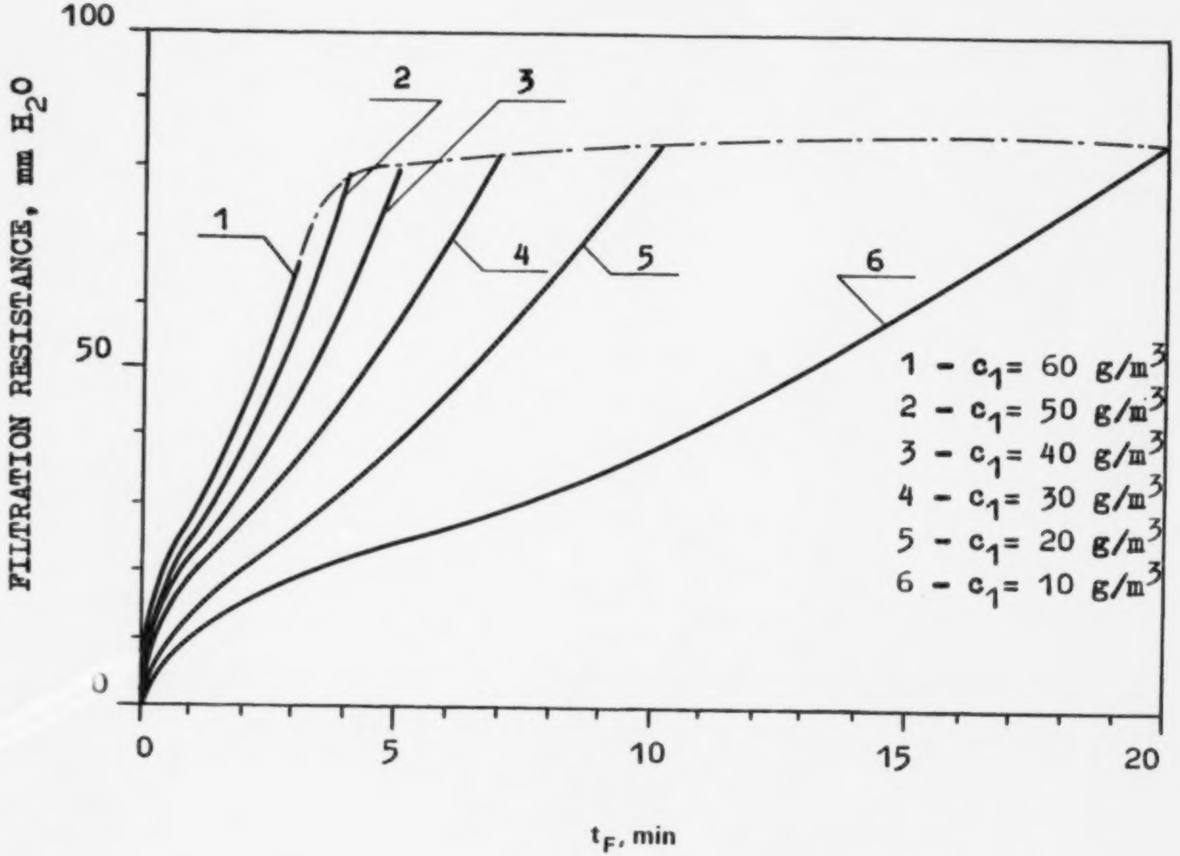

Figure 85. Effect of c_1 on filtration resistance during testing of fabric style ET-30 with separated fly ash.

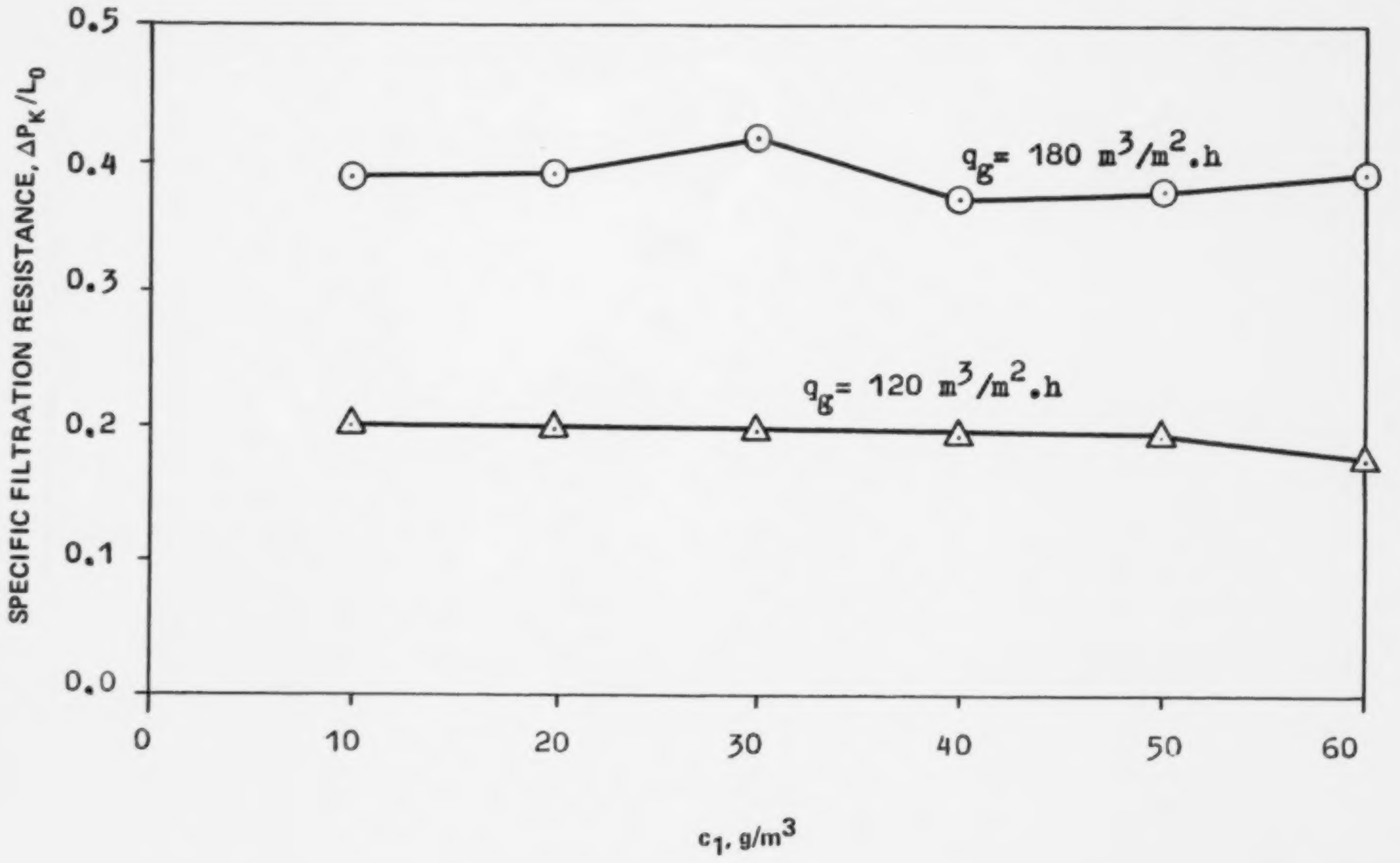

Figure 86. Dependence of specific filtration resistances upon initial concentration during testing of fabric style ET-30 with separated fly ash in two ranges of q_g.

tests to be conducted at low dust loads and at comparable filtration times. Dust collection efficiency was interpreted as a mean for a given filtration cycle and determined as $\bar{L}_o = L_o/2$. Filtration material samples were cleaned uniformly by hand after each test. Thus, a comparison of dust fillings in an individual experiment was possible. Results are shown in Table 19.

When analyzed, the dust collection efficiency as a function of the dust covering (filtration time) was found to be geometrically similar to that variation determined from the probabilistic model (see Figure 87).

However, an actual run suggests variation of dust collection efficiency when formation begins on the fabric surface, influencing the dust cake. When efficiency variation, in terms of hydraulic characteristics, $[(\Delta P_F = f(t_F)]$, is analyzed (Figure 88), some characteristic points connected to qualitative changes of the process are easily distinguished.

The first characteristic point, resulting primarily from variation in dust collection efficiency, is the time when high efficiency is first reached. After that time efficiency variation as a function of time slows. This point is indicated in Figure 87 and Figure 88. Up to this point the filtration resistance increases rapidly, but after this point, resistance increases nearly linearly to inflection point A. From inflection point A on, the increase in resistance is parabolic.

The hypothesis can be offered that when the first characteristic point is reached, the filtration structure has been fully filled with dust (for a given set of process conditions) and the first layer of dust cake is being built. Thus, dust collection efficiency rises. The precipitation of successive layers of dust cake on the fabric surface forces a rapid increase in dust collection efficiency until point A is reached. From the inflection point of hydraulic characteristic A, dust filtration occurs exactly according to the manner described in previous sections. The hypothesis is in accordance with the filtration phases assumed during theoretical deliberations. When the problem of stationary filtration is avoided, the nonstationary filtration phase can easily be distinguished from "ductive" filtration, which occurs next during the experiment.

The rapid increase in efficiency observed until the first characteristic point is reached corresponds to dust filling the filtration material structure. This point is nonstationary filtration, whereby the mechanism of filtration

TABLE 19. LABORATORY EFFICIENCY OF ET-30 DURING TESTING WITH SEPARATED FLY ASH IN THE RANGE OF LOW VALUES, L_o
(At q_g = 60 m^3/m^2h)

t_F (min)	C_1 (g/m^3)	Efficiency (%)	Final pressure drop ΔP_K (mm H_2O)	L_o (g/m^2)	L_N (g/m^2)
0.25	26.16	96.7456	1.78	6.54	5.96
0.5	23.24	98.8100	2.91	11.62	8.89
1.0	21.24	99.4400	3.73	21.24	17.22
2.0	24.17	99.5880	4.54	48.34	22.52
3.0	26.70	99.5897	5.02	61.25	27.44
4.0	23.30	99.7645	5.67	93.21	22.38
10.0	16.87	99.8698	8.42	168.75	26.16

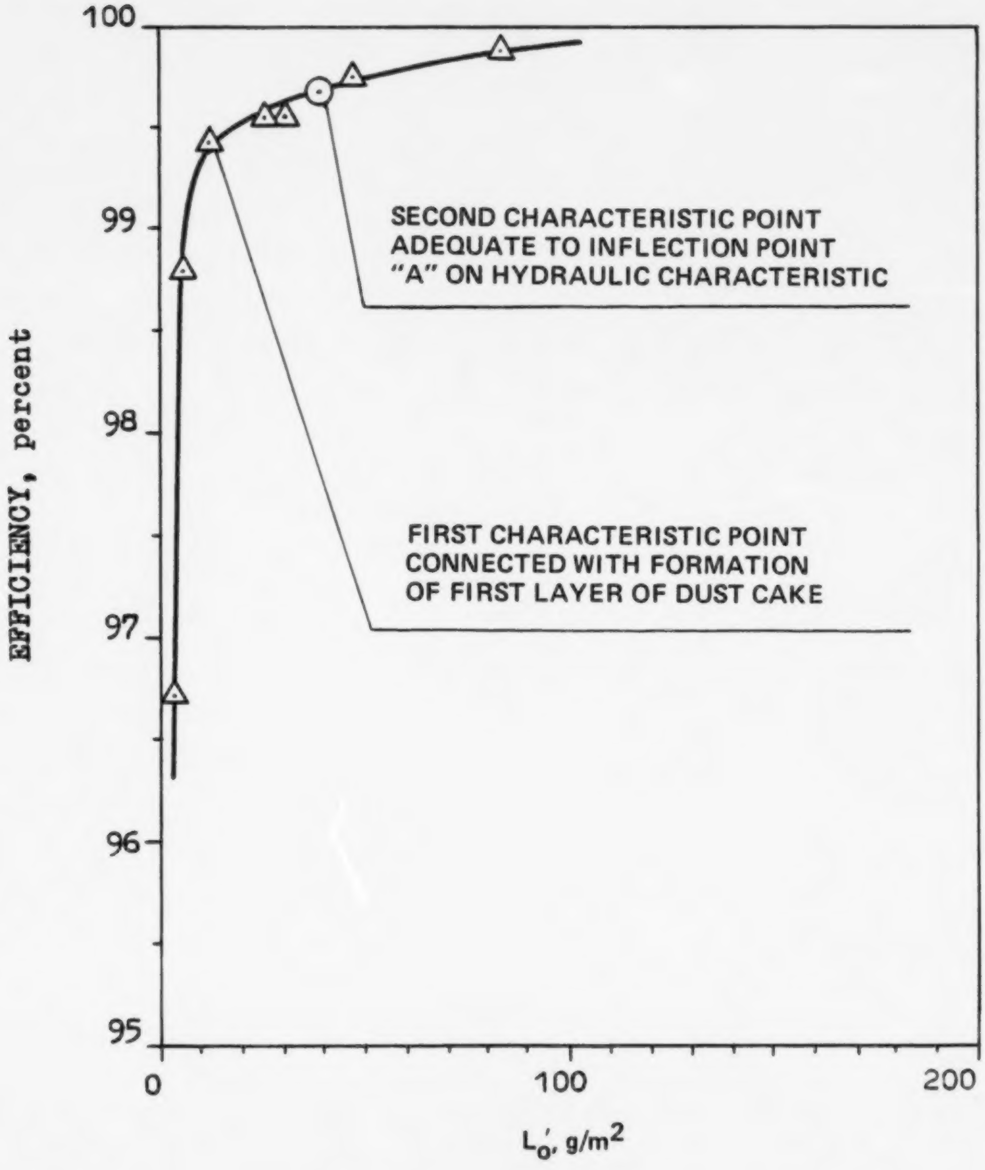

Figure 87. Dust collection efficiency as a function of average value of L_o (low L_o region).

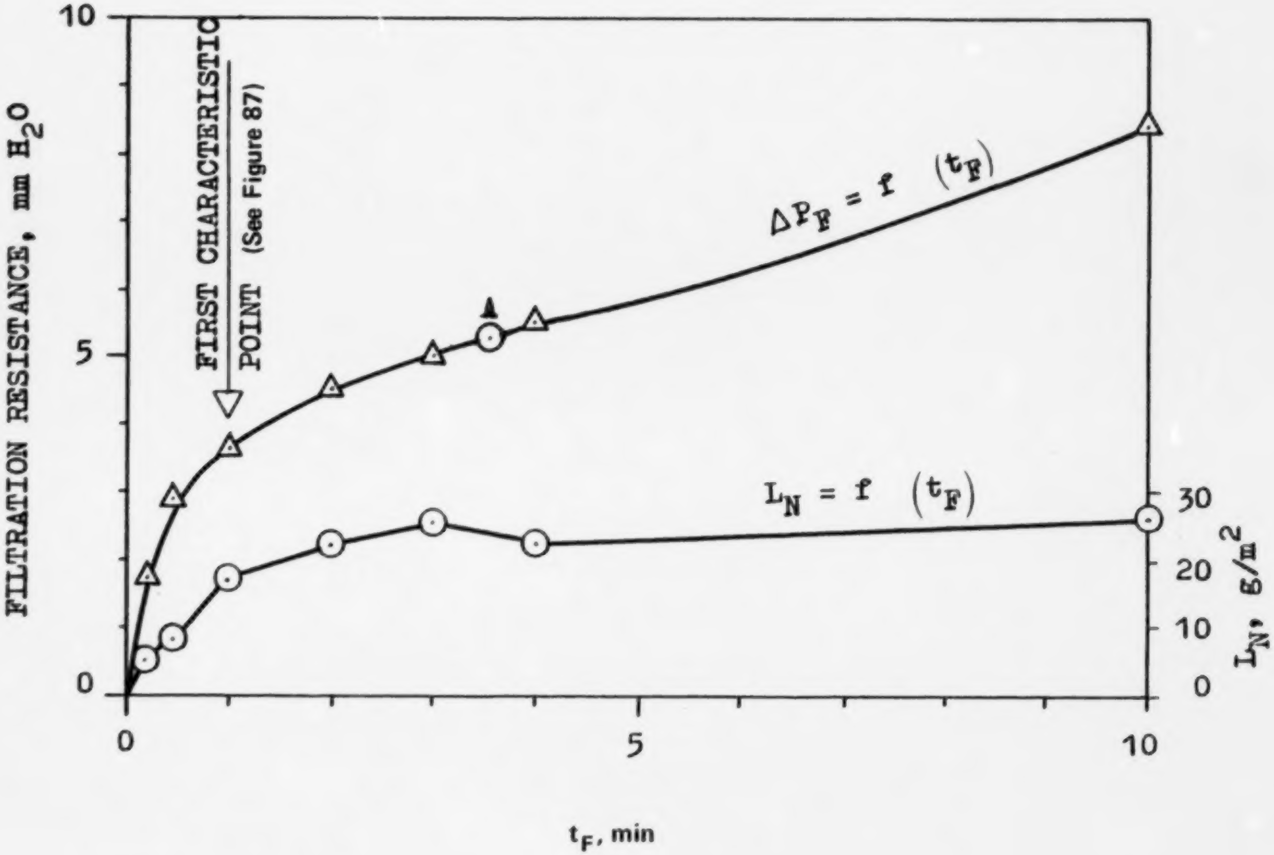

Figure 88. Filtration resistance variation as a function of average L_o in the low L_o region.

efficiency increase is stable in time; e.g., the filtration medium becomes less and less porous. This interpretation is in accordance with assumptions of the classical filtration theory.

The phase of ductive filtration, characteristic of the area above inflection point A and experimentally proven, requires formation of an active dust cake structure. Thus, there is ample time between the first characteristic point and inflection point A. During this period, the dust grains "packing" the filtration material may be dislocated. This possibility is confirmed by filtration resistance variation in time.

The experiments discussed above, which are outside the range of the project, provide interesting information not only regarding confirmation of theoretical studies but also in directing research in Dust Filtration Process Type I.

RECAPITULATION AND CONCLUSIONS

A wide-ranged program, additional laboratory tests, and results of previous examinations allowed a comparatively full description of the peculiarities of Dust Filtration Process Type I. Complex studies of dust filtration made it possible to correlate external parameters (dust collection efficiency and filtration resistances) not only with filtration parameters but also partly with initial aerosol state parameters and structural parameters of the filtration medium and the dust-fabric system. An explanation of process peculiarities can be obtained with application of:

- Mathematical modeling, quantitatively describing phenomena and, because of its empirical character, allowing prediction of process performance over the range of examined parameters; and
- Physical modeling, allowing a hypothesis to be offered over the range of effects between the filtration medium or the dust-fabric system and solid state particles dispersed in the gas.

Three-dimensional probabilistic models for dust collection efficiency and filtration resistances were presented, which included the effect of face velocity and dust covering (filtration time) for polyester fabrics ET-4 and ET-30, both filtering fly ash. As a complement, four-dimensional models illustrating the effect of initial dust concentration on dust collection efficiency variation were developed and presented.

A comparative analysis proved that increased dust dispersion decreases dust collection efficiency and increases filtration resistances. Particular attention was paid to the effect of particle shape on filtration resistances. Numerous statistical analyses conducted during interpretation of results led to some intermediate conclusions and to better interpretation of the physical phenomena. These results helped to distinguish two phases of the filtration cycle, corresponding physically to the stationary and "ductive" canal phase of filtration. The appearance of these two phases in a single Dust Filtration Process Type I is characteristic of this process. The inflection point (A) marked on a hydraulically characterized curve is typical of a given dust-fabric system and certain process conditions. It represents the dust collection efficiency of the fabric and its steady state residual dust load.

This interpretation of dust collection efficiency during a single filtration cycle makes dust collection efficiency predictable at any particular moment of filtration.

An original physical model of the dust-fabric system was prepared that described peculiarities affecting dust collection efficiency and filtration resistance in Dust Filtration Process Type I. Based on the dominant effect of superficial porosity on the process, the model permits delineation of three basic mechanisms of dust filtration:

- Selective precipitation,
- Inertial deposition, and
- Diffusion precipitation.

Although not reflected in the first general model, the influence of electrostatic forces is reflected in the detailed model. Close attention was given dust cake properties and the dust-fabric system. The mechanism of dust cake defects and their influence on external process parameters was described. Because of the basic problems connected with examination of dust cake properties--especially the fact that dust cake occurs in a continuous dynamic process--properties of static cakes obtained by sampling will differ from properties of static cakes during process performance. The examination of dust cakes is therefore possible only with formation and experimental verification of physical models. In dust cakes formed on filtration materials structure this method showed not only compression effects (low values of q_g) but also fluidization effects at high values of q_g.

Additional study of Dust Filtration Process Type I is recommended, to verify not only an extension to partial probabilistic models and the n-dimensional models of filtration but the physical model.

The examinations result in the following conclusions concerning Dust Filtration Process Type I:

- Dust collection efficiency and filtration resistances depend upon the degree of pulverization of the dust in the dispersion medium, the dust concentration, the aerosol particle shape, the face velocity, and the dust covering;
- Dust covering, L_o, is a parameter capable of estimating filtration effects;
- Increased q_g decreases dust collection efficiency, but the character of the variation depends on the structural parameters of the fabric;
- Increased dust concentration increases dust collection efficiency because of an increase in the dust stream, which is characterized by a higher value of dust flux; and
- Increased dust pulverization decreases dust collection efficiency and increases filtration resistances.

SECTION VI

FILTRATION PARAMETERS EFFECT ON DUST FILTRATION PROCESS TYPE III

INTRODUCTION

Dust Filtration Process Type III is characteristic of dust collection in industrial dust collection devices, cyclic dusting, and regeneration of filtration elements composed of certain filtration materials.

Examination of Dust Filtration Process Type III can be conducted directly, either by industrial or "large-scale" testing; i.e., application of filtration elements with commercial dimensions but small numbers (small total active surface area).

Large-scale testing stands are usually suitable for simulating industrial conditions over a wide range of parametric values. They allow broad examination of the process and its relationships and provide more valuable empirical data than do industrial-scale testing stands, where the ranges of process parameters are determined by industrial technology. Compared to laboratory-scale tests, industrial tests require more labor and yield less precise information because of less direct measurements of the operating parameters, which generally incorporate their own additional measurement errors.

Unlike laboratory-scale results, large-scale results can be directly applied to engineering work, without special interpretation. The main purpose of large-scale tests in dust filtration is the determination of the relationship between external and internal process parameters. The characteristic property of Dust Filtration Process Type III is the equilibrium amount of dust remaining in the fabric filter after regeneration because of the cyclic character of the process. Depending on the kind of dust and its physical properties, each filtration medium operating under set conditions (filtration parameters and manner of regeneration) is characterized by a definite steady state residual dust load, L_{NK}, and a corresponding static pressure drop, ΔP_{NK}.

These magnitudes are important with respect not only to a process description but also to its qualitative parameters. The large-scale tests of this project were conducted to discover the large-scale dust filtration relationships corresponding to the filtration relationships obtained in laboratory-scale testing. Thus, large-scale testing was conducted at the same level of initial aerosol state parameters and with similar filtration parameters as for laboratory-scale testing. Testing results were interpreted according to principles established in the theoretical section of this report.

EQUIPMENT AND PROCEDURES

Large-scale testing of selected filtration fabrics was conducted on an apparatus (single-compartment baghouse) specially designed by Instytut Przemysłu Wiążących Materiałów Budowlanych (IPWMB). Illustrated in Figure 89, the apparatus includes:

- Filter chamber,
- Collection hopper,
- Dust feeder,
- Fans,
- Pipelines and valves, and
- Control and measurement system.

The cylindrical filter chamber (0.70 m diameter and 3.52 m length) is composed of four separate elements that can be sealed tightly together. This type of construction enables researchers to conduct experiments on filter bags of various lengths. The last element of the filter chamber is the head, on which an arbitrary mechanical regeneration system can be installed. A collection hopper is located in the lower part of the filter chamber, which is thermally insulated. The test filter bags, 710 mm to 3 250 mm in length and 200 mm in diameter, are installed off center with respect to the filter chamber axis because of an isotopic probe used to measure dust cake thickness deposited on the filter bag. The total maximum filtration area is 2.01 m^2, with a net area of 1.884 m^2. A diagram of the single-compartment baghouse with its control and measurement system is shown in Figure 90. Test dust is circulated through a screw dust feeder with a capacity of 0.5 to 15 kg/hr ± 10 percent. A variable gear regulates the capacity of the screw dust feeder. The single-compartment baghouse is equipped with two fans:

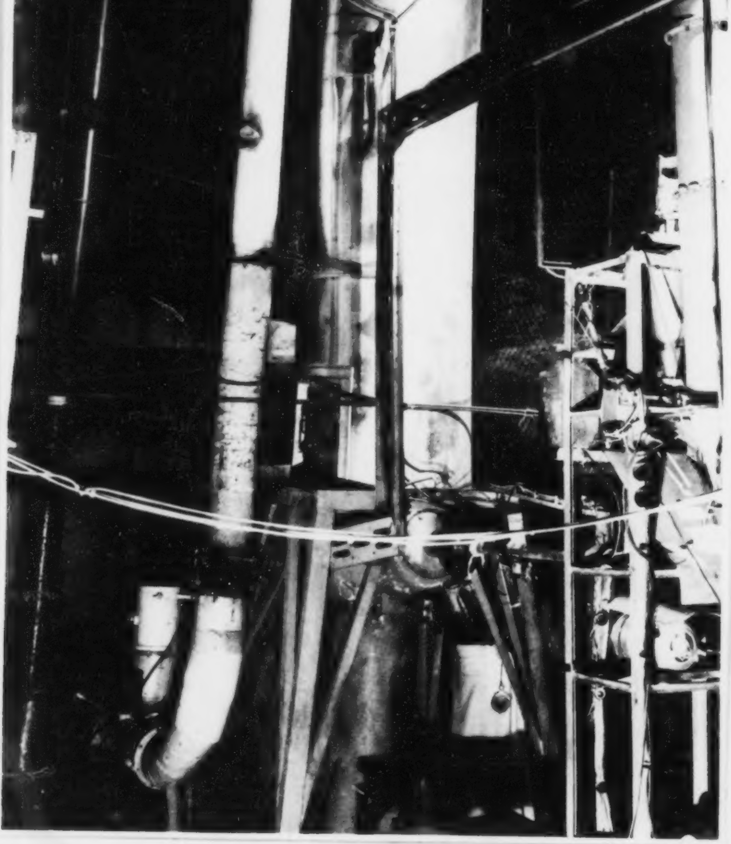

Figure 89. Large-scale stand.

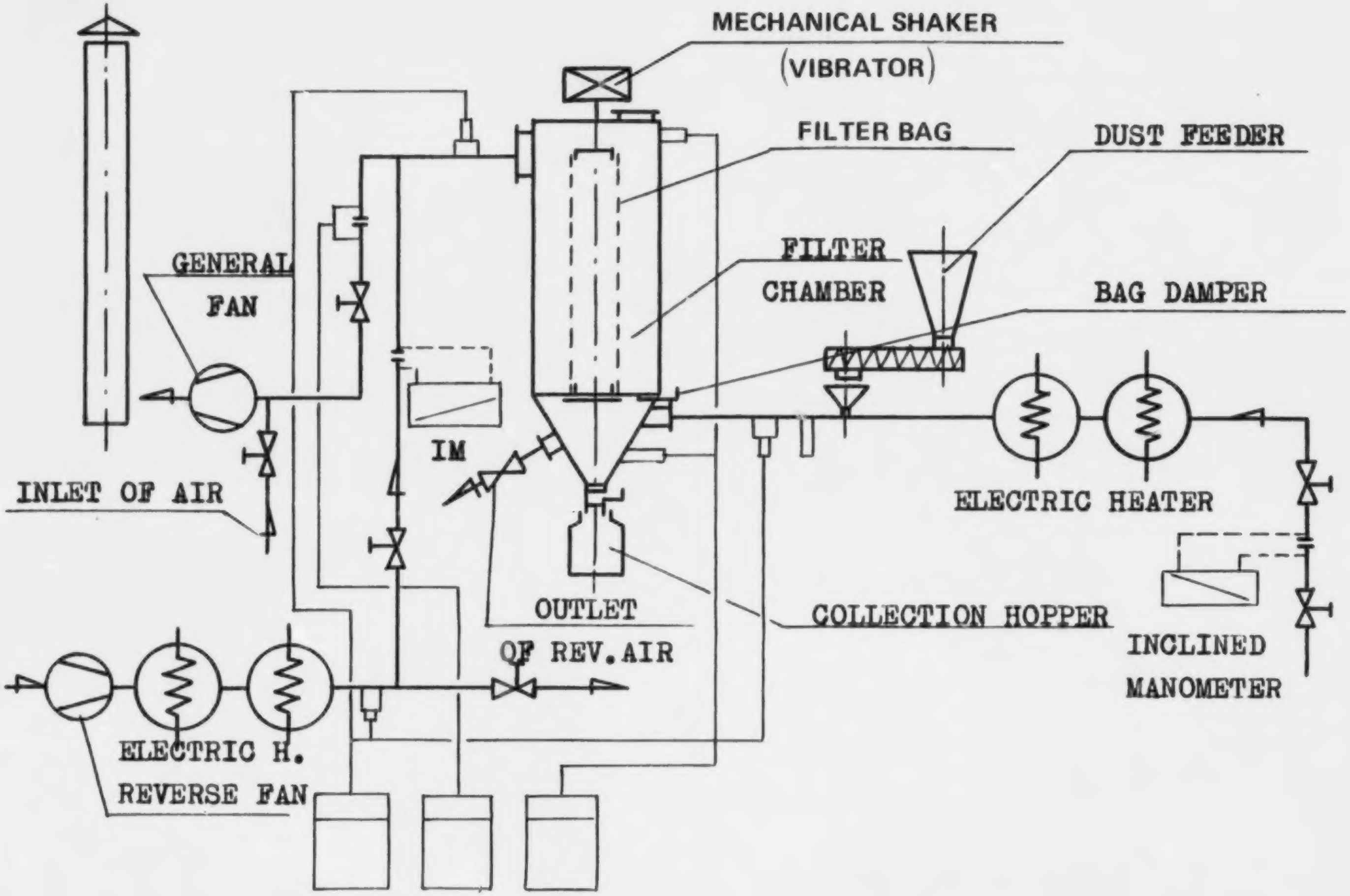
MECHANICAL SHAKER
(VIBRATOR)
FILTER BAG
DUST FEEDER
GENERAL
FAN
FILTER
CHAMBER
BAG DAMPER
IM
INLET OF AIR
ELECTRIC HEATER
OUTLET
OF REV.AIR
COLLECTION HOPPER
INCLINED
MANOMETER
ELECTRIC H.
REVERSE FAN

Figure 90. Diagram of the large-scale test stand.

- The main fan, type MWW 14, is used for maintaining a negative pressure in the test apparatus and for inducing flow through the filter chamber. The main fan capacity is 1 200 m^3/hr, and the total pressure differential achievable is 600 mm H_2O.
- A reverse air fan, type WP 20/1, is used to produce regeneration air flow in the opposite direction of gas flow during filtration. The reverse fan capacity is 1 200 m^3/hr, and the total pressure differential achievable is 300 mm H_2O.

Installations of reverse and circulating gases are equipped with electric heaters, type NP-27, used for maintaining dry filtration in the filter chamber. Control valves on the pipelines permit control of q_g according to programmed values and ensure continuous operation of the fans. The actions of particular systems and instruments of the single-compartment baghouse are remotely controlled from the operational room. The control system permits:

- Operation in the manual control system, and
- Operation in the automatic control system according to one of three variations of filter bag regeneration:
    - Reverse air flow regeneration,
    - Mechanical regeneration, and
    - Mechanical regeneration with simultaneous reverse air flow.

The above test apparatus is equipped with several sensors and control-measurement sets for recording the following parameters:

- Gas humidity,
- Gas temperature,
- Flow rate,
- Static pressure,
- Dust concentration before and after the filter chamber,
- Time of particular filtration cycles, and
- Temperature and humidity of air in the laboratory.

The general experimental conditions were:

- Maximum length of the filter bag: 3 500 mm,
- Regeneration cycle: as shown in Figure 91,
- Construction of the filter bag: as in Figure 92,
- Dispersion medium: unconditioned atmospheric air,
- Reverse air face velocity: 20 percent more than face velocity during filtration,

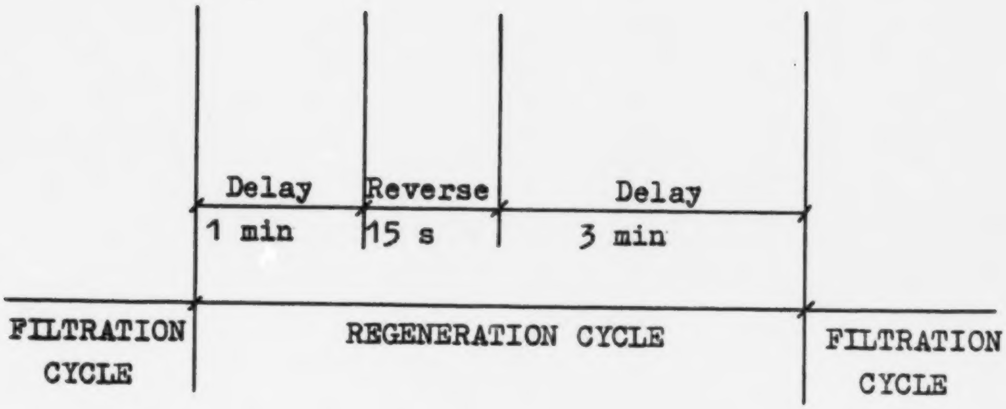
Delay
Reverse
Delay
1 min
15 s
3 min
FILTRATION CYCLE
REGENERATION CYCLE
FILTRATION CYCLE

Figure 91. Diagram of regeneration cycle.

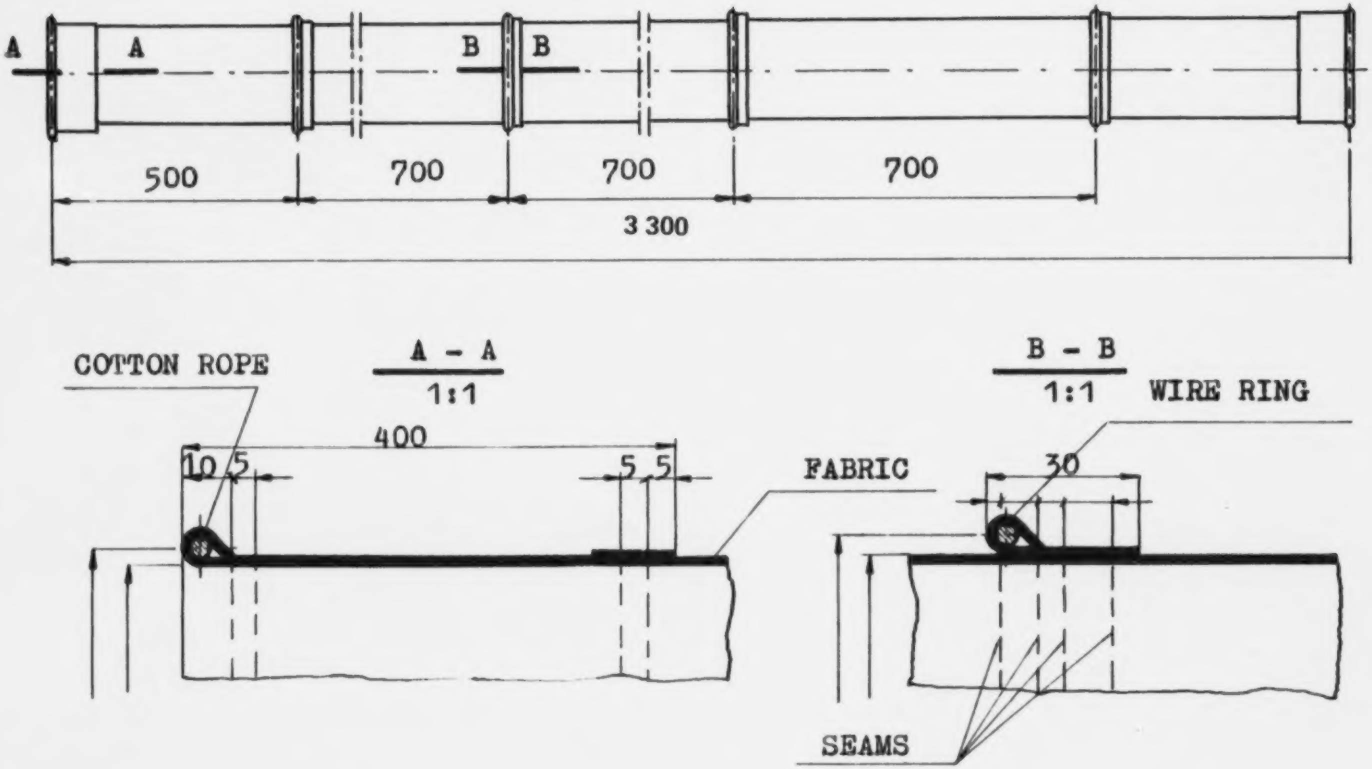
A
A
B
B
500
700
700
700
3 300
COTTON ROPE
A - A
1:1
400
10
5
5
5
FABRIC
B - B
1:1
WIRE RING
30
SEAMS

Figure 92. Construction of bags.

- Measurement of dust concentration behind the filter chamber: by aspiration, and
- Test mode for bags of steady state residual dust load: by multiple repetition of filtration-regeneration cycles.

A detailed description of the preparatory work prior to and the auxiliary work during large-scale fabric testing is included in Section III.

Dust collection efficiency of the single-bag compartment was determined by the weighing method based on the measurement of dust concentration in the cleaned gases.

The total efficiency was calculated from the equation:

$$E_{T1} = \frac{G_c - G_o}{G_c} \cdot 100 = \left(1 - \frac{c_2}{c_i}\right) \cdot 100 \quad , \tag{74}$$

where

E_{T1} = total efficiency, %;
G_c = total weight of the dust introduced into the testing chamber hopper, g;
G_o = weight of dust in cleaned gases--measurement of emission, g;
c_i = initial concentration at the compartment inlet, g/m^3; and
c_2 = outlet concentration at the compartment, g/m^3.

The steady state residual dust load, L_{NK}, was determined by weighing the filtration element after the regeneration system.

$$L_{NK} = \frac{G_1 - G_2}{F} \quad , \tag{75}$$

where

L_{NK} = steady state residual dust load, g/m^2;
G_1 = weight of filtration element after regeneration, g;
G_2 = weight of clean filtration element, g; and
F = filtration element surface, m^2.

Dust collection efficiency was determined by taking the mean of five measurement cycles after a state of equilibrium was reached for the dust-fabric system; i.e., stabilization of the L_{NK} value. According to deliberations in the theoretical section, the mean dust cake parameter is expressed by the following equation:

$$\bar{L}_p = \frac{\left(\frac{1}{n} \sum_{n=1}^{5} L_{o_n} - \frac{1}{n} \sum_{n=1}^{5} L_{NK_n}\right)}{2} , \qquad (76)$$

assuming that $L_o = L_{NK} + L_p$.

RESULTS

Testing results are shown in Tables 20 through 23. Table 20 includes the mean values of dust collection efficiency from five measurement cycles. These efficiencies were obtained in succession at each q_g level with increasing values of the terminal dust load, $L_o = L_{NK} + L_p$.

The values of the final pressure drop, corresponding to a specific dust load at a given q_g, are shown in Table 21. Table 21 also includes true values of the dust load; i.e., the steady state residual dust load plus the areal mass density of the dust cake.

Values of the true steady state residual dust load, L_{NK}, for individual levels of the filtration parameters are shown in Table 22. Table 23 includes values of characteristic dust cake areal mass density, L_p, obtained during measurements.

DISCUSSION OF RESULTS

The Influence of Filtration Parameters Upon Dust Collection Efficiency

The basic filtration parameters, q_g and L_o, affect the external process parameters: efficiency and filtration resistance. As in the laboratory-scale experiments, deliberations in the theoretical section acted as a base for analysis and the resulting probabilistic three-dimensional model of dust collection efficiency for Dust Filtration Process Type III in the form of Equation 39. The general form of the model is similar to the dust collection efficiency model of Dust Filtration Process Type I, so a similar mathematical interpretation of the experimental data was assumed.

The straight line equation can be derived from Equation 39 in the Rosin-Rammler coordinate system.

$$\log \log \frac{100}{E_{III}} = F_4 \log L_p + \log \log (F_1 \cdot F_3) \quad . \qquad (77)$$

TABLE 20. LARGE-SCALE EFFICIENCY (%) OF POLYESTER STYLE ET-4 AND ET-30 TESTED WITH SEPARATED FLY ASH

Kind of fabric	q_g (m^3/m^2h)	Nominal values of characteristic parameter of dust cake, L_p (g/m^2)*					
		100	200	300	400	600	800
ET-4	60	99.9496	99.9841	99.9701	99.9756	99.9799	-
	80	99.9744	99.9981	99.9752	99.9797	99.9684	99.9323
	100	99.9417	99.9184	99.8986	99.9471	99.8695	99.9545
	120	99.8622	99.9088	99.8974	99.8317	99.9353	99.8799
	160	99.7464	99.4738	(98.8154)	99.6966	99.6468	99.8070
ET-30	60	99.9070	99.9967	99.9979	99.9780	99.9785	99.9896
	80	99.9686	99.9684	99.9842	99.9816	99.9963	99.9854
	100	99.9770	99.9876	99.9491	99.9829	99.9193	99.9940
	120	99.8907	99.7074	99,8035	99.7866	99.7718	99.9769
	160	99.8514	99.9102	99.8009	99.7879	99.5197	99.8268

*Real values of characteristic parameter of dust cake are presented in Table 23.

TABLE 21. FINAL PRESSURE DROP IN LARGE SCALE (mm H_2O) FOR POLYESTER STYLE ET-4 AND ET-30 TESTED WITH SEPARATED FLY ASH

Kind of fabric	q_g (m^3/m^2h)	Nominal values of characteristic parameter of dust cake, L_p (g/m^2)					
		100	200	300	400	600	800
ET-4	60	10.4/264.6*	15.3/376.0	22.9/568.0	28.3/716.9	31.8/887.6	-
	80	20.5/303.4	30.3/433.7	40.8/538.5	47.8/640.1	59.6/831.7	65.5/1037.0
	100	29.9/317.2	48.4/430.2	59.2/259.8	74.6/662.6	99.2/876.6	115.2/1043.7
	120	28.2/292.7	45.4/421.5	60.8/539.5	72.1/653.4	95.8/858.2	125.4/1090.7
	160	51.2/387.2	78.7/506.2	95.5/595.7	110.6/696.3	133.8/906.3	166.9/1114.7
ET-30	60	18.8/221.2	23.0/332.8	27.2/438.3	29.3/519.4	39.5/740.1	41.7/848.2
	80	25.4/246.1	34.1/356.3	40.6/457.7	42.0/564.2	53.4/757.9	62.2/936.3
	100	32.7/251.8	45.7/388.4	56.9/497.0	64.3/586.1	85.3/791.5	89.6/985.7
	120	42.3/242.1	51.6/344.5	64.7/492.3	73.9/576.9	93.7/787.0	123.8/1007.7
	160	73.4/261.5	81.9/383.3	117.5/524.5	115.6/597.9	164.6/791.5	206.0/990.8

*Real values of dust covering of filtration area, L_o (g/m^2).

TABLE 22. FILLING OF FABRIC STRUCTURE WITH DUST FOR LARGE-SCALE EXPERIMENTS

Kind of fabric	q_g (m^3/m^2h)	Nominal values of characteristic parameter of dust cake, L_p (g/m^2)					
		100	200	300	400	600	800
ET-4	60	211.0	292.4	295.6	292.9	298.2	-
	80	200.8	232.4	239.6	240.6	241.3	231.4
	100	189.0	223.8	229.4	262.1	274.8	252.4
	120	196.7	226.8	241.1	248.8	256.9	294.3
	160	279.4	300.4	(297.7)	297.3	302.9	299.9
ET-30	60	115.7	124.9	137.6	124.9	128.0	140.6
	80	142.7	147.3	156.0	151.4	155.0	146.8
	100	154.4	185.5	198.8	195.7	192.6	184.0
	120	145.8	159.0	208.4	183.5	192.2	182.5
	160	171.8	181.4	207.9	197.8	204.9	190.6

TABLE 23. REAL VALUES OF CHARACTERISTIC PARAMETER OF DUST CAKE, L_p (in g/m^2), FOR LARGE-SCALE EXPERIMENTS

Kind of fabric	q_g (m^3/m^2h)	Nominal values of characteristic parameter of dust cake, L_p (g/m^2)					
		100	200	300	400	600	800
ET-4	60	53.6	83.6	272.4	424.0	589.4	-
	80	102.6	201.3	298.9	399.5	590.4	805.6
	100	128.2	206.4	300.4	400.5	601.8	791.3
	120	96.0	194.7	298.4	404.6	601.3	796.4
	160	107.8	205.8	298.0	399.0	603.4	814.8
ET-30	60	105.5	207.9	300.7	394.5	612.1	707.6
	80	103.4	209.0	301.7	412.8	602.9	789.5
	100	97.4	202.9	298.2	390.4	598.9	801.7
	120	96.3	185.5	283.9	393.4	594.8	825.2
	160	89.7	201.9	316.6	400.1	586.6	800.2

The intercept of the straight line with the value, $L_p = 1$, determines the value of $(F_1 \cdot F_2)$, which, according to Equation 40, describes the initial dust collection efficiency of the fabric and its steady state residual dust load for fixed operating and regenerative conditions.

Initial efficiency corresponds to a state of equilibrium, described by the constant value, $L_N = L_{NK}$ = constant, so the value applies to $t_F = 0$. Thus, E_{oIII} and L_{NK} are important parameters that describe a filtration material operationally.

Function F_4 is similar to function F_2 in Dust Filtration Process Type I and determines the process performance in time. A negative value of F_4 indicates that dust collection efficiency increases with increasing time (increasing dust cake), in accordance with experimental results of this project.

When Equation 57 was applied to the set of empirical data, certain values of $(F_1 \cdot F_3)$ and F_4 as a function of q_g and constant levels of dust cake parameters were determined. A new interpretation of mean dust collection efficiency for the cycle, resulting from the manner of determination, was considered during the calculations. The mean efficiency in the cycle was related to the mean value of the dust cake parameter; i.e., $\bar{L}_p = L_p/2$. Table 24 includes the values of the functions $(F_1 \cdot F_3)$ and F_4 for the fabrics tested and the levels of q_g, where tested.

A small variation of the function $(F_1 \cdot F_3)$ from its absolute value, indicating high initial efficiency, is typical. If the mean value of the function $(F_1 \cdot F_3)$ is taken for an examined range of q_g, it is possible to determine mean initial efficiency:

For fabric ET-4, $\bar{E}_{oIII} = \frac{1}{1.00449} \cdot 100 = 99.55$ percent, and

For fabric ET-30, $\bar{E}_{oIII} = \frac{1}{1.00599} \cdot 100 = 99.40$ percent.

Despite physically different fabric structures, the initial dust collection efficiencies do not vary much. Therefore, the equalization of spatial and superficial porosity was attributed to dust filling of interthread and interfiber spaces. According to theoretical deliberations, porosity determines process efficiency. The initial efficiency of the dust-filled structures is high, which suggests that mean dust collection efficiency is nearly 100 percent.

TABLE 24. VALUES OF $F_1 \cdot F_3$ AND F_4 FROM EQUATION 39

Kind of fabric	q_g (m^3/m^2h)	$F_1 \cdot F_3$	F_4
ET-4	60	1.00065	-0.2042
	80	1.00020	+0.0312
	100	1.0099	-0.5141
	120	1.0054	-0.3614
	160	1.0063	-0.1401
Average		1.00449	
ET-30	60	1.00125	-0.4709
	80	1.01	-0.8326
	100	1.0034	-0.6201
	120	1.0145	-1.2958
	160	1.0008	+0.1332
Average		1.00599	

TABLE 25. COEFFICIENTS OF PARABOLA EQUATIONS:
$F_1 \cdot F_3 = a_{1\ 3}\, q_g^2 + b_{1\ 3}\, q_g + c_{1\ 3}$
and $F_4 = a_4\, q_g^2 + b_4\, q_g + c_4$

Value of coefficient	Kind of fabric	
	ET-4	ET-30
$a_{1\ 3}$	$-8.0475 \cdot 10^{-7}$	$-3.5032 \cdot 10^{-6}$
$b_{1\ 3}$	$2.3885 \cdot 10^{-4}$	$7.7102 \cdot 10^{-4}$
$c_{1\ 3}$	$9.8931 \cdot 10^{-1}$	$9.6784 \cdot 10^{-1}$
a_4	$9.1151 \cdot 10^{-5}$	$3.2891 \cdot 10^{-4}$
b_4	$-2.0764 \cdot 10^{-2}$	$-6.7841 \cdot 10^{-2}$
c_4	$8.2797 \cdot 10^{-1}$	2.4913

The values $(F_1 \cdot F_3)$ and F_4, presented in Table 24, were obtained by a least squares fit to the following parabolic equations:

$$\begin{aligned} (F_1 \cdot F_3) &= a_{1\,3}\, q_g^2 + b_{1\,3}\, q_g + c_{1\,3} \quad \text{, and} \\ F_4 &= a_4\, q_g^2 + b_4 \cdot q_g + c_4 \quad . \end{aligned} \qquad (78)$$

Coefficients for Equation 78 for fabric ET-4 and ET-30 are shown in Table 25.

Functions $(F_1 \cdot F_3)$ and F_4, which depend on q_g, are shown in Figure 93 and Figure 94. When Equation 78 is derived from Equation 39, the following general probabilistic model of dust collection efficiency for Dust Filtration Process Type III is obtained:

$$E_{III} = 100 \left[a_{1\,3}\, q_g^2 + b_{1\,3} \cdot c_{1\,3}\right]^{\bar{L}_p^{\left[a_4\, q_g^2 + b_4 \cdot q_g + c_4\right]}} \qquad (79)$$

where

E_{III} = instantaneous dust collection efficiency, %;

$\bar{L}_p$ = characteristic parameter of the dust cake, g/m^2; and

q_g = face velocity, m^3/m^2h.

When values of the coefficients in Table 25 are used in Equation 79, models of dust collection efficiency for fabrics ET-4 and ET-30 are obtained that apply to the filtration of separated fly ash at initial concentration, $c_1 = 10\ g/m^2$, and use reverse air flow regeneration at a value 20 percent greater than the forward flow. The above value of initial dust concentration refers to the aerosol concentration in the measurement chamber inlet, so it does not necessarily describe the aerosol concentration immediately in front of the filtration element (bag). The aerosol concentration in front of the filtration element depends on the separation properties of the hopper; i.e., its geometry, the location of the gas inlet and the amount of dust in the hopper.

During the overall large-scale test program of Project P-5-533-4, total hopper efficiency was found to be best determined by the method of dust layer balance during certain phases of the experiment and analysis of the results, according to Equation 74.

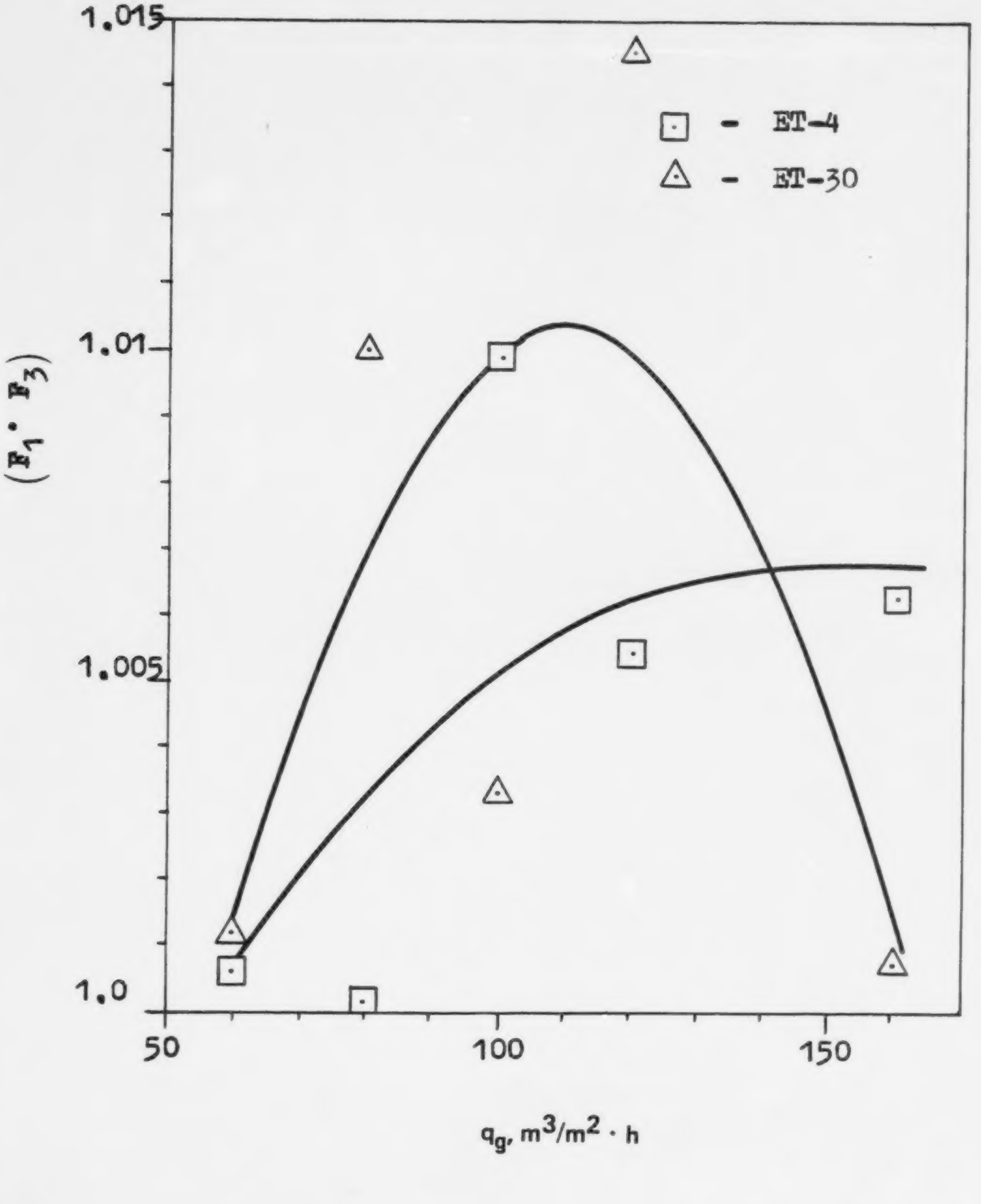

Figure 93. Dependence of $(F_1 \cdot F_3)$ on q_g for fabrics ET-4 and ET-30.

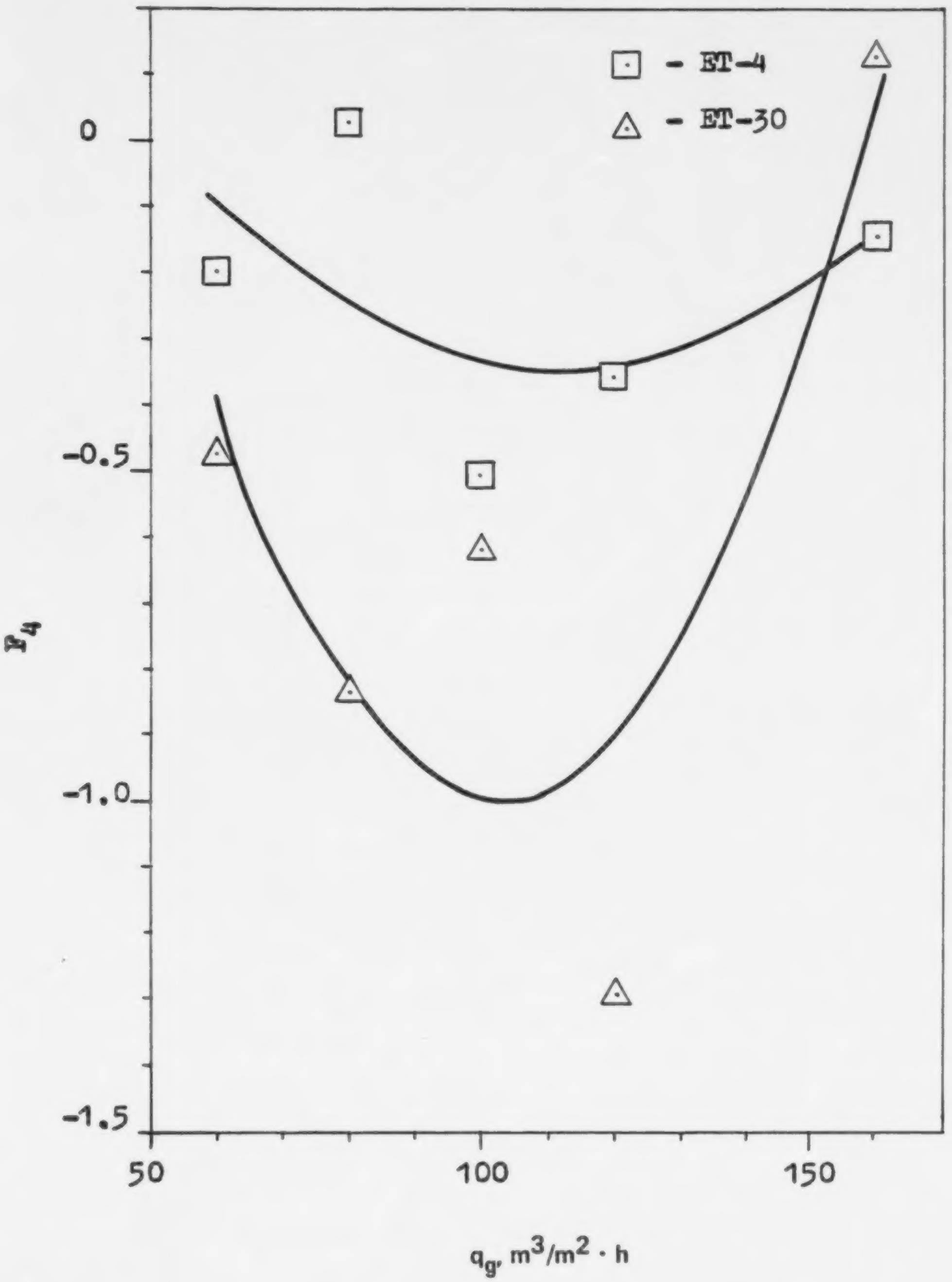

Figure 94. Dependence of F_4 on q_g for fabrics ET-4 and ET-30.

Total hopper efficiency, determined according to the method of dust layer balance for different levels of q_g and different values of L_o, is illustrated in Table 26. Because of the manner of calculating hopper efficiency (the dust balance method over one measurement cycle), the method depends intermediately upon the kind of filtration material, which determines its regeneration properties. This dependency can be verified through a comparison of hopper efficiency values for the tested fabrics.

For fabric ET-4, which has a porous structure and a large surface area of fiber-dust contact, high regeneration is observed and proven by the lack of correlation between hopper efficiency and dust covering for individual levels of q_g. But for fabric ET-30, which is characterized by less spatial porosity and less dust-fiber contact, the dependence of hopper efficiency upon dust load at each level of q_g is apparent.

This apparent dependence results from the fact that during the filtration cycle some of the dust cake slides off the bag and into the hopper because of the good regeneration properties of the fabric. This additional hopper dust influences the dust balance and directly increase hopper efficiency. The mechanism is more obvious when time to reach a certain dust cake thickness is taken into account. During some experiments conducted with fabric ET-30, it was ascertained that the assumed values of L_o would never be reached (at low q_g). In this situation, the reliable hopper efficiency values are the efficiencies obtained at low values of L_o; i.e., 100 g/m². When hopper efficiency as a function of q_g is analyzed, its decrease with increasing q_g is observed. This decrease is understandable, because for a given hopper concentration, increased q_g leads to increased gas velocity in the cross section of the hopper. Thus, the dust grain size and dust concentration at the bag increases. The mean dust concentration on the upstream side of the filtration bag, c_1', determined from hopper efficiency and initial dust concentration on the measurement chamber inlet, is:

For fabric ET-4,

$$c_1' = (1 - E_L) \cdot c_1 = 0.5 \cdot 10 = 5 \text{ g/m}^3 \quad \text{, and}$$

For fabric ET-30,

$$c_1' = (1 - E_L) \cdot c_1 = 0.4 \cdot 10 = 4 \text{ g/m}^3 \quad .$$

TABLE 26. HOPPER EFFICIENCY (%) CALCULATED BY DUST BALANCE

Kind of fabric	q_g (m^3/m^2h)	L_o (g/m^2)	E_L (%)
ET-4	60	100	62.05
		200	71.48
		300	79.54
		400	75.12
		600	74.40
	80	100	57.74
		200	60.63
		300	56.31
		400	55.29
		600	57.06
		800	55.13
	100	100	48.98
		200	49.43
		300	47.67
		400	52.63
		600	50.17
		800	53.28
	120	100	56.95
		200	47.30
		300	48.50
		400	46.50
		600	52.37
		800	54.33
	160	100	45.41
		200	45.29
		300	40.61
		400	37.75
		600	39.96
		800	40.61
ET-30	60	100	56.99
		200	61.08
		300	67.38
		400	64.94
		600	65.59
		800	68.11
	80	100	60.03
		200	53.96
		300	56.88
		400	60.88

(continued)

TABLE 26 (continued)

Kind of fabric	q_g (m^3/m^2h)	L_o (g/m^2)	E_L (%)
		500	65.18
		600	65.57
		800	63.84
	100	100	56.58
		200	61.83
		300	61.72
		400	60.95
		600	61.06
		800	63.96
	120	100	51.06
		200	52.01
		300	56.31
		400	58.75
		600	52.60
		800	60.71
	160	100	49.02
		200	52.26
		300	52.11
		400	49.73
		600	49.30
		800	50.28

The model of dust collection efficiency embodied in Equation 79 depicts efficiency as a function of the parameters, q_g and L_p, for two distinct aerosol states: the initial dust concentration in the measurement chamber inlet (c_1 = 10 g/m^3) and dust concentration at the bag (c_1' = 4 to 5 g/m^3). In the first case, efficiency can be defined as total efficiency of the system, and in the second, as mean efficiency of the dust-fabric system. Analysis of the results from laboratory-scale testing showed that efficiency depended on the value of dust concentration. Therefore, the hypothesis can be offered that a similar dependence is possible in Dust Filtration Process Type III. The model according to Equation 79 describes the variation of dust collection efficiency of the dust-fabric system at the initial concentration, c_1'. Because a constant value of residual dust load (L_{NK} = constant) is one of the model assumptions, the model depicted by Equation 79 can be related to filtration time, t_F, as follows:

$$\bar{L}_p = c_1' \cdot q_g \cdot t_{F/2} = (1 - E_L) \cdot c_1 \cdot q_g \cdot t_{F/2} \quad . \qquad (80)$$

When variations of the ($F_1 \cdot F_3$) functions of the large-scale testing were analyzed, as in laboratory testing, a $q_{g\ extr}$ was found to exist that divided Dust Filtration Process Type III into two ranges. Data from Table 25 were used to calculate $q_{g\ extr}$:

For fabric ET-4,

$$q_{g\ extr} = \frac{2.3885 \times 10^{-4}}{2 \times 8.0475 \times 10^{-7}} = 148.40 \text{ m}^3/\text{m}^2\text{h} \quad , \text{ and}$$

For fabric ET-30,

$$q_{g\ extr} = \frac{7.7102 \times 10^{-4}}{2 \times 3.5032 \times 10^{-6}} = 110.04 \text{ m}^3/\text{m}^2\text{h} \quad .$$

Because initial efficiency is an inverse of the ($F_1 \cdot F_3$) function, the calculated, extreme values of q_g determine the minimum of E_{oIII}. Through application of Equation 79, the plots depicting dust collection efficiency as a function of q_g and at definite levels of the dust cake parameter, L_p, were explained.

Plots are presented in Figures 95 through 116. The points corresponding with measurements are also marked in the figures. Good agreement was obtained among the E_{III} values from experiments and those predicted by the model. Some deviations result from approximation of $(F_1 \cdot F_3)$ and F_4 and can be caused by measuring inaccuracy. During analysis of $E_{III} = f(q_g)$, similarity was observed between its shape and that observed in the laboratory-scale testing. This similarity is especially noticeable at low dust loads and low values of dust cake areal mass (compare Figures 54 and 106 and also Figures 36 and 95). Fabric ET-4 is characterized by maximum efficiency in the range $q_g \sim 80$ to 90 m^3/m^2h, but fabric ET-30 is characterized by an inflection point of the function $E_{III} = f(q_g)$ at $q_g \sim 80\ m^3/m^2h$.

Because the two sets of experiments were conducted with different equipment and under completely different process conditions, the observed similarity can be interpreted as evidence for similar dust cake spatial structure formation, regardless of other factors.

Experimental data as well as the predicted dust collection efficiencies from the model confirm the negative effect of increased q_g on the external process parameters and increased efficiency with increasing dust cake thickness as measured by the value of the parameter, L_p.

However, when Equation $E_{III} = f(q_g)$ is considered for fabric ET-4 at q_g = 80 m^3/m^2h (Figure 102) and for fabric ET-30 at q_g = 100 m^3/m^2h (Figure 114), a discrepancy exists in that efficiency does not increase with increasing dust cake thickness as predicted. The dust cake, under higher pressure differential, is not influenced by compression with a simultaneous decrease in porosity and thus greater efficiency. However, its porosity increases, perhaps either because of some structural defects as observed in the laboratory-scale testing or fluidization. The character of the efficiency variation with $\bar{L}_p$ is discrete, and rebuilding of the dust cake structure at higher values of $\bar{L}_p$ is observed. This process would support the idea that decreased efficiency in the range of high q_g and high values of $\bar{L}_p$ is caused by dust cake defects.

Effect of Filtration Parameters on Filtration Resistance

As in the laboratory-scale testing, no results during large-scale testing gave a linear increase of filtration resistance as a function of dust cake thickness, as measured by the characteristic parameter, L_p (or as a function

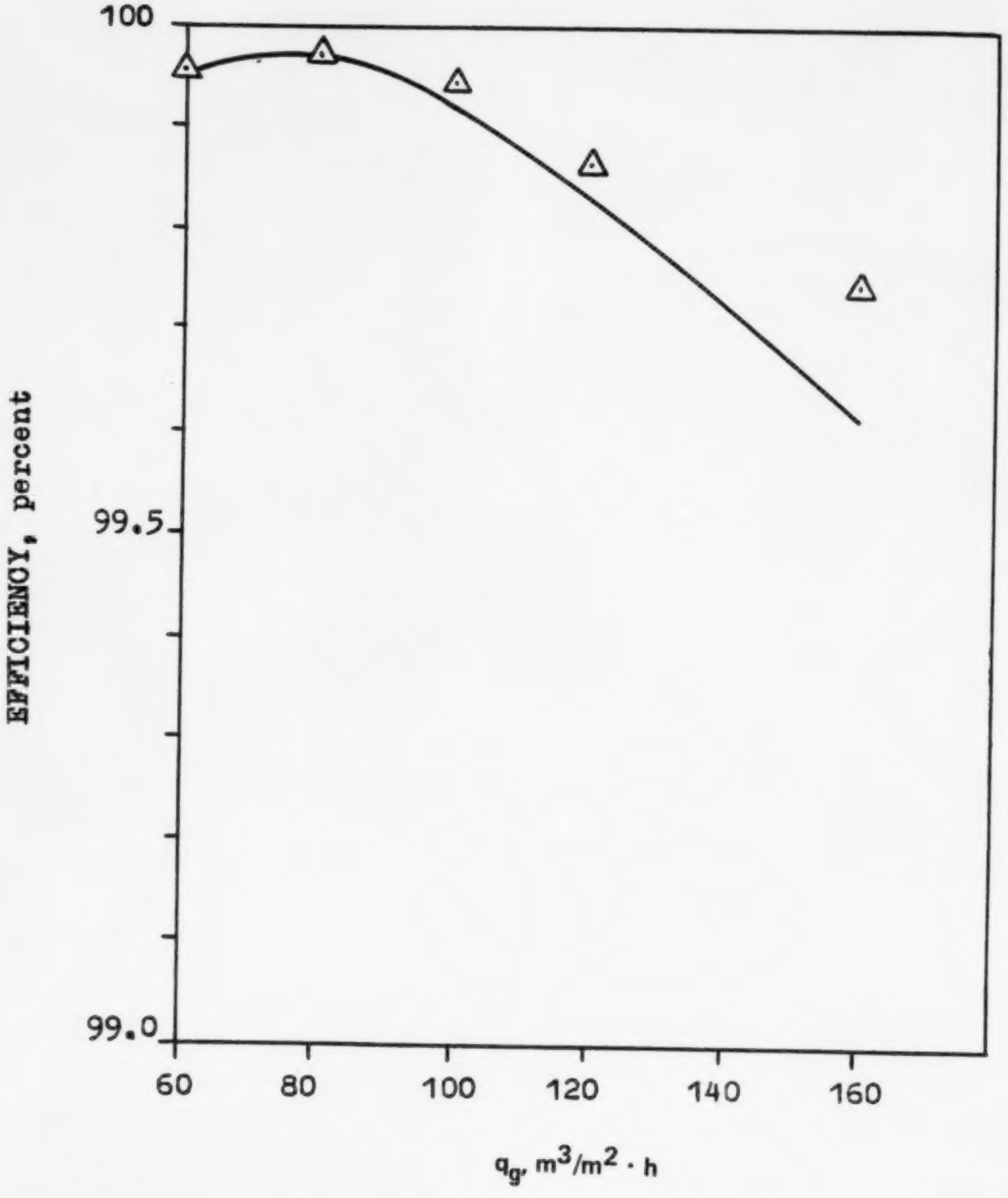

Figure 95. Predicted and experimental efficiencies of ET-4 as a function of q_g for $L_p = 50\ g/m^2$.

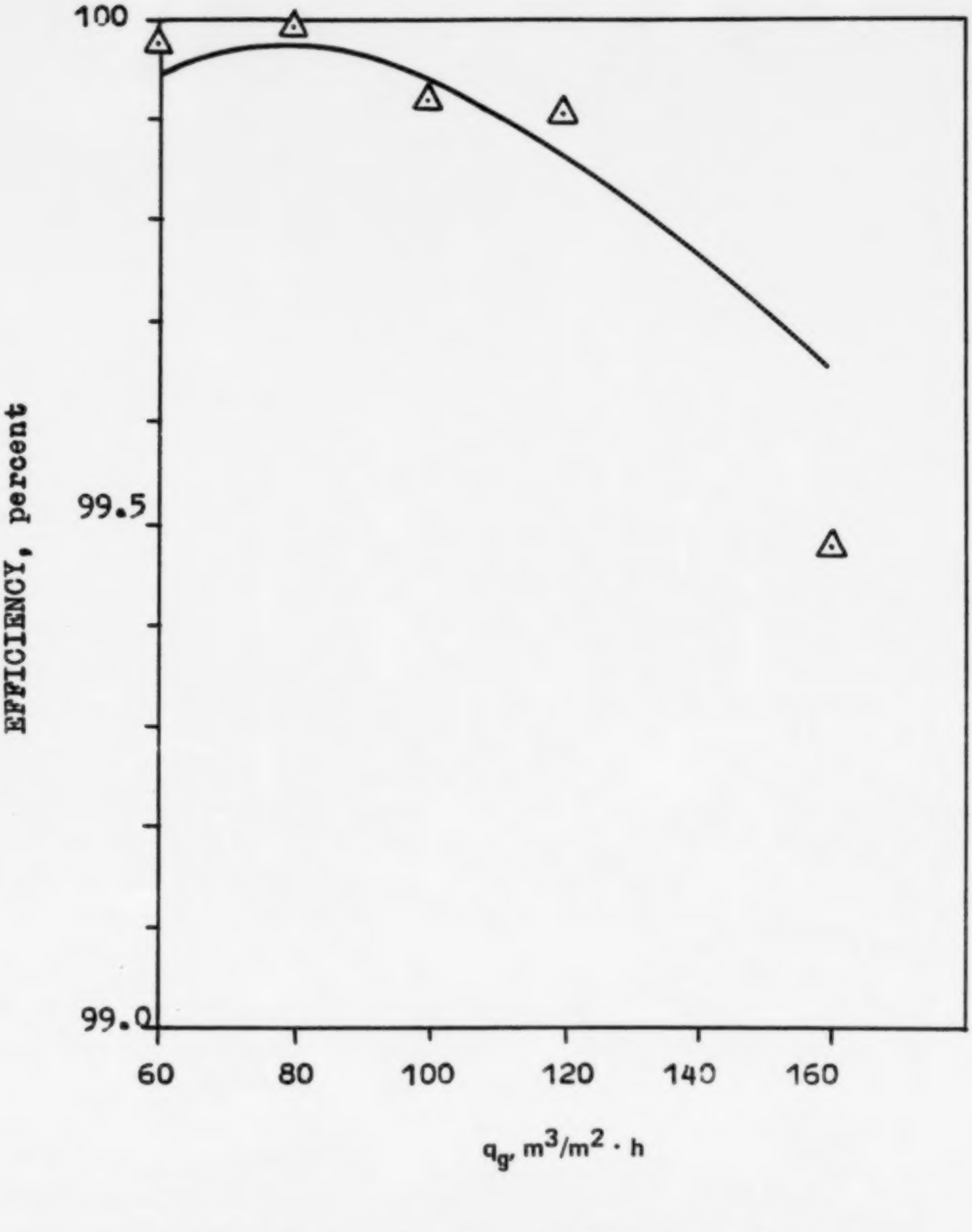

Figure 96. Predicted and experimental efficiencies of ET-4 as a function of q_g for L_p = 100 g/m^2.

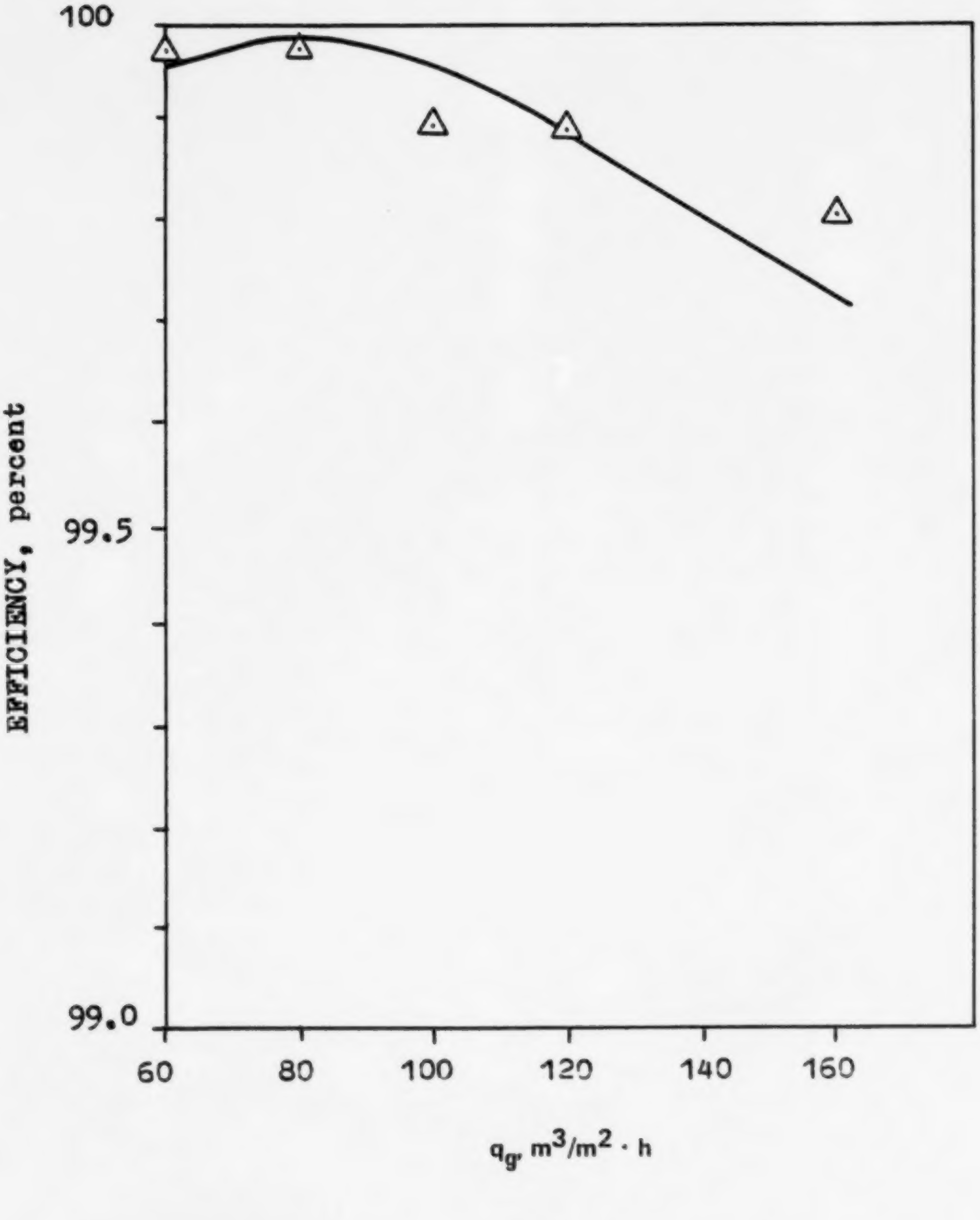

Figure 97. Predicted and experimental efficiencies of ET-4 as a function of q_g for L_p = 150 g/m^2.

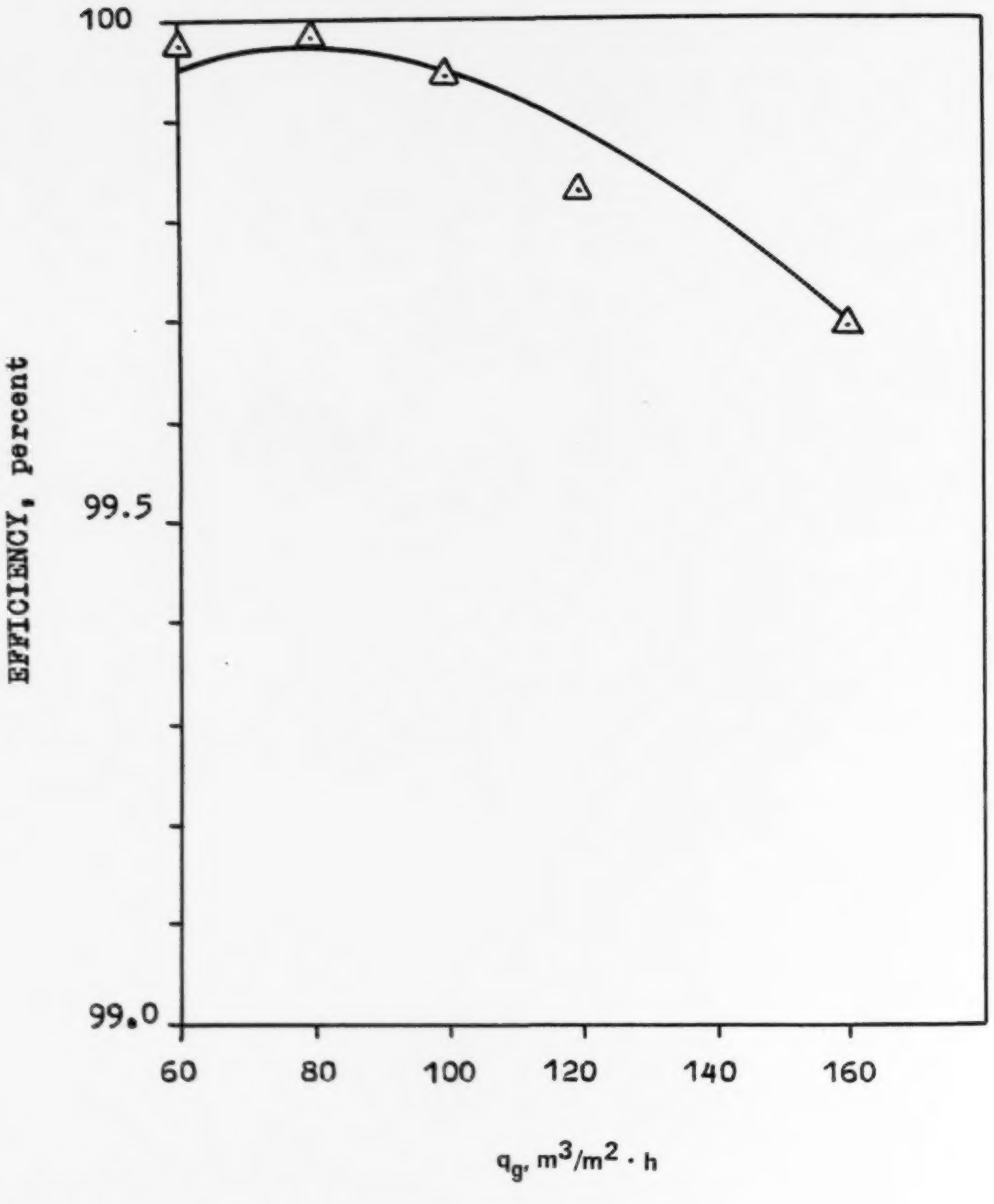

Figure 98. Predicted and experimental efficiencies of ET-4 as a function of q_g for $L_p = 200\ g/m^2$.

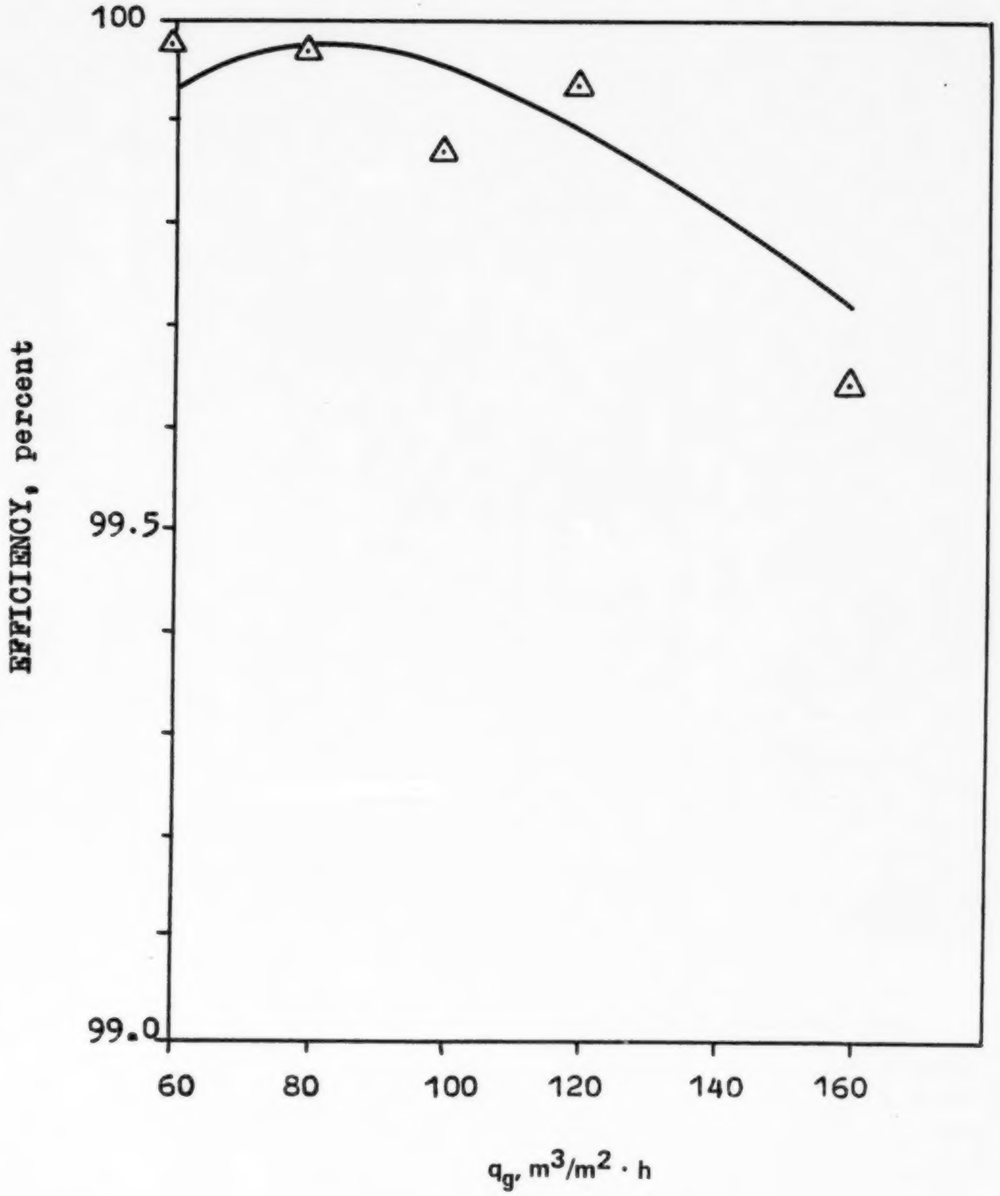

Figure 99. Predicted and experimental efficiencies of ET-4 as a function of q_g for $L_p = 300\ g/m^2$.

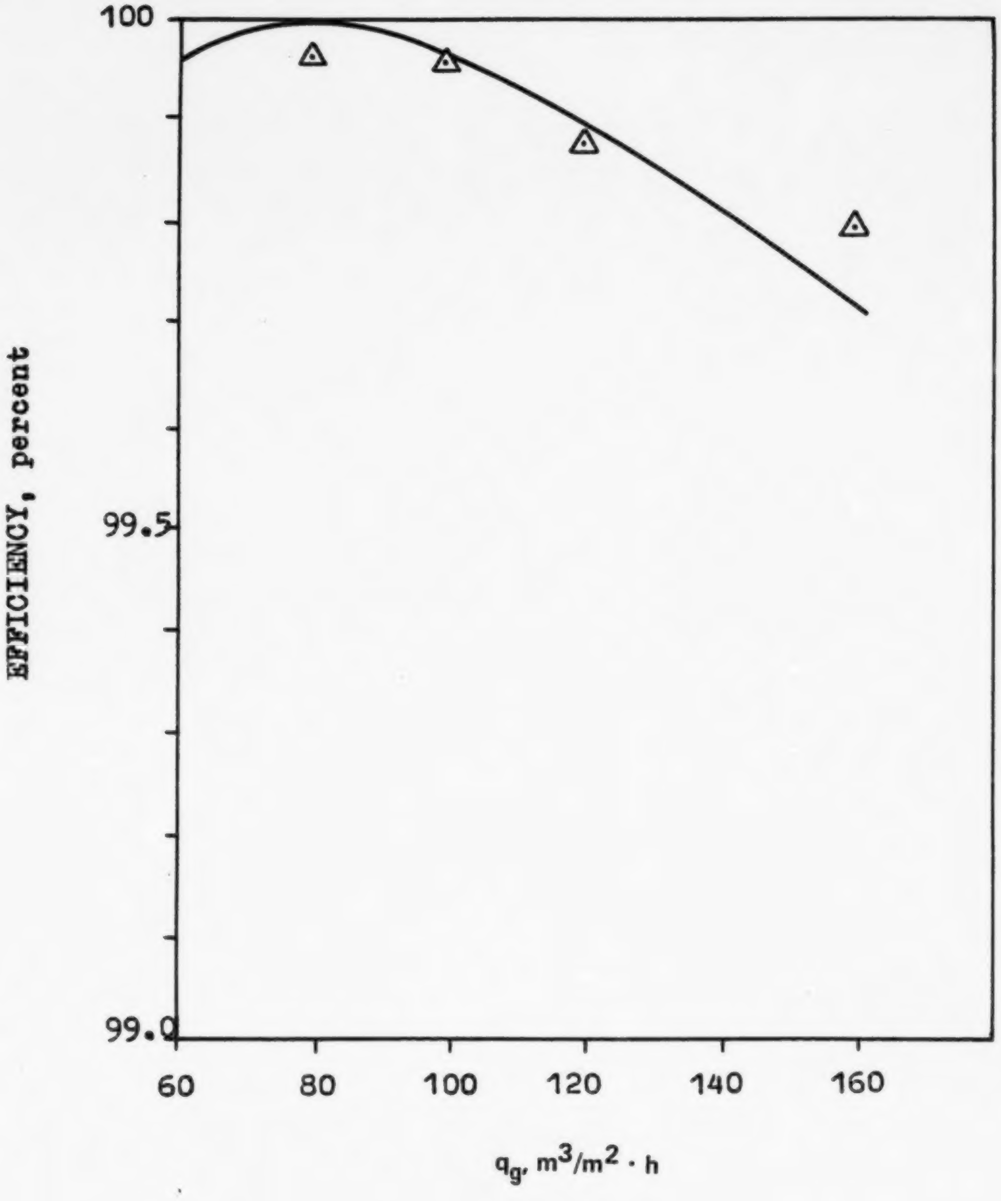

Figure 100. Predicted and experimental efficiencies of ET-4 as a function of q_g for $L_p = 400\ g/m^2$.

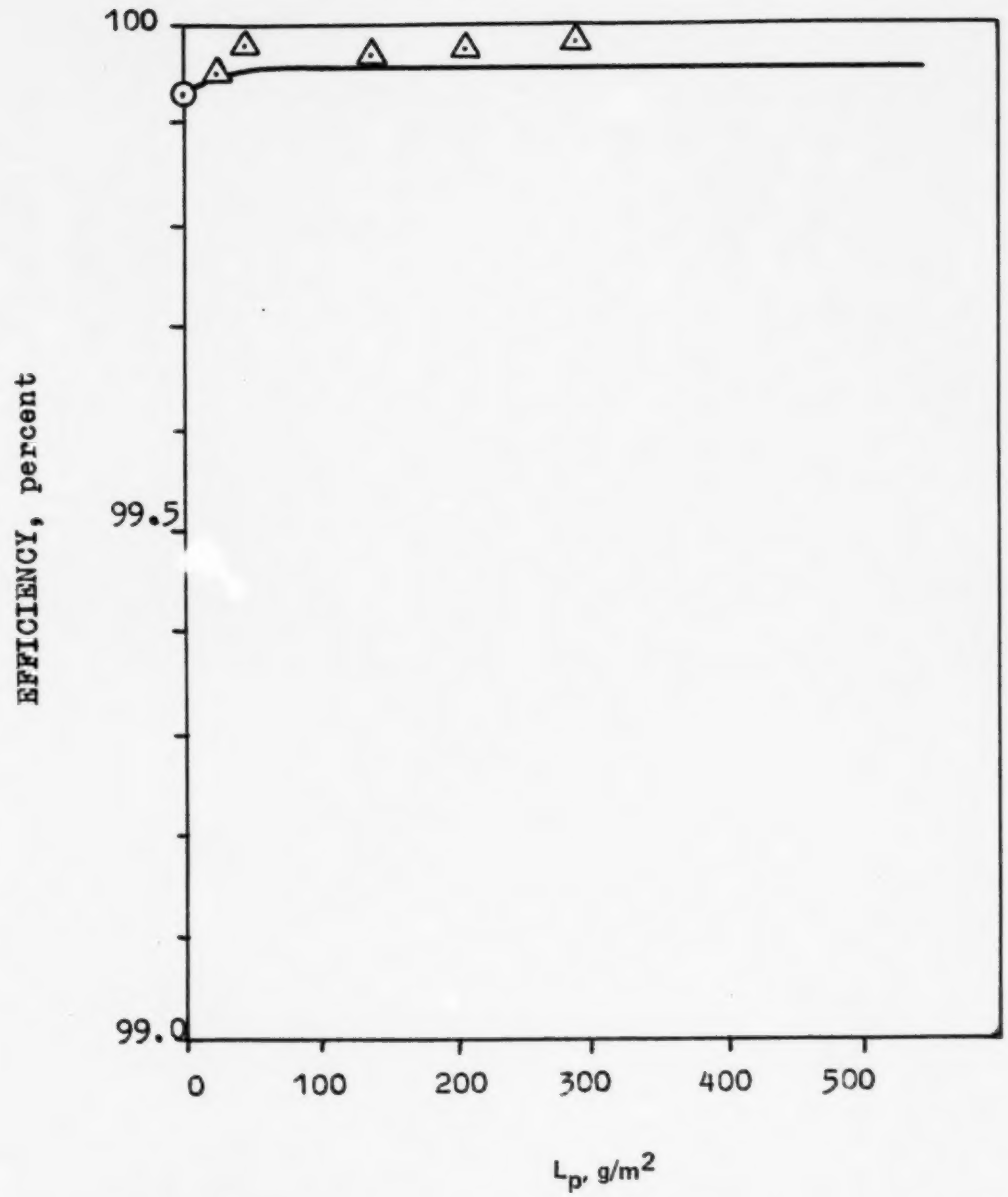

Figure 101. Predicted and experimental efficiencies of ET-4 as a function of L_p for $q_g = 60$ m^3/m^2 · h.

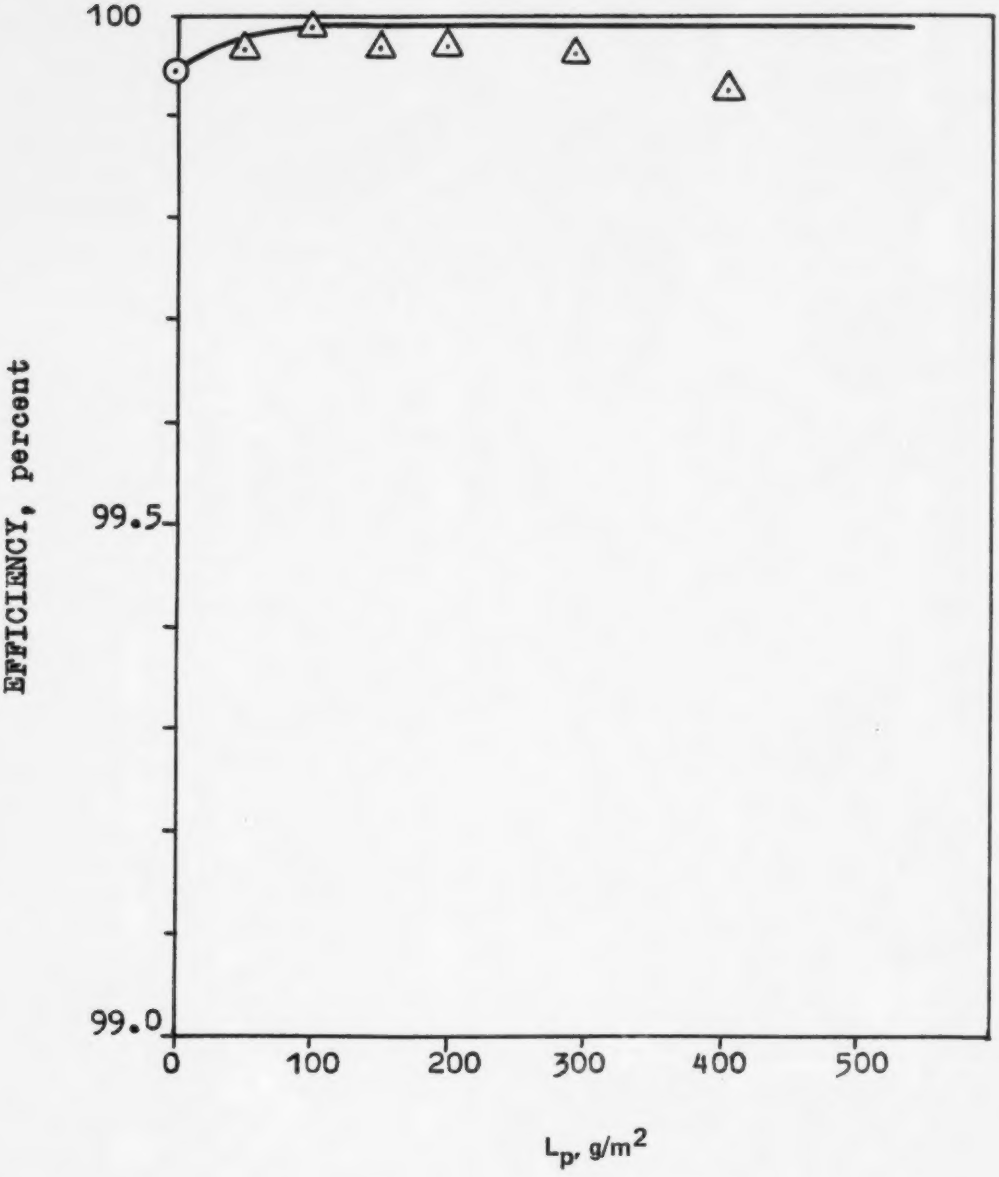

Figure 102. Predicted and experimental efficiencies of ET-4 as a function of L_p for $q_g = 80$ m^3/m^2 · h.

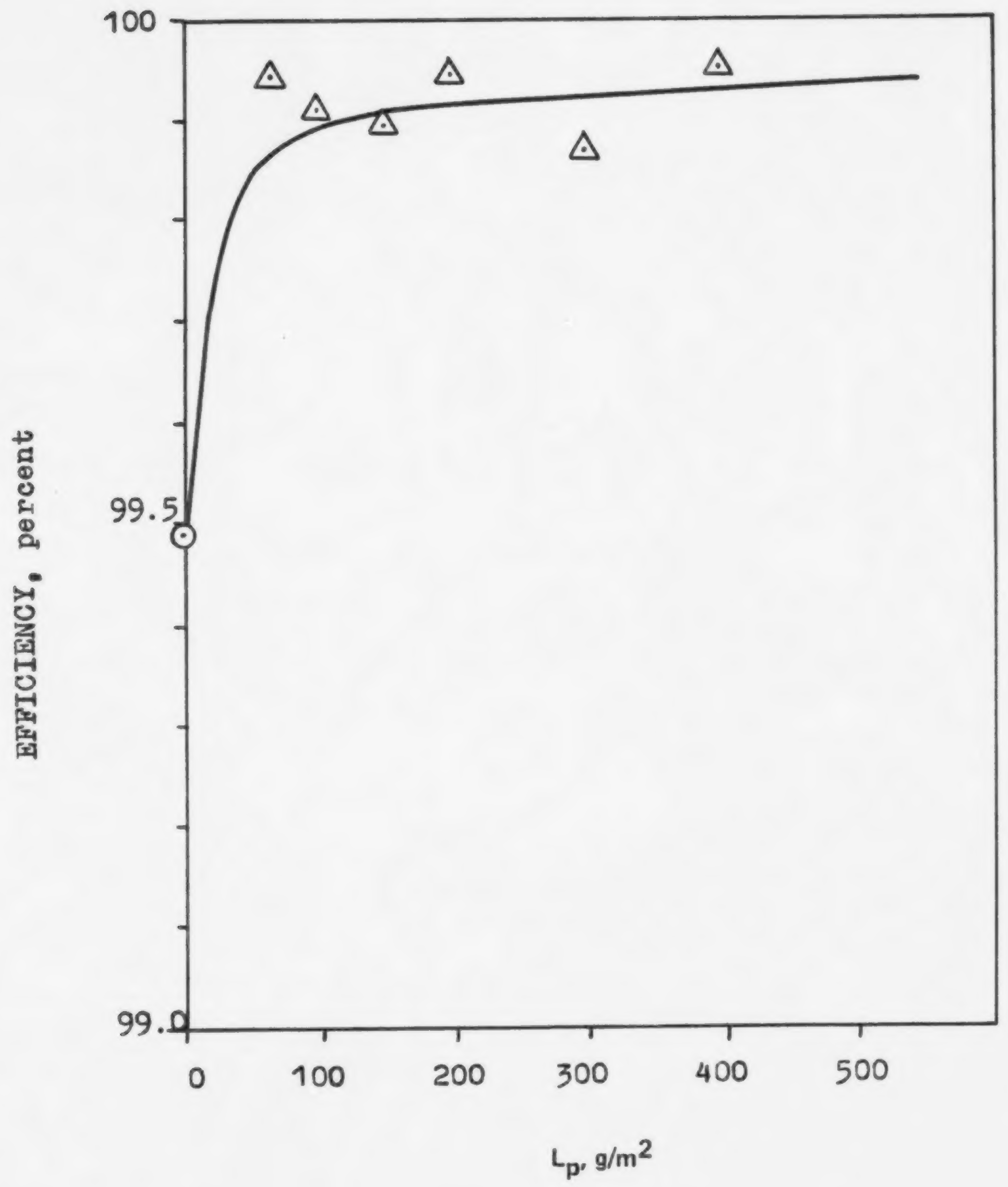

Figure 103. Predicted and experimental efficiencies of ET-4 as a function of L_p for q_g = 100 m^3/m^2 · h.

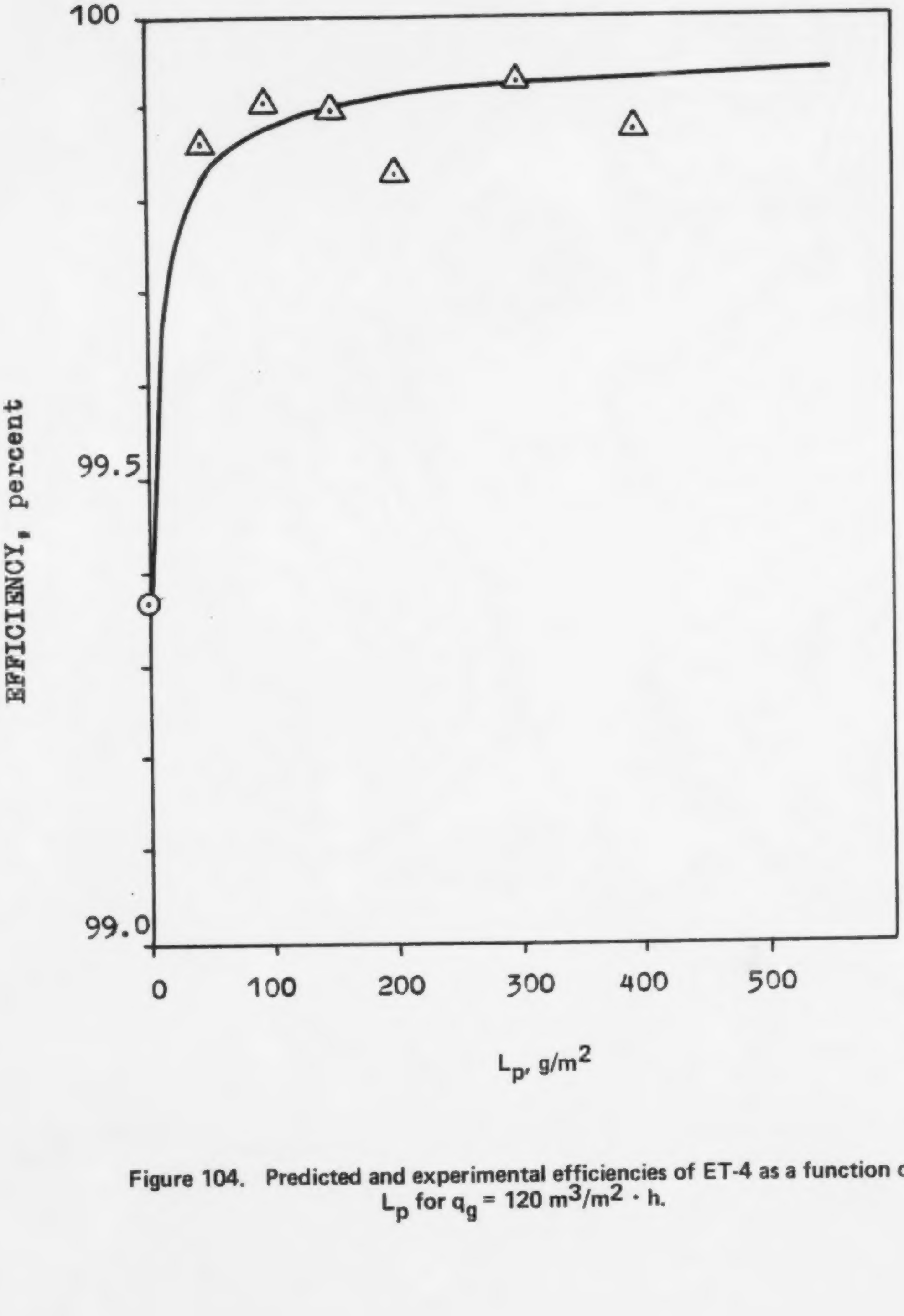

Figure 104. Predicted and experimental efficiencies of ET-4 as a function of L_p for $q_g = 120$ m^3/m^2 · h.

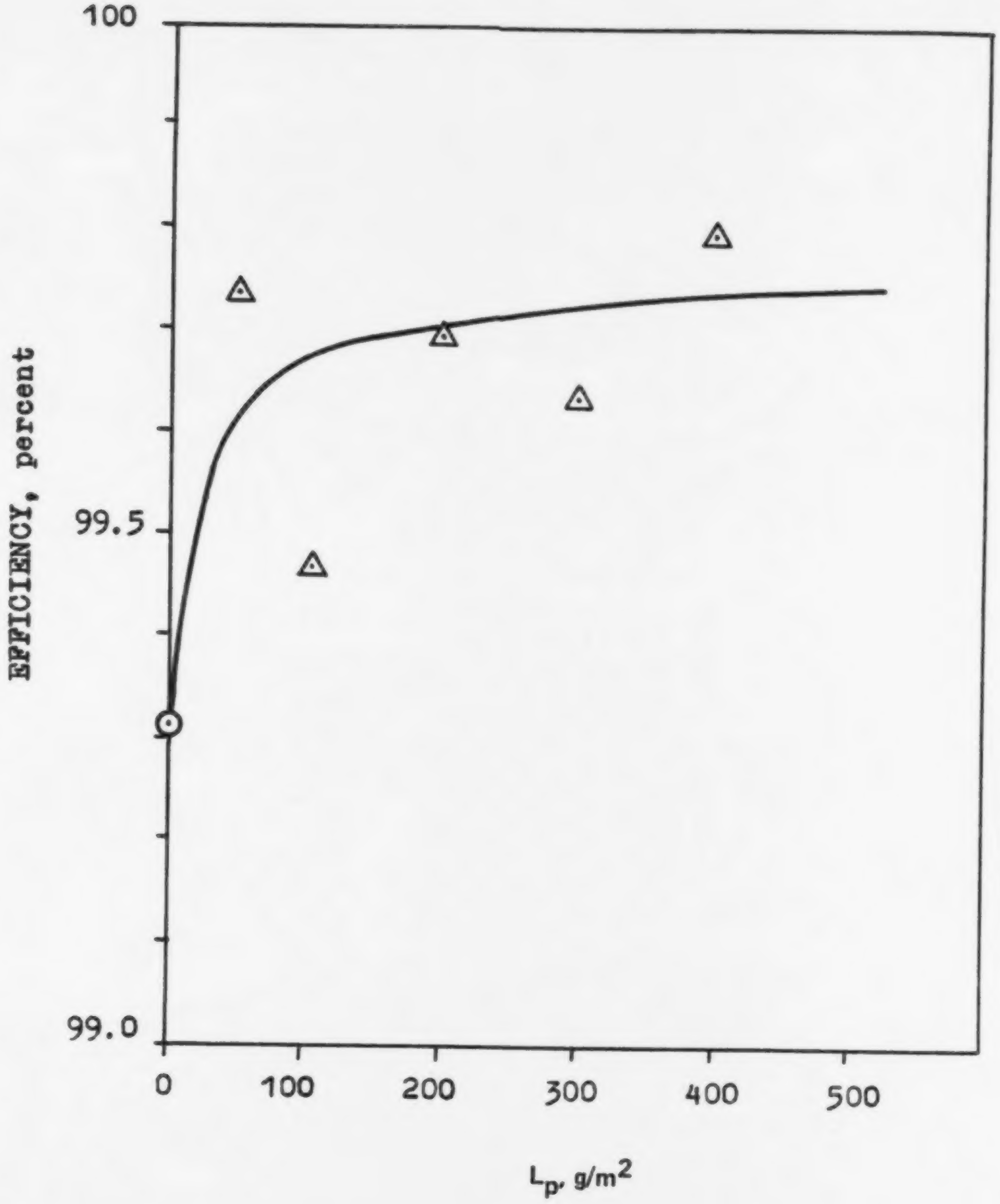

Figure 105. Predicted and experimental efficiencies of ET-4 as a function of L_p for q_g = 160 m^3/m^2 · h.

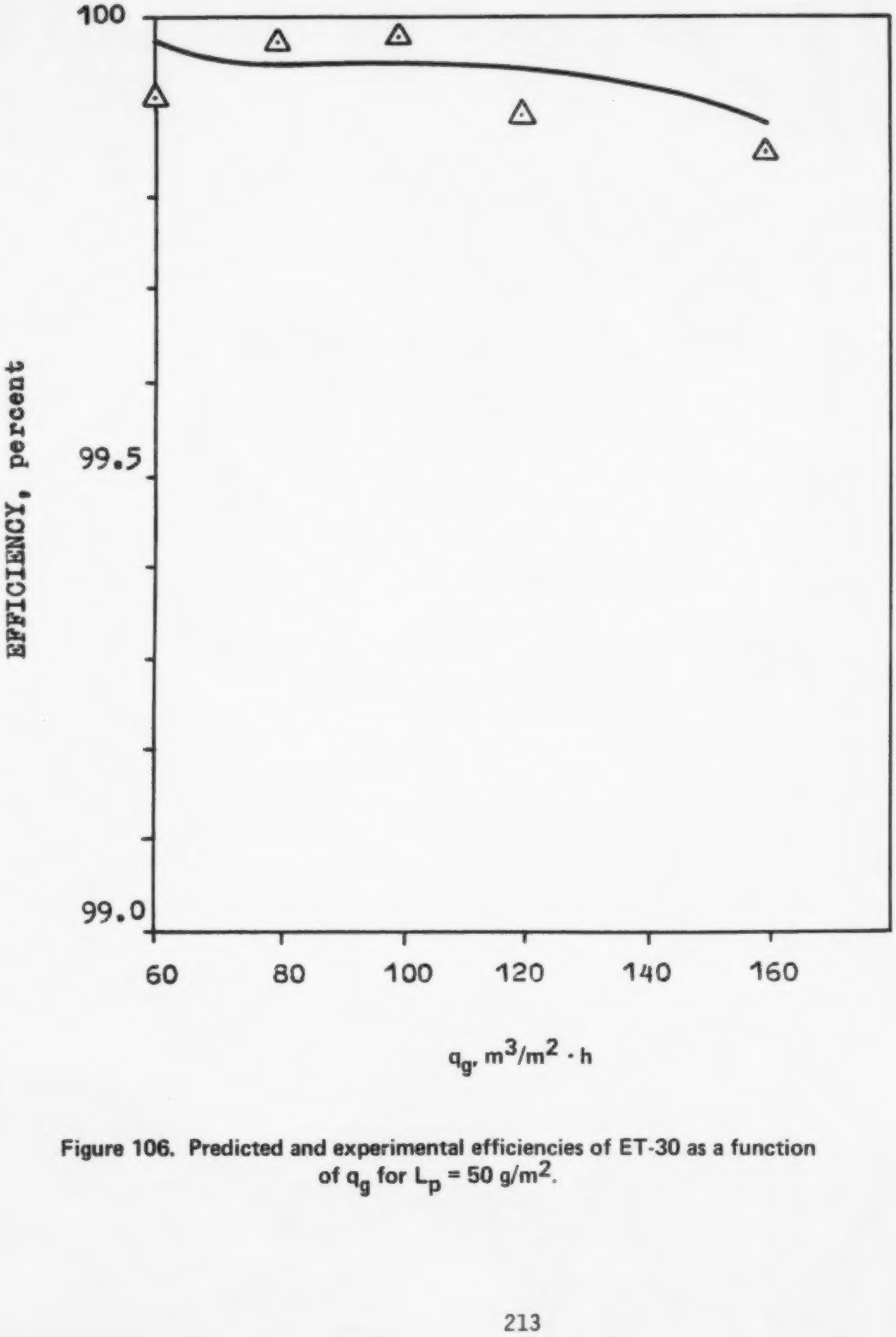

Figure 106. Predicted and experimental efficiencies of ET-30 as a function of q_g for L_p = 50 g/m^2.

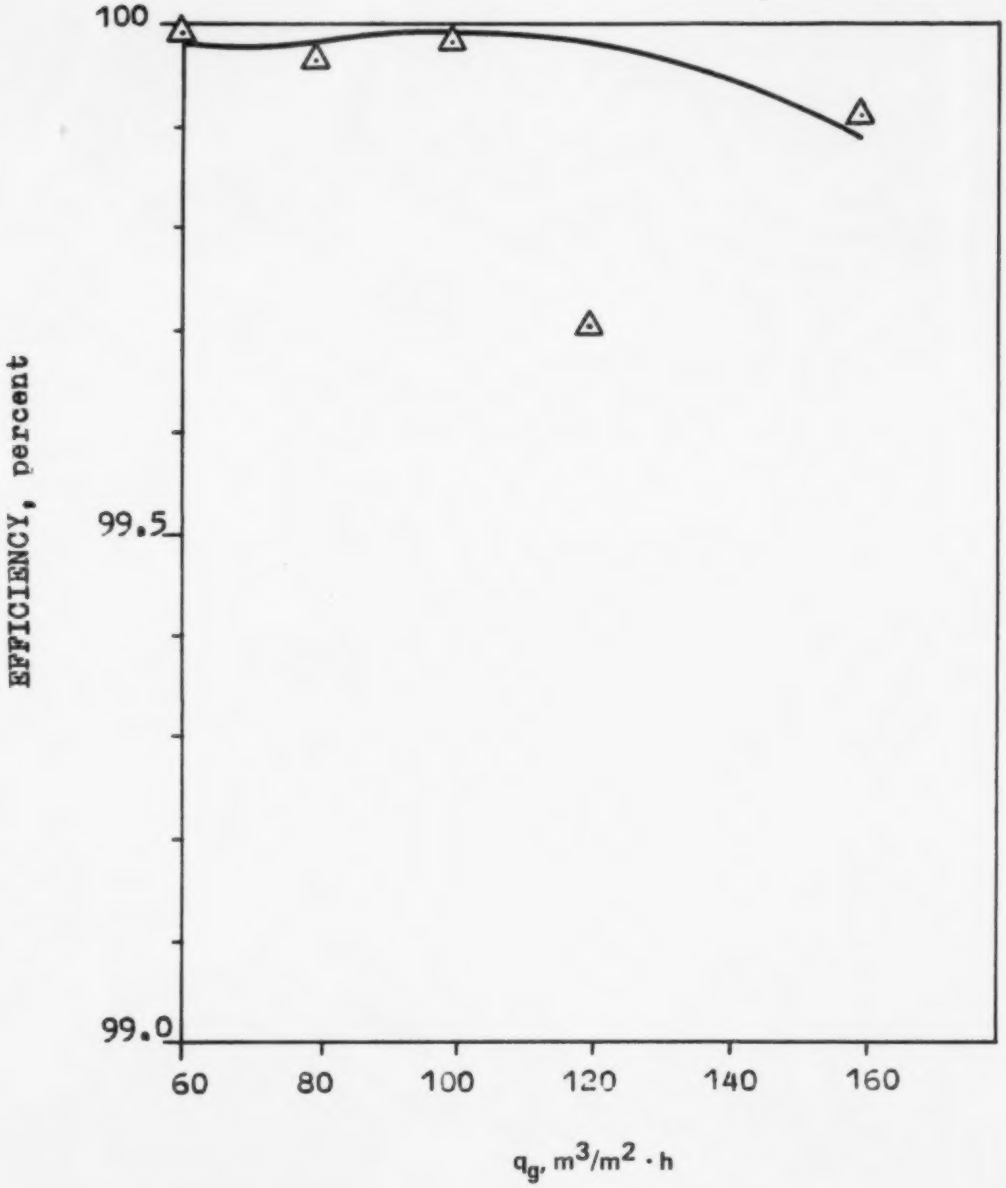

Figure 107. Predicted and experimental efficiencies of ET-30 as a function of q_g for $L_p = 100\ g/m^2$.

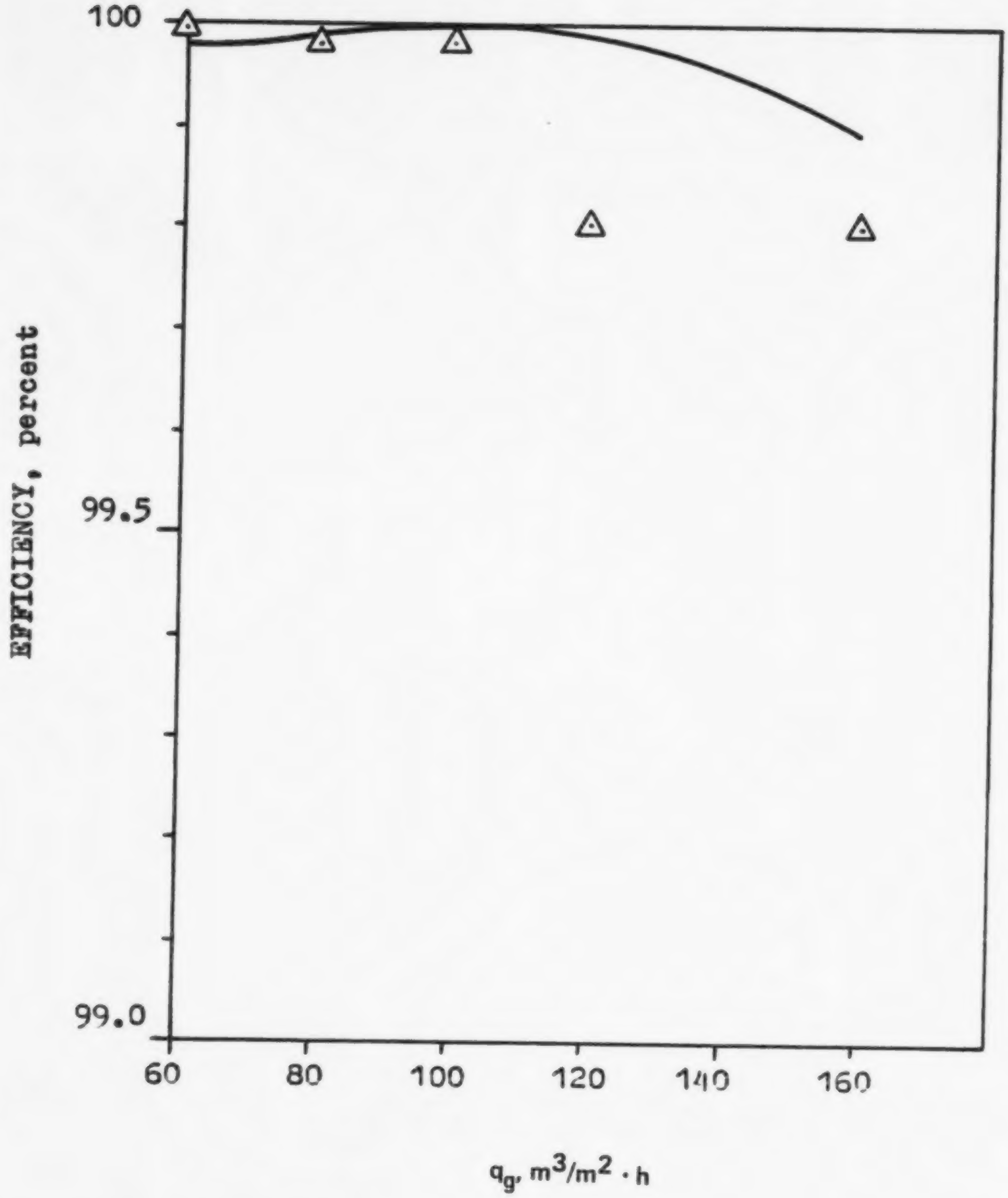

Figure 108. Predicted and experimental efficiencies of ET-30 as a function of q_g for L_p = 150 g/m^2.

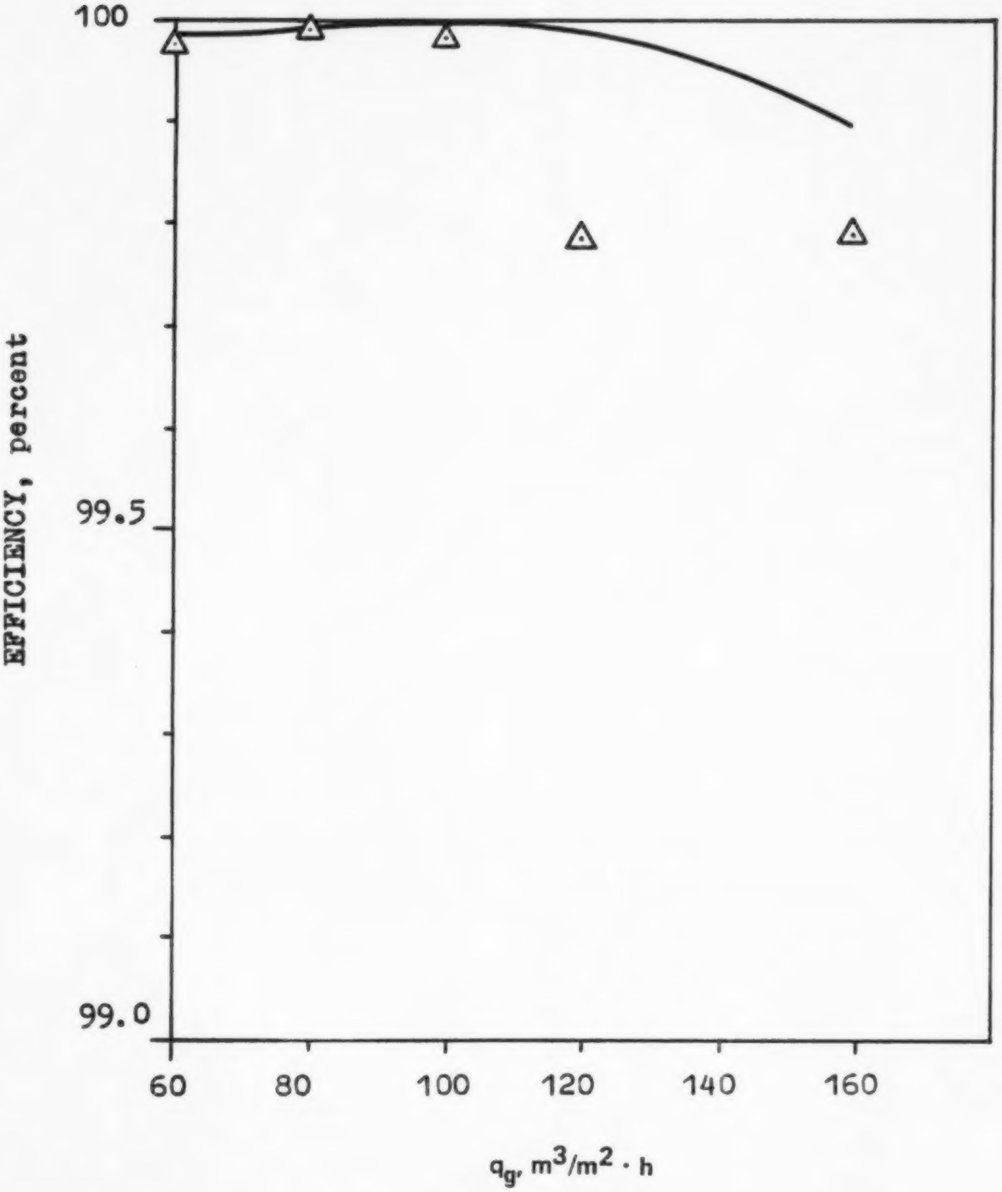

Figure 109. Predicted and experimental efficiencies of ET-30 as a function of q_g for $L_p = 200\ g/m^2$.

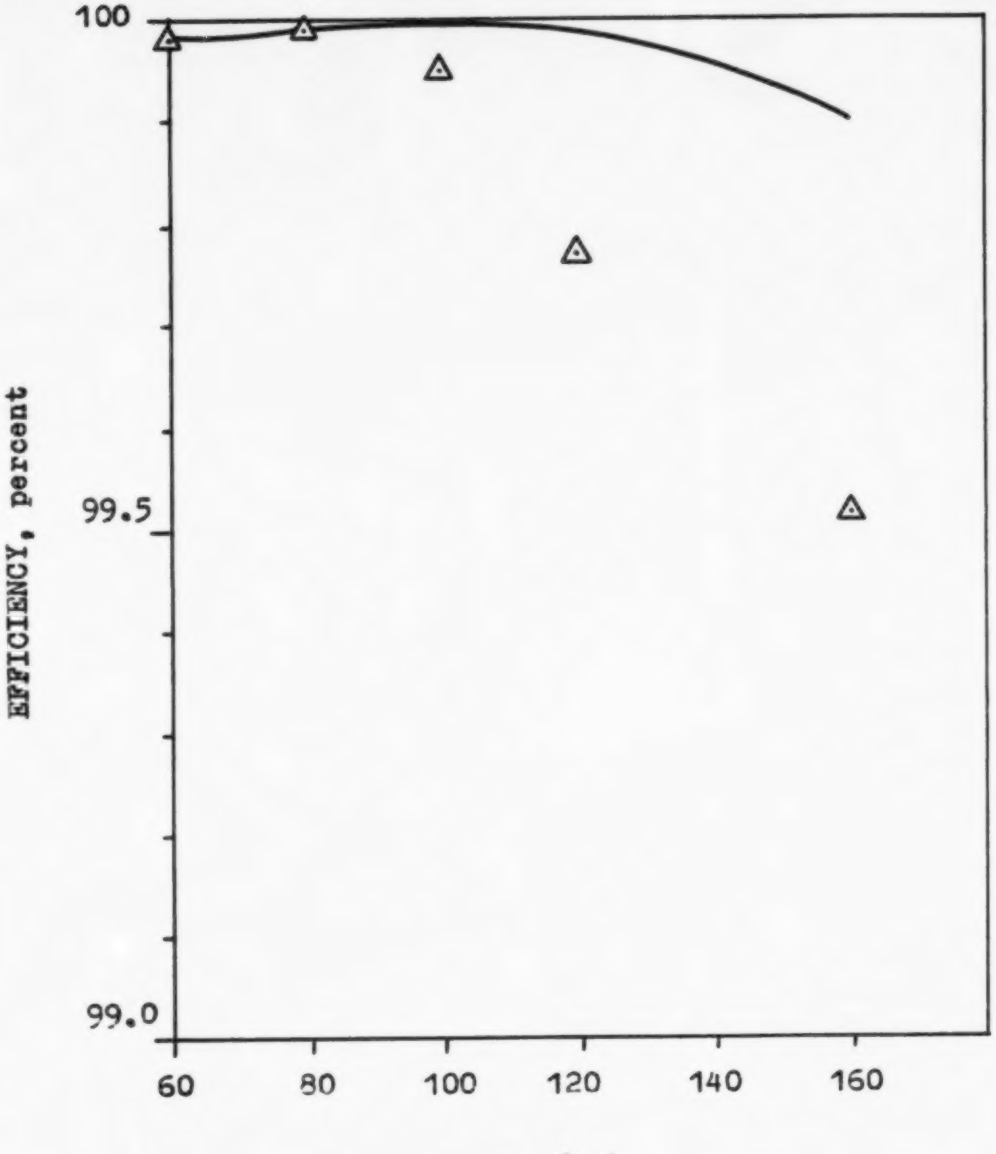

Figure 110. Predicted and experimental efficiencies of ET-30 as a function of q_g for L_p = 300 g/m^2.

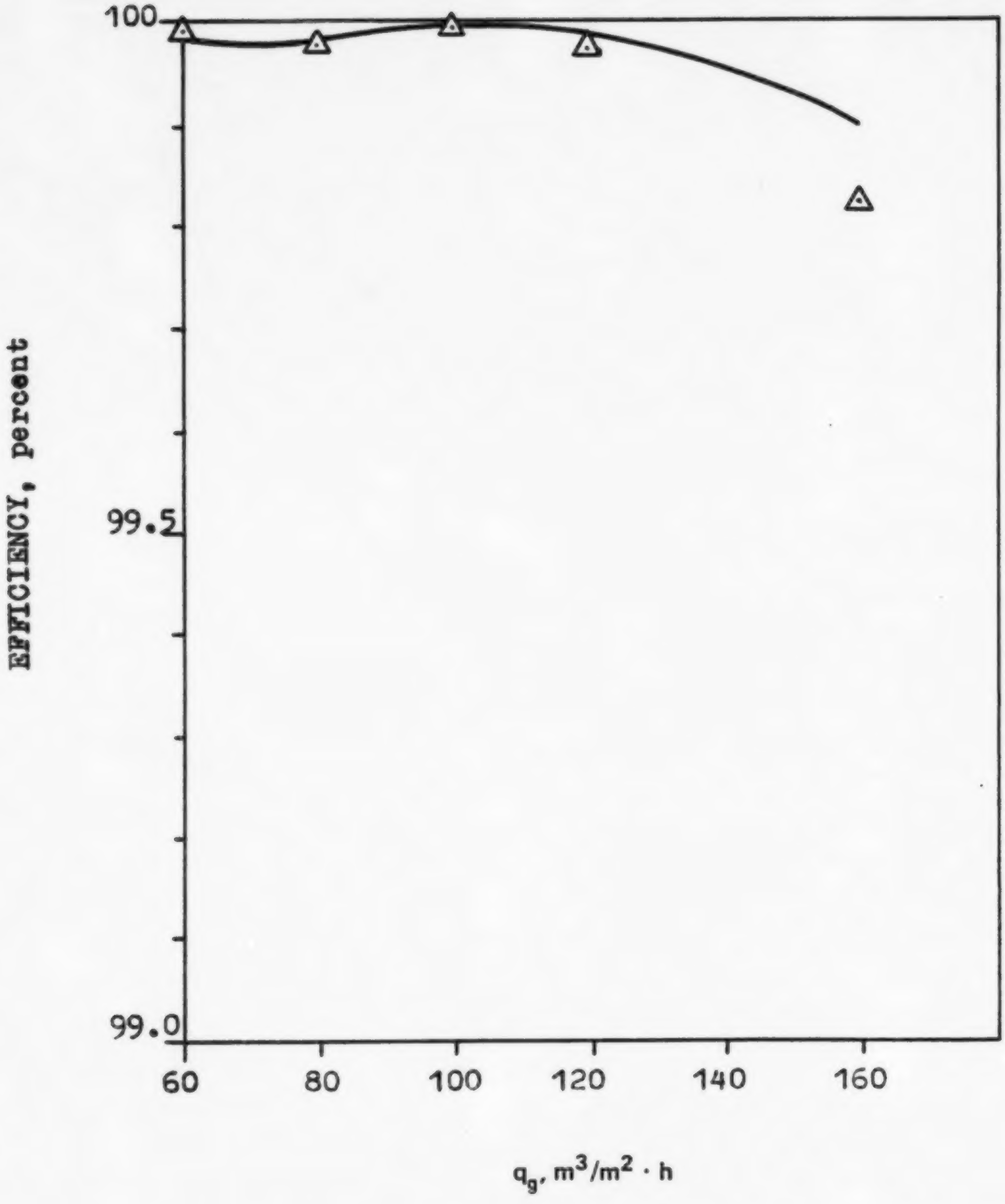

Figure 111. Predicted and experimental efficiencies of ET-30 as a function of q_g for $L_p = 400\ g/m^2$.

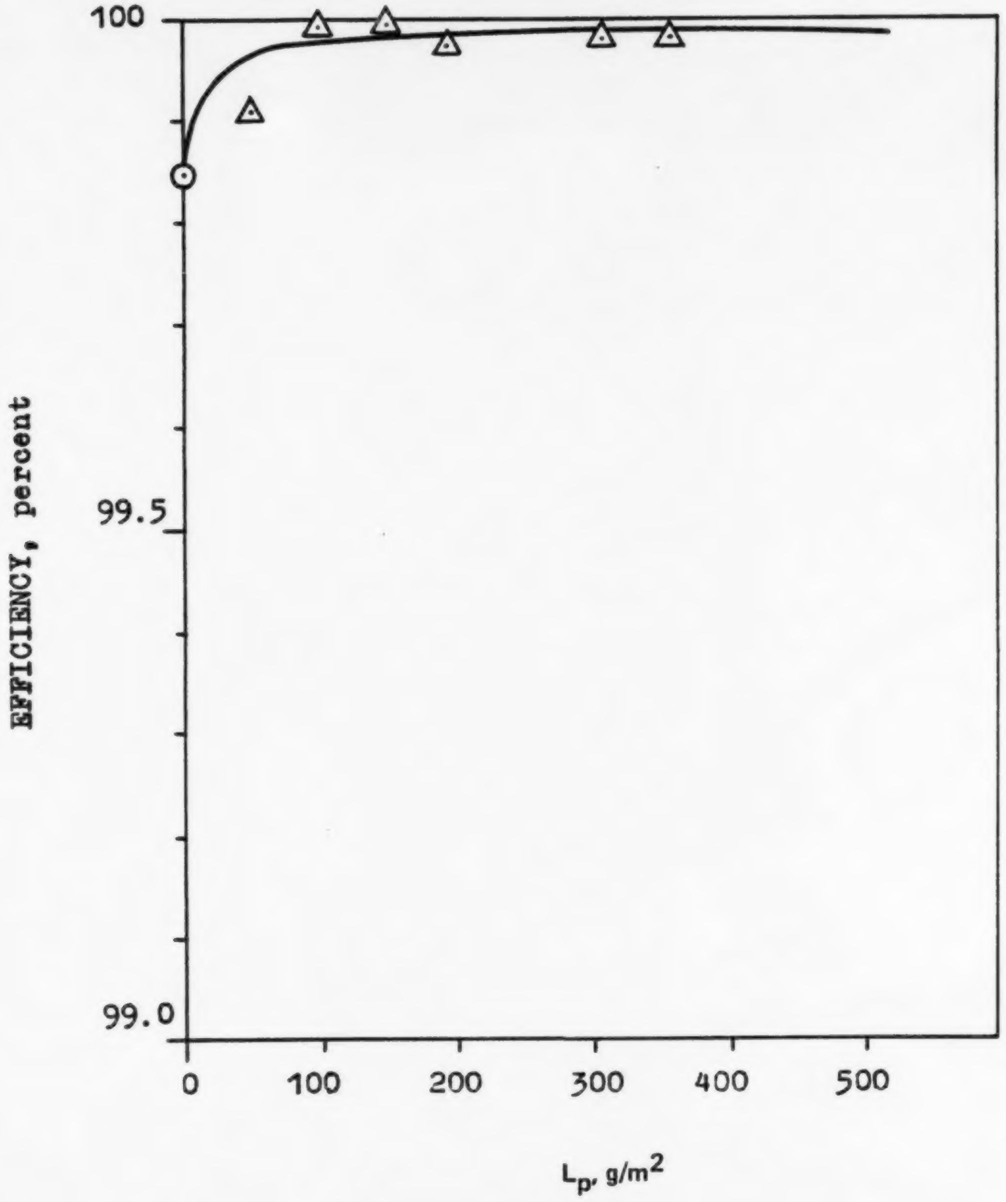

Figure 112. Predicted and experimental efficiencies of ET-30 as a function of L_p for $q_g = 60$ m^3/m^2 · h.

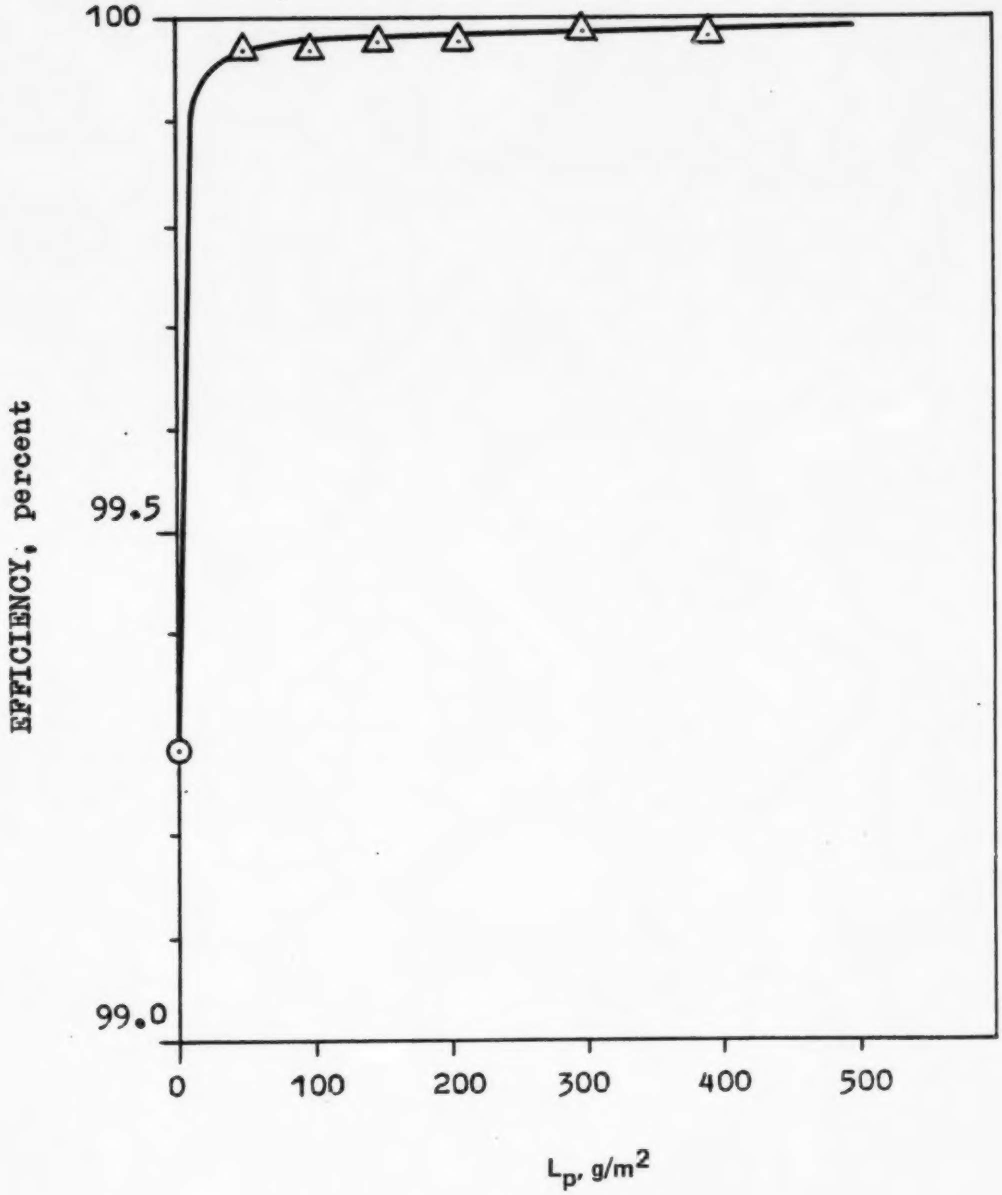

Figure 113. Predicted and experimental efficiencies of ET-30 as a function of L_p for q_g = 80 m^3/m^2 · h.

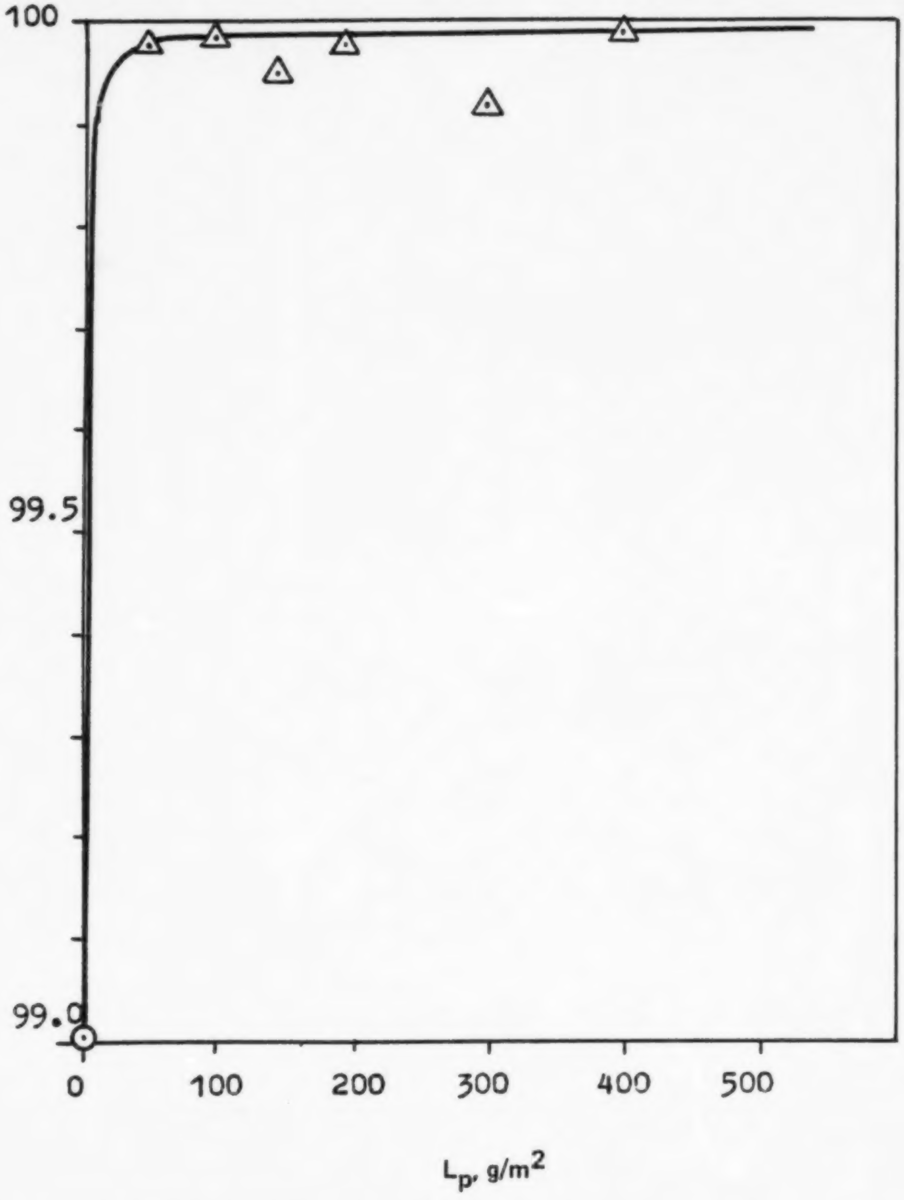

Figure 114. Predicted and experimental efficiencies of ET-30 as a function of L_p for q_g = 100 m^3/m^2 · h.

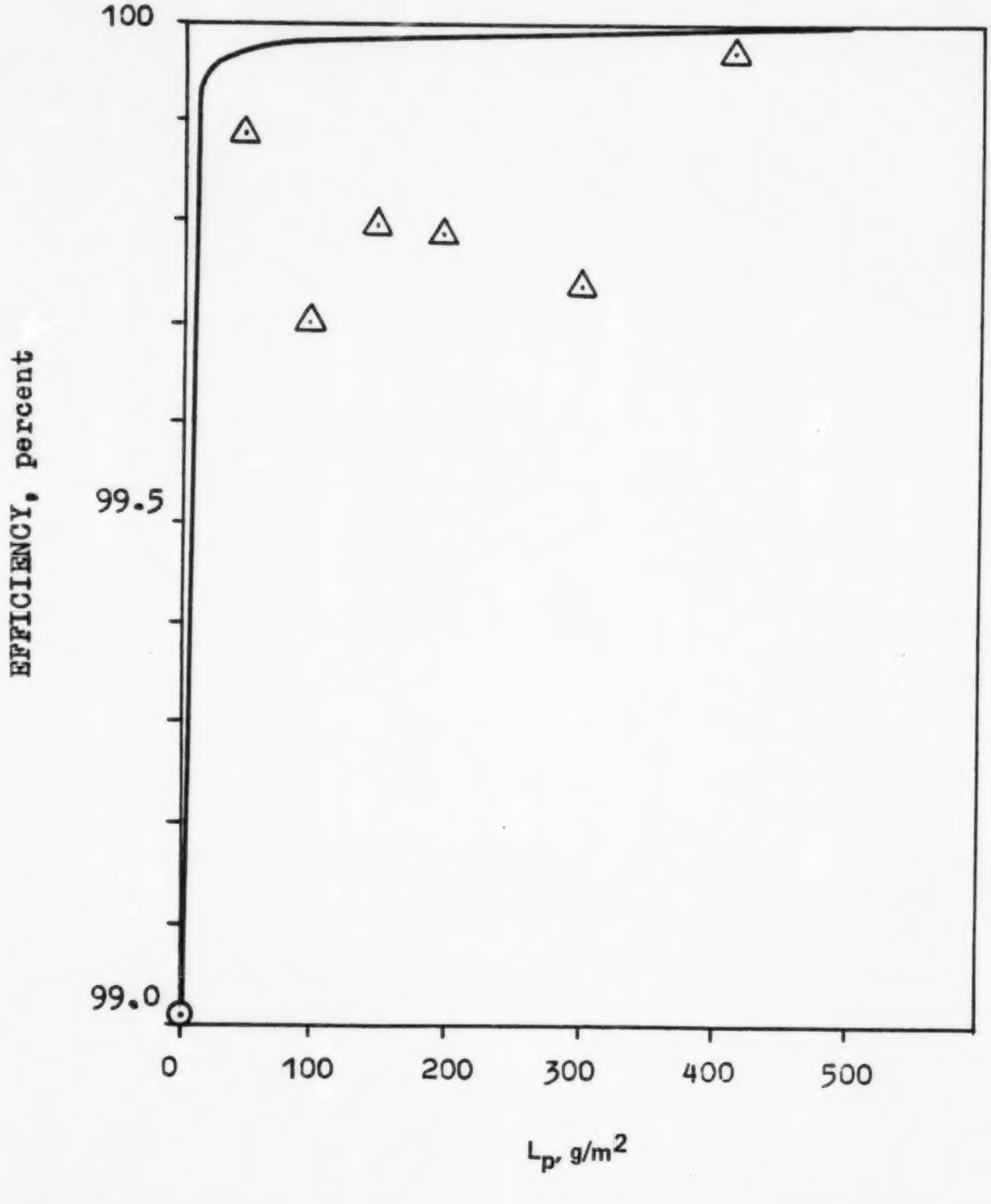

Figure 115. Predicted and experimental efficiencies of ET-30 as a function of L_p for $q_g = 120\ m^3/m^2 \cdot h$.

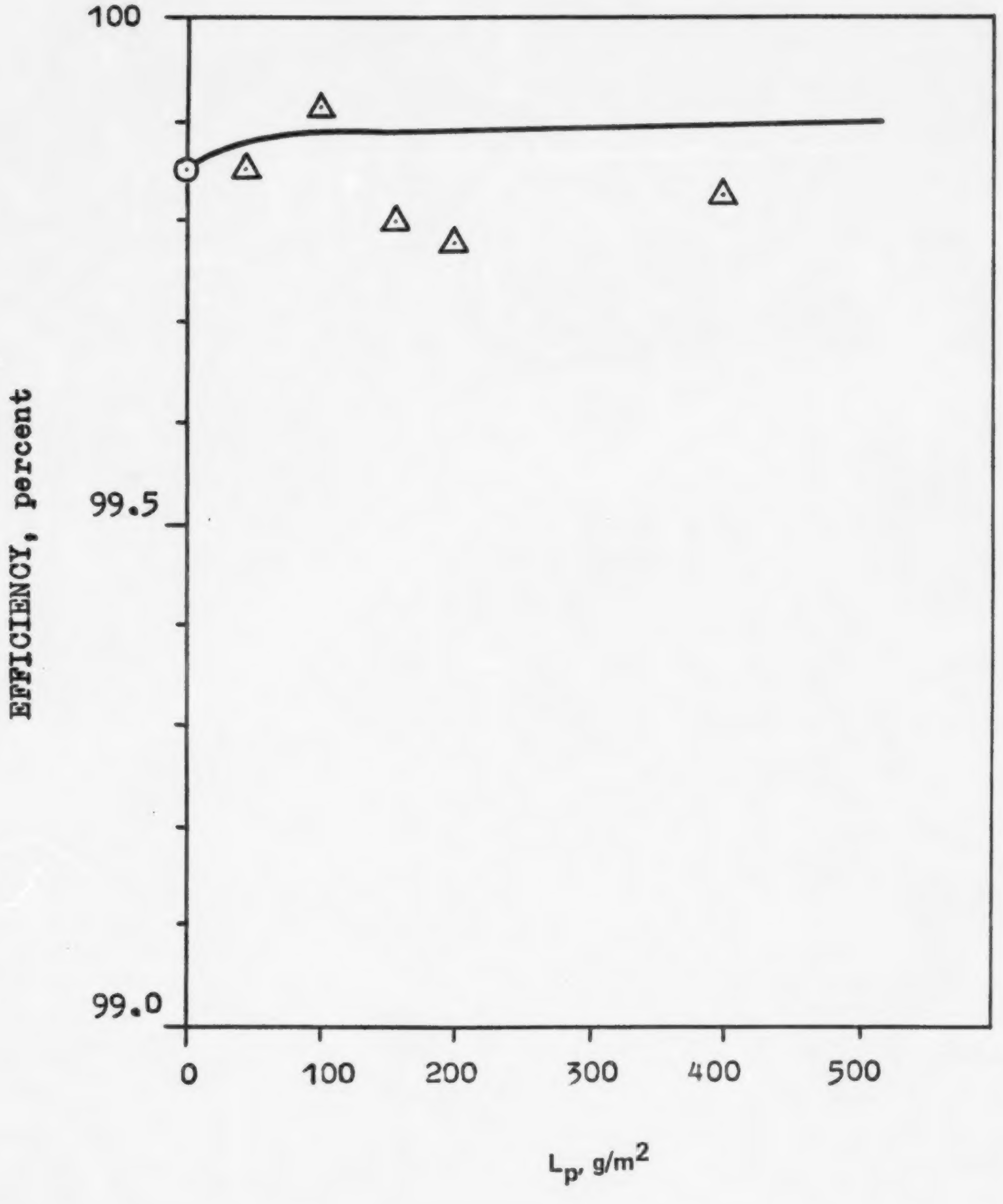

Figure 116. Predicted and experimental efficiencies of ET-30 as a function of L_p for q_g = 160 m^3/m^2 · h.

of time). However, the deliberations recounted in the theoretical section of this report were confirmed. Because of the above, experimental data processing was conducted in a manner similar to that of the laboratory-scale testing. The basic equation is:

$$\Delta P_{F\ III} = f[q_g,\ L_p\ (t_F)]\ . \qquad (81)$$

This equation expresses the effect of the filtration parameters on the filtration resistance. Equation 81 leads to an examination of the second phase of the filtration cycle; i.e., after the inflection point of curve $\Delta P_{F\ III} = f(L_p)$ according to Equation 47. The following general equation is assumed:

$$\Delta P_{F\ III} = A'\ [q_g]^{B'}, \qquad (82)$$

where

$$B' = f[L_p(t_F)] = A_3 \cdot L_p^2 + B_3 \cdot L_p + C_3$$

$$= A_3(q_p \cdot t_F)^2 + B_3(q_p \cdot t_F) + C_3\ ,$$

where

$\Delta P_{F\ III}$ = filtration resistance in Dust Filtration Process Type III, mm H_2O;
q_g = face velocity, m^3/m^2h;
q_p = dust flux, g/m^2h,
t_F = filtration time, h; and
A', A_3, B_3, C_3 = empirical constants characterizing the dust-fabric system.

A linear equation in the log-log system is obtained as follows when the log of both sides of Equation 82 is taken:

$$\log \Delta P_{F\ III} = B' \log q_g + \log A'\ . \qquad (83)$$

Setting $\Delta P_{F\ III} = 0$ in Equation 82 as the origin of the coordinate system led to wide scatter in values of A', as calculated from Equation 83 for abscissa $q_g = 1$. Accordingly, the simple method of displacing the coordinate system that worked well for the laboratory-scale data was not used, but the function $A'(L_p)$ was determined. Thus, a better model was obtained for estimating filtration resistances. The general form of that model can be presented as follows:

$$\Delta P_{F\ III} = \left[a_3 L_p^{\ 2} + b_3 L_p + c_3\right] \cdot q_g^{\left[A_3 L_p^{\ 2} + B_3 L_p + C_3\right]} . \tag{84}$$

All assignations are the same as in the previous equations. Values of the coefficients, A′ and B′, were determined by a regression calculation for certain levels of L_p, as shown in Table 27. The values from Table 27 were fitted to parabolas by the least squares method. The parabolic coefficients are shown in Table 28.

Figure 117 shows both coefficient B′ as a function of L_p, determined by the data fitting and data points. When the constant values from Table 28 are used in Equation 84, a three-dimensional model is obtained describing the effects of q_g and L_p on filtration resistance in Dust Filtration Process Type III.

Equation 82 demonstrates that the true values of q_g and dust covering (parameter characteristic for dust cake) were used for the model, without consideration of the actual filtration times in individual experiments.

The model presented in Equation 84 is the actual mathematical treatment. Equation 84 can be generalized to the following form:

$$\Delta P_{F\ III} = \left[a_3(q_p\ t_F)^2 + b_3(q_p\ t_F) + c_3\right] q_g^{\left[A_3(q_p\ t_F)^2 + B_3(q_p\ t_F) + C_3\right]} \tag{84a}$$

Large-scale testing is not as simple as laboratory-scale testing, because hopper efficiency, which affects the length of the elementary filtration cycle, must be considered. The assumed dust load at lower dust flux, q_p, may be obtained with use of Equation 80 and application of the values of hopper efficiency depicted in Table 27 to determine the true filtration time:

$$L_p = (1 - E_L)\ c_1 \cdot q_g \cdot t_F \quad \text{, and}$$

$$t_F = \frac{L_p}{(1 - E_L)\ c_1 \cdot q_g} .$$

TABLE 27. VALUES OF COEFFICIENTS A´ AND B´ FROM EQUATION 82

	A´		B´	
	ET-4	ET-30	ET-4	ET-30
100	0.0698	0.04172	1.2913	1.4706
200	0.1237	0.05453	1.2538	1.4617
300	0.1455	0.06256	1.2741	1.4706
400	0.1393	0.002537	1.3231	(2.3015)*
600	0.08347	0.06401	1.4850	1.5482
800	0.000036	0.05516	3.0937	1.6188

*No valid B´ at L_o = 400.

TABLE 28. COEFFICIENTS OF EQUATION:
$A' = a_3L_p^2 + b_3L_p + c_3$ and $B' = A_3L_p^2 + B_3L_p + C_3$

	Kind of fabric	
Coefficient	ET-4	ET-30*
a_3	$-8.0426 \cdot 10^{-7}$	$-1.4941 \cdot 10^{-7}$
b_3	$6.0055 \cdot 10^{-4}$	$1.5061 \cdot 10^{-4}$
c_3	$2.7676 \cdot 10^{-2}$	$2.9418 \cdot 10^{-2}$
A_3	$1.5230 \cdot 10^{-6}$	$3.5779 \cdot 10^{-7}$
B_3	$-6.6209 \cdot 10^{-4}$	$9.8881 \cdot 10^{-5}$
C_3	1.3363	1.4719

*No valid B´ at L_o = 400 (see Table 27).

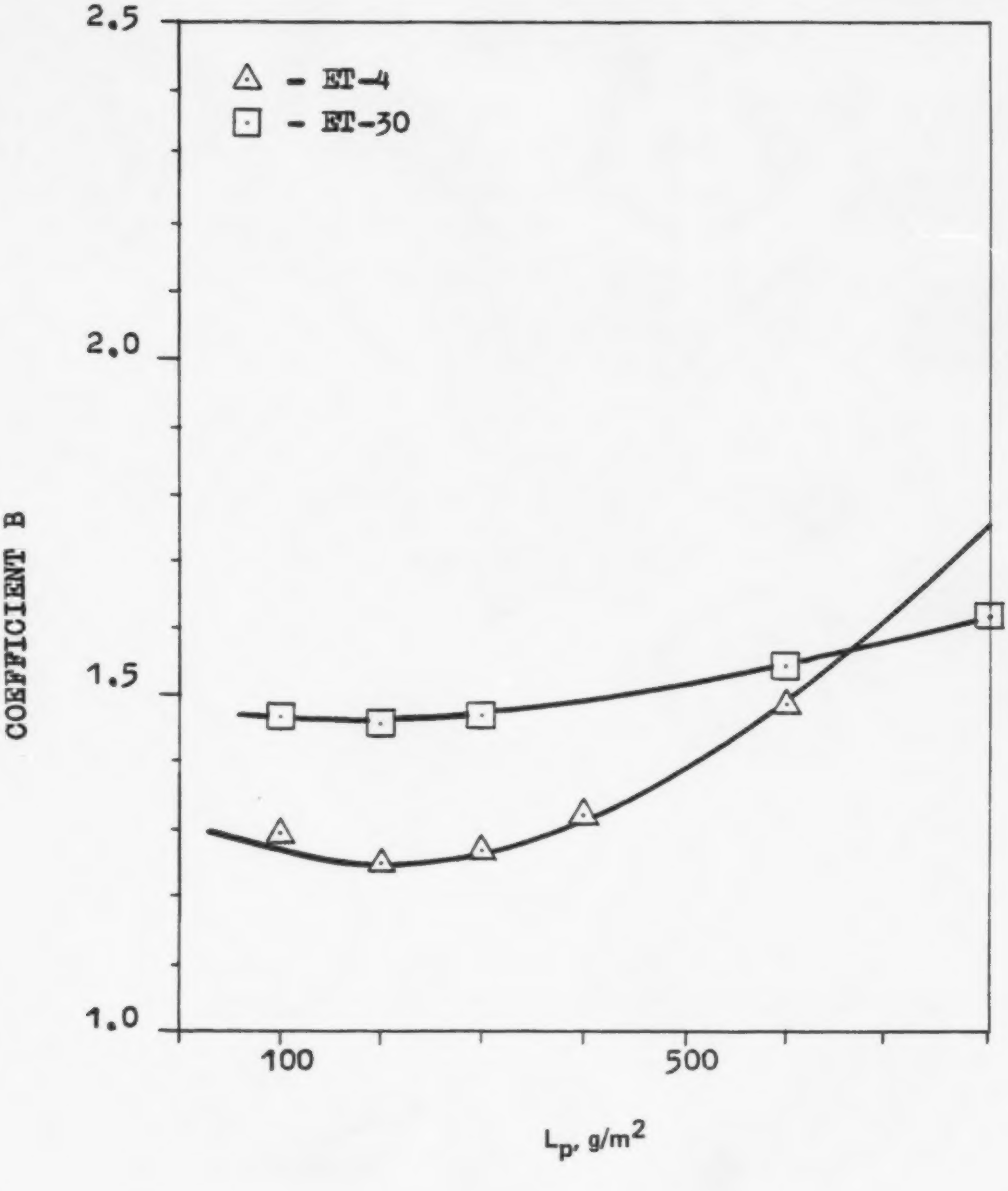

Figure 117. Variation of coefficient B´ as a function of L_p.

Filtration resistance is affected by the actual amount of dust reaching the filtration medium. Thus, a generalized and equivalent form of the model expressed by Equation 84 for Dust Filtration Process Type III, which considers both filtration time and the separation properties of the hopper, can be written as follows:

$$\Delta P_{F\ III} = \left[a_3\ (q_p'\ t_F)^2 + b_3\left(q_p'\ t_F\right) + C_3\right]\ q_g^{\left[A_3\ (q_p'\ t_F)^2 + B_3\ q_p\ t_F + C_3\right]} \qquad (84b)$$

where

$q' = (1 - E_L) \cdot c_1 \cdot q_g$, and
E_L = hopper efficiency.

With the filtration resistance of Equation 84b, model filtration resistance was examined over the range of q_g, in which a drop in dust collection efficiency was observed--probably caused by defects in the dust cake structure. For fabric ET-4, decreased dust collection efficiency was observed above $q_g = 80$ m^3/m^2h. Figure 118 shows predicted and measured filtration resistances as a function of the characteristic dust cake parameter, L_p.

After filtration resistance values of about 65 mm H_2O were reached, a decrease in measured filtration resistances comparable to those predicted was observed. This decrease indicates structural changes in the dust-fabric system, resulting in increased system porosity. This observation confirms the hypothesis of dust cake defect formation. A similar analysis of the data from fabric ET-30 gives a less clear picture of the filtration resistance variation attributable to dust cake defect formation, because of the limits placed on the range of the characteristic dust cake parameter (see Figure 119).

The concept in this report concerning the effect of the dust-fabric system on the dust filtration process requires further examination and verification. However, in both laboratory-scale and large-scale tests, the physical model discussed in the theoretical section answers some peculiarities observed in the behavior of dust collection efficiency and of filtration resistance.

CONCLUSIONS

Large-scale testing was conducted over a narrower range of variables than the laboratory testing, but both test programs were designed to permit development of probabilistic filtration models. The goal was achieved by presentation of dust collection efficiency and filtration resistance models for two kinds

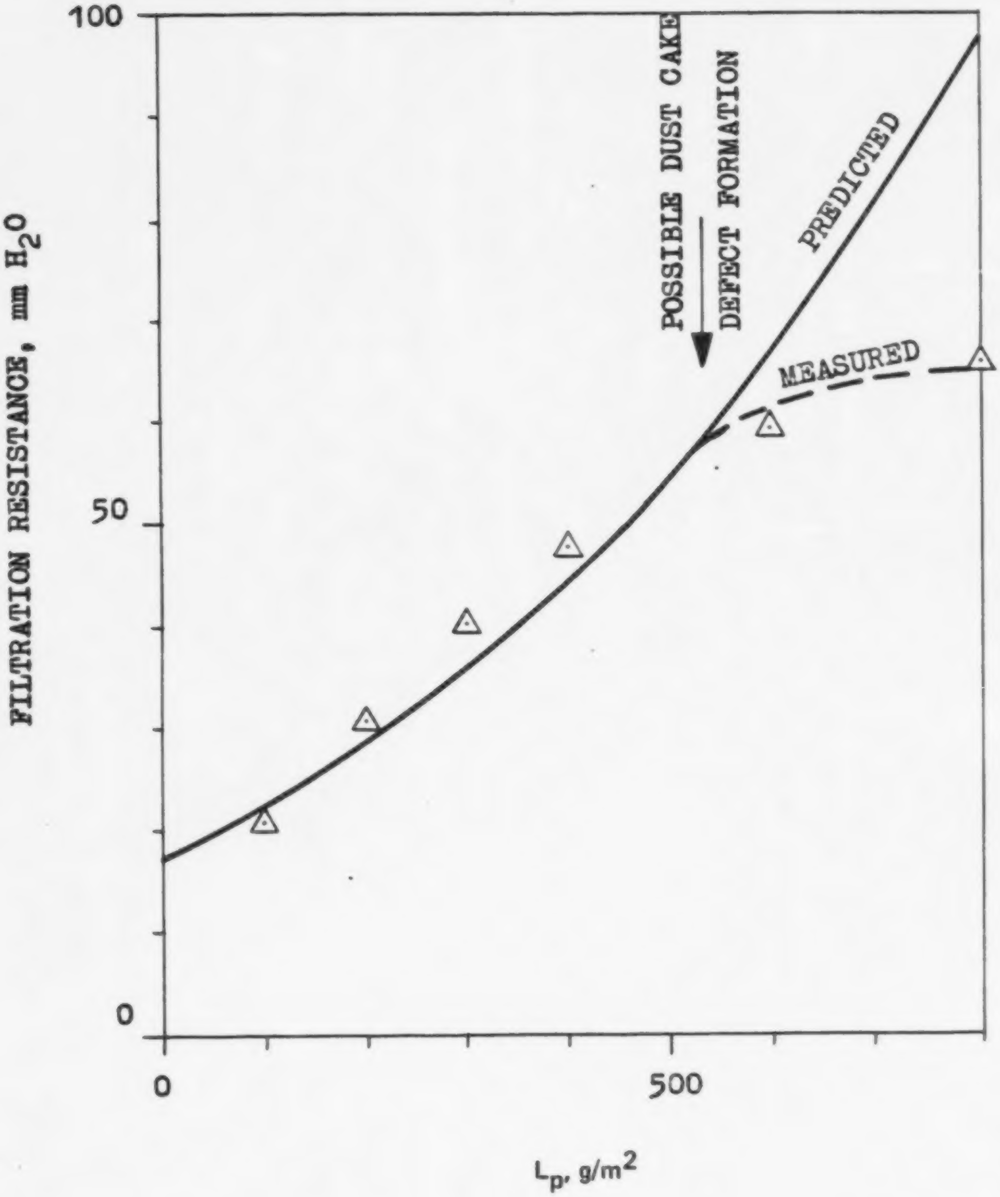

Figure 118. Predicted and measured filtration resistance for ET-4 at $q_g = 80\ m^3/m^2 \cdot h$.

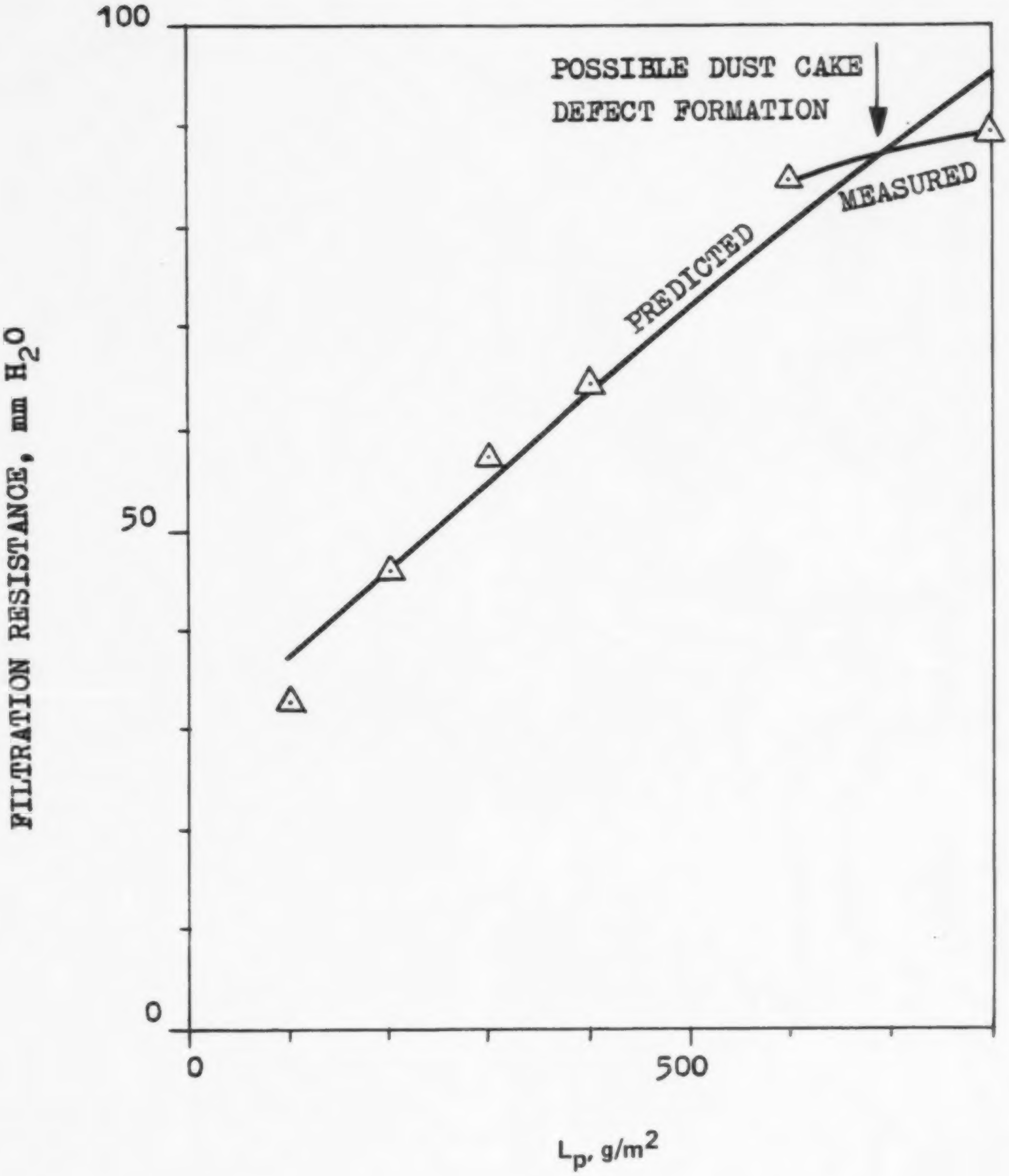

Figure 119. Predicted and measured filtration resistance for ET-30 at $q_g = 100\ m^3/m^2 \cdot h$.

of test fabrics and a description of Dust Filtration Process Type III over the range of the examined filtration parameters. From analysis of the empirical data, the following conclusions were reached concerning Dust Filtration Process Type III:

- Dust Filtration Process Type III is characterized by a high dust collection efficiency of 99.9 percent and more.
- The effect of q_g on dust collection efficiency and filtration resistance is observed, but with increasing q_g, efficiency does not drop below 99.5 percent over the range explored.
- Efficiency as a function of q_g depends on the kind of fabric in the dust-fabric system. The hypothesis can be offered that staple-fiber fabrics, characterized by higher spatial and superficial porosity, will have maximum efficiency at a definite q_g. Fabrics with low permeability and dense construction (small porosity) will not have an extreme efficiency value, but their efficiency will increase with decreasing q_g. The observed phenomenon is valid for laboratory and large-scale testing.
- An increase in the characteristic dust cake parameter, L_p, equivalent to an increase in dust cake thickness, forces an increase in dust cake efficiency in each range of q_g.
- Analysis of the curves $E_{III} = f(q_g)$ and $E_{III} = f(L_p)$ shows that during Dust Filtration Process Type III, formation of dust cake defects, which decreases dust collection efficiency, must be considered. Appearance of dust cake defects is more probable for those dust-fabric systems in which the fabric has high spatial and superficial porosity.

SECTION VII

COMPARISON BETWEEN DUST FILTRATION PROCESS TYPE I AND TYPE III

INTRODUCTION

Probabilistic models of dust collection efficiency and filtration resistance, presented in the two previous sections, allow a prediction of the external parameters of Dust Filtration Process Type I and Type III at a specific time over specific ranges of basic filtration parameters and process conditions.

The empirical character of these models limits their practical application. First, because of the lack of a unique physical structural parameter(s) by which a filtration material can be defined or the dust cake described, these models cannot be generalized. They are not valid for filtration processes occurring in other structures or with other dusts. Second, the models can be applied only for processes operating within certain ranges of the basic filtration parameters. Their application outside these ranges can cause significant errors.

However, regardless of these disadvantages, these models are important research tools, verifying physical models. They explain certain peculiarities of dust filtration and help construct fresh hypotheses based on observed behavior. Further research in defining the physical structural parameters of the filtration materials and dust cakes will help develop a base for generalizing the present models.

The equivalence of Dust Filtration Process Type I and Type III and especially the equivalence among the corresponding external parameters is interesting. In the theoretical section of this report, the above processes were proven dissimilar because of different states of the filtration medium depicted by the structure filling with dust in each dust filtration process. The processes are also dissimilar in values of external parameters, as indicated by the physical analysis of the dust filtration process and previously developed probabilistic models.

The general relationship among the external dust filtration process parameters is illustrated in Equation 11. If a regression function could be determined by Equation 11, it would be possible, based on laboratory tests, to predict the performance of filtration in large-scale and industrial-scale testing. Considering the fact that the models were developed for a comparatively wide range of basic filtration parameters, including practically all ranges common to dust filtration, the development of the required regression functions establishes the conditions important for broader laboratory research. This fact is important for economy of research.

The application of the regression function for developing new qualitative testing methods for filtration materials is closely related to the problem discussed. Air permeability, the commonly applied qualitative parameter, and also the superficial mass of the fabric, seem inadequate for the multiparameter character and peculiarities of the dust filtration process.

This section discusses the external parameters of Dust Filtration Process Type I and Type III based on the empirical results obtained during laboratory and large-scale experiments. The research concentrated on one dust type (separated fly ash) and on two polyester fabrics, differing in spatial structure but not in raw material. Thus, during a discussion of the regression function it was possible to ignore some interaction between the dust particles and elements of the filtration structure.

COMPARISON OF DUST COLLECTION EFFICIENCIES

Based on the dust collection efficiency models in Dust Filtration Process Type I and Type III and on Equation 11, the function, R_E, was sought that best approximates E_I and E_{III} for certain levels of basic filtration parameters, q_g, L_o, and L_p. Equation 11 results in:

$$R_E = \frac{E_I}{E_{III}} \quad , \tag{85}$$

where

E_I and E_{III} are dust collection efficiency models for laboratory and large-scale testing, respectively.

For laboratory-scale testing, value L_o is a characteristic parameter describing the state of the fabric covered with dust, but for large-scale testing, value L_p is the equivalent parameter. A comparison of dust collection efficiencies of the two processes was thus feasible. With consideration of the previously discussed problem of mean efficiency in the filtration cycle, the following mathematical relationships can be formulated:

$$\text{at constant } g_g,\ R_E = f(L)\ \text{, and} \qquad (86)$$

$$\text{at constant } L,\ R_E = f(q_g)\ , \qquad (86a)$$

where

$L = \bar{L}_o = L_o/2$ for laboratory experiments, and

$L = \bar{L}_p = L_p/2$ for large-scale experiments.

Empirical data from laboratory and large-scale tests of fabrics ET-4 and ET-30 were used to calculate the values of R_E for specific levels of g_g and the quantity of dust in the filtration structure. Results are contained in Table 29. The plots in Equation 86 and Equation 86a were developed based on calculated values of R_E from Table 29. Figures 120 and 122 and Figures 121 and 123 illustrate the dependence of R_E upon q_g and L for fabric ET-4 and ET-30, respectively.

For constant levels of q_g the equation, $R_E = f(L)$, demonstrates curvilinear character that, with increasing dust cake thickness, makes laboratory and large-scale processes more and more comparable, tending to the same value of the function, R_E. Equation $R_E = f(q_g)$ for constant levels, $L_o = L_p$, is linear, but two ranges--low q_g and high q_g--can be distinguished. Value $q_{g\ extr}$, which has been discussed before, is a classical value. It is interesting that the problem of two dust filtration process phases appears in a classical discussion of nearly unrelated problems. For the classical range of $q_g < q_{g\ extr}$, which contains no dust cake defects, $R_E = f(q_g)$ is inversely proportional. Therefore, with increasing q_g, laboratory and large-scale processes are concluded to become less similar.

For the range, $q_g > q_{g\ extr}$, a similar but more pronounced behavior of $R_E(q_g)$ is observed. R_E, corresponding to $q_g = q_{g\ extr}$, differs considerably from values determined by the equation in the classical range. The stronger, inversely proportional relationship in the second phase of the process results from a significant decrease in laboratory efficiency because of dust cake defects. A decrease in dust collection efficiency in large-scale testing for the same range is much smaller. Further discussion concerns only the classical range of dust filtration--the most important from a

TABLE 29. VALUES OF FUNCTION R_E

Kind of fabric	q_g (m^3/m^2h)	Terminal dust load, L (g/m^2)					
		100	200	300	400	600	800
ET-4	60	0.9933	0.9978	0.9989	0.9992	0.9993	-
	80	0.9924	0.9973	0.9981	0.9987	0.9993	0.9998
	100	0.9918	0.9927	0.9985	0.9990	1.0000	0.9990
	120	0.9961	0.9973	0.9983	0.9998	0.9990	1.0000
	160	0.9951	0.9990*	-	0.9993*	0.9979*	-
ET-30	60	0.9985	0.9988	0.9988	0.9993	0.9996	0.9999
	80	0.9956	0.9983	0.9988	0.9987	0.9992	0.9996
	100	0.9932	0.9974	0.9992	0.9984	0.9995	0.9994
	120	0.9929	0.9989	0.9997	0.9995	1.00098	0.9994
	160	0.9892	0.9903*	0.9931	0.9952*	1.00093*	-

*Duct/canal formation.

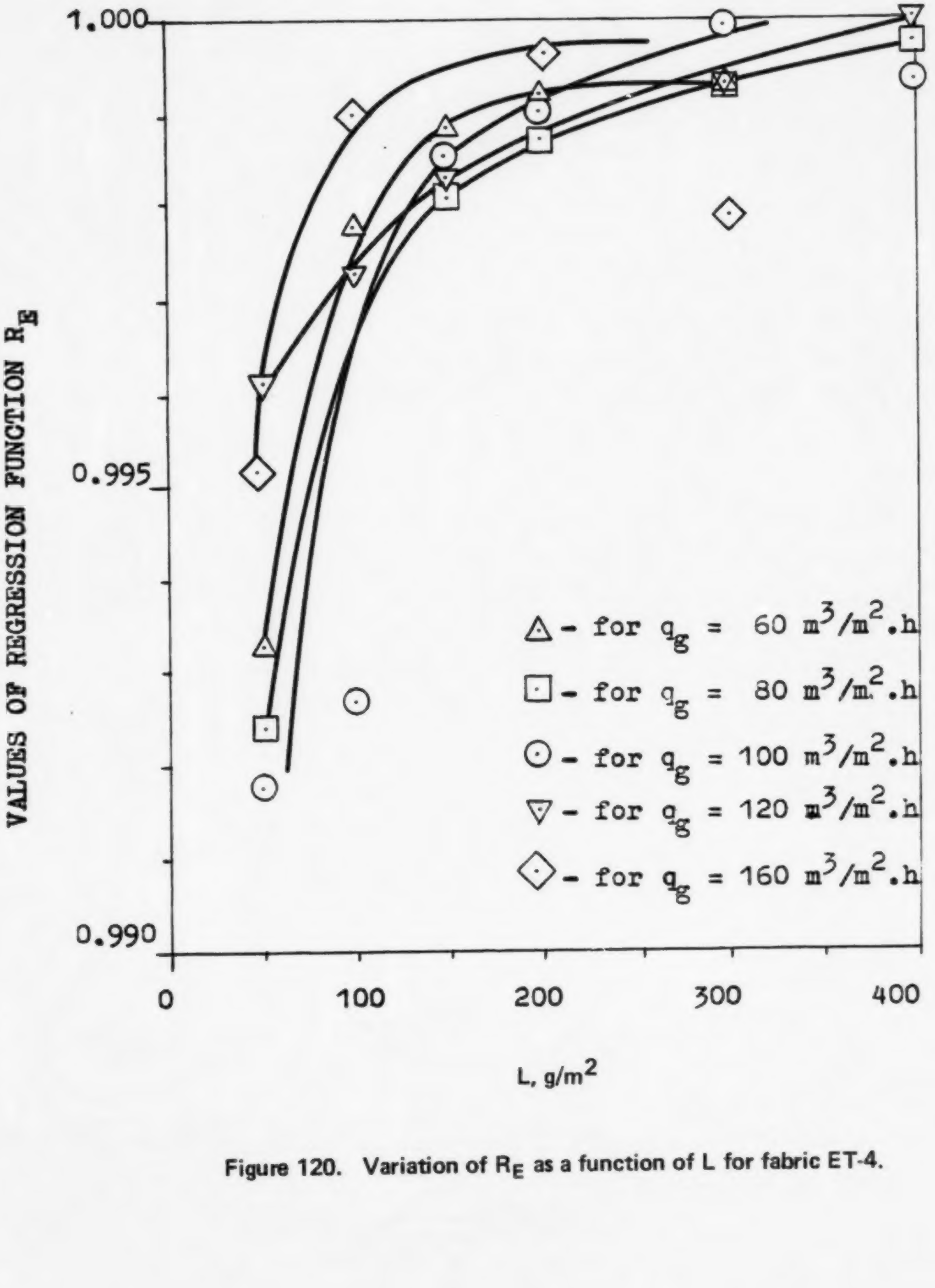

Figure 120. Variation of R_E as a function of L for fabric ET-4.

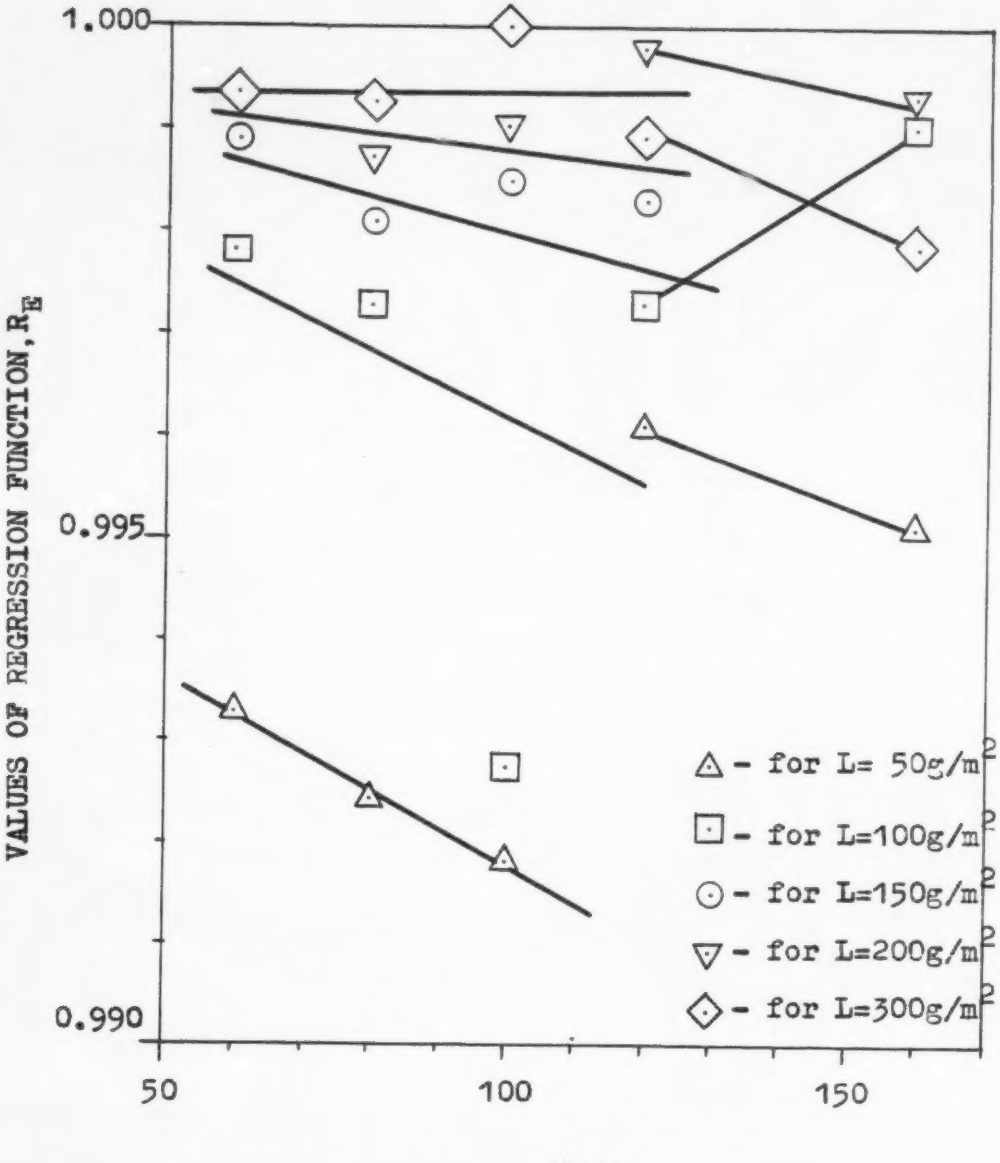

Figure 121. Variation of R_E as a function of q_g for fabric ET-4.

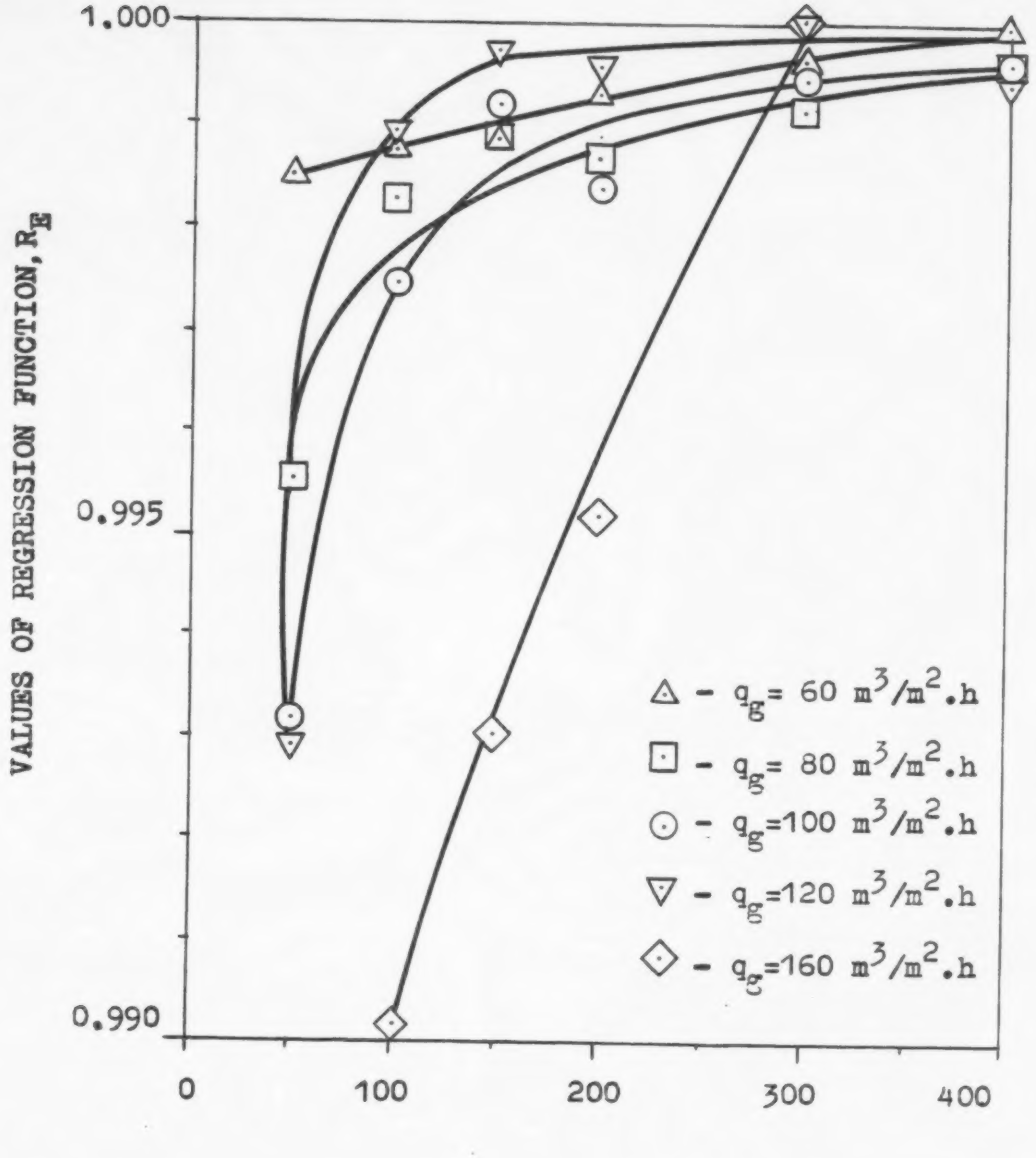

Figure 122. Variation of R_E as a function of L for fabric ET-30.

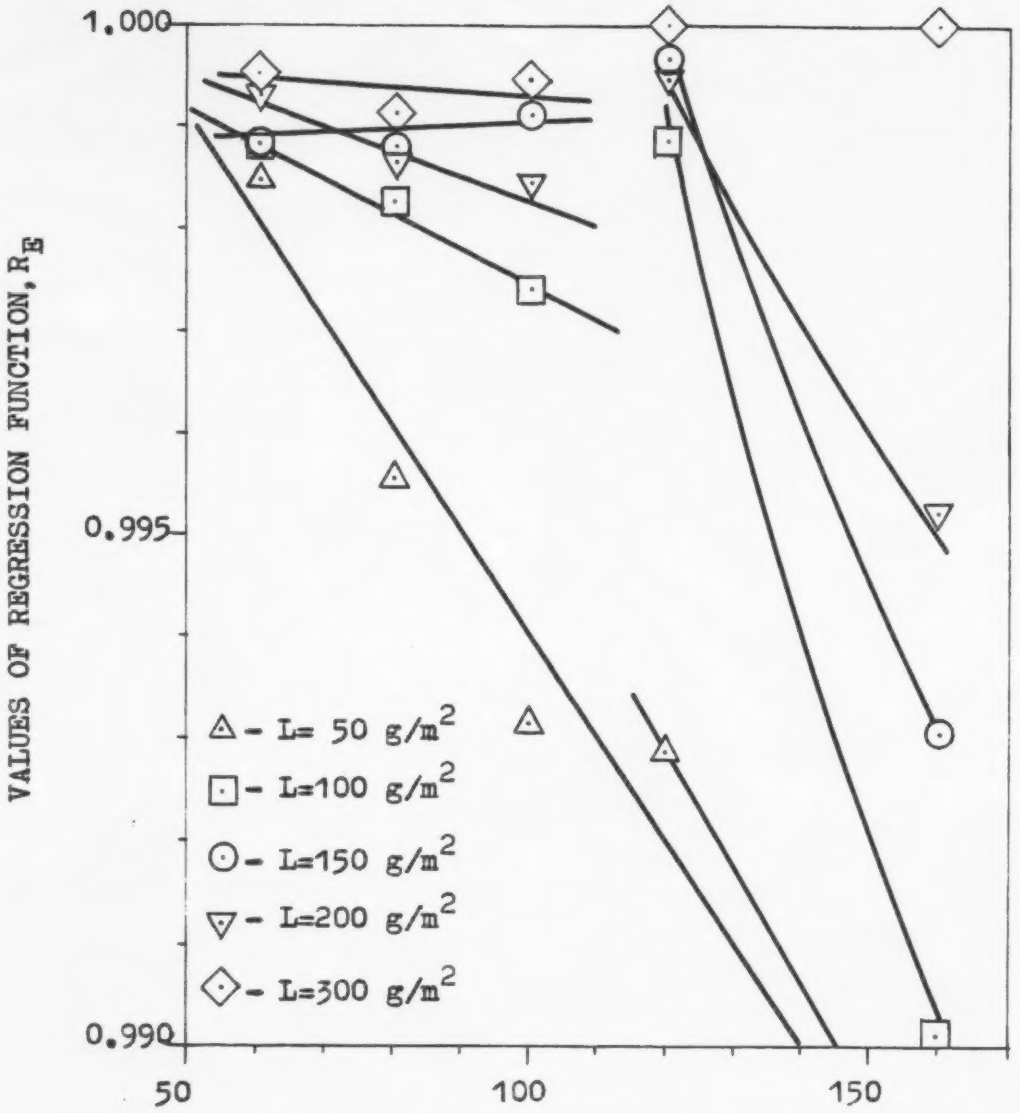

Figure 123. Variation of R_E as a function of q_g for fabric ET-30.

utilitarian viewpoint. Analysis of $R_E(q_g)$ (see Figure 121 and Figure 123) indicates that a dust cake increase decreases the slope of the straight lines. At $\bar{L}_o = L_p = 200$ to 300 g/m², the dust-fabric systems in the range of classical dust filtration achieve a different constant efficiency apart from the constant q_g and R_E. Based on Equation 86a, the regression function can be written as follows:

$$R_E = R_{E_o}(L) - n(L) \cdot q_g \;, \tag{87}$$

where

R_E = regression function,
$R_{E_o}(L)$ = regression function for $q_g = 0$,
$n(L)$ = directional coefficient, and
q_g = face velocity, m³/m²h.

Assuming that the equation, $R_E = f(L)$, is at least second order, Equation 87 can be written:

$$R_E = R_{E_o} - (a_{R2}\bar{L}^2 + b_{R2}\bar{L} + c_{R2}) \cdot q_g \;, \tag{88}$$

where

$\bar{L} = \bar{L}_o = L_o/2$ for laboratory scale, and
$\bar{L} = \bar{L}_p = L_p/2$ for large scale.

Values of coefficients a_{R2}, b_{R2}, and c_{R2} are determined by the least squares method.

Equation 88 in the rectangular coordinate system, $R_E - q_g$, is shown in Figure 124. Table 30 includes values $R_{E_o}(\bar{L}_o)$ and $n(\bar{L})$, which are regression coefficients determined from empirical data. As indicated in Table 29, regression function R_E has a nearly constant value, $R_{E_o}(\bar{L}_o)$, for $q_g = 0$, apart from the dust covering.

Data presented in Table 30 confirm the hypothesis that dust filtration at low values of q_g and at low gradients of static pressure is characterized by a certain dust cake structure depending primarily upon filtration material structure. Mean values of $R_{E_o}(L)$ for the tested fabrics differ:

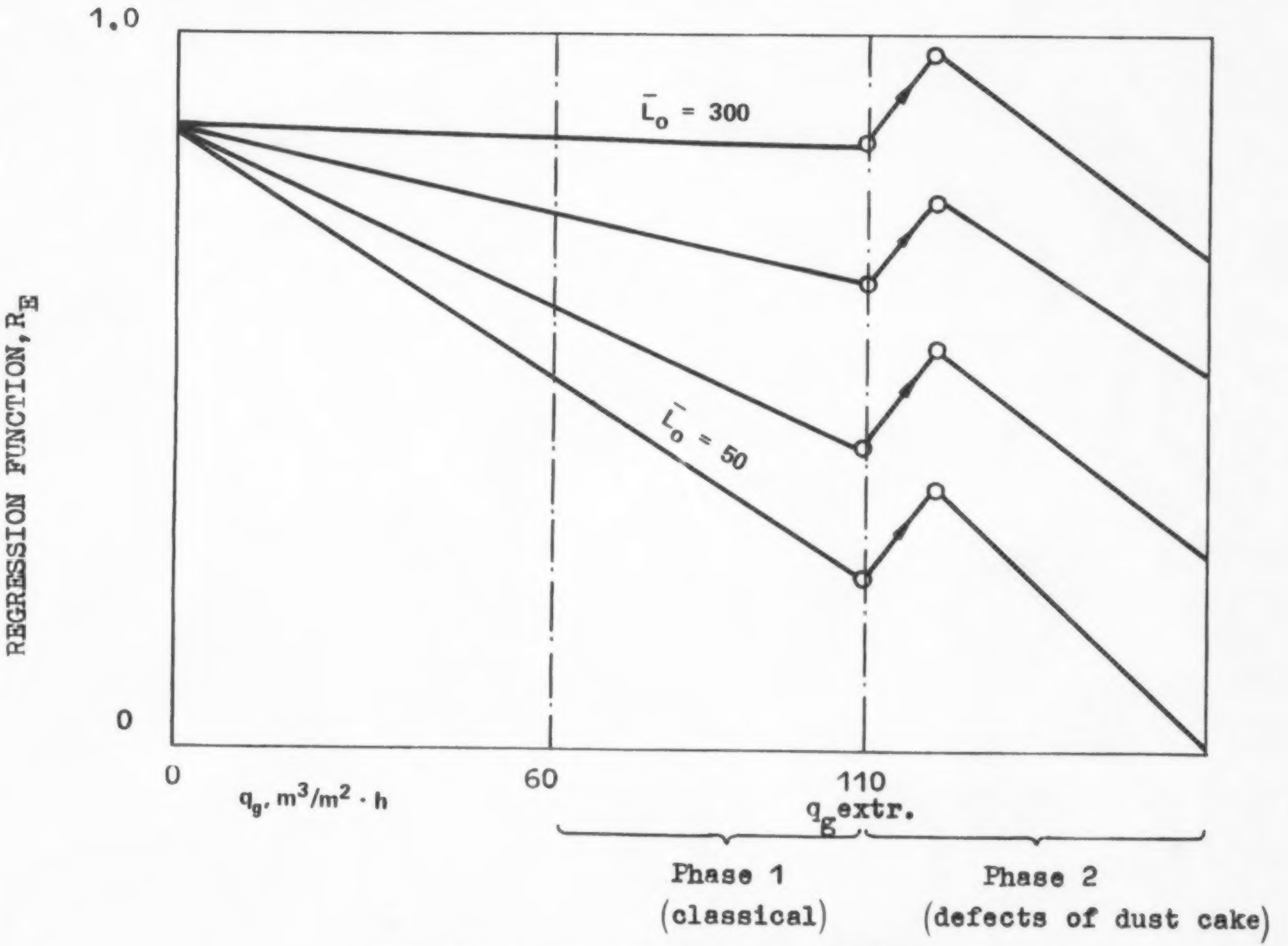

Figure 124. Transition from classical filtration to defect filtration.

TABLE 30. VALUES R_{E_o} AND $n(\bar{L}_o)$ FROM EQUATION 87

Kind of fabric	$\bar{L}$ (g/m²)	R_{E_o}	$n(\bar{L}_o)$
ET-4	50	0.9955	$-3.75 \cdot 10^{-5}$
	100	0.9990	$-3.05 \cdot 10^{-5}$
	150	0.9991	$-0.70 \cdot 10^{-5}$
	200	0.9993	$-0.50 \cdot 10^{-5}$
	300	0.9995	$-0.10 \cdot 10^{-5}$
ET-30	50	1.0036	$-9.60 \cdot 10^{-5}$
	100	1.0009	$-3.50 \cdot 10^{-5}$
	150	-	-
	200	1.0006	$-2.25 \cdot 10^{-5}$
	300	0.9996	$-0.25 \cdot 10^{-5}$

For fabric ET-4, $R_{E_o}(L) = 0.9985$, and

For fabric ET-30, $R_{E_o}(L) = 1.0012$.

The laboratory efficiency of fabric ET-4 degrades more compared to its large-scale efficiency than is true for fabric ET-30. The lower efficiency of fabric ET-4 results from its large pores and, thus, from its dust cake pores, which allow particles to penetrate the dust-fabric system more easily. Difference in the dust cake structure attributable to the filtration material porosity results from the selective precipitation mechanism, which depends on the structural parameters of the filtration material and permits the formation of certain dust-particle spatial structures.

At low values of q_g, dust cakes on the surface of the fabric will have quasi-stable spatial structures. Their efficiency will hinge mainly on mechanisms of selective sedimentation and dust particle diffusion. Inertial sedimentation will decrease with decreasing gas velocity in pores, according to Equation 29.

Variation of coefficients for straight lines, $R_E(L)$, is shown in Figure 125. This figure verifies the assumption that the least squares relationship, n(L), in Equation 88 is accurate. $R_{E_o}(L)$ has a similar parabolic character. In absolute value, the variation of $R_{E_o}(L)$ is small, but because of the precision of Equation 88 this variation was fitted by a parabola. The application of a mean value, R_{E_o}, for individual kinds of fabrics may lead to error in calculating predicted dust collection efficiencies. The final regression function is:

$$R_E = (a_{R1}\bar{L}^2 + b_{R1}\bar{L} + c_{R1}) - (a_{R2}\bar{L}^2 + b_{R2}\bar{L} + c_{R2}) \cdot q_g \; . \qquad (89)$$

Coefficients of Equation 89, determined from empirical data by the least squares method, are presented in Table 31. The resulting regression function permits a calculation of predicted dust collection efficiency in large-scale testing based on experimental data obtained in laboratory-scale testing, according to the equation:

$$E_{III} = \frac{1}{R_E} \cdot E_I \; . \qquad (90)$$

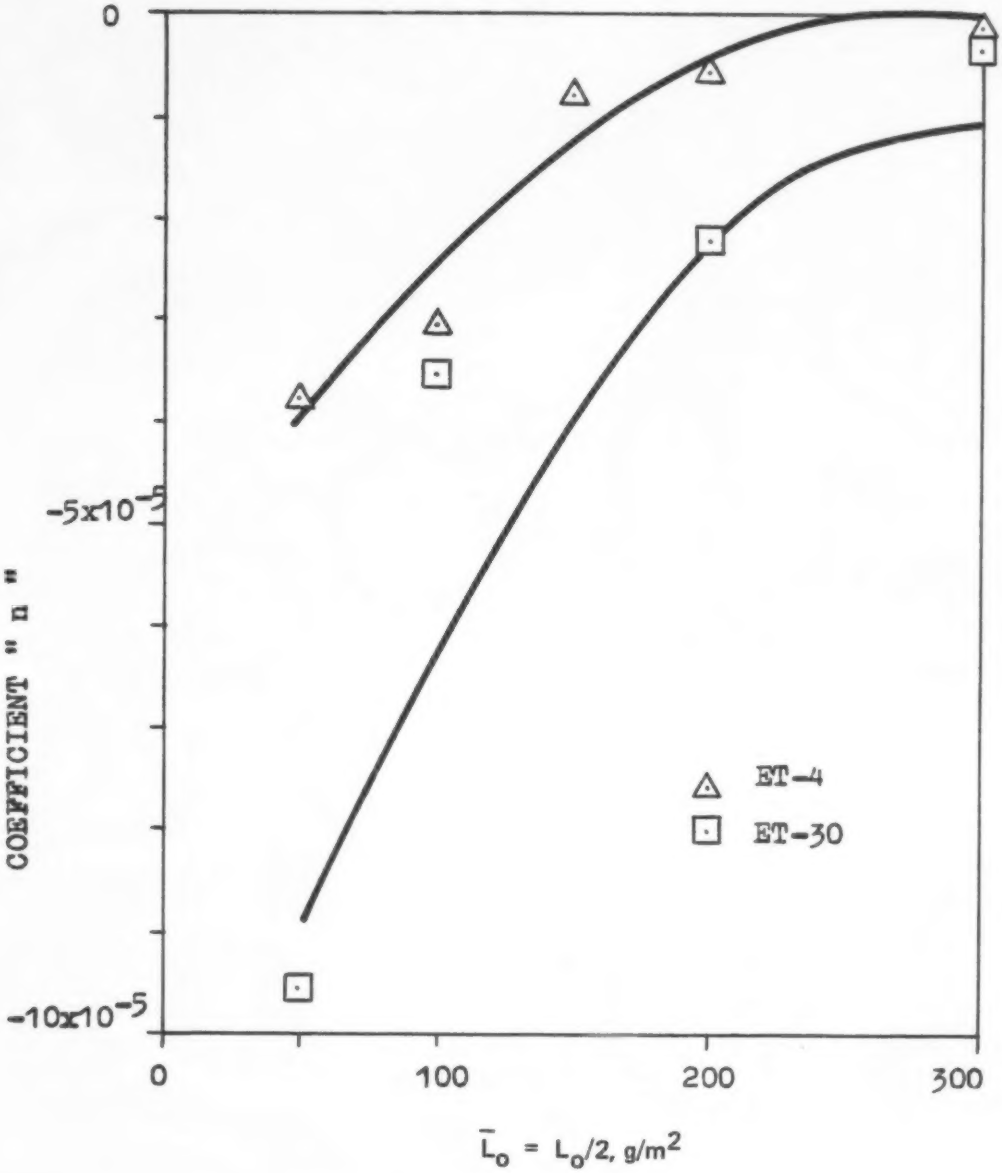

Figure 125. Variation of coefficient "n" as a function of dust covering.

TABLE 31. COEFFICIENTS a_{R1}, b_{R1}, c_{R1}, AND a_{R2}, b_{R2}, c_{R2} FROM EQUATION 89

Kind of fabric		Value
ET-4	a_{R1}	$-1.2701 \cdot 10^{-7}$
	b_{R1}	$5.7573 \cdot 10^{-5}$
	c_{R1}	$9.9347 \cdot 10^{-1}$
	a_{R2}	$-8.1104 \cdot 10^{-10}$
	b_{R2}	$4.4080 \cdot 10^{-7}$
	c_{R2}	$-5.9964 \cdot 10^{-5}$
ET-30	a_{R1}	$7.5597 \cdot 10^{-8}$
	b_{R1}	$-4.0240 \cdot 10^{-5}$
	c_{R1}	1.0051
	a_{R2}	$-4.9216 \cdot 10^{-10}$
	b_{R2}	$5.7357 \cdot 10^{-7}$
	c_{R2}	$-1.1685 \cdot 10^{-4}$

Through application of empirical data from laboratory-scale testing (Series II) and Equation 89 and Equation 90, predicted large-scale test values of dust collection efficiency as a function of q_g were determined for the examined levels of dust covering.

In most cases, the predictions are in accordance with the large-scale experiments. Figures 126 and 127 show excellent dust collection efficiency for fabrics ET-4 and ET-30 for certain values of dust cake parameters.

COMPARISON OF FILTRATION RESISTANCES

As with dust collection efficiency, Equation 11 provided the basic relationship that results in the general regression function for filtration resistance. The regression function is:

$$R_{\Delta P} = \frac{\Delta P_{F_I}}{\Delta P_{F_{III}}} , \tag{91}$$

where

ΔP_{F_I} and $\Delta P_{F_{III}}$ are filtration resistance models in Dust Filtration Process Types I and III, respectively.

The regression function was determined from the empirical data obtained during laboratory and large-scale testing of fabrics ET-4 and ET-30. Values of the regression function were calculated from values of filtration resistances at specific face velocity and dust covering. These values in the coordinate system, $R_{\Delta P} - q_g$ and $R_{\Delta P} - L$, plot the dependence of the regression functions upon q_g and L. For laboratory-scale testing, L_o is a reliable value, and for large-scale testing, L_p is a reliable value. Because the nominal values of L_o and L_p assumed for the testing program are in accordance with the measured values of L_o and L_p (with small deviations), the calculation of function $R_{\Delta P}$ employed no interpolation but used the values of ΔP_F corresponding to the nominal values of L_o and L_p.

Results of the calculations are contained in Table 32. The table does not include the value of the function, $R_{\Delta P}$, for $q_g = 60$ m³/m²h for fabric ET-30. Laboratory testing was conducted for this level of q_g on fabric samples from a different batch, and the test results differ significantly from those obtained for other q_g ranges.

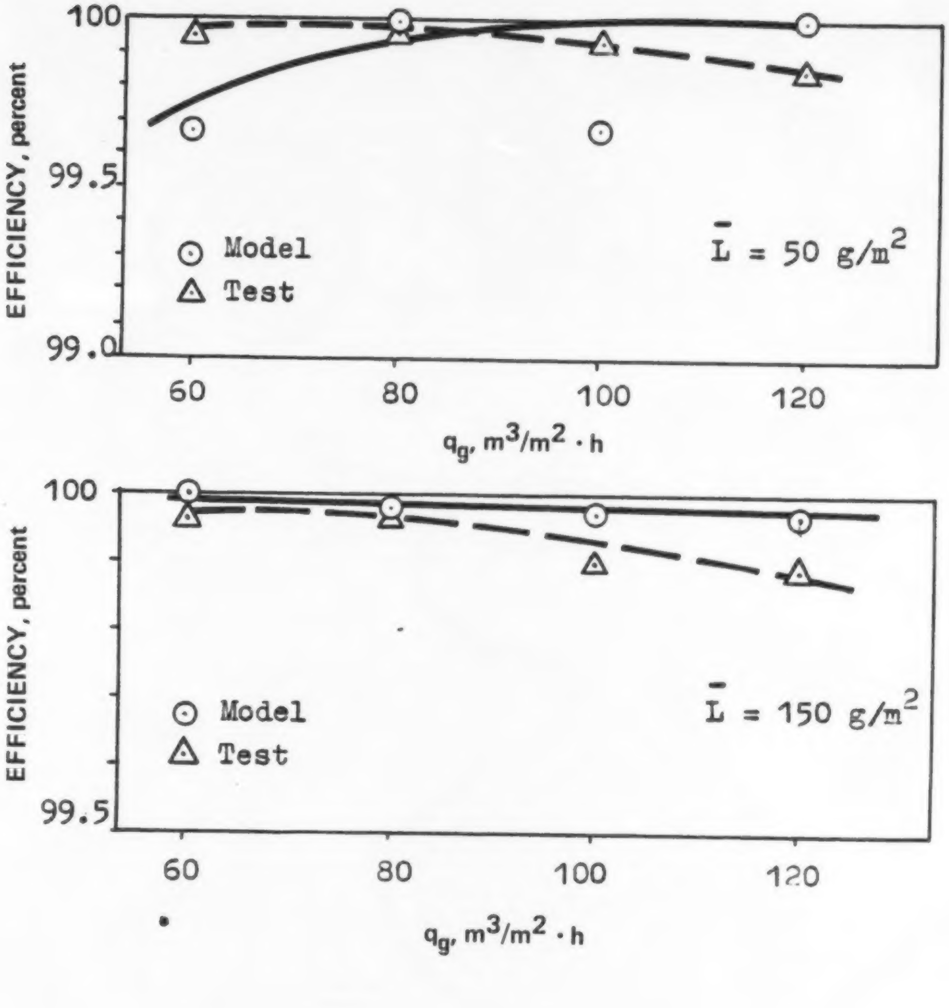

Figure 126. Large-scale dust collection efficiency calculated from Equation 90 for fabric ET-4 tested with separated fly ash.

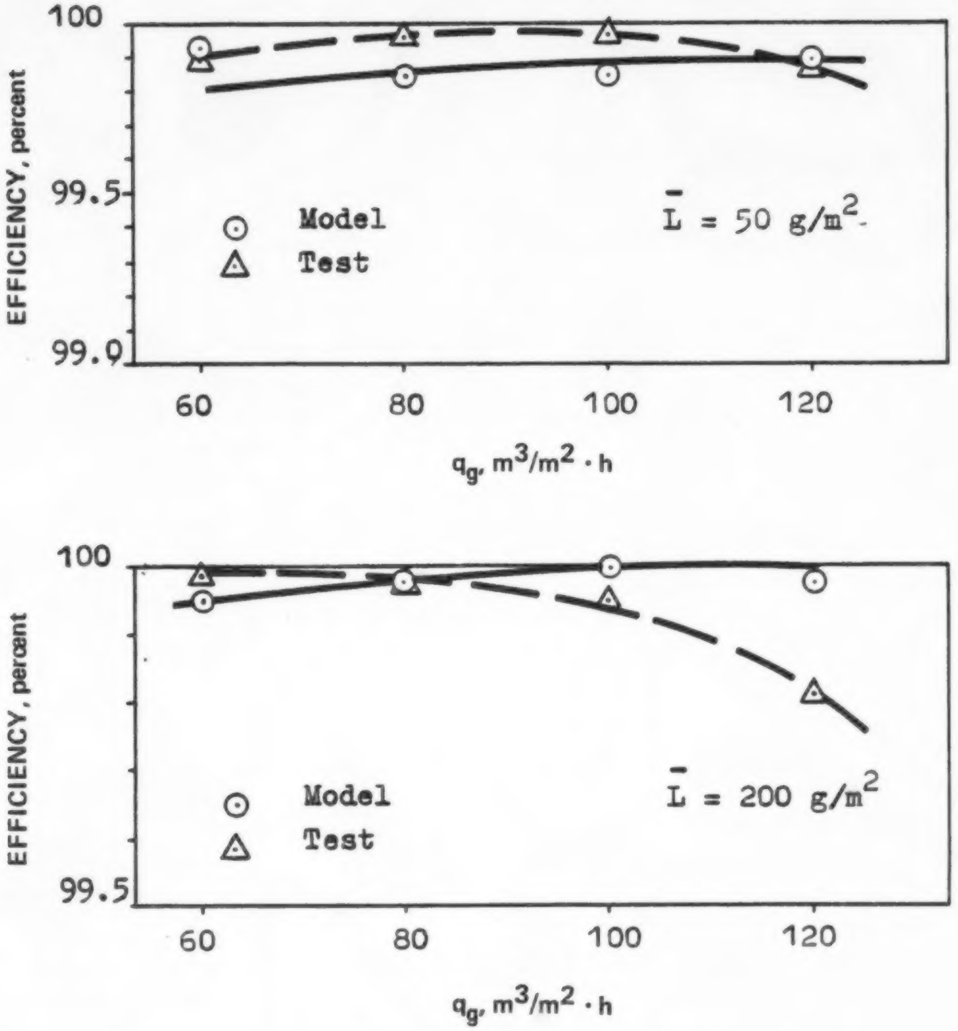

Figure 127. Large-scale dust collection efficiency calculated from Equation 90 for fabric ET-30 tested with separated fly ash.

TABLE 32. VALUES OF FUNCTION $R_{\Delta P}$

Kind of fabric	q_g (m^3/m^2h)	Terminal dust load, L (g/m^2)					
		100	200	300	400	600	800
ET-4	60	0.4115	0.4712	0.4379	0.4593	0.6975	-
	80	0.3936	0.4135	0.4941	0.5864	0.7674	0.9551
	100	0.4080	0.4008	0.4760	0.5104	0.6538	0.7529
	120	0.5169	0.6000	0.6717	0.7638	0.9144	0.9285
ET-30	80	0.4657	0.5049	0.5837	0.7140	0.9304	1.1291
	100	0.5544	0.5639	0.6427	0.7567	0.9201	1.1586
	120	0.5505	0.7486	0.8218	0.9492	1.1416	1.0912

Variations of $R_{\Delta P}$ as a function of dust quantity per unit area of filtration fabric are depicted in Figure 128 and Figure 129 for fabric ET-4 and ET-30, accordingly. These variations can be approximated to the straight line presented below:

$$R_{\Delta P} = R_{o_{\Delta P}} + n \cdot L \ , \tag{92}$$

where

$R_{\Delta P}$ = regression function,

$R_{o_{\Delta P}}$ = value of regression function for $L = 0$,

n = directional coefficient, and

L = quantity of dust in and on the filtration structure.

Calculated values, $R_{o_{\Delta P}}$ and n, for certain levels of q_g have been compiled into Table 33.

Both $R_{o_{\Delta P}}$ and n as functions of q_g are parabolas. With application of the least squares method, $R_{o_{\Delta P}}(q_g)$ and $n(q_g)$ with parabolic coefficients were determined and are contained in Table 34. The parabolas and points corresponding with data from experiments are shown in Figure 130 and Figure 131.

The parabolas fit the empirical data. With consideration of $R_{o_{\Delta P}}(q_g)$ and $n(q_g)$ in Equation 92, the regression functions are:

$$R_{\Delta P} = (a_{p1}\, q_g^2 + b_{p1}\, q_g + c_{p1}) + (a_{p2}\, q_g^2 + b_{p2}\, q_g + c_{p2})\, L \ , \tag{93}$$

where

a_{p1}, a_{p2}, b_{p1}, b_{p2}, c_{p1}, and c_{p2} are coefficients according to Table 34.

Equation 93 is a regression function of filtration resistance that permits predictions of filtration resistances in large-scale testing. These predictions are based on the laboratory experiments for fabric ET-4 and ET-30 tested with separated fly ash at an initial dust concentration of 10 g/m³, and about 60 percent hopper efficiency. The following equation can be applied:

$$\Delta P_{FIII} = \frac{1}{R_{\Delta P}}\ \Delta P_{FI} \ . \tag{94}$$

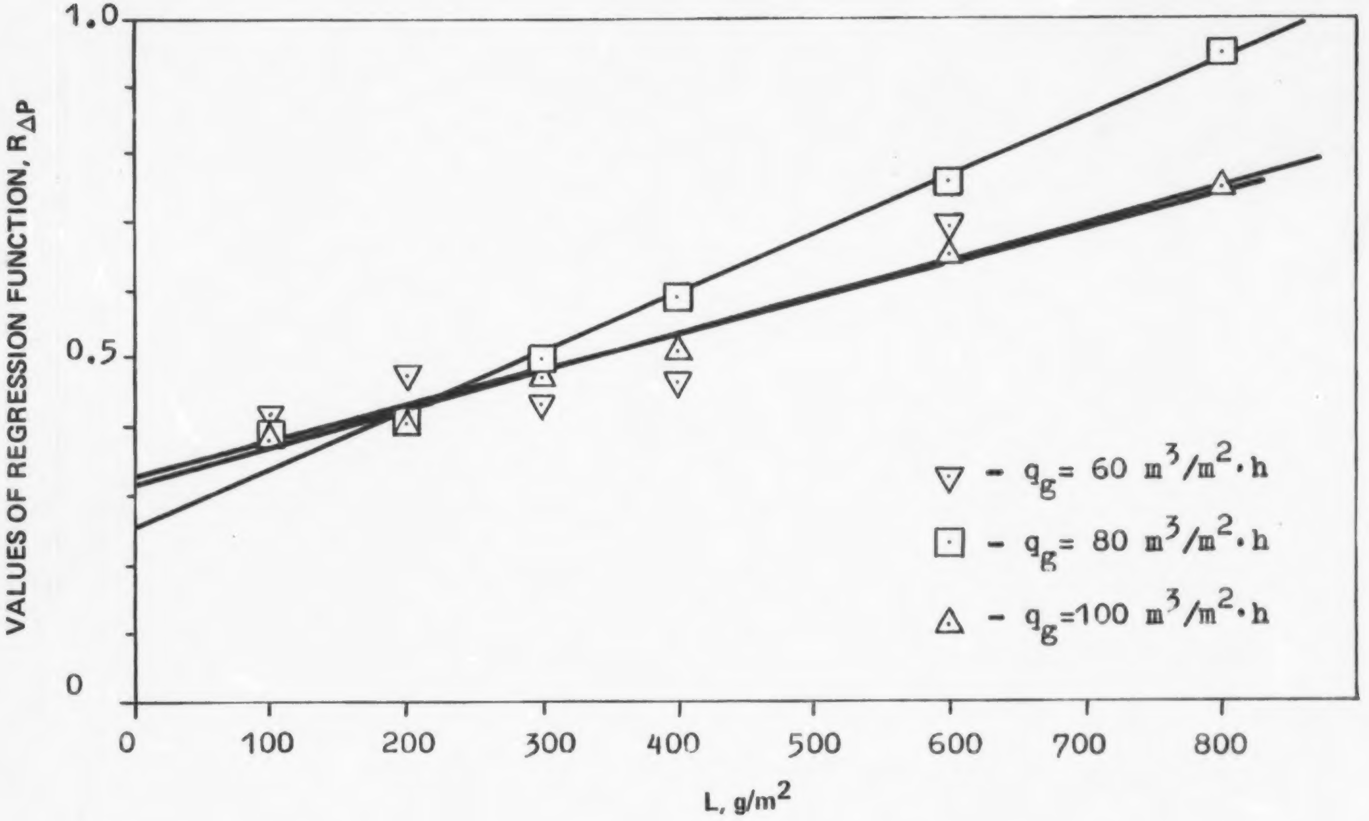

Figure 128. Variation of $R_{\Delta P}$ as a function of L for fabric ET-4.

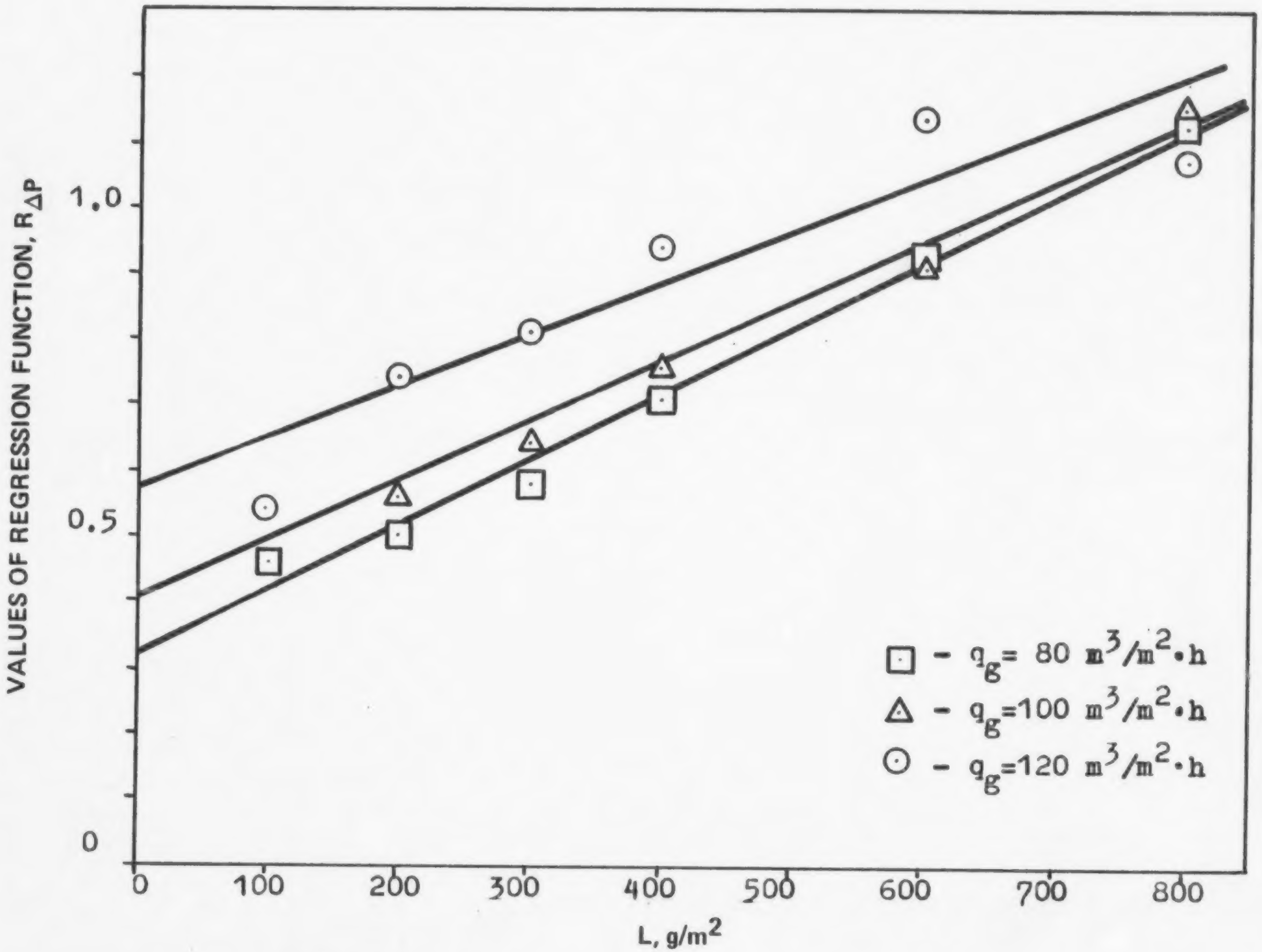

Figure 129. Variation of $R_{\Delta P}$ as a function of L for fabric ET-30.

TABLE 33. VALUES OF $R_{o\Delta P}$ AND $n(q_g)$ FROM EQUATION 92

Kind of fabric	q_g (m^3/m^2h)	Values of $R_{o\Delta P}$	Values of n
ET-4	60	0.3307	$5.1495 \cdot 10^{-4}$
	80	0.2660	$8.3921 \cdot 10^{-4}$
	100	0.3198	$5.3459 \cdot 10^{-4}$
	120	0.4831	$6.2365 \cdot 10^{-4}$
ET-30	80	0.3229	$9.9606 \cdot 10^{-4}$
	100	0.4081	$8.9468 \cdot 10^{-4}$
	120	0.5688	$7.8750 \cdot 10^{-4}$

TABLE 34. COEFFICIENTS a_{p1}, b_{p1}, c_{p1}, AND a_{p2}, b_{p2}, c_{p2} FROM EQUATION 93

Value of coefficient	Fabric	
	ET-4	ET-30
a_{p1}	$3.0761 \cdot 10^{-7}$	$2.1937 \cdot 10^{-4}$
b_{p1}	$2.4996 \cdot 10^{-3}$	$-3.5227 \cdot 10^{-2}$
c_{p1}	$1.2229 \cdot 10^{-1}$	1.7371
a_{p2}	$-9.6660 \cdot 10^{-9}$	$-7.25 \cdot 10^{-9}$
b_{p2}	$2.7993 \cdot 10^{-6}$	$-3.764 \cdot 10^{-6}$
c_{p2}	$4.7136 \cdot 10^{-4}$	1.3436

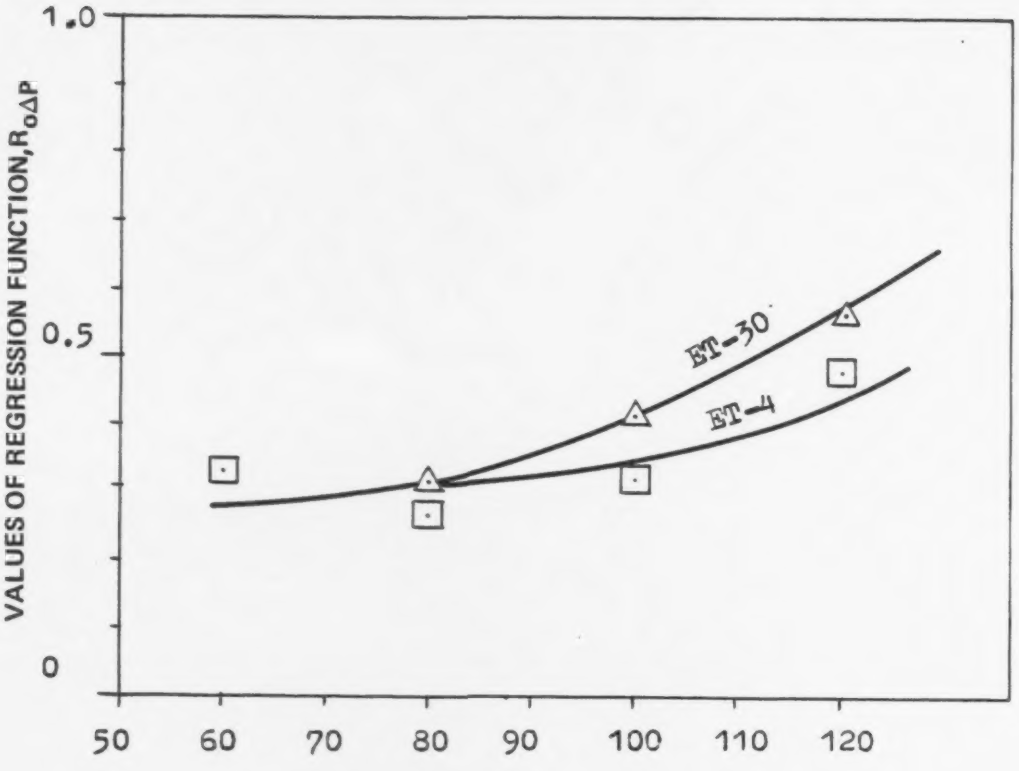

Figure 130. Variation of $R_{\alpha\Delta P}$ as a function of q_g for fabrics ET-4 and ET-30.

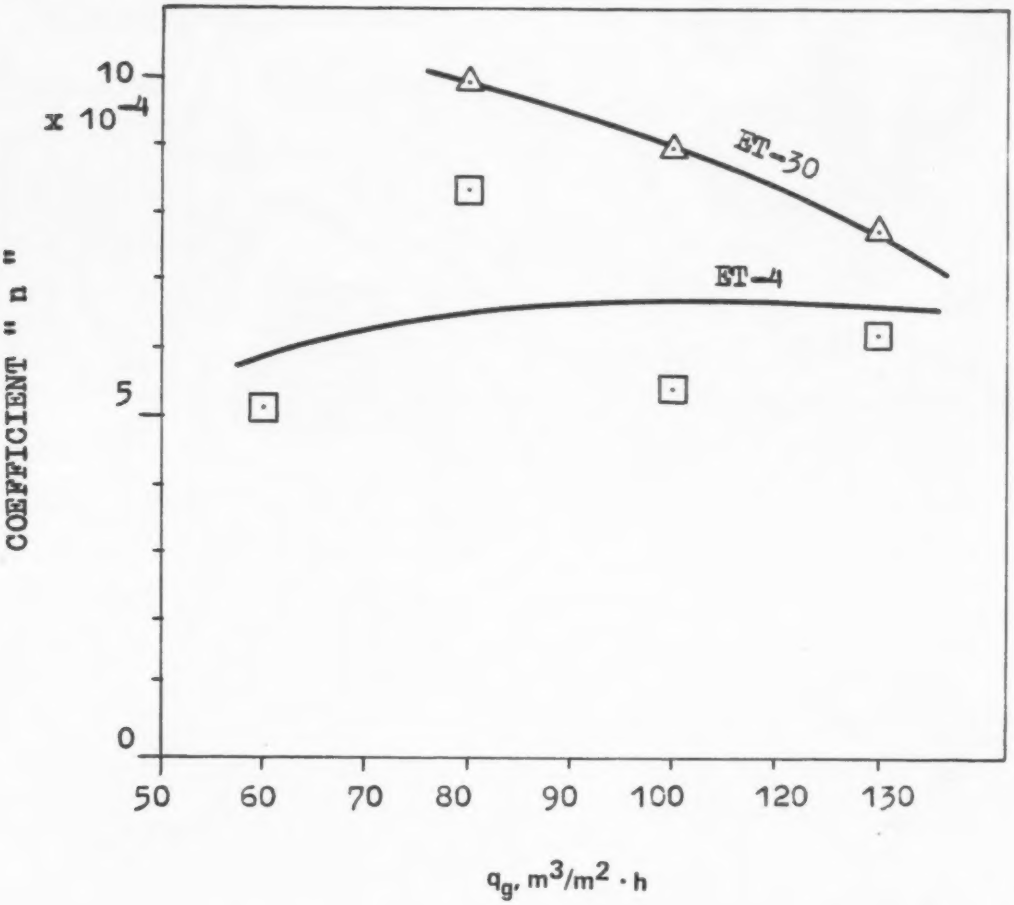

Figure 131. Variation of coefficient "n" from Equation 92 vs. q_g.

$$\Delta P_{FIII} = \frac{1}{R_{\Delta P}} \Delta P_{FI} . \qquad (94)$$

Calculated values of filtration resistances were compared to those obtained from large-scale testing, and the agreement between theoretical and actual runs was usually good. Figure 132 and Figure 133 show excellent agreement between the resistance variations determined from Equation 93 and experiments.

CONCLUSIONS

Dust collection efficiencies and filtration resistances between Dust Filtration Process Type I and Type III were compared for similar initial aerosol state and filtration parameters, based on laboratory and large-scale testing. These tests confirmed theoretical deliberations conducted earlier. Dust Filtration Process Type I and Type III are dissimilar mainly because of different dust filling of the filtration structure, which influences the structural characteristic of the dust cake, and, thus, dust collection efficiency and filtration resistance. The transformation of external process parameters from laboratory to large scale depends on a determination of certain regression functions. The lack of suitable empirical data associated with the description of the structure of filtration material and dust dictated that the presented models of dust collection efficiency and filtration resistance be regarded as detailed. These models acted as certain cross sections of the process described theoretically by a general multiparameter probabilistic model for the dust filtration process.

Thus, the models are first approximations where the constants show the effect of parameters not considered. Despite a limited number of parameters considered in the mathematical structure of the presented models, the model acts as a good process descriptor in agreement between theoretical and empirical values. Parameters considered; i.e., face velocity and dust load, are therefore concluded to dominate dust filtration. Consideration of more parameters is anticipated to permit more precise process modeling. Similar conclusions are reached after analysis of the mathematical structure of the regression dependences, where it is still difficult to give the constants an actual value. As the dust filtration process parameters increase, the effect of these constants will progressively weaken. Research should be performed in the following areas:

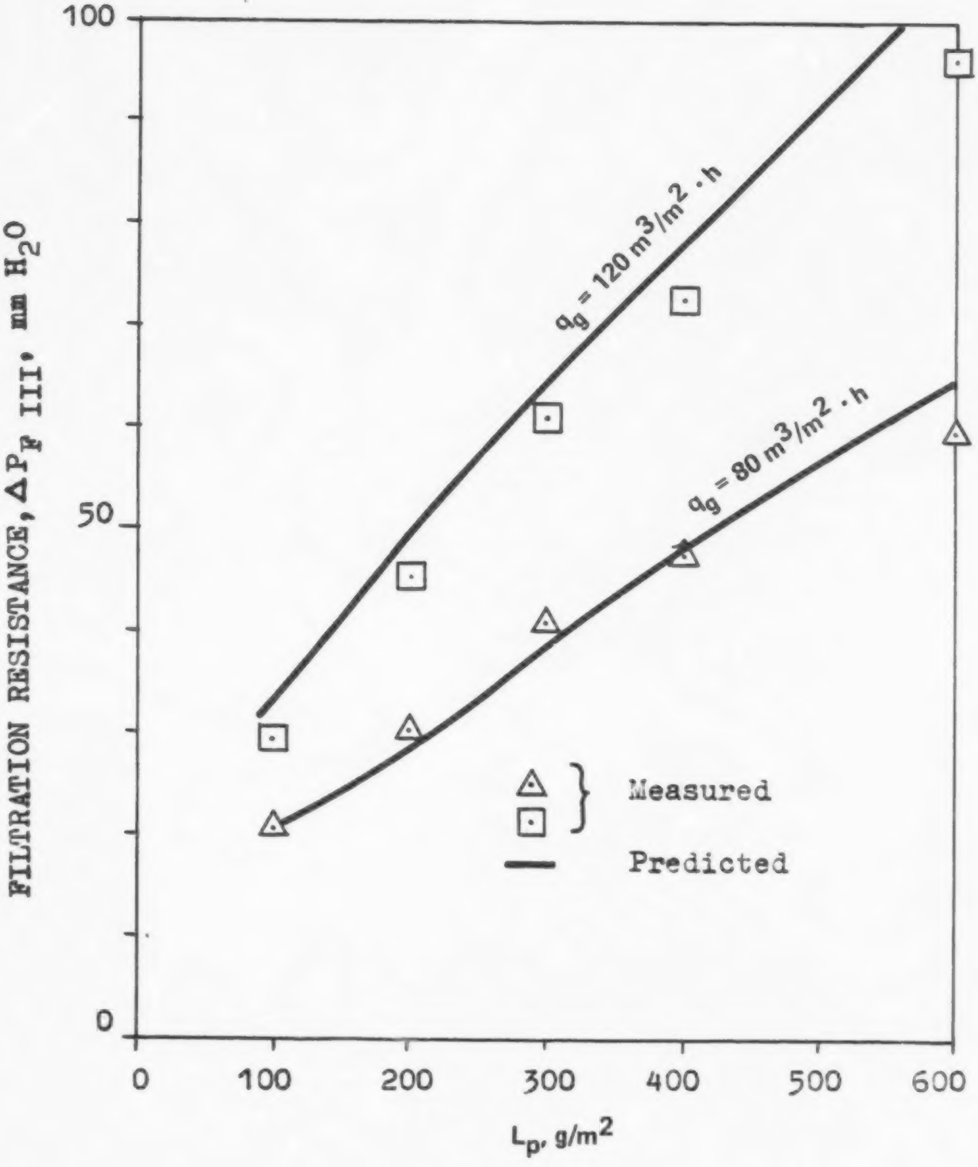

Figure 132. Predicted and measured variations of filtration resistance for fabric ET-4.

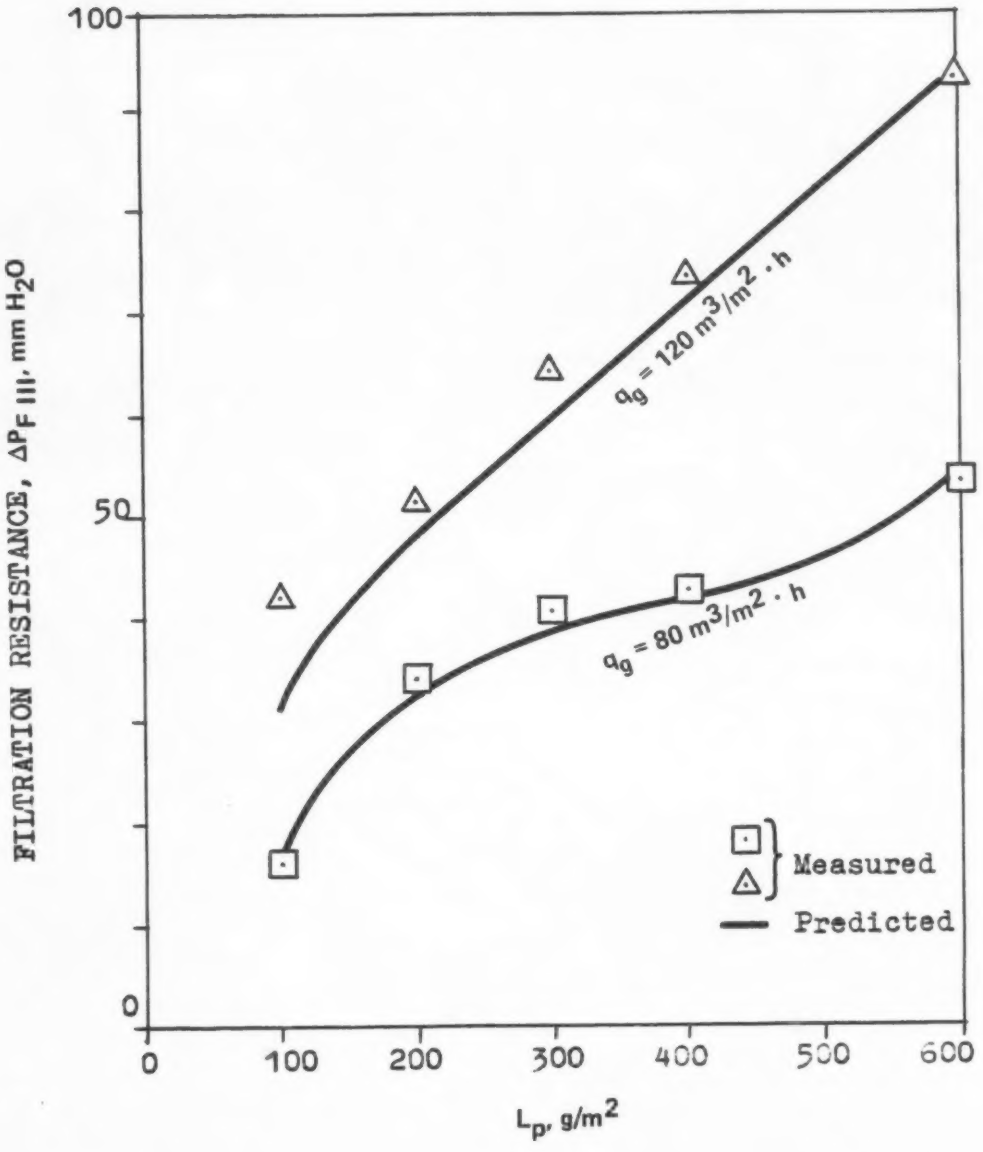

Figure 133. Predicted and measured variations of filtration resistance for fabric ET-30.

- Structural examinations in support of a physiomathematical description of woven and nonwoven fabric structures, eventually leading to a unique physical parameter describing these structures in dust filtration.
- Structural examinations associated with a physiomathematical description of dust cake structures, helping to define an unequivocal parameter characterizing dust cake in dust filtration, and to identify dependencies of the dust cake parameter that correlates with inlet dust particle size distribution.
- Detailed studies of the effect of the initial dust concentration on filtration process performance; i.e., dust collection efficiency and filtration resistance.
- Further verification of dust collection efficiency and resistance models, considering additional process parameters.
- Examination of the effect of dust distribution across the area of a real bag upon the dust collection efficiency and the mean filtration resistance.

Preliminary work in these areas was conducted within this project. Analysis of the results can be useful for future planning.

SECTION VIII
STUDY OF FILTER MEDIUM PARAMETERS

INTRODUCTION

Defining a structural parameter by which the spatial structure of textile filtration materials can be characterized is needed for a general mathematical modeling of dust filtration. For the physical filtration model, with known initial aerosol state parameters, process performance is determined by two sets of parameters: filtration parameters (FPs) and structural parameters of the filtration medium (SPFM).

Simply studying the effect of the filtration parameters on the dust filtration process is the usual method of studying dust filtration, and this method was used in this project. While data are gathered that allow the development of explicit mathematical models for predicting external process parameters over certain ranges of filtration parameters, no basis exists from which a complete general filtration model can be developed and from which the process can be optimized.

Structural parameters of the filtration medium must be defined and their effect on process performance determined. Information about the effect of structural parameters of filtration materials can be obtained from laboratory and large-scale tests, through comparative analysis, but the results are limited to certain structural elements or a particular fabric.

A definition of the structural parameters is crucial for a full description of dust filtration. For several years, Instytut Przemysłu Wiążących Materiałów Budowlanych (IPWMB) has conducted research--including an analysis of sectional character--on woven material structures. This section includes recommendations for solving the current problem and for directing future research.

Generally, textile filtration materials used in dust collection devices can be distinguished in terms of spatial structure as follows:

- Nonwoven fabrics and felts,
- Woven fabrics, and
- Knitted fabrics.

Nonwoven fabrics and felts have the most uniform structure of the filtration materials produced through textile technology. This structure is characterized by a definite ordering of elementary fibers, which permits the assumption of isotropy in spatial structure. Woven fabrics and knitted fabrics have heterogeneous and anisotropic structures, but with definite planes and directions in which homogeneous and isotropic elements can be found. A woven fabric has periodic structure because of the way in which it is made. The structure of a woven filtration material can be described by its technological and physical parameters.

Among the technological parameters are the basic independent variables determining the spatial and superficial composition of the filtration material. Technological parameters of woven fabrics include yarn thickness, thread count per 10 cm, superficial mass, and weave type.

Physical parameters consist of parameters that can be determined physically and that can be introduced directly into analytical equations (mathematical) depicting dust filtration. They include porosity, elementary fiber diameter, and apparent and total density.

The technological parameters of textile materials are usually known or may be determined by known standard methods. Physical parameters characterizing the material require additional assumptions, permitting properties to be related to structure.

The classical filtration theory, which deals primarily with high-efficiency filtration and air filtration through nonwoven filtration materials, is the basis for defining certain structural parameters important to filtration process performance. These parameters (elementary fiber diameter, thickness, and porosity or fiber packing density) are technological as well as physical. This circumstance is of practical importance because it means that routine performance tests can act as a basis for perfecting the process.

Woven filtration materials, the main subject of dust filtration research, have not been described satisfactorily from the viewpoint of spatial structure, despite the fact that fabric peculiarities and their effect on process performance have been discovered.

Generally, two main problems exist with respect to the structure of woven filtration materials:

- Determination of a universal physical parameter(s) that adequately describes the woven structure, and
- Determination of the relationship between this physical parameter and the technological parameters of the woven structure.

Research concerning these problems has already been conducted. Testing of various woven materials by D. C. Draemel[24] led to the proposal of a characteristic parameter called "free area" (FA), which reflects the periodicity of the woven material and depends on certain technological parameters. However, as shown in Project 5-533-4,[13] this parameter is valid only for fabrics made from staple fibers. For continuous filament fabrics, weave deformations cause the calculated value of FAs to differ from FAs determined by measurement of fabric geometry. Detailed examination of continuous filament fabrics exhibiting dust cake defects led to the discovery of the active filtration role of areas between the fill and warp yarns in a plane askew to the fabric surface. These areas are called "basket free areas" (BFAs) and have been confirmed by R. Dennis. Although discovery of BFAs facilitated an interpretation of test results, their value as an empirical parameter to characterize the fabric structure has not yet been considered.

To adequately characterize the woven fabric structure, a physical parameter should:

- Describe the structure satisfactorily either during clean air flow or air flow containing dust concentrations characteristic of dust filtration;
- Be selective, distinguishing between individual fabric structures;
- Be sensitive to variation in important, structure-determining technological parameters; and
- Be easy to measure physically.

Primary attention was given to clean air flow through woven materials, which is the filtration process with an initial dust concentration of zero. Operating test results were interpreted mathematically and examinations of structural geometry were conducted. This report shows the complexity of the problem by reporting not only the present project research but also earlier research not yet published.

FABRIC STRUCTURE: BASIC TECHNOLOGICAL PARAMETERS

Fabric macrostructure depends on the system of fill and warp threads, which are perpendicular to each other and woven in a certain interlaced pattern. Weave of the fill threads through the warp threads determines the pattern, which is characterized by different macrostructural elements in space and varies with fabric thickness.

Figure 134 shows the plan view and cross sections of a plain weave. The fill and warp threads system is characterized by the thread diameter and the distance between the axes of neighboring threads. The diameter of the fill and warp threads is determined either by the number per length (the metrical number) or by direct microscopic measurement (projected diameter) of a single thread.

The relationship between diameter and metrical number is:

$$d_o = \frac{C}{\sqrt{Nm_o}} \quad \text{, and} \tag{95}$$

$$d_w = \frac{C}{\sqrt{Nm_w}} \quad , \tag{96}$$

where

d_o, d_w = warp and fill thread diameter, mm;
Nm_o, Nm_w = metrical number of warp and fill threads, mm^{-1}; and
C = characteristic value, depending upon the fiber, as listed in Table 35, $mm^{\frac{1}{2}}$.

The distance between axes of threads of the fill and warp system is a parameter related to linear warp and fill density (n_o, n_w) defined by the system in thread count per 100 mm of fabric. The distance between thread axis in the individual system can be calculated according to the equation:

$$A_o = \frac{100}{n_o} \quad \text{, and} \tag{97}$$

$$A_w = \frac{100}{n_w} \quad , \tag{98}$$

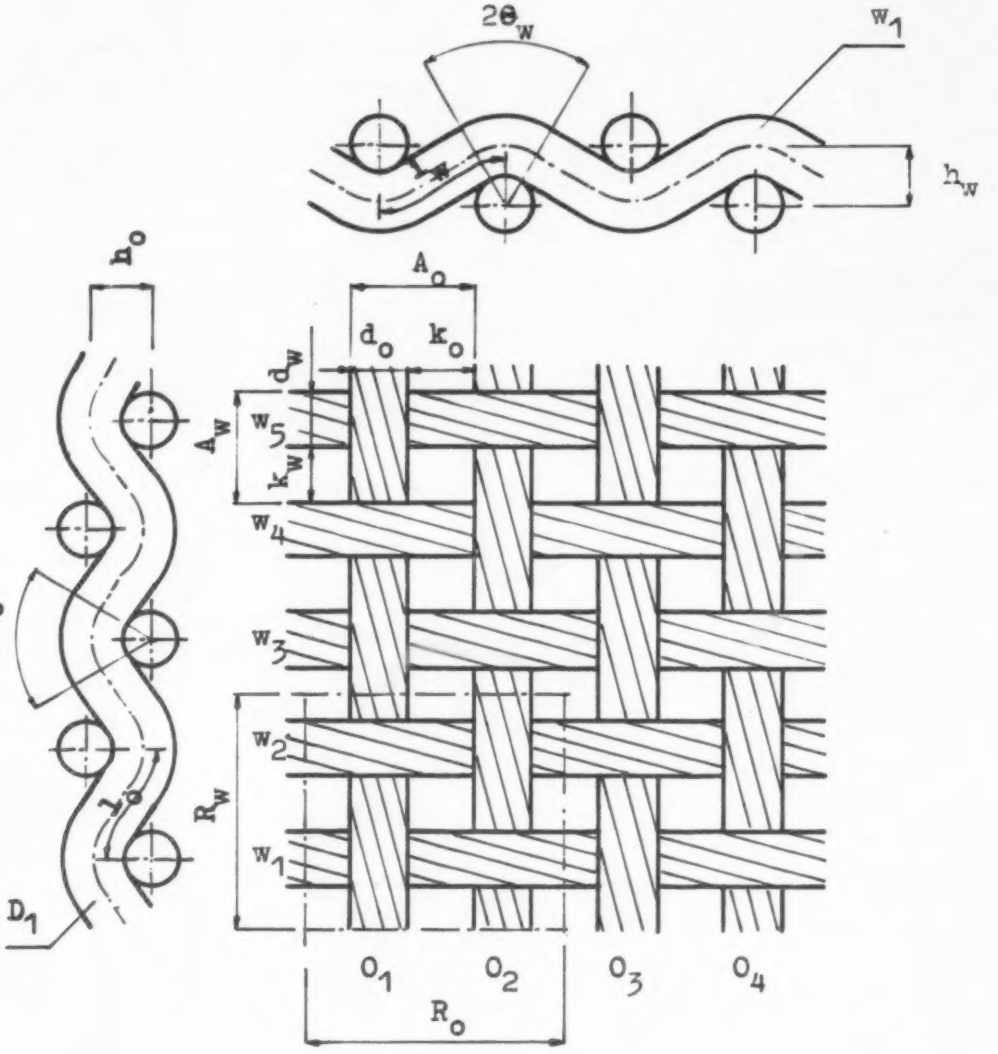

2θ_W
W_1
h_W
h_o
A_o
d_o
k_o
d_W
A_W
W_5
k_W
W_4
2θ_o
W_3
W_2
R_W
l_o
W_1
D_1
O_1
O_2
O_3
O_4
R_o

Figure 134. View and sections of plain weave fabric.

TABLE 35. VALUES OF CHARACTERISTIC FACTOR "C"

Raw materials		"C" value
Cotton and staple viscose		1.25
Worsted wool:	French system	1.26
	British system	1.32
Carded wool		1.36
Polyamid silk, continuous		
Polyester and nomex		1.50
Staple polyester		1.32
Glass		0.705

where

A_o, A_w = distance between adjacent warp or fill threads, mm; and

n_o, n_w = warp or fill thread count per 100 mm of fabric.

The linear dimension of the FAs can be calculated according to the following equations:

$$K_o = A_o - d_o \text{ , and} \tag{99}$$

$$K_w = A_w - d_w \text{ ,} \tag{100}$$

where

K_o, K_w = free area dimension between adjacent warp and fill threads, mm; and

A_o, A_w, d_o, d_w = as in above equations.

The characteristic value of fabric macrostructure is the weave repeat that defines the number of fill and warp threads in the basic unit weave. Warp weave repeat, R_w, calculated along the fill direction, and fill weave repeat, R_o, calculated along the warp direction, identify the macrostructure. The periodicity of the fabric structure is confirmed by the presence of repeating structural elements as defined by the weave repeats. The fact that this repeating structural element is observed throughout the fabric leads to the conclusion that some properties of the material surface, determined by weave repeat, are characteristic of the entire fabric area.

Based on previously presented equations, linear dimensions of the weave pattern area can be calculated according to the following equations:

$$L_o = R_o \cdot A_o \text{ , and} \tag{101}$$

$$L_w = R_w \cdot A_w \text{ ,} \tag{102}$$

where

L_o, L_w = length of warp and fill weave pattern, respectively, mm.

The structural composition of the yarns in the fill and warp thread systems accounts for the complexity of the woven material structures. Yarn, characterized in the fabric macrostructure by diameter, d, is composed of elementary fibers of specific cross-sectional dimensions and lengths.

Table 36 lists the three basic fiber types and subdivides the chemical fibers into groups according to production method.

Natural plant and animal fibers, unlike chemical fibers, are characterized by fixed shapes and properties that are determined by origin. With the exception of natural silk and some plant fibers, they are usually short, ranging from 10 to 300 mm in length. Chemical fibers, on the other hand, can be produced according to any desired cross section and length. They can be produced as either staple or continuous filament (silk-like) fibers and processed by conventional spinning technology into yarns. Yarns obtained from staple fibers differ from those produced from continuous filament fibers (Table 37). Yarn properties to a great extent determine fabric properties. The elementary fibers of a yarn are aligned parallel to the yarn axis. Twist is then applied to the staple fiber yarns (and to some continuous filament fibers) resulting in askew placement of the elementary fibers with respect to the yarn axis. However, a net twist effect on fiber placement in the yarn volume can be avoided by using elementary yarn lengths.

The number of fibers in the yarn cross section is an important yarn parameter. Assuming the diameter of the elementary fiber to be d_f, the fiber filling of a yarn cross section of diameter, d, can be calculated:

$$\alpha = \frac{n \cdot d_f^2}{d^2} \cdot 100 \ , \qquad (103)$$

where

α = coefficient of yarn filling with fiber, %;
n = number of elementary fibers;
d_f = elementary fiber diameter, μm; and
d = yarn diameter, μm.

The coefficient measures volumetric yarn filling with fibers, neglecting any length variation caused by yarn twist. This parameter is similar to parameters characterizing nonwoven filtration materials. The fabric is a permeable filtration medium with periodic distribution of its plastic fiber.

TABLE 36. KINDS OF ELEMENTARY FIBERS

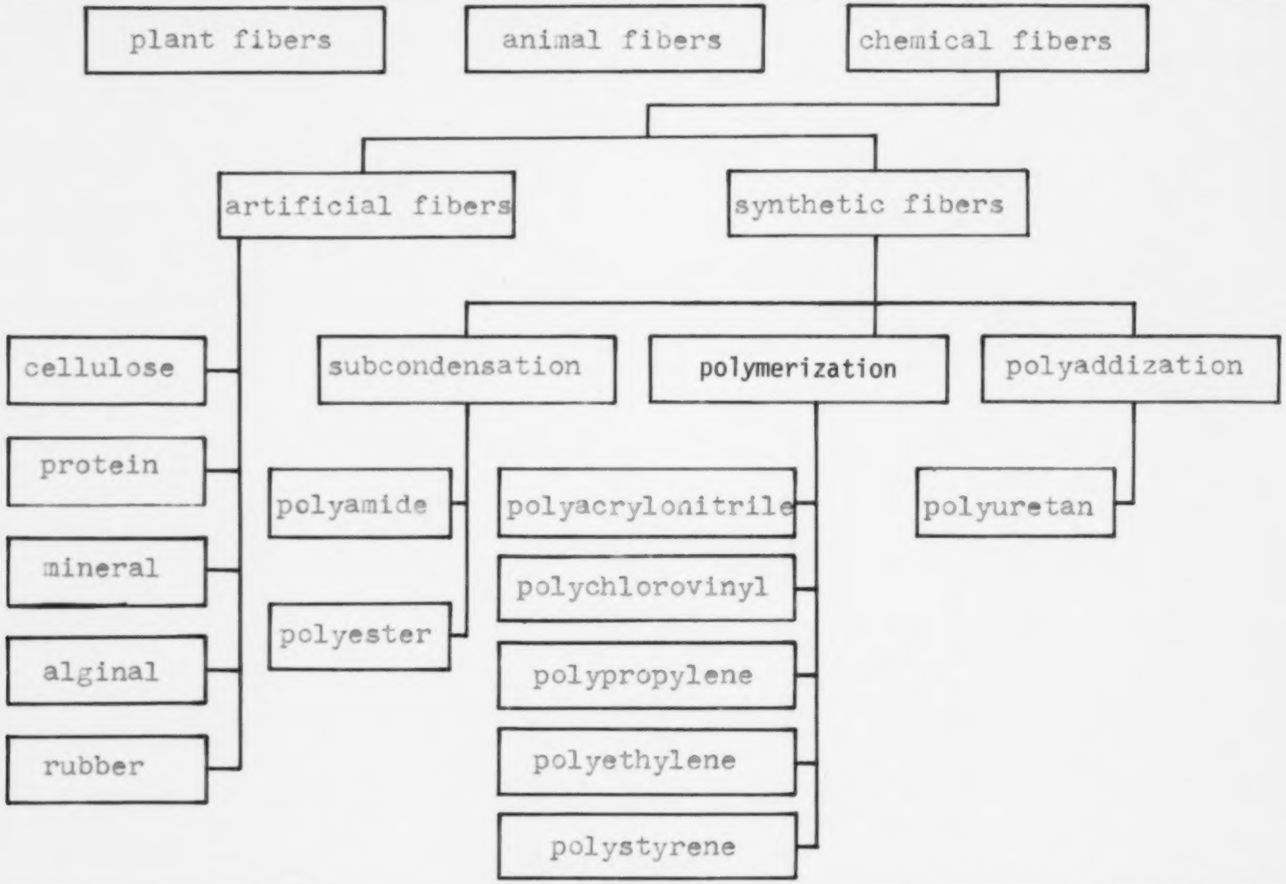
plant fibers
animal fibers
chemical fibers
artificial fibers
synthetic fibers
cellulose
protein
mineral
alginal
rubber
subcondensation
polyamide
polyester
polymerization
polyacrylonitrile
polychlorovinyl
polypropylene
polyethylene
polystyrene
polyaddization
polyuretan

TABLE 37. YARN CHARACTERISTICS OF FABRICS USED IN LABORATORY AND LARGE-SCALE TESTS

Parameter	Kind of fabric			
	ET-4	ET-30	F-tor 5	PT-15
Kind of fiber				
warp	Staple	Staple	Filament	Filament
fill	Staple	Staple	Filament	Filament
Length of fiber (mm)				
warp	32.38	76.87	Silk	Silk
fill	3846.50	76.87	Silk	Silk
Diameter of yarn (mm) (calculated)				
warp	0.4091	0.2864(0.4048)	0.2612(0.3694)	0.2378
fill	0.5742	0.2852(0.4032)	0.2514(0.3355)	0.2405
Diameter of yarn (mm) **(measured** axes of ellipse)				
warp	0.6069 · 0.4013	(0.2344 · 2) · 0.2906	(0.1787·2) · 0.2294	0.2269 · 0.1875
fill	0.8187 · 0.6363	(0.2319 · 2) · 0.2594	(0.3281·2) · 0.2113	0.2825 · 0.1781
Number of fibers in cross-section of yarn				
warp	231	80 " 2	96 " 2	32
fill	383	88 " 2	48 " 2	32
Diameter of fiber (mm)				
warp	17.2	20.1	23.5	29.0
fill	19.5	19.8	22.8	29.0
Fabric porosity, measured using mercury intrusion (%)	66.97	54.94	45.99	42.98
Fabric porosity, calculated from technological parameters (%)				
for circular shape of yarns	61.00	57.62	35.61	39.87
for eliptical shape of yarns	51.82	46.95	10.23	25.66
FA				
for circular shape of yarns	8.11	0.006	0.744	-3.58
for eliptical shape of yarns	0.05	-5.68	-1.03	-2.26

SECONDARY TECHNOLOGICAL PARAMETERS DESCRIBING WOVEN STRUCTURE

Spatial woven structure is too complicated for adequate description by the basic parameters discussed in the previous section. In textile technology other secondary parameters are used; some of them--the most important for further deliberation--are discussed below.[28]

F. T. Pierce, introducing the term "ideal fabric" (i.e., fabric composed of one-dimensional fill and warp yarns of circular cross sections), presented theoretical analyses of the fabric composition of plain weave. Plain weave was considered because its structure is simple and easily distinguished from other kinds of weaves.

Assuming a constant length of weave elements, ℓ_o and ℓ_w (the ideal fabric definition), Pierce obtained the following seven geometrical relationships:

$$\left.\begin{aligned} A_w &= f(D, \Theta_o, \ell_o) \\ A_o &= f(D, \Theta_w, \ell_w) \\ h_o &= f(D, \Theta_o, \ell_o) \\ h_w &= f(D, \Theta_w, \ell_w) \\ W_o &= f(\ell_o, A_w) \\ W_w &= f(\ell_w, A_o) \\ D &= f(d_o, d_w) \end{aligned}\right\} \tag{104}$$

where

A_o, A_w = distance between neighboring warp and fill threads,
ℓ_o, ℓ_w = length of elementary segment of warp and fill (see Figure 135),
Θ_o, Θ_w = angle for warp and fill,
h_o, h_w = deflection of warp and fill thread,
W_o, W_w = takeup degree of warp and fill, and
$D = d_o + d_w$ (sum of warp and fill diameters).

Takeup degree is a percentage defined by the following:

$$W_o = \frac{\ell_o - A_w}{A_w} \cdot 100 \quad \text{, and} \tag{105}$$

$$W_w = \frac{\ell_w - A_o}{A_o} \cdot 100 \quad . \tag{106}$$

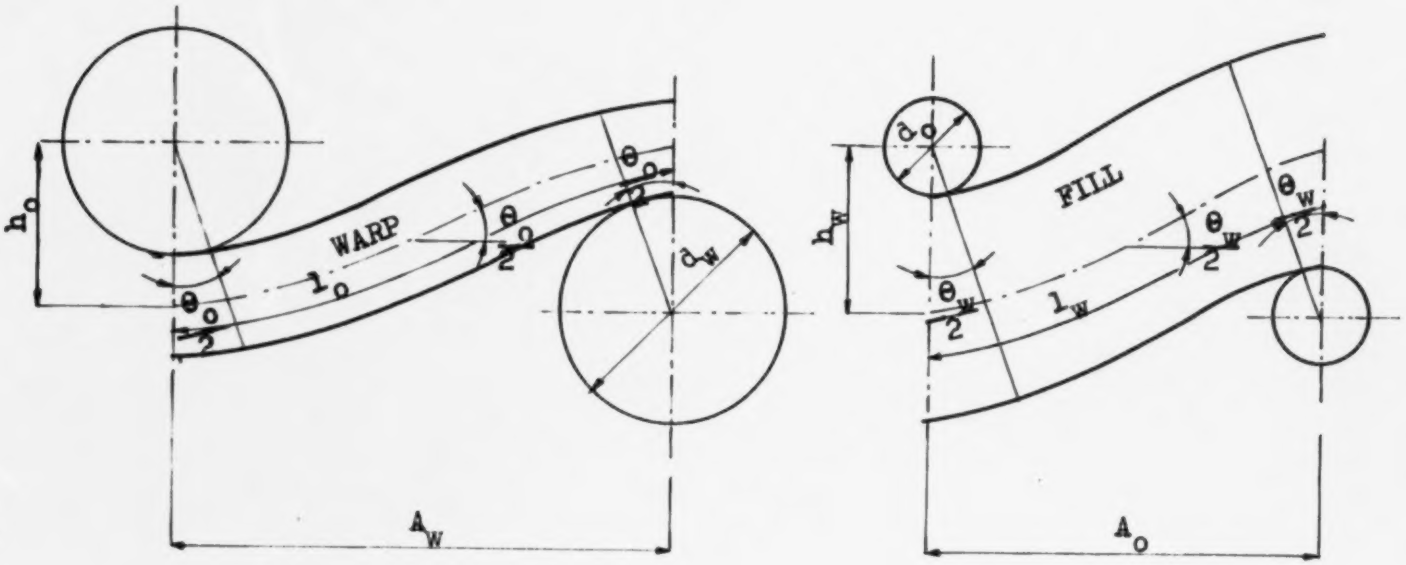
WARP
FILL
h_o
h_w
θ_o
$\frac{\theta_o}{2}$
$\frac{\theta_w}{2}$
θ_w
l_o
l_w
d_o
d_w
A_w
A_o

Figure 135. Characteristic magnitudes of plain weave composition.

The other variables are presented in Figure 135.

Presenting the geometric character of an ideal plain weave fabric in the form of 7 equations with 11 unknowns permits the determination of all interesting parameters, assuming 4 of them. From Pierce's work, E. V. Painter developed a nomogram, which can be used to obtain individual parameters quickly. Painter modified Pierce's equation by introducing the ratios, ℓ/D and h/D. Families of curves were obtained and are represented by the following equations:

$$\frac{\ell}{D}: \qquad \left.\begin{aligned} \frac{\ell_o}{D} &= f(W_o, E'_w) \\ \frac{\ell_w}{D} &= f(W_w, E'_o) \end{aligned}\right\} \qquad (107)$$

$$\theta: \qquad \left.\begin{aligned} \theta_o &= f(W_o, E'_w) \\ \theta_w &= f(W_w, E'_o) \end{aligned}\right\} \qquad (108)$$

$$\frac{h}{D}: \qquad \left.\begin{aligned} \frac{h_o}{D} &= f(W_o, E'_w) \\ \frac{h_w}{D} &= f(W_w, E'_o) \end{aligned}\right\} . \qquad (109)$$

For development of the nomogram, Pierce's equation can be applied:

$$\left.\begin{aligned} h_o &= \frac{13.6\sqrt{W_o}}{n_w} \\ h_w &= \frac{13.6\sqrt{W_w}}{n_o} \end{aligned}\right\} . \qquad (110)$$

Figure 136 shows Painter's nomogram. The variable, E', appearing in Equations 107 through 109, is the reduced fabric filling in the direction perpendicular to that discussed and is calculated as follows:

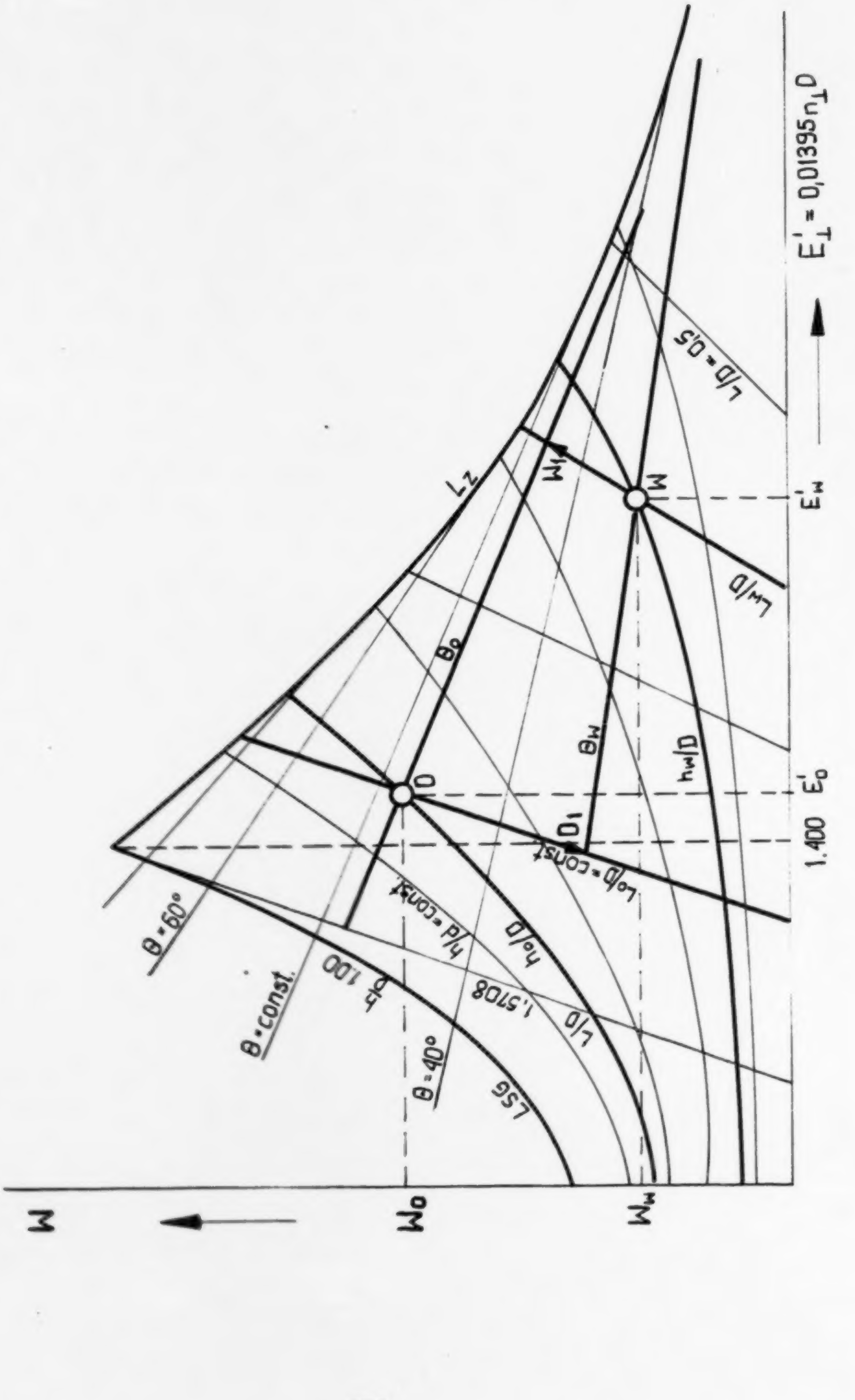
W
Wo
Ww
E'⊥ = 0,01395 n⊥ D
E'w
E'o
1,400
θ = 60°
θ = const.
θ = 40°
LSG
L/D
1,5708
hp 100
h/d = const
ho/D
Lo/D = const
O
O1
θo
θw
hw/D
Lw/D
M
M1
L/D = 0,5
LZ

Figure 136. Painter's nomogram (diagram).

$$\left.\begin{aligned} E_o' &= k \cdot E_o = 0.01395 \cdot n_o \cdot D \\ E_w' &= k \cdot E_w = 0.01395 \cdot n_w \cdot D \end{aligned}\right\} \quad (111)$$

where

E_o and E_w are defined as full filling with yarn, depending upon the kind of weave, and are calculated according to the equations:

$$\left.\begin{aligned} E_o &= \frac{d_o \cdot R_o + p_w \cdot d_w}{R_o \cdot A_o} \cdot 100 \\ E_w &= \frac{d_w \cdot R_w + p_o \cdot d_o}{R_w \cdot A_w} \cdot 100 \end{aligned}\right\} \quad (112)$$

where

E_o, E_w = full filling with warp and fill yarn, %; and

p_o, p_w = number of inflections of warp and fill threads in weave repeat, R_o and R_w.

The fabric in the Painter nomogram is characterized by two points: 0 for the warp and W for the fill. These points, connected with the geometrical parameters, ℓ/D, h/D, and Θ, determine the exact takeup degree and yarn filling of the fabric. Introduction of E' connects both systems of a given fabric (i.e., warp and fill) concerning the parameter's effect.

Painter's nomogram also shows structural changes as a result of external forces. Under tension along the warp or fill threads in one direction, characteristic points 0 and W move along straight lines, ℓ/D, as shown in Figure 136 and according to the assumption of an ideal fabric with stable values ℓ, d_o, and d_w. With fabric tension along the warp thread, the takeup degree deflection and wrapping angle of warp decrease, but the degree of takeup fill and its deflection and wrapping angle increase. Linear yarn densities (n_o and n_w) and fabric dimensions change.

This situation causes shifts of points, $0 \rightarrow 0_1$ and $W \rightarrow W_1$, along constant ℓ/D curves. At the extreme, the tension shifts point 0 to the X-axis, so h_o =

0, W = 0, and the warp system takes the lowest constant value of reduced fabric filling with fill yarn, corresponding to D = constant with the lowest value of linear density of fill yarn, $n_{w\ min}$. This state may be obtained when the fill thread system takes value, h/D = 1, so it is characterized by parameters placing point W on or to the left of curve, $\ell/D = 1.5708$. In other situations, this extreme state cannot be reached.

With the fabric tension along the fill thread, similar analyses may be made. In the case of multidirectional tension; i.e., along warp and fill threads at the same time, the application of Pierce and Painter's assumptions (ℓ = constant and D = constant) predicts structural changes in the ideal fabric, and the system remains in a state of equilibrium but with increasing stress in the thread systems. This conclusion is important to further analysis of real fabric performance.

Fabric thickness and superficial mass are parameters that are not explicitly considered in Pierce and Painter's theory but are often used in the textile industry. Fabric thickness depends upon which thread system--warp or fill--forms the plane tangent to the fabric. Three structural variants can be distinguished (see Figure 137). The fabric thickness is lowest when planes tangent to the fabric surface are formed simultaneously by warp and fill systems. Variant 1 presented in Figure 137 illustrates that kind of structure. Thus, fabric thickness is determined by the following equation:

$$G_{min} = d_o + h_o = d_w + h_w \quad . \tag{113}$$

The greatest fabric thickness appears when the thread system of smaller diameter has deflection, h = 0. This situation is illustrated by variant 3 in Figure 137. In this case, fabric thickness is described by the equation:

$$G_{max} = 2d_w + d_o \ , \tag{114}$$

at $d_w > d_o$.

General fabric thickness is expressed by:

$$G = d_{ps} + h_{ps} \ , \tag{115}$$

where

G = fabric thickness, μm; and

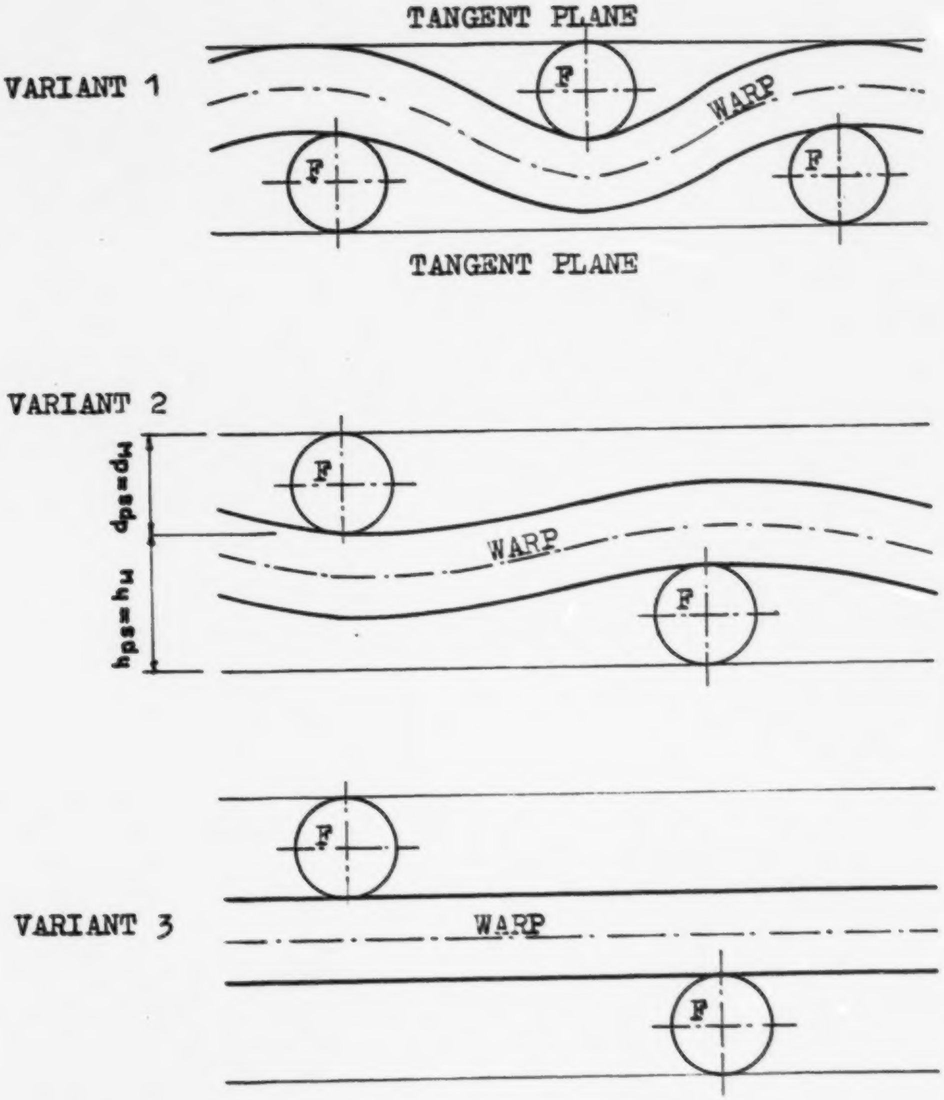
TANGENT PLANE
VARIANT 1
F
WARP
F
F
TANGENT PLANE
VARIANT 2
dps=pw
hps=hw
F
WARP
F
F
VARIANT 3
WARP
F

Figure 137. Geometric interpretation of fabric thickness.

d_{ps}, h_{ps} = thread diameter and deflection of system forming plane tangent to fabric surface (variant 2, Figure 137).

Superficial mass is the sum of the warp and fill thread masses in 1 m² of material:

$$M = M_o + M_w = n_o\ (100 + W_o)\ \frac{1}{10\ Nm_o} + n_w\ (100 + W_w)\ \frac{1}{10\ Nm_w}\ , \tag{116}$$

where

M = superficial mass, g/m².

The discussed technological parameters and the Pierce-Painter theories are concerned with the spatial composition of fabric. However, fabric surface properties are interesting from another point of view. These properties are depicted by two technological parameters: linear and superficial fabric filling with yarn. Linear fabric filling with yarn is considered along both thread systems and is expressed by the following equations:

$$\left.\begin{aligned} Z_o &= \frac{C \cdot n_o}{\sqrt{Nm_o}} = d_o \cdot n_o \cdot 100 \\ Z_w &= \frac{C \cdot n_w}{\sqrt{Nm_w}} = d_w \cdot n_w \cdot 100 \end{aligned}\right\} \tag{117}$$

where

Z_o, Z_w = linear fabric filling with warp and fill yarn, %.

Superficial fabric filling with yarn is a secondary parameter with linear filling that describes the percentage of fabric surface covered totally by warp and fill threads. It is calculated from the equation:

$$Z_t = Z_o + Z_w = 0.01 \cdot Z_o \cdot Z_w\ , \tag{118}$$

where

Z_t = superficial fabric filling with yarn, %.

PHYSICAL PARAMETERS CHARACTERIZING WOVEN FILTRATION STRUCTURE

As reported in the second phase of this project, woven filtration materials are characterized by periodic spatial and superficial structures. Consequently, these materials cannot be regarded as homogeneous, isotropic media. Thus, the required physical parameter must be formulated differently than with nonwoven materials, where in some cases structural homogeneity and isotropy simplify analyses.

D. C. Draemel,[24] in dealing with the problem of the effect of woven material structure, defined a simple and accordingly strong parameter; i.e., free area, expressing in percentage the area not covered with warp and fill yarn. If the nomenclature used previously is applied, FA can be defined as follows:

$$FA = 100 - (n_o \cdot d_o \cdot 10 + n_w \cdot d_w \cdot 10 - n_o \cdot n_w \cdot d_o \cdot d_w) = 1-Z_t \quad . \quad (119)$$

The concept of FA results from the assumed fabric model, illustrated in Figure 138.

It is interesting that free areas can be determined from technological parameters as well as from microscopic measurements. Hence, the basic research problem; i.e., the expression of technological parameters describing a given structure by a physical parameter, was solved and can be expressed as follows:

$$FA\ (n_o,\ d_o,\ n_w,\ d_w) = FA\ (A,\ B) \quad , \qquad (120)$$

where

n_o, n_w, d_o, d_w = technological parameters allowing a theoretical calculation of FA, and

A, B = linear dimensions of elementary pore, established empirically by testing.

Because the calculated value, FA, determined from Equation 119, assumes a circular cross section of warp and fill yarns, Equation 120 indicates that FA is a representative parameter only for those structures in which yarn formation was not changed during the fabric manufacturing process.

However, research, including that conducted on U.S. fabrics under Project 5-544-4, showed that the free area concept is limited to staple fabrics characterized by small yarn irregularities. Because of large yarn irregularities,

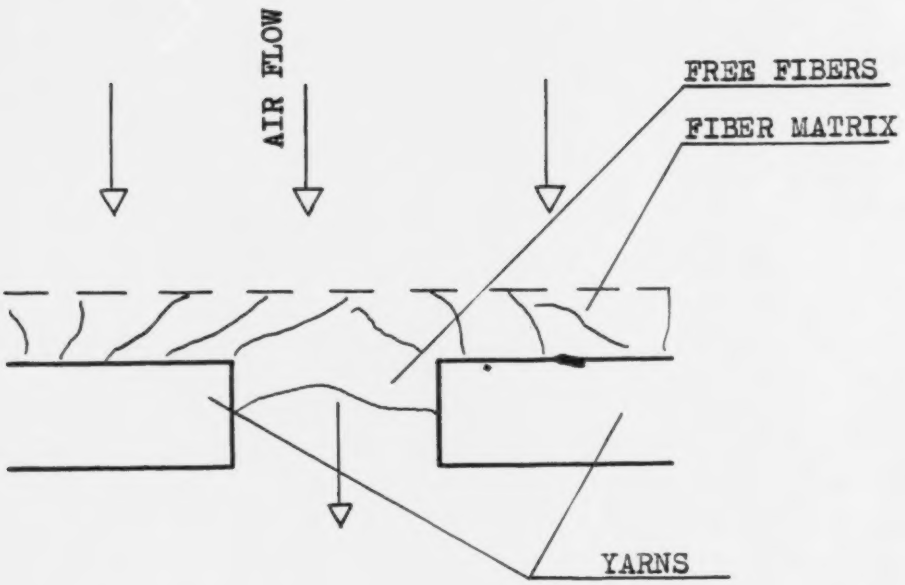
AIR FLOW
FREE FIBERS
FIBER MATRIX
YARNS

Figure 138. Draemel's model of woven filtration structure.

Equation 120 is not valid for continuous filament fabrics and FA is no longer a meaningful physical parameter. Figure 139 and Figure 140 illustrate the effect of yarn irregularity on the calculated value of FA.

With structure 1, which has obvious warp and fill yarn deformation, Equation 119 predicts high FA values using the d_o and d_w values determined from the metrical number of yarns (assuming that the yarn is circular). However, in reality the fabric area is well covered with yarn (negative value of K'_{o1}). Structure 1 is characteristic of continuous filament fabrics of polyester, polyamide, polyamidonitrile types, and glass fabrics.

In the case of fabric 2, characterized by only slight deformation of the warp and fill yarns, the calculated value of FA is in accordance with the true free areas of the fabric, as measured microscopically. Structure 2 is characteristic of natural fibers (except silk) and of synthetic and mineral staple fibers.

This analysis of fabric structure identified the importance of yarn deformation in continuous filament fabrics and helped explain the anomalous dependence of their resistance coefficient, K_1, upon FA in clean air flow. In addition, the analysis showed that, in this situation, FA determined from projected values of d_o and d_w (considering yarn deformation) is a more representative magnitude.

More complete microscopic examinations of woven continuous filament fabrics were prompted by defects observed in the dust cake and led to the discovery of additional free areas in their structure. These areas were called "basket free areas" (BFAs) because of their similarity to wicker products. The characteristic shape of BFAs and a comparison with FAs are presented in Figures 27 and 28 in Section IV of this report. BFAs similar to FAs exist in all woven structures as a consequence of the method of fabric production, so they also exist in staple fabrics. This hypothesis was confirmed by microscopic examinations of fabrics ET-4, ET-30, F-tor 5, and PT-15. Figures 141 through 144 are scanning electron micrographs of these materials, facilitating analyses of their spatial and superficial structures. Staple fabrics show fewer distinctions between FAs and BFAs because their free areas become filled with interthreads--or "free fibers"--and because of the lower longitudinal rigidity of staple fibers, which causes the fabric to have a high degree of takeup and high wrapping angle in both directions of the thread system.

Reproduced from
best available copy.

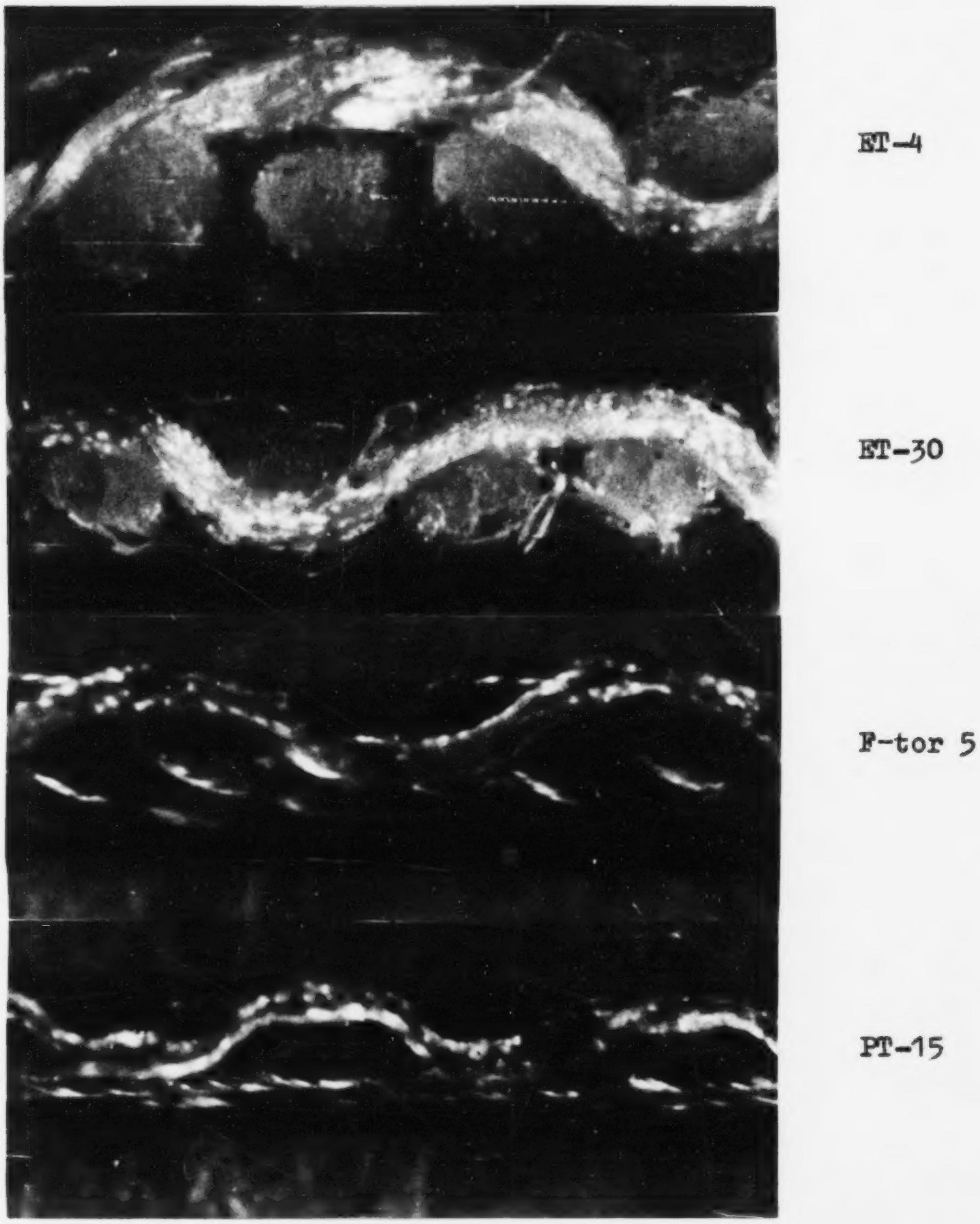
ET-4
ET-30
F-tor 5
PT-15

Figure 139. Comparison of cross sections of threads of examined fabrics (along fill).

STRUCTURE 1

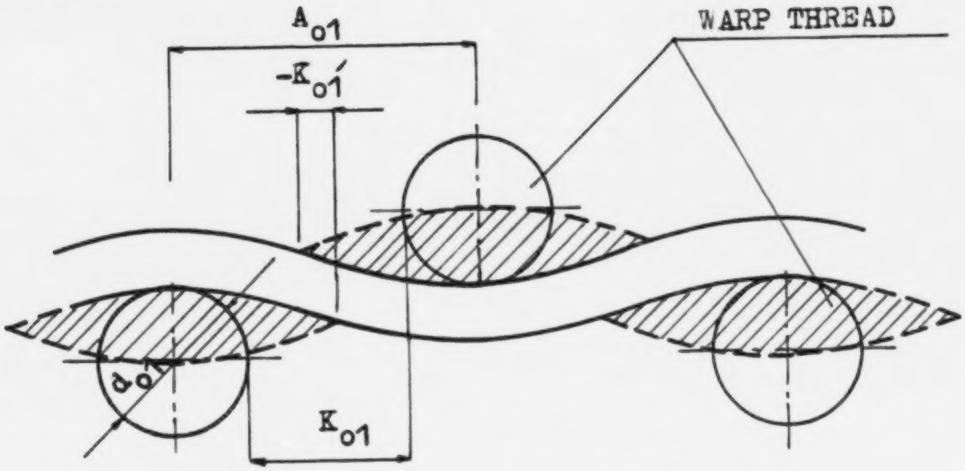
A_{o1}
$-K_{o1}'$
WARP THREAD
d_{o1}
K_{o1}

STRUCTURE 2

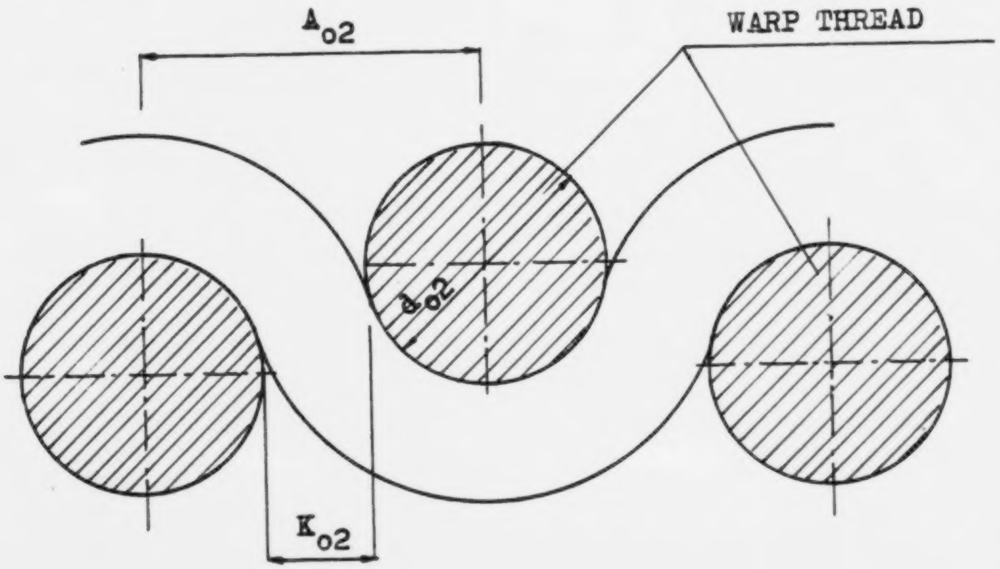
A_{o2}
WARP THREAD
d_{o2}
K_{o2}

Figure 140. Influence of fabric structure deformation on calculated "free area" (FA).

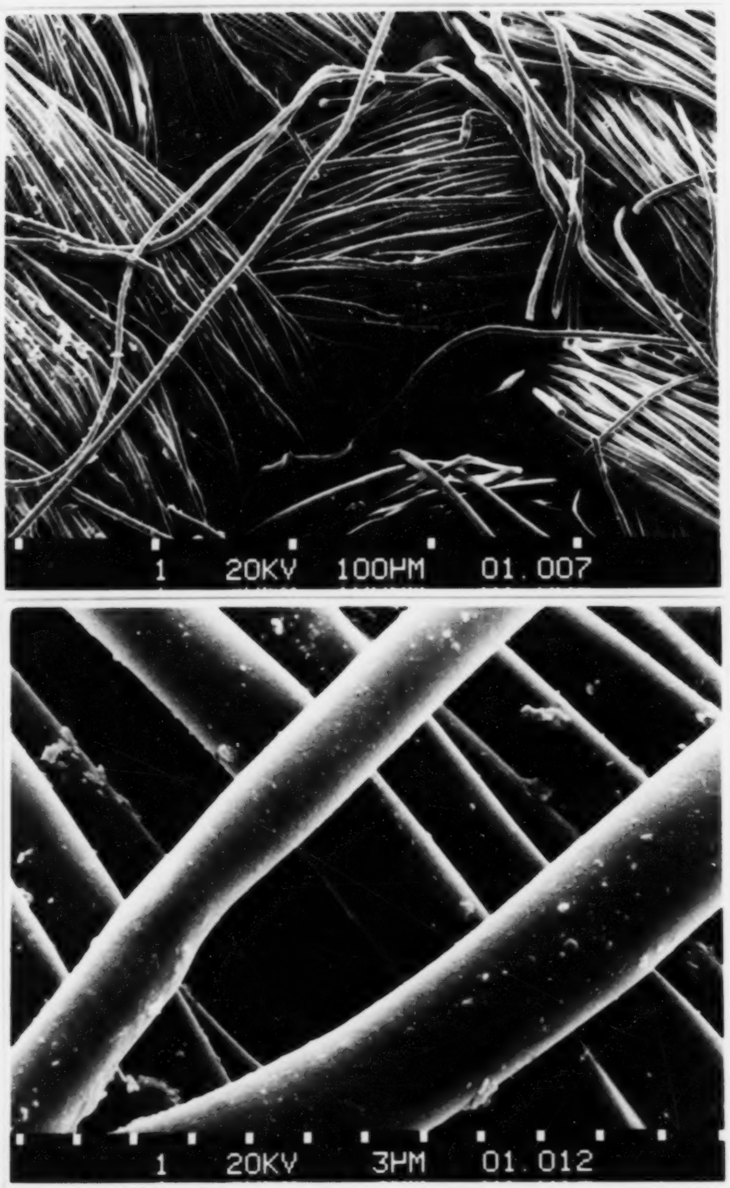
1 20KV 100μM 01.007
1 20KV 3μM 01.012

Figure 141. View of new "basket free area" (BFA) in structure of fabric ET-4.

Photo credit: SEM by K. Skudlarski, Electronic Microscopy
Laboratory of Wrocław Polytechnic.

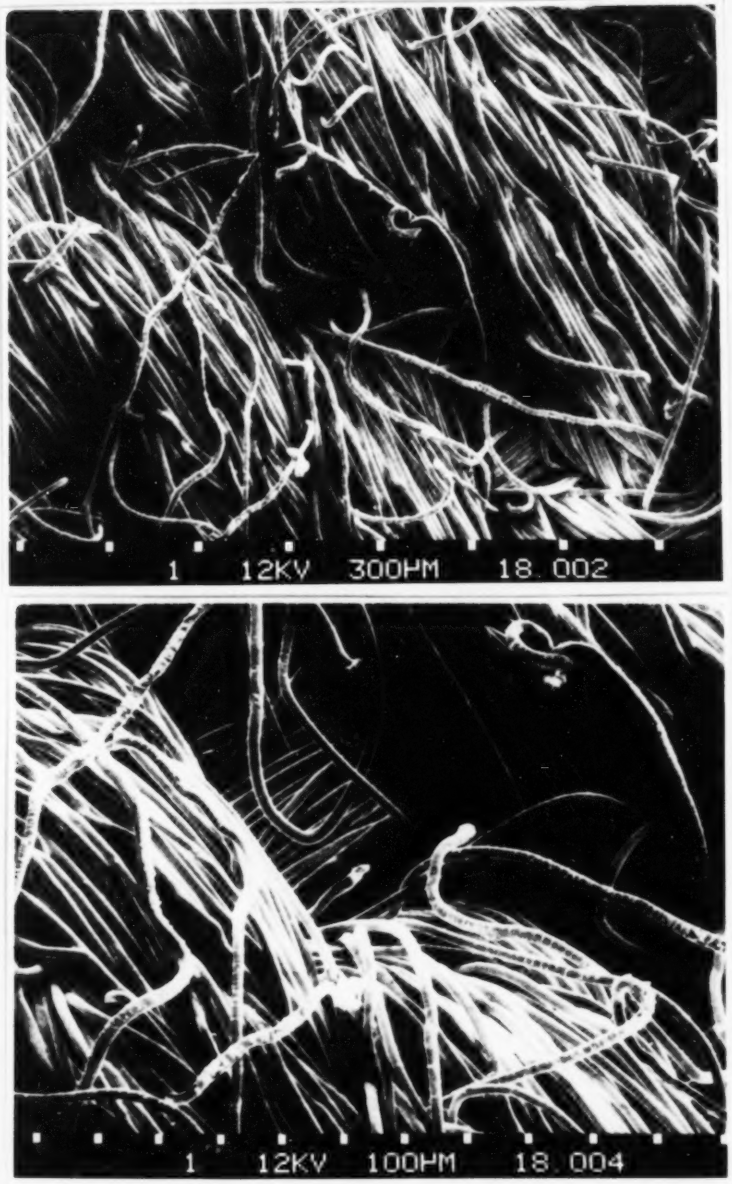
1 12KV 300µM 18.002
1 12KV 100µM 18.004

Figure 142. View of new "basket free area" (BFA) in structure of fabric ET-30.

Photo credit: SEM by K. Skudlarski, Electronic Microscopy
Laboratory of Wrocław Polytechnic.

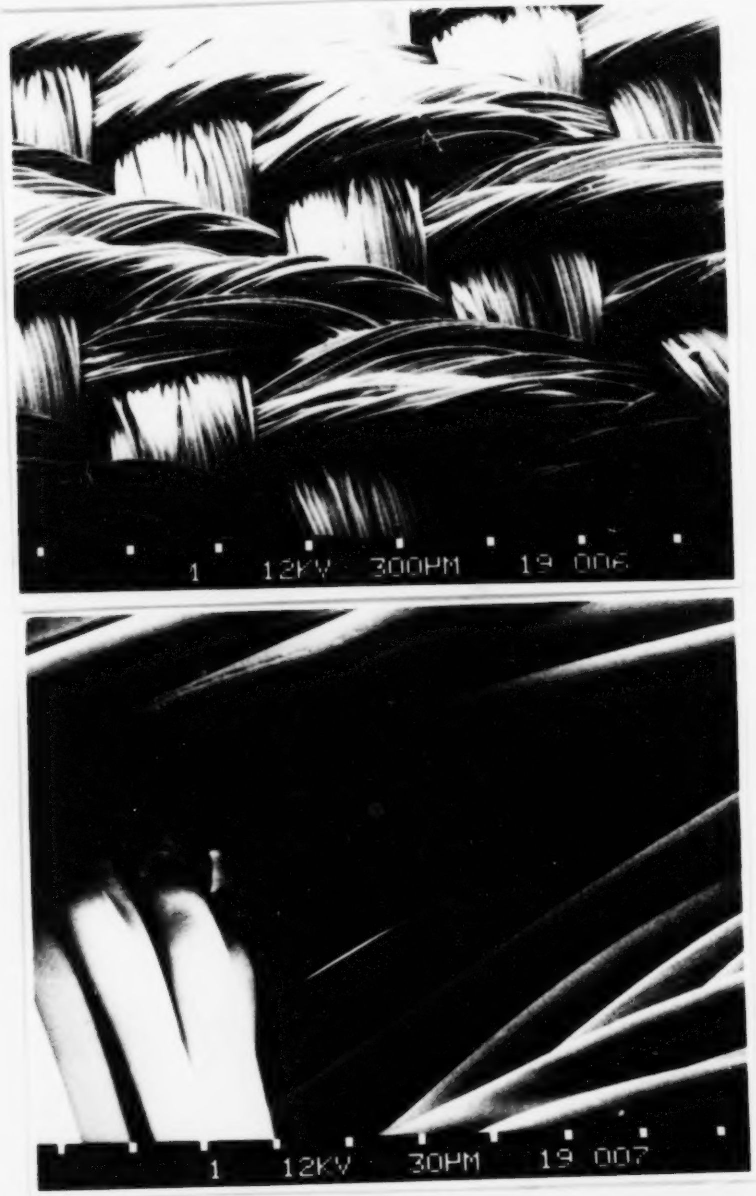
1 12KV 300PM 19 006
1 12KV 30PM 19 007

Figure 143. View of new "basket free area" (BFA) in structure of fabric F-tor 5.

Photo credit: SEM by K. Skudlarski, Electronic Microscopy
Laboratory of Wrocław Polytechnic.

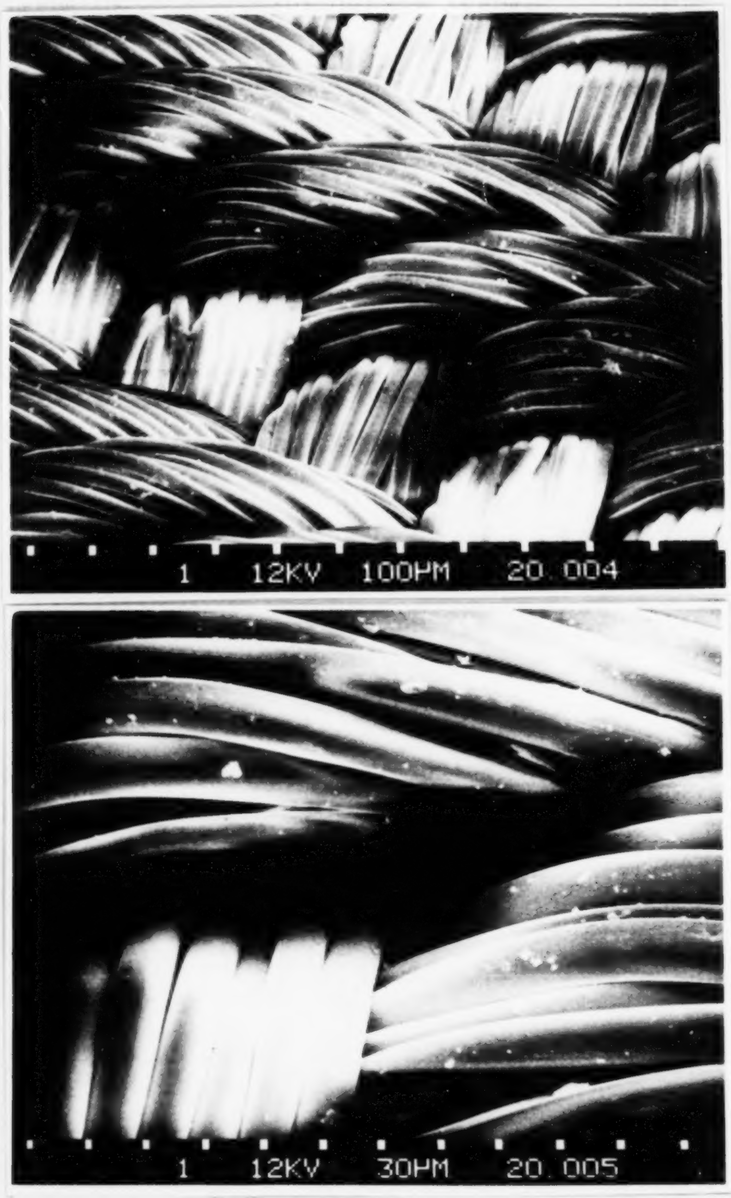
1 12KV 100PM 20.004
1 12KV 30PM 20.005

Figure 144. View of new "basket free area" (BFA) in structure of fabric PT-15.

Photo credit: SEM by K. Skudlarski, Electronic Microscopy
Laboratory of Wrocław Polytechnic.

Lower longitudinal rigidity of yarns made of staple fibers and increased friction between fibers results from successive spinning operations during which the final yarn structure is determined. The operations include carding, combing, and doubling. These operations do not exist in the manufacture of continuous filament yarns, which are characterized by a smooth surface (small interfiber friction) permitting fiber displacement in the cross section of the yarn and threads of the fabric structure.

Figure 145 shows how external forces cause deformation in the circular sections of yarns. The assumed scheme of yarn element bending is in accordance with the distribution of force in the weave process. Yarns composed of staple fibers are either loose or compact, depending on stress. In continuous filament yarns, displacement of the elementary fibers causes changes in the length of the yarn element, and the circular cross section becomes a characteristic lenticular cross section. Yarn irregularities that decrease the true value of FAs also affect the value of BFAs; i.e., FAs are placed in a vertical plane to the fabric surface. Because of their strength, most industrial textile materials are produced with covered warp weave (higher mechanical strength of warp threads). BFAs are observed mainly in the warp plane instead of under fill threads. Figure 146 shows a simplified section of fabric made along the warp thread where yarn areas (placed in the vertical plane to the fabric surface) called BFAs can be seen. The section was made with the assumption that $h_w = 0$ and that the fill and warp yarns have circular cross sections. Because of the geometrical relationships existing in a fabric made with regular yarns and warp covering, a BFA is a function of the following parameters:

$$\mathrm{BFA} = f\left(\frac{d_o}{d_w}, A_w, h_w\right), \qquad (121)$$

where

$\frac{d_o}{d_w}$ = warp diameter to fill diameter ratio,

A_w = distance between fill threads, and

h_w = deflection of fill threads.

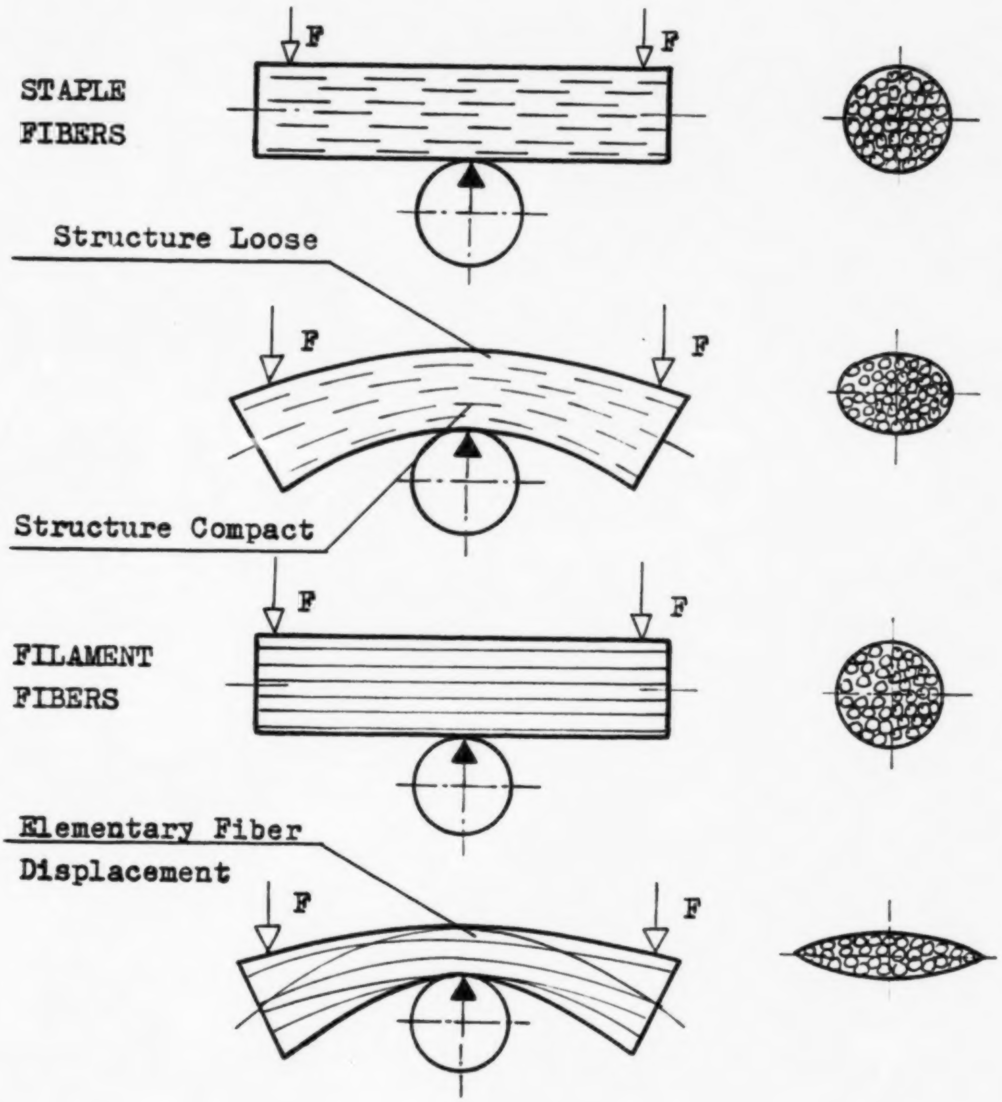
F
F
STAPLE FIBERS
Structure Loose
F
F
Structure Compact
F
F
FILAMENT FIBERS
Elementary Fiber Displacement
F
F

Figure 145. Deformation of yarn sections under external forces.

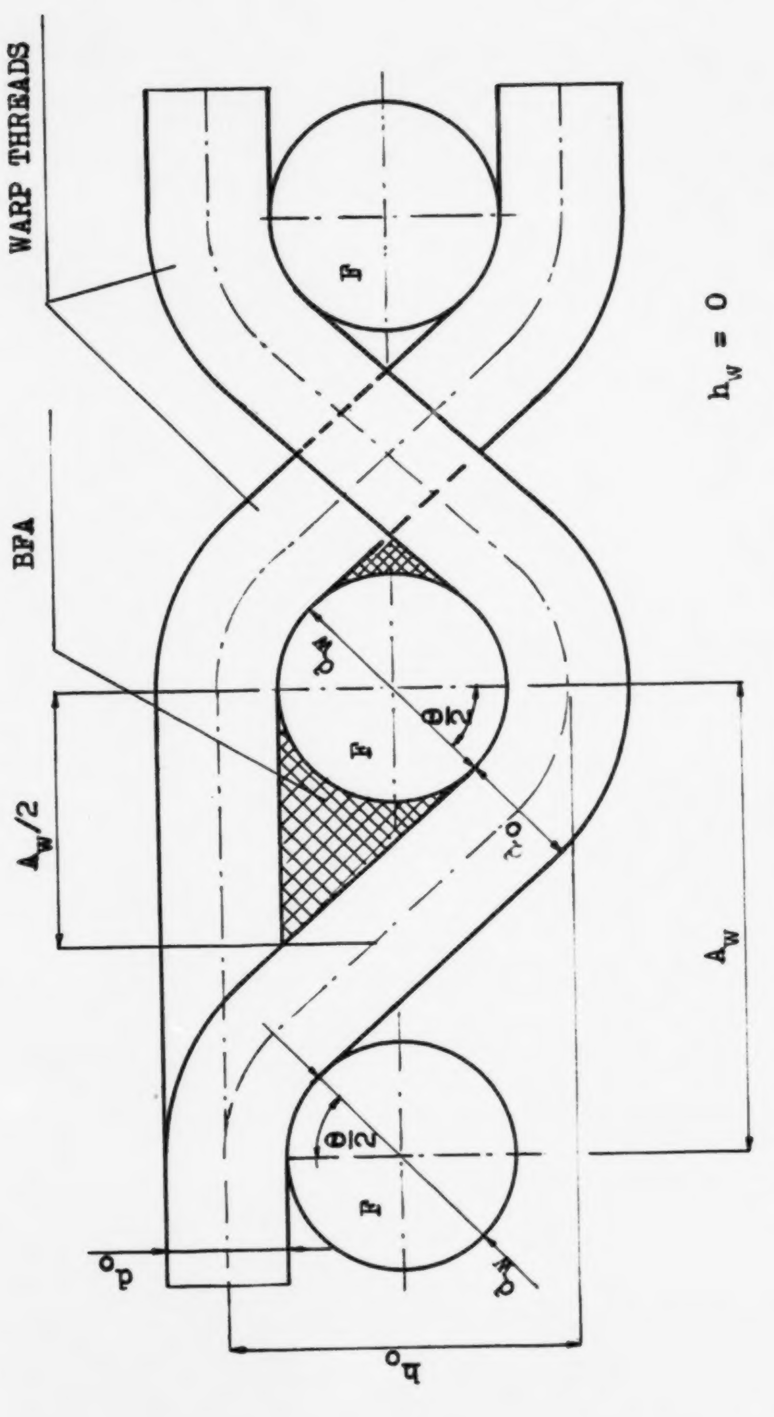
WARP THREADS
BFA
$A_W/2$
A_W
$h_W = 0$
F
F
F
$\frac{\theta}{2}$
$\frac{\theta}{2}$
d_o
h_o
$\frac{d_o}{2}$

Figure 146. Basket free area in woven filtration structure.

The influence of individual variables on a BFA is illustrated in Figure 147, which shows different variants of the same weave but with different $\frac{d_o}{d_w}$, A_w, and h_w. It was found that $\frac{d_o}{d_w}$ and h_w heavily influence BFA, but that A_w has less effect.

The conclusion is that a filtration fabric should be designed to prevent the formation of basket free areas since these BFAs are undesirable for dust filtration. First, fill and warp yarn diameters should not differ greatly. Second, high rigidity with fill yarns should be avoided, which results in lower takeup and smaller values of h_w.

Using smaller distances between fill threads and making the fill yarns of staple fibers helps produce better performing fabrics based on continuous filament fibers. Fabric permeability improves, and BFA is minimized because of the higher degree of fill takeup (longer h_w).

The previously discussed irregularities of circular yarn cross section affect the value of BFAs because they decrease the deflection and wrapping angle in the fabric (see Figure 148).

The value of BFAs can be determined by:

- Geometric measurements (planimetry) from photographs of specially made cross sections of fabric,
- Reproduction of cross sections from scanning photographs of a given fabric (planimetry), and
- Analysis of geometric properties characteristic of a woven structure.

The first two methods require laborious laboratory techniques, still being developed, for preparing unaltered, representative samples. The simpler but less detailed method is the analytical determination of BFA by application of geometric equations. Because of problems with determining the physical parameters of a woven structure from its basic technological parameters, the best way to estimate BFA is from a geometrical relationship. The two methods mentioned first can verify the geometric model of the fabric.

For an idealized fabric structure with $h_w = 0$, BFA (the shaded area in Figure 146) can be determined from the following equation:

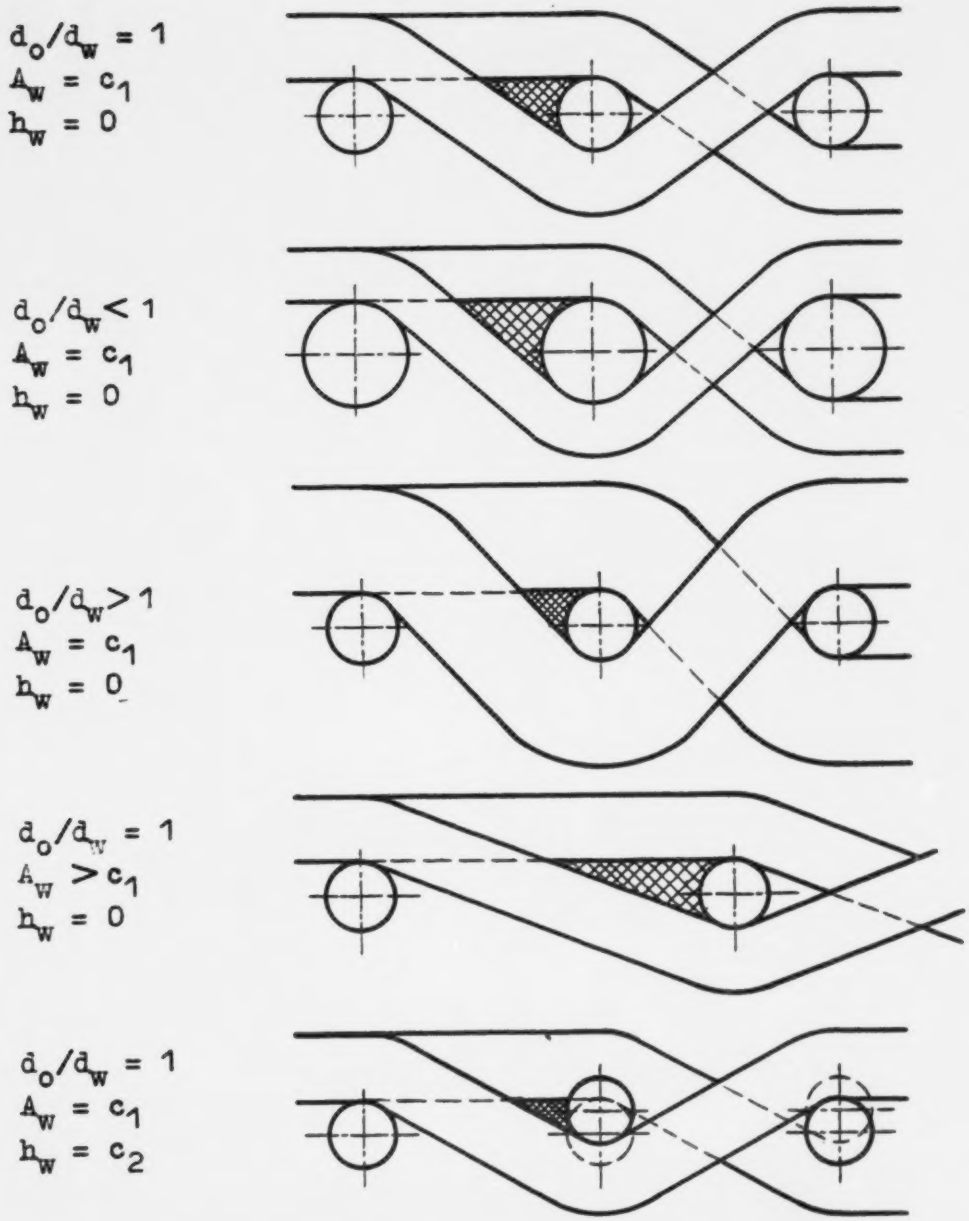
$d_o/d_w = 1$
$A_w = c_1$
$h_w = 0$
$d_o/d_w < 1$
$A_w = c_1$
$h_w = 0$
$d_o/d_w > 1$
$A_w = c_1$
$h_w = 0$
$d_o/d_w = 1$
$A_w > c_1$
$h_w = 0$
$d_o/d_w = 1$
$A_w = c_1$
$h_w = c_2$

Figure 147. Influence of certain structural parameters on BFA (cross sections along warp).

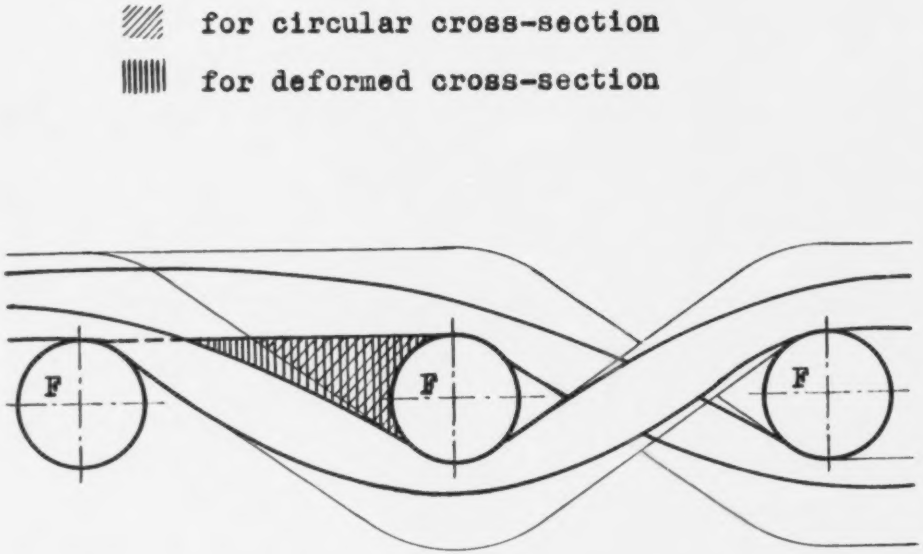
▨ for circular cross-section
▥ for deformed cross-section
F
F
F

Figure 148. Warp yarn deformation effect on BFA.

$$\mathrm{BFA} = \left\{\frac{1}{2} \cdot \frac{A_w}{2} \left[\left(\frac{d_o + d_w}{2}\right) \cot \frac{\theta}{2} + \frac{d_o}{2} \cdot \tan \frac{\theta}{2}\right] \cdot \sin \frac{\theta}{2}\right\} \tag{122}$$

$$- \left\{\frac{1}{2}\left[\frac{\pi \left(180 - \frac{\theta}{2}\right)}{180} - \sin \left(180 - \frac{\theta}{2}\right)\right]\right\},$$

where

BFA = basket free area for one element of weave, mm;
A_w = distance between fill threads, mm;
d_o, d_w = diameter of warp and fill yarns, mm; and
θ = wrapping angle in grads.

Discovery of BFAs as integrally woven, connected elements of a filtration structure (similar to FAs but in addition to FAs) leads to a fabric model different from Draemel's (see Figure 149). This model of fabric structure addresses both FAs and BFAs. Two types of structures--loose Type 1 and compact Type 2--can be distinguished.

Structural elements can be positioned differently depending on the kind of weave and deflection of warp. The model agrees with the concept of pores existing in filtration material and their resultant effect on process performance and dust cake formation.

Based on the verified hypothesis (Project 5-533-4) that both BFA values and the distribution of structural elements have normal distributions (phase II, Project 5-533-3), the FA distribution is anticipated to be normal. Because BFAs and FAs dominate the porosity of woven material, the distribution of pore diameters will be determined by their values. Thus, the porosity of a woven material can be written as:

$$P = f(\mathrm{BFA}, \mathrm{FA}) \quad , \tag{123}$$

where

P = pore diameter distribution, and
BFA, FA = free area distributions.

Pore diameter can be determined physically, but BFA and FA are expressed by equations containing appropriate technological parameters. From the above

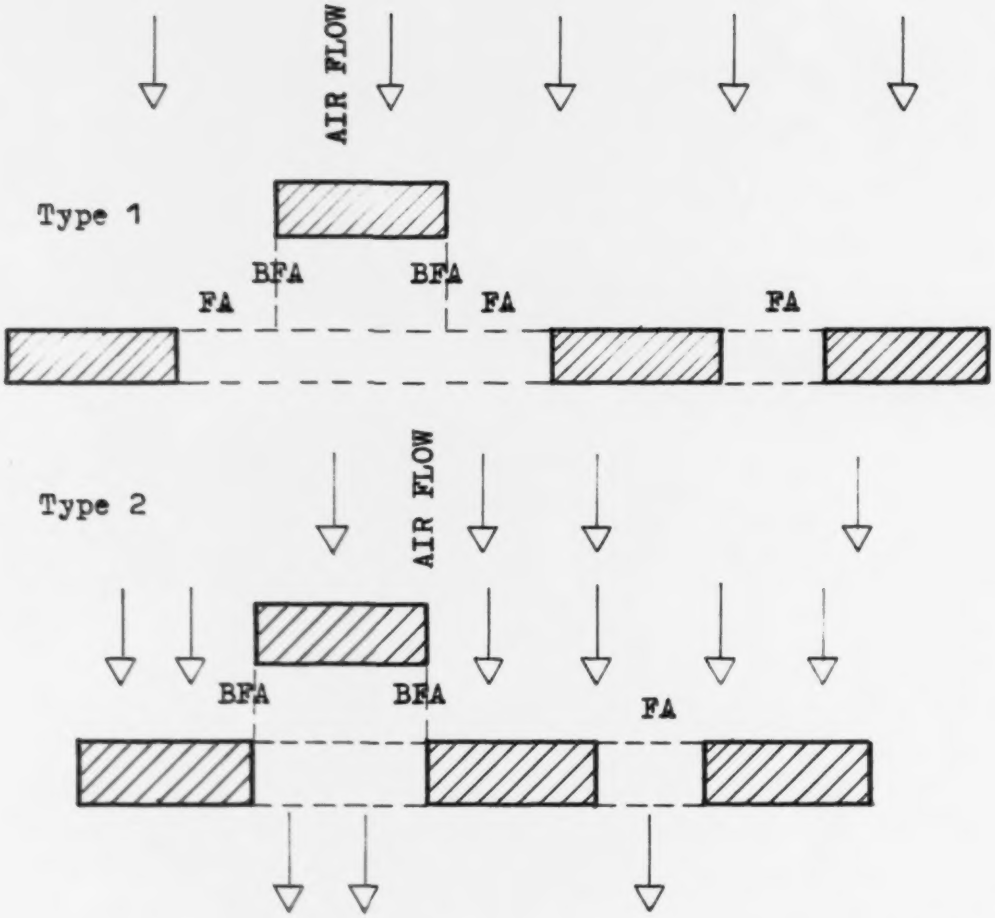
AIR FLOW
Type 1
BFA
BFA
FA
FA
FA
Type 2
AIR FLOW
BFA
BFA
FA

Figure 149. New model of woven filtration structure.

deliberations, the hypothesis can be offered that the porosity distribution will representatively depict woven filtration structure.

COMPARISON OF SOME FABRIC PARAMETERS

The technological and physical parameters discussed above describe fabric macrostructure from two different viewpoints, as defined in the section introduction. Technological parameters, which depend on the type and characteristics of the fiber plastic and the method of fabric production, permit the development of true structural models because of geometric relationships. These geometric models may be ideal, depending upon assumptions. They make it possible to study the deformations observed in woven fabrics and deformations connected with certain fiber properties or the production method.

Physical models, based on physical structural parameters, are usually not in accordance with geometric models. These physical models represent theoretical, simplified structures that highlight some characteristic expressed by a physical parameter that affects or is related to process performance.

Woven filtration structures of many different geometric descriptions exist. This great variety of fabric geometrical description hampers the evaluation of geometrical parameters on dust filtration performance. The influence of a specific parameter on dust filtration performance may be discussed based on testing and later comparative analysis. But some doubts always remain as to whether the discussed parameter is the important one.

Sixteen structures--represented by Polish fabrics that differ according to raw material, weave, and basic technological parameters--were statistically examined to create a basis for further examination of the woven structure of the material. This examination, described in the phase II report of this project, was conducted under the assumption of a circular cross section of fill and warp yarns (yarn diameter determined from metrical number). The following conclusions were formulated:

- Technological and physical parameters (FAs) have normal distribution;
- With the assumption that fabric structural parameters remain constant during evaluation, fabrics can be classified according to structural similarity, and it is possible to develop criteria for levels of similarity; and
- Free area (FA) yields the strongest structural measure of fabric similarity.

Examination verified Draemel's physical model of woven structure. The model evolved from superficial geometric relationships in the fabric structure and was based on the assumption of circular cross section of yarns. Despite the oversimplified fabric spatial structure resulting from the assumption of no yarn irregularities in the fill and warp threads system, statistical examinations supported the hypothesis that macropores formed between fill and warp threads are important structural elements in determining filtration properties. Laboratory testing conducted within the range of this project and Project 5-533-4, together with a microscopic examination of certain woven structures, confirmed the hypothesis concerning BFA, which together with FA, forms a macroporous structure. Because FA and BFA must be discussed in connection with the kind of weave, additional statistical examinations were programmed. These examinations were conducted to show the similarities and differences between test structures of varying structural elements. Testing was carried out on two polyamide fabrics made from continuous filament fibers--PT-15 and PT-41--and for five polyester fabrics:

ET-2	staple fiber
ET-3	staple fiber
ET-4	staple fiber
ET-30	staple fiber
F-tor 5	continuous filament fiber

Seven elements that are characteristically repeated (depending on the kind of fabric) on the fabric surface as part of the weave repeat were distinguished in the fabric structure:

E I = warp and fill thread in hard interlace;

E II = warp and fill threads crossing without the interlace, fill over warp;

E IIa = warp and fill threads crossing without the interlace, fill under warp;

E III = fill thread in area between two neighbor warp threads;

E IIIa = as above but fill thread in inflection;

E IV = warp thread in area between two neighbor fill threads; and

E IVa = as above but warp thread in inflection.

Elements characteristic of the structure are shown in Figure 150. Each element is ascribed to an elementary fiber filling coefficient according to the equation:

$$\alpha_{Ex} = \frac{V_{WEx}}{V_{PEx}} , \qquad (124)$$

where

α_{Ex} = fiber filling of element x coefficient,
V_{WEx} = plastic volume (fiber) in element x, and
V_{PEx} = yarn volume forming given element x.

Values of coefficient α_{Ex} were calculated for two variants:

Variant 1 - circular cross section of yarn determined from metrical number (40 measurements for each thread system), and

Variant 2 - actual yarn cross section based on microscopic measurement of threads from the fabric (100 measurements for each thread system).

Plastic volume and yarn volume of element x were calculated by analyzing the structural composition of each element according to the equations:

$$Vw_o = \frac{\pi}{4} dw_o^2 \cdot Lw_o \cdot Mw_o , \qquad (125)$$

$$Vw_w = \frac{\pi}{4} dw_w^2 \cdot Lw_w \cdot Mw_w , \qquad (126)$$

$$Vp_o = \frac{\pi}{4} d_o^2 \cdot L_o , \text{ and} \qquad (127)$$

$$Vp_w = \frac{\pi}{4} d_w \cdot L_w , \qquad (128)$$

where

Vw_o = fiber volume in warp yarn, mm^3;
Vw_w = fiber volume in fill yarn, mm^3;
dw_o = fiber diameter in warp yarn, mm;
dw_w = fiber diameter in fill yarn, mm;
Lw_o, Lw_w = fiber length in warp and fill, mm;
Mw_o, Mw_w = number of fibers in warp and fill yarn;
Vp_o = warp yarn volume, mm^3;

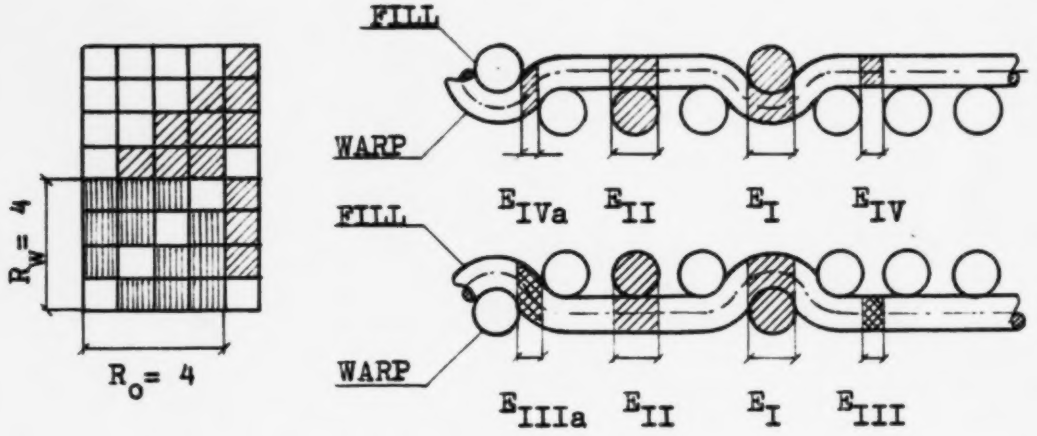
FILL
WARP
$R_W = 4$
$R_o = 4$
E_{IVa}
E_{II}
E_I
E_{IV}
FILL
WARP
E_{IIIa}
E_{II}
E_I
E_{III}

A. The twill weave with characteristic hard interlaces (Element E_I).

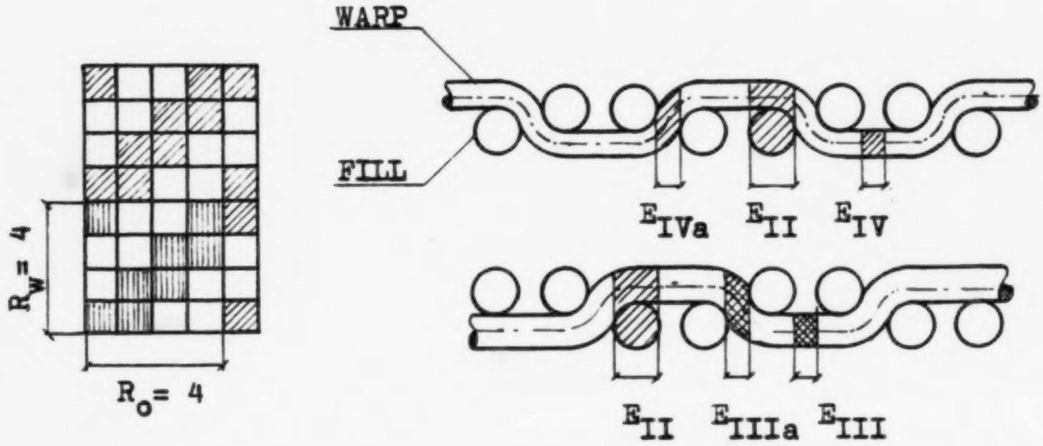
WARP
FILL
$R_W = 4$
$R_o = 4$
E_{IVa}
E_{II}
E_{IV}
E_{II}
E_{IIIa}
E_{III}

B. The twill weave without characteristic hard interlaces (Element E_I is not apparent).

Figure 150. Characteristic elements of structure for woven materials.

Vp_w = fill yarn volume, mm³;

d_o, d_w = warp and fill yarn diameters, mm; and

L_o, L_w = warp and fill yarn length, mm.

Based on microscopic cross sections of warp and fill yarns, it was found that cross sections of irregular yarns can be replaced by elliptical yarns. Thus, Equations 127 and 128 can be:

$$Vp'_o = \pi \cdot a_o \cdot b_o \cdot L_o \text{ , and} \qquad (129)$$

$$Vp'_w = \pi \cdot a_w \cdot b_w \cdot L_w \text{ ,} \qquad (130)$$

where

a_o, a_w = half of smaller ellipse axis for warp and fill, mm; and

b_o, b_w = half of bigger ellipse axis for warp and fill, mm.

Structural elements of fabrics ET-2, ET-30, and F-tor 5 differ from the others because they have two warp or fill threads without twist (instead of one thread) to obtain higher superficial yarn filling and hence higher air permeability. Because of the structure of these fabrics, the yarn diameter in Equations 127 and 128 should equal that of two threads. The substitute diameter can be calculated as:

$$\left.\begin{aligned} d_{o_z} &= \frac{C}{\sqrt{Nm_o/2}} \\ d_{w_z} &= \frac{C}{\sqrt{Nm_w/2}} \end{aligned}\right\} \qquad (131)$$

where

d_{o_z}, d_{w_z} = substitute diameter for warp and fill yarn, mm;

C = constant (see Table 35); and

Nm_o, Nm_w = metrical number of warp and fill yarn for one thread.

For flattening of doubled yarns, the following equations for cross sections were applied to calculate volumes of structural elements:

ET-2 $\quad F'_o = \pi \cdot 2 \cdot a_o \cdot b_o$,

$F'_w = \pi \cdot a_w \cdot b_o$ (single thread is a fill), ET-30 $F'_o = \pi \cdot 2 \cdot a_o \cdot b_o$,

$F'_w = \pi \cdot 2 \cdot a_w \cdot b_w$,

F-tor 5 $F'_o = \pi \cdot 2 \cdot a_o \cdot b_w$, and

$F'_w = \pi \cdot 2 \cdot a_w \cdot b_w$,

where

F'_o F'_w = cross section area of warp and fill yarns, mm.

The following assumptions were made to determine element length and fiber length in these elements:

- Because of small dimensions of the elements, yarn twist was not considered, and
- Fiber length in a yarn is equal to the yarn section length.

The t-Student test was applied after determination of the coefficients, α_{Ex}, for both circular and elliptical yarn cross sections. All two-element combinations of the tested fabrics were considered. The hypothesis of mean value equality in the general population was tested against the reverse hypothesis based on independent sampling, from which statistics, t, were formed. The hypothesis was verified on the level, $\alpha = 0.01$.

Test results are included in Table 38 and Table 39. Sign " - " means that in this case the hypothesis of the same mean value failed. Thus, statistically, these fabrics differ by more than coefficient α_E. In other cases, elements exist for which there is no basis to reject the hypothesis of mean value equality. The conclusion is therefore reached that these fabrics do not differ statistically by α_E.

For analysis of results of a statistical examination, it should be observed that the assumption in variant 1 concerning the circular cross section of yarn in the warp and fill thread system idealizes fabric structures from the viewpoint of spatial geometry as well as from spatial fiber filling. The assumption of elliptical cross section of yarns accurately approximates hypothetical structures to the cross sections of actual yarns.

A comparison of the number of similar structural elements in a group of fabrics composed of staple fibers shows that for variant 1 these fabrics have

TABLE 38. SIMILARITY TABLE OF FABRICS UNDER ASSUMPTION OF CIRCULAR CROSS SECTION OF YARNS

Fabrics	Staple fiber				Continuous filament fiber		
	ET-2	ET-3	ET-4	ET-30	PT-41	PT-15	F-tor 5
ET-2	X	E I	E I E IIIa E IVa	E I E IIIa E IVa	-	-	-
ET-3	E I	X	E I	E I	E II	-	-
ET-4	E I E IIIa E IVa	E I	X	E I E II E III E IIIa E IV E IVa	-	-	-
ET-30	E I E IIIa E IVa	E I	E I E II E III E IIIa E IV E IVa	X	-	-	E IIIa
PT-41	-	E II	-	-	X	-	-
PT-15	-	-	-	-	-	X	-
F-tor 5	-	-	-	E IIIa	-	-	X

TABLE 39. SIMILARITY TABLE OF FABRICS UNDER ASSUMPTION OF ELLIPTICAL CROSS SECTION OF YARNS

	Staple fiber				Continuous filament fiber		
Fabrics	ET-2	ET-3	ET-4	ET-30	PT-41	PT-15	F-tor 5
ET-2	X	E I	E I	E I	-	-	E IVa
ET-3	E I	X	E I	-	-	-	-
ET-4	E I	E I	X	E I E IVa	-	-	-
ET-30	E I	-	E I E IVa	X	E II	E II	E III E IV
PT-41	-	-	-	E II	X	E IIa	-
PT-15	-	-	-	E II	E IIa	X	-
F-tor 5	E IVa	-	-	E III E IV	-	-	X

many common properties. For variant 2, the primary element similar for all fabrics is E I. This distinction results from the fact that the fabrics were made of yarns of similar diameter and weave but with different technological parameters. Therefore, yarn irregularities over the range of discussed structural elements differ in each case except in E I.

In a group of fabrics composed of continuous filament yarns, no similarity was observed for a circular cross section (variant 1). Structural perfection led to completely different models of spatial structures; e.g., fabrics PT-15 and PT-14, although they are characterized by similar composition differing only by yarn thickness.

The same group of fabrics analyzed in terms of changed assumptions (variant 2) showed a similar element E IIa for fabrics PT-15 and PT-41. It should be noted that the assumption of elliptical yarn cross section caused similarity of some structural elements (E II, E III, E IV, E IVa) between fabrics made of staple and continuous filament fibers, but E II was the dominant element represented by two threads crossed without interlace. In conclusion, statistical examinations proved important for spatial structural changes caused by yarn irregularities. Thus, the conclusion is reached that a determination of FA must be based on microscopic measurement of yarn shape when actual structures are analyzed and with the assumption of an elliptical cross section (based on empirical data) in structural design. This conclusion is also valid for determining BFA.

AIR FLOW THROUGH CLEAN FILTRATION STRUCTURES

Air flow through clean filtration fabrics is related to the problem of defining structural parameters for filtration materials. The close relationship results because the equations characterizing flow depend upon the structural parameters of the filtration medium rather than upon other hydraulic properties.

Hydraulic characteristics, determined by measurements of hydraulic resistances and air flow velocity, usually differ for differing filtration materials. Their shape depends upon flow character and the spatial and superficial composition of a particular structure. Analysis of hydraulic characteristics facilitates formulation of close relationships of a functional or stochastic character between parameters of the air flow process--the mathematical modeling of the air flow process. The development of these models is the object of most research conducted in this area.

Regardless of utilitarian significance, the incomplete models of air flow through clean porous structures recently developed have stimulated theoretical work concerning fluid movement in porous structures. They also facilitate statistical examinations that verify hypothesized structural behavior during flow and process peculiarities.

Generally, air flow through porous structures can be molecular, laminar, or turbulent. Molecular flow occurs when the fluid (in this case, air) is not regarded as a continuum; i.e., the equations of classical hydrodynamics do not apply. The condition for molecular flow is $K_n >> 1$ ($K_n = \bar{\lambda}/\bar{r}$, where $\bar{\lambda}$ is the mean free path of molecules and $\bar{r}$ is the mean pore diameter). The above results, concerning true textile filtration materials, indicate that air flow at atmospheric pressure and ambient temperature does not have the character of molecular flow but of laminar and turbulent flows.

Darcy's equation is most frequently applied to depict the correlation between pressure drop and flow velocity in the area of laminar flow. The equation, determined empirically, is:

$$\frac{\Delta P}{L} = \frac{f \cdot \bar{V}_o}{K} , \qquad (132)$$

where

ΔP = hydraulic resistance,

L = porous layer thickness,

v_f = gas viscosity,

$\bar{V}_o$ = mean velocity of gas stream upstream of the porous structure, and

K = permeability coefficient.

Equation 132 was introduced for interpreting assumptions concerning flow conditions:

- The porous structure is regarded as a rigid, stable, homogeneous body; all pores have the same shape and diameter; and the porous layer thickness is constant in time;
- Flow through the porous structure is stable, and the fluid is an incompressible medium; and

- Flow resistances result only from fluid viscosity, without consideration of the effects of inertia (laminar flow).

The criterion for laminar flow is a Reynolds number, $Re < 1$. The Reynolds number for porous materials, sedimentated particles, and fiber can be determined from the following equation:

$$Re = \frac{\rho_f \cdot \bar{V}_p \cdot d_p}{\nu_f}, \qquad (133)$$

where

Re = Reynolds number,
ρ_f = fluid density,
$\bar{V}_p = \frac{\bar{V}_o}{\varepsilon}$ = hypothetical mean gas velocity through pores,
d_p = pore diameter, and
ν_f = gas viscosity.

At a higher Re number and with turbulent flow, the dependence of flow resistance upon velocity is of second order, i.e.:

$$\frac{\Delta P}{L} = \frac{\nu_f \cdot \bar{V}_o^{\,2}}{K}. \qquad (134)$$

With the assumption of constant conditions (small variation of ν_f with ambient temperature) and substitution of $\Delta P/L = \Delta P_i$ (ΔP_i = specific hydraulic resistance of the porous layer), the following equations are obtained:

- For laminar flow, $Re < 1$:

$$\Delta P_i = \frac{1}{K} \cdot \bar{V}_o = K_1 \cdot \bar{V}_o \text{ , and} \qquad (135)$$

- For turbulent flow, $Re > 1$:

$$\Delta P_i = \frac{1}{K} \cdot \bar{V}_o^2 = K_1 \cdot \bar{V}_o^2 , \qquad (136)$$

where

K_1 = resistance coefficient of the porous layer.

The shape of the above equations is illustrated in Figure 151. The crossing point of both curves, A, for material of permeability, K, marks the critical velocities (V_o crit.) and the critical specific hydraulic resistance (ΔP_i crit.) where the laminar flow becomes turbulent. The permeability of coefficient K is equivalent to structural parameters and determines to a certain extent the kind of flow in the porous layer.

Theories of permeability based on various physical models address the problem of determining the value, K, for structural parameters of layers formed with different materials. The Kozeny-Carman theory based on the capillary model and the Brinkman theory based on the model of flow around elements of the porous structure are best known.

For air flow through fabrics, where the mean gas velocity in front of the fabric is equivalent to face velocity, q_g, Equations 135 and 136 can be presented as:

- For laminar flow through fabrics, Re < 1:

$$\Delta P_i = K_1 \cdot q_g \quad \text{, and} \tag{137}$$

- For turbulent flow through fabrics, Re > 1:

$$\Delta P_i = K_1 \cdot q_g^2 \quad , \tag{138}$$

where

K_1 = resistance coefficient of the clean fabrics.

These equations were the basis of studies of air flow through clean fabric structures over the range of this project. Because it was necessary to have a wider empirical base for the statistical analysis, some results of earlier tests and those conducted for Project 5-533-4 were also used. Testing was conducted at two levels of q_g and the corresponding pressure drops:

- Low flow values: $\Delta P = 0 - 10$ mm H_2O, and
- High flow values: $\Delta P > 10$ mm H_2O.

For all data, the recorded value of q_g for a certain pressure drop was the mean of 30 measurements.

In the first phase, 16 different Polish fabrics, each with different technological parameters, were chosen for the high flow tests. From that group, 14 structures were selected for additional testing at low flow values.

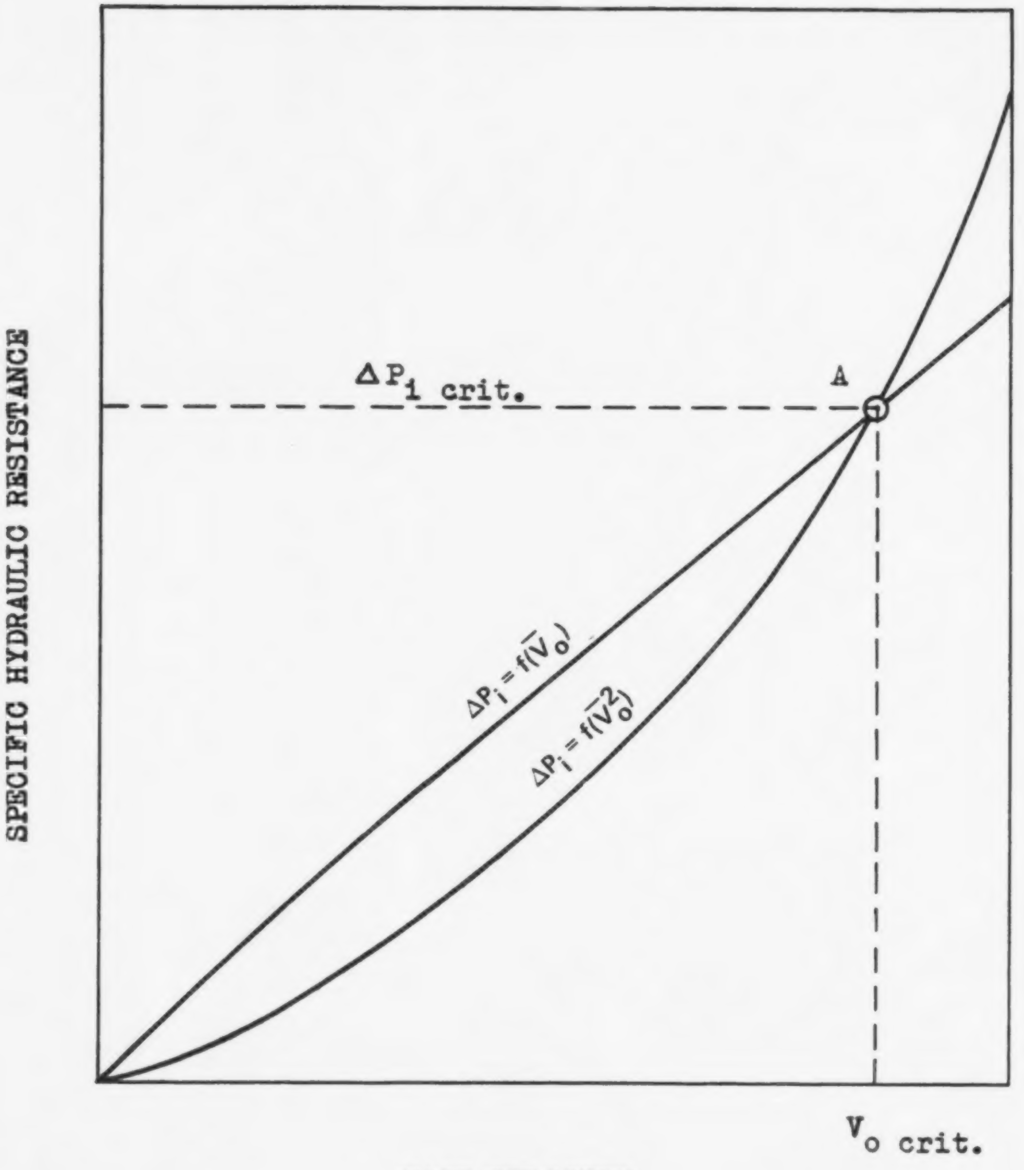

Figure 151. Comparison of hydraulic resistances during laminar and turbulent flow.

The technological parameters of the tested fabrics and the test results are contained in the phase I and II reports of this project. The results were statistically interpreted, with the following conclusions:

- Air flow through clean woven structures is a stochastic, normal process (see phase II report);
- The equation of flow resistances in the range of low flows ($\Delta P <$ 10 mm H_2O) is linear, but for high values of flow ($\Delta P >$ 10 mm H_2O) it is parabolic (the equation was determined by the least squares method);
- Increases in the σ value of the variable, q_g, accompanying increasing ΔP verify the fact that structural changes occur together with increased flow velocity in the fabric pores. Thus, for air flow, the fabric structure cannot be regarded as a physically rigid body.

In the second phase of the work related to air flow through clean filtration structures based on empirical data, the true forms of the function, $\Delta P = f(q_g)$, were determined in the form of regression curves fitted by the least squares method. The true forms of the function for low and high values of flow are shown in Tables 40 and 41 and can be written as:

- For low flows:

$$\Delta P = a \cdot q_g + b \quad , \text{ and} \tag{139a}$$

$$\Delta P_i = a_i \cdot q_g + b_i \quad . \tag{139b}$$

- For high flows:

$$\Delta P = a' \cdot q_g^2 + b' \cdot q_g + c' \quad , \text{ and} \tag{140a}$$

$$\Delta P_i = a_i' \cdot q_g^2 + b_i' \cdot q_g + c_i' \quad . \tag{140b}$$

When free terms are avoided in the above equations (straight lines and parabolas must cross the point, 0,0), the following equations are obtained:

- For low flows:

$$\Delta P = a \cdot q_g \quad , \text{ and} \tag{141a}$$

$$\Delta P_i = a_i \cdot q_g \quad . \tag{141b}$$

- For high flows:

$$\Delta P = a' \cdot q_g^2 + b' \cdot q_g \quad . \tag{142a}$$

$$\Delta P_i = a_1' \cdot q_g^2 + b_i' \cdot q_g \quad . \tag{142b}$$

TABLE 40. TRUE FORMS OF FLOW RESISTANCE FUNCTION
(For Low Values of Flow, $\Delta P < 10$ mm H_2O)

Kind of fabric	Form of function
ET-1	$\Delta P = 0.89\ q_g - 0.07$
ET-2	$\Delta P = 0.76\ q_g - 0.40$
ET-3	$\Delta P = 1.32\ q_g + 0.01$
ET-4	$\Delta P = 0.73\ q_g - 0.34$
ET-30	$\Delta P = 2.49\ q_g + 0.06$
WT-201	$\Delta P = 0.44\ q_g - 0.29$
WT-202	$\Delta P = 1.02\ q_g - 0.18$
WT-203	$\Delta P = 0.60\ q_g - 0.07$
WBT-210	$\Delta P = 0.94\ q_g - 0.08$
BT-57	$\Delta P = 1.57\ q_g - 0.10$
BWA-1539	$\Delta P = 1.87\ q_g + 0.03$
ST-1	$\Delta P = 0.59\ q_g - 0.84$
ST-13	$\Delta P = 0.77\ q_g - 1.53$
ST-41	$\Delta P = 1.32\ q_g - 0.23$

TABLE 41. TRUE FORMS OF FLOW RESISTANCE FUNCTION
(For High Values of Flow, $\Delta P > 10$ mm H_2O)

Fabric	Form of function
ET-1	$\Delta P = 0.0078\ q_g^2 + 1.1866\ q_g - 1.7066$
ET-2	$\Delta P = 0.0070\ q_g^2 + 0.7556\ q_g - 0.8574$
ET-3	$\Delta P = 0.0097\ q_g^2 + 1.4013\ q_g - 0.3358$
ET-4	$\Delta P = 0.0120\ q_g^2 + 0.7812\ q_g - 1.1068$
ET-30	$\Delta P = 0.0336\ q_g^2 + 2.3674\ q_g + 0.2542$
WT-201	$\Delta P = 0.0016\ q_g^2 + 0.3193\ q_g + 0.6428$
WT-203	$\Delta P = 0.0012\ q_g^2 + 0.5377\ q_g + 0.1431$
WT-204	$\Delta P = 0.0014\ q_g^2 + 0.2078\ q_g + 0.6360$
WT-207	$\Delta P = 0.0013\ q_g^2 + 1.0853\ q_g - 4.8650$
WBT-208	$\Delta P = 0.0021\ q_g^2 + 0.8592\ q_g - 1.1991$
WBT-210	$\Delta P = 0.0035\ q_g^2 + 0.8025\ q_g + 0.3572$
BT-57	$\Delta P = 0.0127\ q_g^2 + 1.3312\ q_g + 0.4904$
BWA-1539	$\Delta P = 0.0085\ q^2 + 1.0855\ q_g + 1.6031$
ST-1	$\Delta P = 0.0180\ q_g^2 + 0.0123\ q_g + 2.2286$
ST-13	$\Delta P = 0.0283\ q_g^2 + 0.1442\ q_g + 1.1674$
ST-41	$\Delta P = 0.0498\ q_g^2 + 0.1586\ q_g + 3.7310$

The relationships expressed by Equation 141a and Equation 141b are the same in structure as Darcy's general equation for laminar flows expressed by Equation 137. Coefficient a from Equation 141b corresponds to the resistance coefficient for clean fabrics, K_1. Outside the laminar flow region (Re > 1), Equations 142a and 142b are not similar structurally to Equation 138, which is illustrated by the following:

$$\Delta P_i = K_1 \cdot q_g^2 = a_i' \cdot q_g^2 + b_i' \cdot q_g \quad . \qquad (143)$$

When Equation 136 is transformed, the following is obtained:

$$K_i' = \left(a_i' + \frac{b_i'}{q_g} \right) \quad . \qquad (144)$$

From Equation 137, the resistance coefficient for above-laminar flows depends upon q_g. This relationship, shown in Figure 152, is a hyperbola with asymptotes, $q_g = 0$, $K_i' = a_i'$. Above a certain critical value of q_g (q_g crit.) flows through the fabric are no longer laminar. A transition region extends to q_{gT}, from which the constant value, $K_i' = a_i'$, can be approximated.

When the K_i' (q_g) function of Equation 144 is treated as a resistance function characteristic of woven materials, the following occurs:

$$\left.\begin{array}{lll} \text{For:} & q_g < q_{g\ \text{crit.}} & K_i' = a_i = K_1 \\ & q_{g\ \text{crit.}} < q_g < q_{gT} & K_i' = a_i' + \dfrac{b_i'}{q_g} \\ & q_g > q_{gT} & K_i' = a_i' = K_i'' \end{array}\right\} . \qquad (145)$$

After a certain critical value of q_g ($q_{g\ \text{crit.}}$) is achieved, K_i' reflects the effects of inertia--except for the flow resistance component attributable to gas viscosity. Thus, compared to purely viscous flow, additional energy is lost. When the effects of inertia dominate, the flow becomes turbulent and Bernoulli's equation applies.[29] The resistance function in the transition region of flow depends upon two parameters connected to the structural characteristic of the porous medium. The value of coefficient b_i' considerably influences the shape of the parabolic curve, which determines the placement of characteristic points, $q_{g\ \text{crit.}}$ and q_{gT}. This peculiarity may be examined later based on structural models.

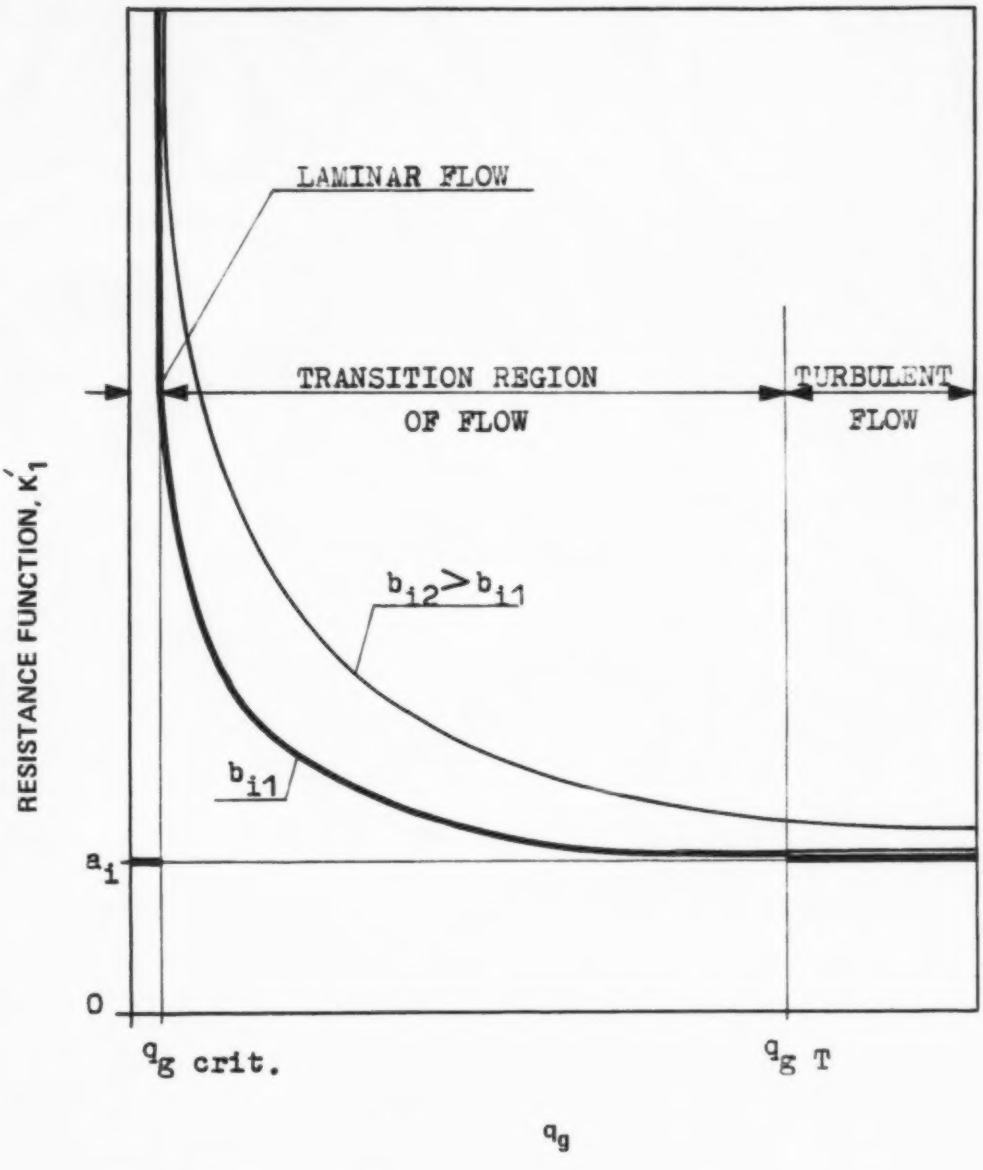

Figure 152. Variation of resistance function of woven filtration materials.

The a_i' coefficient values appear inconsistent when empirical data are used to compare the coefficients, a_i' and b_i', in actual equations of the hydraulic resistance function over the examined range of flows (Tables 40 and 41). It should be noted that Equations 141b and 142b have been developed based on Darcy's equation, which illustrates flow through rigid, homogeneous bodies. Thus, the discrepancy concerning coefficient a_i results from fabric elasticity, which causes structural changes in the tansition region of flow. Moreover, it should be noted that during determination of the specific hydraulic resistance, ΔP_i, fabric thickness was measured as a distance between planes tangent to its surface. This observation confirms the results of previous statistical analysis.

Introductory analysis of flow resistances over specific ranges of q_g reflected the presence of inflection points in the hydraulic characteristics of the fabrics. The hypothesis can thus be offered that the fabric structural changes attributable to increasing differences in pressure are discrete and appear rapidly because structural elements are displaced.

General analysis of the dependence of the fabric resistance coefficient, K_1, upon several structural parameters (conducted under Project 5-533-4) did not show any strong dependences. However, this analysis confirmed some predicted trends, primarily concerning FAs. Consideration of BFAs is presumed to allow the correct inverse function, $K_1 = f(FA)$, which is observed for continuous filament fabrics.

RECAPITULATION AND CONCLUSIONS

Results of testing clean air flow through clean fabric structures confirmed the theory that filtration fabrics are spatially and superficially complicated and cannot be regarded as rigid bodies. The observed deformation of fabric structural elements during manufacture and during air flow, especially in the higher ranges of flow, complicate the hydrodynamic description. Results of this work will contribute to define structural parameters for woven materials. It is noteworthy that some of the problems this project has addressed have not been dealt with by other scientists. The research has allowed formulation of the following basic conclusions, which are important for developing work concerning air flow through the woven structures:

- Woven filtration materials are characterized by periodic spatial and superficial composition, in which the distribution of physical properties (parameters) is normal.
- The basic physical parameters of woven structures that determine hydraulic properties are not-covered-with-yarn-or-fiber areas called free areas (FAs) or basket free areas (BFAs).
- Free areas form macroporous structures, which can be described by a normal pore size distribution function. This function can be expressed in terms of technological parameters, so this part of the overall modeling problems is completed.
- The proposed model of woven structure (considering BFA) meets the requirements of formation and thickening of dust cake, but in the future it will be necessary to reconstruct the static model as a dynamic model according to observed peculiarities of air flow.
- Air flow through clean woven filtration structures is a normal, stochastic process determined by specific fabric properties.
- At low flows, air flow through fabrics can be laminar, but at high flows flow is mainly in the transition region of flow (between laminar and turbulent flows).
- From a hydrodynamic viewpoint, air flow resistance through woven filtration structures is determined by the fabric resistance function, K_1', which is discontinuous over the total range of flows. For laminar and turbulent flows, flow is a constant (K_1 and K_1'', respectively); and in the transition region of flow, it is a hyperbolic function depending upon q_g.
- The characteristic fabric resistance function results from the changed flow character and shifting relative importance of viscosity and inertial forces.

SECTION IX
STUDY OF STRUCTURAL DUST PARAMETERS

INTRODUCTION

When tested with different kinds of dust, similar filtration fabric structures with similar size distributions exhibited different filtration resistances and efficiencies. The dust type (kind of dust raw material) with definite aerosol state and filtration parameters determines the force between particles and the filtration structure and also among individual particles. During this research, electrostatic forces were observed to dominate.

Observations led to the conclusion that although dust layers are usually regarded as heterogeneous, quasi-isotropic media, the dust cake formed on the filtration structure is anisotropic. The anisotropy of the dust cake is caused by the fact that industrial aerosols are polydisperse and local fields of gas velocity exist in front of the filtration material surface. These factors contribute to dust-gas separation and form a dust layer characterized by only local, unidirectional isotropy.

Studying dust cake structure is complicated because of the lack of practical methods of observing the formed structure and the process by which it forms. The preparation of dust cake cross sections from a formed cake invariably displaces dust particles during the preparation of the cross section. Random microscopic examination confirms dust particle separation resulting from the structure of the filtration materials.

Under these conditions, investigations of the filtration and hydraulic properties of dust cakes require certain idealized physical models that make theoretical studies possible. When the assumptions presented in Section IV are considered, the four-element configuration and eight-element configuration of dust cake can be distinguished.

The four-element configuration consists of four individual dust grains whose centers form a regular pyramid-shaped cell. Figure 153 and Figure 154

Reproduced from
best available copy.

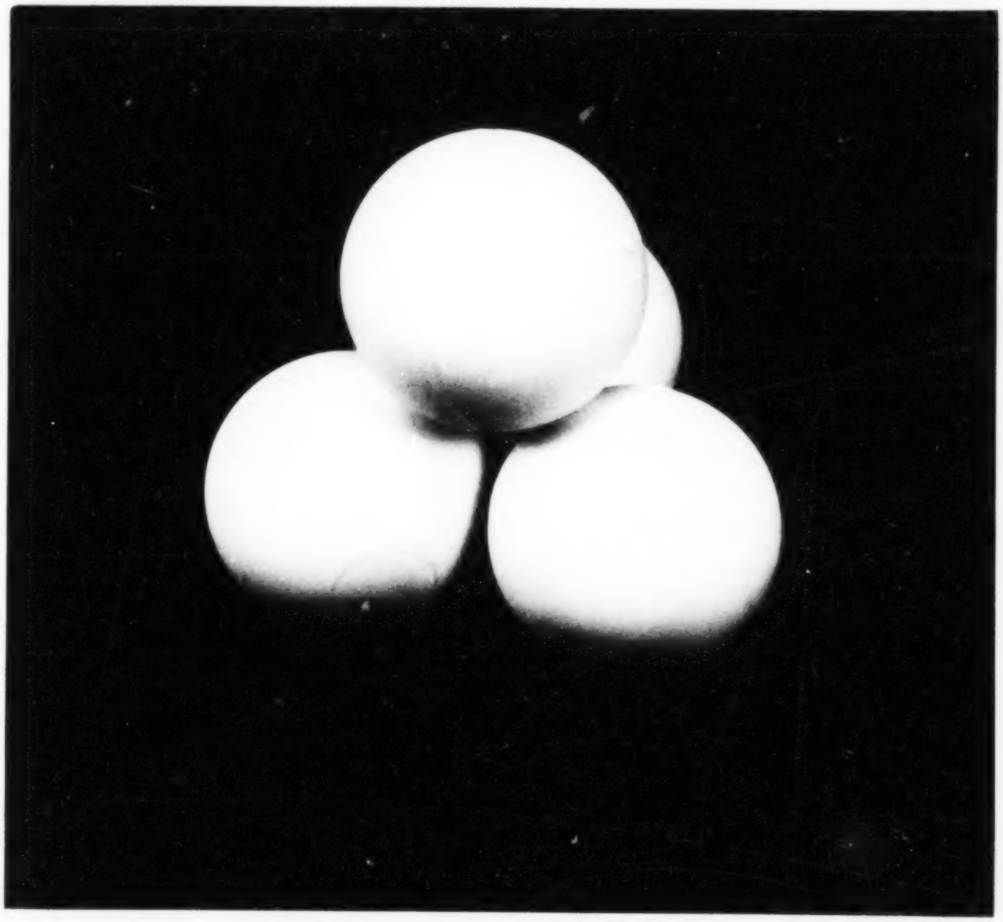

Figure 153. Four-element configuration of dust grains.

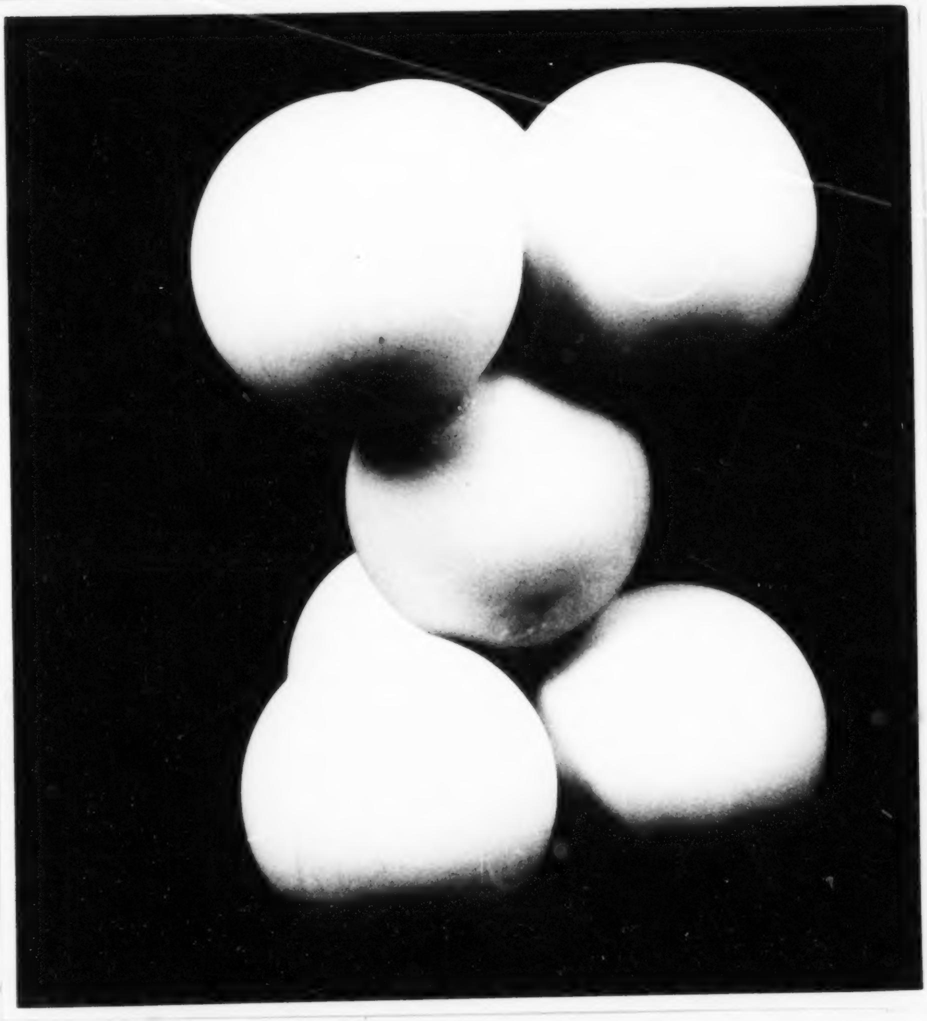

Figure 154. View of dust cake structure made with grains of four-element configuration.

Reproduced from
best available copy.

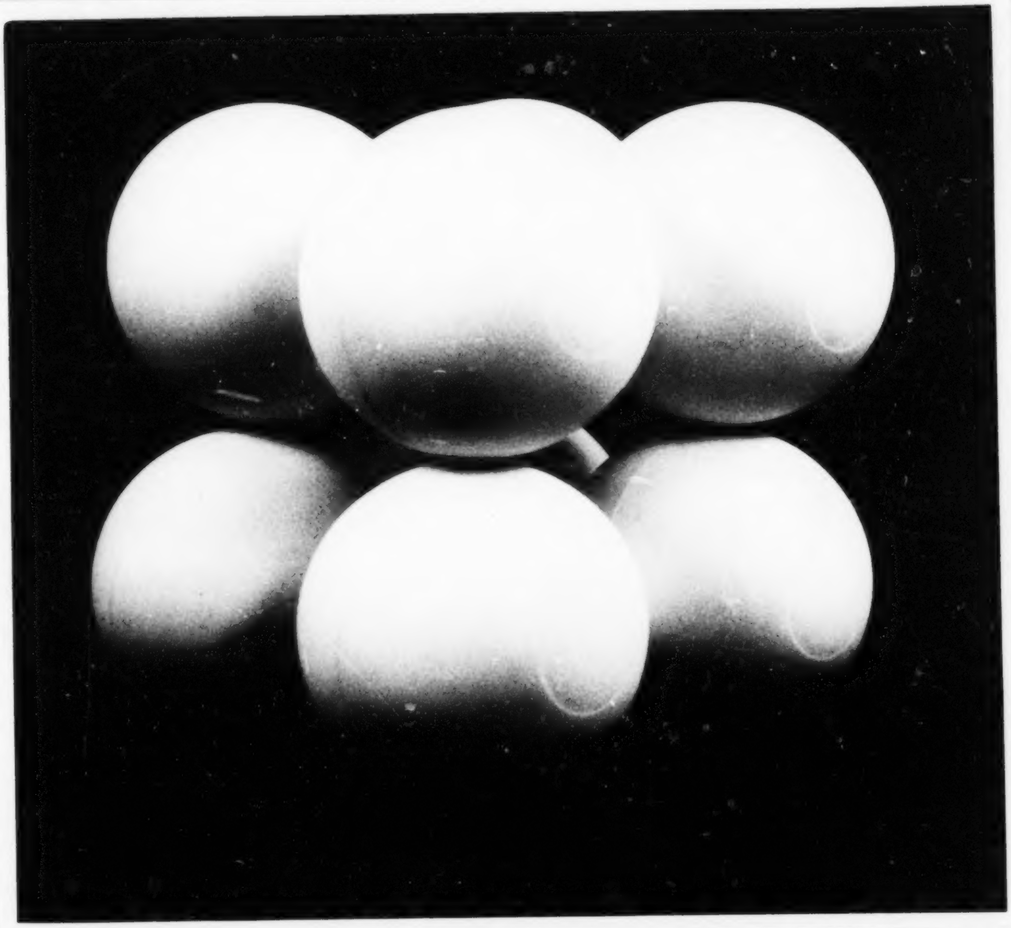

Figure 155. Eight-element configuration of dust grains.

Preceding page blank

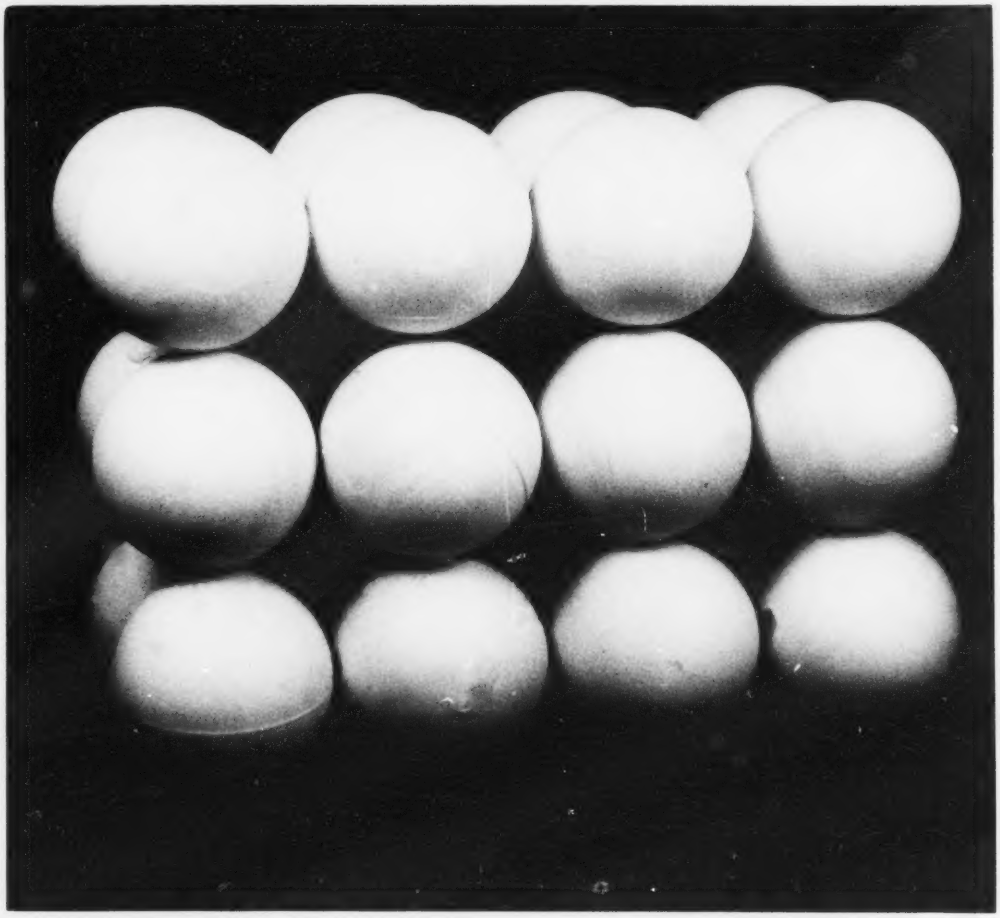

Figure 156. View of dust cake structure made with grains of eight-element configuration.

EQUIPMENT AND PROCEDURES

Fractional analysis of the dust was performed with a Bahco centrifugal separator and a Sartorius sedimentation balance ($d < 5$ μm). The specific static surface was identified by the Establishment of Catalysis and Physics of Surface of the Polish Academy of Sciences in Cracow with use of the Bet apparatus and argon as an adsorbent. The specific kinetic surface was measured with a Lea-Nursea apparatus. The manner of dust separation in Series II is illustrated in Figures 157 through 160.

The change in dust layer porosity was determined by standard apparatus, the basic principle being the determination of the thickness of a jogged dust sample (Polish Standard PN-65/Z-04003). The apparatus is shown in Figure 161. Decreasing thickness of dust layer as a function of shocking (jogging) time was investigated. Experiments were conducted for:

- Five levels of initial thickness of dust layer: $H_o = 30, 50, 70, 90$, and 200 mm; and
- Eight ranges of shocking time: $t_s = 5, 10, 15, 30, 60, 300, 600$, and 2 400 s.

Therefore, the thickness of the dust layer was determined after 5, 15, 30, 60, 120, 420, 1 020, and 3 420 seconds of shocking. The decrease of initial thickness of the dust layer was estimated by the following equation:

$$\Delta h = H_o - h_t \quad , \qquad (146)$$

where

Δh = decrease of initial thickness of dust layer, mm;

H_o = initial thickness of dust layer, mm; and

h_t = thickness of dust layer after a certain shocking time, t_s.

RESULTS AND DISCUSSION

Based on an introductory analysis of results obtained during Series I (see Table 42), the following partial conclusions can be presented:

- Stationary (static) specific surface, the total area of dust sample covered by a monomolecular layer of adsorbent, is for all ranges of dust particle diameters higher than the specific kinetic surface. Its absolute value depends on the dust type (raw material), so it

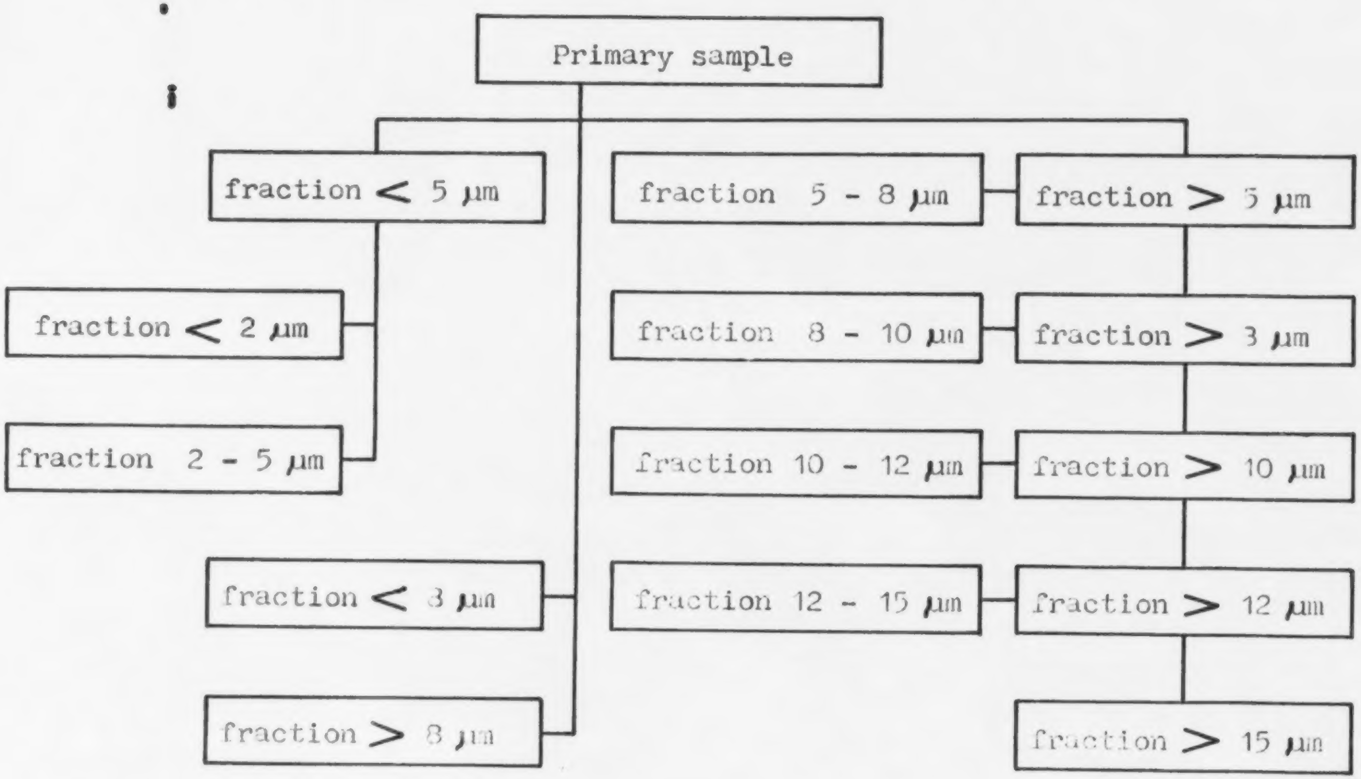
Primary sample
fraction < 5 µm
fraction < 2 µm
fraction 2 - 5 µm
fraction < 3 µm
fraction > 8 µm
fraction 5 - 8 µm
fraction 8 - 10 µm
fraction 10 - 12 µm
fraction 12 - 15 µm
fraction > 5 µm
fraction > 3 µm
fraction > 10 µm
fraction > 12 µm
fraction > 15 µm

Figure 157. Scheme of cement dust separation.

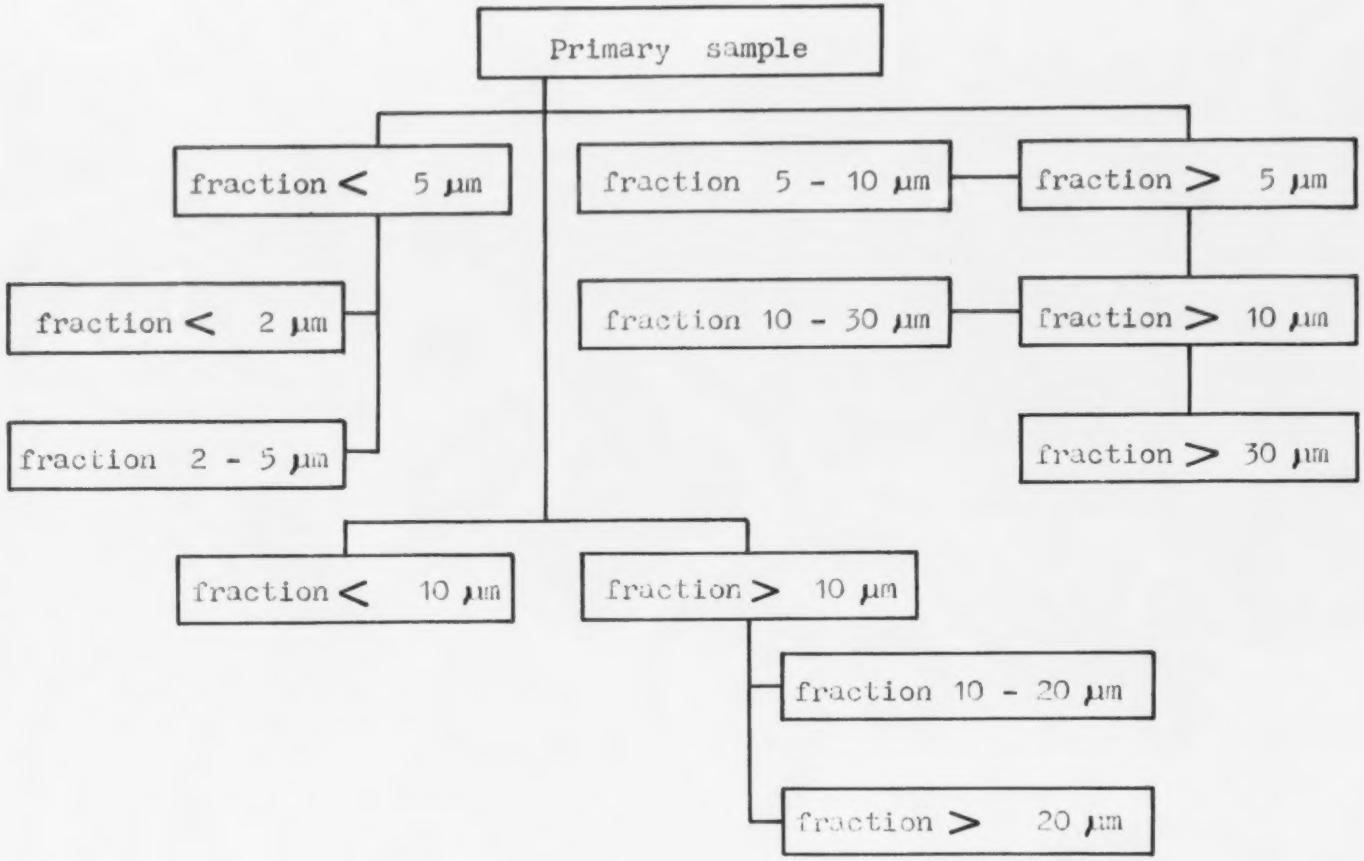
Primary sample
fraction < 5 µm
fraction < 2 µm
fraction 2 - 5 µm
fraction 5 - 10 µm
fraction > 5 µm
fraction 10 - 30 µm
fraction > 10 µm
fraction > 30 µm
fraction < 10 µm
fraction > 10 µm
fraction 10 - 20 µm
fraction > 20 µm

Figure 158. Scheme of coal dust separation.

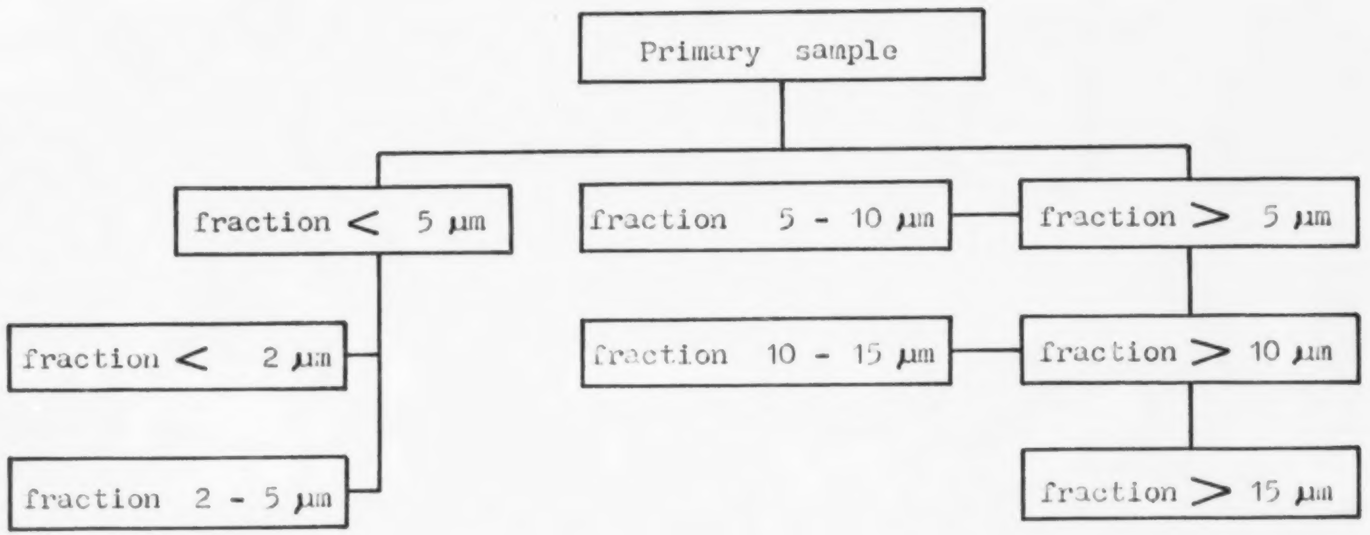
Primary sample
fraction < 5 µm
fraction 5 - 10 µm
fraction > 5 µm
fraction < 2 µm
fraction 10 - 15 µm
fraction > 10 µm
fraction 2 - 5 µm
fraction > 15 µm

Figure 159. Scheme of talc separation.

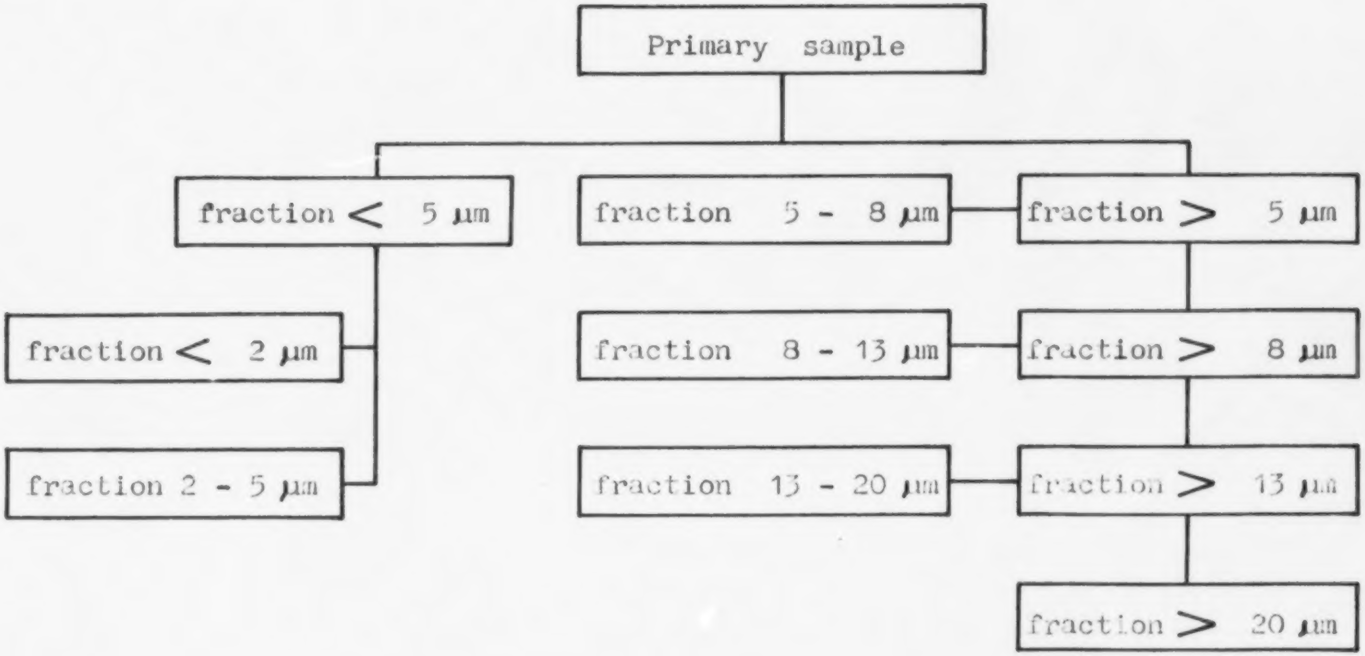
Primary sample
fraction < 5 µm
fraction 5 - 8 µm
fraction > 5 µm
fraction < 2 µm
fraction 8 - 13 µm
fraction > 8 µm
fraction 2 - 5 µm
fraction 13 - 20 µm
fraction > 13 µm
fraction > 20 µm

Figure 160. Scheme of fly ash separation.

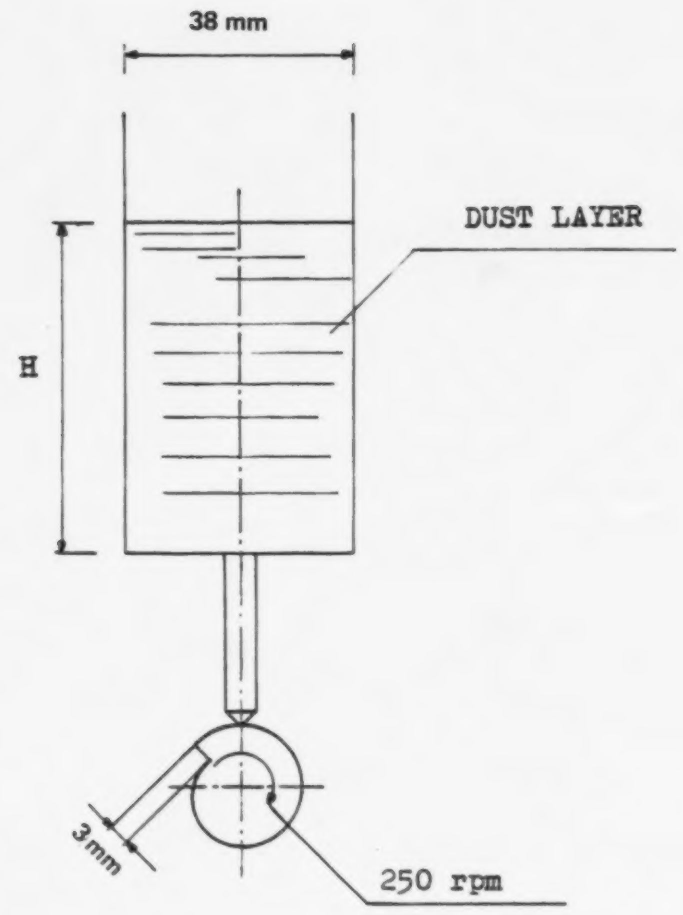
38 mm
DUST LAYER
H
3mm
250 rpm

Figure 161. Apparatus for determination of the jogged dust weight.

TABLE 42. KINETIC AND STATIC SPECIFIC SURFACE FOR DUSTS: CEMENT AND COAL (Series I)

Kind of dust and fraction	Average value of static specific surface (cm^2/g)	Average value of kinetic specific surface (cm^2/g)	MMD (μm)	Part of fraction less than d_{lim} = 20 μm (%)
Cement:				
Nonfractionated	-	7 082	22.00	48.0
Fraction < 5 μm	-	27 556	2.25	-
Fraction < 10 μm	-	19 429	4.80	100.0
Fraction < 20 μm	36 390 ± 1 280	11 952	6.50	99.7
Fraction > 20 μm	-	1 467	48.00	15.0
Coal:				
Nonfractionated	-	7 423	30.00	40.0
Fraction < 10 μm	-	24 775	5.20	100.0
Fraction < 20 μm	63 950 ± 2 400	15 775	7.00	98.0
Fraction < 30 μm	-	11 007	10.00	78.0
Fraction > 30 μm	-	1 539	80.00	6.0

characterizes superficial properties of the dust structure. Thus, this value is not of interest to the project because it includes surfaces that do not affect gas flow through the porous layer.

- Specific kinetic surface, the total external surface of the particles without consideration of porosity, is the value that varies according to the degree of dust dispersion, represented by d_{50}.

With regard to the above statments, the hypothesis can be offered that specific kinetic surface depends exponentially on the parameter characterizing the degree of dust dispersion; its dependence on MMD is fixed for each dust.

The following empirical dependences were obtained from a statistical analysis of results obtained during Series I:

- For the degree of dispersion determined as M_d (percentage of sample particles with diameter less than the assumed limiting diameter, d_{lim}),

$$S = a\,(M_d)^{b}, \tag{147}$$

where

S = specific kinetic surface, cm^2/g;
M_d = percent particles with diameter less than d_{lim} = 20 μm, %; and
a,b = coefficients.

- For the degree of dispersion determined as d_{50},

$$S = a\,(d_{50})^{-b}, \tag{148}$$

where

S = specific kinetic surface, cm^2/g;
d_{50} = MMD, μm; and
a,b = coefficients.

The equation for the degree of dust dispersion in a dispersed state, determined as d_{50}, was verified with results of Series II, shown in Tables B-25 through B-28. The theoretical curve, $S = f(d_{50})$, agreed with results from specific kinetic surface measurements for specific dust classes. The curves are shown in Figures 162 through 165. Values of coefficients a and b for Equation 148 were determined empirically (see Table 43).

From microscopic examination of the test dusts, a strong dependence is evident between coefficient a and the shape of the dust particle.

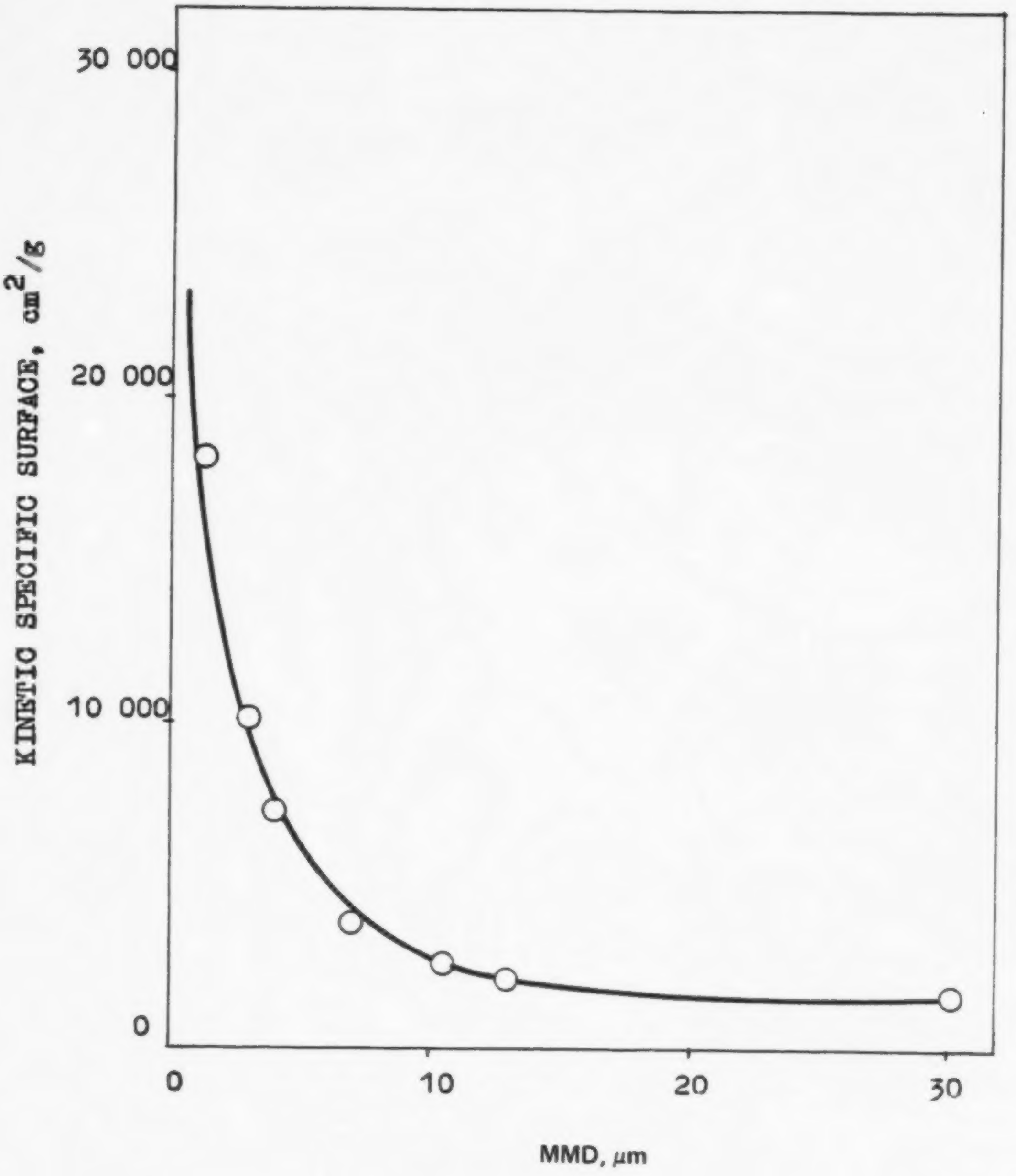

Figure 162. Theoretical dependence, $S = f(d_{50})$, for cement (Series II).

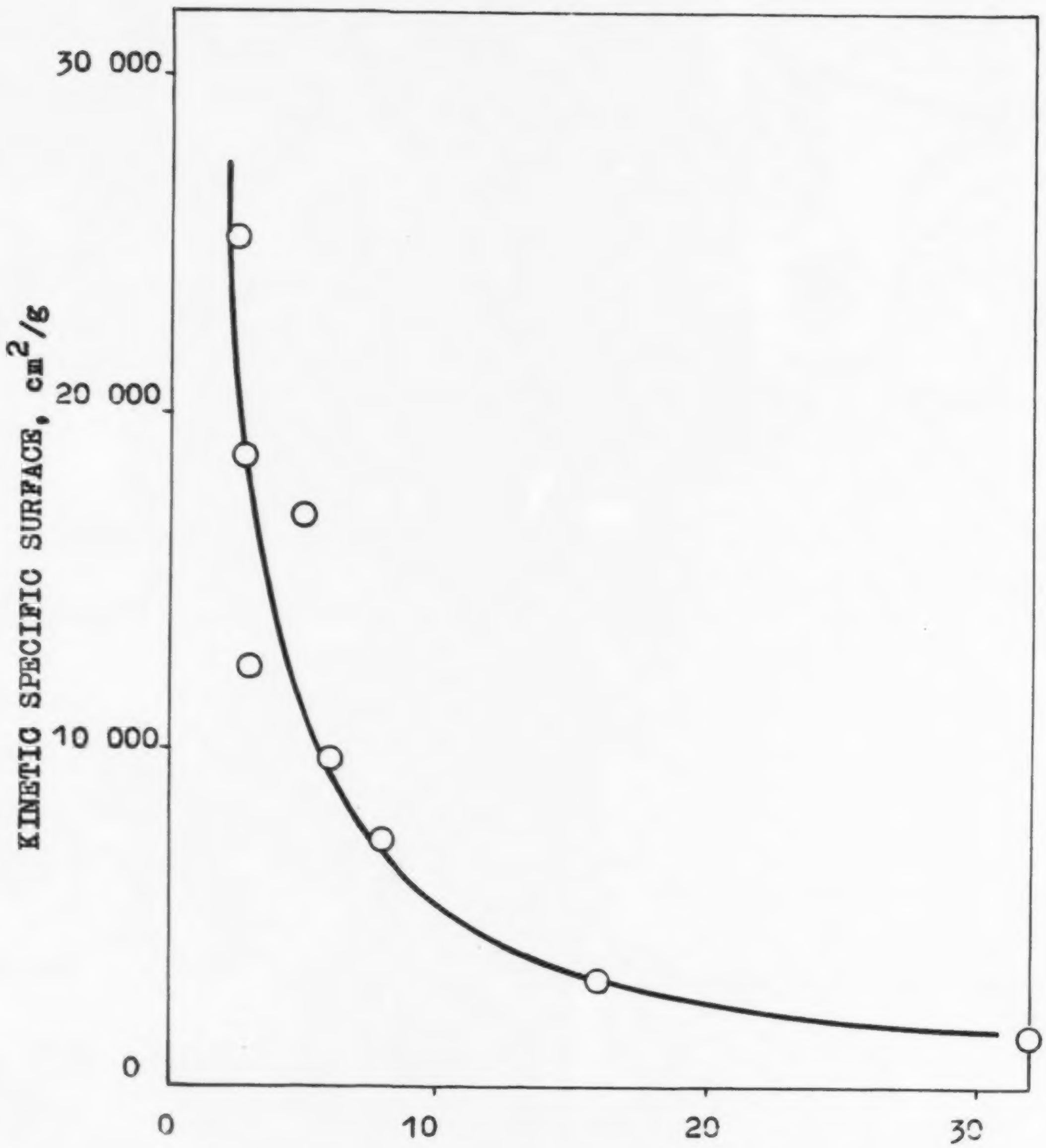

Figure 163. Theoretical dependence, $S = f(d_{50})$, for coal (Series II).

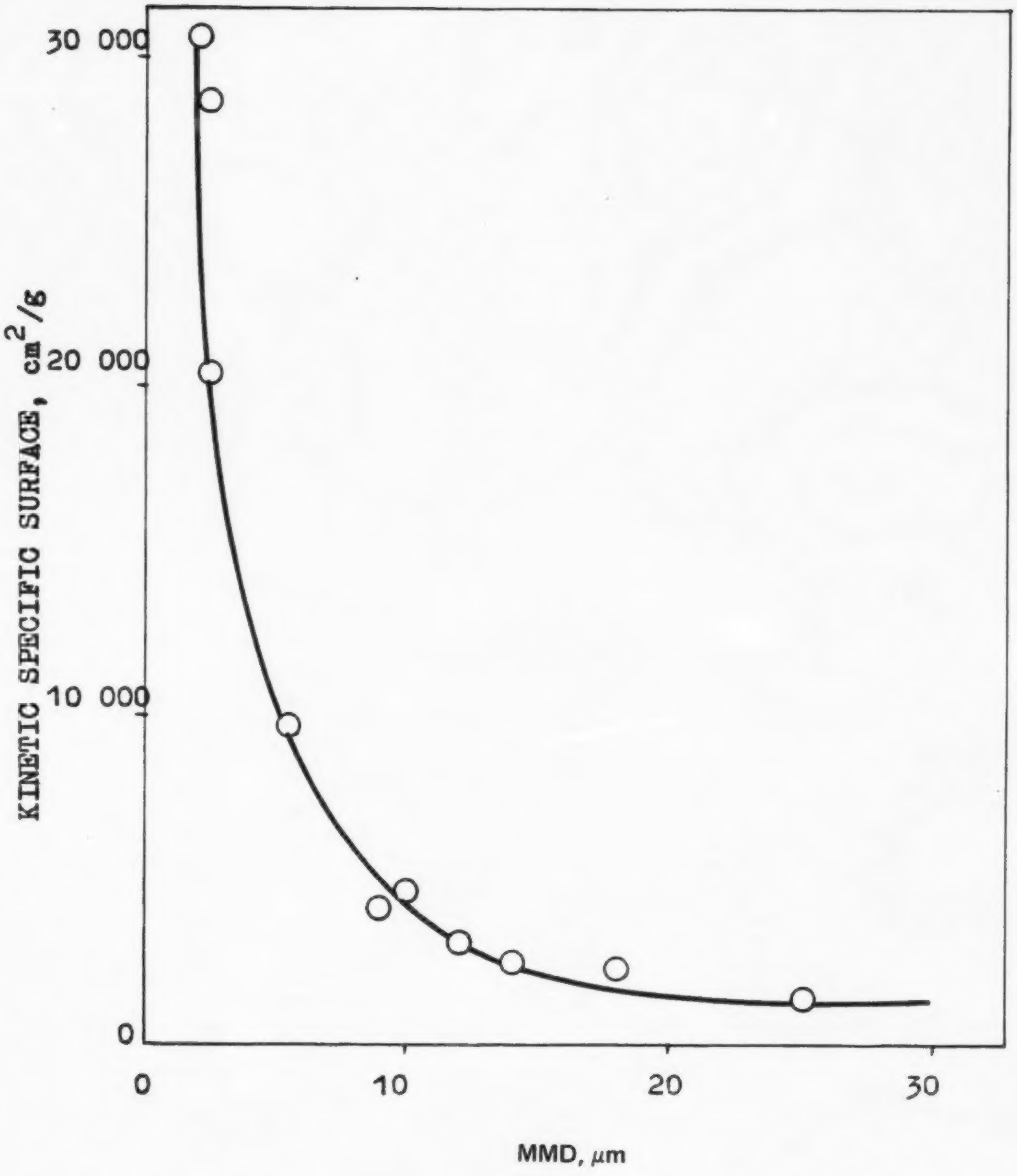

Figure 164. Theoretical dependence, $S = f(d_{50})$, for talc (Series II).

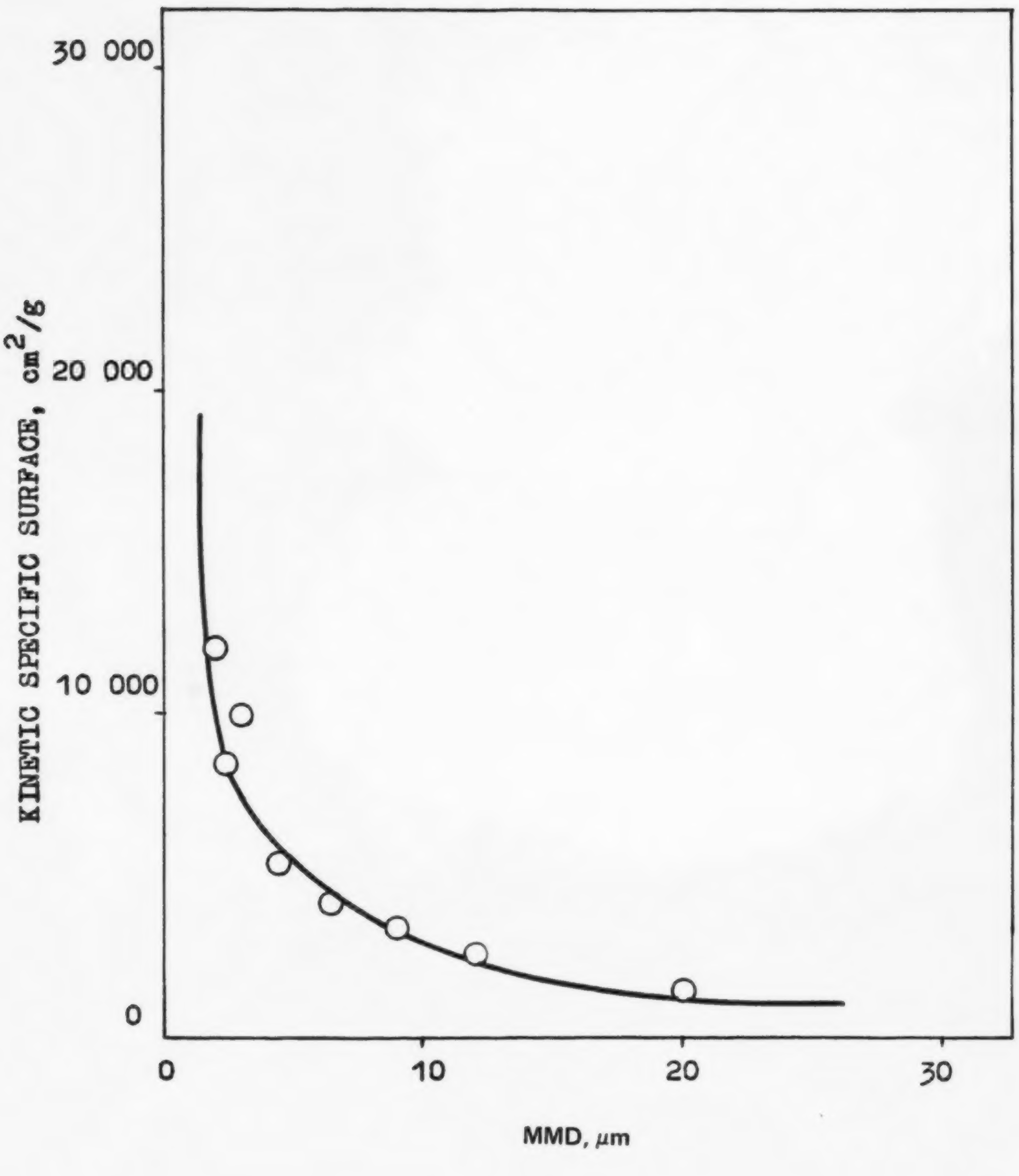

Figure 165. Theoretical dependence, $S = f(d_{50})$, for fly ash (Series II).

TABLE 43. COEFFICIENTS a AND b FOR EQUATION 148

Kind of dust	a	b
Cement	23.440	-0.89
Talc	71.640	-1.23
Coal	41.020	-0.86
Fly ash	21.040	-0.87

TABLE 44. CHANGES OF DUST LAYER POROSITY DURING SHOCKING

Initial dust layer thickness	Kind of dust					
	Cement		Coal		Fly ash	
	Separated	Unseparated	Separated	Unseparated	Separated	Unseparated
0*	0.74	0.69	0.74	0.61	0.75	0.71
$H_o = 30$†	0.56	0.51	0.59	0.48	0.61	0.55
$H_o = 50$	0.59	0.50	0.62	0.47	0.63	0.59
$H_o = 70$	0.60	0.47	0.64	0.44	0.65	0.57
$H_o = 90$	0.60	0.52	0.64	0.47	0.64	0.57
$H_o = 200$	0.60	0.55	0.62	0.41	0.63	0.61

*Calculated initial value of dust layer porosity.

†Calculated final value of dust layer porosity during shocking.

The lowest value of a is observed for fly ash, which usually consists of spherical particles. The highest value of a is observed for talc, which usually consists of plate-needle-shaped particles. Cement particles have a more regular geometric shape than coal particles, a characteristic that governs the variation of value a.

Value b characterizes the effect of d_{50} on S. At higher values of b, smaller changes of d_{50} cause considerable variation in S. Talc dusts exhibit this property, which may result from inadequate fractional composition analysis and inadequate knowledge of the true sizes of the dust particles. Coefficient b should therefore be regarded as a property of each specific kind of dust.

In all cases, the differences in particle dust distribution with d_{50} less than 10 μm can be regarded as unimportant for corresponding values of specific kinetic surface. Above this value, variation in particle size distribution causes significant differences in the values of specific kinetic surface. Further investigation is planned of the correlation between a given parameter characteristic for dust cake specific kinetic surface and the filtration properties of dust-fabric systems.

The porosity of a dust layer can be calculated from the following equation:

$$\varepsilon = 1 - \alpha = 1 - \frac{\rho_i}{\rho_m} \quad , \tag{149}$$

where

ε = porosity,

α = fraction of solids in the dust layer,

ρ_i = packing density of the dust layer in g/cm^3, and

ρ_m = absolute density of dust in g/cm^3.

Equation 149 was used to calculate the initial porosity of the dust layer formed with a certain kind of dust. Values ρ_i and ρ_m are magnitudes characteristic of the dusts.

With Equation 149, the porosity of a shocked dust layer can be determined from the decreased dust layer thickness caused by shocking. The following equation can be used:

$$\varepsilon_t = 1 - \alpha_t = 1 - \frac{V_1 \cdot \rho_i}{V_2 \cdot \rho_m} \quad ,$$

where

ε, α, ρ_i, and ρ_m as previously;

V_1 = initial volume of dust layer in cm^3 (calculated for initial thickness of dust layer, H_0); and

V_2 = final volume of dust layer in cm^3 (calculated for thickness of dust layer, h_t; i.e., after a certain shocking time, t_s).

Results of calculations are contained in Table 44. The decrease in initial thickness of the dust layers during shocking is shown in Tables B-29 through B-34 and in Figures 166 through 171. For all cases, initial porosity, ε_i, reaches values as high as 0.61 to 0.75. However, porosity values are higher for separated than for unseparated dusts because some free spaces between large grains are filled with smaller grains. The change in initial porosity of the dust during shocking is rapid and nearly independent of dust layer thickness. Differences observed in the first phase of shocking probably result from packing of nonuniform dust grains in the dust layer (see Figure 172). After about 2½ minutes of shocking, a stable value of porosity is reached. Longer shocking time does not cause further differences in porosity. These results typify the range of true porosity values for industrial dust layers. It is noteworthy that the porosity of the shocked dust layer changes until the range of 0.41 to 0.59 is reached. Porosity of the dust cake in dust filtration probably has a value between that of the initial porosity and that of the porosity after shocking.

CONCLUSIONS

- Mean mass diameter, d_{50}, is a parameter that characterizes dust in a state of suspension.
- Specific kinetic surface, S, is a suitable parameter correlated functionally with d_{50} for describing dust in a state of suspension.
- The specific kinetic surface of the dust cake can be determined from the particle size distribution of the aerosol by a known functional dependence when the mean porosity of the dust cake is about 0.55.
- Porosity of the dust layer depends on the dust type and its particle size distribution. Porosity is greater for a more uniform dust (separated dusts) than for a less uniform dust.
- During shocking, the dust layers reached a stable value of porosity, which was usually about 20 percent less than their initial porosity.

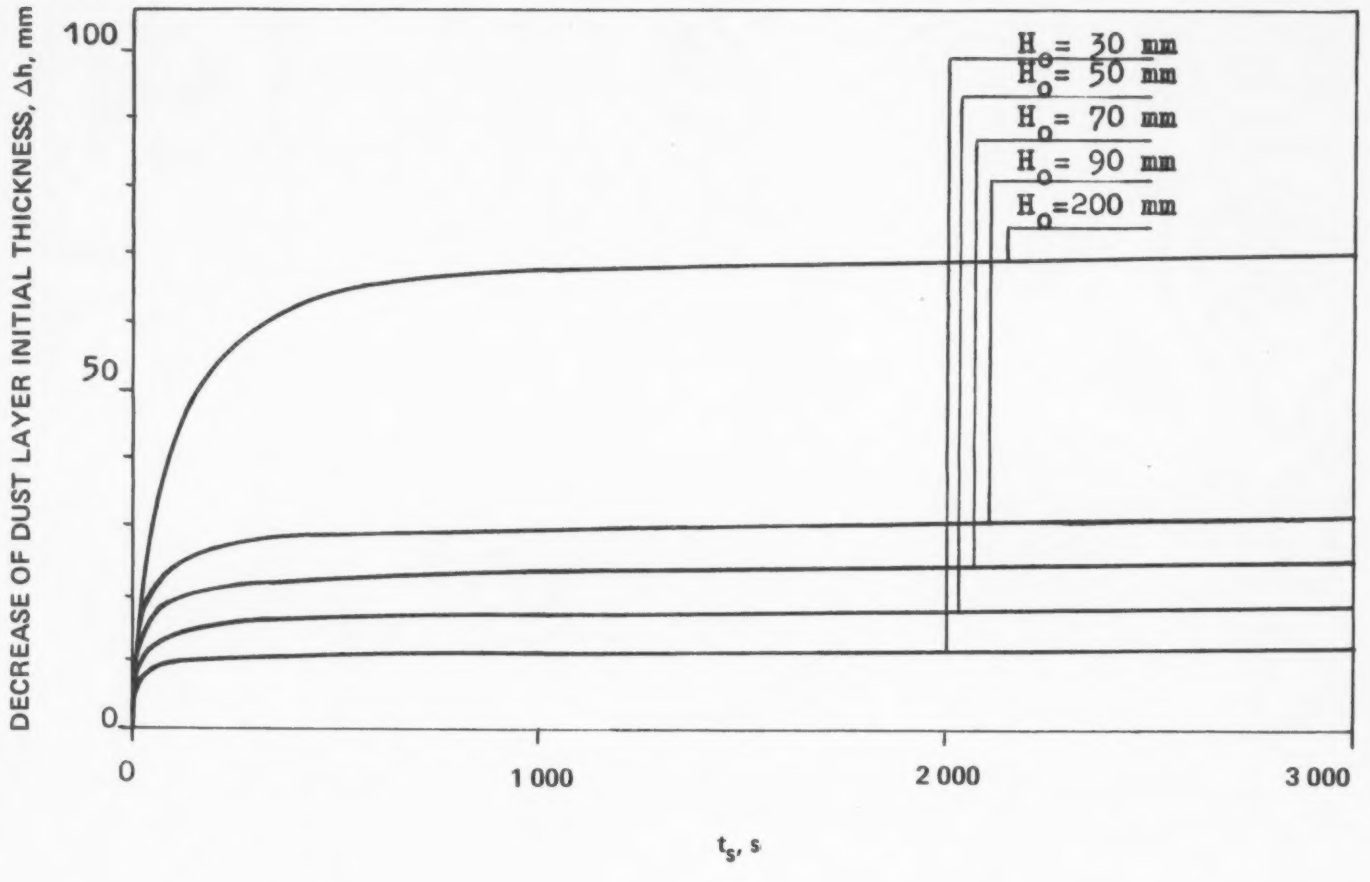

Figure 166. Variation of Δ h vs. shocking time for separated cement.

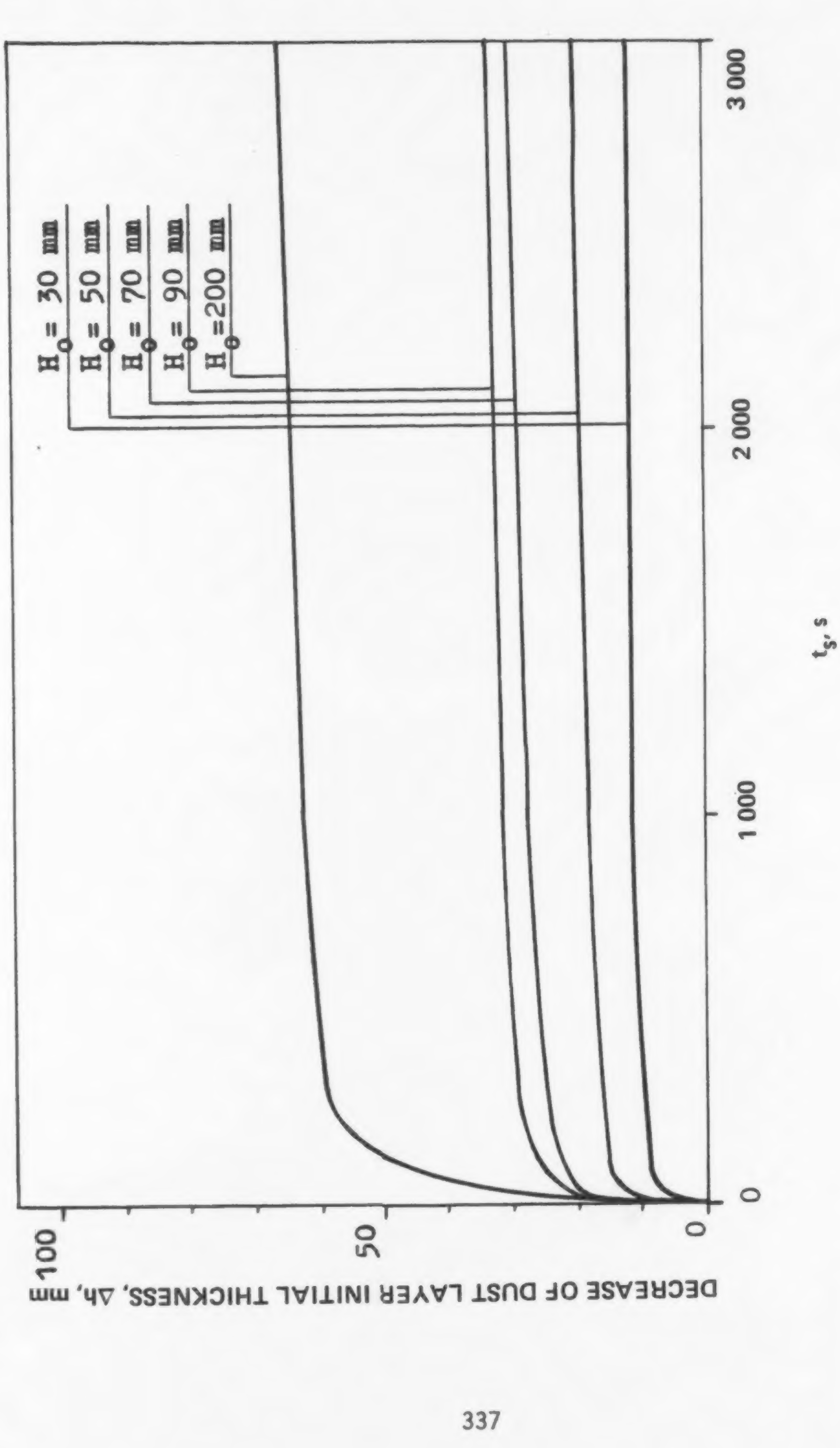

Figure 167. Variation of Δ h vs. shocking time for unseparated cement.

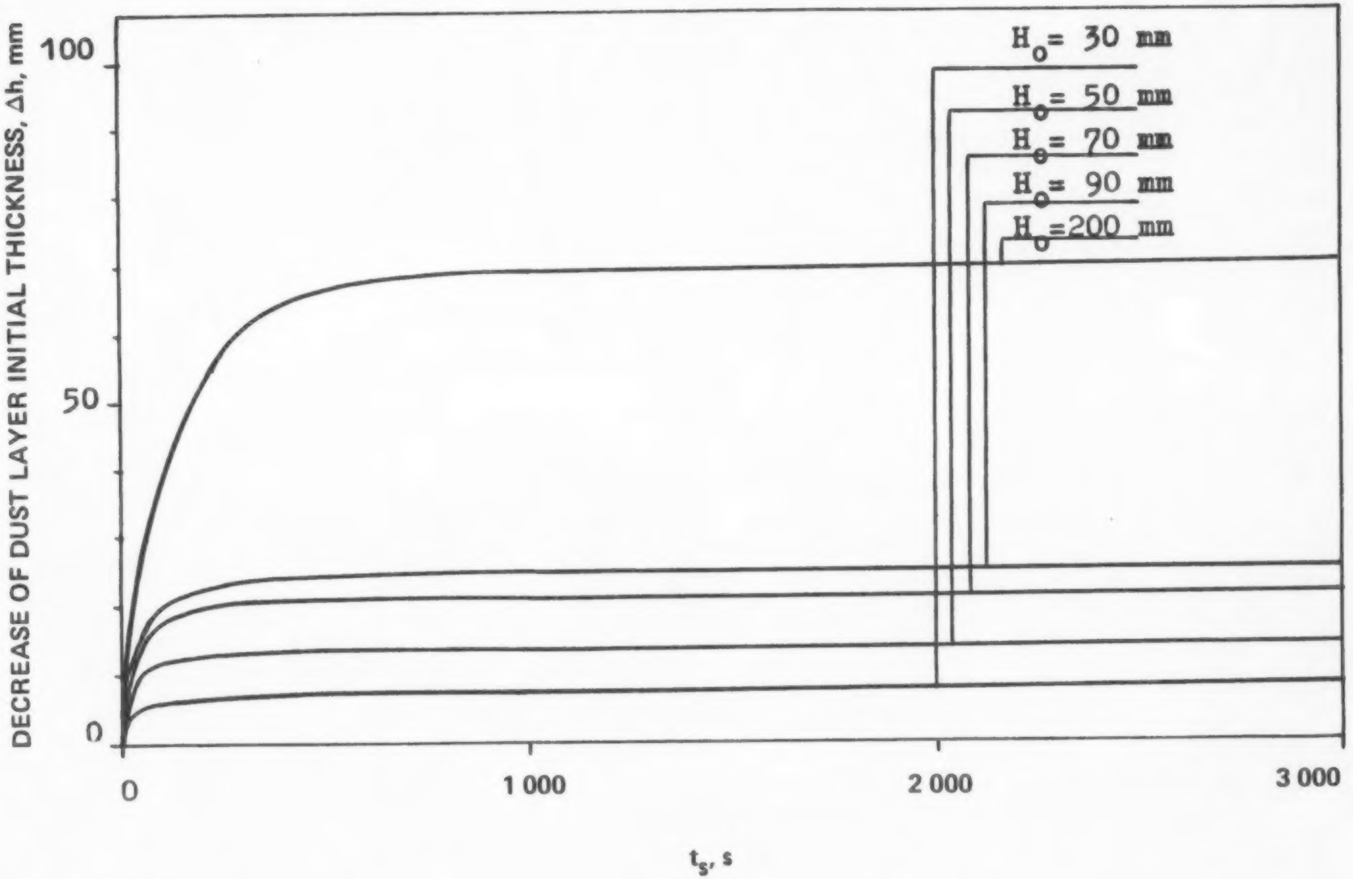

Figure 168. Variation of Δ h vs. shocking time for separated coal.

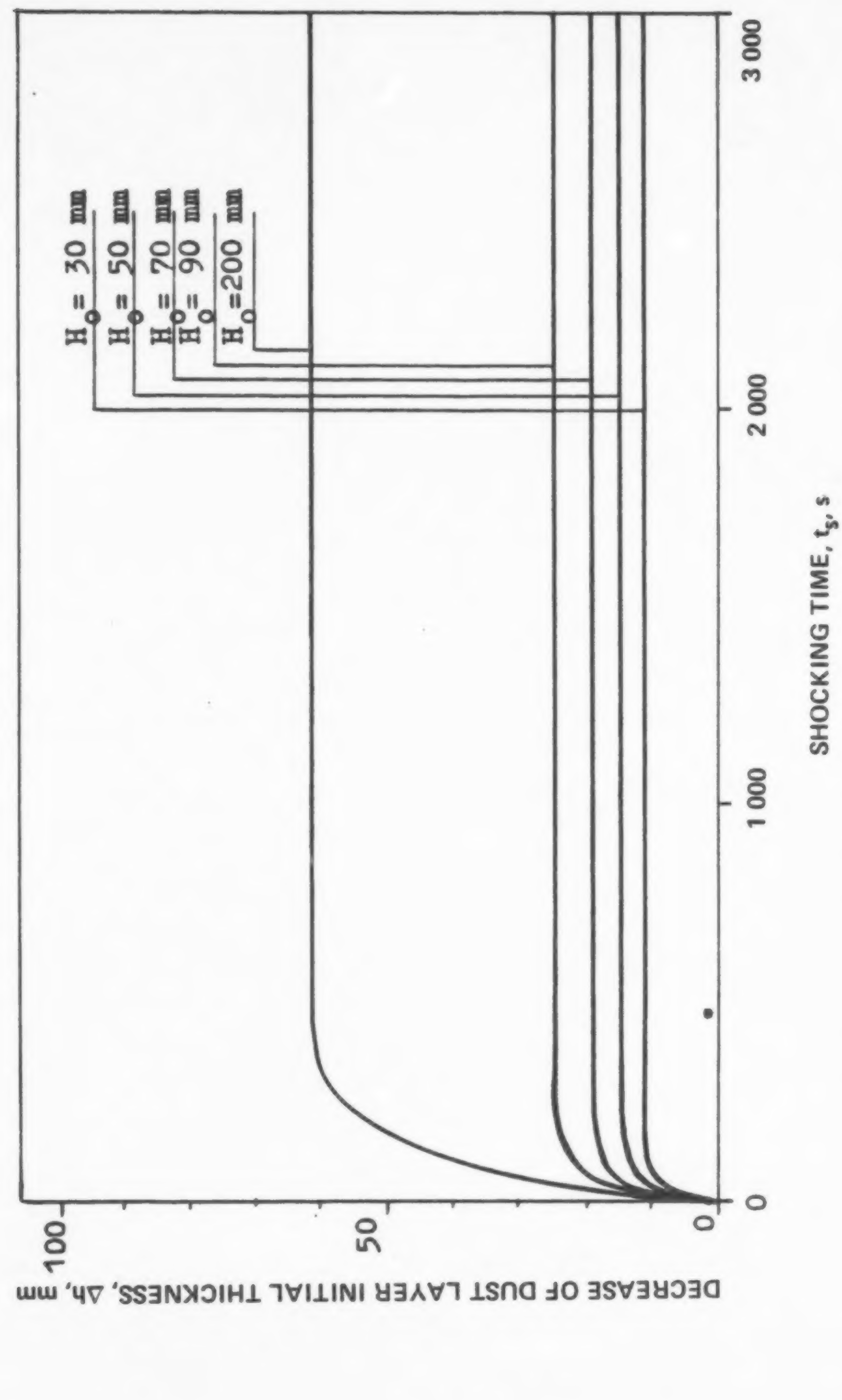

Figure 169. Variation of Δh vs. shocking time for unseparated coal.

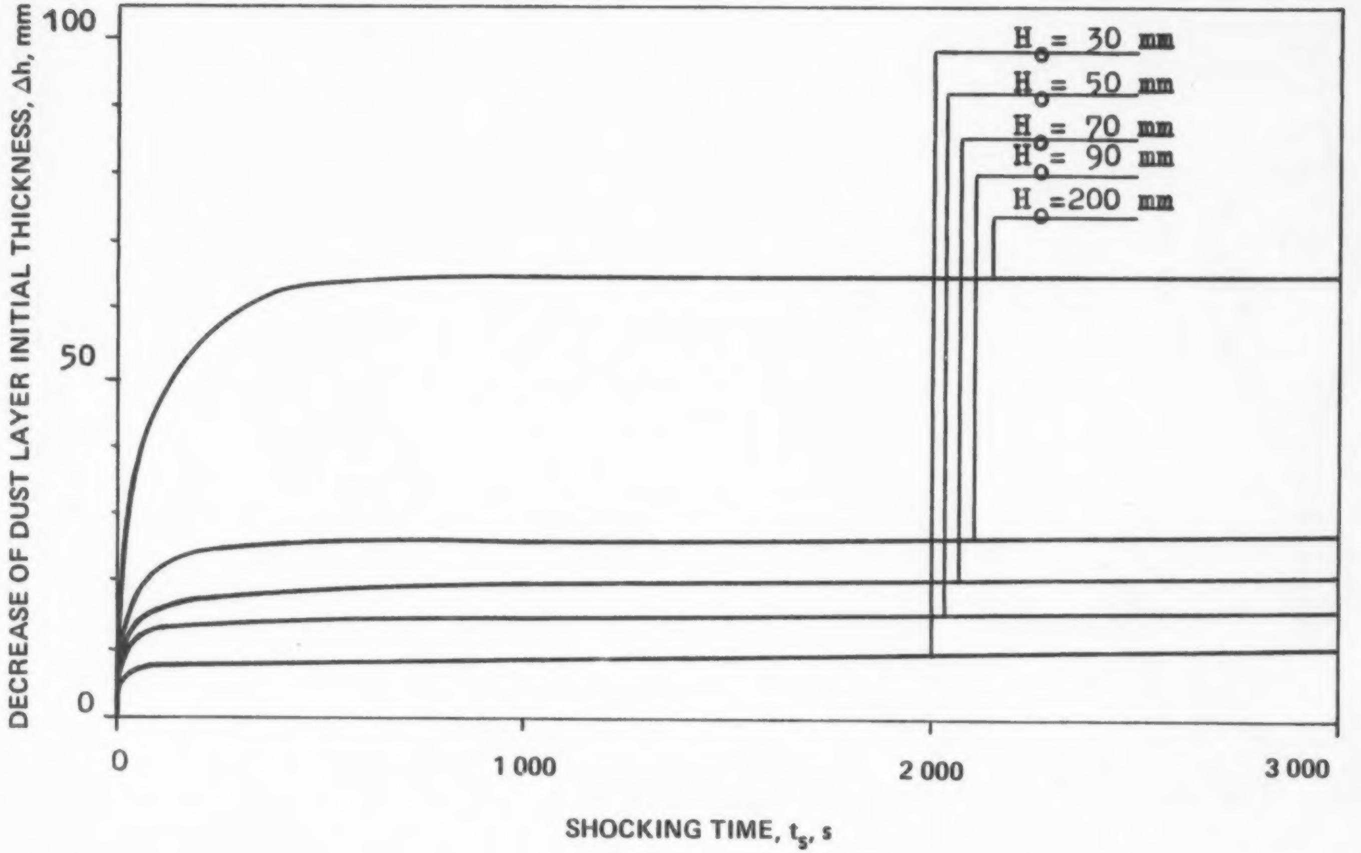

Figure 170. Variation of Δh vs. shocking time for separated fly ash.

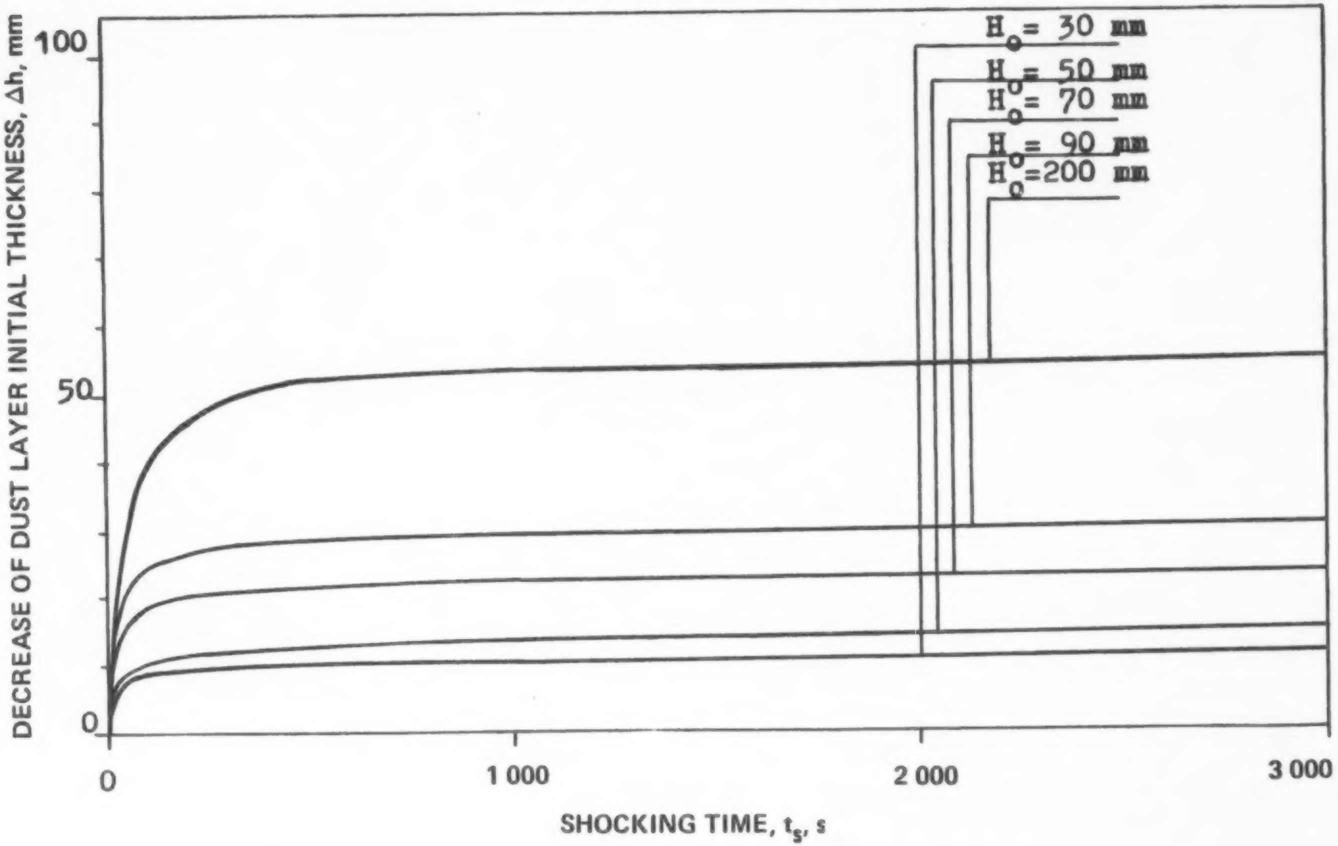

Figure 171. Variation of Δh vs. shocking time for unseparated fly ash.

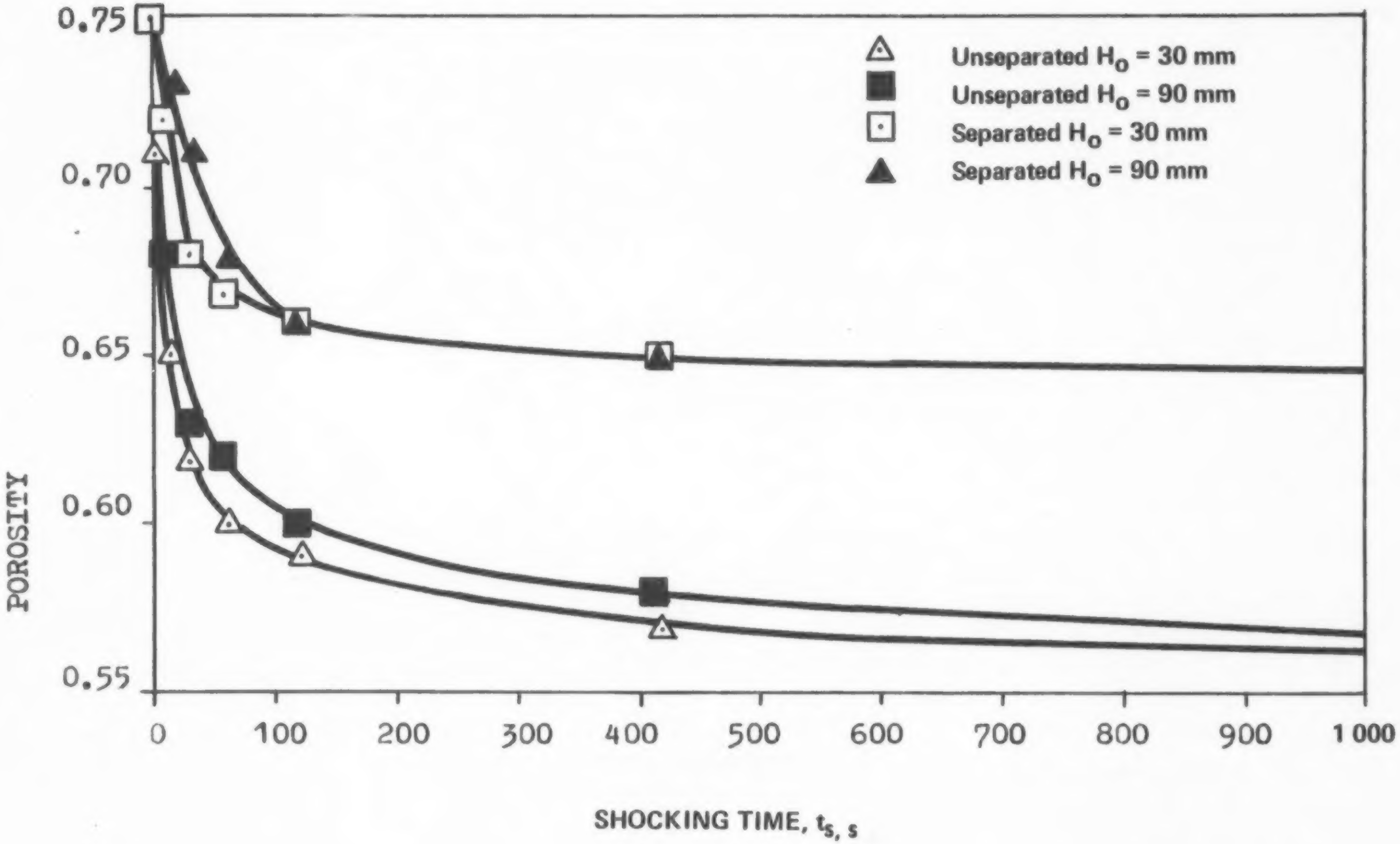

Figure 172. Change of dust layer initial porosity during shocking (separated and unseparated fly ash).

SECTION X

MODEL OF DUST COLLECTION EFFICIENCY*

This section deals with dust collection efficiency problems. A mathematical model is presented of dust collection efficiency as a partial filtration model. The model is based on stationary random fields, which are isotropic or quasi-isotropic. The theory of fields is presented below in abbreviated form.

THEORETICAL BACKGROUND

Let (E,P,A) be probabilistic spaces. Each function f: $IR^n \times E \rightarrow IR^1$, where for each $p \in IR^n$, function $e \rightarrow f(p, e)$ is a random variable in E, is called a random field. The random field understood in this manner is designated as f(p). The random field on plane IR^2 can be deduced as follows: let C(e) be a coordinate system in IR^2 according to e E. It can be assumed that the axes of the system, C(e), are parallel to the system, 0,x,y put in IR^2. But the origin of coordinates, C(e), varies randomly (according to e E); i.e., the origin is placed randomly in points of the set, D_1. The system, C(e), can be chosen randomly so the probability of placing the origin of coordinates in a borelion field of subsets, B in set D_1, amounts to $\mu(B)/\mu(D_1)$. Thus, the mean value and variance, f(p), will be constant under the condition that f is an integrable function. Analogically, as in IR^2, the random field can be put in IR^n $(n > 2)$.

The correlation coefficients of random variables f(p) and f(q) are designated as r[f(p), f(q)] and are:

$$r[f(p),\ f(q)] = \frac{\int_E \left\{ \left[f(p) - m_p\right] \left[f(q) - m_q\right] \right\} dP(e)}{\left\{ \int_E \left[f(p) - m_p\right]^2 dP(e) \right\}^{\frac{1}{2}} \int_E \left[f(q) - m_q\right]^2 dP(e) \Big\}^{\frac{1}{2}}} , \qquad (151)$$

---

*Prepared by Eugeniusz Szczepankiewicz, Institute of Mathematics of WSP in Opole.

where

$$m_p = \int_E f(p)\, dP(e),\ m_q = \int_E f(q)\, dP(e).$$

E[f(p)] is considered an expected value of field f(p), and D^2 [f(p)] is its variance, so:

$$E[f(p)] = \int_E f(p)\, dP(e) \quad \text{, and} \tag{152}$$

$$D^2\ [f(p)] = \int_E [f(p) - m_p]^2\, dP(e)\ . \tag{153}$$

Definition I. The random field, f(p), is considered stationary if E[f(p)] = constant, D^2 [f(p)] = constant > 0, and for each p, q ϵ IR^n:

$$r[f(p),\ f(q)] = r(p\vec{\ }q)\ ; \tag{154}$$

i.e., the correlation coefficient depends only on the vector, $p\vec{\ }q$, connecting points p and q.

Definition II. The random field, f(p), considered stationary, is isotropic when correlation coefficient r[f(p), f(q)] depends only on the length $|p\vec{\ }q|$ of vector $p\vec{\ }q$, so:

$$r[f(p),\ f(q)] = r(|p\vec{\ }q|)\quad , \tag{155}$$

for each p, q ϵIR^n.

Equation 154 and Equation 155 are referred to as the correlation functions of the random field, f(p).

Their magnitude is calculated as:

$$|\vec{y}|^{\ 2} = \sum_{i,j=1}^{n} a_{ij}\, y_i\, y_j > 0\ , \tag{156}$$

when only $\vec{y} \neq o$; i.e., (a_{ij}) is a positive matrix of definite square form. The magnitude of Equation 156 is called the elliptical distance of points p and q, if:

$$\|p\ q\|^2 = \sum_{i,j=1}^{n} a_{ij}\,(u_i - v_i)\,(u_j - v_j) \quad , \tag{157}$$

where

$p = (u_1 \ldots,\ u_n)$, and $q = (v_1 \ldots,\ v_n)$.

Definition III. The random field, f(p), considered stationary, is called quasi-isotropic, if the correlation function, r[f(p), f(q)], depends only on the elliptical distance, i.e.:

$$r[f(p),\ f(q)] = r(\|p\ q\|) \ . \tag{158}$$

The random field, f(p), is called continuous if:

$$\lim_{\vec{pq} \to 0} r[(p\ q)] = 1 \quad , \tag{159}$$

where (p, q) represents:

$$|\vec{p\,q}| \quad \text{or} \quad \|\vec{p\,q}\| \quad .$$

The definitions presented above should be regarded as approximate; i.e., they are correct but simplified and not addressed to mathematicians. More precise definitions can be found in supplements to this report.

Various problems can be solved by this model. The following integral is usually estimated:

$$V(D) = {}_{D}\, f(p)\ \ dp \ , \tag{160}$$

where

$dp = dx\ dy$, or:

$$V(D) = \frac{1}{|D|}\int_D f(p)\ dp \qquad\qquad 0 < |D| < \infty \ . \tag{161}$$

V(D) is called the integral or mean value of the characteristic in set D. The estimators of Equation 161 are:

$$M_1(D) = c_1\ f_1 + \ldots . + c_m\ f_m \quad , \tag{162}$$

but $c_1 + \ldots . + c_m = 1$ and the non-negative constants, c_i $(i = 1, \ldots,\ n)$, are selected so that:

$$s_1^2 = \min_{c_1 \ \ldots .\ \ c_m} E\ [c_1\ f_1 + \ldots . + c_m\ f_m - M(D)]^2 \quad , \tag{163}$$

$$E\,[c_1\, f_1 + \ldots + c_m\, f_m] = E[M(D)] \quad , \qquad (164)$$

and

$$M_2(D) = c[f_1 + \ldots + f_m] \quad . \qquad (165)$$

Then when Equation 164 is satisfied:

$$s_2^2 = E[c(f_1 + \ldots + f_m) - M(D)]^2 \quad . \qquad (166)$$

The expected value is designated E.

The best estimator of Equation 161 is an arithmetic value, $M_2(D)$, expressed by Equation 165. The main element of the random field is its correlation function. Bochner and Chinczyn proved that the correlation function of a stationary random field satisfies the integral equation:

$$r(\vec{x}) = \int_{IR^n} \exp[i(\vec{u} \mid \vec{x})] \; dF(\vec{u}) \quad , \qquad (167)$$

where

$(\vec{u}\;\vec{x})$ is a scalar product of the vectors, $\vec{u}$ and $\vec{x}$, and $F(\vec{u})$ is a distribution function of an n-directional random vector.

It was proven that the following functions can be correlation functions of either isotropically or quasi-isotropically stationary random fields:

$$r(\vec{x}) = \exp \; -A\|\vec{x}\|^{2^{-k+1}} \quad , \text{ and} \qquad (168)$$

$$r(\vec{x}) = \frac{1}{1 + A\,\|\vec{x}\|^{2^{-k+1}}} \quad , \qquad (169)$$

where

$k = 0, 1, 2, \ldots \; A > 0.$

Equations 168 and 169 are correlation functions of isotropic fields when $\|\vec{x}\| = \|\overrightarrow{pq}\|$ and correlation functions of quasi-isotropic fields when $\|\vec{x}\| = \|\overrightarrow{pq}\|$, where $\|\overrightarrow{pq}\|$ is given by Equation 157.

The correlation function of a random field is regarded as a function that equalizes the correlation coefficients calculated between states of the field but is chosen from the class defined by Equation 168.

The correlation coefficients between states of random fields are estimated with magnitude ρ_{ij}, which is calculated from the following equation:

$$\rho_{ij} = \frac{\frac{1}{n}\sum_{1}^{n}\left[f_k^{(i)}(p) - m\right]\left[f_k^{(j)}(p) - m\right]}{\sqrt{\frac{1}{n^2}\left\{\sum_{1}^{n}\left[f_k^{(i)}(p) - m\right]^2\right\}\left\{\sum_{1}^{n}\left[f_k^{(j)}(p) - m\right]^2\right\}}} , \qquad (170)$$

where

$f_k^{(i)}(p)$ and $f_k^{(j)}(p)$ are values of the random field in states i and j of the random field, respectively.

The values of the random field are thus separated by a distance of $|\vec{pi\,pj}|$.

Coefficients of ρ_{ij} are equalized by Equations 168 and 169 by application of the method of maximum likelihood.

The following function is minimized with respect to A and K (see Equations 168 and 169):

$$Q = \frac{1}{N}\sum_{1}^{N}\left[r\left(\left|\overrightarrow{p_i\,p_j}\right|\right) - \rho_{ij}\right]^2 \quad . \qquad (171)$$

The correlation function governs the random field (which is stationary). This primary function can be used to evaluate the probability density of the random field.

With knowledge of the correlation function of the random field, the best samples are, in order: random, stratified, and systematic. According to a previous paper, the worst sample is the random sample. For the sample points that are somewhat "distant," the stratified sample is better than the systematic sample. For more "distant" points, the best sample is the systematic sample.

From the best sample the regression curves (i.e., analytically describing the relationships occurring between filtration parameters) can be plotted. Let the parameters be: dust collection efficiency: E; face velocity, q_g; dust loading of the filtration area, q_p; the structure covered with dust, L_o; filtration time, t_F; and the initial dust concentration, c_i. The regression curves are understood as follows: let $f_i(p_j)$ $(i = 1,\ldots,s,\ j = 1,\ldots,m)$ be a value of the random field, $f_i(p)$, describing the i filtration parameter through the fabric at point p_j. The following coordinates can be determined:

$$\begin{cases} m_{\ell k}[f_k(p_j)] = E[f_\ell(p) \mid f_k(p) = f_k(p_j)] = \sum_j f_\ell(p_i)\, \dfrac{p_{ij}}{p_j} \\ \\ m_{k\ell}[f_\ell(p_j)] = E[f_k(p) \mid f_\ell(p) = f_\ell(p_j)] = \sum_j f_k(p_j)\, \dfrac{f_{ij}}{p_j} \end{cases} \quad , \tag{172}$$

where

$$p_{ij} = p[f_\ell(p) = f_\ell(p_i),\ f_k(p) = f_k(p_j)] \quad \text{, and}$$

$$p_i = \sum_j p_{ij},\ p_j = \sum_i p_{ij} \quad .$$

From Equation 172, two sets of points are obtained:

$$f_\ell(p) = m_{\ell k}[f_k(p_j)] \text{ and } f_k(p) = f_k(p_j) \quad \text{, and} \tag{173}$$

$$f_\ell(p) = f_\ell(p_j) \text{ and } f_k(p) = m_{k\ell}[f_\ell(p_j)] \quad , \tag{174}$$

which determine regression curves of random fields, $f_k(p)$ and $f_1(p)$. Because the random fields, $f_k(p)$ and $f_\ell(p)$, are continuous, Equation 172 is considered an estimator of expressions:

$$\begin{cases} m_{\ell k}\ [f_k(p)] = \displaystyle\int_{IR^n} f_\ell(p)\, \frac{f[f_\ell(p),\ f_k(p)]}{f_2[f_k(p)]}\, dp \\ \\ m_{k\ell}\ [f_\ell(p)] = \displaystyle\int_{IR^n} f_k(p) \frac{f[f_\ell(p),\ f_k(p)]}{f\ [f_\ell\ (p)]}\, dp \end{cases} \quad , \tag{175}$$

where

$f[f_\ell(p),\ f_k(p)]$ is a density of the random variable $[f_k(p),\ f_\ell(p)]$, and

$$\begin{cases} f_1[f_\ell(q)] = {}_{IR^n} f[f_\ell(q),\ f_k(p)]dp \\ f_2[f_k(p)] = {}_{IR^n} f[f_\ell(p),\ f_k(q)]dp \end{cases} \quad , \tag{176}$$

where

n is a space dimension in which random fields, $f_k(p)$, are placed.

Determination of regression curves involves the following procedure: the sets of point pairs $[f_\ell(p_i),\ f_k/p_j]$ ($\ell, k = 1,\ldots,s;\ i,j = 1,\ldots,m$) plot the curves. The curves plotted in the coordinate system identify the class of the curve. Because the regression curves satisfy the condition of minimalization, the procedure for determining optimum regression curves minimizes Equation 171, where $r\ (|\overrightarrow{p_i\ p_j}|)$ is replaced by $f_k(p_j)$ and q_{ij} by the curve with its general parameters.

Thus, Equation 171 takes the following form:

$$Q = \frac{1}{N} \sum_{j=1}^{n} [f_k(p_j) - K\ (A_1,\ldots,\ A_r,\ p_j)]^2 \quad , \tag{177}$$

where

$K\ (A_1,\ldots,\ A_r,\ p_j)$ is a curve depending upon parameters $A_1,\ldots\ A_r$ at point p_j.

Equation 177 is minimized because of the procedure by which parameters $A_1,\ldots,\ A_r$ are calculated.

The above method for calculating regression curves is called the method of maximum likelihood. The curve obtained through this method can be proven to be the most probable relationship between the parameters fitted.

The above discussion illustrated the determination of only one regression curve. Usually we are interested only in this equation, so the second curve is not determined.

MODEL APPLICATION TO FABRIC FILTRATION

Empirical data obtained from large-scale testing are given in Table B-35. Dust collection efficiency, E, is listed in column 1. Face velocity, q_g; dust flux, q_p, the terminal dust load, L_o(g/m^2); the steady state residual dust load, L_N (g/m^2); the dust cake, L_p (g/m^2); filtration time, t_F; and initial dust concentration, c_i (g/m^3); are contained in columns 2 through 8. Tests were conducted for fabrics ET-30 and ET-4.

The following notations were introduced: $x_2 = q_g$, $x_3 = q_p$, $x_4 = L_o$, $x_5 = L_N$, $x_6 = L_p$, $x_7 = t_F$, and $x_8 = c_i$. The efficiency, E, is assumed to depend on $x_2,\ldots,x_8$ according to:

$$E = 1 - \exp\ [-\ f(x_i)] \quad , (i = 2,\ldots,8) \quad . \tag{178}$$

As a result, random variables $x_2,\ldots,x_8$ are assumed to be independent (this assumption is a simplification).

When a Maclaurin series expansion is used for the terms of Equation 178,

$$f(x) = f(0) + \frac{f'(0)}{1!}x + \frac{f''(0)}{2!}x^2 + \ldots + \frac{f^{(n-1)}(0)}{(n-1)!}x^n + \frac{f^{(n)}(\theta x)}{n!}x^n \quad , \tag{179}$$

where

> The nth derivative is calculated at point θx, while all lower order derivatives are calculated at point 0, and when the first three terms are taken (the series is known to be converging), a parabola of the following form is obtained:

$$E = ax_i^2 + bx_i + c \quad . \tag{180}$$

This dependence of E on x_i is compared to the parabola obtained from Equation 177.

$$E = \acute{a}x_i^2 + \acute{b}x_i + \acute{c} \quad . \tag{181}$$

Equations $\acute{a}$ to $\acute{a}$, $\acute{b}$ to $\acute{b}$, and $\acute{c}$ to c yields the following curves:

For fabric ET-4,

$$E = -0.8 \times 10^{-2}x_2^2 - 0.3\text{x}10^2x_2 + 0.3 \times 10^4 \ ,$$

$$E = -0.9 \times 10^{-4}x_3^2 - 3x_3 + 0.3 \times 10^4 \ ,$$

$$E = -0.3 \times 10^{-3}x_4^2 - 66x_4 + 0.4 \times 10^5 \ ,$$

$$E = -0.2 \times 10^{-2}x_5^2 - 77x_5 + 0.2 \times 10^5 \ ,$$

$$E = -0.8 \times 10^{-3}x_6^2 - 89x_6 + 0.4 \times 10^4 \ ,$$

$$E = -0.02x_7^2 - 18x_7 + 0.14 \times 10^4 \ ,$$

$$E = -x_8^2 - 0.3 \times 10^5x_8 + 0.3 \times 10^6 \ , \text{ and}$$

For fabric ET-30, (182)

$$E = -0.9 \times 10^{-2}x_2^2 - 24x_2 + 0.3 \times 10^6 \ ,$$

$$E = -0.84 \times 10^{-4}x_3^2 - 2.4x_3 + 0.3 \times 10^4 \ ,$$

$$E = -0.33 \times 10^{-3}x_4^2 - 0.2 \times 10^3x_4 + 0.11 \times 10^6 \ ,$$

$$E = -0.4 \times 10^{-2}x_5^2 - 76x_5 + 0.15 \times 10^5 \ ,$$

$$E = -0.6 \times 10^{-3}x_6^2 - 418x_6 + 0.2 \times 10^6 \ ,$$

$$E = -0.2x_7^2 - 29x_7 + 0.22 \times 10^4 \ , \text{ and}$$

$$E = -x_8^2 - 0.14 \times 10^6x_8 + 0.14 \times 10^7 .$$

From Equation 182, the following are obtained:

$$E = 1 - \frac{1}{7}\Big[e^{-0.8 \times 10^{-2}\ x_2+1875^2} + e^{-0.9 \times 10^{4}\ x_3+1432^2}$$

$$+\ e^{-0.3 \times 10^{-3}\ x_4+1100^2} + e^{-0.2 \times 10^{-2}\ x_5+38500^2} \qquad (183)$$

$$+\ e^{-0.8 \times 10^{-3}\ x_6+640^2} + e^{-0.02\ x_7+900^2} + e^{-\ x_8+0.15^2}\Big].$$

for fabric ET-4, and

$$E = 1 - \frac{1}{7}\Big[e^{-0.9 \times 10^{-2} xz\ +1\ 333^2} + e^{-0.84 \times 10^{-4} x_3\ +\ 14285^2}$$

$$+\ e^{-0.33 \times 10^{-3} x_4\ +\ 30300^2} + e^{-0.4 \times 10^{-2} x_5\ +\ 9500^2} \qquad (184)$$

$$+\ e^{-0.6 \times 10^{-3} x_6+34830^2} + e^{-0.2x_7\ +\ 12.5^2} + e^{-x_8\ +4900^2}\Big],$$

for fabric ET-30.

Assuming that $E = x_1$, the correlation functions of random fields are determined accordingly:

$R(x_1) = \exp\ [-42.1|x_1|^{1/2}]$, fabric ET-4 (dust collection efficiency, E) , and

$R(x_1) = \exp\ [-690|x_1|^{1/2}]$, fabric ET-30 (dust collection efficiency, E) . (185)

$R(x_2) = \exp\ [\frac{3}{2}|x_2|^{1/2}]$, fabric ET-4 (face velocity, q_g) , and

$R(x_2) = \exp\ [-|x_2|^{1/2}]$, fabric ET-30 (face velocity, q_g.) . (186)

$R(x_3) = \exp\ [-\ \frac{1}{2}|x_3|^{1/2}]$, fabric ET-4 (dust loading of filtration area, q_p) , and

$R(x_3) = \exp\ [-0.4|x_3|^{1/2}]$, fabric ET-30 (dust loading of filtration area, q_p) .(187)

$R(x_4) = \exp\ [-1.7|x_4|^{1/2}]$, fabric ET-4 (structure covered with dust, L_o) , and

$R(x_4) = \exp\ [-|x_4|^{1/2}]$, fabric ET-30 (structure covered with dust, L_o) . (188)

$R(x_5) = \exp\ [-2|x_5|^{1/2}]$, fabric ET-4 (structure filled with dust, L_N) , and

$R(x_5) = \exp\ [-0.9|x_5|^{1/2}]$, fabric ET-30 (structure filled with dust, L_N) . (189)

$R(x_6) = \exp\,[-3.1\,|x_6|^{\frac{1}{2}}]$, fabric ET-4 (dust cake, L_p) , and

$R(x_6) = \exp\,[-3\,|x_6|^{\frac{1}{2}}]$, fabric ET-30 (dust cake, L_p) . (190)

$R(x_7) = \exp\,[-1.8\,|x_7|^{\frac{1}{2}}]$, fabric ET-4 (filtration time, F), and

$R(x_7) = \exp\,[-\,|x_7|^{\frac{1}{2}}]$, fabric ET-30 (filtration time), F . (191)

$R(x_8) = \exp\,[-15\,|x_8|^{\frac{1}{2}}]$, fabric ET-4 (initial dust concentration, c_i) , and

$R(x_8) = \exp\,[-0.6\,|x_8|^{\frac{1}{2}}]$, fabric ET-30 (initial dust concentration, c_i) . (192)

The function of the multiplex correlation for ET-4 is:

$$R(x_1,\ldots.,x_8) = \exp\left[-42.1\,|x_1|^{\frac{1}{2}} - \frac{3}{2}\,|x_2|^{\frac{1}{2}} - \frac{1}{2}\,|x_3|^{\frac{1}{2}} - 1.7\,|x_4|^{\frac{1}{2}} - 2\,|x_5|^{\frac{1}{2}} - 3.1\,|x_6|^{\frac{1}{2}} - 1.8\,|x_7|^{\frac{1}{2}} - 15.5\,|x_8|^{\frac{1}{2}}\right] . \qquad (193)$$

For ET-30 it is:

$$R(x_1,\ldots.,x_8) = \exp\left[-690\,|x_1|^{\frac{1}{2}} - |x_2|^{\frac{1}{2}} - 0.4\,|x_3|^{\frac{1}{2}} - |x_4|^{\frac{1}{2}} - 0.0\,|x_5|^{\frac{1}{2}} - 3\,|x_6|^{\frac{1}{2}} - |x_7|^{\frac{1}{2}} - 0.6\,|x_8|^{\frac{1}{2}}\right] ,$$

with x_i as an absolute value of x_i.

The full proofs of the theorems and conclusions, on which these models are based, can be found in the supplements to this report.

CONCLUSIONS

The model equations are valid within the ranges of the empirical data but should also be valid over other ranges. The assumption that random variables, $x_2,\ldots.,x_8$, are independent cannot be satisfied generally, but this assumption was necessary numerically. At this point in the research, these curves adequately describe the random field of dust collection efficiency.

Further work is proposed to define correlation equations between parameters, $x_1,\ldots.,x_8$, for improving these models. The correlation functions given in Equations 185 through 192 quickly assume values near 0, which means that clear structural changes could occur during dust filtration.

SECTION XI

ELECTROSTATIC PROPERTIES OF DUSTS AND FABRICS*

INTRODUCTION

Literature searches show that most research concerning filtration ignores electrostatic effects between dusts and fibers. Dust precipitation on fibers is usually explained by four mechanisms:

- Interception,
- Impaction,
- Gravitational sedimentation, and
- Diffusion.

Few publications address the electrical effects between dust particles and fibers.[16 31 32 33 34 35 36]

However, electrical effects during filtration and regeneration of the filtration medium should not be ignored because:

- Dust particles carried by a gas medium are always charged; when deposited, they pass an electrical charge to the filtration material.
- Dust particle deposition on fibers, their penetration into the filtration structure, and gas medium flow through this structure can cause electrification of the fibers and dust particles.
- Recombination and charge dissipation occurring together with electrification in a state of dynamic equilibrium may not lead to complete electrical neutralization of the filtration material. Accordingly, the filtration process occurs in the presence of an electric field formed between the filtration element and its housing and also of a strong local field in the pores of the filtration material.
- Removal of the dust layer during regeneration may increase the electrification of the filtration material.

DEFINITION OF FORCES BETWEEN DUST PARTICLES AND FIBERS BECAUSE OF ELECTROSTATIC PHENOMENA

Between a charged dust particle that carries charge q, and charged fibers, the following electrical forces exist:

---

*Prepared by Józef Malcher, Anna Sycińska-Trojniak, Anna T. Szaynok, and Ryszard Zuczkowski, Institute of Physics of Wrocław Polytechnic.

- Coulomb force:

$$F_c = q \cdot E \quad , \tag{195}$$

where

E is a local value of the electric field intensity.

For a single rectilinear cylindrical fiber charged uniformly with linear charge density Q_L[C/m], the coulomb force is radial and is given by:

$$F_c = \frac{q \cdot Q_L}{2\Pi\ \varepsilon_o \varepsilon \cdot x} \quad , \tag{196}$$

where

ε_o = permittivity of vacuum ($\varepsilon_o = 8.85 \times 10^{-12}$ F/m),
ε = dielectric constant (for air, $\varepsilon = 1$), and
x = distance between particle and fiber axis.

- Force F_p connected with particle polarization in the electric field. For a spherical particle of radius r placed in a nonhomogeneous electric field, the polarization force is expressed by the equation:

$$F_p = \frac{1}{2}\,\varepsilon_o\ \frac{\varepsilon_1 - \varepsilon}{\varepsilon_1 + 2\varepsilon}\ r^3 \text{ grad } E^2 \quad , \tag{197}$$

where

ε_1 = dielectric constant of the particle material ($\varepsilon_1 > 1$).

When the electric field formed by the above-mentioned charged single fiber is placed in air, the particle force becomes:

$$F_p = -\frac{Q_L{}^2 \cdot r^3}{4\Pi^2\ \varepsilon_o\ x^3} \cdot \frac{\varepsilon_1 - 1}{\varepsilon_1 + 2} \quad . \tag{198}$$

The negative sign means that the force, F_p, is attractive. When the particle is conductive, $\varepsilon_1 \to \infty$ and $\frac{\varepsilon_1 - 1}{\varepsilon_1 + 2} \to 1$.

- Force F_i of the "electric picture" of the particle in the fiber material. This force is fiber polarization caused by the charged particle. Force F_i can be expressed by a simple equation when the particle diameter and its distance, x, from the cylindrical fiber are small compared to the fiber radius. In this case, for the particle in air, the equation is:

$$F_i = -\frac{\varepsilon_2 - 1}{\varepsilon_2 + 1} \cdot \frac{q^2}{16\Pi\ \varepsilon_o\ x^2} \quad , \qquad (199)$$

where

ε_2 = dielectric constant of the fiber material ($\varepsilon_2 > 1$). Force F_i is also positive.

In studies[33 36] of electrical forces in filtration, simplified models are used because of the complexity of the problem. With the assumption that dust particles are not charged, the forces, F_c and F_i, are avoided. Local values of the electric field are calculated as the disturbances of a homogeneous external field caused by the insertion of a cylindrical fiber. The cylindrical fiber of the radius, R, is placed perpendicularly to the direction of the external electric field intensity, E, and is treated as a linear dipole with dipole moment, m_1, per unit length:

$$m_1 = \frac{1}{2}\varepsilon_o \frac{\varepsilon_2 - 1}{\varepsilon_2 + 1}\ R \cdot E \quad . \qquad (200)$$

Near the fiber dipole, the electric field is distorted because of the superposition of the external field and the dipole field. A neutral, spherical dust particle placed in this field experiences force, F_p, as expressed by Equation 197.

The effect of the electric field on filtration can be measured by the dimensionless coefficient, β. This coefficient is the ratio between the dust particle velocity attributable to the electric field at the cylinder surface and medium flow velocity, assuming the flow to be perpendicular to the cylinder axis. The coefficient is expressed as:

$$\beta = 2\varepsilon_o \frac{(\varepsilon_1 - 1)(\varepsilon_2 - 1)}{(\varepsilon_1 + 1)(\varepsilon_2 + 1)} \cdot \frac{E^2 r^2 u}{vR} \quad , \qquad (201)$$

where

v = medium flow velocity, and
u = mechanical mobility of the particle.

In the theory of filtration, the mobility of a spherical particle of radius, r, moving in a gas medium is described by the following empirical equation:

$$u = \frac{1 + A\frac{\lambda}{r} + B\frac{\lambda}{r}\exp\left(-C\frac{\lambda}{r}\right)}{6\Pi\mu \cdot r}, \qquad (202)$$

where

λ = the mean free path of the gas particles,
μ = gas viscosity coefficient, and
A, B, C = constants (A = 1.246, B = 0.42, and C = 0.87).

The collection efficiency for a single fiber is calculated as:

$$\eta = 0.5\,\beta \quad . \qquad (203)$$

In the case of a system of parallel fibers, the correction for the electric field distortion must be introduced to Equation 201:

$$E' = E\left(1 - \frac{\Pi\,\alpha}{4\sqrt{3}}\right)^{-1} \quad , \qquad (204)$$

where

α = fiber packing density.

With tightly packed fibers, fiber-to-fiber electrical interactions should be considered, which complicates the problem. For the simpler, symmetrical, parallel fiber systems, the spatial distribution of electrical forces can be calculated analytically.

Differential equations depicting dust particle motion under even the simpler parallel fiber case are still complicated and can only be solved numerically with a digital computer.[36] Two such problems are solved in Reference 33:

- Case a: electric field oriented perpendicular to the gas flow, and
- Case b: electric field oriented parallel to the gas flow.

In case a, the maxium flow velocity occurs in regions where the electrical forces favor particle collection. Enhanced particle reentrainment then negates the improved collection efficiency introduced by the electrical forces. In case b, however, the electrical forces collect particles on the leading and trailing edges of the fiber where the entrainment forces are lowest. Case b therefore maximizes the effect of electrical forces on the process.

The complex field distribution between the fibers of an actual filtration structure leads to the assumption that conditions similar to those in case b will be partly satisfied, which will create a smaller electrical effect on dust collection efficiency than that considered in studies of ideal models.

Experimental results[33 35] confirm the increase of dust collection efficiency in actual structures resulting from application of an external electric field.

The primary reasons for not considering electrical effects in the filtration process are the theoretical problems in extending ideal models to actual systems and the lack of experimental data concerning the electrical properties of dusts and filtration materials under operating filtration conditions. However, future work cannot disregard these important effects. Correct correlation of electrostatic phenomena and known filtration mechanisms is the only way to increase dust collection efficiency in actual dry filtration processes.

ELECTRICAL PROPERTIES OF INDUSTRIAL DUSTS AND FILTRATION MATERIALS

For determining the effect of electrical forces during filtration, it is necessary to understand the electrical interactions between the fibers and the dust. The value and sign of dust particle charge, the degree of fiber electrification, the rate of accumulation and decay of fiber charge, and the ability to conduct electrical charges must be known for the fiber/fiber, dust/dust, and fiber/dust systems.

Thus, research conducted by the Institute of Physics of Wrocław Polytechnic, under the direction of Dr. Anna Szaynok, included the following problems:

- Determination of the electrical properties of industrial dusts,
- Determination of the electrical properties of filtration materials, and
- Study of the dust-fabric system.

Results of this research are contained in the phase II report of Project 5-533-3 and were published[37] [38] and presented at both international and domestic meetings. A brief recap of these results follows.

Determination of the Electrical Properties of Industrial Dusts

Cement, fly ash, coal, talc, lime, bituminous meal, and dusts from cement rotary kilns were the subject of this research.

The research program included the following measurements:

- The dependence of dust electrification on dust particle diameter, contact with various materials, and degree of ionization of the atmosphere. Measurement was taken according to the Kunkel and Hansen method, which permits measurement of the sign and value of charge and the size of a single dust particle.
- Dust resistivity as a function of pressure, humidity, temperature, and electric field intensity. Resistivity is measured by a method that permits the pressure of the dust to be controlled and changed.
- Dust resistivity as a function of humidity and temperature under conditions of assumed compression. Measurements were taken in a specially designed chamber that provided a constant volume of measurement space.

A detailed description of the methods and results is contained in the phase II report of Project P-533-3. The experiments led to the following conclusions:

- Electrical charge distribution on dust particles has normal distribution.
- The mean and standard deviation of both the positive and negative dust charge increase linearly with increasing particle diameter over the range of 5 to 15 μm.
- Regarding standard deviation as a measurement of dust electrification, coal dust shows the highest electrification and cement dust the lowest.
- In test dust clouds, a slight excess of charges of the same sign is noted. The sign and magnitude of this excess depend on the conditions under which the dust is generated. The arithmetic mean charge, $\bar{q}$, is considered a measurement of the excess charges of the same sign.
- Dust contact with different materials (metal or porcelain) causes σ and $\bar{q}$ to vary. Contact with procelain causes an increase and contact with metal cause a decrease in standard deviation.

- Increased concentration of ions in the atmosphere, resulting from spark discharge or exposure to ultraviolet radiation, increases the electrification of dust previously weakly electrified (cement) and decreases the electrification of dust previously strongly electrified (coal).
- Resistivity of dust layers depends strongly on pressure. At low pressures (about 10^6 N/m^2), decreased resistivity with increasing pressure is clearly observed, but for pressures above 2×10^6 N/m^2, resistivity is constant.
- The resistivity of dust layers depends on the electric field intensity at which it is measured, so its magnitude does not uniquely determine the electrical properties of the materials.
- The resistivity of dust layers depends on humidity and temperature. Increased temperature increases resistivity, but increased humidity decreases resistivity.
- Coal dusts show the highest resistivity, cement dust shows a lower resistivity, and dusts from electrostatic precipitators show the lowest resistivity.

Determination of Electrical Properties of Filtration Materials

Polyester, polyamid, and glass fiber fabrics were examined. Some fabrics were finished with silicone or graphite.

The following measurements and examinations were made:

- Measurement of volume resistivity, ρ_α, and surface resistance of unit fabric area, R_s, in a measurement configuration having a flat electrode system with a protective ring. The measurement was conducted at different electric field intensities. The effects of electrode pressure and humidity upon resistivity were examined.
- Measurement of fabric surface resistivity, ρ_1, using jaw electrodes under conditions of assumed humidity.
- Measurement of static dielectric constant for selected high-resistivity fabrics. Measurements were made by the methods of charge accumulation and linear increase of voltage.
- Study of fabric charge decay curves, U(t), by the method of condenser self-discharge.

Methods and measurement results are included in the phase II report of Project 5-533-3.

These experiments led to the following conclusions:

- Volume resistivity of filtration fabrics does not depend upon the intensity of the electric field up to 2 000 V/cm.
- Volume resistivity decreases with increased pressure caused by the electrodes. Constant resistivity is observed for pressures higher

than 10^5 N/m^2. After the pressure is released, hysteresis on the order of 10 to 15 percent exists.

- Values of fabric ρ_d, R_s, and ρ_L decrease as air humidity increases. Air humidity had the smallest influence on polyester fabrics and the largest on glass fabrics, which proves that electrical conduction for fibrous materials is superficial.
- Measurements of fabric R_s and ρ_1 for known fibers depend upon the structure, finishing, and materials used for impregnation.
- At an assumed air relative humidity (of 51 percent and an ambient temperature between 20° and 23° C), measured values of R_s and ρ_1 characterize the resistivity properties of a given kind of filtration material.
- When measured values of R_s and ρ_1 increase with time with a tendency to stabilize, two measurement values are usually enough--a first after 60 seconds, and a second after 600 seconds. This phenomenon was observed for some unwoven fabrics.
- Static dielectric constant for the examined fabrics ranged between 1.2 (polyester fabrics) and 5.8 (glass fabrics).
- Curves, U(t), obtained by the capacitor self-discharge method (through the fabric) were not usually exponential.

Study of Dust-Fabric Systems

Dust-fabric systems were examined based on materials and measurement results described above. The following examinations and measurements were conducted:

- Examination of voltage decay curves, U(t), on fabrics covered by layers of dusts (by the capacitor self-discharge method);
- Measurement of charge buildup on filtration fabrics during dusty air flow using various dusts and concentrations and at different flow velocities; and
- Measurement of charge accumulation on fabrics after dust layer removal.

The methods and results of the measurement of voltage decay on fabrics covered with dust layers are discussed in the periodical report under phase II of Project 5-533-3.

The measurement of charge accumulation on filtration fabrics both during air flow (regarded as the dispersion medium) and at the moment of dust cake removal from the fabric surface was the subject of the last phase of this project. The measurement of charge buildup on the fabric during air flow was conducted on a special stand (see Figure 173). This stand includes:

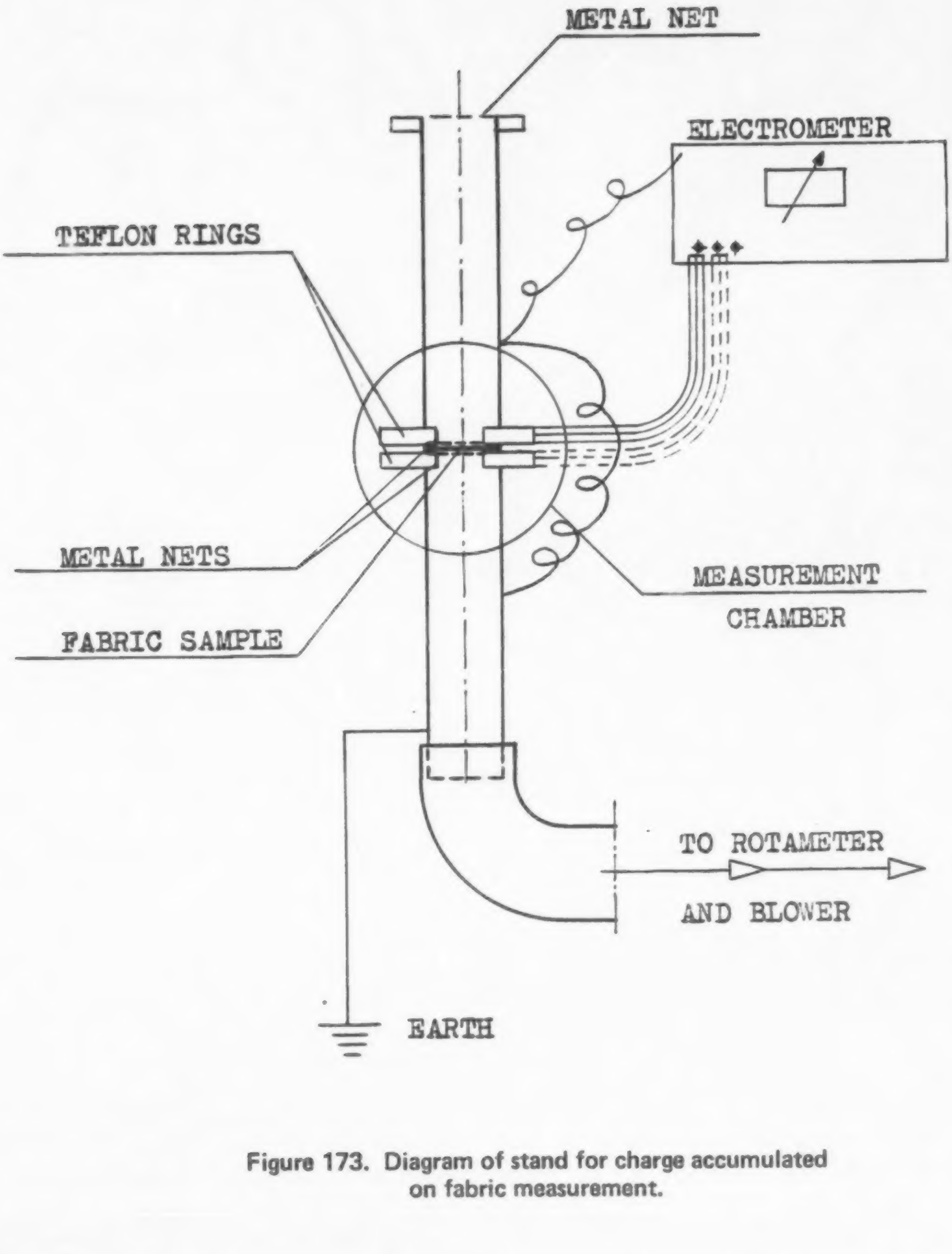
METAL NET
ELECTROMETER
TEFLON RINGS
METAL NETS
FABRIC SAMPLE
MEASUREMENT CHAMBER
TO ROTAMETER AND BLOWER
EARTH

Figure 173. Diagram of stand for charge accumulated on fabric measurement.

- A vertical metal pipe with a metal net in its upper part, a measurement chamber in its middle part, and an outlet air duct in its lower part;
- A rotameter for measuring air flow;
- A suction air blower with regulated rotation; and
- An electrometer for measuring electrical charge.

The dusty air flows through the pipe and rotameter connected with the blower. The required air flow velocity through the filtration fabric is obtained by regulating blower rotation. Air flow velocity is measured with the rotameter. A dust sample of known weight is put on the metal net in the upper part of the pipe to achieve the required dust concentration.

The measurement chamber consists of two teflon rings that hold the round fabric sample. During dusty air flow the dust is collected on the fabric. The measurement chamber is screened for protection from external electric fields, which can disturb the measurement. The fabric is placed between two metal nets connected to the duct to carry away the electric charge accumulated on the fabric. An electrometer shows the value of the accumulated electric charge given by the dust collected on the filtration fabric.

Typical charge measurements are on the order of 10^{-8} to 10^{-9} coulombs. The capacitance of the measurement system is about 100 pF, introducing an error of 1 to 10 percent, respectively. But because the measurement scatter usually exceeds 10 percent for the individual measurement, the error resulting from this capacitance was neglected. Each measurement of charge for a certain fabric, at a given flow velocity and dust type and concentration, was repeated two to four times, depending upon the repeatability of the results. The filtration fabric area, on which dust is precipitated during measurement, amounted to 20.42 cm^2. The measured values of charge (C) are for this fabric area, from which a charge density is calculated (C/cm^2).

Measurements were conducted on the following separated dusts: talc, coal, cement, and fly ash. The following fabrics were used: polyester (ET-1 and ET-30) and glass (ST-13 and FL-14). Tables 45 to 48 show the mean values of the charge measurements. The measurement scatter forming the mean value ranged from 0 to 50 percent, depending upon the kind of dust. Measurements conducted for talc, cement, and fly ash were more easily repeated than those of coal dust.

TABLE 45. CHARGE ACCUMULATING ON FILTRATION FABRICS DURING DUSTING WITH TALC AIR FLOW

Initial concentration (g/cm^3)	q_g (m^3/m^2h)	Kind of fabric							
		ET-1		ET-30		ST-13		FL-14	
		q $(10^{-9}$ C)	q/f $(10^{-10}$ C/cm$^2)$	q $(10^{-9}$ C)	q/f $(10^{-10}$ C/cm$^2)$	q $(10^{-9}$ C)	g/f $(10^{-10}$ C/cm$^2)$	q $(10^{-9}$ C)	q/f $(10^{-10}$ C/cm$^2)$
10	60	-1.25	-0.61	-0.41	-0.20	-0.525	-0.25	-1.65	-0.80
	120	-1.83	-0.84	-2.11	-1.03	-0.615	-0.30	-1.65	-0.80
	180	-2.15	-1.05	-1.30	-0.63	-0.58	-0.28	-1.82	-0.89
	300	-2.30	-1.12	-2.10	-1.02	-1.67	-0.81	-1.60	-0.78
30	60	-1.88	-0.92	-3.08	-1.50	-0.72	-0.35	-3.40	-1.62
	120	-4.80	-2.35	-3.00	-1.46	-1.20	-0.58	-3.30	-1.61
	180	-5.10	-2.49	-3.35	-1.64	-1.70	-0.83	-3.55	-1.73
	300	-3.20	-1.12	-5.25	-2.57	-3.60	-1.76	-4.00	-1.95

TABLE 46. CHARGE ACCUMULATING ON FILTRATION FABRICS DURING DUSTING WITH CEMENT AIR FLOW

Initial concentration (g/cm^3)	q_g (m^3/m^2h)	Kind of fabric							
		ET-1		ET-30		ST-13		FL-14	
		q (10^{-9} C)	q/f (10^{-10} C/cm^2)	q (10^{-9} C)	q/f (10^{-10} C/cm^2)	q (10^{-9} C)	g/f (10^{-10} C/cm^2)	q (10^{-9} C)	q/f (10^{-10} C/cm^2)
10	60	-1.75	-0.85	-2.215	-0.129	-0.525	-0.25	-0.65	-0.32
	120	-2.02	-0.98	-0.27	-0.13	-0.615	-0.30	-0.706	-0.345
	180	-3.15	-1.54	-0.125	-0.06	-0.58	-0.28	-0.65	-0.32
	300	-3.03	-1.48	-2.60	-1.27	-1.67	-0.81	-1.025	-0.50
30	60	-4.15	-2.03	-0.46	-0.22	-0.72	-0.35	-1.96	-0.96
	120	-5.25	-2.57	-0.75	-0.36	-1.20	-0.58	-1.80	-0.88
	180	-3.80	-1.86	-1.23	-0.60	-1.70	-0.82	-2.00	-0.98
	300	-4.10	-2.00	-6.05	-2.96	-3.60	-1.76	-3.40	-1.60

TABLE 47. CHARGE ACCUMULATING ON FILTRATION FABRICS DURING DUSTING WITH FLY ASH AIR FLOW

Initial concen-tration (g/cm^3)	q_g (m^3/m^2h)	Kind of fabric							
		ET-1		ET-30		ST-13		FL-14	
		q $\left(10^{-9}\ C\right)$	q/f $\left(\begin{matrix}10^{-10}\\ C/cm^2\end{matrix}\right)$	q $\left(\begin{matrix}10^{-9}\\ C\end{matrix}\right)$	q/f $\left(\begin{matrix}10^{-10}\\ C/cm^2\end{matrix}\right)$	q $\left(\begin{matrix}10^{-9}\\ C\end{matrix}\right)$	g/f $\left(\begin{matrix}10^{-10}\\ C/cm^2\end{matrix}\right)$	q $\left(\begin{matrix}10^{-9}\\ C\end{matrix}\right)$	q/f $\left(\begin{matrix}10^{-10}\\ C/cm^2\end{matrix}\right)$
10	60	-0.60	-0.29	-1.65	-0.80	-1.52	-0.74	-2.32	-1.13
	120	-0.70	-0.34	-1.65	-0.80	-1.72	-0.84	-2.25	-1.10
	180	-1.07	-0.52	-2.10	-1.02	-2.12	-1.03	-2.60	-1.27
	300	-1.85	-0.90	-3.17	-1.55	-2.95	-1.44	-3.45	-1.68
30	60	-1.45	-0.71	-3.96	-1.93	-3.45	-1.68	-5.70	-2.79
	120	-2.25	-1.10	-4.15	-2.03	-3.83	-1.87	-5.70	-2.79
	180	-3.15	-1.54	-4.35	-2.13	-4.80	-2.35	-5.90	-2.88
	300	-6.00	-2.93	-8.20	-4.01	-7.50	-3.67	-8.15	-3.99

TABLE 48. CHARGE ACCUMULATING ON FILTRATION FABRICS DURING DUSTING WITH COAL AIR FLOW

Initial concentration (g/cm³)	q_g (m³/m²h)	Kind of fabric							
		ET-1		ET-30		ST-13		FL-14	
		q $(10^{-9}$ C)	q/f $(10^{-10}$ C/cm²)	q $(10^{-9}$ C)	q/f $(10^{-10}$ C/cm²)	q $(10^{-9}$ C)	g/f $(10^{-10}$ C/cm²)	q $(10^{-9}$ C)	q/f $(10^{-10}$ C/cm²)
10	60	-0.90	-0.44	-2.35	-1.15	-0.52	-0.25	-1.45	-0.71
	120	-2.15	-1.05	-1.05	-0.51	-0.86	-0.42	-4.15	-2.03
	180	-0.50	-0.24	-1.26	-0.61	-0.20	-0.097	-0.38	-0.18
	300	-0.70	-0.34	-3.25	-1.59	-1.65	-0.81	-3.90	-1.90
30	60	-0.90	-0.44	-2.10	-1.02	-0.32	-0.15	-2.45	-1.19
	120	-1.70	-0.84	-1.70	-0.83	-0.35	-0.17	-5.00	-2.44
	180	-0.50	-0.24	-1.95	-0.95	-1.10	-0.53	-0.72	-0.35
	300	-	-	-6.50	-3.18	-2.95	-1.44	-5.10	-2.49

The measurement of charge accumulation on filtration fabrics during dust cake removal from the fabric surface was also conducted on the stand (see Figure 173) described above. To make this measurement, a certain amount of dust is put on the fabric sample and distributed uniformly on its surface. Next, any existing electrical charge is taken away by connecting both sides of the material with earthed metal electrodes. After the electrodes are removed, the measurement chamber is placed on the stand where it remains 0.5 hour to achieve a state of electrical equilibrium. Then, after the electrometer, the recorder, and the blower are turned on, the measurement is taken. Just after the blower is switched on, the dust cake from the fabric comes off and the electrometer indicates the charge remaining on the fabric. Even with a long period of blower operation (30 s), the charge does not alter.

For fabrics ET-4 and ET-30, the time required for the charge to reach equilibrium is several tens of seconds. This time depends not on air flow but on fabric resistivity.

Cement, hydrated lime, bituminous meal, and coal were measured and 0.1, 0.2, 0.5, and 1 g of dust were placed on the surface of the filtration material. The surface area contacted with dust was 20 cm^2. The tests concerned polyester fabrics ET-4 and ET-30. Measurement results contained in Table 49 and Table 50 lead to the following conclusions:

- The presence of dust on the fabric alters, to varying degrees, the shape of the U(t) curves obtained for clean fabrics. Variations did not depend linearly upon dust resistivity.
- For fabrics of high surface resistance, R_s (above 10^{14} Ω cm^2), the presence of dust always caused a faster capacitor discharge.
- The electrical charge accumulated on the fabric increased with increasing dust concentration and increasing dusty air flow velocity. In some cases, the increase was linear.
- Clean air flow did not appear to change fabric charge.
- Electrical charges collected on polyester and glass fiber fabrics were always negative.
- Change of fabric or dust affected the value of accumulated charge, but the changes were not great, never exceeding one order of magnitude.
- In most cases, the value of the accumulated charge increased as the amount of dust removed from the fabric increased.

TABLE 49. ELECTRIC CHARGE ACCUMULATING ON FABRIC ET-4 AT THE MOMENT OF DUST CAKE REMOVAL FROM FABRIC SURFACE

	Electric charge (10^{-9} coulomb) for quantity of dust				
Kind of dust	0.1 g	0.2 g	0.5 g	1.0 g	1.5 g
Cement - batch I*	-	-3.80	-7.40	-9.70	-13.7
Cement - batch II	-1.40	-3.00	-5.50	-7.30	-
Hydrated lime - batch I	-15.00	-19.20	-11.50	-13.30	-
Hydrated lime - batch II	-9.20	-14.10	-21.50	-16.80	-
Bituminous meal - batch I	+1.10	+2.30	+3.90	+7.00	-
Bituminous meal - batch II	+0.28	+1.03	+1.40	+1.15	-
Coal - batch I	+0.92	+3.70	+6.00	+6.40	-
Coal - batch II	+1.74	+3.60	+5.80	+8.20	-

*Dusts of batch I were preserved a long time.

TABLE 50. ELECTRIC CHARGE ACCUMULATING ON FABRIC ET-30 AT THE MOMENT OF DUST CAKE REMOVAL FROM FABRIC SURFACE

	Electric charge (10^{-9} coulomb) for quantity of dust				
Kind of dust	0.1 g	0.2 g	0.5 g	1.0 g	1.5 g
Cement - batch I*	-	-2.90	-7.50	-10.50	-9.70
Hydrated lime - batch II	-13.50	-8.30	-14.30	-14.30	-
Bituminous meal - batch I	+1.80	+1.30	+3.00	+3.70	-
Coal - batch I	+3.20	+3.10	+4.50	+9.20	-

*Dusts of batch I were preserved a long time.

- Values and signs of accumulated charge after dust layer removal differed for various dust-fabric systems. Results obtained for the same dust-fabric system were easily repeated.
- Time of charge flow from fabric to the electrometer (after dust layer removal) was longer for fabrics with higher resistivity.

FINAL REMARKS AND DISCUSSION OF FURTHER RESEARCH

After research and compilation of results, the following conclusions can be made:

- Fabric electrification during filtration is connected to electric charge transfer in the dust particle-fiber system and to generation of charges in these systems triboelectrically. The effect of the carrying medium movement on electrification is minimal.
- The value of excessive electric charge accumulated on a fabric in a state of equilibrium is correlated with the resistive (ρ, ρ_L, and R_s) and dielectric (ε_s) properties of the fabrics and dusts. High values of accumulated charge correspond to high values of ρ, ρ_L, R_s, and ε_s.
- Parameters ρ, ρ_L, R_s, and ε_s will be reliable when they are determined appropriately at specified values of electric field intensity, temperature, and humidity.
- The appropriate method for determining dust resistivity is the method that assumes a constant degree of compression. If the dust layer electric conduction is assumed to increase as areal contact increases between dust particles, the degree of layer compression expressed by the ratio, $\Delta V/V$ (where V is the volume of the layer after compression and ΔV is the volume loss resulting from compression), measures this areal increase. Measurement of resistivity for different dusts with assumed pressure gives various uncontrolled degrees of compression, which leads to inconsistent values of resistivity.
- Measurement of the static dielectric constant of fabrics or dust-fabric systems should be conducted by the method of accumulation or the method of linear intensity increase because of slow polarization effects in these materials.

Electric microfields formed triboelectrically between charged fibers and oppositely charged dust particles precipitated on the filter play a more important role than the field created by excess charges. Electric microfields are strong nonhomogeneous electric fields with short ranges; their presence can be marked by uniformly distributed dust particles and fibers. In these fields even neutral dust particles are influenced by electric forces, according to Equation 197. The difficulties of dust layer removal during regeneration and of the high charge remaining on the filter after dust layer removal prove that these fields exist.

Thus, determining the effect of measured parameters, σ, $\bar{q}$, ρ, ρ_L, R_s, and ε_s, that characterize the electrical properties of dusts and fabrics, on filtration performance is not a simple problem. The number of parameters considered must be larger. Because of theoretical difficulties, further experimental research and model development are necessary. The following problems appear most important:

- Study of the effect of parameters σ and $\bar{q}$ on the value of the excessive charge accumulated on the filter;
- Study of the kinetic electrical charge in the filtration material;
- Study of the triboelectric mechanism of dust-fabric system electrification and its description by measurable parameters;
- Determination, by modeling studies, of the relative importance of coulomb force, F_c; polarization, F_p; and "picture" force, F_i; in the filtration process;
- Study of electric field distribution in model and real dust-fabric systems; and
- Development of contactless methods for measuring the electrical properties of dusts and fabrics.

The above studies will help researchers overcome difficulties that impede fuller understanding of electrostatic effects in the filtration process and develop improved dust collection devices.

SECTION XII
ADDITIONAL WORK

INTRODUCTION

For this project, the Institute had access to a helium-air pycnometer* for determining absolute dust density. In Poland, absolute dust density is determined by the liquid pycnometer, according to Polish Standard PN-74/Z-04002/01. These two methods of determining dust density were compared for accuracy. Measurements were conducted by the Laboratory of Physico-Chemical Dust Properties of Instytut Przemysłu Wiążących Materiałów Budowlanych (IPWMB) in Opole under the direction of J. Zareba, MSc, who also statistically analyzed the results.

MEASUREMENT CONDITIONS

Cement, coal, and talc were selected for measurement because of their different chemical and granulometric composition.

The mean pulverization according to the median particle size distribution of the selected dusts was:

- Unseparated portland cement "250" - d_{50} = 30 μm,
- Unseparated coal dust - d_{50} = 22 μm,
- Unseparated coal dust - d_{50} = 49 μm,
- Unseparated coal dust - d_{50} = 7.0 μm, and
- Technical talc (fraction < 20 μm) d_{50} = 9.0 μm.

Granulometric composition of the above dusts is illustrated in Figure 174.

Lighting kerosene "Prymusówka" produced in Poland was used as a pycnometric liquid for measurement with a liquid pycnometer. Measurements were conducted at a temperature of 20° C ± 2° C. The sample was weighed on an analytical balance with an accuracy of ±0.0002 g.

---

*Model 1302, manufactured by the Micrometrics Instrument Corporation, Coulter Electronics Limited.

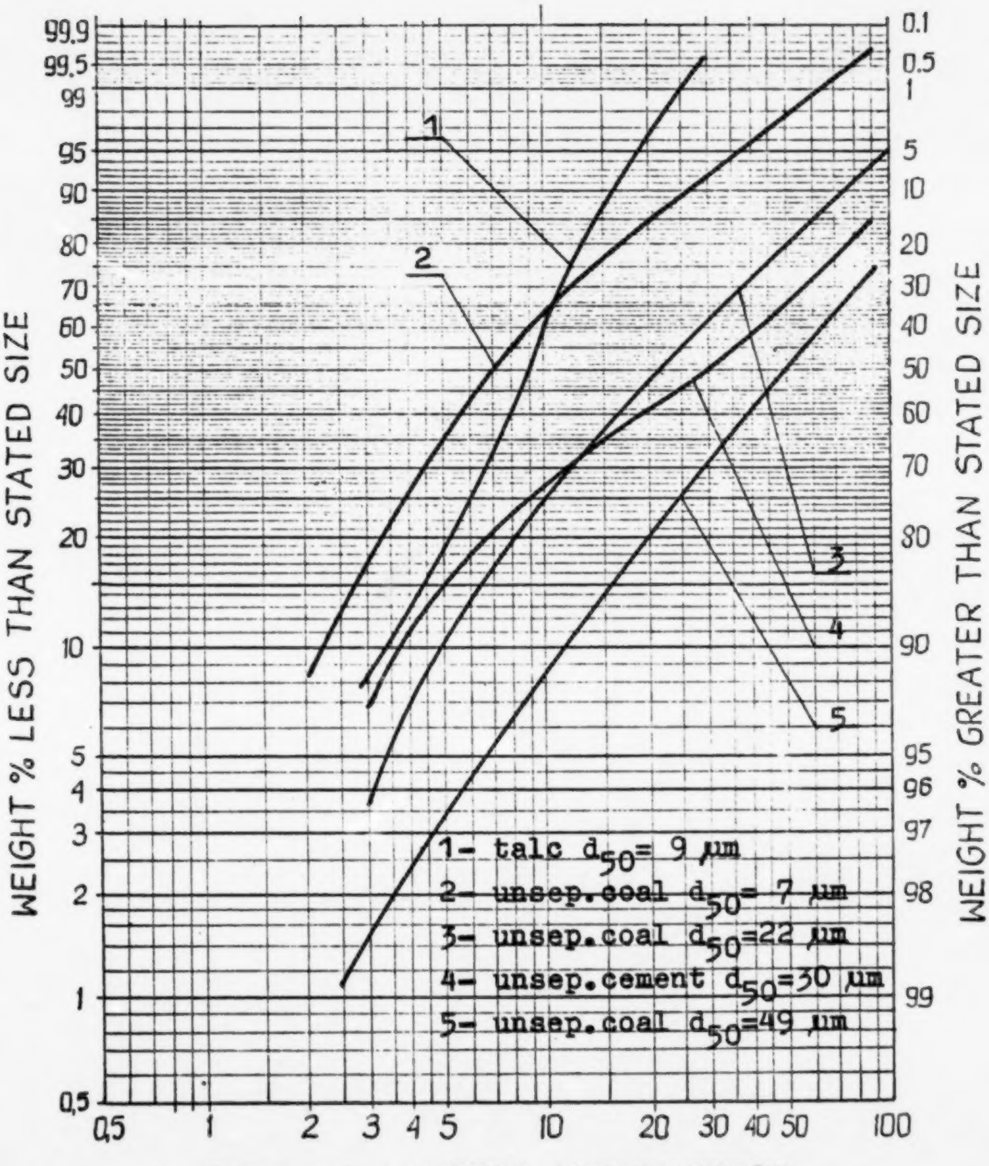

Figure 174. Particle size distribution of test dusts.

RESULTS AND DISCUSSION

Density was determined for five different kinds of material, and measurement results were compiled separately for each kind of dust in Tables B-36 through B-40. Each table includes the absolute dust density measured by both methods. The measurement for one kind of dust was repeated 10 to 24 times.

The means calculated from the total series of measurements showed that dust densities determined by air and liquid pycnometers differ slightly. In two cases (i.e., for unseparated coal dust, d_{50} = 22 μm; and for unseparated coal dust d_{50} = 7 μm), the mean densities obtained by both methods were the same. For unseparated portland cement "250," the mean value of density obtained by the air pycnometer was 0.05 higher than the value obtained by the liquid pycnometer. The largest differences in mean density were observed for the technical talc fraction less than 20 μm; these differences amounted to 0.11 μm.

The higher density values obtained from the air pycnometer can be explained by better deaeration of the sample; thus, the measured volume of the examined material is lower than the volume measured by the liquid pycnometer, which directly influences calculated density. In one case, the mean calculated from measurements made with the liquid pycnometer is higher than the mean calculated from the air pycnometer; and the difference of 0.01 is observed for unseparated coal dust, d_{50} = 49 μm.

Statistical analysis of the absolute dust density as determined by both methods showed that the mean square deviation, σ, for values obtained with the liquid pycnometer is 0.0052 to 0.0087, and deviation from the mean $\Delta\rho$ ranges from 0.012 to 0.018 for probability, $\alpha = 0.95$. The mean square deviation, σ, for values obtained by the air pycnometer, was 0.0070 to 0.279, and the deviation from the mean, $\Delta\rho$, = 0.015 to 0.060 for the same probability as above; i.e., $\alpha = 0.95$. The probability of higher and lower values than $\rho = \bar{\rho} \pm \Delta\rho$ is 0.05; i.e., 5 percent. Statistical analysis also showed that the highest result scatter was observed for densities measured by the liquid pycnometer for unseparated portland cement "250," d_{50} = 30 μm; and for unseparated coal dust, d_{50} = 7 μm. For the air pycnometer, the highest scatter of results was observed for technical talc (fraction less than 20 μm).

The relationship between density values obtained by both methods is shown in Figure 175. As shown in this figure, results are completely equivalent,

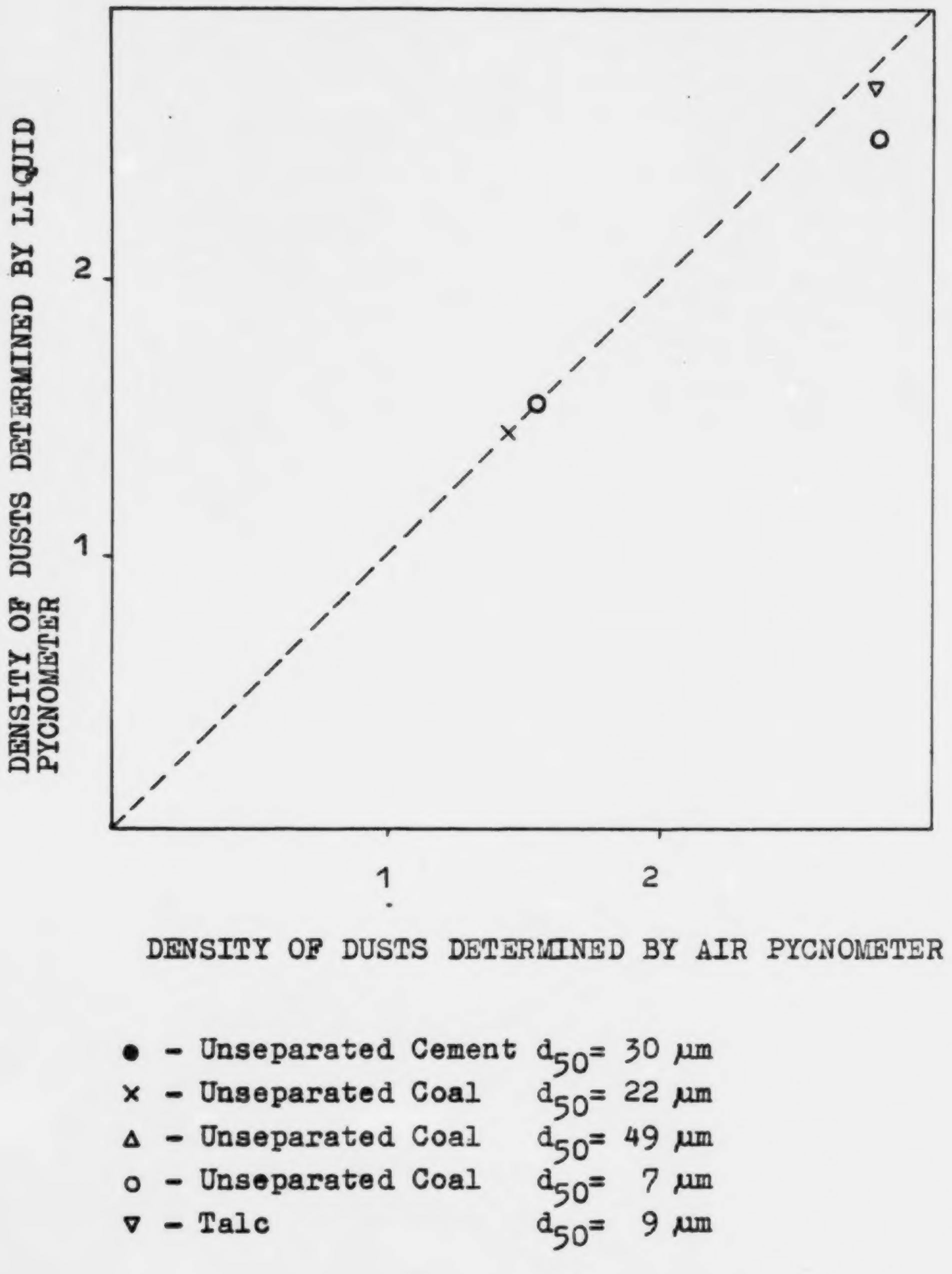

Figure 175. Correlation between two methods of measuring absolute dust density.

which suggests that the two methods of dust density determination are also equivalent. For completion of the above material, a linear correlation coefficient was calculated. The coefficient values for each kind of examined dusts are:

- Portland cement "250" $d = 30$ µm; $r = -0.725$.
- Unseparated coal dust $d_{50} = 22$ µm; $r = +0.8298$.
- Unseparated coal dust $d_{50} = 49$ µm; $r = +0.793$.
- Unseparated coal dust $d_{50} = 7$ µm; $r = +0.9571$.
- Technical talc (fraction < 20 µm), $d_{50} = 9$ µm; $r = +0.0234$.

Calculated values of the linear correlation coefficient prove that density values obtained by both methods are well correlated, except for measurements of the technical talc fraction. In this case, because of a high scatter of results obtained from the air pycnometer and possibly because of random errors connected to individual measurements, the correlation is weak. The above equivalent methods should be confirmed by wider empirical data.

CONCLUSIONS

- The values of mean density obtained from both methods differ by an insignificant amount. However, higher values were obtained for measurements conducted with an air pycnometer.
- The liquid pycnometer is more readily available in Poland and can be successfully used in plant laboratories for checking dust density.

SECTION XIII

REFERENCES

1. Friedlander, S. K. Smoke, Dust, and Haze. A Wiley-Interscience Publication, New York, London, Sydney, Toronto, 1977.

2. Fuchs, N. A. The Mechanics of Aerosols. Pergamon Press, Oxford, London, Edinburgh, New York, Paris, Frankfurt, 1964.

3. Davies, C. N. Aerosol Science. Academic Press, London and New York, 1966.

4. Kouzov, P. A. The Basics of Particle Size Distribution of Industrial Dusts and Grinding Materials. (in Russian) Izd. "Chimija", Leningrad, U.S.S.R., 1974.

5. Kościanowski, J. R., L. Kościanowska, and E. Szczepankiewicz. Filtration Parameters for Dust Cleaning Fabrics. EPA-600/7-79-031, U.S. Environmental Protection Agency, January 1979.

6. White, P. A. F., and S. E. Smith. High-Efficiency Air Filtration. Butterworths, London, 1964.

7. Billings, C. E., and J. Wilder. Handbook of Fabric Filter Technology, Vol. I, Fabric Filter Systems Study. EPA Publication APTD 0690, NTIS No. PB-200 648, U.S. Environmental Protection Agency, December 1970.

8. Billings, C. E. Fabric Filter Installations for Flue Gas Fly Ash Control, Status Report. Powder Technology, 18:79-110, 1977.

9. Kościanowski, J. R., and L. Kościanowska. Effect of Filtration Parameters on Dust Cleaning Fabrics. EPA-600/2-76-074, U.S. Environmental Protection Agency, March 1976.

10. Valentine, F. H. H. Cloth Filtration of Fine Aerosols. British Chemical Engineering, 7:268-271, 1962.

11. Leith, D., S. N. Rudnick, and M. W. First. High-Velocity High-Efficiency Aerosol Filtration. EPA-600/2-76-020, U.S. Environmental Protection Agency, January 1976.

12. Kościanowski, J. R., L. Kościanowska, and M. Szablewicz. Test of Fabric Filtration Materials. EPA-600/7-78-056, U.S. Environmental Protection Agency, March 1978.

13. Kościanowski, J. R., L. Kościanowska, and M. Szablewicz. Test of Fabric Filtration Materials. EPA-600/7-79-087, U.S. Environmental Protection Agency, March 1979.

14. Harris, D. B. Procedures for Cascade Impactor Calibration and Operation in Process Streams. EPA-600/2-77-004, U.S. Environmental Protection Agency, January 1977.

15. Shannon, L. J. Control Technology for Fine Particulate Emissions. EPA-650/2-74-027, U.S. Environmental Protection Agency, May 1974.

16. Turner, J. H. Extending Fabric Filters Capabilities. In: Proceedings: Symposium on the Use of Fabric Filters for the Control of Submicron Particulates (April 8-10, 1974, Boston, Massachusetts), L. M. Seale, ed. EPA-650/2-74-043, U.S. Environmental Protection Agency, May 1974.

17. Dennis, R., and J. Wilder. Fabric Filter Cleaning Studies. EPA-600/2-75-009, U.S. Environmental Protection Agency, January 1975.

18. Spaite, P. W., and G. W. Walsh. Effect of Fabric Structure on Filter Performance. American Industrial Hygiene Association J., 24:357-365, 1963.

19. Penney, G. W. Electrostatic Effects in Fabric Filtration, Vol. I, Fields, Fabrics, and Particles. EPA-600/7-78-142a, U.S. Environmental Protection Agency. Frederick, E. R. Vol. II, Triboelectric Measurement and Bag Performance. EPA-600/7-78-142b, U.S. Environmental Protection Agency.

20. Dennis, R., R. W. Cass, D. W. Cooper, R. R. Hall, V. Hampl, H. A. Klemm, J. E. Langley, and R. W. Stern. Filtration Model for Coal Fly Ash With Glass Fabrics. EPA-600/7-77-084, U.S. Environmental Protection Agency, August 1977.

21. Stephan, D. G., G. W. Walsh, and R. D. Derrick. Concepts of Fabric Air Filtration. American Industrial Hygiene Association J., 21:1-14, 1960.

22. Robinson, J. W., R. E. Harrington, and P. W. Spaite. A New Method for Analysis of Multicompartment Fabric Filtration. Atmospheric Environment, 1:499-508, 1967.

23. Holland, C. R., and E. Rothwell. Model Studies of Fabric Dust Filtration. 1. Flow Characteristics of Dust Cake Uniformly Distributed on Filter Fabrics. Filtration and Separation, 14(1):30-36, January/February 1977.

24. Draemel, D. C. Relationship Between Fabric Structure and Filtration Performance In Dust Filtration. EPA-R2-73-288, U.S. Environmental Protection Agency, July 1973.

25. Mohamed, M., and E. Afify. Efficient Use of Fibrous Structures in Filtration. EPA-600/2-76-204, U.S. Environmental Protection Agency, July 1976.

26. Andrew, E. D. Textile Media for Air Filters and Dust Collectors. Filtration and Separation, 13(1):21-22, January/February 1976.

27. Davis, W. T., P. J. LaRosa and K. E. Noll. The Generation and Evaluation of Fabric Filter Performance Curves from Pilot Plant Data. Filtration and Separation, 13(6):555-560, November/December 1976.

28. Poradnik Inzyniera - Włókiennictwo. Handbook of Engineer-Textile Industry. WNT, Warszawa, Poland, 1978.

29. Kościanowski, J. R., and L. Kościanowska. Some Aspects of Dust Filtration Processes. Paper 78-76.4. Presented to 71 APCA Meeting, Houston, Texas, June 1978.

30. Szczepankiewicz, E. Pewna Klasa N-Wymiarowych Pól Losowych i Próba Ich Zastosowania. Rozprawy i Monografie Zeszytów Naukowych WSP, Opole. 1972.

31. Gillespie, T. The Role of Electric Forces in the Filtration of Aerosols by Fiber Filters. J. Colloid Science, 10:299-314, 1955.

32. Silverman, L., E. W. Conners, and D. M. Anderson. Electrostatic Mechanism in Aerosol Filtration by Mechanically Charged Fabric Media and Related Studies. Industrial and Engineering Chemistry, 47:952, 1955.

33. Havlicek, V. The Improvement of Efficiency of Fibrous Dielectric Filters By Application of An External Electric Field. International J. Air Water Pollution, 4:225-236, 1961.

34. Frederick, E. R. How Dust Filter Selection Depends on Electrostatics. Chemical Engineering. 107-114, June 26, 1961.

35. Kirsch, A. A. The Influence of an External Electric Field on the Deposition of Aerosols in Fibrous Filters. J. Aerosol Science, 3:25-29, 1972.

36. Ariman, T., and L. Tang. Collection of Aerosol Particles by Fabric Filters in an Electrostatic Field. Atmospheric Environment, 10:205-210, 1976.

37. Ciesielska, E., J. Kościanowski, M., Kryszałowicz, J. Malcher, A. Szaynok, and W. Wolniewicz. Badania Nad Elektryzacja Pyłow Przemysłowych Cementowni. Prace Naukowe Institute. Fizyki Technicznej Politechniki Wrocławskiej Nr. 6, Studia i Materiały Nr. 5. Wrocław, Poland, 1973. pp. 9-14.

38. Kościanowski, J., J. Malcher, L. Szaro, and A. Szaynok. Pomiary Rezystywności Warstw Pyłowych Pyłow Przemysłowych Cementowni. Prace Naukowe Institute. Fizyki Technicznej Politechniki Wrocławskiej Nr. 6, Studia i Materiały Nr. 5. Wrocław, Poland, 1973. pp. 47-52.

APPENDIX A

DATA PLOTS

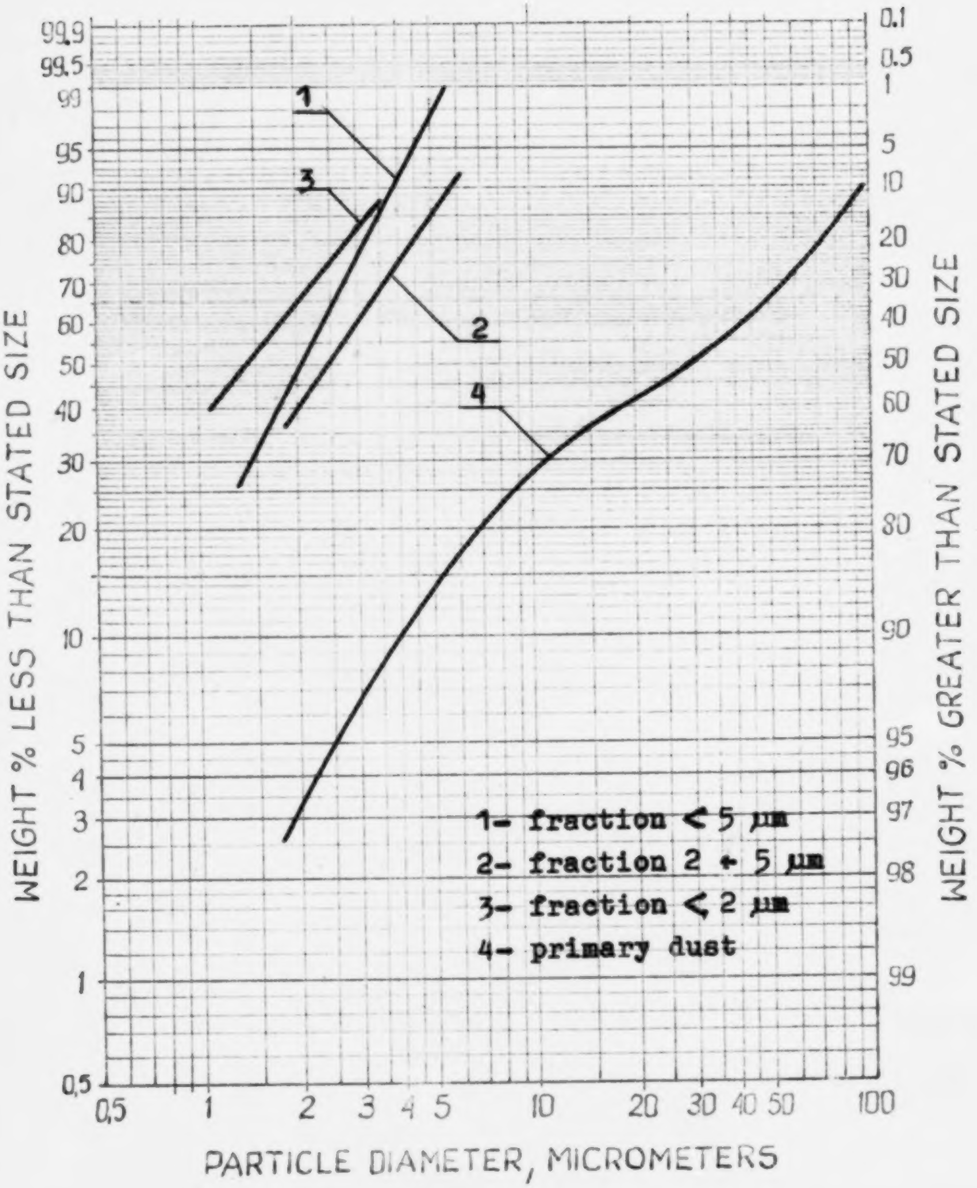

Figure A-1. Particle size distribution of cement test dusts (first separation).

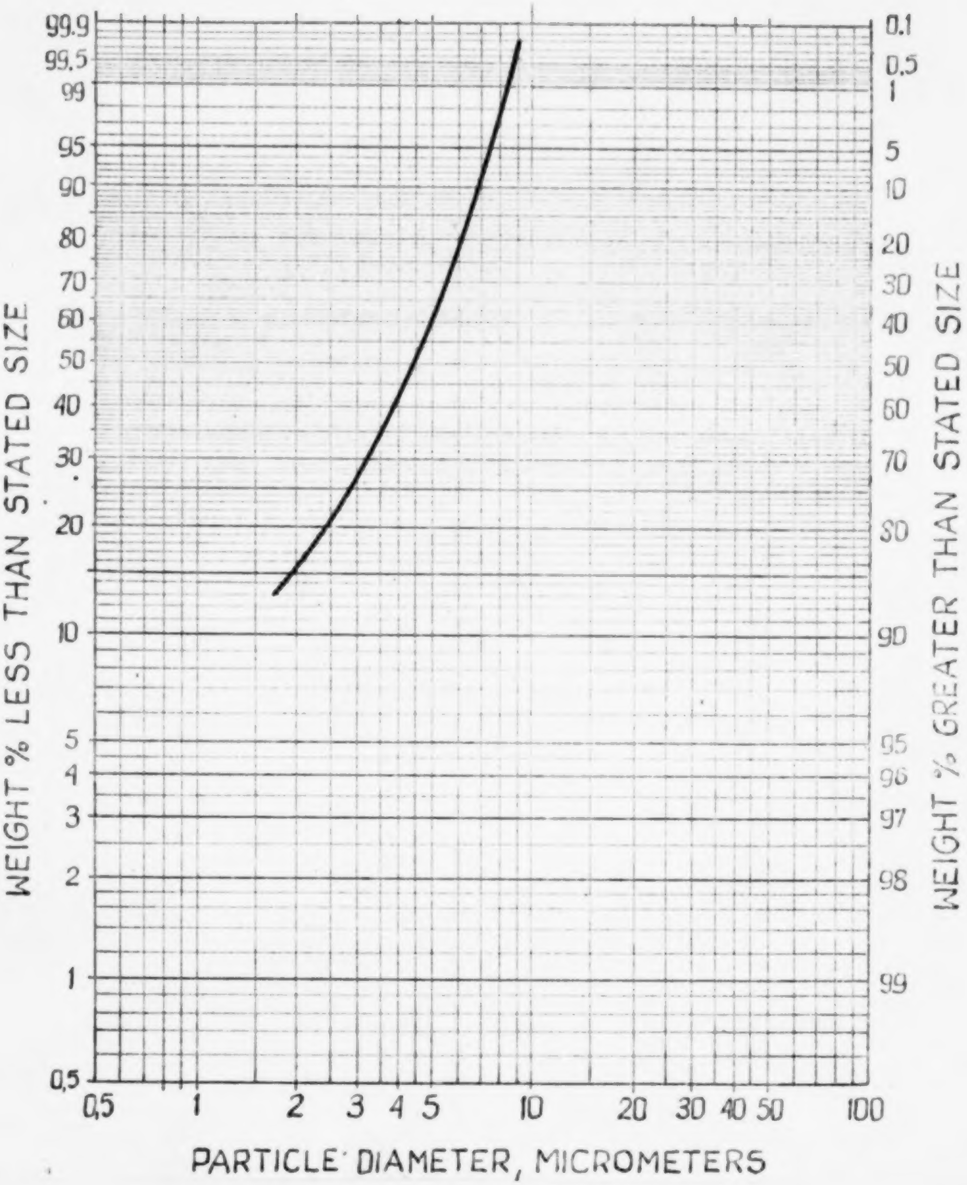

Figure A-2. Particle size distribution of cement test dusts (fraction < 8 μm), (second separation).

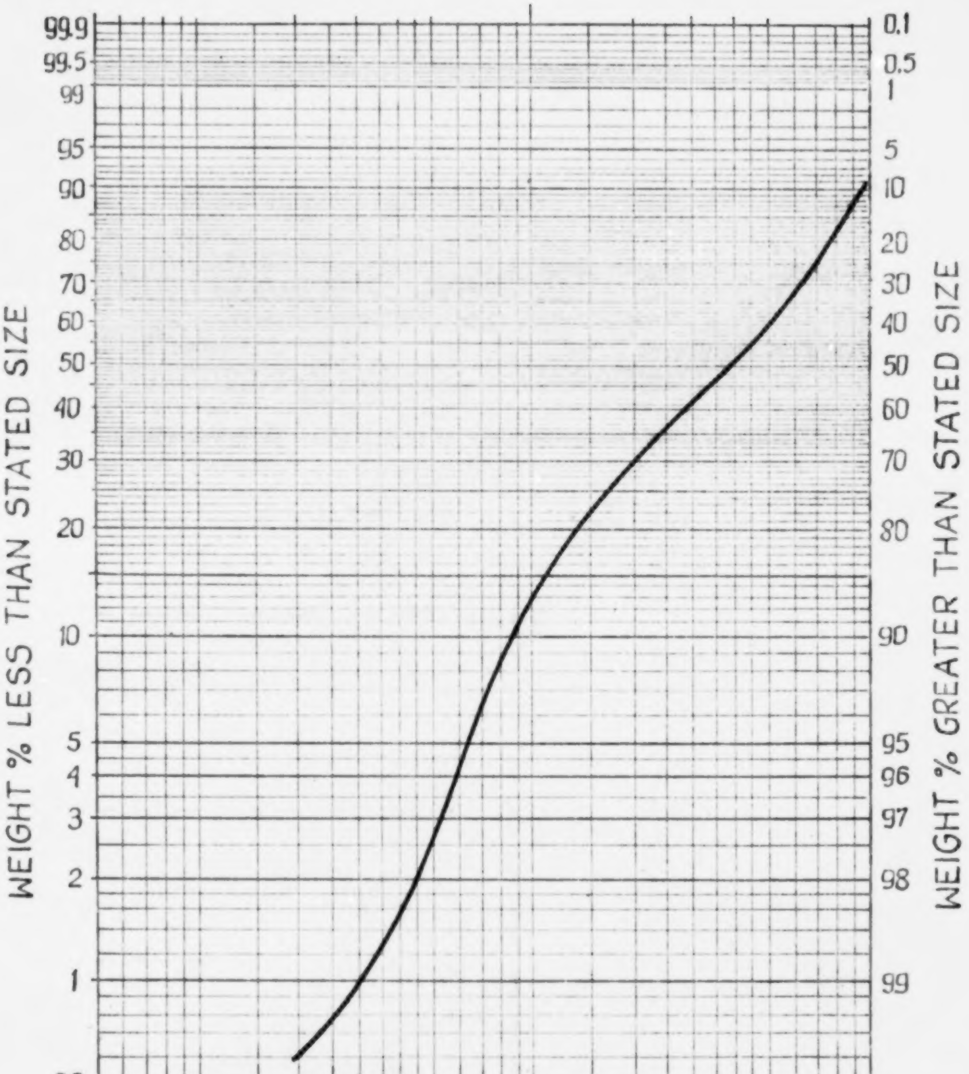

Figure A-3. Particle size distribution of cement test dusts (fraction > 8 μm), (third separation).

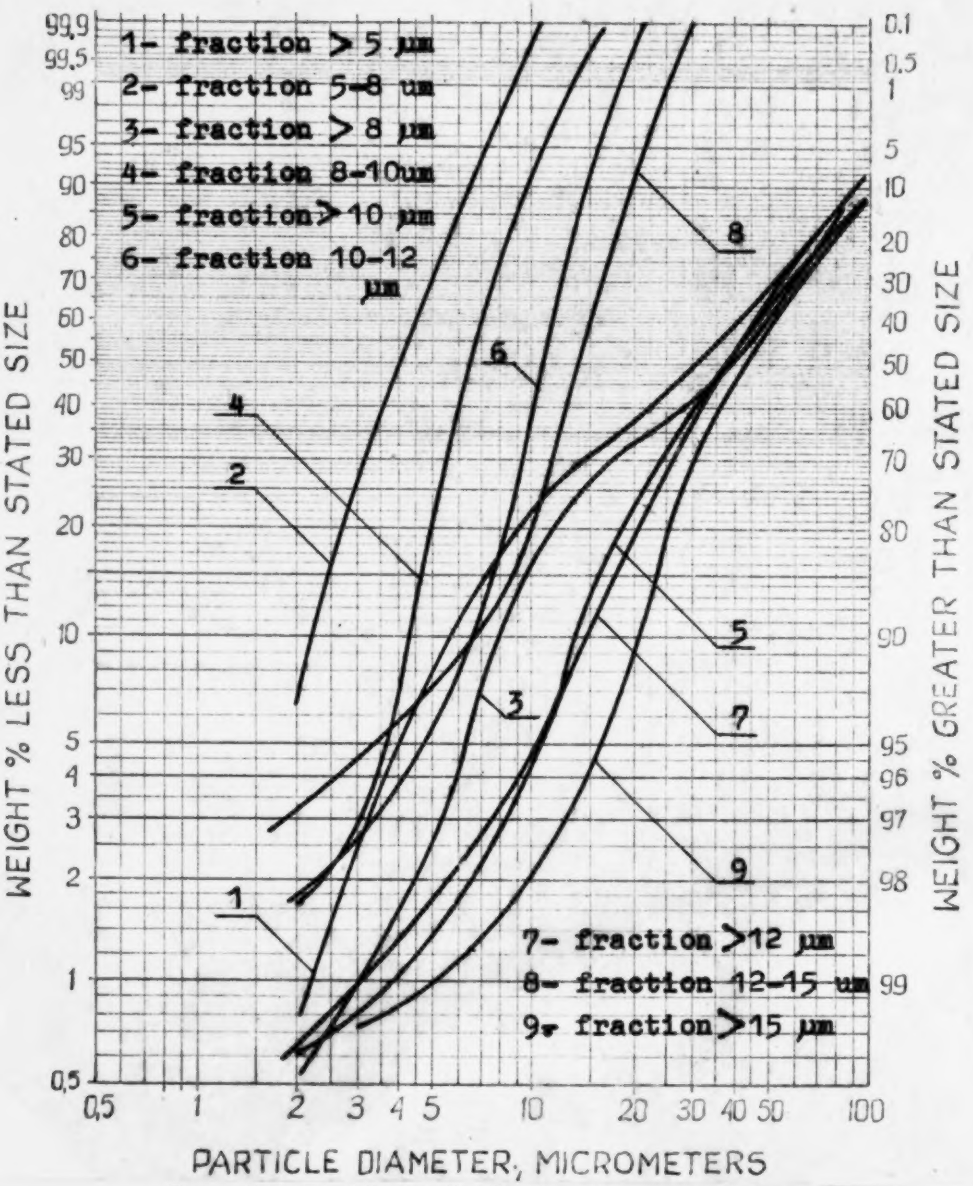

Figure A-4. Particle size distribution of cement test dusts (fourth separation).

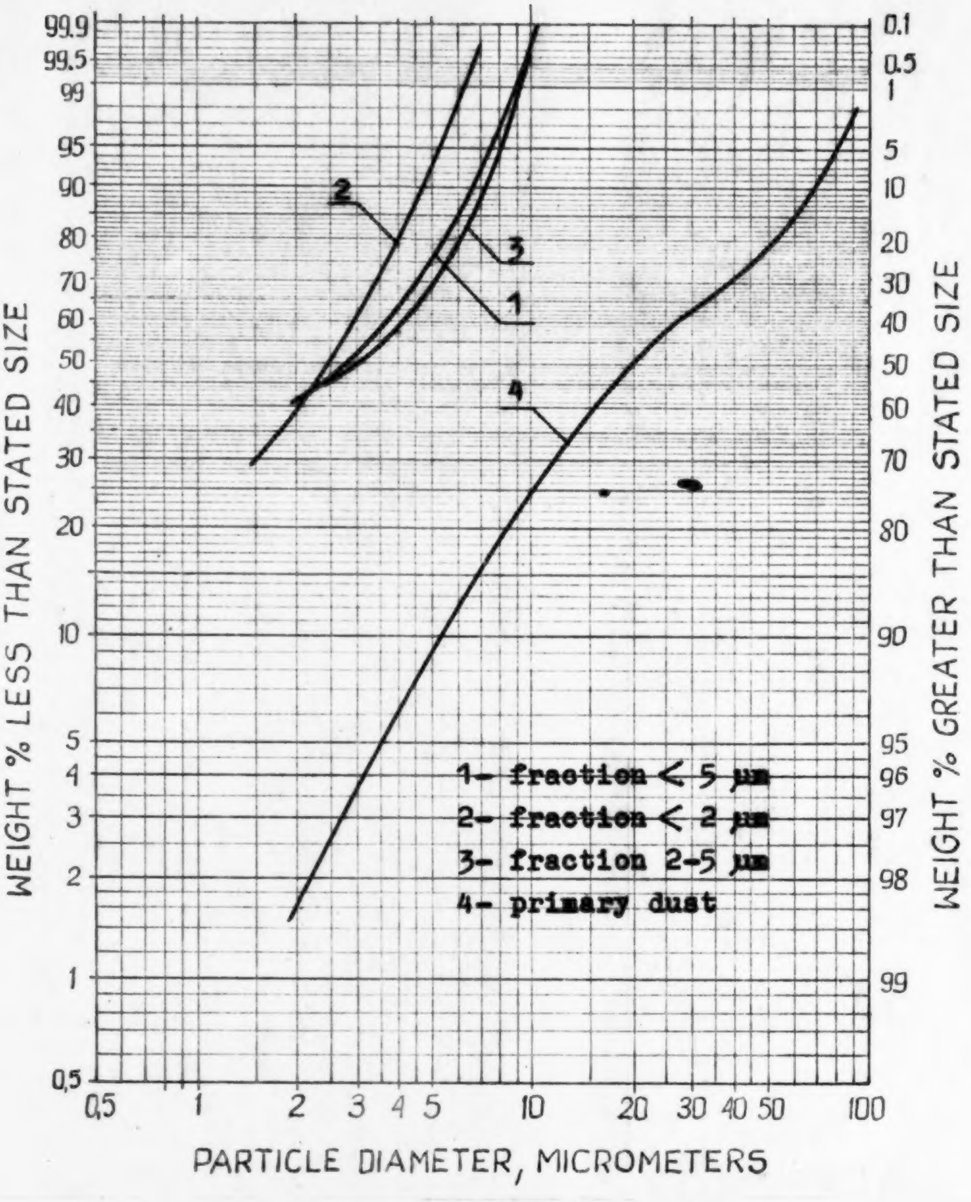

Figure A-5. Particle size distribution of coal test dusts (first separation).

Reproduced from best available copy.

(6)

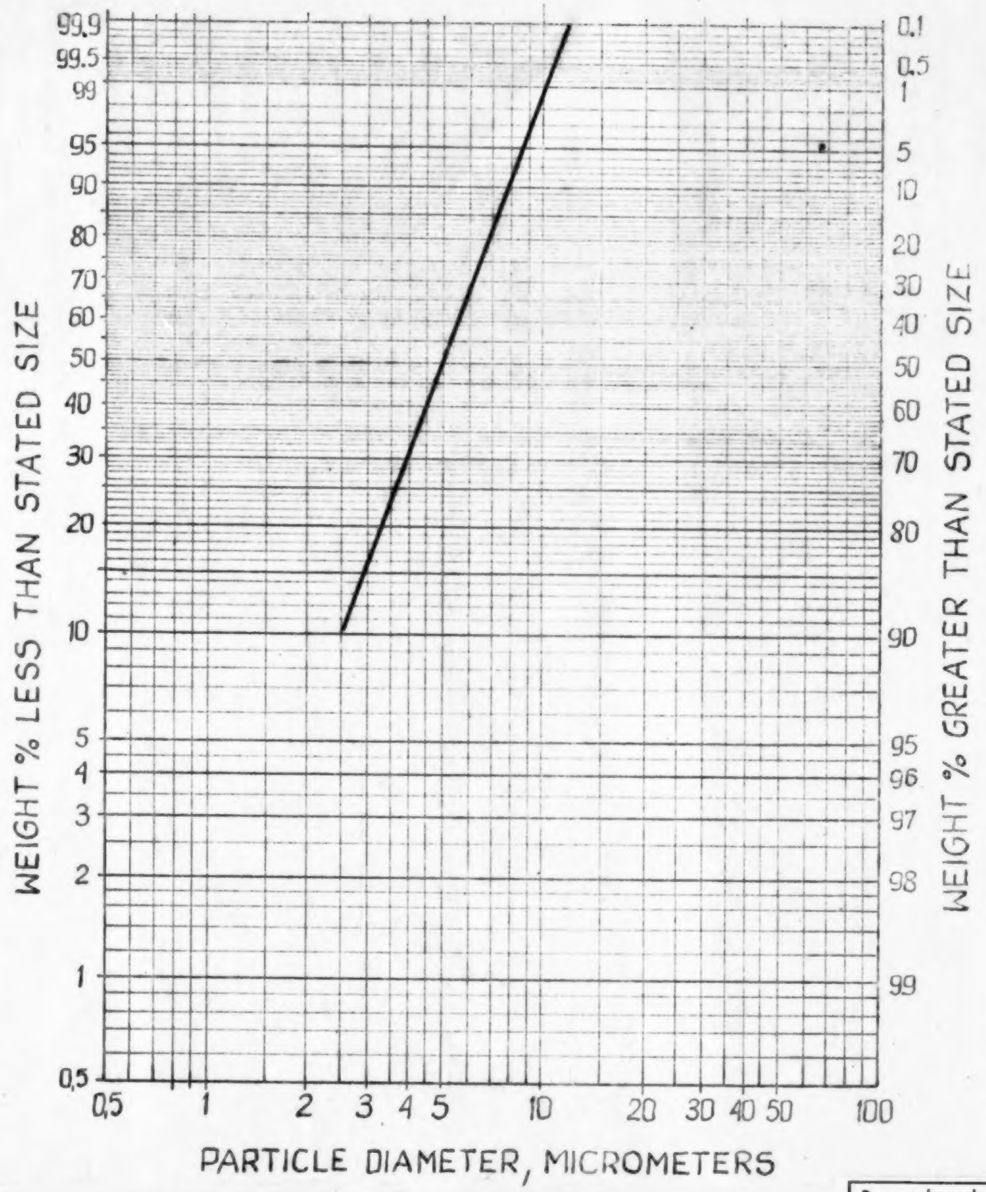

Figure A-6. Particle size distribution of coal test dusts (fraction < 10 μm), (second separation).

Reproduced from best available copy.

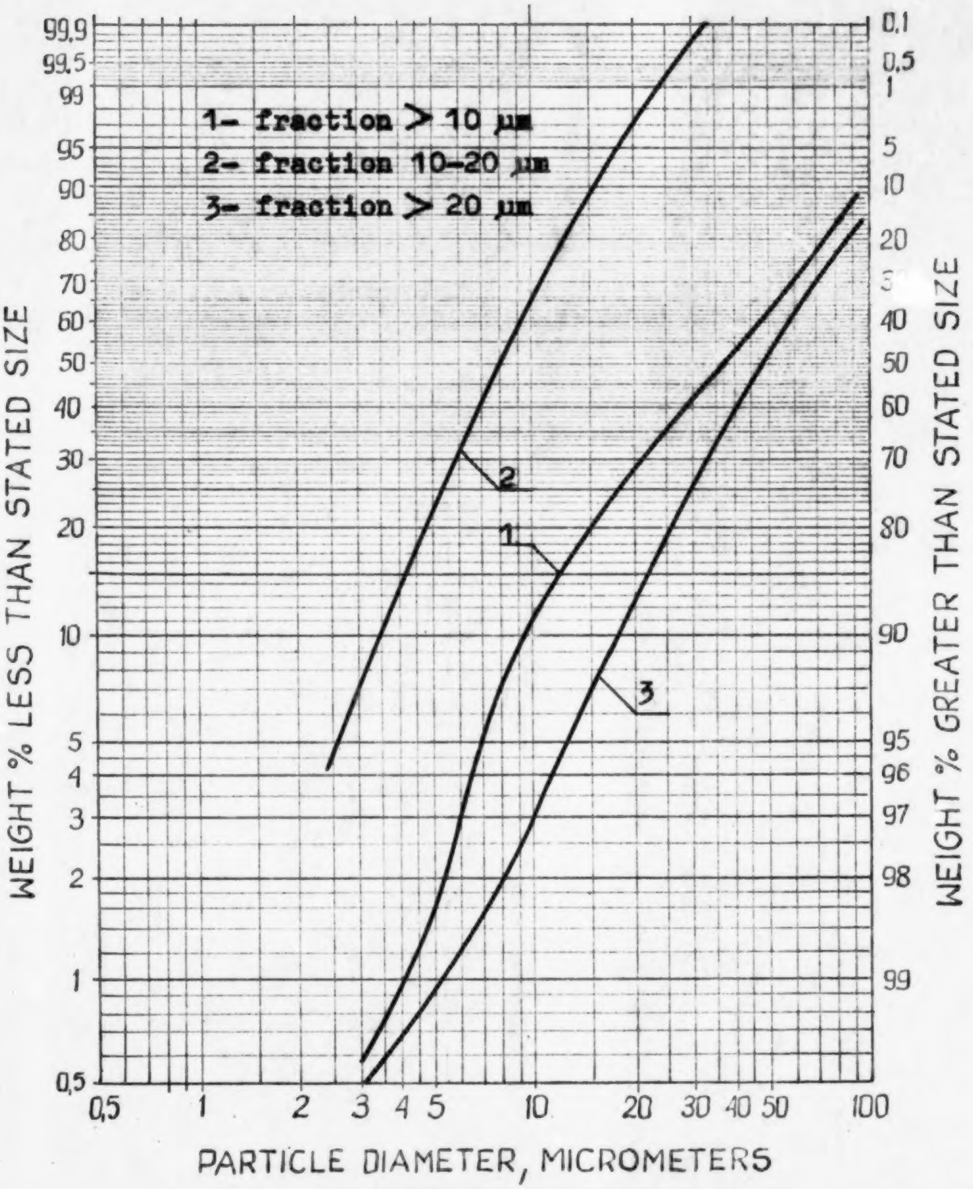

Figure A-7. Particle size distribution of coal test dusts (third separation).

Reproduced from best available copy.

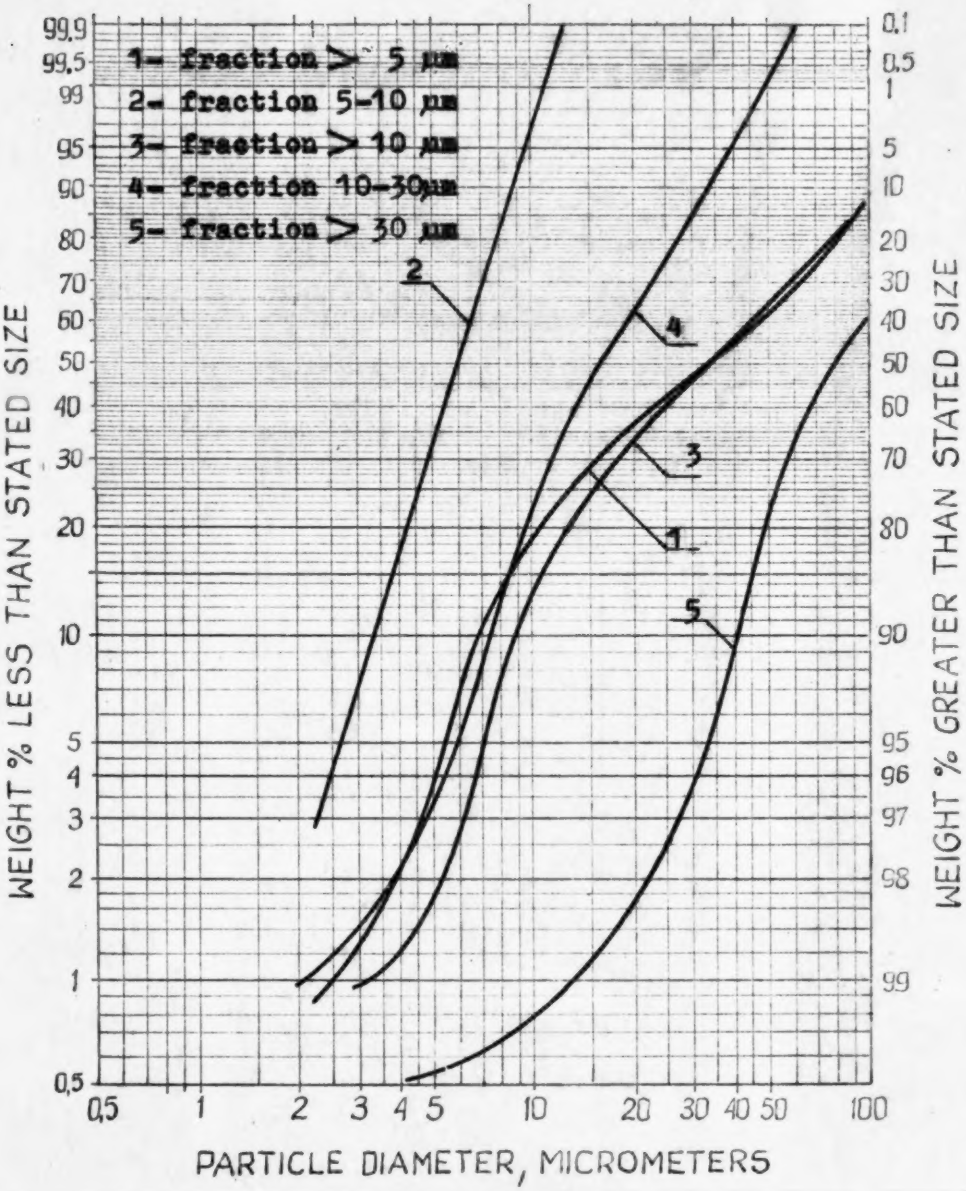

Figure A-8. Particle size distribution of coal test dusts (fourth separation).

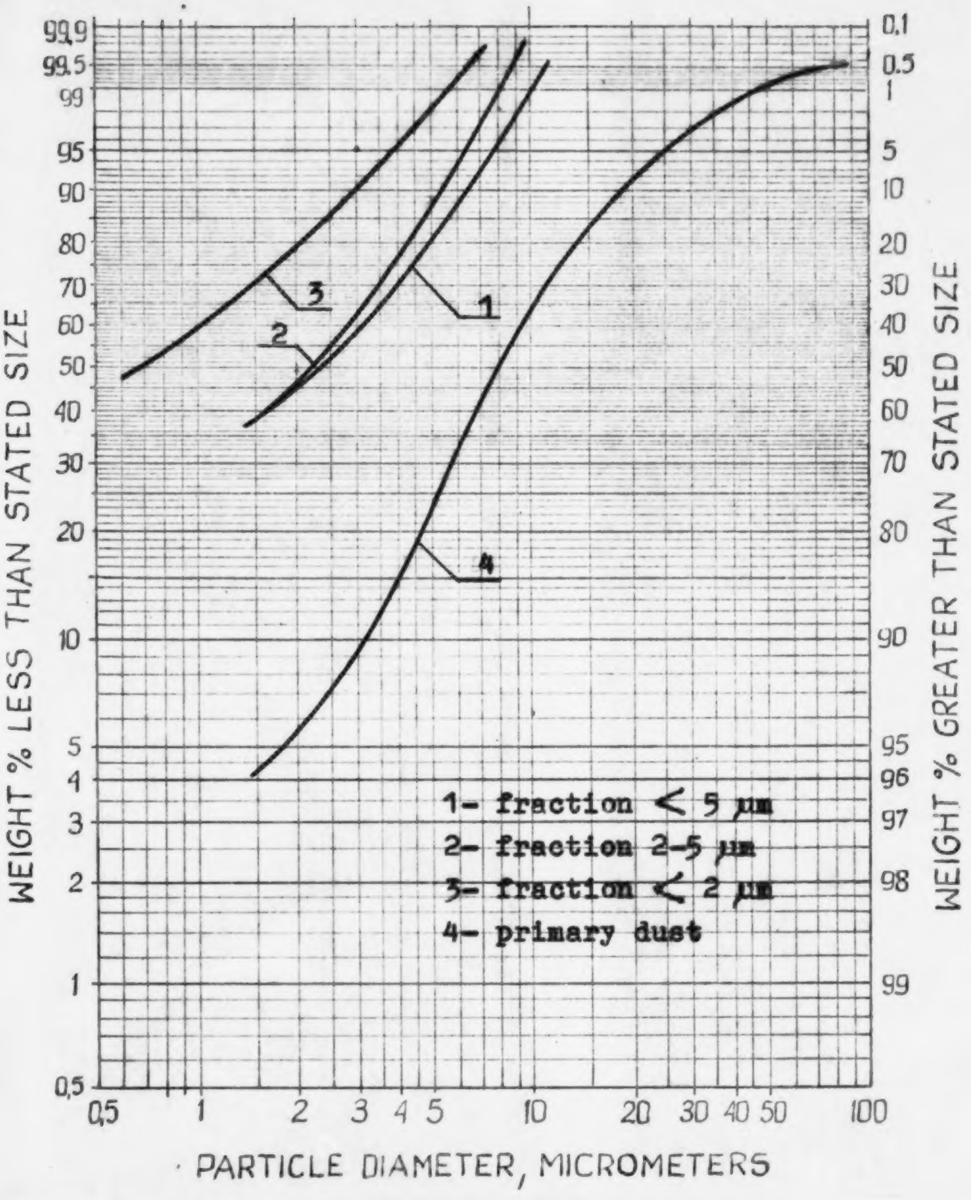

Figure A-9. Particle size distribution of talc test dusts (first separation).

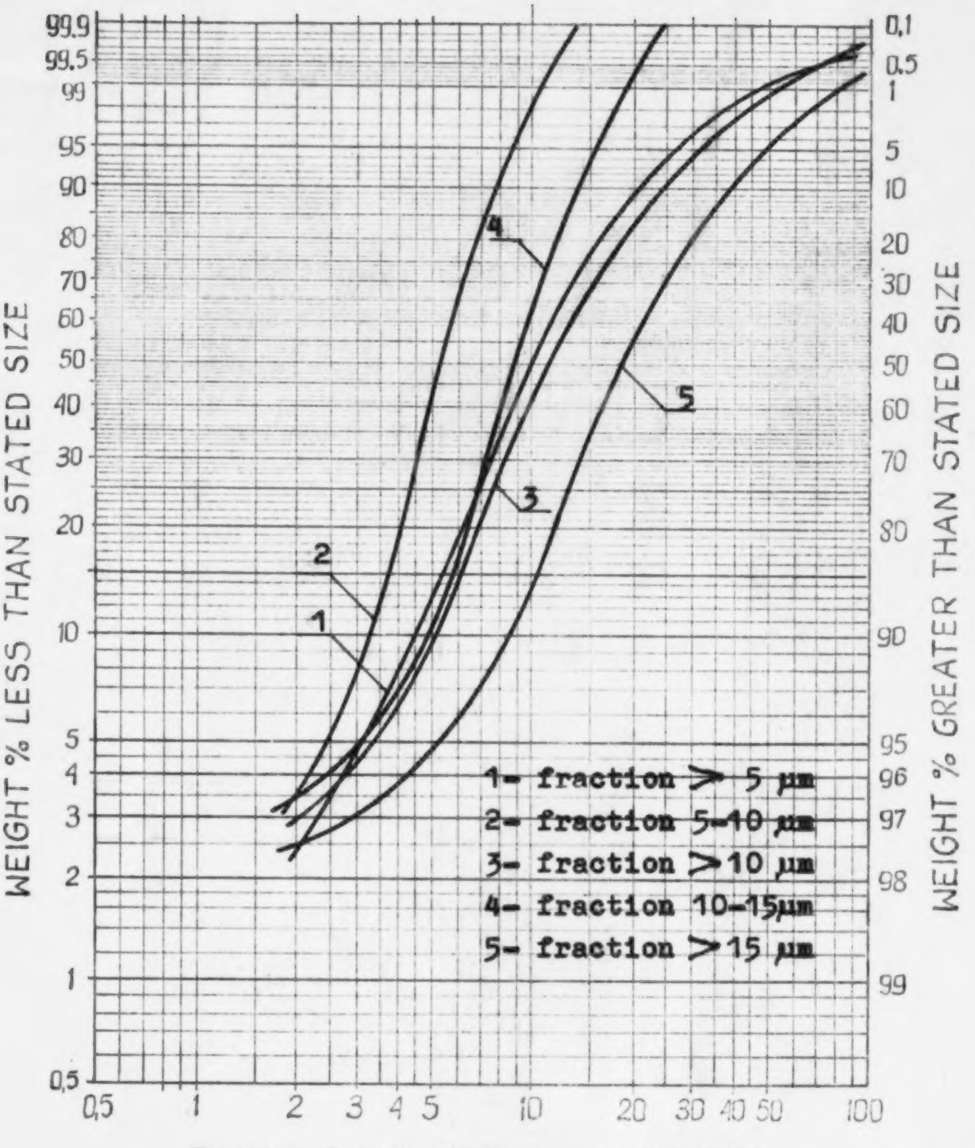

Figure A-10. Particle size distribution of talc test dusts (second separation).

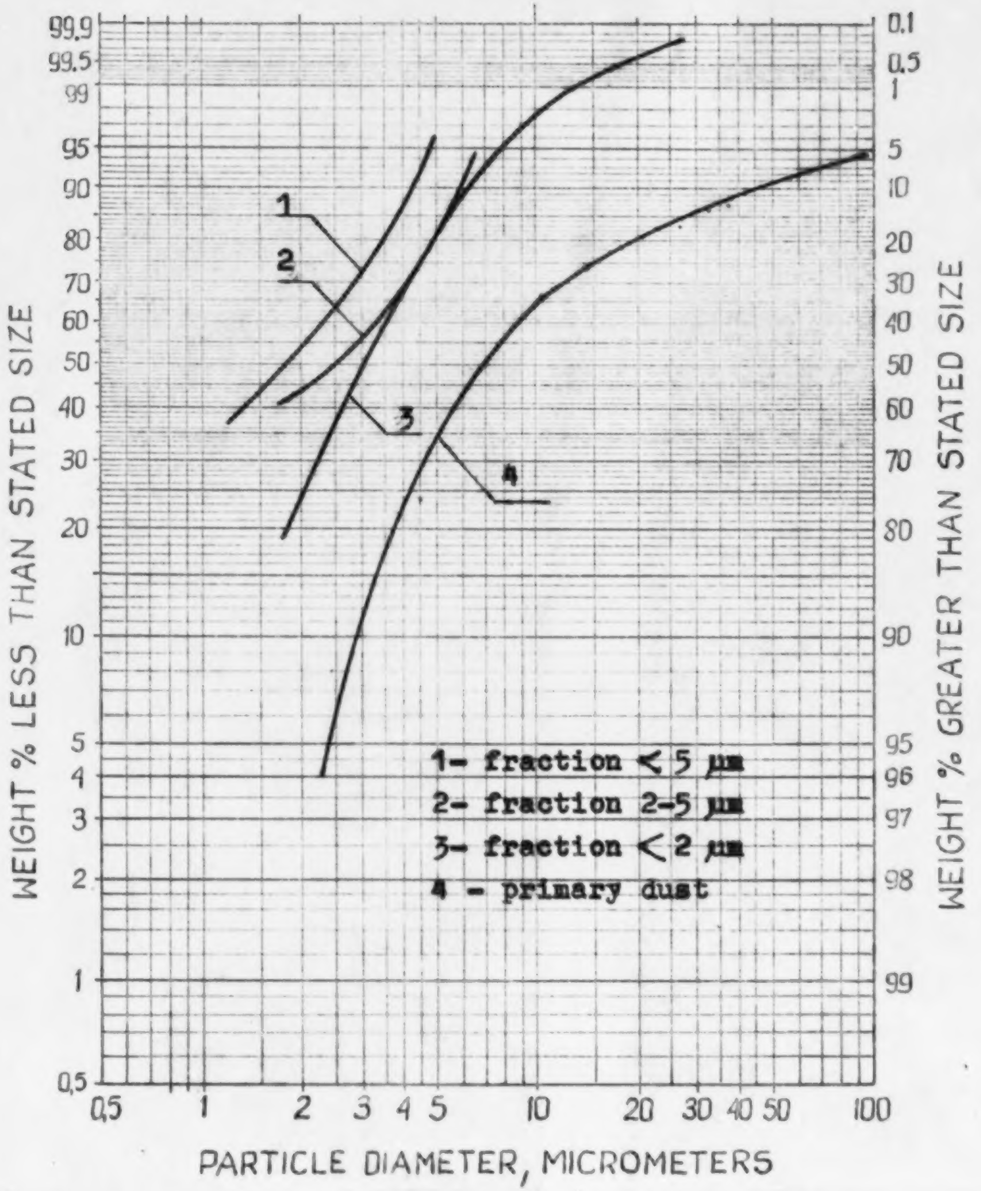

Figure A-11. Particle size distribution of fly ash test dusts (first separation).

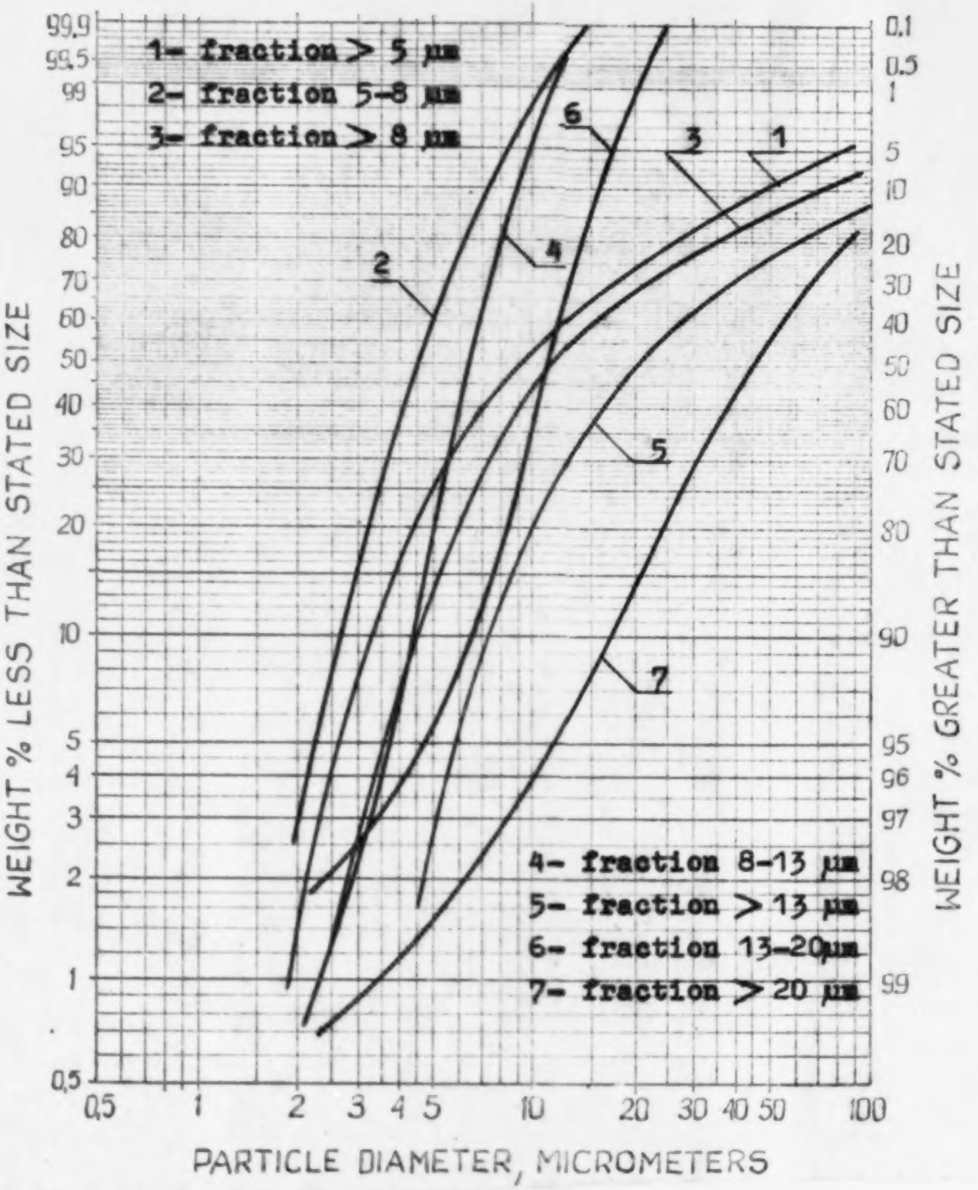

Figure A-12. Particle size distribution of fly ash test dusts (second separation).

APPENDIX B

DATA TABULATION

Preceding page blank

TABLE B-1. PARTICLE SIZE DISTRIBUTION OF TEST DUSTS

Before separation					After separation				
Range of particle size (μm)	Percent by weight				Range of particle size (μm)	Percent by weight			
	Cement	Coal	Talc	Fly ash		Cement	Coal	Talc	Fly ash
<5	12.0	9.0	23.0	19.0	<5	26.0	24.0	32.5	40.0
5 - 10	12.0	16.0	33.0	45.5	5 - 10	36.5	40.0	37.5	50.0
10 - 20	16.0	24.5	30.0	15.0	10 - 20	33.0	34.5	25.0	9.7
20 - 30	9.5	13.0	8.5	5.0	>20	4.5	1.5	5.0	0.3
30 - 40	10.0	7.5	2.5	3.0					
40 - 50	10.0	6.5	1.2	2.0					
50 - 60	7.5	4.5	0.5	1.5					
>60	23.0	19.0	1.3	9.0					

TABLE B-2. LABORATORY EFFICIENCY (%) OF POLYESTER STYLE ET-4 (Unseparated Dust, c_1 = 30 g/m^3)

		Kind of dust	
q_g (m^3/m^2/h)	L_o (g/m^2)	Unseparated cement dust	Unseparated coal dust
60	100	99.84	99.65
	400	99.96	99.84
	700	99.93	99.93
80	100	99.27	99.58
	400	99.88	99.91
	700	99.94	99.94
120	100	99.28	99.54
	400	99.82	99.73
	700	99.88	99.76

TABLE B-3. LABORATORY EFFICIENCY (%) OF POLYESTER STYLE ET-30 (Unseparated Dust, c_1 = 30 g/m^3)

		Kind of dust	
q_g (m^3/m^2/h)	L_o (g/m^2)	Unseparated cement dust	Unseparated coal dust
60	100	99.79	99.88
	400	99.97	99.97
	700	99.98	99.98
80	100	99.63	99.88
	400	99.91	99.96
	700	99.95	99.98
120	100	99.82	99.72
	400	99.93	99.91
	700	99.93	99.94

TABLE B-4. LABORATORY EFFICIENCY (%) OF POLYESTER STYLE F-tor-5
(Unseparated Dust, c_1 = 30 g/m³)

		Kind of dust	
q_g (m³/m²/h)	L_o (g/m²)	Unseparated cement dust	Unseparated coal dust
60	100	99.62	99.85
	400	99.87	99.95
	700	99.95	99.90
80	100	98.49	98.56
	400	99.88	98.68
	700	99.95	99.67
120	100	96.23	94.49
	400	99.89	98.47
	700	99.70	99.73

TABLE B-5. LABORATORY EFFICIENCY (%) OF POLYAMIDE STYLE PT-15
(Unseparated Dust, c_1 = 30 g/m³)

		Kind of dust	
q_g (m³/m²/h)	L_o (g/m²)	Unseparated cement dust	Unseparated coal dust
60	100	99.88	99.92
	400	99.99	99.96
	700	99.99	99.97
80	100	98.59	99.77
	400	99.90	99.92
	700	99.99	98.99
120	100	99.89	99.93
	400	99.93	99.94
	700	99.95	99.97

TABLE B-6. FINAL PRESSURE DROP IN LABORATORY TESTING (mm, WATER) FOR POLYESTER STYLE ET-4
(Unseparated Dust, c_1 = 30 g/m^3)

		Kind of dust	
q_g (m^3/m^2/h)	L_o (g/m^2)	Unseparated cement dust	Unseparated coal dust
60	100	5.40/98.00*	4.15/105.00
	400	15.20/397.00	16.80/391.50
	700	25.30/717.00	20.40/748.50
80	100	8.60/98.00	7.20/100.00
	400	33.12/412.00	27.04/389.00
	700	49.50/693.00	41.90/690.00
120	100	17.20/99.00	14.30/98.00
	400	57.50/400.00	47.80/412.00
	700	92.30/728.00	68.40/716.50

*Real value of L_o for experiment.

TABLE B-7. FINAL PRESSURE DROP IN LABORATORY TESTING (mm, WATER) FOR POLYESTER STYLE ET-30
(Unseparated Dust, c_1 = 30 g/m^3)

		Kind of dust	
q_g (m^3/m^2/h)	L_o (g/m^2)	Unseparated cement dust	Unseparated coal dust
60	100	13.60/101.00*	6.20/100.0
	400	23.70/404.00	21.00/398.00
	700	38.80/687.00	24.50/656.00
80	100	23.40/106.00	12.40/110.00
	400	51.00/385.00	34.20/380.00
	700	71.70/743.00	51.40/700.00
120	100	50.30/99.00	37.20/102.50
	400	104.00/403.00	84.40/408.00
	700	121.00/710.00	94.00/726.00

*Real value of L_o for experiment.

TABLE B-8. FINAL PRESSURE DROP IN LABORATORY TESTING (mm, WATER) FOR POLYESTER STYLE F-tor-5 (Unseparated Dust, c_1 = 30 g/m³)

		Kind of dust	
q_g ($m^3/m^2/h$)	L_o (g/m^2)	Unseparated cement dust	Unseparated coal dust
60	100	11.80/102.00*	12.45/100.42
	400	24.85/413.00	29.20/399.08
	700	36.60/695.00	33.10/675.32
80	100	21.80/108.00	19.49/94.42
	400	47.70/387.00	47.30/403.99
	700	72.00/675.00	64.06/702.29
120	100	44.20/105.00	41.08/95.33
	400	93.50/409.00	99.54/401.65
	700	128.00/707.00	135.88/688.10

*Real value of L_o for experiment.

TABLE B-9. FINAL PRESSURE DROP IN LABORATORY TESTING (mm, WATER) FOR POLYAMIDE STYLE PT-15 (Unseparated Dust, c_1 = 30 g/m³)

		Kind of dust	
q_g ($m^3/m^2/h$)	L_o (g/m^2)	Unseparated cement dust	Unseparated coal dust
60	100	17.80/98.00*	10.90/98.70
	400	29.80/386.00	22.70/429.00
	700	46.30/702.00	30.90/696.00
80	100	32.80/98.00	35.63/97.88
	400	62.20/412.00	67.86/390.58
	700	86.10/687.00	96.54/704.40
120	100	68.80/105.00	57.50/100.00
	400	117.00/400.00	89.20/396.00
	700	156.70/734.00	124.00/706.00

*Real value of L_o for experiment.

TABLE B-10. LABORATORY EFFICIENCY (%) OF POLYESTER STYLE ET-4
(Separated Dust, $c_1 = 10\ g/m^3$: Series I)

q_g ($m^3/m^2/h$)	L_o (g/m^2)	Kind of dust			
		Separated cement dust	Separated coal dust	Separated talc dust	Separated fly ash dust
60	100	99.72	99.63	99.71	99.48
	400	99.93	99.85	99.95	99.82
	700	99.97	98.62	99.975	99.91
80	100	99.86	98.45	99.48	99.62
	400	99.96	97.66	99.66	99.91
	700	99.94	96.47	99.80	99.94
120	100	99.12	96.01	97.94*	99.23
	400	99.44*	96.03	96.98*	99.82
	700	99.17*	87.53	97.34*	99.79*

*Ducts/canals.

TABLE B-11. LABORATORY EFFICIENCY (%) OF POLYESTER STYLE ET-30 (Separated Dust, $c_1 = 10$ g/m^3: Series I)

q_g (m^3/m^2/h)	L_o (g/m^2)	Kind of dust: Separated cement dust	Separated coal dust	Separated talc dust	Separated fly ash dust
60	100	99.78	99.82	99.93	99.54
	400	99.92	99.96	99.97	99.91
	700	99.96	99.96	99.98	99.98
80	100	99.81	99.74	99.71	99.74
	400	99.96	99.96	99.89	99.90
	700	99.98	99.97	99.95	99.95
120	100	99.89	99.50	99.82	99.66
	400	99.95	99.93	99.92	99.90
	700	99.97	99.97	99.95	99.94

TABLE B-12. LABORATORY EFFICIENCY (%) OF POLYESTER STYLE F-tor-5
(Separated Dust, c_1 = 10 g/m^3: Series I)

q_g ($m^3/m^2/h$)	L_o (g/m^2)	Kind of dust			
		Separated cement dust	Separated coal dust	Separated talc dust	Separated fly ash dust
60	100	99.65	98.41	99.53	99.62
	400	99.90	99.65	99.47	99.91
	700	99.93	99.93	99.81	99.94
80	100	97.92	94.50	98.80	99.55
	400	99.48	99.81	99.70	99.85
	700	99.65	99.91	99.80	99.90
120	100	93.18	98.46	94.51*	99.18
	400	99.47	98.15	98.82*	99.74
	700	99.38*	98.64	96.94*	99.79

[*] Ducts/canals.

TABLE B-13. LABORATORY EFFICIENCY (%) OF POLYAMIDE STYLE PT-15
(Separated Dust, $c_1 = 10\ g/m^3$: Series I)

q_g $(m^3/m^2/h)$	L_o (g/m^2)	Kind of dust: Separated cement dust	Kind of dust: Separated coal dust	Kind of dust: Separated talc dust	Kind of dust: Separated fly ash dust
60	100	99.80	99.85	99.91	99.93
	400	99.96	99.96	99.986	99.97
	700	99.98	99.98	99.946	99.97
80	100	99.84	99.89	99.80	99.70
	400	99.98	99.98	99.98	99.93
	700	99.98	99.99	99.98	99.96
120	100	99.90	99.94	99.82	99.83
	400	99.98	99.96	99.92	99.94
	700	99.98	99.98	99.95	99.96

TABLE B-14. FINAL PRESSURE DROP IN LABORATORY TESTING (mm, WATER) FOR POLYESTER STYLE ET-4
(Separated dust, $c_1 = 10$ g/m^3: Series I)

q_g (m^3/m^2/h)	L_o (g/m^2)	Kind of dust: Separated cement dust	Separated coal dust	Separated talc dust	Separated fly ash dust
60	100	8.06/101.15*	6.1/101.44	5.89/99.22	5.55/103.58
	400	28.50/396.46	39.1/390.67	32.71/411.72	14.16/392.12
	700	63.50/693.79	81.1/687.07	65.09/682.73	28.09/693.28
80	100	13.60/109.38	14.6/102.73	10.71/106.60	9.84/106.01
	400	48.50/414.86	67.3/401.73	55.30/405.36	29.58/402.03
	700	100.33/714.34	128.0/712.99	132.25/727.83	60.12/734.07
120	100	28.50/100.73	27.8/91.45	22.04/101.00	19.84/100.40
	400	118.30/408.45	122.2/382.63	119.59/407.95	69.76/412.08
	700	212.36/728.68	190.0/664.63	221.80/690.08	125.45/709.94

*Real value of L_o for experiment.

TABLE B-15. FINAL PRESSURE DROP IN LABORATORY TESTING (mm, WATER) FOR POLYESTER STYLE ET-30
(Separated Dust, $c_1 = 10$ g/m³: Series I)

q_g (m³/m²/h)	L_o (g/m²)	Kind of dust			
		Separated cement dust	Separated coal dust	Separated talc dust	Separated fly ash dust
60	100	16.88/99.81*	15.30/89.94	10.24/103.23	9.10/99.67
	400	46.25/404.87	48.10/381.19	45.11/420.26	17.41/405.66
	700	77.13/699.09	87.20/687.04	85.64/707.51	30.18/712.57
80	100	28.24/106.07	27.00/103.59	20.03/107.03	19.05/106.65
	400	67.90/409.99	80.20/387.14	71.41/410.42	41.16/403.97
	700	123.06/751.60	149.20/702.07	115.81/716.28	68.49/720.64
120	100	54.80/104.74	55.56/92.82	44.95/104.09	41.06/97.95
	400	130.00/394.80	174.70/386.07	156.58/405.28	89.82/395.33
	700	229.00/697.91	340.30/730.68	281.80/709.34	159.53/716.56

*Real value of L_o for experiment.

TABLE B-16. FINAL PRESSURE DROP IN LABORATORY TESTING (mm, WATER) FOR POLYESTER STYLE F-tor 5
(Separated Dust, $c_1 = 10$ g/m^3: Series I)

q_g (m^3/m^2/h)	L_o (g/m^2)	Kind of dust Separated cement dust	Kind of dust Separated coal dust	Kind of dust Separated talc dust	Kind of dust Separated fly ash dust
60	100	18.64/99.65*	19.10/100.24	14.41/101.93	11.50/98.43
	400	41.23/387.66	49.90/389.02	45.82/398.35	22.50/403.19
	700	70.00/694.57	102.70/737.49	89.90/709.73	39.34/686.84
80	100	25.56/104.22	27.06/104.95	25.40/106.32	23.00/107.77
	400	73.71/412.48	94.60/407.99	77.88/418.24	43.53/415.92
	700	122.40/705.53	166.00/731.81	134.61/713.69	67.78/712.50
120	100	60.72/98.11	76.60/105.35	46.57/100.31	42.34/100.59
	400	163.40/411.59	199.70/384.21	173.74/395.14	88.32/401.88
	700	269.00/698.01	331.00/674.55	319.00/704.38	150.42/701.22

*Real value of L_o for experiment.

TABLE B-17. FINAL PRESSURE DROP IN LABORATORY TESTING (mm, WATER) FOR POLYAMIDE STYLE PT-15
(Separated Dust, $c_1 = 10$ g/m³: Series I)

q_g (m³/m²/h)	L_o (g/m²)	Kind of dust			
		Separated cement dust	Separated coal dust	Separated talc dust	Separated fly ash dust
60	100	27.02/103.68*	28.40/104.56	19.24/100.01	16.65/101.4
	400	53.40/401.20	67.1/410.07	45.98/406.07	27.25/400.89
	700	79.50/714.44	110.3/733.40	85.16/692.23	42.26/711.08
80	100	48.40/107.29	53.5/107.60	32.23/110.92	33.34/105.79
	400	79.30/414.27	111.4/407.20	87.22/409.64	51.27/416.87
	700	150.40/740.80	183.2/721.63	155.95/737.80	83.27/733.67
120	100	110.70/102.36	111.4/107.49	79.47/102.74	77.74/101.07
	400	219.80/408.75	256.2/399.42	192.60/390.16	128.45/407.42
	700	290.00/680.02	408.0/718.47	312.20/691.19	206.75/705.20

*Real value of L_o for experiment.

TABLE B-18. LABORATORY EFFICIENCY (%) OF POLYESTER STYLE ET-4
(Separated Fly Ash, c_1 = 10 g/m^3: Series II)

q_g (m^3/m^{2}h)	L_o (g/m^2) 50	70	100	200	300	400	500	700	800
60	98.72	99.33	99.28	99.77	99.86	99.90	99.89	99.93	99.94
70	98.40	98.84	99.22	99.73	99.79	99.85	99.90	99.90	99.91
80	98.99	98.79	99.71	99.60	99.80	99.83	99.86	99.91	99.92
100	98.90	98.77	99.13	99.19	99.75	99.85	99.87	99.90	99.86
120	98.52	98.76	99.47	99.64	99.73	99.82	99.84	99.92	99.91
200	97.87	97.77	97.81	98.17*	97.45*	97.82*	97.91*	99.06*	98.60*

*Ducts/canals formation.

TABLE B-19. LABORATORY EFFICIENCY (%) OF POLYESTER STYLE ET-4
(Separated fly ash, $c_1 = 10$ g/m³: Series II)

q_g (m^3/m^2h)	L_o (g/m^2)								
	50	70	100	200	300	400	500	700	800
60	99.63	99.78	99.76	99.88	99.88	99.91	99.94	99.94	99.98
70	99.33	99.47	99.72	99.83	99.84	99.87	99.91	99.93	99.94
80	99.57	99.18	99.53	99.80	99.87	99.85	99.89	99.94	99.95
100	99.27	99.23	99.30	99.73	99.87	99.82	99.85	99.89	99.94
120	98.50	98.92	99.19	99.60	99.78	99.74	99.86	99.88	99.92
200	95.55	96.12	96.74	97.49*	98.38*	98.54*	98.80*	99.05*	98.93*

*Ducts/canals formation.

TABLE B-20. FINAL PRESSURE DROP IN LABORATORY TESTING (mm, WATER) FOR POLYESTER STYLE ET-4 (Separated Fly Ash, c_1 = 10 g/m^3: Series II)

q_g (m^3/m^2/h)	L_o (g/m^2)								
	50	70	100	200	300	400	500	700	800
60	3.24/49.94	3.73/71.78	4.28/100.73	7.21/205.47	10.03/301.66	13.40/393.95	17.44/484.77	26.92/717.76	29.23/808.81
70	3.79/49.54	4.40/69.88	5.16/103.10	9.94/204.12	15.34/300.93	22.17/409.41	27.72/510.96	40.76/731.00	47.00/791.15
80	5.85/50.03	6.44/67.77	8.07/104.60	12.59/202.17	20.16/299.61	28.03/401.96	36.10/517.04	55.38/704.45	62.56/830.63
100	9.44/51.29	11.11/70.16	12.20/98.17	19.40/204.28	28.18/302.28	38.08/400.49	52.14/515.52	77.58/711.53	86.74/817.64
120	9.18/51.36	11.04/67.84	16.27/101.11	27.24/208.31	40.84/302.55	55.07/402.41	68.09/500.59	107.12/713.56	116.44/780.17
200	20.77/50.69	23.63/71.57	29.76/96.75	53.48/196.45	80.08/296.98	113.44/395.36	166.21/513.92	287.80/707.65	314.8/814.07

*Real value of L_o for experiment.

TABLE B-21. FINAL PRESSURE DROP IN LABORATORY TESTING (mm, WATER) FOR POLYESTER STYLE ET-30 (Separated Fly Ash, c_1 = 10 g/m^3: Series II)

q_g (m^3/m^2/h)	L_o (g/m^2)								
	50	70	100	200	300	400	500	700	800
60	11.38/50.95*	11.58/70.21	9.34/99.34	13.11/193.37	19.11/305.65	23.63/392.86	26.67/497.29	34.92/712.07	39.10/807.90
70	6.40/51.14	6.85/70.88	7.87/99.46	11.36/196.67	19.05/297.94	24.68/404.20	30.67/499.20	44.24/716.58	49.53/775.96
80	8.75/49.36	9.97/70.64	11.83/99.79	17.22/204.72	23.70/297.51	29.99/403.47	39.57/495.29	59.80/703.70	70.23/792.35
100	13.97/49.61	14.63/71.65	18.13/100.68	25.75/204.03	36.57/312.04	48.66/398.57	63.91/518.07	93.06/709.85	103.81/812.35
120	17.32/50.21	19.69/71.10	23.29/101.44	38.63/209.20	53,17/302.54	70.15/400.53	95.12/499.80	118.82/720.02	135.09/808.54
200	28.28/48.17	35.60/69.29	43.69/100.69	74.34/199.68	110.44/297.01	163.53/405.44	214.00/503.54	330.00/712.79	421.00/818.59

*Real value of L_o for experiment.

TABLE B-22. LABORATORY EFFICIENCY (%) OF POLYESTER STYLE ET-4 AND ET-30
(Separated Fly Ash, c_1 = 10 g/m³: Series III)

Kind of fabric	q_g (m^3/m^2h)	L_o (g/m^2) 100	300	500	700
ET-4	140	99.3194	99.8050*	99.5796*	99.8856
	160	99.2612	99.4875*	99.1771*	99.1014*
	180	99.0990	99.7990	99.6220*	99.3690*
ET-30	140	99.0459	99.6604	99.8194	99.8550
	160	98.7745	99.1108*	99.5148*	99.7099
	180	98.5151	99.4416	99.4516*	99.5300

*Ducts/canals formation.

TABLE B-23. FINAL PRESSURE DROP IN LABORATORY TESTING (mm, WATER)
FOR POLYESTER STYLE ET-4 AND ET-30
(Separated Fly Ash, c_1 = 10 g/m³: Series III)

Kind of fabric	q_g (m³/m²/h)	L_o (g/m²)			
		100	300	500	700
ET-4	140	20.02/95.27*	61.07/309.44	116.48/496.26	205.60/719.84
	160	25.56/104.42	67.47/279.97	139.14/496.54	241.80/714.83
	180	26.81/88.31	88.29/297.90	185.20/511.26	296.00/709.63
ET-30	140	28.04/96.23	76.38/307.24	146.80/528.72	237.60/728.35
	160	36.93/106.51	84.64/281.66	175.28/524.08	260.49/696.64
	180	39.69/90.28	105.79/295.75	213.80/500.85	342.80/721.34

*Real value of L_o for experiment.

TABLE B-24. VALUE OF K_2 FOR EXPERIMENTS IN SERIES I, II, AND III

Kind of fabric	q_g (m^3/m^2h)	$P_n - P_{n-1}$	$L_{o_n} - L_{o_{n-1}}$	K_2'	Comments
Series I: cement					
ET-4	60	20.44	295.31	0.0692	
		35.00	297.33	0.1547	
	80	34.90	305.48	0.1142	
		51.83	299.48	0.1730	
	120	89.80	307.75	0.2918	Ducts/canals
		94.06	320.23	0.2937	
ET-30	60	29.37	305.06	0.0963	
		30.88	294.22	0.1050	
	80	39.66	303.92	0.1305	
		55.16	341.61	0.1615	
	120	75.20	290.06	0.2593	
		99.00	303.11	0.3266	
F-tor 5	60	22.59	288.01	0.0785	
		28.77	306.91	0.0937	
	80	48.15	308.26	0.1562	
		48.69	293.07	0.1661	
	120	102.68	313.48	0.3275	Ducts/canals
		105.60	286.42	0.3687	
PT-15	60	26.38	297.52	0.0887	
		26.10	313.24	0.0833	
	80	30.90	306.98	0.2930	
		71.10	326.53	0.2177	
	120	109.10	306.39	0.3560	
		70.20	271.27	0.2588	
Series I: coal					
ET-4	60	33.00	289.23	0.1341	
		42.00	296.40	0.1417	
	80	52.70	299.00	0.1763	
		60.70	311.26	0.1950	
	120	94.40	291.18	0.3242	
		67.80	282.00	0.2404	

(continued)

TABLE B-24 (continued)

Kind of fabric	q_g (m^3/m^2h)	$P_n - P_{n-1}$	$L_{o_n} - L_{o_{n-1}}$	K_2'	Comments
ET-30	60	32.80	291.25	0.1126	
		39.10	305.85	0.1278	
	80	53.20	283.55	0.1876	
		69.00	314.93	0.2191	
	120	119.14	293.25	0.4063	
		165.60	344.61	0.0018	
F-tor 5	60	30.80	288.78	0.1067	
		52.80	348.47	0.1515	
	80	67.54	303.04	0.2229	
		71.40	323.82	0.2205	
	120	123.10	278.86	0.4414	
		131.30	290.34	0.4522	
PT-15	60	38.70	305.51	0.1267	
		43.20	323.33	0.1336	
	80	57.90	299.60	0.1933	
		71.80	314.43	0.2283	
	120	144.80	291.93	0.4960	
		151.80	319.05	0.4758	
		Series I: talc			
ET-4	60	26.82	312.50	0.0858	
		32.38	271.01	0.1195	
	80	44.59	298.76	0.1493	
		76.95	322.47	0.2386	
	120	97.55	306.95	0.3178	Ducts/canals
		102.21	282.13	0.3623	
ET-30	60	34.87	317.03	0.1100	
		40.53	287.25	0.1411	
	80	51.38	303.39	0.1694	
		44.40	305.86	0.1452	
	120	111.63	301.19	0.3706	
		125.32	304.06	0.4122	

(continued)

TABLE B-24 (continued)

Kind of fabric	q_g (m^3/m^2h)	$P_n - P_{n-1}$	$L_{o_n} - L_{o_{n-1}}$	K_2'	Comments
F-tor 5	60	31.41	296.42	0.1060	
		44.08	311.38	0.1416	
	80	52.48	311.92	0.1682	
		56.73	295.45	0.1920	
	120	127.17	348.57	0.3648	Ducts/canals
		145.26	309.24	0.4697	
PT-15	60	26.74	306.06	0.0874	
		39.18	286.16	0.1369	
	80	54.99	298.72	0.1841	
		68.73	328.16	0.2094	
	120	113.13	287.42	0.3936	
		119.60	301.03	0.3973	
Series I: fly ash					
ET-4	60	8.61	288.54	0.0298	
		13.93	301.16	0.0463	
	80	19.72	296.02	0.0666	
		30.56	322.04	0.0920	
	120	49.92	311.68	0.1602	
		55.69	297.86	0.1870	
ET-30	60	8.31	305.99	0.0272	
		12.77	306.91	0.0416	
	80	22.11	297.32	0.0744	
		27.33	316.67	0.0863	
	120	48.76	297.38	0.1640	
		69.51	321.33	0.2163	
F-tor 5	60	11.00	304.76	0.0361	
		16.84	283.65	0.0594	
	80	20.53	308.15	0.0666	
		24.25	296.58	0.0818	
	120	45.98	301.29	0.1526	
		62.10	299.34	0.2075	

(continued)

TABLE B-24 (continued)

Kind of fabric	q_g (m^3/m^2h)	$P_n - P_{n-1}$	$L_{o_n} - L_{o_{n-1}}$	K_2'	Comments
PT-15	60	10.60	299.49	0.0354	
		15.01	310.19	0.0484	
	80	17.93	311.08	0.0576	
		32.00	316.80	0.1010	
	120	50.71	306.05	0.1657	
		78.30	298.08	0.2627	
		Series II and III: fly ash			
ET-4	60	0.49	21.84	0.022	
		0.55	28.95	0.019	
		2.93	104.74	0.028	
		2.82	96.19	0.029	
		3.37	92.29	0.036	
		4.04	90.82	0.044	
		9.48	232.99	0.041	
		2.31	91.05	0.025	
	70	0.61	20.34	0.303	
		0.76	33.22	0.023	
		4.78	101.02	0.047	
		5.40	96.81	0.056	
		6.83	108.48	0.063	
		5.55	101.55	0.055	
		13.04	220.04	0.059	
		6.24	60.15	0.104	
	80	0.59	17.74	0.033	
		1.63	36.83	0.044	
		4.52	97.57	0.046	
		7.57	97.44	0.078	
		7.87	102.35	0.077	
		8.07	115.08	0.070	
		19.28	187.41	0.103	
		7.18	126.18	0.057	
	100	1.67	18.87	0.027	
		1.09	28.01	0.039	
		7.20	106.11	0.068	
		8.78	98.00	0.089	
		9.90	98.21	0.101	
		14.06	115.03	0.122	
		25.44	196.01	0.130	
		9.16	106.11	0.086	

(continued)

TABLE B-24 (continued)

Kind of fabric	q_g (m³/m²h)	$P_n - P_{n-1}$	$L_{o_n} - L_{o_{n-1}}$	K_2'	Comments
	120	1.86	16.48	0.113	
		5.23	33.27	0.157	
		10.97	107.20	0.102	
		13.60	94.24	0.144	
		14.23	99.86	0.142	
		13.02	98.18	0.133	
		39.03	212.97	0.183	
		9.32	66.61	0.140	
	140	41.05	214.17	0.192	Ducts/canals
		55.41	186.82	0.297	
		89.12	223.58	0.399	
	160	41.91	175.55	0.239	Ducts/canals
		71.67	216.57	0.331	
		102.66	218.29	0.470	
	180	61.48	191.59	0.321	Ducts/canals
		96.91	213.36	0.454	
		110.80	198.37	0.559	
	200	2.86	20.88	0.137	Ducts/canals
		6.13	25.18	0.243	
		23.72	99.70	0.238	
		26.60	100.53	0.265	
		33.36	98.38	0.339	
		52.77	118.56	0.445	
		121.59	193.73	0.628	
		27.00	106.42	0.253	
ET-30	70	0.45	19.74	0.023	
		1.02	28.58	0.036	
		3.49	97.21	0.036	
		7.69	101.27	0.076	
		5.63	106.26	0.053	
		5.99	95.00	0.063	
		13.57	217.38	0.062	
		5.29	59.38	0.089	
	80	1.22	21.28	0.057	
		1.86	29.15	0.064	
		5.39	104.93	0.051	
		6.48	92.79	0.070	
		6.29	105.96	0.059	
		9.58	91.82	0.104	
		20.23	208.41	0.097	
		10.43	88.65	0.118	

(continued)

TABLE B-24 (continued)

Kind of fabric	q_g (m^3/m^2h)	$P_n - P_{n-1}$	$L_{o_n} - L_{o_{n-1}}$	K_2'	Comments
	100	0.66	22.04	0.030	
		3.50	29.03	0.121	
		7.62	103.35	0.074	
		10.82	108.01	0.100	
		12.09	86.53	0.140	
		15.25	119.50	0.128	
		29.15	191.78	0.152	
		10.75	102.50	0.105	
	120	2.37	20.89	0.113	
		3.60	30.34	0.119	
		15.34	107.76	0.142	
		14.54	93.34	0.156	
		16.98	97.99	0.173	
		24.97	99.27	0.251	
		23.70	220.22	0.108	
		16.27	88.52	0.184	
	140	48.34	211.01	0.229	
		70.42	221.48	0.318	
		90.80	199.63	0.455	
	160	47.71	175.15	0.272	
		90.64	242.42	0.374	
		85.21	172.56	0.494	
	180	66.10	205.47	0.322	
		108.01	205.10	0.527	
		129.00	220.49	0.585	
	200	7.32	21.12	0.347	
		8.09	30.80	0.263	
		30.65	19.59	0.308	
		36.10	97.33	0.371	
		53.09	108.43	0.490	
		50.47	98.10	0.514	
		116.00	209.25	0.554	
		91.00	105.80	0.860	

TABLE B-25. KINETIC SPECIFIC SURFACE OF CEMENT DUST (Series II)

Fraction (μm)	d_{50} (μm)	Porosity	Kinetic specific surface (cm^2/g)
< 2	1.3	0.690	18 147.0
2 - 5	3.0	0.622	10 104.6
> 5	30.0	0.405	1 640.2
5 - 8	4.0	0.589	7 302.8
> 8	38.0	0.412	1 000.2
8 - 10	6.3	0.540	3 784.0
> 10	36.0	0.400	898.0
10 - 12	10.5	0.506	2 678.0
> 12	36.0	0.432	692.0
12 - 15	13.0	0.511	2 094.0
> 15	46.0	0.427	662.0
> 8	37.0	0.431	1 331.0

TABLE B-26. KINETIC SPECIFIC SURFACE OF COAL DUST (Series II)

Fraction (μm)	d_{50} (μm)	Porosity	Kinetic specific surface (cm^2/g)
< 2	2.5	0.682	25 522.10
2 - 5	2.9	0.572	12 556.50
< 5	2.8	0.640	18 840.20
5 - 10	6.0	0.564	9 787.70
> 10	32.0	0.348	1 665.80
10 - 30	16.0	0.444	3 244.10
> 30	80.0	0.414	931.25
< 10	5.0	0.592	16 948.40
10 - 20	8.0	0.497	7 321.83
> 20	47.0	0.403	1 414.00

TABLE B-27. KINETIC SPECIFIC SURFACE OF TALC (Series II)

Fraction (μm)	d_{50} (μm)	Porosity	Kinetic specific surface (cm^2/g)
< 2	2.0	0.731	30 667.80
2 - 5	2.5	0.668	20 392.00
< 5	2.3	0.694	28 687.60
> 5	10.0	0.591	4 687.83
5 - 10	5.5	0.664	9 743.67
> 10	12.0	0.597	3 149.00
10 - 15	9.0	0.608	4 221.20
> 15	18.0	0.557	2 340.83
15 - 20	14.0	0.559	2 464.00
> 20	25.0	0.563	1 394.40

TABLE B-28. KINETIC SPECIFIC SURFACE OF FLY ASH (Series II)

Fraction (μm)	d_{50} (μm)	Porosity	Kinetic specific surface (cm^2/g)
< 2	2.0 (1.8)	0.5443	12 145.50
2 - 5	2.5	0.486	8 337.90
< 5	3.0	0.503	9 955.90
> 5	9.0	0.453	3 319.17
5 - 8	4.5	0.489	5 349.00
> 8	12.0	0.473	2 538.00
8 - 13	6.5	0.503	4 161.00
> 13	20.0	0.480	1 451.00

TABLE B-29. DECREASE OF DUST LAYER INITIAL THICKNESS DURING SHOCKING FOR UNSEPARATED CEMENT

Shocking (s)	Time t_s(s)	Initial thickness of dust layer, H_o (mm)				
		30	50	70	90	200
5	5	2.5	4.0	8.5	9.0	8.5
10	15	5.5	9.5	13.5	14.0	18.0
15	30	7.5	12.5	18.5	19.5	25.5
30	60	8.5	14.0	21.5	24.5	38.0
60	120	9.0	15.5	23.5	27.0	51.5
300	420	10.0	17.0	25.5	29.5	59.5
600	1 020	11.0	18.0	27.5	31.0	62.5
2 400	3 420	11.5	19.5	30.0	32.5	65.5

TABLE B-30. DECREASE OF DUST LAYER INITIAL THICKNESS DURING SHOCKING FOR SEPARATED CEMENT

Shocking (s)	Time t_s(s)	Initial thickness of dust layer, H_o (mm)				
		30	50	70	90	200
5	5	2.5	2.0	2.0	2.0	8.0
10	15	6.0	6.0	6.5	8.0	14.0
15	30	8.5	10.0	11.5	13.0	21.5
30	60	9.5	13.0	17.5	21.0	32.5
60	120	10.0	14.5	20.0	26.0	47.0
300	420	11.0	16.5	22.0	29.0	63.5
600	1 020	11.5	17.0	23.5	30.0	68.0
2 400	3 400	12.5	18.5	25.5	32.5	71.0

TABLE B-31. DECREASE OF DUST LAYER INITIAL THICKNESS DURING SHOCKING FOR UNSEPARATED COAL

Shocking (s)	Time t_s(s)	Initial thickness of dust layer, H_o (mm)				
		30	50	70	90	200
5	5	2.0	2.0	4.0	3.8	4.0
10	15	3.5	4.5	6.2	7.0	16.0
15	30	4.5	7.5	9.0	10.0	20.0
30	60	5.5	10.8	15.1	15.5	27.2
60	120	6.0	12.8	19.0	21.5	39.0
300	420	7.5	13.3	20.6	24.0	66.0
600	1 020	7.5	13.3	21.2	24.3	69.0
2 400	3 420	7.5	13.8	21.3	24.3	70.0

TABLE B-32. DECREASE OF DUST LAYER INITIAL THICKNESS DURING SHOCKING FOR SEPARATED COAL

Shocking (s)	Time t_s(s)	Initial thickness of dust layer, H_o (mm)				
		30	50	70	90	200
5	5	1.0	2.0	3.0	3.5	10.0
10	15	3.0	5.0	6.0	8.0	12.0
15	30	6.0	9.0	10.0	12.0	24.0
30	60	10.0	12.0	15.0	18.0	32.5
60	120	11.0	14.0	17.5	23.0	46.6
300	420	11.0	15.0	19.0	24.5	61.0
600	1 020	11.0	15.0	19.0	24.5	61.0
2 400	3 420	11.0	15.0	19.0	24.5	61.0

TABLE B-33. DECREASE OF DUST LAYER INITIAL THICKNESS DURING SHOCKING FOR NONSEPARATED FLY ASH

Shocking (s)	Time t_s(s)	Initial thickness of dust layer, H_0 (mm)				
		30	50	70	90	200
5	5	1.5	2.0	3.0	4.5	6.5
10	15	5.5	5.0	7.5	9.0	13.5
15	30	7.5	8.0	12.0	14.5	20.0
30	60	8.5	10.0	17.0	21.5	30.0
60	120	9.0	11.0	19.5	25.5	42.5
300	420	10.0	12.5	21.5	28.5	51.5
600	1 020	10.5	13.9	22.5	29.5	53.5
2 400	3 420	11.0	14.9	23.5	30.5	55.0

TABLE B-34. DECREASE OF DUST LAYER INITIAL THICKNESS DURING SHOCKING FOR SEPARATED FLY ASH

Shocking (s)	Time t_s(s)	Initial thickness of dust layer, H_0 (mm)				
		30	50	70	90	200
5	5	1.5	2.5	2.0	3.0	10.0
10	15	3.5	6.0	5.5	7.0	18.0
15	30	6.5	10.0	9.5	11.5	26.5
30	60	7.5	12.5	14.5	18.5	36.5
60	120	8.0	13.5	17.0	23.5	49.0
300	420	8.5	14.5	19.0	25.5	63.0
600	1 020	9.0	15.0	19.5	26.0	64.5
2 400	3 420	10.5	16.0	20.5	27.5	64.5

TABLE B-35. EXPERIMENTAL RESULTS FROM LARGE-SCALE TESTS

E (%)	q_g (m^3/m^2h)	q_p (g/m^2h)	L_o (g/m^2)	L_N (g/m^2)	L_p (g/m^2)	t_F (min)	c_1 (g/m^2)
			Fabric ET-4 tested with fly ash				
99.9515	61.0	602.7	314.0	211.0	103.0	25	9.88
99.9830	60.5	607.4	482.3	292.4	189.9	80	10.04
99.9835	59.1	614.0	568.0	295.6	272.4	110	10.39
99.9756	59.3	613.2	716.9	292.9	424.0	165	10.34
99.9799	58.5	613.7	887.6	298.2	589.4	218	10.49
99.9744	80.8	760.3	303.4	200.8	102.6	20	9.41
99.9981	80.5	783.3	433.7	232.4	201.3	41	9.73
99.9752	80.8	783.0	538.5	239.6	298.9	54	9.69
99.9987	80.1	827.4	640.1	240.6	399.5	65	10.33
99.9979	79.9	758.3	831.7	241.3	590.4	110	9.49
99.9963	80.5	821.1	1 037.0	231.4	805.6	132	10.20
99.9450	101.3	976.5	317.2	189.0	128.2	14	9.64
99.9184	101.7	973.3	430.2	223.8	206.4	25	9.57
99.8988	101.3	986.7	529.8	229.4	300.4	35	9.74
99.9471	101.3	995.8	662.6	262.1	400.5	51	9.83
99.8695	102.0	977.2	976.6	274.8	601.8	75	9.58
99.9555	102.2	1 011.8	1 043.7	252.4	791.3	100	9.90
99.8622	120.0	1 155.6	292.7	196.7	96.0	12	9.63
99.9088	121.8	1 149.8	421.5	226.8	194.7	20	9.44
99.8974	121.4	1 136.3	539.5	241.1	298.4	31	9.36
99.8324	121.1	1 120.2	653.4	248.8	404.6	40	9.25
99.9353	120.0	1 226.4	858.2	256.9	601.3	61	10.22
99.8799	119.3	1 152.4	1 090.7	294.3	796.4	92	9.66
99.7464	163.3	1 569.3	387.2	279.4	107.8	8	9.61
99.4738	161.3	1 490.4	506.2	300.4	205.8	15	9.24
98.8154	161.7	1 534.5	595.7	297.7	298.0	20	9.49
99.6966	160.8	1 532.4	696.3	297.3	399.0	25	9.53
99.6468	161.7	1 524.8	906.3	302.9	603.4	40	9.43
99.8070	161.3	1 590.4	1 114.7	299.9	814.8	52	9.86

(continued)

TABLE B-35 (continued)

E (%)	q_g (m^3/m^2h)	q_p (g/m^2h)	L_o (g/m^2)	L_N (g/m^2)	L_p (g/m^2)	t_F (min)	c_1 (g/m^2)
Fabric ET-30 tested with fly ash							
99.9070	59.6	582.9	221.2	115.7	105.5	25	9.78
99.9967	61.4	608.5	332.8	124.9	207.9	52	9.91
99.9979	61.4	633.0	438.3	137.6	300.7	89	10.31
99.9780	61.4	608.5	519.4	124.9	394.5	110	9.91
99.9785	61.0	624.0	740.1	128.0	612.1	171	10.23
99.9896	59.6	600.2	848.2	140.6	707.6	223	10.07
99.9660	79.0	790.8	246.1	142.7	103.4	20	10.01
99.9684	80.1	791.4	356.3	147.3	209.0	35	9.88
99.9842	80.8	770.0	457.7	156.0	301.7	54	9.53
99.9816	79.9	827.0	564.2	151.4	412.8	78	10.35
99.9857	78.5	769.3	644.2	151.4	492.8	110	9.80
99.9963	79.7	838.4	757.9	155.0	602.9	126	10.52
99.9845	80.3	833.5	936.3	146.8	789.5	157	10.38
99.9769	100.2	914.8	251.8	154.4	97.4	16	9.13
99.9875	99.9	1 047.0	388.4	185.5	202.9	31	10.48
99.9491	99.5	1 017.9	497.0	198.8	298.2	45	10.23
99.9829	99.5	988.0	586.1	195.7	390.4	60	9.93
99.9139	99.8	1 032.9	791.5	192.6	598.9	90	10.35
99.9944	102.2	1 029.2	985.7	184.0	967.3	130	10.07
99.8907	123.1	1 143.6	242.1	145.8	96.3	10	9.29
99.7074	124.5	1 174.0	344.5	159.0	185.5	20	9.43
99.8035	123.2	1 188.9	492.3	208.4	283.9	35	9.65
99.7869	121.2	1 164.7	576.9	183.5	393.4	50	9.61
99.7723	120.0	1 254.0	787.0	192.2	594.8	78	10.45
99.9771	121.6	1 212.4	1 007.7	182.5	825.2	104	9.97
99.8513	160.0	1 552.0	261.5	171.8	89.7	7	9.70
99.9106	157.6	1 528.7	383.3	181.4	201.9	17	9.70
99.8009	156.5	1 565.0	524.5	207.9	316.6	25	10.00
99.7878	157.2	1 586.1	597.9	197.8	399.1	30	10.09
99.5197	157.3	1 617.0	791.5	204.9	586.6	43	10.28
99.8270	160.7	1 597.4	990.8	190.6	800.2	60	9.94

TABLE B-36. DETERMINATION OF ABSOLUTE DENSITY OF UNSEPARATED CEMENT WITH d_{50} = 30 µm

N_o of sample	Density determined by liquid pycnometer (g/cm^3)	$x_i - \bar{x}$	$(x_i - \bar{x})^2$	Density determined by air pycnometer (g/cm^3)	$x_i - \bar{x}$	$(x_i - \bar{x})^2$
1	2.78	0.00	0.0000	2.90	0.07	0.0049
2	2.74	0.04	0.0016	2.88	0.05	0.0025
3	2.80	0.02	0.0004	2.78	0.05	0.0025
4	2.78	0.00	0.0000	2.86	0.03	0.0009
5	2.76	0.02	0.0004	2.74	0.09	0.0081
6	2.78	0.00	0.0000	2.69	0.14	0.0196
7	2.84	0.06	0.0036	2.72	0.11	0.0121
8	2.78	0.00	0.0000	2.87	0.04	0.0016
9	2.78	0.00	0.0000	2.78	0.05	0.0025
10	2.78	0.00	0.0000	2.94	0.11	0.0121
11				2.77	0.06	0.0036
12				2.86	0.03	0.0009
13				2.83	0.00	0.0000
14				2.92	0.09	0.0081
15				2.92	0.09	0.0081
16				2.86	0.03	0.0009
17				2.84	0.01	0.0001
18				2.78	0.05	0.0025
Σ	27.82	0.14	0.0060	50.94	1.10	0.0910
$\bar{x}$	2.78			2.83		

Mean square deviation, σ, = 0.0082.

Deviation from mean, Δρ, = 0.018.

In 95 of 100 determinations made by this method, results were in the range, ρ = 2.78 ± 0.018.

Mean square deviation, σ, = 0.0172.

Deviation from mean, Δρ, = 0.036.

In 95 of 100 determinations made by this method, results were in the range, ρ = 2.83 ± 0.036.

TABLE B-37. DETERMINATION OF ABSOLUTE DENSITY OF UNSEPARATED COAL WITH d_{50} = 22 μm

N_o of sample	Density determined by liquid pycnometer (g/cm³)	$x_i - \bar{x}$	$(x_i - \bar{x})^2$	Density determined by air pycnometer (g/cm³)	$x_i - \bar{x}$	$(x_i - \bar{x})^2$
1	1.45	0.00	0.0000	1.46	0.01	0.0001
2	1.43	0.02	0.0004	1.44	0.01	0.0001
3	1.45	0.00	0.0000	1.46	0.01	0.0001
4	1.42	0.03	0.0009	1.49	0.04	0.0016
5	1.45	0.00	0.0000	1.45	0.00	0.0000
6	1.46	0.01	0.0001	1.39	0.06	0.0036
7	1.47	0.02	0.0004	1.40	0.05	0.0025
8	1.47	0.02	0.0004	1.44	0.01	0.0001
9	1.46	0.01	0.0001	0.44	0.01	0.0001
10	1.46	0.01	0.0001	0.44	0.01	0.0001
11				1.48	0.03	0.0009
12				1.45	0.00	0.0000
13				1.44	0.01	0.0001
14				1.48	0.03	0.0009
15				1.49	0.04	0.0016
16				1.41	0.04	0.0016
17				1.44	0.01	0.0001
Σ	14.52	0.12	0.0024	24.6	0.37	0.0135
$\bar{x}$	1.45			1.45		

Mean square deviation, σ, = 0.0052.

Deviation from mean, Δρ, = 0.012.

In 95 of 100 determinations made by this method, results were in the range, ρ = 1.45 ± 0.012.

Mean square deviation, σ, = 0.0070.

Deviation from mean, Δρ, = 0.015.

In 95 of 100 determinations made by this method, results were in the range, ρ = 1.45 ± 0.015.

TABLE B-38. DETERMINATION OF ABSOLUTE DENSITY OF UNSEPARATED COAL WITH d_{50} = 49 μm

No of sample	Density determined by liquid pycnometer (g/cm³)	$x_i - \bar{x}$	$(x_i - \bar{x})^2$	Density determined by air pycnometer (g/cm³)	$x_i - \bar{x}$	$(x_i - \bar{x})^2$
1	1.45	0.01	0.0001	1.43	0.02	0.0004
2	1.45	0.01	0.0001	1.47	0.02	0.0004
3	1.41	0.05	0.0025	1.38	0.07	0.0049
4	1.45	0.01	0.0001	1.40	0.05	0.0025
5	1.47	0.01	0.0001	1.48	0.03	0.0009
6	1.46	0.00	0.0000	1.46	0.01	0.0001
7	1.58	0.12	0.0144	1.46	0.01	0.0001
8	1.42	0.04	0.0016	1.41	0.04	0.0016
9	1.44	0.02	0.0004	1.44	0.01	0.0001
10	1.46	0.00	0.0000	1.44	0.01	0.0001
11	1.43	0.03	0.0009	1.42	0.03	0.0009
12	1.45	0.01	0.0001	1.45	0.00	0.0000
13	1.43	0.03	0.0009	1.43	0.02	0.0004
14	1.43	0.03	0.0009	1.43	0.02	0.0004
15	1.40	0.06	0.0036	1.40	0.05	0.0025
16	1.42	0.04	0.0016	1.42	0.03	0.0009
17	1.40	0.03	0.0009	1.55	0.10	0.0100
18	1.47	0.01	0.0001	1.47	0.02	0.0004
19	1.48	0.02	0.0004	1.45	0.00	0.0000
20	1.48	0.02	0.0004	1.48	0.03	0.0009
21	1.48	0.02	0.0004	1.46	0.01	0.0001
22	1.48	0.02	0.0004	1.46	0.01	0.0001
23	1.48	0.02	0.0004	1.47	0.02	0.0004
24	1.49	0.03	0.0009	1.50	0.05	0.0025
Σ	35.00	0.64	0.0312	34.76	0.66	0.0306
$\bar{x}$	1.46			1.45		

Mean square deviation, σ, = 0.0075.
Deviation from mean, Δρ, = 0.016.
In 95 of 100 determinations made by this method, results were in the range, ρ = 1.46 ± 0.016.

Mean square deviation, σ, = 0.0074.
Deviation from mean, Δρ, = 0.015.
In 95 of 100 determinations made by this method, results were in the range, ρ = 1.45 ± 0.015.

TABLE B-39. DETERMINATION OF ABSOLUTE DENSITY OF UNSEPARATED COAL WITH d_{50} = 7.0 µm

No of sample	Density determined by liquid pycnometer (g/cm^3)	$x_i - \bar{x}$	$(x_i - \bar{x})^2$	Density determined by air pycnometer (g/cm^3)	$x_i - \bar{x}$	$(x_i - \bar{x})^2$
1	1.54	0.01	0.0001	1.54	0.01	0.0001
2	1.54	0.01	0.0001	1.54	0.01	0.0001
3	1.56	0.01	0.0001	1.54	0.01	0.0001
4	1.64	0.09	0.0081	1.74	0.19	0.0361
5	1.56	0.01	0.0001	1.55	0.00	0.0000
6	1.66	0.11	0.0121	1.66	0.11	0.0121
7	1.53	0.02	0.0004	1.52	0.03	0.0009
8	1.54	0.01	0.0001	1.54	0.01	0.0001
9	1.54	0.01	0.0001	1.53	0.02	0.0004
10	1.53	0.02	0.0004	1.53	0.02	0.0004
11	1.51	0.04	0.0016	1.53	0.02	0.0004
12	1.46	0.09	0.0081	1.44	0.11	0.0121
13	1.54	0.01	0.0001	1.55	0.00	0.0000
14	1.50	0.05	0.0025	1.48	0.07	0.0049
15	1.53	0.02	0.0004	1.54	0.01	0.0001
16	1.52	0.03	0.0009	1.52	0.03	0.0009
17	1.55	0.00	0.0000	1.55	0.00	0.0000
18	1.56	0.01	0.0001	1.55	0.00	0.0000
19	1.55	0.00	0.0000	1.60	0.05	0.0025
20	1.55	0.00	0.0000	1.55	0.00	0.0000
21	1.55	0.00	0.0000	1.55	0.00	0.0000
22	1.55	0.00	0.0000	1.56	0.01	0.0001
Σ	34.01	0.55	0.0353	34.11	0.71	0.0713
$\bar{x}$	1.55			1.55		

Mean square deviation, σ, = 0.0087.
Deviation from mean, Δρ, = 0.018.
In 95 of 100 determinations made by this method, results were in the range, ρ = 1.55 ± 0.018.

Mean square deviation, σ , = 0.0124.
Deviation from mean, Δρ, = 0.026.
In 95 of 100 determinations made by this method, results were in the range, ρ = 1.55 ± 0.026.

TABLE B-40. DETERMINATION OF ABSOLUTE DENSITY OF SEPARATED TALC WITH d_{50} = 9.0 μm

N_o of sample	Density determined by liquid pycnometer (g/cm^3)	$x_i - \bar{x}$	$(x_i - \bar{x})^2$	Density determined by air pycnometer (g/cm^3)	$x_i - \bar{x}$	$(x_i - \bar{x})^2$
1	2.69	0.01	0.0001	2.62	0.19	0.0361
2	2.69	0.01	0.0001	2.91	0.10	0.0100
3	2.69	0.01	0.0001	2.94	0.13	0.0169
4	2.71	0.01	0.0001	2.89	0.08	0.0064
5	2.71	0.01	0.0001	2.65	0.16	0.0256
6	2.74	0.04	0.0016	2.87	0.06	0.0036
7	2.69	0.01	0.0001	2.91	0.10	0.0100
8	2.69	0.01	0.0001	2.75	0.06	0.0036
9	2.70	0.00	0.0000	2.72	0.09	0.0081
10	2.69	0.01	0.0001	2.85	0.04	0.0016
11				2.94	0.13	0.0169
12				2.90	0.09	0.0081
13				2.85	0.04	0.0016
14				2.63	0.18	0.0324
15				2.75	0.06	0.0036
16				2.86	0.05	0.0025
Σ	27.00	0.12	0.0024	45.04	1.56	0.1870
$\bar{x}$	2.70			2.81		

Mean square deviation, σ, = 0.0052.

Deviation from mean, Δρ, = 0.012.

In 95 of 100 determinations made by this method, results were in the range, ρ = 2.70 ± 0.012.

Mean square deviation, σ, = 0.0279.

Deviation from mean, Δρ, = 0.060.

In 95 of 100 determinations made by this method, results were in the range, ρ = 2.81 ± 0.060.

APPENDIX C
GLOSSARY OF TERMS

APPENDIX C

GLOSSARY OF TERMS

Different terms are used in the literature concerning dust filtration through filtration media and the parameters and stages characteristic of the dust filtration processes. Accordingly, these terms and their definitions are listed as used in this project. The proposed terms have physical meaning according to the processes and phenomena occurring during the dust filtration process (which differs from other filtration processes, such as air filtration).

Terms commonly used in English are used in this report, but the glossary also lists parenthetically the literal English translation of the corresponding Polish term.

Aerosol	A two-phase system, composed of a gas and a solid-dispersed phase, which under certain conditions can be treated as stable or quasi-stable (dry filtration).
Filtration	Removal of solid particles from an aerosol stream by deposition in or on the structure of a porous medium.
Air Filtration	Filtration of atmospheric aerosols.
Dust Filtration	Filtration of industrial aerosols.
Dust Filtration Type I	The initial phase of the complete dust filtration process when the fabric first begins operation as a filter medium. This phase ends when the pressure drop reaches a predetermined level immediately prior to the first regeneration cycle.
Dust Filtration Type II	The second phase begins with the first regeneration cycle and continues until the fabric attains a steady state residual dust load (is fully filled with dust).
Dust Filtration Type III	The third phase begins after a stable level of residual dust load has been reached so the pressure drop returns to a constant level after regeneration. This process is typical of industrial dust collectors.

Face velocity (Polish term [not used in this report]: gas loading of filtration area)	Mean calculated value of gas quantity, in cubic meters, passing through a square meter of filtration medium per hour (air-to-cloth ratio [A/C]).
Dust flux (Polish term [not used in this report]: dust loading of filtration area)	Mean calculated value of dust quantity, in grams, deposited on a square of filtration medium per hour.
Filtration velocity	The actual local velocity of an aerosol, in meters per second, passing through a filter medium (measured under actual conditions).
Residual dust load (Polish term: structure filled with dust)	The areal mass density of the dirty filter including all dust retained after regeneration but without dust cake (g/m^2).
Steady state residual dust load (Polish term: structure fully filled with dust)	Residual dust load after steady state operation is reached (g/m^2).
Terminal dust load (Polish term: structure covered with dust)	The areal mass density of dust accumulated on the filter, including the dust cake, prior to regeneration (g/m^2).
Dust cake	The porous dust layer built up on the fabric surface during dust filtration. Its characteristics depend on the kind of fabric, the kind of dust, and the process parameters.
Free area effect	Decrease of dust filtration efficiency caused by interyarn free area viewed in the plane of the fabric.
Basket effect	Decrease of dust filtration efficiency caused by interyarn free area viewed askew to the fabric plane.

APPENDIX D
LIST OF NOMENCLATURE

APPENDIX D

LIST OF NOMENCLATURE

A_o = Distance between warp threads

A_w = Distance between fill threads

BFA = Basket free area

C = Velocity of particle migration affected by external forces

C = Primary factor of fiber raw material

C = Cunningham slip correction factor

c_1 = Initial dust concentration

c_2 = Final dust concentration

d = Yarn diameter

$\bar{d}$ = Mean particle diameter

$d_{eqv.\ p}$ = Equivalent pore diameter

$d^m_{eqv.\ p}$ = Median of equivalent pore diameter

d_f = Elementary fiber diameter

d_{Lim} = Limited dust particle diameter

dN = Number of particles in voluminal unit of fluid for particles from d_p to $d_p + (d_p)$

d_o = Warp diameter

d_p = Particle diameter

d_p = Pore diameter

d_w = Fill diameter

D = Diffusion coefficient

E = Filtration efficiency

E = Local value of electric field intensity

$\bar{E}$ = Mean dust collection efficiency

E_o = Initial dust collection efficiency

$E_{o\ I}$ = Initial dust collection efficiency in Dust Filtration Process Type I

$E_{o\ III}$ = Initial dust collection efficiency in Dust Filtration Process Type III

E_I = Filtration efficiency of Dust Filtration Process Type I

E_{II} = Filtration efficiency of Dust Filtration Process Type II

E_{III} = Filtration efficiency of Dust Filtration Process Type III

E_L = Hopper efficiency

E_o = Full filling with warp yarn

E_w = Full filling with fill yarn

f_L = Percentage by weight of dust cake, which is not regenerated during regeneration cycle

F = Active filtration surface

F = Pore area

F = Filtration element surface

F_c = Dust cake area

F_C = Coulomb force

F_p = Pore area in field, F_c

FA = Free area

G = Fabric thickness

G_1 = Weight of filtration element after regeneration

G_2 = Weight of clean filtration element

G_c = Weight of dust fed into the testing chamber

G_o = Weight of dust collected on the control filter

G_z = Weight of dust collected on the fabric

h = Thickness of dust cake

Δh = Decrease of dust layer initial thickness

h_o = Deflection of warp thread

h_t = Thickness of dust layer after a certain shocking time

h_w = Deflection of fill thread

H_o = Initial thickness of dust layer

k = Carman constant

K = Permeability for the dust-fabric system

K_1 = Resistance coefficient of porous layer (fabric)

K_1' = Resistance function of woven filtration materials

K_2 = Resistance coefficient for dust-fabric system

K_2'' = Resistance coefficient of dust-fabric system for second phase of Dust Filtration Process Type I

K_2''' = Resistance coefficient of dust-fabric system for second phase of Dust Filtration Process Type III

K_n = Knudsen number

K_o = Dimension of free areas between warp threads,

K_w = Dimension of free areas between fill threads

l_o = Length of elementary segment of warp

l_w = Length of elementary segment of fill

L = Porous layer thickness

L = Distance of nozzle from static element

L = Length of pore

L = Amount of dust in filtration structure

L_N = Residual dust load (Polish term: "structure filling with dust")

L_{NK} = Steady state residual dust load ("final filtration structure filling with dust")

L_o = Terminal dust load ("structure covered with dust")

L_o = Length of warp weave repeat

$\bar{L}_o$ = Mean value of structure covered with dust in filtration cycle

L_p = Characteristic parameter of dust cake

$\bar{L}_p$ = Mean value of characteristic dust cake parameter during the filtration cycle

L_w = Length of fill weave repeat

m_1 = Dipole moment

M = Superficial mass of fabric

M_d = Part of fraction less than the limited value of diameter

MMD = d_{50} = Mass median diameter of dust

n = Particle size distribution

n = Number of elementary fibers

n_o = Warp thread count per 100 cm of fabric

n_w = Fill thread count per 10 cm of fabric

Nm_o = Metrical number of warp threads

Nm_w = Metrical number of fill threads

O = Wetted perimeter of pore

p_o = Number of inflections of warp threads in weave repeat, R_o

p_w = Number of inflections of fill threads in weave repeat, R_w

P = Pore diameter distribution

ΔP = Pressure drop

ΔP_F = Filtration resistance

ΔP_{FI} = Filtration resistance of Dust Filtration Process Type I

ΔP_{FII} = Filtration resistance of Dust Filtration Process Type II

ΔP_{III} = Filtration resistance of Dust Filtration Process Type III

ΔP_i = Specific hydraulic resistance

ΔP_o = Initial pressure drop in dust filtration process for pure filtration structure

ΔP_N = Pressure drop corresponding to residual dust load in dust filtration process

ΔP_{NK} = Pressure drop corresponding to steady state residual dust load in dust filtration process

ΔP_K = Final pressure drop in dust filtration process corresponding to terminal dust load

ΔP_{LIM} = Limit gradient of pressure

q = Electric charge

q_g = Face velocity (Polish term: "gas loading of the filtration area")

q_{gA} = Face velocity during formation of static dust cake

$q_{g\ crit.}$ = Critical value of q_g (boundary value for laminar transition region flows)

$q_{g_{extr}}$ = Extreme value of q_g

q_{gT} = Critical value of q_g (boundary value for transition region to turbulent flows)

qp = Dust flux (Polish term: "dust loading of the filtration area")

Q = Mean flow intensity

Q_L = Linear charge density

r = Particle radius

$\bar{r}$ = Mean pore diameter

r = Polar coordinates

R = Average pore radius

R = Particle radius

R = Radius of cylindrical fiber

Re = Reynolds number

R_E = Regression function for dust collection efficiency

R_{E_o} = Value of regression function for $q_g = 0$

$R_{o\Delta P}$ = Value of regression function for $L = 0$

$R_{\Delta P}$ = Regression function for filtration resistance

R_o = Weave repeat along warp

R_w = Weave repeat along fill

R_s = Surface electric resistance of fabric area unit

S = Drag of dust-fabric system

S = Specific kinetic surface

S_o = Specific kinetic surface

t = Time

t_F = Filtration time

t_{FA} = Filtration time corresponding with point of inflection of hydraulic characteristic in Dust Filtration Process Type I

t_{FB} = Filtration time corresponding with point of inflection of hydraulic characteristic in Dust Filtration Process Type III

t_{FC} = Filtration time for definite filtration cycle

Δt_{PR} = Empirical gradient of dispersion medium temperature in real filtration process

t_R = Highest possible temperature of dew point

t_s = Shocking time

T_{PR} = Initial temperature of dispersion medium during the filtration process

u = Mechanical mobility of particle

v = Medium flow velocity

V = Gas velocity before the filtration structure

V = Gas velocity distribution

$\vec{V}$ = Gas velocity field

V_1 = Initial volume of the dust layer

V_2 = Final volume of the dust layer

$\bar{V}_o$ = Mean gas velocity of gas stream before the filtration structure

V_p = Gas velocity in pore

$\bar{V}_p$ = Mean gas velocity in porous structure

W_o = Takeup degree of warp

W_w = Takeup degree of fill

Z_o = Linear fabric filling with warp yarn

Z_w = Linear fabric filling with fill yarn

Z_t = Superficial fabric filling with yarn

x = Distance between particle and fiber axis

α = Coefficient of yarn filling with fibers

α = Fraction of solids in the dust layer

α = Degree of space packing with fiber

β_i = Ratio of actual residual dust load to the steady state residual dust load for a filtration/regeneration schedule

β_r = β_i estimated from hydraulic pressure data

ε = Porosity

ε = Medium permeability

ε_1 = Permeability of particle material

ε_o = Electric constant of vacuum,

ε_p = Superficial porosity

ε_v = Spatial porosity

η = Collection efficiency for single fiber

θ_o = Angle of wrap for warp

θ_w = Angle of wrap for fill

$\lambda, \bar{\lambda}$ = Mean free path of molecules

μ, v, v_f = Gas viscosity coefficient

ρ_α = Cross-resistivity of fabric

ρ_f = Fluid density

ρ_i = Packing density of dust layer

ρ_1 = Surface resistivity of fabric

ρ_m = Absolute density of dust

ρ_p = Density of particle

Σ_g = Geometrical standard deviation

Σ_p = Geometric standard deviation of equivalent pore size distribution

Ψ = Stokes impaction parameter